# METALLOGENY, GEOLOGICAL EVOLUTION, AND THERMOCHRONOLOGY OF THE CHILEAN ANDES BETWEEN LATITUDES 21° AND 26° SOUTH, AND THE ORIGIN OF MAJOR PORPHYRY COPPER DEPOSITS

by

VICTOR MAKSAEV



Submitted in partial fulfilment
of the requirements for the degree of
Doctor of Philosophy
at
Dalhousie University
Halifax, Nova Scotia, Canada
August, 1990

# METALLOGENY, GEOLOGICAL EVOLUTION, AND THERMOCHRONOLOGY OF THE CHILEAN ANDES BETWEEN LATITUDES 21° AND 26° SOUTH, AND THE ORIGIN OF MAJOR PORPHYRY COPPER DEPOSITS

by

VICTOR MAKSAEV



Submitted in partial fulfilment
of the requirements for the degree of
Doctor of Philosophy
at
Dalhousie University
Halifax, Nova Scotia, Canada
August, 1990

**DALHOUSIE UNIVERSITY**

**FACULTY OF GRADUATE STUDIES**

The undersigned hereby certify that they have read and recommend to the Faculty of Graduate Studies for acceptance a thesis entitled" Metallogeny, geological evolution, and thermochronology of the Chilean Andes between latitudes 21° and 26° South, and the origin of major porphyry copper deposits"

by Victor Maksaev

in partial fulfillment of the requirements for the degree of Doctor of Philosophy.



Dated 20th August '90

External Examiner

Research Supervisor

Examining Committee

[redacted]

DALHOUSIE UNIVERSITY

Date August 20, 1990

Author Victor Maksaev

Title METALLOGENY, GEOLOGICAL EVOLUTION, AND THERMOCHRONOLOGY OF THE CHILEAN ANDES BETWEEN LATITUDES 21° AND 26° SOUTH, AND THE ORIGIN OF MAJOR PORPHYRY COPPER DEPOSITS

Department or School: Geology

Degree: Ph.D. Convocation October Year 1990

Permission is herewith granted to Dalhousie University to circulate and to have copied for non-commercial purposes, at its discretion, the above title upon the request of individuals or institutions.

To Myriam, Igor and Nicolas

TABLE OF CONTENTS

## LIST OF FIGURES

## LIST OF TABLES

TABLES OF CHEMICAL ANALYSES

## ABSTRACT

The geologic evolution of the Antofagasta segment of the Chilean Andes (21°-26°S) has been dominated by persistent subduction-related calc-alkaline magmatism. The position of the magmatic front migrated subsequent to tectonic pulses that are recorded in the stratigraphy. Hydrothermal processes associated with over 300 Ma of virtually continuous igneous activity generated most of the metallic ore deposits. These include some of the world's largest porphyry copper deposits and significant concentrations of gold, silver, copper, iron, and sulphur.

Field observations and new $^{40}Ar$-$^{39}Ar$, K-Ar, and fission track data indicate that the most important metallic mineral deposits of this Andean segment were formed during three discrete metallogenic epochs: (1) Middle to Late Jurassic copper stratabound and vein copper deposits of the Coastal Cordillera Metallogenic Belt (2) Paleocene epithermal silver and gold vein deposits, and sub-economic porphyry copper type, and breccia pipe deposits in the western section of the Domeyko Cordillera Metallogenic Belt; and (3) Late Eocene-Early Oligocene giant porphyry copper deposits along the Domeyko Cordillera Metallogenic Belt.

The metallogenic analysis suggests that geologic, tectonic, and geomorphic factors influenced arc-related magmatic activity, hydrothermal, and supergene processes. This accounts for the extraordinary specialization and recurrence of copper mineralization of the region. The thermochronological data are consistent with formation of major porphyry copper deposits following uplift. Geochemical and isotopic data support the hypothesis that porphyry copper mineralization resulted from a period of deep magma generation after a crustal thickening event. Characteristic magmas with restricted Sr, Nd, and Pb isotopic compositions and optimum proportions of volatiles extracted metals from their source, transported their loads to near-surface where late-magmatic/hydrothermal processes concentrated metals and sulphur. Limited regional denudation resulting from aridity since the Late Cretaceous contributed to the formation and preservation of rich supergene ores.

## ACKNOWLEDGEMENTS

I am very thankful to my advisor Dr. Marcos Zentilli for constant enthusiasm, support, and encouragement throughout the duration of this project. I am very grateful to Dr. Casey Ravenhurst who provided advice on many aspects of the fission track dating method and sample preparation. Dr. Ravenhurst together with his wife Dr. Mary Harrington kindly helped me adjust to Canadian life. I thank Carlos Ulriksen, former Assistant Director of the "Servicio Nacional de Geología y Minería" (SERNAGEOMIN), who encouraged me to get involved in both the metallogenic study of the Antofagasta Region, and graduate studies at Dalhousie. I am indebted to Maria Teresa Cañas, former Director of the SERNAGEOMIN, and to Jorge Skarmeta and José Corvalán, former Assistant Directors of the same institution for granting leave of absence to do this thesis. I especially thank the geologists Ricardo Boric and Felipe Diaz, who also took active part in the study of the Antofagasta Region, provided valuable information about ore deposits, and collaborated with the sampling. I thank Carlos Perez de Arce who performed the conventional K-Ar dating and to Alvaro Puig who provided the use of the geochronological laboratory of the SERNAGEOMIN (Chile). I particularly thank my wife Myriam Brockway who assisted with the time-consuming mineral separation and tolerated the innumerable domestic inconveniences created by my graduate studies.

Dr. Peter Reynolds provided the use of the geochronology facilities at Dalhousie University and critically reviewed the manuscript. Keith Taylor provided advice on numerous aspects of sample preparation, laboratory techniques, and handled radioactive material. Dr. Raymond Donelick provided software and advice on the interpretation of fission track data. I thank Dr. Rebecca A. Jamieson, Dr. Jarda Dostal, and Milton Graves for their encouragement and critical reading of the manuscript.

Nicolas Marinovic contributed with samples and major element analyses of intrusive rocks from the Coastal Cordillera south of Antofagasta. Dr. Constantino Mpodozis provided REE analyses of Early Tertiary volcanic rocks. Dr. Charles N. Alpers supplied samples from La Escondida porphyry copper deposit. Moyra Gardeweg provided apatite samples from El Laco and Incahuasi iron deposits. Their collaboration is truly appreciated.

The sampling and field examination of ore deposits was helped by several mining geologists and mining companies. Particularly Orlando Alvarez, Chief Geologist of Chuquicamata; Enrique Tidy, Chief Research Geologist of CODELCO; Hans Dreyer, Chief Geologist of Compañia Minera de Michilla; Jose Miguel Ojeda, Chief Geologist of La Escondida (Utah Minera de Chile Inc.); Compañía Minera de Tocopilla; and Eulogio Gordo y Cia., División Minera.

Financial contributions to this research were made through the operating grant of Dr. Marcos Zentilli from the Natural Sciences and Engineering Research Council of Canada (NSERC Grant A-9036), SERNAGEOMIN (Chile), a Dalhousie Graduate Fellowship, and the Izaak Walton Killam Memorial Scholarship. Dr. James Walker (Northern Illinois University) financed the travel expenses for the last field season in 1986. The Intergovernmental Committee for Migration (ICM) provided reduced air fares to travel to Canada and back to Chile for the author and his family.

# CHAPTER 1. INTRODUCTION

## 1.1 GENERAL STATEMENT

The occurrence of abundant hydrothermal mineral deposits genetically related to igneous activity at active continental margins, such as the western border of South America, implies a genetic link between broad-scale subduction processes and metallic mineralization. The purpose of this project was to investigate, from a regional point of view, the relationships between the rich metallic mineralization and the geological evolution of a segment of the western flank of the Central Andes in northern Chile (Antofagasta Region; 21°-26°S) (Fig. 1.1). Particular attention was devoted to the metallogeny of major porphyry copper deposits.

The Antofagasta Region comprises 125,305 square kilometres. It is part of the Atacama desert where the high peaks of the Main Andes rise to altitudes above 6,000 m (from 200 to 300 km east of the Pacific coast). In a sharp contrast, the Chile-Peru oceanic trench 100 km offshore reaches a depth of 8,066 m. The 14,000 m difference of level between the deep trench and high mountains is the greatest on Earth.

The western flank of the Central Andes in northern and central Chile and southern Peru has long been recognized as a metallogenic province dominated by copper (e.g., Stoll, 1964, 1965; Ruiz and Ericksen, 1962). The segment of the Chilean Andes between 21° and 26° South (Antofagasta Region) is one of the richest sections of this copper-specialized metallogenic province, possessing more than 750 known metallic ore deposits of various types and different metals, including some of the largest and highest grade porphyry copper deposits in the world.

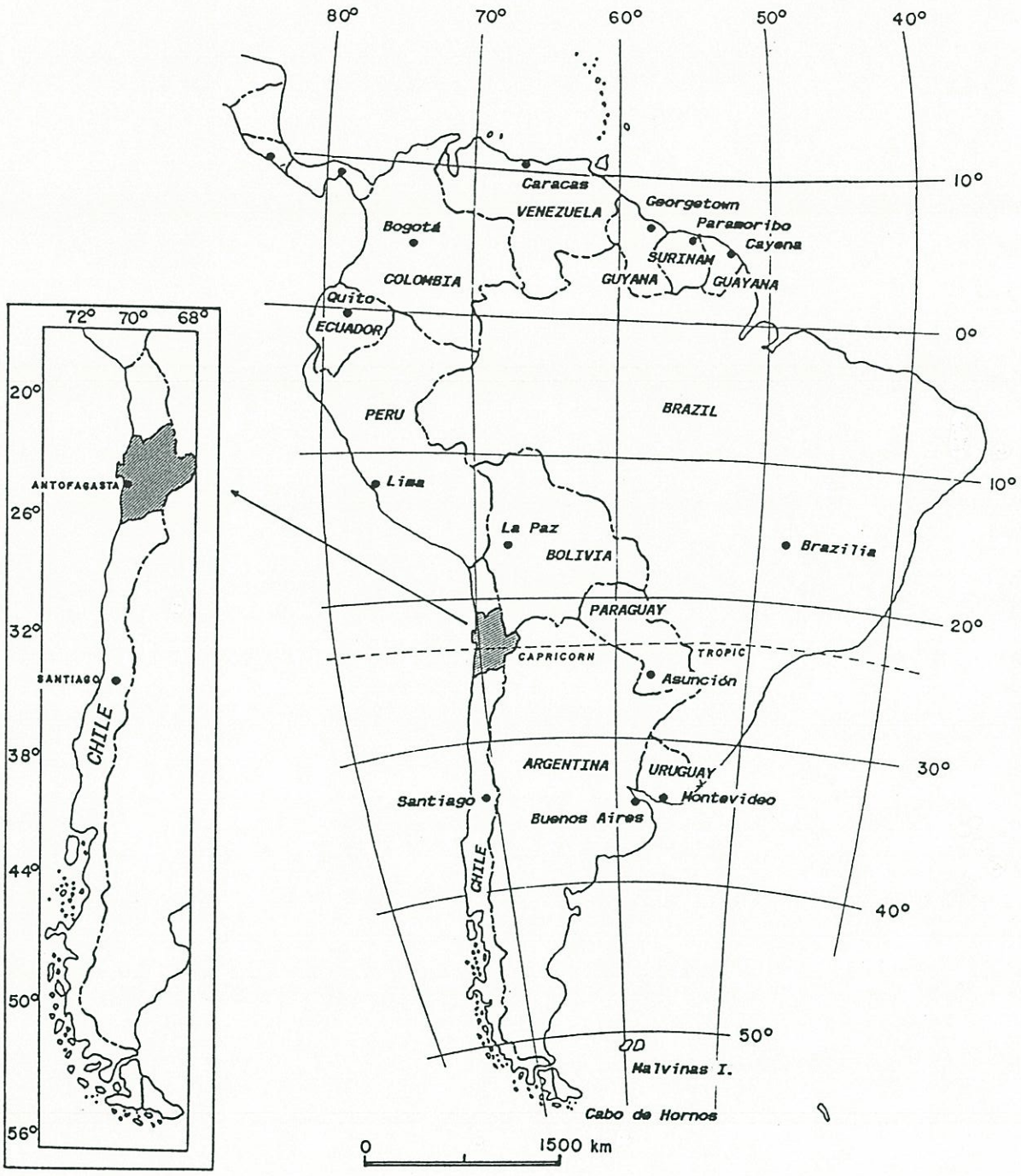


**Figure 1.1.** Location map of the Antofagasta Region, northern Chile.

The study area is a richly mineralized segment of the western flank of the Andes, and probably is a type area for continental margin metallogeny along a convergent plate boundary.

A wide range of geologic, thermochronological, isotopic, and petrochemical data have been used in this study for interpreting the geologic and metallogenic evolution of the Antofagasta Region. K-Ar, $^{40}Ar$-$^{39}Ar$ and fission track methods were used to constrain the age of major mineralizing, tectonic, erosive, and igneous processes. In addition, a conceptual model for the origin of major porphyry copper deposits was developed. Field work and sampling were done during 1984 and 1986, followed by extensive laboratory time preparing samples for $^{40}Ar$-$^{39}Ar$ dating, chemical analyses, and fission-track dating. Previous knowledge of the regional geology and ore deposits of the area come from my active involvement in various exploration programs in the region since 1976.

This project documented three distinct, major mineralizing events for the study area. They are related to the emplacement of Jurassic, Paleocene, and Upper Eocene - Lower Oligocene igneous rocks. The conceptual model developed in this study relates tectonic processes to the origin of major porphyry copper deposits and is probably valid for other active continental margins.

The thesis is organized in eight chapters. (1) Introduction and description of the general physiographic, climatic and hydrologic characteristics of the study area, as well as its mining history. (2) Description and interpretation of the regional geology. (3) Description of the distribution and general characteristics of the metallic mineral deposits that characterize the region. (4) $^{40}Ar$-$^{39}Ar$, and K-Ar dating of mineralized areas and definition of major metallogenic epochs. (5) Constraints on the erosion-uplift events of the region based on fission track thermochronology. (6) Discussion and summary of the general metallogenic conclusions that stem from the investigation. (7) Analysis of the constraints on the porphyry copper mineralization and

development of a conceptual genetic model. (8) Summary of the main contributions of the present study.

## 1.2 TECTONIC SETTING OF THE ANTOFAGASTA REGION

The Antofagasta Region (21°-26° S) is a segment of the mid-section of the Central Andes (Fig 1.2). The Central Andes (about 2° to 45° S) provides a classic example of a "simple" orogen developed along a convergent plate margin (Dewey and Bird, 1970; James, 1971). These are non-collisional mountain belts formed over a long-lived, currently active, subduction system whose distinctive feature is the existence of an enormous volume of igneous rocks generated throughout their geologic history. Therefore the Andes have been referred to as a "magmatic mountain range" (Zeil, 1979) or a "vulcano-plutonic orogen" (Sillitoe, 1976). Most of the metallic ore deposits have an inherent and temporal relationship to the magmatic activity, and they are believed to derive their metallic content from underlying subduction-related processes (Sillitoe, 1972b, 1974, 1976; Clark and Zentilli, 1972).

The Central Andes are continuous for more than 4,000 km (from about 2°S to 45°S), but at present distinct broad-scale tectonic segments exist. They coincide with major along-strike variations in the dip of the Benioff zone (Barazangi and Isacks, 1976; Jordan and others, 1983). The coincidence of lateral variations in the geometry of the descending Nazca plate and changes of Andean physiography and geology is remarkable. There are five major segments as inferred from the spatial distribution of intermediate depth earthquakes (Stauder, 1973; Barazangi and Isacks, 1976, 1979). Three volcanically active segments underlain by steeper dipping Benioff zones are separated by segments with flat-slab subduction without volcanism (Thorpe and others, 1982) (Fig. 1.2). From about 2°S to 15°S and 27°S to 33°S, the Benioff zone dips only about 5° to 10° to the east, whereas from 5°N to 2°S, 15°S to 27°S, and south of 33°S, the zone is inclined 30° to the east.

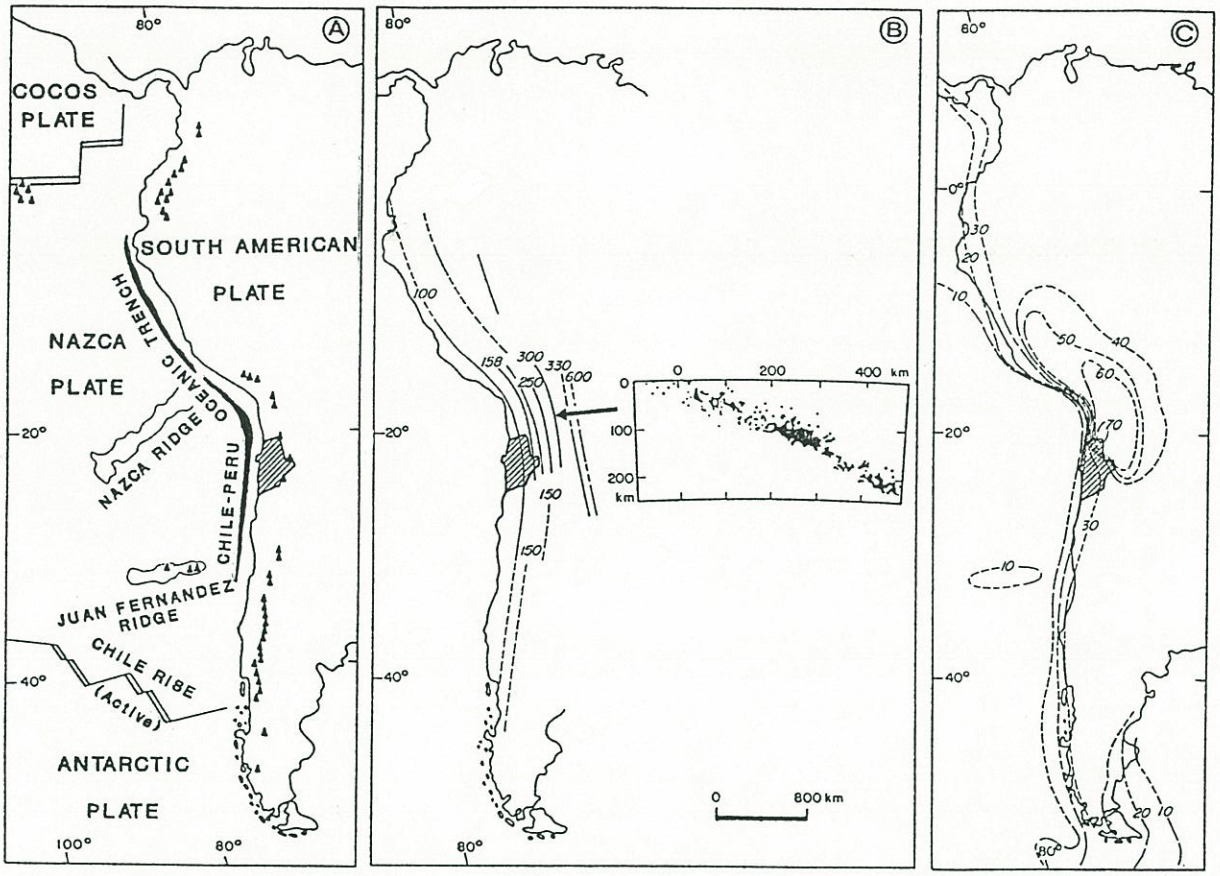


**Figure 1.2.** Tectonic setting of the study area. Figure modified after Thorpe and others (1982). (A) Converging Nazca oceanic plate and South American continent. The Chile-Peru oceanic trench marks the destructive plate boundary. Active volcanoes on the continental margin indicated by filled triangles (after Thorpe and others, 1982). (B) Profile showing the distribution of seismicity from the oceanic trench (0 km) inland (After Barazangi and Isacks, 1976); lines show contours of hypocentral depth (in km) to top of inclined seismic zone. Dashed lines indicate that contours are based on fewer data than those shown by solid lines. (C) Crustal thickness in South America. Thicknesses (in km) are from Cummings and Schiller (1971).

The different segments have distinct morphological and tectonic characteristics as well (Jordan and others, 1983). Comparable tectonic segmentation related to along-strike variations of plate interactions probably occurred in the past, and may have determined the igneous and metallogenic characteristics of distinct segments of the Andes. Sillitoe (1974) identified 16 tectonic transverse boundaries along the Central Andes, and attributed longitudinal variations in the nature of metallogenic belts in the Andes to the tectonic segmentation of this mountain belt. Although one of the tectonic boundaries proposed by Sillitoe (1974) intersects the Antofagasta Region at about 25° Lat. south, most rock units and major structures of this region are longitudinally unbroken. Thus the Antofagasta Region can be regarded as an undivided tectonic segment of the Andes.

The Antofagasta Region is characterized by recurrent seismicity and volcanism, a consequence of the steady subduction of oceanic lithosphere under the South American continent (Fig. 1.2). The hypocentres of earthquakes plotted against depth reveal the existence of a well defined Benioff zone dipping 30° eastward under the continental edge (Barazangi and Isacks, 1976; Jordan and others, 1983). Analyses of global plate motions have shown that the rate of convergence between the South American continent and the oceanic Nazca plate averaged about 9-10 cm/yr during the Neogene (Pilger, 1983, 1984; Pardo-Casas and Molnar, 1987).

Two major longitudinal fault systems, namely Atacama Fault System and Domeyko Fault System, constitute the most conspicuous structural features of the Antofagasta Region. They are at about 140 and 240 km east of the Chile-Peru oceanic trench respectively, and influence the regional mineral deposit distribution (see Section 2.16).

## 1.3 PHYSIOGRAPHY

The topography of the Antofagasta Region is rugged and characterized by north-south trending mountain ridges and intervening sedimentary troughs. Six north-south trending main physiographic units can be defined (from west to east): the Coastal Cordillera, the Intermediate Depression, the Domeyko Cordillera, the Intermontane Basins, the Main Andean Cordillera and a high plateau known as the Altiplano or the Puna (Fig. 1.3).

The **Coastal Cordillera**, about 50 km in width, is a subdued, block-faulted mountain range that rises up to 3,114 m at 24°30' S, although its summits usually lie at about 2,000 to 2,500 m a.s.l.. The western boundary of this mountain range is an abrupt escarpment that falls either to narrow coastal terraces or, more rarely, directly to the sea. In contrast, the highlands of the Coastal Cordillera have a topography characterized by smooth longitudinal ranges flanked by extensive piedmont alluvial plains. These ranges decrease steadily in altitude eastward, so that the eastern boundary of the Coastal Cordillera interfingers with the alluvial surface of the Intermediate Depression at about 1,000 m of altitude. Between 23°00' and 23°30' is the **Mejillones Peninsula**, which is an isolated area of mountainous relief separated from the bulk Coastal Cordillera by a sedimentary (Miocene-Pliocene) marine terrace (Fig. 1.3).

The **Intermediate Depression** in the northern part of the Antofagasta Region is essentially a single, 50 km wide, extensive piedmont alluvial plain known as Pampa del Tamarugál, which flanks the Domeyko Cordillera and slopes westwards from about 2,100 m to 1,000 m of altitude. South of the Loa river (22°30' S) the Intermediate Depression is a composite unit consisting of small, interconnected basins (Pampas) lying between longitudinal ranges and often interrupted by isolated hills. Mountains break the continuity of the Intermediate Depression at 25° Lat. S, where the Coastal and Domeyko Cordilleras are practically connected.

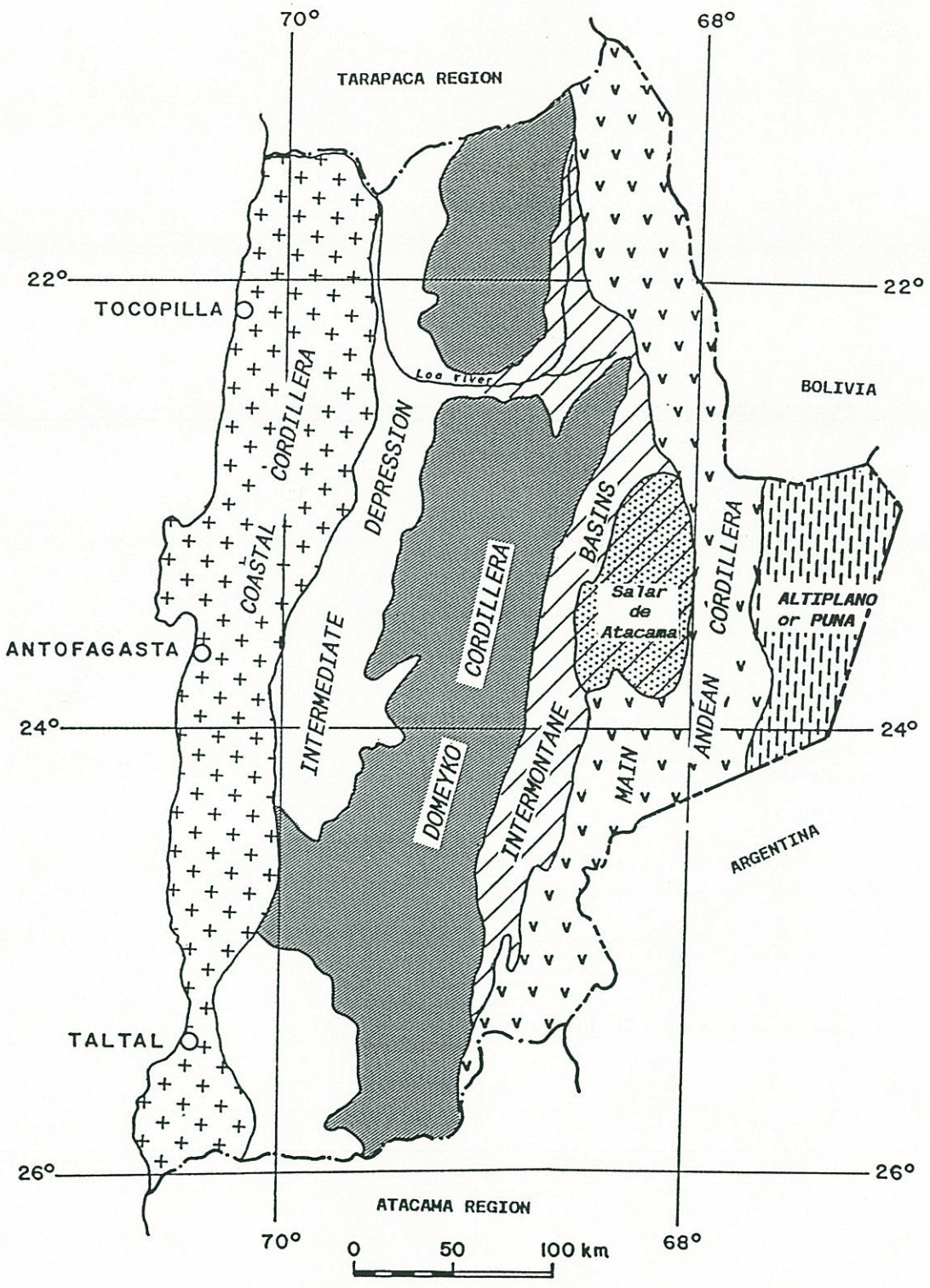


Figure 1.3. Main physiographic units of the Antofagasta Region: western slope of the Central Andes in northern Chile.

The **Domeyko Cordillera** has a rugged relief with longitudinal mountain ranges rising to 4,500 m. Although forming part of the High Andes, this mountain chain is a separate physiographic unit from the Main Andean Cordillera only between 21° and 26° Lat. S.

The **Intermontane Basins** are depressions with altitudes ranging between 2,500 and 3,500 m, located between the Domeyko Cordillera and the Main Andean Cordillera. The northernmost is known as Calama basin (Mortimer, 1980). It contains the upper course of the Loa river, which is the only water course of this region flowing to the sea. The rest are basins with internal drainage occupied by extensive flat, salt-encrusted playas, i.e., Salar de Atacama, Salar de Punta Negra, or the more restricted Salar de Imilac.

The **Main Andean Cordillera** in the Antofagasta Region (Western Cordillera of the Andes) has an undulating plateau-like topography with a base altitude of 3,900 to 4,300 m. On this surface a large number of strato-volcanoes and north-trending ridges are located. The volcanic peaks range from about 4,000 to 6,739 m of altitude. Erosional summits are between 4,000 and 4,500 m. Salt lakes occur in several small endorheic basins (with internal drainage) surrounded by volcanoes. These salt-flats lie at about 4,000 m of altitude; i.e., Salar de Carcote, Salar de Ascotan, and Salar de Pedernales.

The **Altiplano** high plateau lies east of the Main Andean Cordillera and continues into Argentina and Bolivia. It has a relatively smooth relief lying at between 4,000 and 4,500 m a.s.l.; The Altiplano is the only example in the world of a continental plateau unrelated to continental collision.

## 1.4 CLIMATE

This segment of the Andes has a protracted history of aridity. The arid conditions obviously limited the extent of erosion, but have had a positive effect on the operation of secondary enrichment and preservation of metallic ore deposits, making the discussion of the climate important to this metallogenic study.

### 1.4.1 Present Climate

The Antofagasta Region is the most arid segment of the Andes, being part of the Atacama desert, reputed to be the Earth's driest desert (Stoertz and Ericksen, 1974; Trewartha, 1981; Mortimer and Saric, 1975). Its climate has been termed hyper-arid (UNESCO, 1980; Alpers and Brimhall, 1988) being characterized by the extreme infrequency of precipitation, relatively low annual temperatures, small annual ranges of temperature, and the presence along the coastal area of low stratus clouds and fog. Even the High Andes at these latitudes are extremely arid in comparison with other mountain ranges of equal elevation. The snowline is near 6,000 m of altitude on the high volcanic peaks, perhaps the highest snowline in the world. Perennial snow and ice are found on only a few peaks above 6,300 m. These are relatively small in area and in depth of snow and ice (Stoertz and Ericksen, 1974). Because of the extreme aridity the area is practically devoid of vegetation, but extensive alluvial piedmont sediments and colluvial deposits cover much of the rock outcrop.

The mean annual temperatures of the Antofagasta Region are relatively low, usually below 18°C (Fuenzalida, 1965). The temperature is moderated by the cold surface waters offshore, and altitudes over 1,000 m inland. Winter temperatures are mild, generally dropping below 0°C during the winter nights, but usually only at elevations above 1,000 m above sea level. The Intermontane Basins at higher altitude (2,500 -

3,500 m a.s.l.) are cooler. Stoertz and Ericksen (1974) estimated a mean annual range of temperature from 8° to 14°C for the Salar de Atacama Basin, probably averaging about 11°C. The Andean Highlands have a very cold climate, which is closely related to the meteorological conditions that dominate on the Bolivian Altiplano, and differ markedly from those of areas below 3,000 m of altitude. There are large annual variations in its monthly average temperatures (e.g., Ollagüe 23.5°C in January and -32.3°C in June; Caviedes, 1973). The absolute temperatures are also extreme, resulting in a large daily range (25°C in January and 35.5°C in August; Caviedes, op. cit.).

The paucity of meteorologic stations makes it difficult to determine reliable long-term rates of precipitation in this region. Stoertz and Ericksen (1974) have shown that precipitation rate is strongly dependent on altitude. The latter authors estimated that areas below 3,600 m receive less than 50 mm/yr; whereas in areas above 4,000 m precipitation increases abruptly up to about 250 mm/yr. The narrow coastal zone has a remarkably high atmospheric relative humidity, which remains almost constant throughout the year (68 to 78%; Caviedes, 1973). Coastal cloudiness is equally high, generally at low altitude (500 - 1,000 m), but it is not sufficient to cause precipitation. Mean annual precipitation along the coast ranges from 4 mm/yr in Antofagasta to about 25 mm/yr in Taltal (Fuenzalida, 1965). Here, as elsewhere in the Coastal Cordillera and Intermediate Depression, very variable amounts of rainfall may occur as infrequently as every 5 to more than 10 years. The Coastal Cordillera is only slightly less arid than the littoral area. It is characterized by heavy fogs, known as "Camanchaca", which are a daily phenomenon usually from May to September (winter months of the southern hemisphere), and both higher in altitude and less persistent during the summer. The fog is the result of warm air from the open ocean being chilled as it blows over the cool current lying alongshore, and mixes with the cold air immediately above it. It forms a low uniform stratus deck whose base averages between 350 and 550 m above sea level and whose top lies just below the higher peaks of the Coastal Cordillera. The fog may extend inland as far as 80 km, but usually does not extend beyond the

crest of the Coastal Range. The fog rarely, if ever, causes measurable precipitation at these latitudes (Trewartha, 1981). The lowest part of the Intermediate Depression, where salt-encrusted playas (salars) occur, is slightly drier than the Coastal Cordillera: the average annual precipitation may be less than 3 mm/yr. Mean annual precipitation for the Intermediate Depression as a whole is probably less than 6 mm/yr (Stoertz and Ericksen, 1974), and in a sharp contrast with the coastal area, the atmospheric relative humidity is low (annual average 39%; Fuenzalida, 1965). The Atacama Desert, near Calama, is included in The Guiness Book of Records (1990, p. 65) as the driest place on Earth experiencing a drought for some 400 years up to 1971.

The higher Intermontane Basins have a climate more humid than the Intermediate Depression but more arid than the Andean Highlands. Furthermore, the climates of the western and eastern rims of the basins differ markedly, even at the same altitude. The western side is extremely arid, whereas the eastern side is semiarid. Stoertz and Ericksen (1974) have estimated that the basin of the Salar de Atacama has a mean annual precipitation ranging from 8 to 50 mm. In the High Andes, the air has very low humidity (averaging about 27%) and cloudiness is rare, except during the summer (December to March). Precipitation records at 21°S from Collahuasi (altitude 4,805 m) and Ollagüe (altitude 3,695 m) meteorological stations show an annual rainfall of about 100 mm, concentrated between January and March (Caviedes, 1973). The summer rainfall is related to convectional storms (cumulonimbus clouds), known in this region as the "Bolivian Winter."

### 1.4.2 Causes of aridity

A combination of interdependent factors produces the extreme aridity in the Antofagasta Region. Of primary importance is the influence of the strong subsidence (ca. 2 km/day) of cold, dry air associated with the eastern limb of a fixed, subtropical anticyclone in

the southeast Pacific Ocean. The stability of the anticyclone cell is enhanced by the Andean Cordillera and its westward curvature north of 18° S. The Andean mountains are able to impede and divert the normal zonal flow pattern of the southeast Pacific anticyclone into distinct migratory cells. Consequently this cell remains as a permanent feature, which is terminated on the east abruptly by the Andes, and whose position fluctuates only slightly throughout the year. This strong, fixed position of the eastern end of the anticyclone cell, with consequent perennial high atmospheric pressure and clear skies, is by itself capable of producing more than moderate aridity (Trewartha, 1981). Another factor that strongly contributes to the aridity along the coast is the presence of unusually cold upwelling waters of the Humboldt Current derived from the Antarctic (Thompson, 1978; Alpers and Brimhall, 1988). The surface waters within 50 km of the Chilean Coast remain cold (as much as 8°C cooler than water 100 km seaward) because of upwelling driven by southerly to southwesterly winds. Surface stresses produced in response to these shore-parallel winds combined with Coriolis force produce a drift effect (Eckman drift effect; Thompson, 1978) that drives the surface waters away from the coast. Upwelling replaces these surface waters with cooler, deeper waters, supplied by the Humboldt Current. Its obvious effect is to chill and stabilize the surface air, thereby intensifying and lowering the temperature inversion (often reaching down to sea level). Air masses pick up little evaporative moisture from the perennially cold surface waters and tend to remain dry as they heat up moving in an easterly direction. In the normal weather pattern there is little chance for cloud formation or precipitation (Alpers and Brimhall, 1988). In addition, the High Andes provide a rain shadow, effectively shielding the region from most precipitation associated with moist air masses derived from the Amazon Basin and Central Argentina. The abrupt coastal escarpment tends to trap the coastal fog and enhances the aridity of the continental interior, and the strong coincidence between the eastern margin of the subtropical anticyclone cell and the coastline results in maximum atmospheric subsidence over the coastal area, and strengthened upwelling of cold water (Trewartha, 1981; Alpers and Brimhall, 1988). In summary, the extreme

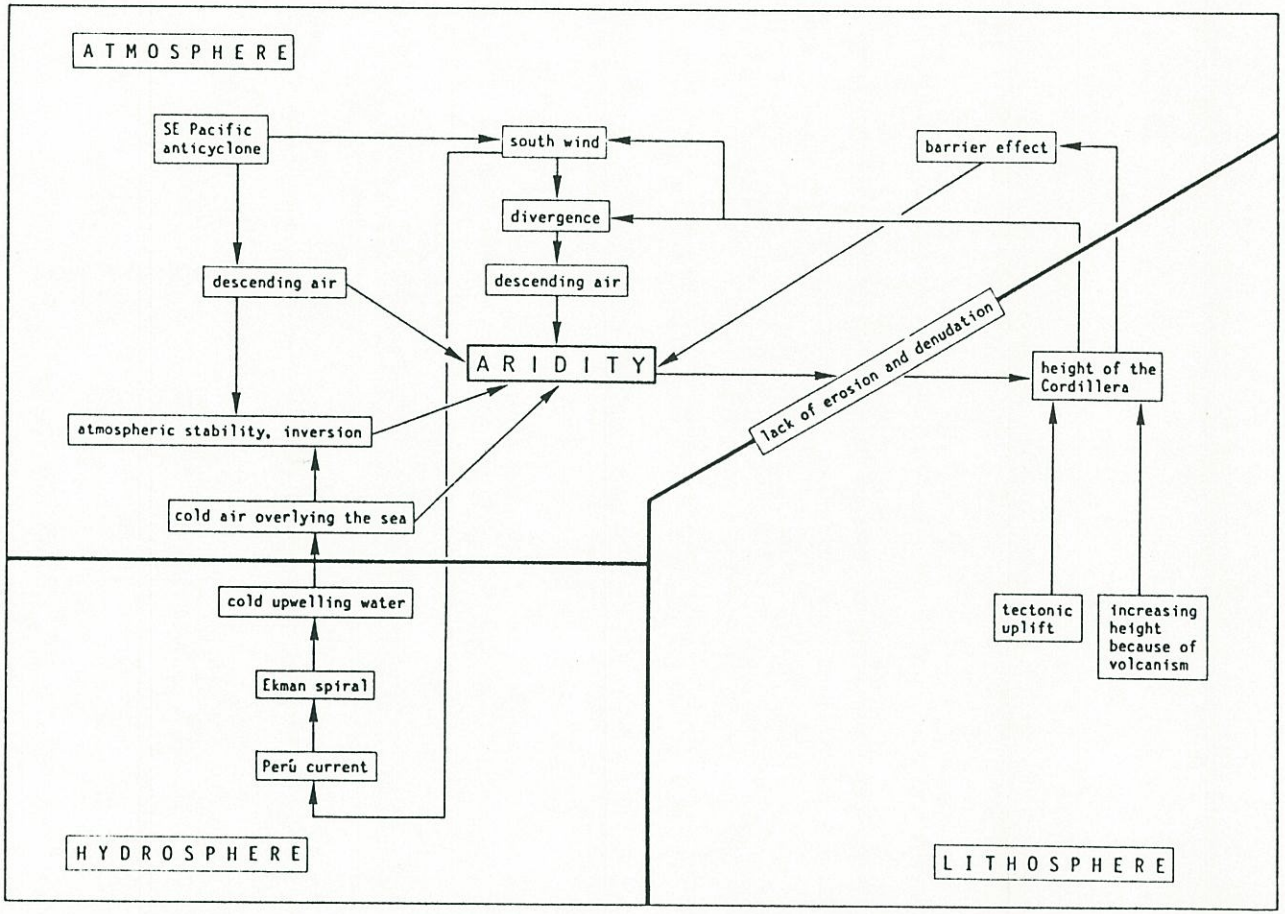


**Figure 1.4.** The interdependent causes of aridity on the western slope of the Central Andes (After Abele, 1989).

aridity prevailing in the Antofagasta Region is related to a unique combination of circumstances, all elements of which are closely interrelated and with each reinforcing the others (Fig. 1.4; Abele, 1989).

### 1.4.3 Paleoclimate

An arid to semi-arid climate seems to have prevailed in the region since the Cretaceous. Intercalations of evaporite deposits of gypsum are found within terrestrial red beds of Early Cretaceous (Arca Formation; Maksaev, 1978), Late Cretaceous - Early Tertiary (Purilactis Formation; Marinovic and Lahsen, 1984), and Oligocene - Middle Miocene ages (Sichal, San Pedro, and Tambores Formations; Maksaev, 1978; Dingman, 1963; Ramirez and Gardeweg, 1982). However, relatively wet periods must have existed to account for the alluvial deposition of the clastic portions of these formations. The Cenozoic paleoclimate of this region has been discussed extensively by Alpers and Brimhall (1988). These authors showed that hyper-arid conditions prevailed in this area since the Middle Miocene, following a desiccation that changed the previous arid to semiarid climate to hyper-arid conditions. Alpers and Brimhall (*op. cit.*) relate this Middle Miocene desiccation to a pronounced decrease in temperature of coastal waters supplied by the Humboldt Current and an increase in upwelling intensity as the Antarctic ice cap became established at approximately 15 to 13 Ma. The Central Andes Cordillera probably attained at least half its present elevation prior about 15 Ma (see Section 2.17) to provide a rain shadow to protect the region from precipitation from the east and to stabilize the southeastern Pacific subtropical anticyclone cell.

The implications of arid conditions for the last ca. 100 Ma and hyper-arid conditions for the last ca. 15 Ma are significant. The dry climate slowed rates of regional erosion, enhanced processes of secondary enrichment, and contributed to preserve the metallic ore deposits of this region.

## 1.5 HYDROLOGY

The water resources of the Antofagasta Region are limited because of the extremely arid climate. Scanty precipitation is chiefly restricted to the High Andes, whereas in the rest of the region precipitation is very infrequent and high rates of evaporation dominate. Most of the drainage systems of the region are endorheic (intermontane basins), because of the barrier effect of longitudinal mountains (Domeyko Cordillera and Coastal Cordillera). Runoff water that reaches these internal drainage basins evaporates at high rates resulting in salt-encrusted playas or salars. The largest of these is the Salar de Atacama (about 4,200 $km^2$), followed by the Salar de Punta Negra (about 300 $km^2$). Several salars also exist within the Intermediate Depression but their water supply comes from groundwater flow. Perennial water courses are sparse, and almost completely restricted to the High Andes and Altiplano.

The only perennial water course that reaches the sea is the Loa river (Fig. 1.3), which is the most important water resource of this arid region. This river is about 400 km in length and has rates of flow ranging from 0.5 to 5 cumecs (cubic metres per second). It follows an extended U-shaped route, and finally flows west through a deep gorge cut across the Coastal Cordillera. Its main tributaries are the San Pedro, El Salado (salty), and San Salvador rivers which contribute volumes of 1.43, 0.35, and 0.7 cumecs respectively (Klohn, 1972). Although the combined runoff of the Loa river and its tributaries is relatively small, it provides irrigation for some minor farming at Toconce, Caspana, Aiquina, San Salvador, Chiu-Chiu, Calama, and Quillagua. It also constitutes the main source of drinking and industrial water for Chuquicamata, Calama, Maria Elena, Antofagasta, and Tocopilla. The human settlement and industrial developments within this desert region rely on this water resource.

Other minor surface water courses exist on the Main Cordillera and Altiplano: i.e., Zapaleri stream (0.6 cumecs) flowing into

Salar de Tara, and both Quipiaco (0.1 cumecs) and Alitar streams (0.1 cumecs) flowing into Salar de Pujsa. Several minor water courses flow into the Salar de Atacama, such as the streams of San Pedro (0.9 cumecs), Vilama (0.25 cumecs), Hecar (0.23 cumecs), Socaire (0.15 cumecs), and Llonas (0.09 cumecs; Klohn, 1972). Minor water sources exist along some creeks on the eastern flank of the Domeyko Cordillera and on the perimeter of salars.

The rest of the regional water resources are underground. Groundwater occurs chiefly within permeable layers within sedimentary deposits in salars of the Intermontane Basins and the Intermediate Depression.

## 1.6 MINING HISTORY

Archaeologic evidence shows that since about 2,400 years ago Atacameño Indians extracted native copper and turquoise from the oxidized zone of some deposits such as Chuquicamata, El Abra, and El Salvador (Fig. 3.7) mainly for ornamental purposes (Peña y Lillo, 1927; Perry, 1960). Mining developed rapidly in Chile after the arrival of the Spaniards in the sixteenth century. However, mining attempts in the desert of the Antofagasta Region were discouraged by the lack of water to sustain mining operations. The exploitation of mineral resources started only by the mid 19th century only after the depletion of the richer sections of deposits located farther south. The deposits mined at that time were high-grade copper veins of the Coastal Cordillera (Gatico, Tocopilla, Naguayan, Julia, and Canchas districts; Figs. 3.1, 3.4) and silver and gold veins of the Domeyko Cordillera (Caracoles, El Inca, Cahinal de la Sierra, Vaquillas, and Guanchaquita districts; Figs. 3.1, 3.6). Mining of these veins pursued rich pockets and stringers that produced high-grade oxidized ores for direct smelting. Usually no predetermined working plans were followed and much of the ore extraction

was carried out by hand. Nearly all the small mines hand-sorted their ore. Only a few large mines were partially mechanized.

Mining of veins declined by the end of the 19th century due to decrease of ore grades, depletion of oxidized ores, higher exploitation costs as a result of deepening of mine workings, and the lack of mechanization. The war between Chile and the Peru-Bolivian coalition (1879-1883) and the Chilean Revolution of 1891 also had negative effects on mining and many mining operations ceased during these conflicts. At the beginning of the 20th century the mining of veins continued to decline and stopped almost completely by 1930 because of the world's economic crisis. During the same time, however, the regional mineral production increased as a result of the discovery of low-grade, large tonnage, porphyry deposits. Their exploitation was made possible with the development of metallurgical processes such as the froth flotation, which enabled large-scale exploitation of ores with grades less than 2% Cu and that permitted the economic recovery of minor constituents (e.g., molybdenum, gold, and silver). In northern Chile the porphyry copper at Chuquicamata was brought in operation in 1915, followed by Potrerillos in 1927, and El Salvador in 1960. La Escondida, a new deposit, is at present under development. The enormous Chuquicamata porphyry copper deposit has produced, since 1915, more than 15 million metric tons of metallic copper, 126,000 tons of molybdenum, and significant volumes of gold and silver. At present Chuquicamata produces about 550,000 tons/yr of copper, being the world's largest individual copper producer. It also produces 9,955 ton/yr of molybdenum, 550 kg/yr of gold, and 165,000 kg/yr of silver (SERNAGEOMIN, 1989).

The exploitation of stratabound copper deposits of the Coastal Cordillera (e.g., Mantos Blancos, Buena Esperanza, Susana, and Santo Domingo; Figs. 3.1, 3.4) started only in the 1950s, after metallurgical problems for exploiting ores with a high proportion of copper chlorides and silicates were solved. Currently these stratabound copper deposits are a second source of copper production in the region (ca. 100,000 tons/yr of copper). At about the same time, the working in the

oxidized zones of copper breccia-pipes and stockworks (e.g., Sierra Gorda, Lomas Bayas, Quetena, Copucha, Silvita; Fig. 3.6) was initiated. However, the latter were abandoned during the seventies following the decline of copper prices. Occasional small-scale exploitation of many copper, sulphur, iron, and manganese deposits has occurred throughout the last century in this region, but their minor production has only been significant during periods of high metal prices.

The increase of gold and silver prices during the last decade and the improvement of the heap leaching processes have lead to the renewal of mining and/or to the reprocessing of old tailings and dump ores within several districts containing epithermal silver and gold vein deposits (e.g., Guanaco, Sierra Esmeralda, Sierra Overa, Sierra Gorda, San Cristobal, El Inca, Caracoles, Cachinal de la Sierra, and Juncal; Fig. 3.6).

The regional mining production in 1988 was: 627,386 metric tons of copper, 9,955 tons of molybdenum, 684.4 kg of gold, 251,165.7 kg of silver, and 22,600 tons of iron ore (SERNAGEOMIN, 1989). This production represents the highest annual production in the mining history of this region and represent 42.6% of the copper, 64.1% of the molybdenum, 3.3% of the gold, 47.6% of the silver, and 0.28% of the iron ore produced by Chile during 1988. Several mineral deposits, such as La Escondida porphyry copper deposit (Fig. 3.7) and El Lince stratabound copper deposit (Michilla district; Fig. 3.1), are presently under development so that a further increase in the metal production may be anticipated.

# CHAPTER 2: GEOLOGICAL EVOLUTION OF THE ANTOFAGASTA REGION

## 2.1 INTRODUCTION

This chapter provides a synthesis of the geological evolution of the Andean segment studied (Antofagasta Region) as a necessary framework to discuss the metallogeny. The regional geological, geomorphological, and metallogenic characteristics of this area were determined by the tectonics of the active continental margin (Fig. 1.2). Since the Late Carboniferous successive magmatic arcs were developed on the continental border (Fig.2.1). Recurrent copper mineralization accompanied the development of these arcs. Magmatic processes have prevailed throughout the geological history of the region. Most of the metallic mineral deposits are genetically related to hydrothermal processes associated with the igneous activity.

For descriptive purposes the geologic history of this Andean segment has been arbitrarily divided into seven intervals. The boundaries are discrete periods of tectonism that produced significant paleogeographic changes.

**Precambrian (?) to Silurian:** Submarine clastic sedimentation, volcanism, and plutonism; superimposed regional metamorphism.

**Ocloyic** tectonic event (Ordovician-Silurian boundary)

**Devonian to Early Carboniferous:** Detrital marine sedimentation, absence of widespread magmatic activity.

**Chanic** tectonic event (Late Devonian-Early Carboniferous)

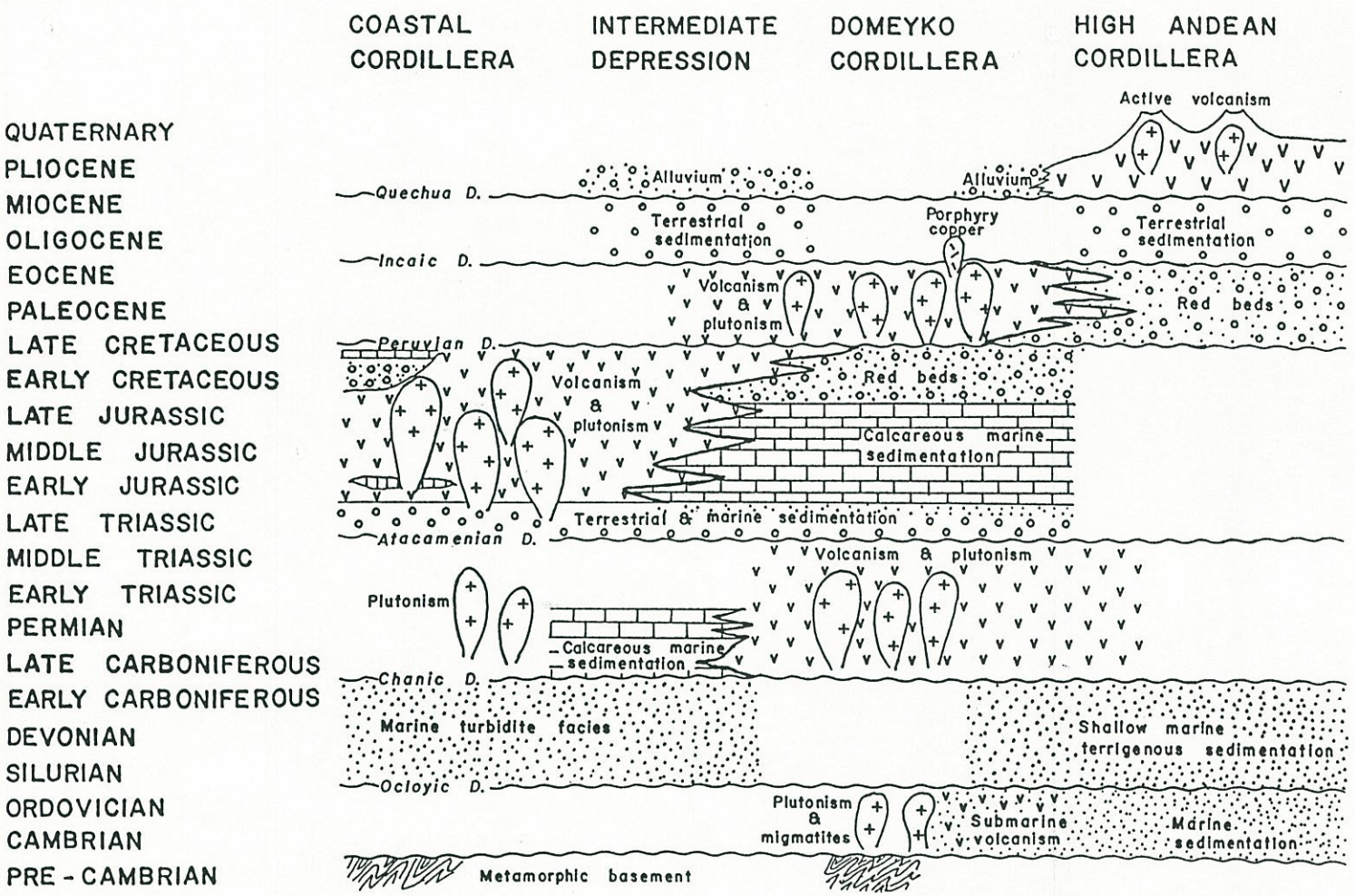


Figure 2.1. Summary diagram of the general geologic evolution of the Antofagasta Region: western slope of the Central Andes (not to scale).

**Late Carboniferous to Middle Triassic:** Intense volcano-plutonic activity in the Domeyko Cordillera accompanied by terrestrial sedimentation. Marine calcareous sedimentation in the present-day Intermediate Depression and Coastal Cordillera.

**Atacamenian** tectonic event (Middle-Late Triassic)

**Late Triassic to Early Cretaceous:** Intense volcano-plutonic activity in the Coastal Cordillera. Marine and terrestrial sedimentation in the present Intermediate Depression and Domeyko Cordillera.

**Peruvian** tectonic event (Late Cretaceous)

**Late Cretaceous to Eocene:** Volcano-plutonic activity in the Intermediate Depression and Domeyko Cordillera. Red bed sedimentation in the eastern section of the region.

**Incaic** tectonic event (Late Eocene-Early Oligocene)

**Oligocene:** Terrestrial sedimentation (alluvial deposits and evaporites) and conspicuous decline of magmatic activity compared to the previous period. Emplacement of porphyritic stocks with associated rich copper mineralization within the domain of an active regional strike-slip fault system.

**Quechua** tectonic event (Late Miocene)

**Miocene to Quaternary:** Active volcanism in the easternmost part of the region. Deposition of extensive piedmont alluvial and mudflow deposits, hyper-arid climate and meager erosion. Restricted marine sedimentation (subsidence) in the Mejillones peninsula.

These seven intervals of geological time are used below as a framework in the description of representative lithologic units of

the study area. An interpretative summary of the geologic history and paleogeography ends the discussion of the rocks formed during each interval. Volcanic and plutonic rocks are emphasized, because they are most relevant for the metallogeny of the region. The discussion incorporates data obtained during this study.

## 2.2 PRECAMBRIAN (?) TO SILURIAN

Sedimentary, volcanic, metamorphic, and plutonic rocks were formed during this first interval of the geological evolution of the Antofagasta Region. However, their precise ages and significance are still open to interpretation because of poor geologic control and the inherent difficulties in dating rocks that have been thermally overprinted.

### 2.2.1 Precambrian (?) - Lower Paleozoic metamorphic rocks

Isolated outcrops of metamorphic rocks occur in the northern section of the Domeyko Cordillera (Sierra de Moreno, Cerros de Chuquicamata, Cerros de Limon Verde) and in the Mejillones Peninsula (Fig. 2.2). No metallic mineral deposits are associated with these rocks in the study area.

The metamorphic rocks of the Sierra de Moreno area (Challo Formation; Maksaev, 1978) occur in the northernmost part of the Domeyko Cordillera (Fig. 2.2). They are quartz-mica schists and subordinate greenschists characterized by penetrative foliation and segregation banding. These rocks show folds at diverse scales, cleavage, crenulations, and boudinage. According to Skarmeta (1983) these resulted from four superimposed deformative events. The rocks have been subjected to a regional, low-grade metamorphism, but primary sedimentary structures

(such as cross-bedding and graded bedding in the quartz-mica schists, and amygdules in greenstones) have been locally preserved. The protolith is sedimentary with volcanic intercalations (Skarmeta, 1983). The metamorphic rocks of Sierra de Moreno are locally migmatized and intruded by Ordovician-Silurian muscovite granites (511 to 431 Ma; Appendix 2). Several K-Ar, Rb-Sr, and U-Pb dates (Appendix 2), obtained in both the metamorphic rocks and migmatites, suggest a Silurian minimum age (Skarmeta, 1983; Damm and others, 1986) and zircon U-Pb dates of 1260 ± 30 and 1213 ± 28 Ma obtained in the migmatites (upper intercept of the discordia line; Damm and others, 1986), suggest a maximum Middle to Late Proterozoic age for these rocks.

The Limon Verde and Chuquicamata area (Fig. 2.2) is underlain by an assemblage of mica schists and amphibolites with scarce quartzite and metaconglomerate intercalations (Limon Verde and Chuquicamata Metamorphic Complex; Marinovic and Lahsen, 1984). These rocks are intruded by extensive bodies of Upper Carboniferous granitic to granodioritic rocks and in part the metamorphic rocks are roof-pendants within the granitic plutons. The metamorphic rocks are strongly folded and foliated as a result of at least two superimposed deformation events (Baeza and Venegas, 1985). Studies of the area of Limon Verde (Herve, 1982; Baeza, 1984; Rogers, 1985; Damm and others, 1986) suggest a single-phase, medium-grade metamorphism. The protolith of the schists and quartzites is clastic and volcanoclastic sediments, whereas the amphibolites represent volcanic rocks whose trace-element fractionation is similar to alkaline within-plate basalts (Baeza, 1984; Rogers, 1985; Damm and others, 1986). The contact relationships and K-Ar and Rb-Sr ages (Appendix 2) indicate a Late Carboniferous minimum age for these metamorphic rocks (Marinovic and Lahsen, 1984; Herve and others, 1985; Rogers, 1985) and a zircon U-Pb age of 777 ± 36 Ma (upper intercept of discordia line; Damm and others, 1986) suggests a maximum Late Proterozoic age.

The metamorphic rocks of the Mejillones peninsula (Fig. 2.2) (Jorgino Formation of Ferraris and Di Biase, 1978) have been separated into two series with different lithologies and metamorphic

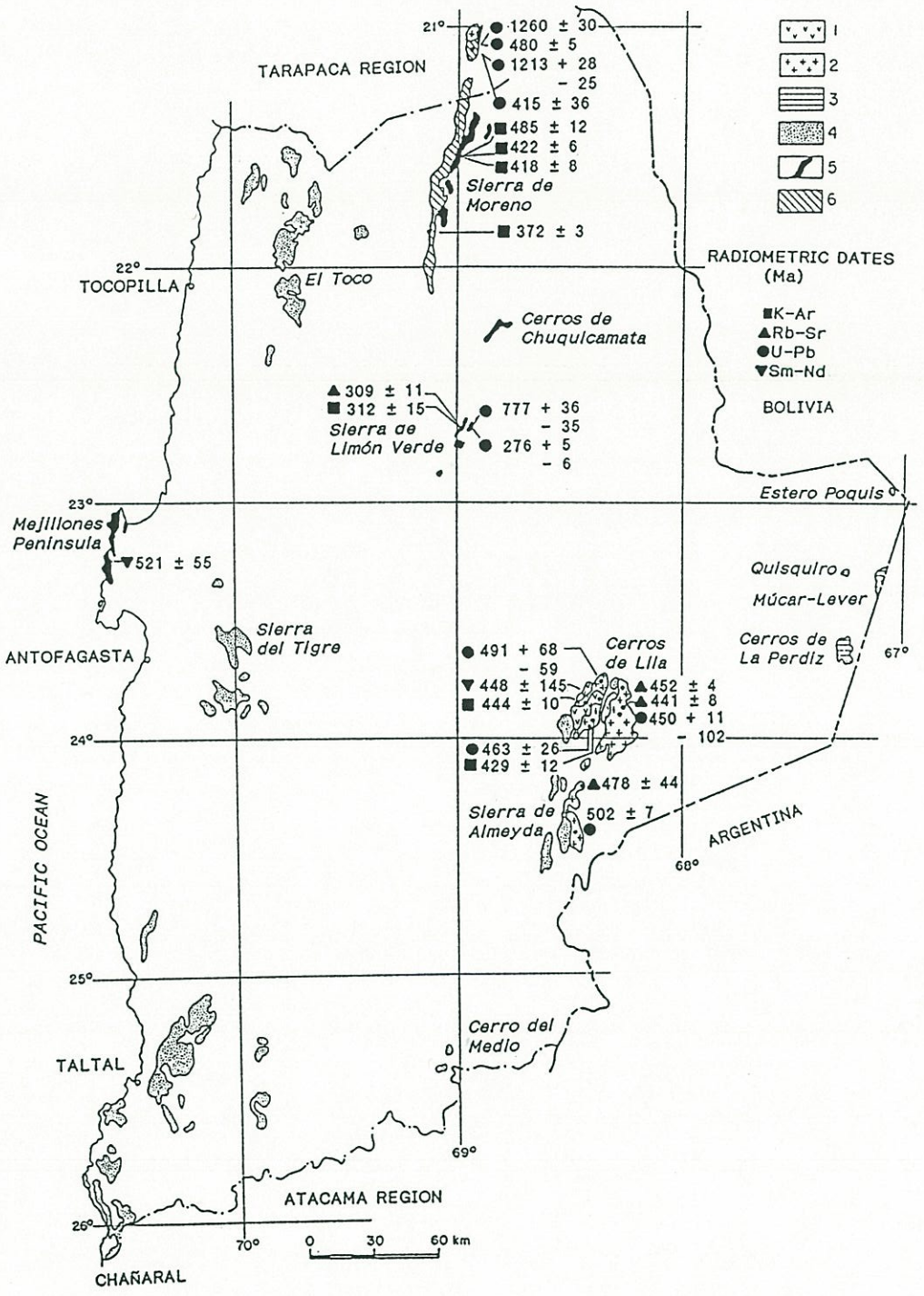


Figure 2.2. Distribution of Precambrian (?) to Lower Carboniferous rocks. (1) Cambrian-Ordovician Volcanic rocks. (2) Ordovician-Silurian plutons. (3) Ordovician marine sedimentary rocks. (4) Devonian to Lower Carboniferous sedimentary rocks. (5) Precambrian (?) - Lower Paleozoic metamorphic rocks. (6) Paleozoic migmatites.

grades by Baeza (1984). One series occurs in the central part of the peninsula and includes gneisses and amphibolites of low to medium metamorphic grade. The other series outcrops in the northern section of the peninsula and is composed of mica schists and scarce amphibolites and quartzites intruded by a Jurassic tonalite. These show a thermal metamorphism superimposed on regional low-grade metamorphic features. All metamorphic rocks of the Mejillones peninsula are folded, foliated, and boudinaged as a result of three superimposed deformation stages (Baeza and Venegas, 1985). Their protolith appears to be clastic sedimentary and volcanic rocks. The petrochemical characteristics of the amphibolites is similar to tholeiitic within-plate basalts (Baeza, 1984; Damm and others, 1986). K-Ar dates from 177 to 167 Ma have been obtained in the metamorphic rocks of the Mejillones peninsula (Diaz and others, 1985); however, a Sm-Nd isochron of 521 ± 55 Ma obtained for the gneisses (Damm and others, 1986) suggests an Early Paleozoic minimum age.

### 2.2.2 Paleozoic migmatites

Extensive outcrops of migmatites occur in the northernmost portion of the Domeyko Cordillera (Fig. 2.2). They include injection gneisses that show local mylonitization and agmatites (Skarmeta, 1983). Their paleosome is composed of the previously described metamorphic rocks of Sierra de Moreno, whereas the neosome is formed of Paleozoic intrusions of granitic to dioritic composition. The migmatites were formed during two thermal-plutonic events (Skarmeta and Marinovic, 1981). Radiometric dates are Ordovician-Silurian (511 to 431 Ma; Appendix 2) and Late Carboniferous-Permian (297-269 Ma; Vergara, 1978; Skarmeta, 1983) in age. During the first stage a *lit-par-lit* injection of granitic magma into the schist occurred under ductile conditions producing migmatites and injection gneisses that are strongly deformed and show evidence of rotation, stretching, boudinage, and folding. The second thermal-plutonic event took place under more brittle conditions generating agmatites whose paleosome is made of migmatites formed during the first stage, and whose

neosome is granite, granodiorite, or pegmatite that clearly crosscut the previously formed migmatitic structures (Skarmeta and Marinovic, 1981).

### 2.2.3 Cambrian-Ordovician volcanic rocks

The oldest non-metamorphic igneous rocks in the Antofagasta Region occur in the Cordon de Lila mountain range south of the Salar de Atacama (Fig. 2.2). A Lower Paleozoic volcanic sequence outcrops in this area. It is more than 2,000 m in thickness and composed of spilitic lavas (some with pillow structures), rhyolitic lavas and hyaloclastites. The felsic volcanic rocks are more abundant towards the top of the sequence. Minor marine sandstones, limestones, pelites, and chert beds are intercalated. In addition, several subvolcanic stocks of gabbro, diorite, rhyolitic porphyry and diabasic dikes are spatially related to the volcanic rocks (Niemeyer and others, 1985; Damm and others, 1986; Breitkreuz and others, 1989).

According to Damm and others (1986) the petrochemical characteristics show that, despite their strong alteration, the trace-element fractionation of the spilites compares to typical within-plate basalts. However, recent geochemical data of Breitkreuz and others (1989) indicate that the Cambro-Ordovician volcanic rocks of Cordon de Lila can be divided into a group of weakly alkaline basaltic-andesitic rocks and a calc-alkaline dacitic-rhyolitic group of rocks. The apparent tholeiitic character of one sample was attributed by the latter authors to a secondary iron enrichment. The trace-element fractionation of the basic-intermediate rocks is similar to a typical high-K calc-alkaline andesite of Gill (1981) and the submarine siliceous volcanoclastic rocks are similar to evolved igneous rocks of active continental margins (Breitkreuz and others, *op. cit.*).

The age of the volcano-plutonic unit of the Cerros de Lila is not well constrained: Its stratigraphic position, unconformably underlying a marine, fossiliferous, Devonian sedimentary sequence implies at least an Early Paleozoic age. A Sm-Nd errorchron of 448 ± 145 Ma was obtained by Damm and others (1986) for the spilites, which has little chronological value because of marked scattering of the data points. A U-Pb zircon age of 491 +60/-59 Ma was obtained by the same authors for a dioritic stock emplaced within these volcanic rocks. A Cambro-Ordovician age as proposed by Niemeyer and others (1985) based on the stratigraphic position of the sequence seems reasonable for this submarine volcanism, but the range may also be extended up to the Silurian.

The Lower Paleozoic volcano-plutonic unit may be partially equivalent to the Ordovician-Silurian volcano-plutonic belt that outcrops in the northwestern Argentinian Altiplano ("Faja Eruptiva de la Puna," Turner and Mendez, 1979). In Argentina these rocks appear to be genetically related to a stage of continental stretching responsible for the formation of an ensialic intracratonic Early Paleozoic basin that extended north into Peru and Bolivia (Dalmayrac and others, 1980, 1980b; Carlier and others, 1982) and probably a short-lived oceanic basin in northern Argentina, followed by eastward subduction, and basin closing (Dalziel and Forsythe, 1985; Ramos and others, 1986). The Chilean submarine volcanic rocks and related subvolcanic intrusions may be representatives of magmatic activity that took place along the western side of this Early Paleozoic marine trough during both the continental stretching and subsequent convergence.

The basic ingredients for the formation of massive sulfide ores existed during the development of this Lower Paleozoic submarine volcanism. So far none has been recognized and, therefore, this unit is regarded as lacking metallogenic importance.

### 2.2.4 Ordovician-Silurian plutonism

The Ordovician-Silurian plutonism is represented by some scattered plutons that occur along the Domeyko Cordillera and High Andes (Sierra de Moreno, Cordon de Lila, and Sierra de Almeyda areas; Fig. 2.2). Stocks of muscovite granite outcrop in the Sierra de Moreno area and were emplaced within schist of probable Precambrian age, either with sharp cross-cutting relationships or forming extensive migmatites. Huete and others (1977) obtained a biotite[1] K-Ar age of 438 ± 10 Ma for one of these stocks. The migmatites have yielded an amphibole K-Ar age of 452 ± 11 Ma (Skarmeta, 1983) and zircon U-Pb ages (lower discordia intercepts) of 415 ± 36 and 480 ± 5 Ma (Damm and others, 1986).

The plutons of the Cordon de Lila and Sierra de Almeyda areas in the High Andes are biotite syenogranites, muscovite monzogranites, and biotite-hornblende granodiorites (Mpodozis and others, 1983). K-Ar, Rb-Sr, and U-Pb radiometric ages of these plutons are in the range 502 to 452 Ma (Appendix 2; Halpern, 1978; Mpodozis and others, 1983; Damm and others, 1986). The ratio Al/(Na+K+(Ca/2)) is greater than 1.1, normative corundum is above 2.5%, and modal garnet is present (Damm and others, 1986). These indicate their peraluminous character and affinity to S-type granitoids (classification of Chappel and White, 1974; White and Chappel, 1977). High initial $^{87}Sr/^{86}Sr$ ratios of the granitic plutons of Cerros de Lila area (0.7102 - 0.7113; Mpodozis and others, 1983) suggest a crustal derivation for the granitic magmas. The biotite-hornblende granodiorites, however, compare to I-type granitoids (Mpodozis and others, 1983; Damm and others, 1986). The origin of these granodiorites is still obscure but may be related to Early Paleozoic subduction (active continental margin setting).

The question of whether the Ordovician-Silurian plutonism was genetically related to Lower Paleozoic submarine volcanism

---

[1] Age recalculated using the decay constants of Steiger and Jäger, 1977.

and plutonism described in the previous section cannot be solved solely based on the available data. The data suggest the involvement of multiple magma sources during the Ordovician-Silurian igneous activity.

The Ordovician-Silurian plutonism coincides in part with the **Ocloyic** tectonic event that took place at about the Ordovician-Silurian boundary. This tectonism produced the folding and low-grade metamorphism of Ordovician sedimentary rocks in the northern part of Argentina and Chile (Coira and others, 1982).

Only minor vein-type mineralization of Sn, Fe, Cu, and Sb appears to be genetically related to the Ordovician - Silurian plutonism in the Argentinian Altiplano (Turner and Mendez, 1979). The plutons that outcrop in northern Chile are apparently barren and seem to lack metallogenic importance.

### 2.2.5 Ordovician marine sedimentary rocks

Marine sedimentary rocks of Ordovician age belong to the Aguada de la Perdiz and Poquis Formations (Gardeweg and Ramirez, 1985) and are restricted to the localities of Cerros de la Perdiz, Mucar-Lever, and Estero Poquis in the Altiplano of the Antofagasta Region (Fig. 2.2). This sedimentary unit is about 2,000 m in thickness and unconformably underlies Upper Cretaceous sedimentary rocks and Neogene ignimbrites; its base is not exposed. The sequence is well stratified and composed of sandstones, shales, and conglomerates; intercalations of tuffs occur throughout the succession. The sandstones are mainly lithic or feldspathic graywackes (arkosic wackes) and subordinate lithic, arkosic, or tuffaceous arenites. The clastic material is primarily of volcanic origin. The occurrence of Arenigian marine fossil graptolites within the lower part of the exposed sequence indicates the Ordovician age of these sedimentary rocks (Garcia and others, 1962; Marinovic, 1979; Perez, 1983; Gardeweg and Ramirez, 1985). According to Gardeweg and Ramirez (1985) the rocks and fossils

indicate a deposition from turbidity currents, probably in a deep submarine fan.

In the Cerros de la Perdiz area the Ordovician strata show tight folds with north-northwest and north-south axes. The outcrops of Poquis show isoclinal folds with subvertical limbs whose strike is N15°W (Gardeweg and Ramirez, 1985). This deformation has been ascribed to the Ocloyic tectonic event that took place at about the Ordovician-Silurian boundary (Coira and others, 1982).

## 2.3 PRECAMBRIAN TO SILURIAN GEOLOGICAL AND PALEOGEOGRAPHIC SYNOPSIS

The metamorphic rocks of the northern part of the Domeyko Cordillera and the Mejillones Peninsula are the oldest exposed rocks of the Antofagasta Region. They were formed between the Late Proterozoic and the Early Paleozoic but their precise age is not yet determined. These rocks record events of clastic sedimentation, volcanism, and low- to medium-grade regional metamorphism. However, the paleogeographical and geotectonic significance of these metamorphic rocks is uncertain, since the relationship among the different outcrops is obscure. The metamorphic rocks of the Domeyko Cordillera may be correlated with the Belen Schists (Rb-Sr 1,000 Ma; Pacci and others, 1980; Sm-Nd 1,460 ± 447 Ma, Damm and others, 1986), which outcrop 430 km north of the Antofagasta area.

The metamorphic units may be either an integral part of the South American Craton (Coira and others, 1982) or represent exotic terranes to the South American continent accreted during the Early Paleozoic (Coira and others, 1982; Ramos and others, 1986; Ramos, 1988; Herve, 1988). The metamorphic rocks of the Mejillones Peninsula, which have chemical composition compatible with oceanic floor origin (Baeza, 1984), also may represent a block accreted to the South American continent during the Paleozoic (Baeza and Venegas, 1985; Damm and others, 1986).

An extensive marine trough existed during the Cambrian-Ordovician in the area of present-day southwestern Bolivia and northwestern Argentina. This trough was the site of deposition of clastic sediments and tholeiitic volcanic rocks (Coira and others, 1982). It is apparent that the basin extended to the present-day Altiplano of the Antofagasta Region where a detrital sequence was deposited during the Ordovician in a deep submarine fan. The dominance of volcanoclastic materials indicates the occurrence of synchronous volcanism. The Cambro-Ordovician sequence of submarine basalts, rhyolites, and marine sedimentary rocks of Cerros de Lila was also deposited within this extensive Lower Paleozoic marine trough.

According to the compiled geochronological data (Appendix 2), the Ordovician to Lower Silurian granitic and granodioritic plutons were emplaced in the Sierra de Almeyda and Cordon de Lila areas as the first phase of migmatization of the schists of Sierra de Moreno occurred. This plutonic-thermal event partly coincides with an important deformation affecting strata of northern Chile and northwestern Argentina (**Ocloyic Orogeny** of Turner and Mendez, 1979). This compressive tectonic event produced major paleogeographic changes. The Cambro-Ordovician sedimentary basin became an area of positive relief ("Arco Puneño"; Davidson and others, 1981a). Some interpretations suggest that this stage of deformation and magmatism may be associated with collision of an exotic terrane with the South American border (Arequipa Microplate; Coira and others, 1982; Mpodozis and others, 1983; Mpodozis and Ramos, in press). However, the stratigraphic data now available (Cobbing, 1985) do not support the exotic nature of the Arequipa metamorphic massif (southern coast of Peru). Cobbing (1985) suggests that this metamorphic massif has been an integral part of the South American continent at least since the Early Paleozoic. The Ocloyic tectonic event in the Peruvian Andes is represented only by an Ashgillian hiatus in the Lower Paleozoic sedimentary sequence (Laubacher and others, 1982; Laubacher and Megard, 1985). A more plausible alternative interpretation has been advanced by Dalziel

and Forsythe (1985) who consider the Arequipa massif as a parautochthonous peninsula of South America separated from the main South American continent by a short-lived Early Paleozoic oceanic basin in northern Argentina. According to this interpretation the Ordovician-Silurian plutonism could be, in part, arc magmatism related to Early Paleozoic subduction, and also crustal melting associated with closing of the oceanic basin and terrane accretion. No matter what type of terrane was accreted (allochthonous or parautochthonous), a significant modification of the continental border is apparent (see next section), with the consequent paleogeographic changes, and probable readjustment of plate interactions.

The rocks of this first interval of the geological history of the Antofagasta Region lack metallic mineralization. Although the Cambrian-Ordovician volcanic rocks appear to be promising for massive sulfide mineralization, the overall impression is that this sequence has no metallogenic importance. Veins with minor tin, iron, copper, and antimony occur only in the Argentinian Altiplano and these would be genetically related to the Ordovician - Silurian plutonism (Turner and Mendez, 1979).

## 2.4 DEVONIAN TO EARLY CARBONIFEROUS

This interval is characterized by the deposition of thick terrigenous marine sedimentary deposits, which are exposed now along the Coastal Cordillera, and in the western flank of the Main Andean Cordillera (Cordon de Lila, Sierra de Almeyda; Fig. 2.2).

### 2.4.1 Devonian-Lower Carboniferous sedimentary and metasedimentary rocks

These rocks occur along the Coastal Cordillera, where previous studies have defined the following formations: El Toco (Harrington, 1961), Las Tortolas (Ulriksen, 1979; Naranjo and Puig, 1984), Britania (Chong, 1973), and the Salar de Navidad Strata (Ferraris and Di Biase, 1978). They also crop out in the southern part of the Main Andean Cordillera: Lila Formation (Moraga and others, 1974; Ramirez and Gardeweg, 1982), Zorritas Formation (Ceccioni and Frutos, 1975), and Cerro del Medio Strata (Naranjo and Puig, 1984) (Fig. 2.2). In the High Andes the sequence overlies Ordovician-Silurian granitoids and is covered unconformably by Upper Carboniferous-Middle Triassic volcanic rocks. In the Coastal Cordillera the base of this unit is not exposed and it is covered unconformably by Upper Triassic sedimentary rocks or Jurassic volcanic rocks (Cifuncho and La Negra Formations; Maksaev and Marinovic, 1980; Naranjo and Puig, 1984).

The diverse outcrops in the Antofagasta Region show a rather uniform lithology dominated by an alternation of fissile sandstones and shales with intercalations of calcareous sandstones, limestones (some with cone in cone structures), fine conglomerates, and scarce chert beds. The sandstones are primarily graywackes (Maksaev and Marinovic, 1980; Boric, 1981; Davidson and others, 1981a, 1981b; Bell, 1982). These rocks are dominantly greenish grey in colour and well stratified in medium to fine beds. They have many primary sedimentary structures, such as ripple marks, cross-bedding, and graded-bedding that are characteristic of marine turbidites. Pillowed alkaline basaltic rocks are associated with these sedimentary rocks in the Coastal Cordillera at Taltal and Chañaral (Bell, 1982; Naranjo and Puig, 1984) . The within-plate basalt geochemical characteristics of the lavas led Bell (1987) to propose an ocean island origin, whereas Breitkreuz and others (1989), based on new geochemical data claim that these volcanic rocks were formed in an active continental margin setting (ensialic marginal basin). The latter authors ascribe an

Early Carboniferous age to these volcanic rocks based on the presence of conodonts in strata underlying the lavas.

In the Coastal Cordillera this sedimentary sequence is intensely deformed into recumbent chevron folds, which have southwest vergence and northwest-trending axes. It also has been subjected to low-grade metamorphism so that the rocks have partially been transformed to metasandstones, phyllites, slates, and rare schists. However, primary sedimentary structures were largely preserved. In the Chañaral area these rocks are extensively disjointed and have been interpreted by Bell (1982, 1984, 1987) as a tectonic melange (Chañaral Melange). In contrast to the coastal area, the sequence exposed in the High Andes does not show significant folding or metamorphism.

The thickness of this sedimentary sequence is about 3,000 to 3,500 m in the northern part of the Coastal Cordillera (Boric, 1981; Maksaev and Marinovic, 1980) and about 2,000 m in the High Andes (Ramirez and Gardeweg, 1982).

Many Devonian marine fossils have been reported in the outcrops of the High Andes and also in the Sierra del Tigre area of the Coastal Cordillera (Fig. 2.2) (Ceccioni and Frutos, 1975; Ferraris and Di Biase, 1978). In the rest of the Coastal Cordillera, only transported fossil plants and trace fossils have been discovered (Maksaev and Marinovic, 1980; Boric, 1981; Naranjo and Puig, 1984). The fossils and the contact relationships indicate a Devonian to Early Carboniferous age.

In the area of the present-day High Andes the Devonian to Early Carboniferous terrigenous sedimentation took place in a shallow marine environment (Davidson and others, 1981a). The source of sediments was probably located farther east in the Argentinian Altiplano (Ocloyic orogen). In the Coastal Cordillera a marine deltaic environment has been postulated (Ulriksen, 1979; Maksaev and Marinovic, 1980; Boric, 1981). These rocks have also been interpreted as distal or proximal turbidites (Bell, 1982; Breitkreuz and Bahlburg, 1985). Sedimentation in abyssal

submarine fans seems unlikely because of frequent calcareous intercalations and transported fossil plants. The overall Devonian to Lower Carboniferous terrigenous sedimentation appears to have taken place on the shelf and perhaps the continental slope of the Gondwana supercontinent. Although basic submarine volcanism and the disjointing of the sedimentary strata at Chañaral suggest an Early Carboniferous subduction complex (Bell, 1987), no active subduction was apparent during Devonian times. The Devonian is a distinct period of magmatic quiescence in the Central Andes between latitudes 17°and 27° S (Breitkreuz, 1985).

## 2.5 DEVONIAN TO EARLY CARBONIFEROUS GEOLOGICAL AND PALEOGEOGRAPHIC SYNOPSIS

During this interval most of the study area was under the sea. The deposition of a clastic sedimentary sequence probably accompanied the denudation of the Ocloyic orogen. The shallow marine facies of the Main Andes are compatible with the existence of a positive area in the present-day Argentinian Altiplano ("Arco Puneño", Salfity as quoted in Davidson and others, 1981a). Deeper turbidite facies seem to be represented in the Coastal Cordillera. The striking absence of Devonian magmatic activity in most of the region, and in the whole segment of the Central Andes between latitudes 17° and 27° S (Breitkreuz, 1985) suggests that the margin of the Gondwana supercontinent during the Devonian evolved primarily as a passive plate margin. However, the low-grade metamorphism, the strong deformation in the coastal area, the presence of Lower Carboniferous basic volcanic rocks, and the formation of the Chañaral Melange are phenomena that have been interpreted by Bell (1982; 1987) as related to a subduction complex. Thus it seems that, in the Early Carboniferous, active subduction of oceanic crust under the new continental edge (modified after the Ocloyic collision) occurred.

The folding and low-grade metamorphism that affected the Devonian - Lower Carboniferous sedimentary rocks in the coastal area can

be correlated with the Late Devonian-Early Carboniferous **Chanic** tectonic event (Turner and Mendez, 1975; **Eohercynic** phase of Dalmayrac and others, 1980). The deformation could be the result of the hypothesized change from a passive to an active continental type of margin. The Chañaral Melange represents the Early Carboniferous subduction complex.

## 2.6 LATE CARBONIFEROUS TO MIDDLE TRIASSIC

The Late Devonian-Early Carboniferous **Chanic** tectonic event was followed by the reactivation of magmatic processes in this Andean segment. Thus during the Late Carboniferous to Middle Triassic a dominantly subaerial volcanism, accompanied by synchronous plutonism, took place in the Domeyko Cordillera. Granitic plutons were emplaced in the Coastal Cordillera but there is no record of volcanism. Only minor outcrops in the Intermediate Depression and Coastal Cordillera evidence the deposition during this interval of calcareous and terrigenous marine sediments, whereas terrestrial sediments were deposited in the Domeyko Cordillera.

### 2.6.1 Upper Carboniferous-Middle Triassic volcanic rocks

Upper Carboniferous to Triassic volcanic rocks occur in a north-south belt along the Domeyko and Main Andean Cordilleras (Fig. 2.3). They belong to the following formations (defined in previous studies): Collahuasi (Vergara, 1978; Vergara and Thomas, 1984), Macata (only eastern outcrops; Vergara, 1978), Peña Morada (Maksaev, 1978), Arca (only eastern outcrops; Maksaev, 1978), Cas (Moraga and others, 1974), Agua Verde (Lahsen, 1969), Tuina (Raczynski, 1963), Bardas Negras (Chong, 1973), La Tabla (Garcia, 1967), Peine (Ramirez and Gardeweg, 1982), and Pular Formations (Harrington, 1961) and El Bordo Strata (Fortt, 1981). Some of the above units were attributed in previous studies either to the

Late Triassic, Jurassic, or Cretaceous, but according to field observations and new geochronological, and paleontologic data they are ascribed by the writer to the Late Carboniferous to Middle Triassic.

The base of this volcanic sequence is exposed in the Sierra de Almeyda area (High Andes), where it unconformably overlies Devonian sedimentary rocks. In the Domeyko Cordillera these volcanic rocks are overlain unconformably by Upper Triassic sedimentary and volcanic rocks. The Upper Carboniferous - Middle Triassic volcanic unit is composed of rhyolitic and dacitic tuffs, breccias, lavas, and porphyritic subvolcanic intrusions, and subordinate andesitic and basaltic lavas and breccias with calcareous and clastic sedimentary intercalations. The thickness of the sequence is variable: a maximum of 2,500 m was estimated in the Cerros de Tuina area (Raczynski, 1963). Dacites and rhyolites dominate. These are massive, porphyritic, or banded and include many intercalations of volcanic breccias, tuffs, and ignimbrites. The ignimbrites are made up of lithic fragments within a felsic, devitrified, or recrystallized matrix. Andesitic porphyritic lavas are usually restricted to the lower portion of the sequence. Olivine basalts are intercalated with the lower andesitic section of the sequence in the Cerros de Tuina area (Marinovic and Lahsen, 1984). Many rhyolitic and dacitic porphyritic intrusive bodies either intrude, or are covered by, or show a lateral gradation with the silicic volcanic rocks indicating a common origin. Intercalated sedimentary horizons are more common in the localities of El Bordo, Cerros de Tuina, Sierra de Almeyda, and Sierra de Argomedo (Fig. 2.3) where they sum up to 200 m in thickness. The sedimentary strata are composed of sandstones and conglomerates derived from volcanic rocks, calcareous sandstones, shales, and limestones. These sedimentary rocks contain invertebrate, vertebrate, and plant fossils indicative of both saline and fresh water lacustrine environments (Marinovic and Lahsen, 1984; Casamiquela, 1980; Osorio and Rivano, 1985).

This assemblage of volcanic and subvolcanic rocks has been ascribed to the Late Carboniferous to Middle Triassic because of its stratigraphic position and fossils and plutons that have yielded

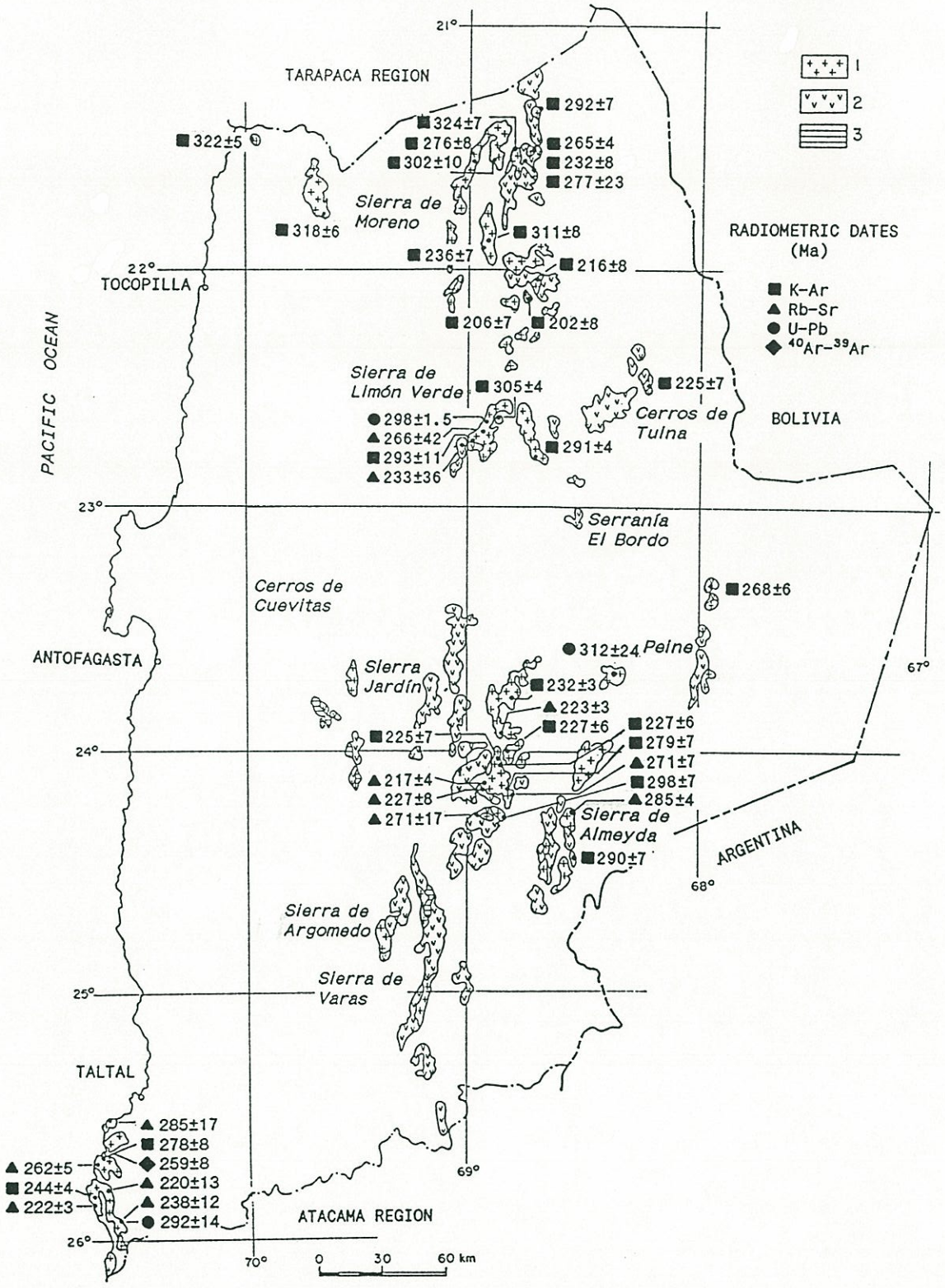


**Figure 2.3.** Distribution of Upper Carboniferous to Middle Triassic Rocks. (1) Plutons. (2) Volcanic rocks. (3) Sedimentary rocks.

radiometric dates (K-Ar and Rb-Sr) from 287 to 223 Ma (Appendix 2). In addition, radiometric dating of ignimbrites and rhyolites in the Imilac area has yielded values of 290 ± 7 and 268 ± 6 Ma (biotite, K-Ar), as well as 271 ± 17 and 227 ± 8 Ma (whole rock Rb-Sr; Davidson, personal communication). The lithologic and paleontologic characteristics suggest that this unit represents primarily subaerial volcanism. A few small basins accumulated lenticular lacustrine (fresh and saline water) sedimentary deposits at the same time.

According to Breitkreuz and others (1989) the petrochemical characteristics of the Upper Carboniferous to Triassic volcanic rocks of the Domeyko Cordillera reveal a typical calc-alkaline trend from basaltic andesites to rhyolites with the more siliceous compositions dominant. The basic-intermediate lavas display trace element characteristics similar to those of continental rift basalts (relatively high P, Ti, and Zr contents). The REE patterns are similar to those of evolved calc-alkaline rocks of active continental margin settings. A setting of an active continental margin subjected to extensional stress has been inferred for the volcanism (Breitkreuz and others, 1989). On the other hand, Kay and others (1989) attributed the dominance of silicic magmatism during the Late Paleozoic to Triassic as effect of extensive crustal melting induced by the accumulation of basaltic magmas at the mantle-crust interface during an extensional period resulting from reduced convergence rates on the active margin of the Gondwana supercontinent. Initial ratios $^{87}Sr/^{86}Sr$ reported by Davidson and others (1985) from both volcanic and plutonic Late Paleozoic rocks of the Domeyko Cordillera are relatively low, ranging between 0.7046 and 0.7055, congruent with arc magmas. Rogers (1985) reported higher initial $^{87}Sr/^{86}Sr$ (from 0.70600 to 0.70649) for the Late Carboniferous Limon Verde granitic pluton ($\epsilon^{i}_{Sr}$ = +23 to + 30.0). The initial $^{143}Nd/^{144}Nd$ of this pluton varies from 0.512195 to 0.512229 ($\epsilon^{i}_{Nd}$ = -2.0 to -1.3). Rogers (1985) interpreted these isotopic data as indicative of crustal contamination, but advocated a primarily mantle source for the parental magma.

The Upper Carboniferous - Middle Triassic volcanic unit is sparsely mineralized. It hosts minor copper and manganese in vein and irregular deposits (Guacazul, Caspana, and Tuina districts; Fig. 3.3). The largest deposits are those of the Tuina district (Raczynski, 1963; Marinovic and Lahsen, 1984).

### 2.6.2 Upper Carboniferous-Middle Triassic intrusive rocks

Extensive Upper Carboniferous-Middle Triassic plutons occur along the Domeyko and Main Andean Cordilleras. Isolated intrusive bodies occur also along the Coastal Cordillera (Fig. 2.3). The plutons of the Domeyko and Main Andean Cordilleras include coarse- to medium-grained monzogranites, syenogranites, granodiorites, tonalites, quartz-diorites, and diorites whose main ferromagnesian mineral phases are usually biotite and hornblende. The plutons intruded Lower Paleozoic intrusive rocks and Devonian sedimentary rocks and they are covered unconformably by Upper Triassic sedimentary and volcanic rocks. Their age range is constrained by these contact relationships and many K-Ar and Rb-Sr dates ranging from 318 to 217 Ma (Appendix 2; Fig. 2.3). Their distribution coincides with that of the Upper Carboniferous to Middle Triassic volcanic rocks described in the previous section. Petrochemical data from the central portion of the Domeyko Cordillera show the calc-alkaline nature of these intrusive rocks and affinity to I-type granites (Davidson and others, 1985; Baeza, 1984; Rogers, 1985).

In the Coastal Cordillera, about 100 km west of the main Upper Carboniferous to Middle Triassic magmatic belt, several leucocratic monzogranite and syenogranite plutons occur, which have radiometric ages ranging between 322 and 222 Ma (Cifuncho Plutonic Group after Naranjo and Puig, 1984). Berg and others (1983) reported high initial $^{87}Sr/^{86}Sr$ ratios (>0.710) and advocated S-type affinity for the coastal plutons of Chañaral implying a crustal origin for the magmas. However, the more recent study of the same rocks by Brown (1989), including new isotopic data, failed to

confirm the S-type signature or high $^{87}Sr/^{86}Sr$ initial ratios. Brown (*op. cit.*) claims that petrochemical characteristics of Late Paleozoic intrusive complexes of the Coastal Cordillera and Main Andes are similar (calc-alkaline, I-type intrusions). He suggested that igneous rocks from a single broad Paleozoic magmatic arc were tectonically separated during Mesozoic crustal stretching.

Despite the great extent of the outcrops of Upper Carboniferous to Middle Triassic igneous rocks (Fig. 2.3), they are only sparsely mineralized. Thus from a metallogenic point of view they appear unimportant. Several small copper and silver-lead veins are associated with the plutons of the Domeyko Cordillera (Moctezuma, Sierra de Argomedo districts and El Aromo and Vizcachas mines; Fig. 3.3). In addition, a quartz-dioritic porphyry in the Imilac area hosts a tourmaline breccia-pipe with an copper-bearing vein on its southeastern border (La Casualidad mine; Fig. 3.3). Sericite from this vein has yielded a K-Ar age of 298 ± 7 Ma (Davidson and others, 1985). The granitic plutons of the Coastal Cordillera host only a few small veins with silver-lead (Cerro Camino and Cifuncho mines) (Fig. 2.3).

Carboniferous-Permian porphyry copper deposits in the Argentinian Andes are associated with Upper Paleozoic calk-alkaline igneous rocks (Sillitoe, 1977, 1981). This led Sillitoe (1977) to conclude that they were generated in a convergent plate margin characterized by eastward subduction, closely comparable to the Meso-Cenozoic and present-day plate boundaries in the Central Andes. This interpretation has been reinforced by more recent work (e.g., Ramos and others, 1986; Breitkreuz and others, 1989; Brown, 1989) and is favoured by the writer.

### 2.6.3 Upper Carboniferous-Permian sedimentary rocks

These rocks occur in small isolated hills within the Intermediate Depression (Fig. 2.3), and within the Coastal Cordillera

(Cerros de Cuevitas) and in the Domeyko Cordillera (Sierra de Varas). The sequence exposed in the Intermediate Depression overlies Paleozoic rhyolites (possibly Carboniferous) and underlies Upper Triassic to Jurassic sedimentary rocks (Niemeyer and others, 1985). It consists of 430 m of sandstones, shales, and limestones with intercalations of conglomerates and breccias with rhyolitic clasts (Niemeyer and others, 1985). The limestones include abundant fossils (bryozoan, brachiopods, foraminifers, and algae) suggesting that the deposition of the sequence took place during the Carboniferous to Permian in a neritic marine environment (Davidson and others, 1981b).

## 2.7 LATE CARBONIFEROUS TO MIDDLE TRIASSIC GEOLOGICAL AND PALEOGEOGRAPHIC SYNOPSIS

This interval was preceded by the Chanic tectonic event and was characterized by intense magmatic activity in the Domeyko and Main Andean Cordilleras. This igneous activity involved extensive rhyolitic-dacitic and subordinate andesitic-basaltic volcanism (including subaerial pyroclastic flows) and the synchronous emplacement of extensive lithologically diverse calc-alkaline plutons. The chronological and spatial relationships between the volcanic and intrusive rocks, along with their petrochemical characteristics, suggest that these igneous rocks represent arc magmatism related to steady subduction of oceanic crust under the edge of the Gondwana supercontinent. This is further supported by the extent of these igneous rocks from the northernmost part of a magmatic belt in northern Chile about 4,000 km to Neuquen in southern Argentina (Coira and others, 1982; Mpodozis and Ramos, in press). Geochemical analyses suggest calk-alkaline magmatism (Coira and Kouharsky, 1976; Caminos, 1979; Breitkreuz and others, 1989). Initial ratios $^{87}Sr/^{86}Sr$ ranging between 0.7046 and 0.7065 from both volcanic and plutonic rocks (Davidson and others, 1985; Rogers, 1985) suggest primarily sub-crustal magma derivation. Thus these rocks very probably represent a magmatic arc developed on the border of the Gondwana supercontinent: the "Gondwana

Magmatic Arc" of Ramos and others (1986). The dominance of silicic magmatism during this period has been recently interpreted by Kay and others (1989) to reflect extensive crustal melting within an extensional regime; however, no corroborating data were presented by these authors, who did not exclude subduction in their interpretation but envisaged intra-arc extension during a period of reduced convergence rates. The apparently continuous and recurrent magmatic activity in the same geographic location for ca. 100 Ma suggests a static (non-migrating) magmatic front and a relatively stable subduction system.

Jesinkey and others (1987) have shown that the Upper Carboniferous-Middle Triassic volcanic and intrusive rocks of the Domeyko Cordillera have concordant South American Late Paleozoic paleomagnetic poles, which indicate that these igneous rocks have been *in situ* with respect to the rest of the continent since their formation (autochthonous igneous rocks).

The emplacement of granitic plutons during the Late Carboniferous to Middle Triassic in the Coastal Cordillera, about 100 km west of the Domeyko Cordillera, is problematic. These plutons intrude the Chañaral Melange interpreted as part of a subduction complex by Bell (1982, 1987). The melange was probably part of the Upper Paleozoic accretionary wedge interpreted by Herve and others (1981) and Forsythe (1982) from outcrops of metamorphic and sedimentary rocks along the coastal area between 28° and 36° S. The position of the Upper Carboniferous to Middle Triassic coastal plutons would correspond to the place of least heat-flow in a typical active continental margin. This setting may suggest the hypothetical generation of magmas by the interaction of the accretionary wedge with an active oceanic ridge in a similar manner to the Paleocene magmatism of the Kodiak islands in Alaska (Moore and others, 1983). Brown (1989) suggested that the coastal granitic plutons represent part of a broad Late Paleozoic arc that was split by Mesozoic crustal stretching. This hypothesis presupposes hypothetical extension in excess of 100 km during the Mesozoic. However, none of the above speculations are supported by conclusive geological data.

The paucity of mineral deposits is attributable mainly to a deep erosion level of the Upper Paleozoic to Triassic igneous rocks. Carboniferous-Permian porphyry copper deposits in the Argentinian Andes indicate that mineralizing processes were active at that time.

## 2.8 LATE TRIASSIC TO EARLY CRETACEOUS

The Late Triassic to Early Cretaceous interval was characterized by intense magmatic activity in the Coastal Cordillera and marine and terrestrial sedimentation within a trough that occupied the area of the present-day Intermediate Depression and Domeyko Cordillera. This paleogeography implies a major change from the Late Carboniferous to Middle Triassic interval, including a 100 to 150 km westward displacement of the magmatic front and the formation of a marine trough in the area where subaerial volcanism was formerly active. This major paleogeographic change is related to crustal movements that took place during the Middle-Late Triassic, **Atacamenian** tectonic event, which is recorded by an unconformity at the base of Upper Triassic strata.

### 2.8.1 Upper Triassic volcanic and sedimentary rocks

The most extensive outcrops of Upper Triassic rocks occur along the Domeyko Cordillera and western flank of the Main Andean Cordillera. Minor outcrops are also present in the southern part of the Coastal Cordillera (Fig. 2.4). This unit includes the following lithostratigraphic units: Agua Dulce Formation (Garcia, 1967); Cerros Negros Strata (Ramirez and Gardeweg, 1982), and Quebrada del Salitre Formation (Naranjo and Puig, 1984).

The Upper Triassic sequence unconformably overlies Upper Carboniferous to Middle Triassic volcanic, sedimentary, and plutonic rocks and is conformably covered by Lower Jurassic sedimentary rocks. The sequence includes volcanic rocks (lavas, tuffs, and breccias) of andesitic, rhyolitic, and trachytic composition; paraconglomerates and orthoconglomerates; and volcanoclastic sandstones. Minor intercalations of mudstones, marine limestone, and chert occur in the Cerros de Caracoles area. The clastic materials are mainly locally derived from the erosion of the Upper Carboniferous to Middle Triassic volcanic and intrusive rocks. The maximum thickness of this sequence is 1,600 m, but rapid thickness variations are typical, and locally the Jurassic rocks directly overlie Paleozoic rocks. The strata show open to tight folds, with north-south trending axes (Ramirez and Gardeweg, 1982). The lithology varies from north to south. The northernmost outcrops are mainly volcanic rocks with only minor sedimentary intercalations (Agua Dulce Formation, and Cerro Negro Strata), whereas to the south, the number and thickness of sedimentary intercalations increase. This is particularly true in the lower portion of the sequence in which sedimentary rocks dominate to the south (Quebrada del Salitre Formation). Mudstone beds contain fossil flora and limestone horizons are found with abundant marine invertebrate fossils (Naranjo and Puig, 1984; Chong and Hillebrandt, 1985). The stratigraphic position and fossil content define the Late Triassic age of this volcano-sedimentary sequence. Rocks and fossils indicate dominantly terrestrial sedimentation (Ramirez and Gardeweg, 1982), but some fossiliferous limestones were deposited in a sublittoral marine environment (Naranjo and Puig, 1984).

The sequence exposed in the Coastal Cordillera (Cifuncho Formation) unconformably overlies Devonian metasedimentary rocks and underlies Hettangian sedimentary strata. This unit, 1,000 m thick, is composed of conglomerates (polymictic orthoconglomerates); red sandstones with thin levels of shale, cherts and lacustrine limestones; and intercalations of andesitic to dacitic lavas, tuffs, and breccias. The sedimentary rocks include primary sedimentary structures (cross-bedding,

graded-bedding, ripple-marks, load-casts, and paleochannels) and fossil flora. These sedimentary rocks were probably deposited in terrestrial alluvial and lacustrine environments. They are ascribed to the Late Triassic since the sequence conformably underlies Hettangian sedimentary rocks. According to Naranjo and Puig (1984), a preliminary analysis of their fossil flora corroborates the Late Triassic age.

### 2.8.2 Jurassic volcanic rocks

A Jurassic volcanic sequence, 3,000 to 10,000 m thick, is exposed along the Coastal Cordillera (Fig. 2.4) (La Negra Formation; Garcia, 1967). This sequence is composed chiefly of lavas, breccias, and subordinate tuffs of basaltic-andesite, basaltic, and andesitic composition. Dacites are less common and are generally restricted to the easternmost outcrops (Cerro Cisne, Boric, 1981; Mantos Blancos District, Chavez, 1984). Beds of volcanoclastic conglomerates, sandstones, and breccias form intercalations to thicknesses of a few metres. Locally (west of Quillagua, Michilla District, and southwest of Taltal) the basal section of the volcanic sequence includes lenticular intercalations of sandstones, shales, and marine fossiliferous limestones up to 160 m in thickness (Maksaev and Marinovic, 1980; Astudillo, 1984; Naranjo and Puig, 1984). Pillow lavas have been described in the lower and middle portion of this volcanic sequence (Ferraris and Di Biase, 1978; Naranjo and Puig, 1984).

The volcanic rocks typically include variable amounts of epidote, chlorite, calcite, quartz, albite, sericite, prehnite, pumpellyite, and actinolite as secondary minerals usually concentrated in brecciated and amygdaloidal sections of lava flows. This widespread alteration has been attributed to low- to very low-grade regional metamorphism (prehnite-pumpellyite facies) (Losert, 1973, Palacios, 1977), and has been ascribed to burial (Levi and others, 1989). Burial metamorphism of the thick Jurassic volcanic sequence may indeed account for at

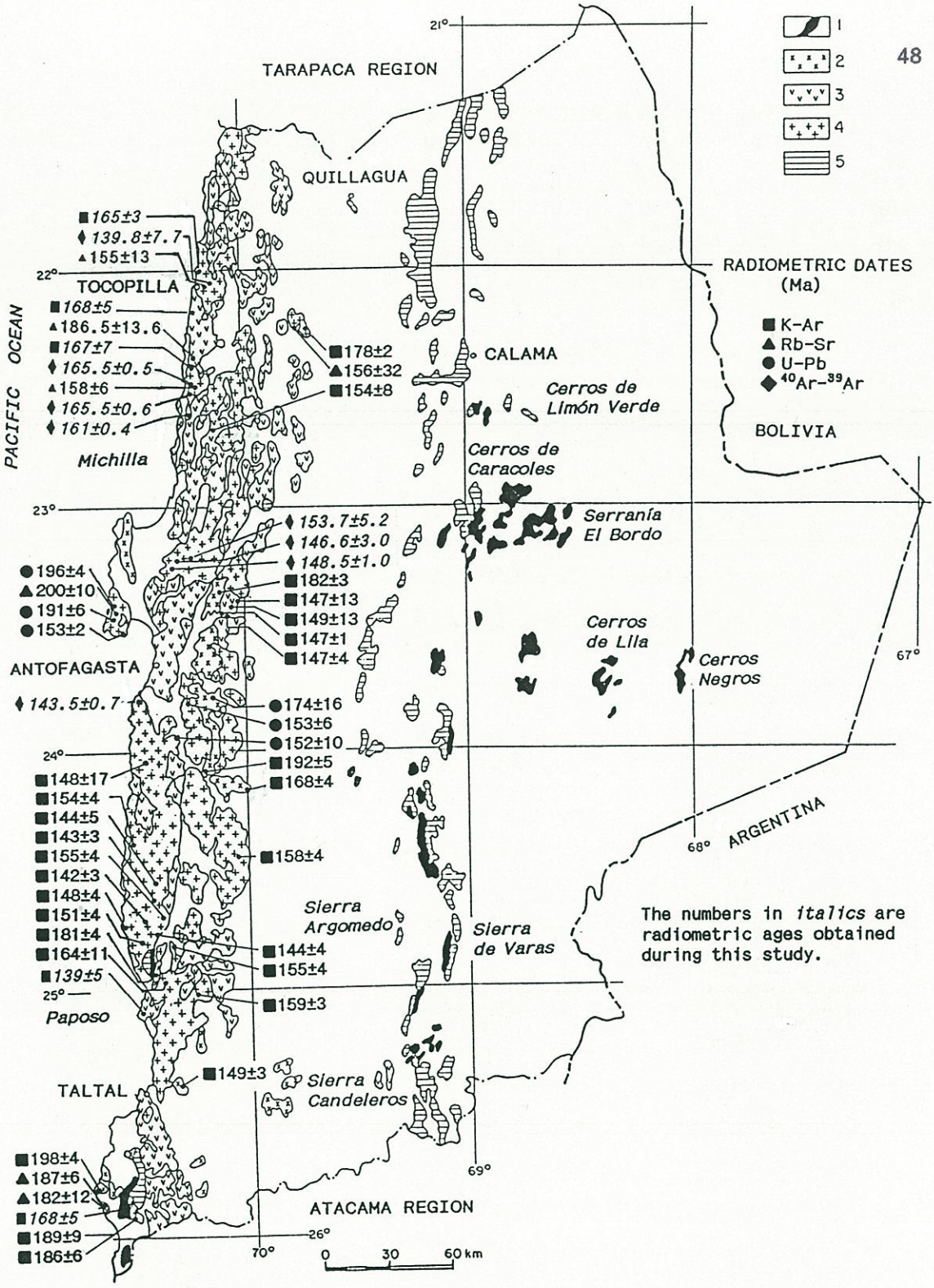


**Figure 2.4.** Distribution of Upper Triassic to Upper Jurassic rocks. (1) Upper Triassic volcanic and sedimentary rocks. (2) Upper Triassic-Lower Jurassic plutons. (3) Jurassic volcanic rocks. (4) Jurassic plutons. (5) Marine sedimentary rocks.

least part of regional alteration of the volcanic rocks, but part of this alteration may also be of deuteric origin and from metasomatic-alteration aureoles associated with extensive Jurassic and Lower Cretaceous batholiths (Figs. 2.4, 2.5). Buchelt and Tellez (1988), in a petrographic and geochemical study of the Jurassic volcanic rocks of Antofagasta, argued that no minerals typical of the zeolite or greenschist metamorphic facies were observed in any of their studied samples. According to these authors, although the alteration (propylitization) of the Jurassic volcanic rocks is widespread, and locally very intense, the minerals that occur (epidote, clinozoisite, and chlorite) are products of hydrothermal and metasomatic processes.

The Jurassic volcanic sequence is stratified in thick layers (25 to 30 m). Different fault-bounded blocks of these volcanic strata display homoclinal disposition, with north-trending strike, and dips 20° to 35° either to the west or east. Dikes, sills, sheets, and subvolcanic stocks of basaltic and andesitic compositions, are emplaced within the volcanic rocks. Some of these have been interpreted as volcanic feeder conduits (Palacios and Definis, 1981). The thick individual basaltic and andesitic lava flows are usually porphyritic. They have a brecciated base, a massive central portion and a brecciated, and amygdaloidal upper part (aa type lavas).

The fossils in the calcareous intercalations (*ammonites*) and the stratigraphic position of this volcanic sequence, indicate an age range from Sinemurian to Kimmeridgian (Bobenrieth, 1980; Maksaev and Marinovic, 1980; Naranjo and Puig, 1984). Support for this age range is provided by a whole-rock Rb-Sr isochron of 186 ± 14 Ma (south of Tocopilla, Rogers, 1985) and K-Ar dates from 165 to 133 of dikes and stocks emplaced within the volcanic rocks (Astudillo, 1984; Chavez, 1984; this work) (Appendix 2).

The volcanic rocks were produced by intense primarily subaerial, basaltic to andesitic volcanism. Minor clastic terrestrial

sedimentation, probably derived from the erosion of the same volcanic rocks, occurred between some lava flows. Marine calcareous intercalations and pillow lavas, particularly in the lower part of the sequence, show that part of the volcanic pile was also deposited in a submarine environment.

The Jurassic lavas are dominantly calc-alkaline to high-K calc-alkaline. Different authors agree that this volcanism was related to a subduction zone that was active during the Jurassic. Interpretations differ, however, on the tectonic setting of this volcanism. It has been compared with an island arc (Palacios, 1982); ascribed to volcanism within an ensialic marginal basin (Rogers, 1985; Rogers and Hawkesworth, 1989); or attributed to a magmatic arc on an active continental margin, but with trace-element fractionation similar to within plate basalts and back arc volcanism (Buchelt and Zeil, 1986). From a geochemical point of view the Jurassic lavas are more like island-arc rocks than other volcanic sequences in the Andes of northern Chile (e.g., Dostal and others, 1977) but they probably represent a magmatic arc developed on the continental border. There is no evidence that this volcanic sequence is an exotic terrane.

The Jurassic volcanic rocks host many important stratabound copper deposits (e.g., Mantos Blancos, Buena Esperanza, Santo Domingo). Less important copper-bearing vein deposits are also known (see Section 3.2.2).

### 2.8.3 Jurassic intrusive rocks

Jurassic intrusive rocks form most of the coastal batholith (Fig. 2.4). They are emplaced within the Jurassic volcanic rocks, and Triassic and Jurassic sedimentary sequences. They range from

gabbros to granites (gabbros, diorites, quartz-diorites, granodiorites, tonalites, and granites). The contacts between different lithologies are both sharp or gradational. In general mafic units (gabbros, diorites) are relatively older than the felsic units (granodiorites, granites) (Arabasz, 1971; Palacios, 1973; Vergara, 1985). These intrusive rocks are commonly medium-grained, including hornblende, biotite, and locally clinopyroxene. They are cut by many dikes and sills (andesitic, basaltic, rhyodacitic, microdioritic, granitic, syenitic, and aplitic; Pichowiak and Breitkreuz, 1984) and show an incipient to moderate alteration-metasomatism with assemblages of chlorite, epidote, sericite, and clay minerals.

The Jurassic gabbroic rocks form an intrusive complex exposed along the coast from the southern end of the Mejillones Peninsula to Paposo Cove (Fig. 2.4). These rocks commonly show penetrative vertical foliation due to ductile deformation associated with sinistral shearing (Herve, 1987a; Scheuber and Andriessen, 1990). The conspicuous foliation of these Jurassic gabbros led previous authors to erroneously regard them as Paleozoic metamorphic rocks (e.g., Bolfin Formation; Ferraris and Di Biase, 1978).

Many radiometric dates ranging from 200 to 138 Ma by K-Ar, Rb-Sr, U-Pb and $^{40}Ar$-$^{39}Ar$ methods prove the Jurassic age of these intrusive rocks (Appendix 2). The older ages have been obtained in gabbros of the Mejillones Peninsula (200 ± 10 Ma, whole rock Rb-Sr; Diaz and others, 1985; 199 ± 4 Ma, zircon U-Pb, Damm and others, 1986). The abundant radiometric data (Appendix 2) suggest continuous plutonism from Early Jurassic to Early Cretaceous time.

The Jurassic intrusive rocks are characterized by low initial $^{87}Sr/^{86}Sr$ ratios (0.7032-0.7049) and calc-alkaline geochemistry (Palacios and Espinoza, 1982; Shibata and others, 1984; Ishihara and others, 1984; Berg and Breitkreuz, 1983; Berg and others, 1983; Rogers, 1985; Rogers and Hawkesworth, 1989). Most investigators agree that these granitoids represent arc plutonism genetically related to mantle-derived

magmas during the subduction of oceanic crust below the active continental margin of South America.

The Middle to Upper Jurassic plutons host many copper-bearing veins. Minor veins host silver, gold, iron, and cobalt (see Section 3.2.2).

### 2.8.4 Jurassic sedimentary rocks

The Jurassic sedimentary rocks are exposed mainly along the Domeyko Cordillera. Minor outcrops also occur in the Intermediate Depression and Coastal Cordillera (Fig. 2.4). They constitute the following lithostratigraphic units: Rencoret Strata (Tobar, 1966), Paposo Strata (Ferraris, 1978), Pan de Azucar Formation (Naranjo, 1978), Posada de los Hidalgo (Garcia, 1967; Naranjo and Puig, 1984), Cholita Formation (Garcia, 1967), Quehuita Formation (Vergara, 1978), Quinchamale Formation (Maksaev, 1978), Sierra San Lorenzo Strata (Marinovic and Lahsen, 1984), Cerritos Bayos Formation (Biese, 1961; Garcia, 1967), Caracoles Group (Ramirez and Gardeweg, 1982, Marinovic and Lahsen, 1984), Sierra El Cobre Formation (Tobar, 1966), Profeta Formation (Chong, 1973), and Candeleros Formation (Naranjo and Puig, 1984).

In the Domeyko Cordillera the Jurassic sequence conformably overlies Upper Triassic volcanic and sedimentary rocks or unconformably overlies Upper Carboniferous-Middle Triassic volcanic and intrusive rocks. The sequence paraconformably underlies Lower Cretaceous sedimentary rocks. Along the Domeyko Cordillera the sequence is composed of alternating limestones and calcareous sandstones. These rocks are intercalated, particularly in the basal section, with marls, shales, sandstones, and conglomerates. The largely calcareous lower to middle portion of the sequence includes abundant marine invertebrate and subordinate vertebrate fossils. The upper section includes gypsum, mudstones, conglomerates, and red sandstones. Some of these have cross-

bedding and desiccation cracks. Fossil flora (without chronostratigraphic value) occur in this section. In the southern part of the area (Sierra Candeleros), andesitic pillow lavas and dacitic tuffs are intercalated (Naranjo and Puig, 1984). The sequence exposed along the Domeyko Cordillera is well stratified in thin beds and commonly shows tight folds with north-south trending axes, locally overturned and reversely faulted, making estimates of thickness unreliable. A maximum thickness of 3,500 m has been estimated by Naranjo and Puig (1984) in the Sierra de Candeleros area, but the sequence is usually 1,500 to 2,000 m thick.

In the Intermediate Depression Jurassic sedimentary rocks occur south of Quillagua, where they are only 270 m thick and made up of well stratified fossiliferous limestones and sandstones, with intercalations of thick andesite and volcanoclastic conglomerate beds (Maksaev and Marinovic, 1980).

In the Coastal Cordillera most of the stratified Jurassic rocks are volcanic but at Paposo (Fig. 2.4), a 1,700 m thick alternation of sandstones, shales, calcareous sandstones, limestones, and conglomerates underlies the volcanic sequence (Arabasz, 1971). These rocks are well stratified in fine beds and include abundant marine fossils.

The sedimentary sequence of the Coastal Cordillera is Early Jurassic in age according to its fossil content (Hettangian to Pliensbachian), whereas in the Domeyko Cordillera the lower to middle calcareous portion of the sequence has an age from Hettangian to Oxfordian. The upper section, which includes gypsum levels and clastic sedimentary rocks without fossils of chronostratigraphic value, is ascribed to the Oxfordian-Tithonian based on their stratigraphic position.

The petrographic characteristics and fossil content of this sedimentary sequence suggest the deposition in a neritic marine environment. During the Oxfordian, a general regression of the sea took place, and accumulation of evaporites (gypsum) and clastic terrestrial

deposits sedimentary rocks were deposited. The Jurassic calcareous rocks host many silver-bearing veins and minor stratiform deposits with copper, iron, or manganese (see Chapter 3).

### 2.8.5 Lower Cretaceous volcanic rocks

The Lower Cretaceous volcanic rocks outcrop in a north-northeast trending discontinuous belt extending from the Coastal Cordillera in the southern part of the area to the Domeyko Cordillera in the northern part (Fig. 2.5). These rocks outcrop as the following stratigraphic units: Macata Formation (western outcrops; Vergara, 1978), Arca Formation (western outcrops; Maksaev, 1978), Santa Isabel Sequence (Boric, 1981), Quebrada Seca and Quebrada Mala Formations (Montaño, 1976), and Aeropuerto Formation (Ulriksen, 1979; Naranjo and Puig, 1984). Some of these units were previously regarded as Jurassic, Late Cretaceous, or Early Tertiary but, according to the writer's field observations, they are Early Cretaceous. These volcanic rocks conformably overlie Tithonian to Lower Cretaceous sedimentary rocks and underlie Upper Cretaceous - Lower Tertiary volcanic rocks with marked unconformity. They include andesites, dacites and scarce basalts and are thus similar to the Jurassic volcanic rocks except that andesitic compositions dominate and dacites are more abundant. The volcanic rocks form thick lava flows (ca. 20 to 30 m) that alternate with andesitic and dacitic breccias and tuffs. Intercalations of conglomerates, sedimentary breccias, and red volcanoclastic sandstones are common. In addition, intercalations of marine fossiliferous limestones occur in the Coastal Cordillera south of Taltal (Aeropuerto Formation; Ulriksen, 1979; Naranjo and Puig, 1984).

The maximum thickness of the sequence is about 3,000 to 3,200 m. The volcanic strata show a homoclinal disposition generally striking north and dipping either to the east or west in different structural blocks.

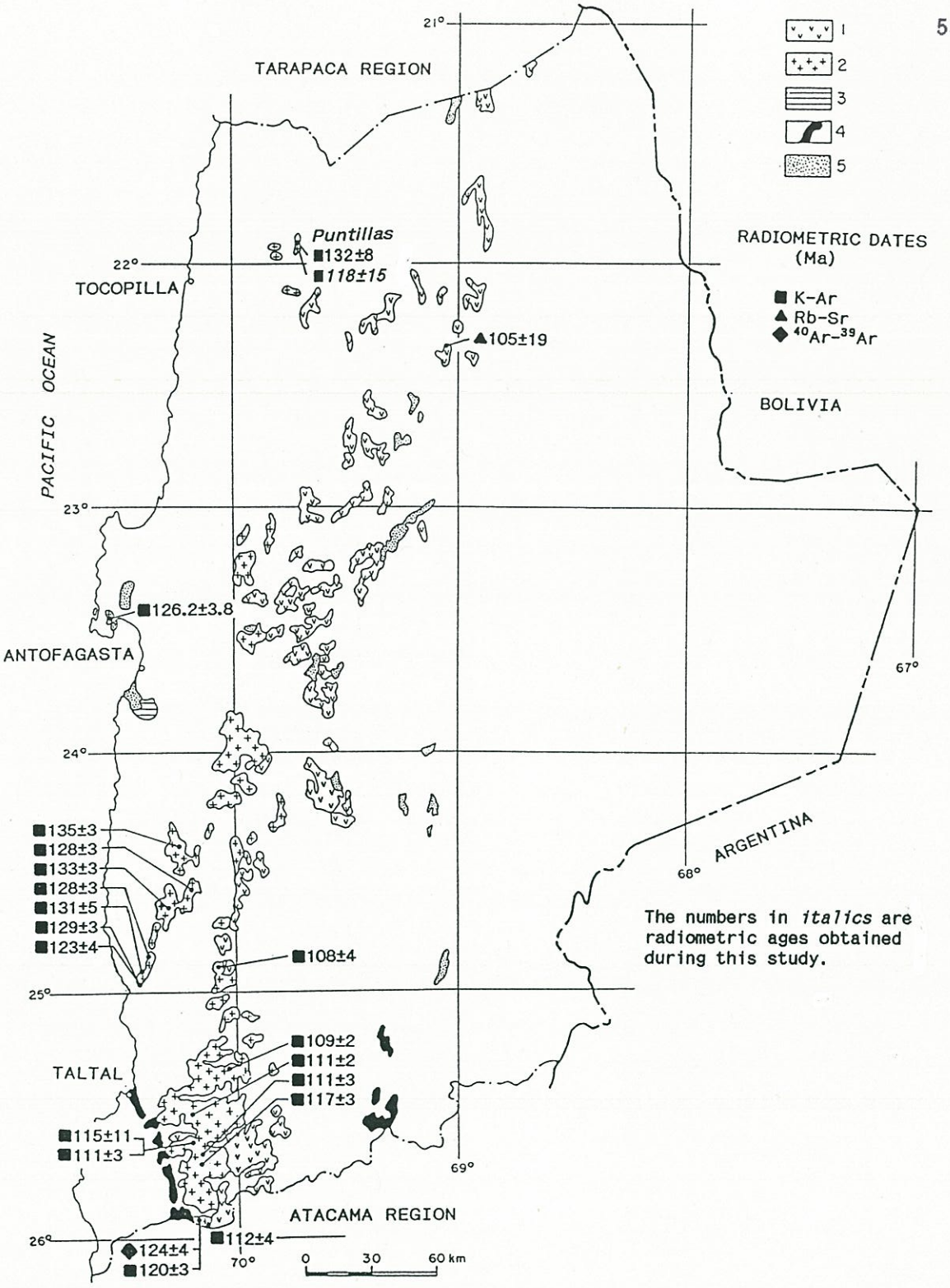


**Figure 2.5.** Distribution of Lower Cretaceous rocks. (1) Volcanic rocks. (2) Intrusive rocks. (3) Marine sedimentary rocks. (4) Volcanic rocks with marine sedimentary intercalations. (5) Terrestrial red beds.

The Early Cretaceous age ascribed to these volcanic rocks is based on their stratigraphic position, dates ranging from 124 to 108 Ma for plutons that intrude them, and $^{40}Ar$-$^{39}Ar$ dating of lavas has yielded total gas ages of 111 ± 3 Ma and 106 ± 3 Ma (Ulriksen, 1979) (Appendix 2). Furthermore, they can be correlated to the south with volcano-sedimentary sequences that contain Neocomian fossils (Naranjo and Puig, 1984).

The lithology of this sequence indicates that it was formed by subaerial volcanic activity and associated terrestrial clastic sedimentation. In the southern part of the area the volcanism alternated with shallow marine sedimentation (Ulriksen, 1979).

The Lower Cretaceous volcanic rocks at latitude 22° S are of K-rich calk-alkaline affinity (Rogers, 1985). A Rb-Sr errorchron of 105 ± 19 Ma was obtained for these rocks, with an initial $^{87}Sr/^{86}Sr$ ratio of 0.7043 by Rogers (1985).

The Lower Cretaceous volcanic rocks host many small copper, silver, gold, iron, and manganese deposits (vein, stratiform and irregular bodies) in the southern section of the Coastal Cordillera (see Section 3.2.3).

### 2.8.6 Lower Cretaceous intrusive rocks

Lower Cretaceous plutons of diverse lithology (granites, granodiorites, tonalites, quartz-monzodiorites, diorites, and quartz-monzonites) are exposed along the Coastal Cordillera (Fig. 2.5). They intrude Jurassic volcanic and intrusive rocks and Lower Cretaceous

volcanic rocks. These plutonic rocks usually are medium-grained and have hornblende and biotite as main mafic minerals. Some plutons located near the Atacama Fault System are foliated (ductile shear strain; see Section 2.16.1), whereas others have abundant mafic inclusions that according to Arabasz (1971) distinguishes them from the Jurassic plutons. There are gradational contacts within some plutons and also sharp contacts, especially of microgranitic stocks with older plutons.

Small stocks of granodiorite, diorite and tonalite porphyries that outcrop in the northern part of the region have also been ascribed to the Early Cretaceous. Some of these intrusives have been interpreted as volcanic necks (Maksaev and Marinovic, 1980).

The Lower Cretaceous intrusions represent the continuation in time of the plutonic activity that began in the Jurassic along the Coastal Cordillera. Many K-Ar and $^{40}Ar-^{39}Ar$ dates that range from 136 to 109 Ma indicate their Early Cretaceous age (Appendix 2). The petrochemical data of Berg and Breitkreuz (1983) demonstrate their calk-alkaline nature. Their $^{87}Sr/^{86}Sr$ initial ratios are in the range 0.7033 to 0.7055 (Munizaga and others, 1985; Berg and Breitkreuz, 1983) suggesting a subcrustal origin.

Many veins hosting copper, gold, silver, and iron occur within Lower Cretaceous plutons. A granodioritic porphyry at Puntillas (Lat. 22° S) has low-grade copper mineralization and strong hydrothermal alteration (argillic, sericitic, and minor potassic). This porphyry-type alteration-mineralization (Maksaev and Marinovic, 1980) has yielded K-Ar dates ranging between 132 and 118 Ma (Munizaga and others, 1985; Table 4.1)

### 2.8.7 Lower Cretaceous sedimentary rocks

Lower Cretaceous sedimentary rocks are exposed on the western flank of the Domeyko Cordillera and within the Intermediate Depression. Minor outcrops occur in the Coastal Cordillera south of the port of Antofagasta, and in the Mejillones Peninsula. They are represented by the following lithostratigraphic units: Caleta Coloso Formation (Garcia, 1967; Ferraris and Di Biase, 1978), El Way Formation (Garcia, 1967), Continental Sequence of Cerritos Bayos (Biese, 1961), Quebrada Mala Formation (Montaño, 1976), Upper part of the Sierra El Cobre Formation (Tobar, 1966), Member 1 of the Profeta Formation (Chong, 1973), and Santa Ana Formation (Naranjo and Puig, 1984).

The sequence in the Domeyko Cordillera paraconformably overlies sedimentary rocks ascribed to the Kimmeridgian. It conformably underlies Lower Cretaceous volcanic rocks. In the Coastal Cordillera the Lower Cretaceous sedimentary rocks overlie with a slight angular unconformity Jurassic volcanic rocks (Garcia, 1967) and their top is the present erosion surface.

In the Domeyko Cordillera and Intermediate Depression the sequence is 1,500 to 1,800 m thick. It is composed of sandstones, conglomerates, and breccias. The component clastic materials are dominantly of volcanic origin and intercalations of porphyritic andesitic lavas are common. In the southern part of the region the lower part of the sequence includes shales and calcareous sandstones with marine fossils (Santa Ana Formation; Naranjo and Puig, 1984). In the northern part of the Domeyko Cordillera evaporitic gypsum beds are intercalated with these rocks (Arca Formation; Maksaev, 1978). The Lower Cretaceous sedimentary rocks form a well stratified, reddish sequence folded along dominant north-south trending axes.

In the Coastal Cordillera the sequence includes a lower portion, 600 to 2,000 m thick, composed of thick red beds of volcanoclas-

tic conglomerates and thin horizons of red sandstones and mudstones. These red-beds host stratiform copper deposits (El Way district; see Section 3.2.3). South of Antofagasta the red-beds are conformably overlain by 240 m of limestones, marls, and calcareous sandstones with intercalations of shales (El Way Formation; Garcia, 1967). These rocks include abundant Lower Cretaceous marine fossils (Brüggen, 1950; Alarcon and Vergara, 1964; Garcia, 1967; Jurgan, 1974). Part of the Early Cretaceous red beds and the upper calcareous marine sedimentary deposits filled a rhombic 10 by 15 km pull-apart basin (see Section 2.16.1).

The fossil content of the rocks of both the Domeyko and Coastal Cordilleras indicate an Early Cretaceous age (Brüggen, 1950; Alarcon and Vergara, 1964; Garcia, 1967; Jurgan, 1974; Chong, 1976; Naranjo and Puig, 1984); however, the stratigraphic relationships indicate that the sequence probably also includes Tithonian rocks. The lithology indicates mainly terrestrial alluvial sedimentation but in the southern part of the Antofagasta Region periods of neritic marine sedimentation are also represented (Alarcon and Vergara, 1964; Naranjo and Puig, 1984).

## 2.9 LATE TRIASSIC TO EARLY CRETACEOUS GEOLOGICAL AND PALEOGEOGRAPHIC SYNOPSIS

The Late Triassic is a transitional epoch, which has been traditionally regarded as the boundary between the "Hercynian" and "Andean" orogenic cycles (e.g., Coira and others, 1982; Suarez and others, 1985; Aguirre, 1985). The separation of orogenic cycles in the Andes is inherited from outdated cyclic and deterministic geosynclinal interpretations (e.g., Aubouin and others, 1973). This arbitrary division is not favoured by the writer because the Andean evolution can be interpreted in terms of continuous plate interactions.

Recent interpretations suggest that the Late Paleozoic evolution of the Andes was characterized by the formation of an

accretionary prism at the edge of the South American continent (Herve and others, 1981; Forsythe, 1982; Mpodozis, 1984; Dalziel and Forsythe, 1985; Ramos and others, 1986; Herve, 1988; Ramos, 1988), whereas the Mesozoic and Cenozoic history is one of subduction erosion of the continental border (Coira and others, 1982; Mpodozis, 1984).

During the Late Triassic the Coastal Cordillera, Intermediate Depression, and Domeyko Cordillera were the site of terrestrial clastic sedimentation that alternated with volcanic activity. Minor periods of shallow marine sedimentation are also recorded in the Domeyko Cordillera. These geological processes are intimately related to crustal movements that took place at the Middle-Late Triassic, which the writer terms **Atacamenian** tectonic event. The denudation of the Upper Carboniferous to Middle Triassic igneous rocks and coeval deposition of coarse clastic sediments during the Late Triassic suggest that these crustal movements were essentially block faulting related to extensional tectonics. This process has been inferred by Charrier (1979) for the Late Triassic of central Chile, but the precise paleogeography for the Antofagasta Region is still obscure. Most of the Late Triassic volcanism was scattered along the Domeyko Cordillera, but minor volcanic deposits also occur in the southern part of the Coastal Cordillera (Cifuncho Formation; Ulriksen, 1979; Naranjo and Puig, 1984; Suarez and others, 1985).

At the onset of the Jurassic the Intermediate Depression and Domeyko Cordillera were inundated by the sea and volcanic activity ceased completely along the Domeyko Cordillera. In contrast, along the Coastal Cordillera intense volcanism and plutonism began, which persisted during all the Jurassic and Early Cretaceous.

Jurassic to Early Cretaceous magmatism along the area of the present Coastal Cordillera signifies a westward displacement of about 100 to 150 km of the magmatic front, relative to its previous position along the Domeyko Cordillera. The specific reason for this westward shift of the magmatic front is unknown, but probably was the result of a Late

Triassic major reorganization of plate interactions involving the westward migration of the subduction zone itself. This problem has not been addressed by previous studies, but is very important for understanding the geological history of this Andean segment. Possible causes are speculative: one possibility is the accretion of an exotic crustal block to the continental border; however, there is no conclusive geological evidence supporting terrane accretion. Another possible explanation may be the subduction of an active oceanic ridge during the Triassic that inhibited subduction due to the buoyancy of the hot materials and resulted in subsequent development of a new subduction zone further west.

The characteristics of Jurassic and Early Cretaceous calc-alkaline magmatism of the Coastal Cordillera are consistent with an active continental margin setting. These igneous rocks are thought to represent arc magmatism related to the subduction of oceanic crust under the South American continental border (e.g., Coira and others, 1982). Some recent interpretations suggest that the Jurassic volcanic rocks were deposited within an ensialic marginal (back-arc) basin rather than in an actual volcanic arc (Rogers, 1985; Rogers and Hawkesworth, 1989; Buchelt and Zeil, 1986). This idea follows the interpretation, on petrochemical grounds, by Atherton and others (1983) of the Cretaceous Puente de Piedra Formation of Central Peru. The Jurassic volcanic rocks of the Antofagasta Region are petrochemically similar to the Cretaceous rocks of central Peru. However, the volcanism in the Jurassic and Early Cretaceous was dominantly subaerial in the Antofagasta segment of the Andes and there is no conclusive geological evidence supporting a back-arc setting. On the contrary, the marginal basin interpretation opens questions about the significance of coeval calc-alkaline plutonism and would imply the subsequent complete removal of the Jurassic volcanic arc from the South American border.

The foliation of Jurassic and Lower Cretaceous igneous rocks due to ductile shear strain, and the associated development of a major trench-linked strike-slip fault system along the Coastal Cordillera (Atacama Fault System; see Section 2.16.2) has been attributed to a

hypothetical period of southeasterly-directed oblique plate convergence during the Late Jurassic and Early Cretaceous (Naranjo and others, 1984; Herve, 1987a; Scheuber and Andriessen, 1990).

The Intermediate Depression and Domeyko Cordillera were a back-arc sedimentary basin that from the Hettangian to the Callovian, was the site of mostly calcareous marine sedimentation. During the Oxfordian a general regression of the sea took place and the deposition of evaporites (gypsum) and clastic sediments ensued. Lower Cretaceous terrestrial red-beds covered the Upper Jurassic deposits, but in the southern part of the region Lower Cretaceous terrestrial conditions alternated with shallow marine sedimentation. A Lower Cretaceous calcareous marine sequence was also deposited within the Coastal Cordillera (El Way Formation, Garcia, 1967) but these rocks are restricted to a 10 by 15 km pull-apart basin (see Section 2.16.2).

Abundant copper mineralization is spatially related to Middle to Upper Jurassic igneous rocks. Indeed, the largest number of individual metallic mineral deposits of the Antofagasta Region is hosted by these rocks (see Section 3.2.2).

## 2.10 LATE CRETACEOUS TO EOCENE

A Late Cretaceous compressive tectonic event (**Peruvian** or **Subhercynian** phase; Vicente and others, 1973) introduced major paleogeographic changes in this Andean segment, including the uplift of the Jurassic-Early Cretaceous back-arc sedimentary basin and the eastward shift of the magmatic front by about 100 km. These changes initiated a new interval characterized by active subaerial volcanism in the Intermediate Depression and Domeyko Cordillera and deposition of red-beds in the Main Andes and Altiplano.

### 2.10.1 Upper Cretaceous-Eocene volcanic rocks

Upper Cretaceous to Eocene volcanic rocks occur along a north-northeast belt in the Intermediate Depression and Domeyko Cordillera (Fig. 2.6). They comprise the following formations: Icanche (Maksaev, 1978), Cerro Cinchado (Montaño, 1976), Augusta Victoria (Garcia, 1967), Chile-Alemania (Naranjo and Puig, 1984), Azabache (Ferraris and Di Biase, 1978), and Cerro Islote (Chong, 1973). This volcanic sequence overlies, with a marked angular unconformity, Jurassic and Lower Cretaceous sedimentary and volcanic sequences. Locally, in the northeastern part of the region, it conformably overlies Upper Cretaceous red beds (Tolar Formation, Maksaev, 1978). These volcanic rocks unconformably underlie Oligocene to Middle Miocene terrestrial sedimentary rocks.

The volcanic sequence is composed of lavas, tuffs, ignimbrites, breccias, and volcanic agglomerates, which range in composition from pyroxene-bearing basalts and basaltic-andesites to rhyolites. Andesitic and dacitic compositions dominate. The lavas are commonly massive and porphyritic, although brecciated, vesicular, and amygdaloidal flows are not unusual. The tuffs are either vitreous, crystalline, or lithic and a large proportion of them are welded pyroclastic flows (ignimbrites). The existence of both rhyolitic and dacitic ignimbrites distinguishes this volcanic unit from Jurassic and Lower Cretaceous volcanic sequences, which virtually lack this type of pyroclastic rock.

Many small, subvolcanic, usually porphyritic, coeval intrusive bodies are emplaced within the volcanic sequence. These stocks range in composition from gabbroic-diorite to granite and have been interpreted as volcanic centres by Naranjo and Puig (1984). Some rhyolitic and dacitic domes also occur. Sedimentary intercalations are scarce, lenticular, and composed of volcanoclastic conglomerates and sandstones. The volcanic strata are massive or thickly stratified. The thickness of these strata is variable reaching a maximum of 3,900 m in the

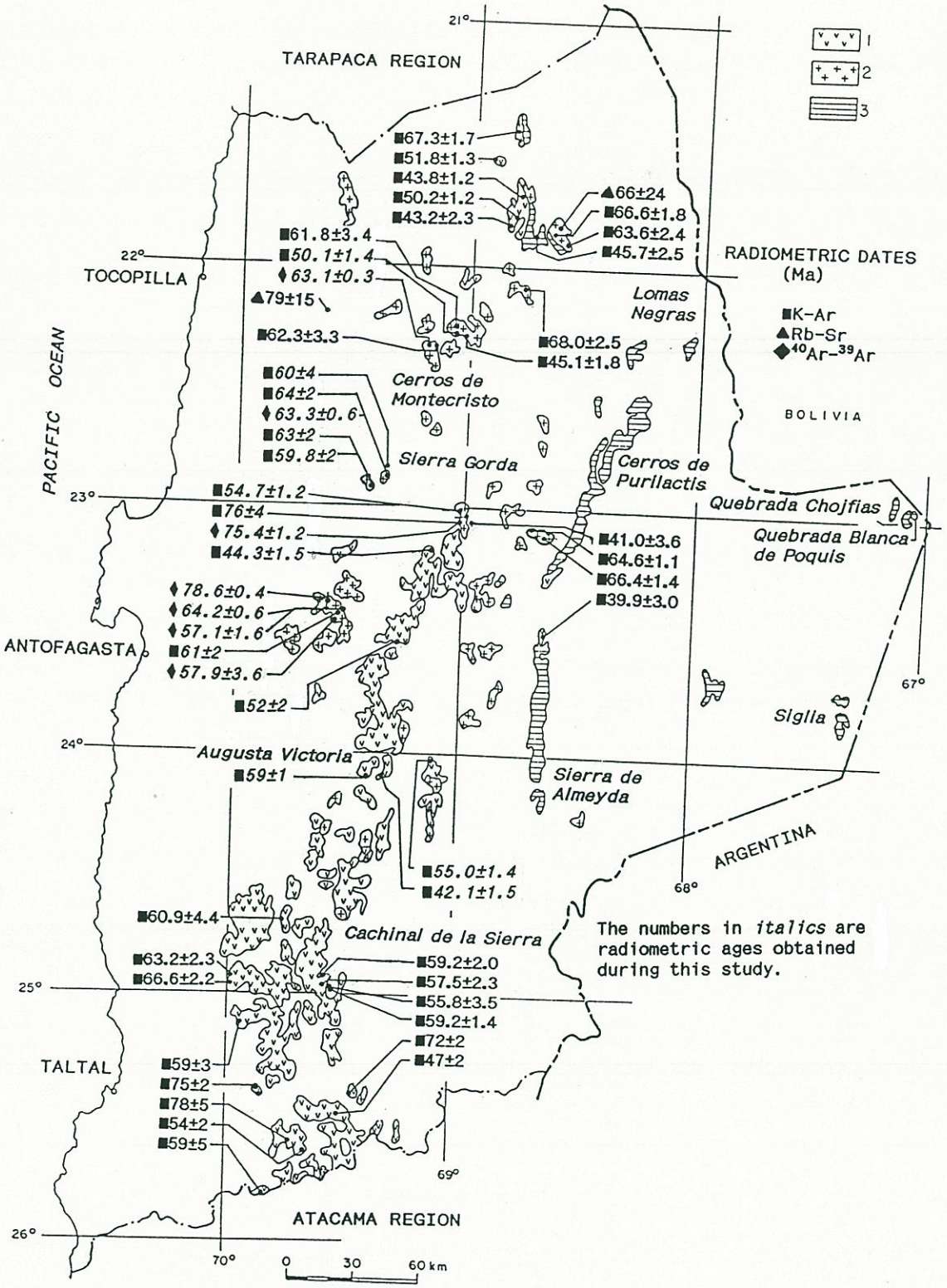


**Figure 2.6.** Distribution of Upper Cretaceous to Eocene rocks. (1) Volcanic rocks. (2) Intrusive rocks (3) Terrestrial red beds.

northern part of the Domeyko Cordillera. The volcanic strata located within the Intermediate Depression are usually sub-horizontal, whereas those in the Domeyko Cordillera are deformed in large open folds with north- or northeast-trending axes.

The volcanic sequence is ascribed to the Late Cretaceous - Eocene by its stratigraphic position and a great number of K-Ar radiometric dates that range from 78 to 39.9 Ma (Appendix 2; Table 4.1). Even though volcanism began in the Late Cretaceous (about 78 Ma), locally the basal rocks of this sequence yield K-Ar biotite ages of 55.0 ± 1.4 Ma and 59 ± 1 Ma (this work; Table 4.1). Most available radiometric dates range between the Paleocene and Eocene, which probably represents the interval of maximum volcanic activity.

The first description of these volcanic rocks was advanced by Garcia (1967) who defined the Augusta Victoria Formation. Garcia (*op. cit.*) ascribed a preliminary "Middle to Late Cretaceous" age to this unit, based on its unconformable position overlying Upper Jurassic and Lower Cretaceous rocks and correlation with volcanic rocks exposed farther south in the Atacama Region. Unfortunately the authors of subsequent regional studies erroneously assumed a Cretaceous age for this unit. Thus different volcanic units were mapped and correlated with the Augusta Victoria Formation, some of them with very different lithology from that described by Garcia (1967). In addition, new formation names were given to equivalent volcanic rocks, even to volcanic strata that have lateral continuity with outcrops in the Augusta Victoria area (e.g., Azabache Formation, Ferraris and Di Biase, 1978). This confusion complicates stratigraphic interpretation of the region, particularly the volcanic history of the region. Field revision, coupled with radiometric dating, has allowed this author to recognize this important Late Cretaceous - Early Tertiary volcanic event.

The lithologic characteristics of the volcanic sequence show that it is the result of subaerial volcanism developed on a continental margin (Maksaev, 1978, Montaño, 1978). The existence of

ignimbrites suggests that calderas were associated with this volcanism. Calderas have been recently identified in the area of the mining districts of Cachinal de la Sierra (Ag) and El Guanaco (Au) (Puig and others, 1987; 1988).

The petrochemical characteristics of the volcanic rocks indicate their calk-alkaline to high-K calc-alkaline affinity, and compare well to volcanic rocks of magmatic arcs developed on active continental margins (see Section 7.2.7; also Herrmann and Zeil, 1989).

Many alteration zones are associated with this volcanic unit. The volcanic rocks in these zones are bleached and strongly silicified-argillized. This hydrothermal alteration seems to be related to paleo-geothermal fields. Important gold and silver deposits (epithermal veins) and small veins hosting copper and lead-zinc are associated with some of the alteration zones (see Section 3.2.5).

### 2.10.2 Upper Cretaceous-Eocene intrusive rocks

Intrusive rocks of Upper Cretaceous to Eocene age occur as stocks that outcrop along the Domeyko Cordillera and the Intermediate Depression in a discontinuous belt that coincides with the previously described volcanic rocks (Fig. 2.6). These stocks intrude Jurassic, Lower Cretaceous, and Upper Cretaceous sedimentary and volcanic units and are covered by Oligocene and Miocene sedimentary rocks. Some stocks are also emplaced within coeval volcanic rocks. The intrusive rocks have a wide compositional range, including diorites, tonalites, monzodiorites, granodiorites, granites, syenites, monzonites, gabbros, and their porphyritic varieties. Commonly they are medium to fine-grained rocks and their mafic components are hornblende, biotite, and locally pyroxene (augite). The accessory minerals are usually apatite, sphene, opaque minerals (magnetite), and zircon. The rocks are usually fresh, but

alteration zones (argillization, sericitization, and silicification) are associated with some Paleocene porphyries as well as copper mineralization (porphyry copper deposits, breccia pipes) and silver-bearing veins. The contacts between different igneous lithologies are either gradational or sharp suggesting multiple pulses of intrusion.

These stocks are ascribed to the Late Cretaceous to Eocene based on their contact relationships and radiometric dates ranging between 79 and 44 Ma (Appendix 2). According to the petrochemical data of Rogers (1985), the stocks of the northern part of the region are calk-alkaline and their magmas appear to have a subcrustal origin.

### 2.10.3 Upper Cretaceous to Lower Tertiary sedimentary rocks

Upper Cretaceous to Lower Tertiary sedimentary rocks occur in the easternmost portion of the Domeyko Cordillera and in the Main Andean Cordillera with minor outcrops in the Altiplano (Fig. 2.6). This sedimentary sequence unconformably overlies Upper Carboniferous to Middle Triassic volcanic and sedimentary rocks, and conformably underlies Palaeogene volcanic rocks. It is represented by following formations: Tolar (Maksaev, 1978), Aiquina (Dingman, 1963), Purilactis (Marinovic and Lahsen, 1984), Pampa de los Burros (Raczynski, 1963), Lomas Negras (Lahsen, 1969), Siglia (Hoffstetter and others, 1957), and Chojfias (Marinovic, 1979), as well as the Quebrada Blanca de Poquis and Quepe Strata (Gardeweg and Ramirez, 1985; Ramirez and Gardeweg, 1982).

The maximum thickness of this sequence is 3,900 m in the Cerros de Purilactis area. It is composed of sandstones, conglomerates, and mudstones. These strata have intercalations of gypsum, salt (halite), calcareous sandstones, and andesitic lavas and tuffs. The conglomerates and sandstones are poorly sorted and polymictic. Some conglomerate clasts include Jurassic and Lower Cretaceous marine fossils (Ramirez and

Gardeweg, 1982; Marinovic and Lahsen, 1984). These sedimentary rocks are reddish-brown and show primary sedimentary structures, such as cross-bedding, desiccation cracks, and rain imprints.

The rocks that outcrop on the Altiplano (Quebrada Blanca de Poquis Strata) and Main Andean Cordillera (Lomas Negras Formation) unconformably overlie Ordovician sedimentary rocks and unconformably underlie Miocene volcanic rocks. They constitute a well stratified sequence 500 m thick, composed of alternating red sandstones and conglomerates both with intercalations of marls and limestones. These calcareous rocks contain Upper Cretaceous marine fossils (Marinovic and Lahsen, 1984; Gardeweg and Ramirez, 1985). A few andesitic lavas are also found in this sequence.

The lithologic characteristics indicate that this sequence was deposited in a terrestrial alluvial and lacustrine environments with clastic materials derived from the west and northwest (Marinovic and Lahsen, 1984). The easternmost outcrops indicate Late Cretaceous marine sedimentation, which correlates with fossiliferous marine sedimentary deposits exposed farther east in Bolivia (Chaunaca and El Molino formations) and Argentina (Lecho and Yacoraite formations) (Marinovic and Lahsen, 1984; Gardeweg and Ramirez, 1985; Salfity and others, 1985; Marquillas and Salfity, 1988).

## 2.11 LATE CRETACEOUS TO EARLY TERTIARY GEOLOGICAL AND PALEOGEOGRAPHIC SYNOPSIS

During the Late Cretaceous, major paleogeographic changes took place in this Andean segment. The active magmatism that persisted during the Jurassic and Early Cretaceous in the Coastal Cordillera ceased at about 100 Ma. A Late Cretaceous tectonic event (Peruvian tectonic event; *cf.* Steinmann, 1929) produced folding and uplift

of the pre-existing stratified units, particularly the Jurassic and Lower Cretaceous sedimentary strata. The Peruvian tectonic event is reflected by a marked unconformity between the Jurassic to Lower Cretaceous strata and the Upper Cretaceous to Lower Tertiary formations. This compressive deformation correlates with increased oceanic spreading rates between Africa and South America at about 100 Ma (Larson and Pitman, 1972) and a contemporaneous change in the pole of rotation of South America with respect to Africa (Dalziel, 1986). According to the latter author these phenomena would have resulted in an increased convergence rate all along the Pacific margin of South America, and thus increased compressive stress at a high angle to the continental margin producing crustal shortening and uplift. Thus the extensional or "neutral" state during the break up of the Gondwana supercontinent appears to have been followed by compression at a high angle to the South American continental margin in the Late Cretaceous. The linear extent of this compression along ca. 7,500 km of the Pacific margin rules out local events as the cause of the compression (Dalziel, 1986).

The Late Cretaceous uplift of the Coastal Cordillera and Intermediate Depression area led to alluvial sedimentation in the easternmost part of the region (east of the Domeyko Cordillera). This terrestrial sedimentation took place within a large basin, which extended farther east in Bolivia and Argentina (Salta Basin; Marquillas and Salfity, 1988). Campanian-Maastrichtian shallow marine sedimentation is recorded into Argentina and Bolivia (Salfity, 1982; Macellari, 1988; Marquillas and Salfity, 1988) and also in the easternmost part of the Antofagasta Region.

The magmatic activity resumed at about 78 Ma (Late Cretaceous) and persisted until the Late Eocene. It took place in the Intermediate Depression and Domeyko Cordillera, which implies an eastward shift of 100 km of the magmatic front relative to the Jurassic-Early Cretaceous front position. The magmatic activity included both subaerial calk-alkaline volcanism (basaltic to rhyolitic) and subvolcanic plutonism resulting in the formation of a volcanic chain with similar setting and

lithology to the currently active Neogene-Quaternary Central Volcanic Zone of the Andes (CVZ; *cf.* Thorpe and others, 1984). This volcano-plutonic belt is interpreted here as a magmatic arc on the continental border, related to the steady subduction of the Farallon oceanic plate under the South American continent.

The Lower Tertiary igneous rocks host the most important silver and gold epithermal deposits of this Andean segment. Sub-economic porphyry copper deposits and copper-bearing breccia pipes are also present (see Section 3.2.5).

## 2.12 LATE EOCENE TO OLIGOCENE

This interval of the geological history of the Antofagasta Region was characterized by diminished magmatic activity, active faulting, and reactivated erosion-sedimentary processes. It was initiated by a compressive deformation event (**Incaic** tectonic event; Maksaev, 1979) that produced major physiographic changes in northern Chile, including the uplift of the Domeyko Cordillera crustal block (Mortimer and Saric, 1975; Maksaev, 1979).

### 2.12.1 Upper Eocene-Early Oligocene intrusive rocks

Upper Eocene-Oligocene stocks are scattered along the Domeyko Cordillera (Fig. 2.7). These stocks are of great metallogenic importance, because some of them have generated the largest porphyry copper deposits of this Andean segment. These stocks are emplaced within Paleozoic, Mesozoic and Lower Tertiary rocks, and are locally covered by Upper Miocene alluvial gravels. They often are composite porphyritic stocks formed by multiple intrusive pulses, and show significant textural and compositional variations. Their dominant lithology is granodioritic,

but rocks of quartz-dioritic, tonalitic, granitic, and monzonitic compositions also occur. The monzonitic-syenitic and granitic facies have been interpreted as products of strong potassic metasomatism (hydrothermal alteration) developed during the cooling of the intrusive bodies (Ambrus, 1979).

The porphyries include phenocrysts of quartz, orthoclase, plagioclase, biotite, and rare hornblende commonly within a felsic aphanitic mesostasis. Strong hydrothermal alteration of potassic, quartz-sericitic, argillic, and propylitic types, as well as disseminated copper sulfides, are typically associated with these intrusive rocks. Often the porphyries are emplaced next to, or within, Upper Eocene biotite-hornblende granodioritic or quartz-dioritic stocks having medium-grained equigranular texture, such as the Fortuna Granodiorite at Chuquicamata and the Southern Granodiorite at El Abra. These are biotite-hornblende granodiorites showing weak potassic and propylitic alteration. The porphyry copper deposits are distributed within the domain of a regional fault system (Domeyko Fault System; see Section 2.16.2).

Many K-Ar and $^{40}Ar$-$^{39}Ar$ radiometric dates of these stocks (see Chapter 4), ranging between 41 Ma (El Salvador) and 31 Ma (Chuquicamata) fix their Late Eocene-Early Oligocene age and show that the major porphyry copper mineralization took place during a discrete interval of geological time (see Chapters 4 and 7).

### 2.12.2 Oligocene-Lower Miocene sedimentary rocks

The Oligocene-Lower Miocene sedimentary rocks are exposed at the eastern and western foothills of the Domeyko Cordillera (Fig. 2.7). They are represented by the following Formations: Sichal (Maksaev, 1978), Tambores (Dingman, 1963), San Pedro (Brüggen, 1942), Quebrada Justo (Lahsen, 1969), and Pampa Mulas (Chong, 1977). The sequence unconformably overlies Paleocene-Eocene volcanic rocks and

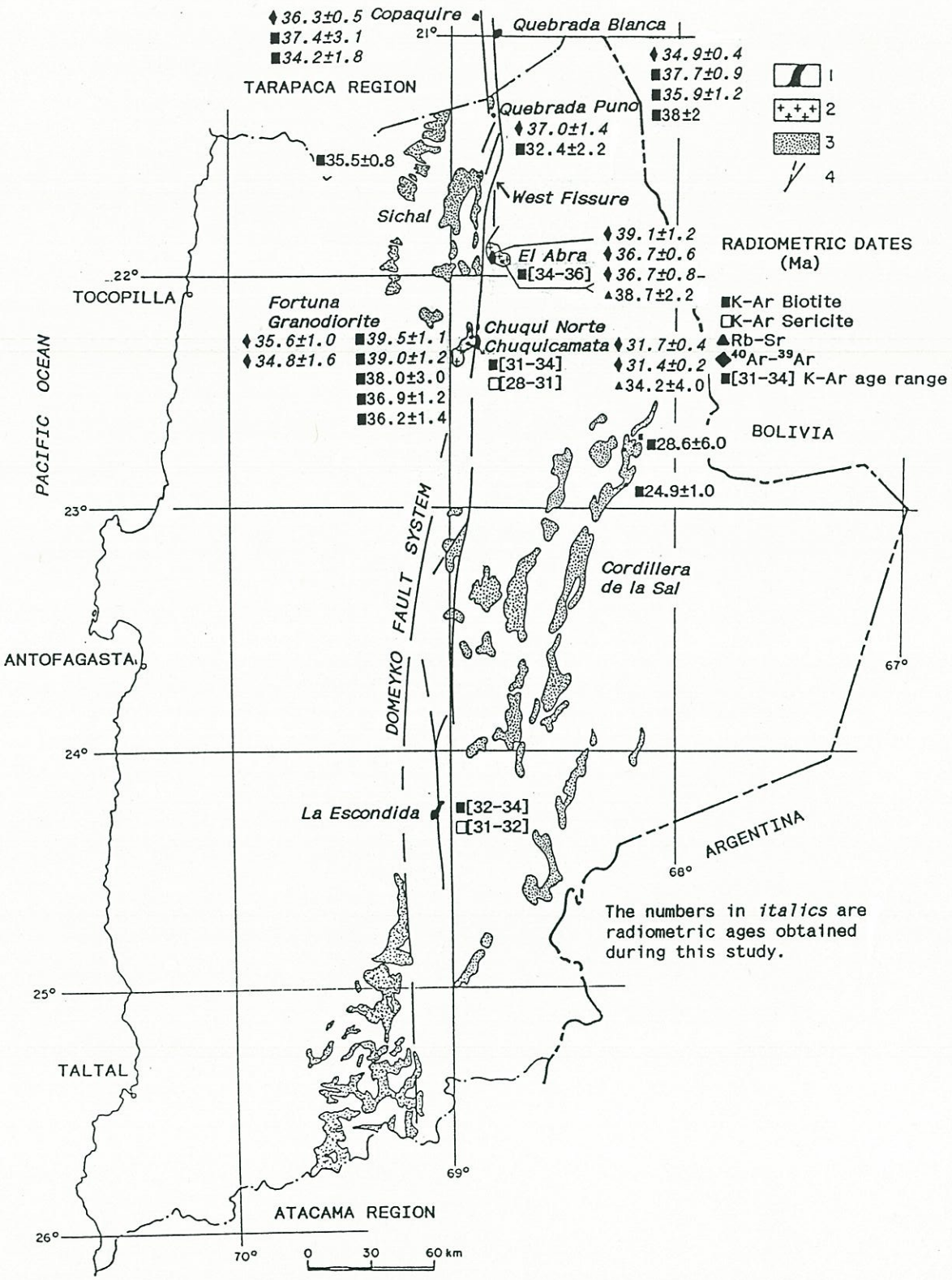


**Figure 2.7.** Distribution of the Upper Eocene - Oligocene rocks. (1) Porphyritic stocks. (2) Upper Eocene - Lower Oligocene granodiorites. (3) Terrestrial sedimentary rocks. (4) Faults of the Domeyko Fault System.

unconformably underlies Middle Miocene volcanic rocks. It is composed of polymictic, brown or reddish-brown conglomerates, breccias, sandstones, and mudstones, as well as scarce intercalations of tuffs. The upper portion of the sequence includes gypsum and halite beds alternating with red mudstones. This unit is variable in thickness with a maximum of 2,100 m exposed in the Cordillera de la Sal area (Ramirez and Gardeweg, 1982; Marinovic and Lahsen, 1984). The sedimentary strata are deformed into folds with north-south to northeast axes, but also occur as sub-horizontal beds in the western foothills of the Domeyko Cordillera. Native copper mineralization occurs within sandstone horizons of the middle portion of the sequence in the San Bartolo area (see Section 3.2.7).

The Oligocene-Early Miocene age of this sedimentary sequence is based on its stratigraphical position and radiometric dates of tuff intercalations ranging from 35.5 to 24 Ma (Appendix 2).

The lithological characteristics of this unit demonstrate an initial terrestrial alluvial sedimentation followed by the deposition of terrestrial evaporites (gypsum, halite), silt, and clays, within ancient salt-flats (Maksaev, 1978; Ramirez and Gardeweg, 1982; Marinovic and Lahsen, 1984; Flint, 1985b). This suggests a progressive climatic desiccation in the region, whose significance for the development of supergene processes and the preservation of mineral deposits has been stressed by Alpers and Brimhall (1988).

## 2.13 LATE EOCENE - OLIGOCENE GEOLOGICAL AND PALEOGEOGRAPHIC SYNOPSIS

This stage of the geologic history of the Antofagasta Region began with compressive deformation (Incaic tectonic event; Maksaev, 1979). This tectonic event was characterized by differential uplift of fault-bounded crustal blocks. The major physiographic units of this Andean segment were established, except for the Altiplano where terres-

trial sedimentation persisted during the Oligocene (Mortimer, 1980; Jordan and Alonso, 1987), implying that its main uplift probably post-dated the Incaic tectonic event. The uplift of the Domeyko Cordillera block produced terrestrial sedimentation bordering the newly created mountains. The widespread volcanic activity of the Paleocene and Eocene virtually ceased. Late Eocene - Oligocene magmatism was limited to the emplacement of subvolcanic stocks along the Domeyko Cordillera. These are primarily of granodioritic composition and represent the last magmatic activity along the Domeyko Cordillera. Major porphyry copper deposits were formed during this last phase of diminished magmatism (see Section 7.2.3).

The Incaic tectonic event correlates with a global plate reorganization that occurred primarily during the Middle and Late Eocene (Rona and Richardson, 1978; Cande and others, 1982; Schwan, 1985; Zonenshayn and others, 1984; 1985). Global plate reconstructions, based on ocean floor paleomagnetic data, show that during the Late Eocene - Oligocene a northwest-southeast-trending spreading ridge between the Farallon and Pacific oceanic plates was active (Mammerickx and others, 1980). Consequently a northeast-directed oblique subduction of the Farallon plate under the western border of the South American continent prevailed (Pilger, 1983, 1984; Cande, 1983; Cande and Leslie, 1986; Pardo-Casas and Molnar, 1987). Maximum convergence rates of 12 cm/yr were achieved between anomaly 18 and 13 (ca. 42 to 36 Ma) (Cande, 1983). A regional trench-linked strike-slip fault system was formed along the magmatic arc during this period of fast oblique convergence (Domeyko Fault System; see Section 2.16.2).

## 2.14 MIOCENE TO HOLOCENE

The last interval of the geologic history of the Antofagasta Region began with a compressive tectonic event (Quechua tectonic event; Maksaev, 1979), which was followed by the development of a volcanic chain along the Main Andean Cordillera and western section of the Altiplano. This implies a new, eastward shift of the magmatic front of 100 to more than 150 km. Extremely arid climate has prevailed since the Middle Miocene in this Andean segment resulting in minimal erosion rates. Extensive alluvial piedmont deposits were laid down at the foothills of the mountains, giving rise to the present-day plains ("Pampas") within the Intermediate Depression and Intermontane Basins. Extensive salar were formed within the lower sections of basins with internal drainage.

### 2.14.1 Miocene-Holocene volcanic rocks

The youngest volcanic rocks of the area are limited to the easternmost part of the Antofagasta Region (Fig. 2.8), but their outcrops extend farther east into Bolivia and Argentina. These volcanic rocks are part of the Central Volcanic Zone of the Andes (CVZ; *cf.* Thorpe and others, 1984). Many strato-volcanoes, of andesitic, dacitic, and subordinate rhyolitic or minor basaltic composition, whose lavas are interstratified with dacitic and rhyolitic ignimbrites, form an elevated volcanic chain over a pre-Miocene basement. Subordinate dacitic and rhyolitic domes and basaltic pyroclastic cones also occur. The ignimbrites spread laterally to great distances from the volcanic chain covering extensive areas on the western foothills of the High Andes and also far eastward into Argentina and Bolivia.

Pyroxene and hornblende andesites (usually porphyritic) are the dominant andesite types. They compose "aa" type and blocky lava

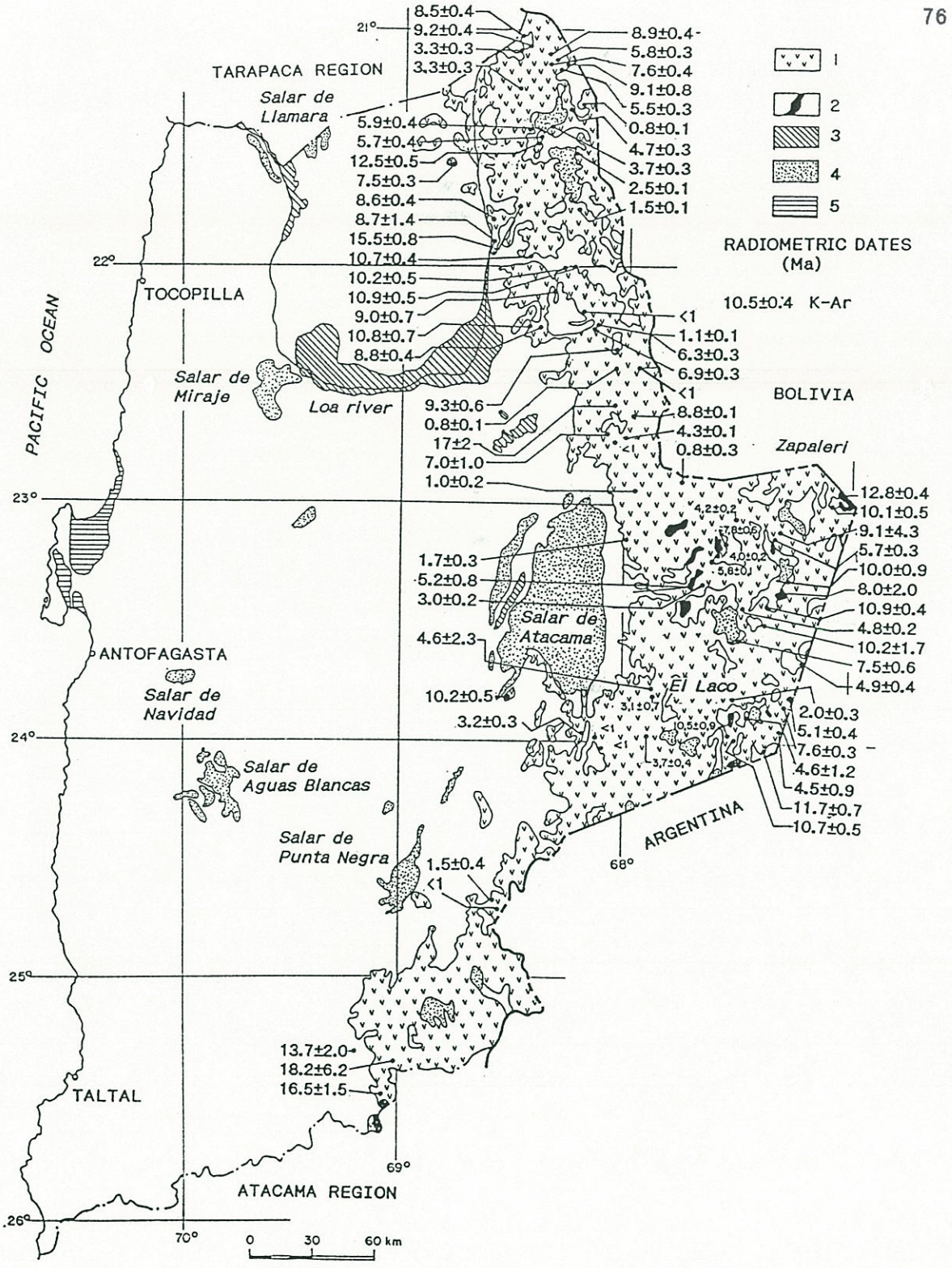


**Figure 2.8.** Distribution of Miocene to Holocene deposits (except for alluvium). (1) Volcanics. (2) Subvolcanic intrusives. (3) Lacustrine deposits. (4) Salt flats. (5) Miocene-Pliocene marine sedimentary rocks.

flows, up to 100 m thick in strato-volcanoes and more rarely in lava domes. The dacites, usually containing hornblende and biotite, form short, lobate lava flows, up to 250 m thick, either in strato-volcanoes or lava domes. The basalts (with pyroxene and olivine) form "aa" type and blocky lavas. Porphyritic or vitrophyric rhyolites are associated with lava domes. The ignimbrites form extensive plateaus, with 2° to 5° slopes, among the strato-volcanoes and extending to the foothills of the volcanic chain. These pyroclastic flow deposits occur either as individual beds from 2 to 50 m thick or as series of strata up to 150 m in thickness. They fill old creeks and depressions, as well as abutting the flanks of older features of positive relief. The dacitic and rhyolitic ignimbrites have various degrees of welding, and include phenocrysts and pumice fragments in a dominantly vitreous matrix. The ignimbrites were generated by explosive volcanism, thought to be related to collapse calderas, such as the 1.5 Ma, 25 km diameter Cerro Purico Caldera (Baker, 1981; Hawkesworth and others, 1982) and the 4.5 Ma, 35 by 60 km La Pacana Caldera (Gardeweg and Ramirez, 1987).

Many strato-volcanoes, particularly where partially eroded, show solfataric alteration zones produced by fumarolic, solfataric, and geothermal activity related to eruptive processes. Solfataras are still active in some volcanoes (e.g., Ollagüe, Putana, Lascar, Lastarria). Many sulphur deposits are associated with the alteration zones and solfataras (see Section 3.7.3). Unusual lava flows and subvolcanic bodies of massive magnetite occur at El Laco volcano (Park, 1961; Ruiz and others, 1965; Henriquez and Martin, 1978; Gardeweg and Ramirez, 1985).

A great number of radiometric dates are available in the literature for these volcanic rocks (Appendix 2). They range from 18.2 to less than 1 Ma for the strato-volcanoes, and from 24 to less than 1 Ma for the ignimbrites. The older ignimbrites (24 to 18 Ma) are restricted to the southern part of the area, where they are intercalated within Miocene

alluvial sediments west of the main volcanic chain (Naranjo and Puig, 1984; Gardeweg, personal communication). In the segment between latitudes 21°00' and 24°30' S, the onset of volcanism seems to have occurred at about 15 Ma.

Diverse petrochemical studies have shown the calc-alkaline nature of these volcanic rocks, and they commonly are considered to be typical volcanic rocks of active continental margins (Thorpe and others, 1982, 1984; Ramirez and Gardeweg, 1982, Marinovic and Lahsen, 1984; Gardeweg and Ramirez, 1985). Owing to the progressive eastward increase in $K_2O$ in the easternmost part of the area (Zapaleri and Nevados de Poquis area) the volcanic rocks have shoshonitic affinities (Munizaga and Marinovic, 1979) typical of the Cenozoic volcanic rocks of Bolivia that crop out farther east (Deruelle, 1982).

### 2.14.2 Miocene-Pliocene subvolcanic intrusive rocks

Some small porphyritic stocks of rhyolitic, dacitic andesitic, and monzonitic composition occur in the High Andean Cordillera and Altiplano (Fig. 2.8). The stocks intrude Miocene lavas and underlie Pliocene and Quaternary volcanic rocks (Gardeweg and Ramirez, 1985). Their mineralogy commonly includes quartz, plagioclase, biotite, hornblende, and pyroxene phenocrysts in a felsic or vitreous mesostasis. Their radiometric dates range from 12.8 to 4.8 Ma (Appendix 2).

The stocks represent the subvolcanic roots of Miocene-Pliocene strato-volcanoes that have been exposed by erosion, landslides, or explosive volcanic eruptions. The petrochemistry of these intrusive rocks is similar to the coeval volcanic rocks. They are mostly calc-alkaline rocks, whereas the easternmost stocks are shoshonitic (Poquis

area, Gardeweg and Ramirez, 1984; Munizaga and Marinovic, 1979). Small veins bearing silver, antimony and iron are related to these porphyries.

### 2.14.3 Miocene-Pliocene marine sedimentary rocks

This sedimentary unit is restricted to the Mejillones Peninsula and coastal terraces to the north (Fig. 2.8) and is represented by La Portada and Mejillones Formations (Ferraris and Di Biase, 1978). This 420 m thick marine sedimentary sequence unconformably overlies Paleozoic and Mesozoic rocks and its top coincides with the present erosion surface. Lithologies include sandstones, calcareous sandstones, coquina beds, limestones, gypsum, mudstones, scarce conglomerates, and lenticular beds of phosphorite. These sub-horizontal strata contain abundant marine fossils. This sequence represents marine littoral sedimentation and the fossils are of Miocene-Pliocene age (Ferraris and Di Biase, 1978; Valdebenito, 1979; Martinez, 1978).

### 2.14.4 Miocene-Pleistocene lacustrine sedimentary rocks

Lacustrine sedimentary deposits occur mainly along the course of the Loa River and in the Cordillera de la Sal area; minor occurrences are scattered throughout the Antofagasta Region (Fig. 2.8). These deposits southeast of the Salar de Atacama unconformably overlie Oligocene sedimentary rocks. They include the following formations: El Loa (Fuenzalida in Hoffstetter and others, 1957), Chiu-Chiu (Naranjo and Paskoff, 1981), El Campamento (Brüggen, 1942), Vilama, El Tambo (Moraga and others, 1974), and Pampa Margarita Strata (Naranjo and Puig, 1984).

The lithology of these deposits is heterogeneous, including partially consolidated, lenticular sandstones, mudstones, conglomerates, breccias, calcareous sandstones, marls, limestones, gypsum,

diatomites, travertine, chert, and intercalations of tuffs and volcanic ash. The upper part of the sequence is composed of unconsolidated materials (gravels, sand, silt and clay). The sequence is well stratified in lenticular beds up to 20 m thick and includes many fresh and salt water fossils (Wetzel, 1927; Courty, 1907; Frenguelli in Hoffstetter and others, 1957; Marinovic and Lahsen, 1984; Moraga and others, 1974; Naranjo and Puig, 1984). The maximum thickness of these deposits is 150 m south of Calama city (Naranjo and Paskoff, 1981). These sediments are usually sub-horizontal, but within the Calama basin, gravitational domes and centroclines have been described (Naranjo and Paskoff, 1981) and in the Cordillera de la Sal area (western section of the Salar de Atacama salt-flat) they show *en echelon* open folds with northeast-trending axes.

The deposits along the Loa River have been ascribed to the Late Miocene-Pleistocene because of their fossils and intercalations of tuffs with radiometric ages ranging from 8.9 to 5.6 Ma (Marinovic and Lahsen, 1984). The rest of these deposits are ascribed to the Pliocene-Pleistocene based on their stratigraphic position. The lithology and fossil content of these units indicate a sedimentation within shallow lakes of variable salinity. Intercalations of pyroclastic materials are from the synchronous volcanic activity in the Neogene volcanic chain of the easternmost part of the Antofagasta Region.

### 2.14.5 Miocene-Holocene unconsolidated sediments

Diverse accumulations of unconsolidated detrital sediments, mainly of mudflow and alluvial origin, and subordinate colluvial, eolian, glacial, and laharic derivation cover more than one third of the surface of the Antofagasta Region. These sediments unconformably overlie Palaeogene sedimentary, volcanic, and intrusive rocks, and either overlie or interdigitate with Miocene-Quaternary volcanic rocks or lacustrine sediments.

The mudflow, alluvial, and colluvial sediments that occur within the Intermediate Depression and Intermontane Basins are composed of a heterogeneous mixture of polymictic gravels, sands, silts, and clays. Intercalations of fine volcanic ash are often present. These sediments are poorly sorted, have been deposited mainly by mudflows, and constitute extensive alluvial plains and piedmont slopes. The older deposits have some degree of coherence and form terraces or plateaus, which are dissected by the present-day creeks. The deposits of the Intermediate Depression are locally cemented by salts (nitrates, halite, sulphates, and subordinate borates). They constitute important sodic nitrate deposits ("caliche") that have been exploited with grades of 8-15% $NaNO_3$. A description and discussion of their origin has been presented by Ericksen (1981, 1983). In Chuquicamata and El Tesoro areas, alluvial gravels are cemented by copper oxides, forming important exotic copper-ore bodies (see Section 3.2.7).

Most of the unconsolidated sediments of the Antofagasta Region have been traditionally regarded as Quaternary, but recent dating of intercalations of volcanic ash has yielded ages ranging from 19 to 2.9 Ma (Appendix 2) indicating that their accumulation began at least in the Miocene.

The rest of the unconsolidated deposits have a more restricted distribution. Eolian dunes are rare, but some occur in the vicinity of the Salar de Atacama and locally in the Coastal Cordillera. Glacial and laharic deposits are restricted to the volcanic chain of the High Andean Cordillera.

### 2.14.6 Pliocene-Holocene salt deposits

Salt deposits occur within several salars located within the Intermontane Basins, Altiplano and Intermediate Depression (Fig. 2.8). They overlie or interdigitate with Miocene-Quaternary volcanic rocks and

alluvial or lacustrine sediments (Vila, 1974; Skarmeta and Marinovic, 1981; Gardeweg, personal communication).

The salars are composed of salt crusts of chlorides, sulphates, carbonates, and nitrates (Vila, 1974; Stoertz and Ericksen, 1974). These saline crusts have variable areal extent and thickness. The largest is the Salar de Atacama, which has salt deposits, 60 m thick, covering a surface of 3,200 $km^2$ (Ramirez and Gardeweg, 1982).

The salars formed within basins with internal drainage because of the high evaporation prevailing in this extremely arid region (Stoertz and Ericksen, 1974). The persistence of a hyper-arid climate since the Middle Miocene (Alpers and Brimhall, 1988) contributed to their development and preservation.

The salt deposits were traditionally regarded as Quaternary. However, the basins existed since the Late Miocene so their accumulation probably followed the Middle Miocene desiccation recognized by Alpers and Brimhall (1988) in this Andean segment. Detailed information about the composition, structure, and origin of the salars can be found in the studies of Vila (1974) and Stoertz and Ericksen (1974).

## 2.15 MIOCENE TO HOLOCENE GEOLOGICAL AND PALEOGEOGRAPHIC SYNOPSIS

During the Middle to Late Miocene a compressive tectonism occurred (**Quechua** tectonic event; Maksaev, 1979). It was accompanied by thrust faulting along the Domeyko Cordillera and High Andes. This tectonic event correlates with a major reorganization and reorientation of the spreading system in the East Pacific ocean. This was due to the gradual extinction of the Oligocene northwest-southeast trending spreading ridge in the Pacific oceanic floor, and the subsequent development of a new north-northeast-trending spreading ridge. At the

same time the ancient Farallon plate fragmented into the Cocos and Nazca oceanic plates (Mammerickx and others, 1980; Pilger, 1983; Whitman and others, 1983). The northeast-directed oblique convergence that persisted during the Oligocene changed to straight east-west subduction in Miocene times. Maximum convergence rates of 12 cm/yr were achieved between anomaly 8 and 3 (ca. 26 to 4 Ma) (Cande, 1983).

The magmatic front shifted eastward from 100 to more than 150 km following the Quechua tectonic event and a volcanic chain was formed along the High Andes and western section of the Altiplano. This volcanic chain is part of the active Central Volcanic Zone of the Andes (CVZ; *cf.* Thorpe and others, 1984).

Sedimentary processes were limited to the deposition of alluvial piedmont, lacustrine sediments, accumulation of salt crusts, and shallow marine sedimentation on coastal terraces. The limited extent of sedimentation was the result of minimal denudation attributable to the prevalence of a hyper-arid climate since the Middle Miocene (Alpers and Brimhall, 1988), coupled with the barrier effect of the Coastal and Domeyko Cordilleras, which isolated the regional drainage from marine baselevel (Mortimer, 1980; Abele, 1988, 1989). The virtual lack of erosion allowed the preservation of surficial rock units, supergene enrichment blankets, epizonal porphyry copper deposits, and silver and gold epithermal deposits.

## 2.16 MAJOR REGIONAL STRUCTURES

The most important structural features of the Antofagasta Region are the Atacama Fault System and the Domeyko Fault System. Varying degrees of deformation affect the rocks of the area due to the several tectonic events described in the preceding sections. Only the

largest structures relevant to the metallogenic evolution are discussed here.

### 2.16.1 Atacama Fault System

The Atacama Fault System is composed of a main trace and many north-south trending vertical or sub-vertical faults, as well as branches trending either to the north-northeast or north-northwest, which are exposed mainly in a belt about 12 km wide along the Coastal Cordillera (Fig. 2.9). Near the faults, but not coincident with their present traces, are rocks displaying the effects of ductile dynamic deformation, such as mylonitic gneisses and mylonites. The foliation is the result of preferred orientation (and bending) of feldspar and recrystallization of biotite, amphibole, and quartz into preferred orientation in the rocks. The protoliths are dominantly Jurassic intrusive rocks and subordinate Jurassic volcanic rocks (Arabasz, 1971; Uribe and Niemeyer, 1984; Scheuber and Andriessen, 1990). Elongate bodies of Lower Cretaceous intrusive rocks occur parallel to the faults either along or near their traces. These intrusive rocks show marked foliation and mylonitization in shear zones adjacent to the faults (Herve and Marinovic, 1988, 1989). The shear zones, and horizontal to sub-horizontal slickensides within the fault planes suggest important sinistral strike-slip motion (Arabasz, 1971; Scheuber and Andriessen, 1990).

In most of the Antofagasta Region the trace of the Atacama Fault outcrops within intrusive or volcanic Jurassic rocks but locally the fault juxtaposes Jurassic lavas with Devonian sedimentary rocks. Devonian rocks occur on either side of the fault suggesting opposing senses of vertical displacements in different sections along the fault.

The Atacama Fault system of northern Chile (Fig. 2.9) has been long recognized as a major structural feature of the Circum-

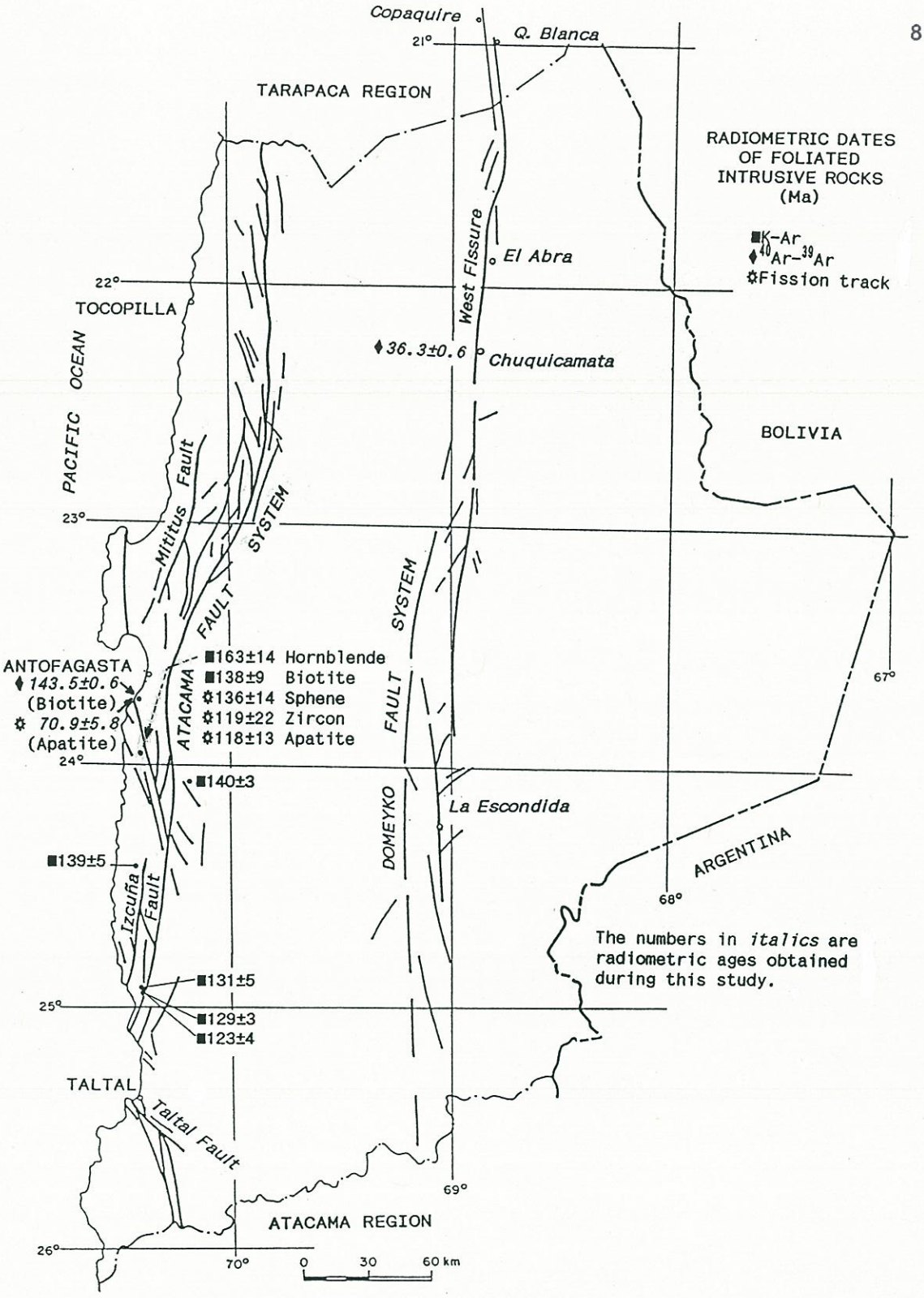


**Figure 2.9.** Major regional fault systems of the Antofagasta Region and radiometric dates of foliated intrusive rocks.

Pacific Region. It was initially considered to be analogous to regional transcurrent faults such as the San Andreas Fault of California and the Alpine Fault of New Zealand (St. Amand and Allen, 1960; Allen 1962, 1965; Arabasz, 1968, 1971; Arabasz and Allen, 1972; Ulriksen, 1979). The fault system extends along the Coastal Cordillera between latitudes 20° and 29° S, being about 110 km east from, and parallel to, the Chile-Peru oceanic trench. Recently it has been classified as a trench-linked strike-slip fault (Woodcock, 1986; Sylvester, 1988; Scheuber and Andriessen, 1990). Trench-linked strike-slip faults accommodate only a component of the total displacement at convergent plate boundaries, whereas "boundary transform" faults like the San Andreas and Alpine Faults accommodate total horizontal displacements between plates (Woodcock, 1986; Sylvester, 1988). Boundary transform faults are active longer and have larger displacements than trench-linked faults.

Minor veins hosting copper, silver, and gold occur along the Atacama Fault System south of Taltal (Taltal, La Isla, and Sierra del Pingo districts). These deposits are especially numerous farther south in the Atacama Region where they are accompanied by iron deposits associated with the fault zone (Diaz and others, 1981; Colley and others, 1989; Diaz in preparation). Within the Antofagasta Region, the Atacama Fault System is largely devoid of significant metallic mineralization. However, since it constitutes the eastern limit of the block that contains most of the mineral deposits of the Coastal Cordillera (Fig. 3.4) this fault system does exert a control on the regional mineral distribution of this Andean segment.

### 2.16.2 Evolution of the Atacama Fault System

Recrystallized biotite from a foliated gabbro at Cerro Coloso (south of the port of Antofagasta port; Fig. 2.9) has given a well defined $^{40}Ar$-$^{39}Ar$ age plateau at 143.5 ± 0.6 Ma (see Chapter 4). Comparable gabbros in the southern tip of the Mejillones peninsula (26 km NNW of

Cerro Coloso) have yielded zircon U-Pb ages of 196 ± 4 and 196 ± 6 Ma (Damm and others, 1986) and a whole rock Rb-Sr isochron of 200 ± 10 Ma (Diaz and others, 1985). Thus the 143.5 ± 0.6 Ma $^{40}Ar$-$^{39}Ar$ plateau age on recrystallized biotite most probably represents a stage of mylonitic ductile deformation of the gabbro. The latter date agrees with the whole rock K-Ar age of 139 ± 5 Ma obtained by Herve (1987a) for a mylonite north of Paposo (25°S). Herve (*op. cit.*) has shown a 34 km sinistral strike-slip displacement of the fault system from 144 to 131 Ma ago, based on the distribution of a faulted Lower Cretaceous pluton and K-Ar dates of foliated and non-foliated intrusive rocks. Scheuber and Andriessen (1990) report new radiometric dates on a foliated gabbro 15 km south of Cerro Coloso: recrystallized hornblende yielded a K-Ar age of 163 ± 14 Ma, and recrystallized biotite produced a K-Ar age of 138 ± 9 Ma. Fission track ages reported were of: sphene 136 ± 14 Ma, zircon 119 ± 22 Ma, and apatite 118 ± 13 Ma. These authors interpreted the K-Ar age of recrystallized amphibole to represent Jurassic ductile shear strain and based on the mineral assemblage estimated amphibolite facies conditions during deformation (pressure <3 Kb, temperature about 500°C). The biotite K-Ar age was interpreted in terms of subsequent Early Cretaceous shear. According to Scheuber and Andriessen (*op. cit.*) the mineral assemblage in the Early Cretaceous foliated intrusive rocks indicates ductile deformation under greenschist facies conditions. The concordance, within error limits, of the fission track ages with the biotite K-Ar date was interpreted as the effect of rapid Early Cretaceous cooling, implying that uplift of the Coastal block took place mainly during the latest Jurassic and the Early Cretaceous.

The development of the Atacama Fault System has been attributed to a period of oblique plate convergence during the Early Cretaceous (Naranjo and others, 1984; Herve, 1987a). Alternatively, Scheuber and Andriessen (1990) inferred Late Jurassic to Early Cretaceous oblique convergence.

Previous studies based on stratigraphic analyses (Arabasz, 1971; Ulriksen, 1979) suggested several thousand metres of

upthrow of the eastern block of the Atacama Fault at the latitude of Taltal (25°30' S). Ulriksen (1979) argued that this hypothetical vertical displacement took place in pre-Early Cretaceous times, based on the absence of about 5,000 m of Jurassic and Triassic strata on the eastern block of the fault in the Taltal area, and the deposition of the Lower Cretaceous sediments directly onto Paleozoic basement. This interpretation assumes that the Jurassic and Triassic sediments were previously deposited there, which may not be the case. Recently, Colley and others (1989) indicated instead that the Atacama fault zone has an overall downthrow to the east in the segment between latitudes 26° and 27° S. These authors suggest that the dominant displacement along the major fault traces parallels prominent downdip stretching lineations. On the other hand, farther north in the Coastal Cordillera (latitude 23°45' S.; south of the Antofagasta port) the deposition of marine sediments with Hauterivian-Barremian marine fossils (El Way Formation; Garcia, 1967) overlying Lower Cretaceous terrestrial red beds (Caleta Coloso Formation; Garcia, 1967) immediately west of the Atacama fault zone could be interpreted in terms of downthrow of the western block of the Atacama Fault during the Early Cretaceous. However, a closer look reveals that the latter sedimentary deposits may have filled a rhombic (10 by 15 km) pull-apart basin related to the left-lateral displacement of the fault system (Salar del Carmen and Coloso faults; Fig. 2.10). Local subsidence during the Early Cretaceous cannot be extrapolated to the rest of the Coastal Cordillera. One critical factor that should be considered when analyzing regional vertical displacements along strike-slip faults is that when several scarps are present within a strike-slip fault zone they typically have opposite senses of vertical displacements ("scissors" geometry) resulting from topographic irregularities or because of the variable oblique displacements on the faults themselves (Sylvester, 1988). Strike-slip faults may (and usually do) display reversals of the direction of throw along their traces, particularly along discontinuous segments (Segall and Pollard, 1980). Relatively uplifted blocks may subsequently slide by gravity or be thrust onto adjacent down-dropped blocks (Sylvester *op. cit.*), therefore vertical displacements inferred solely from the stratigraphic record of restricted areas may have no regional signifi-

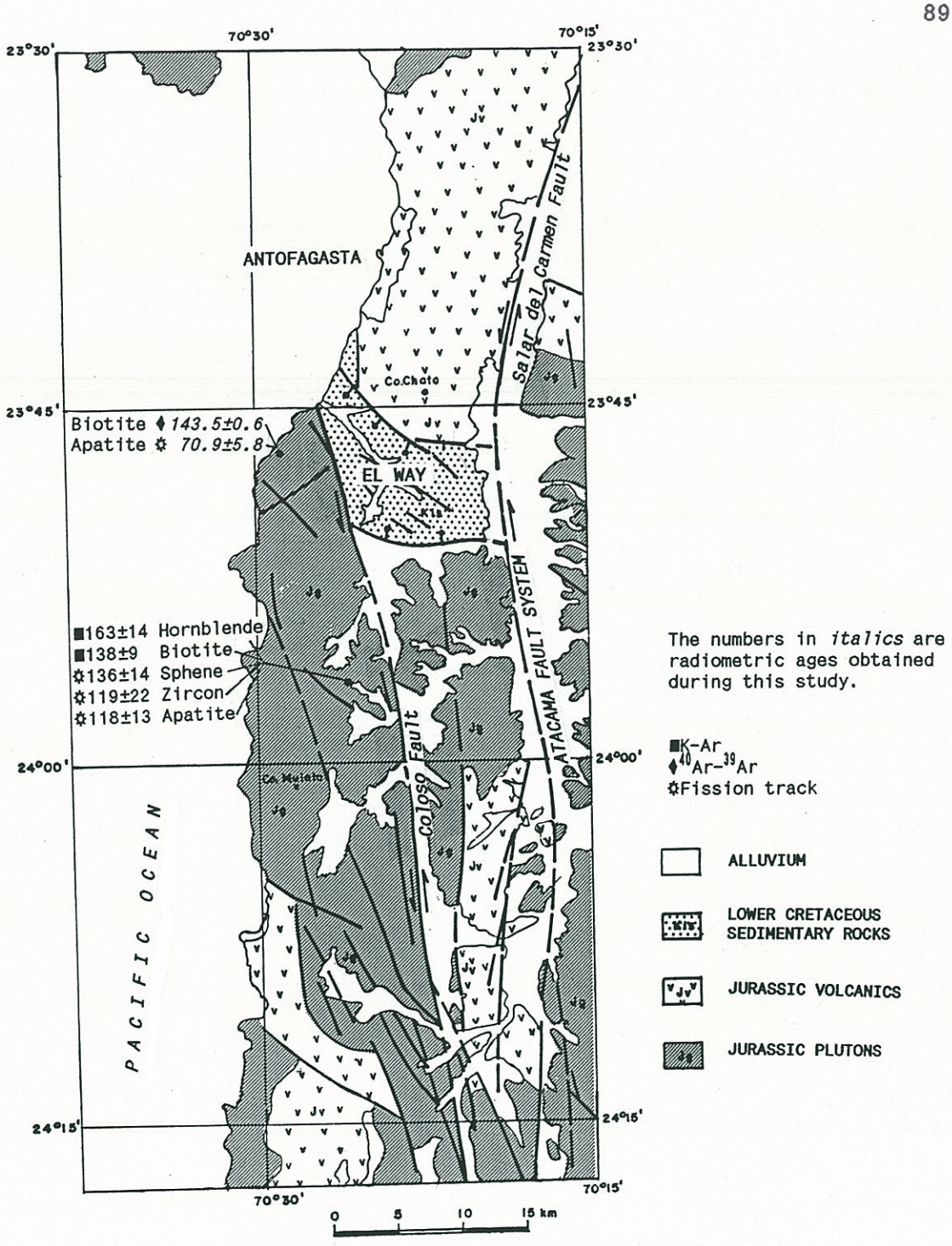


**Figure 2.10.** Lower Cretaceous pull-apart basin of El Way in the Coastal Cordillera area, formed during sinistral strike-slip displacements of the Atacama Fault System. Geology modified after Ferraris and Di Biase (1978).

cance. The same effect on the stratigraphy may be produced by local accommodation of individual blocks, or by the relative horizontal displacement of ancient topographic heights along the fault, without significant vertical displacement of the fault. This does not rules out possible early vertical displacements along the Atacama Fault, particularly on local sections, but rather shows that despite conclusions based on stratigraphic data of previous authors, there is no conclusive evidence for an overall relative vertical displacement of thousands metres between the blocks bounded by this strike-slip structure.

A Miocene vertical displacement across the Atacama Fault System, a 300 m upthrow of the western block, has been documented from geomorphological analysis and K-Ar dating of tuffs (Herve, 1987). This late displacement defines the present-day trace of the faults. The occurrence of undisturbed Late Miocene to Pleistocene sediments (El Loa Formation) overlying the fault in the northern section of the Antofagasta Region shows that all the significant displacements of the Atacama Fault occurred before the Late Miocene (Maksaev and Marinovic, 1980), which has been corroborated by the geomorphological analyses of Herve (1987) and Naranjo (1987). Between latitudes 23° and 24° S, the Salar del Carmen Fault shows a 3 m-high scarp within Miocene to Quaternary gravels (upthrow of the western side and minor left-lateral displacement (Armijo and Thiele, 1990) these minor neotectonic movements may have little to do with the original displacement of the fault system.

### 2.16.3 Domeyko Fault System

The Domeyko Fault System is composed of a series of faults that bound uplifted crustal blocks along the Domeyko Cordillera between latitudes 21°00' and 26°30' S (Fig. 2.9). The fault system includes the renowned West Fissure of Chuquicamata (Taylor, 1935; Perry, 1952; Sillitoe, 1973; Alvarez and others, 1980), the less known Cerro Castillo Fault located east of the El Salvador porphyry copper (Tobar,

1977, Perello and Müller, 1984), and the Sulfato fault at Copaquire (Hollister and Bernstein, 1975). The faults trend N5°E, are steeply-dipping or vertical and Paleozoic basement outcrops east of the main faults indicate upthrow of the eastern block, even though the opposite case also occurs locally (e.g., Cordon del Millo; Maksaev, 1978). The relative displacement (either horizontal or vertical) probably attains several thousand metres based on the local juxtaposition of Upper Paleozoic rocks with Lower Tertiary volcanic rocks along faults belonging to this system (e.g., the area of Pampa Augusta Victoria and Pampa Loreto; 24°00' to 24°30' S). The faults displace Lower Tertiary volcanic rocks (e.g. 59 ± 1 and 42.1 ± 1.5 Ma K-Ar ages; Table 4.1) clearly indicating Tertiary activity of the faults. Displacement along the Domeyko Fault System associated with the **Incaic** tectonic event (Late Eocene) has been established by K-Ar dates and the analysis of erosion-sedimentation features (Maksaev, 1979). The Domeyko Fault System accommodated the uplift of the Domeyko Cordillera crustal block at that time (see Section 2.17). Brecciated sections and zones of hydrothermal alteration occur along faults of this system (e.g., Punta Colorada alteration zone; Maksaev, 1978, and NW of El Abra alteration zone; Ambrus, 1977). In addition, many minor intrusive bodies of dioritic to monzonitic composition outcrop along the fault zone. Therefore past magmatic and thermal activity along these regional structures is apparent. The major porphyry copper deposits of the Antofagasta Region also occur within the domain of this regional fault system (e.g., Quebrada Blanca, Copaquire, El Abra, Chuquicamata, La Escondida; Fig. 3.7).

### 2.16.4 Evolution of the Domeyko Fault System

The Domeyko Fault System probably has a protracted history of strike-slip and/or vertical displacements amounting to thousands of metres. However, precise magnitudes are still to be determined. At Chuquicamata, close to the West Fissure there are (N10°E/vertical) shear zones, multiple fractures, and other textural

evidence for ductile deformation of both the Fortuna Granodiorite and the Chuquicamata mineralized porphyry. The fracture pattern (Fig. 7.24) is compatible with dextral shear as suggested by Lopez (1939, 1942; also Hollister,1978; Sibson, 1987). A dextral strike-slip fault (Sulfato Fault), parallel to the West Fissure, was also recognized by Hollister and Bernstein at Copaquire (120 km north of Chuquicamata), where the mineralization developed along the fault. The $^{40}Ar$-$^{39}Ar$ and K-Ar dating on biotite from igneous rocks affected by shear strain indicates that the strike-slip fault was active at least between 36 to 31 Ma ago (see Section 4.3.1).

Upper Paleozoic basement rocks exposed on the eastern block of the West Fissure suggest that the main vertical displacement of this fault was the upthrow of the eastern block, during the uplift of the Domeyko Cordillera in the Mid-Late Eocene. However, the West Fissure constitutes the abrupt western limit of the Oligocene Chuquicamata porphyry copper (Perry, 1952; Sillitoe, 1973), and the local geology suggests a post-intrusion upthrow of the western block. This is attributed to a late reactivation of the fault, probably during the Miocene Quechua compression.

The West Fissure is covered by Upper Miocene ignimbrites between Quebrada Blanca and El Abra, and even though the trace of the fault is clearly visible within these pyroclastic deposits there is no significant displacement of them. Thus the fault has been inactive at least since the Late Miocene. The above inferred displacements and ages of the West Fissure are compatible with the statement of Perry (1952) that "the West Fissure was an early, pre-porphyry structure along which profound, primary crustal adjustment occurred. The evidence is strong for believing that it controlled emplacement of the porphyry, quartz and sulfides, ending its activity in final relief of stresses after close of the mineralizing epoch."

Some authors have claimed a left-lateral strike-slip displacement for the West Fissure (Ambrus, 1979; Hunt and others, 1983; Baker and Gilbert, 1987). However, the presently available data indicate a dextral shear along the Domeyko Fault System, at least during the Oligocene (Lopez, 1939, 1942; Hollister and Bernstein, 1975; Hollister, 1978; Sibson, 1987; this work).

The Domeyko Fault System was primarily developed as a dextral transcurrent fault along the Late Eocene - Early Oligocene magmatic arc. It is regarded as a trench-linked, strike-slip fault according to the classification of Woodcock (1986).

### 2.16.5 Significance of the regional strike-slip fault systems

Strike-slip faulting is now recognized as a ubiquitous process in volcanic arcs of most subduction zones that have a continental overriding plate. This is because periods of oblique convergence are likely to occur at some point in their protracted tectonic history (Jarrard, 1986; Sylvester, 1988; Holly and Scholl, 1989; Busby-Spera and Saleeby, 1990). Trench-linked faults nucleate and develop along the weak zone formed by the volcanic arc and accommodate the horizontal component of the displacement at convergent plate margins during periods of oblique convergence (Woodcock, 1986; Beck, 1986; Busby-Spera and Saleeby, 1990). Thus strike-slip faulting and associated shear strain concentrate along thermally weakened zones within magmatic arcs related to subduction. This is consistent with theoretical models of Fitch (1972), Walcott (1978), Dewey (1980), and Beck (1983, 1986) as well as with examples of the Central Aleutian Arc (the Hawley Ridge shear zone; Holly and Scholl, 1989), Sumatra (Fitch, 1972) and coastal California (Beck, 1986).

The Atacama Fault System has been attributed to a hypothetical period of oblique plate convergence during the Late Jurassic and Early Cretaceous (Naranjo and others, 1984; Herve, 1987a; Scheuber and

Andriessen, 1990). The development of the Domeyko Fault System correlates with a period of fast northeasterly-directed oblique convergence (ca. 12 cm/yr; Cande 1983) between the South American continent and the oceanic Farallon plate from about 42 to 26 Ma (anomaly 18 to 13) based on paleomagnetic reconstructions of movements of the oceanic floor (Pilger, 1983, 1984; Cande, 1983; Cande and Leslie, 1986; Pardo-Casas and Molnar, 1987). Each of these major strike-slip fault systems developed along the magmatic front at the time of oblique convergence, thus ultimately accounting for the spatial association of coeval igneous rocks with the fault system.

## 2.17 ANDEAN UPLIFT: A REVIEW

### 2.17.1 Introduction

Early analyses of the evolution of the Andean orogenic belt were interpreted in terms of geosynclinal theory. Accordingly, an "Andean Geosyncline" was defined, with a western *eugeosynclinal* domain where volcanic activity was prevalent, and an eastern *miogeosynclinal* sedimentary platform (Ruiz and others, 1965; Corvalan, 1965). The idea that the initial stages of Andean evolution involved the development of a trough, filled by a marine and terrestrial stratigraphic sequence more than 22 km thick, was a basic assumption of this interpretation (e.g., Ruiz and others, 1965; Corvalan, 1965; Levi and Corvalan, 1968). Widespread burial metamorphism was inferred (e.g., Levi and Corvalan, 1964; Levi, 1969, 1970). Andean uplift was regarded as a relatively rapid process related solely to the final phases of the "Andean Orogenic Cycle," particularly to a Pliocene-Quaternary extensional event, the "Geographic Phase" of Vicente (1970; 1972) or "Taphrogenic Phase" of Frutos and Tobar (1975) and Frutos (1982). This opinion was widely accepted during the 1950s, 1960s, less commonly in the 1970s (Brüggen, 1950; Muñoz-Cristi, 1950, 1956; Ruiz and others, 1965; Rutland and others, 1965; Corvalan,

1965; Corvalan and others, 1968; Aubouin and Borello, 1966; Charrier and Vicente, 1970; Frutos, 1970; Frutos and Tobar, 1975; Aubouin and others, 1973; Aguirre and others, 1974; Charrier, 1973), and still advocated by some authors in the 1980s (e.g., Charrier, 1981; Aguirre, 1985; Frutos, 1981, 1982, 1985).

The introduction of modern geochronologic methods, particularly the K-Ar dating of ignimbrites deposited onto several distinct erosion surfaces in northern Chile (e.g., Dingman, 1963, 1965; Galli, 1967), demonstrated that some surfaces now uplifted and tilted, were undoubtedly in existence by the Late Miocene. Although the perceived duration of Andean uplift was greatly extended, it was still maintained that the magnitude of Late Pliocene-Pleistocene uplift exceeded the preceding phases (e.g., Galli, 1967; Hollingworth and Rutland, 1968). Studies that integrated geologic and geomorphologic investigations with K-Ar dating of volcanic rocks further demonstrated a complex landform chronology, and indicated that considerable relief existed prior to the Late Miocene in northern Chile (Clark and others, 1967a, 1967b, 1976; Sillitoe and others, 1968; Rutland, 1971; Mortimer, 1973, 1980; Mortimer and others, 1974; Mortimer and Saric, 1972, 1975; Maksaev, 1979), southern Peru (Laharie, 1976; Tosdal and others, 1984), and central Peru (Myers, 1976; Farrar and Noble, 1976; Noble and others, 1978, 1979; McKee and Noble, 1982). In addition, Clark and others (1967b) showed that tectonic activity in Pliocene and more recent times has been of little fundamental importance in the Atacama Region of northern Chile.

### 2.17.2 Timing of uplift events

Several studies have contributed to the knowledge of the timing of uplift events in the Andes of northern Chile. Rutland (1971) advanced one of the first field-based accounts of a protracted uplift history of the Antofagasta segment of the Andes. He showed that in the Late Cretaceous or Early Tertiary the western and eastern Andes became

positive areas subject to repeated uplift and erosion, while the Puna plateau and Sub-Andean zones (eastern flank of the present Andes) became sedimentary basins with marine deposition during the Late Cretaceous. According to Rutland (*op. cit.*), the present Intermediate Depression and associated topographic features did not develop as basins until Miocene times, when the main uplift of the Altiplano began. Block faulting was initiated in the Early Tertiary and the uplift of the Domeyko Cordillera at that time resulted in the filling of intermontane troughs during the Oligocene or Miocene (Tambores, San Pedro and Lower Loa Formations). Intermittent tectonism in the east of the segment accompanied the deposition of the Pliocene San Bartolo and Upper Loa Formations. Although Rutland's chronology of uplift events is not completely correct, owing to the paucity of paleontologic and radiometric constraints in the early 1970s, his account of the uplift history of the Antofagasta segment coincides remarkably well with the presently available geological and radiometric data.

Geomorphologic studies of northern Chile by Galli (1967) and Mortimer and Saric (1972) showed the existence of a planated surface (Tarapaca Pediplain in the Coastal Cordillera; Saric, 1971; Mortimer and Saric, 1972, and Choja Pediplain in the easternmost section of the Intermediate Depression; Galli, 1967). Early Miocene K-Ar ages determined for ignimbrites intercalated within alluvial deposits overlying this surface were used to infer that the erosion surface probably developed during the Oligocene (Mortimer and others, 1974). However, the same erosional surface is covered by Early Tertiary volcanic rocks in the Intermediate Depression of the Antofagasta Region (K-Ar ages 55.0 ± 1.4 and 52 ± 2 Ma; Chapter 4, Table 4.1), therefore this surface already existed at the beginning of the Tertiary. Block faulting of this surface was ascribed to the Oligocene-Miocene boundary and the beginning of sedimentation within the Intermediate Depression was taken to indicate that the Coastal Cordillera was uplifted relative to the rest of the Andean system at that time (Mortimer and others, 1974; Mortimer and Saric, 1975). Consequently a major change in the physiography of northern Chile, the uplift of the Domeyko Cordillera, and the establishment of the major

longitudinal physiographic units were ascribed to the Oligocene-Miocene boundary (Mortimer and Saric, 1975). The present study implies instead that these events occurred somewhat earlier (see below). The K-Ar dates of ignimbrite flows intercalated within the upper part of the alluvial deposits of the Pampa del Tamarugal (Intermediate Depression) indicated that the aggradation of the Intermediate Depression throughout the length of northern Chile virtually ceased after the close of the Middle Miocene. This has been attributed to a climatic change by Mortimer and Saric (1975) and corroborated by Alpers and Brimhall (1988).

Based on geologic relations and K-Ar dates from the northern part of the Domeyko Cordillera Maksaev (1979) showed that most of the uplift was related to two Cenozoic compressive events. The older was ascribed to the Late Eocene-Oligocene boundary from an angular unconformity between Paleocene-Eocene volcanic rocks and overlying Oligocene terrestrial sedimentary strata. This compressive event was characterized by the differential uplift of major crustal blocks bounded by sub-vertical faults, formation of the Domeyko Cordillera, and tilting of Paleocene-Eocene volcanic strata. Subsequent erosion of the Domeyko Cordillera produced Oligocene to Early Miocene terrestrial alluvial and evaporite deposits on its foothills. These deposits cover extensive areas east and west of the Domeyko Cordillera with variable thickness from 280 to 2,100 m (Fig. 2.7).

The above compressive event correlates with the **Incaic** tectonic event of the Peruvian Andes as named by Steinmann (1929). Geologic observations and K-Ar dating by Noble and others (1974, 1978, 1979) indicated that the "**Incaic** pulse" of compressive deformation, and consequent uplift and erosion of the Andes of Central Peru, took place before 40 to 41 Ma ago. Based on these data, and his own observations, Megard (1987) ascribed the **Incaic** tectonic event to the Middle to Late Eocene. This compressive event is commonly considered the main Cenozoic tectonic phase of shortening in the Peruvian and Bolivian Andes (Megard, 1987, 1989; Audebaud and others, 1973; Ellison and others, 1989). A Middle-Late Eocene age for the **Incaic** tectonic event is compatible with

the available geologic data from the Antofagasta Region and with regional cooling determined from apatite fission-track thermochronology on basement rocks of the Domeyko Cordillera (see Chapter 5). Consequently a major change in the physiography and establishment of the major longitudinal units of relief in the Antofagasta Region is ascribed to the Late Eocene, earlier than the Oligocene-Miocene age previously inferred by Mortimer and others (1974) and Mortimer and Saric (1975).

The second compressive event took place at about Middle-Late Miocene, and was accompanied by high-angle reverse faulting and localized folding within the Domeyko and Main Andean Cordilleras. This compressive tectonic event correlates with the **Quechua** compression of the Peruvian Andes (Steinmann, 1929), and the Andes of central Chile (Charrier and Vicente, 1970). The occurrence in the Andes of Peru of sedimentary deposits with intercalated ignimbrites has allowed identification of three "**Quechua**" compressive pulses (e.g., Megard and others, 1984): the **Quechua** 1 in the Early Miocene, the **Quechua** 2 in the Late Miocene, and the **Quechua** 3 in the Pliocene. Similar discrete pulses may have occurred also in the Antofagasta Region, but so far they have not been confirmed by stratigraphic data.

The Miocene **Quechua** compression either obliterated or reactivated some of the structures formed during the previous **Incaic** tectonic event and increased by further uplift the previously formed relief. This additional uplift of the Western Andes and the virtual lack of aggradation or degradation since the Late Miocene may appear at first sight as a single relief forming event (e.g., Mortimer and others, 1974; Mortimer and Saric, 1975). Subsequent tectonic activity in the Antofagasta segment of the Andes was insignificant (Maksaev, 1979).

Mortimer's (1980) detailed study of drainage evolution in northern Chile showed that the Central Andes began to form in the Cretaceous, with uplift of Mesozoic sedimentary and volcanic rocks that had been deposited peripheral to the western margin of South American continent. A proto-Andean divide was established some distance west of

the present Main Andean Cordillera (Western Andes). During the Late Cretaceous and the Paleogene, the erosion of the original mountain mass produced thick accumulations of terrestrial sediments in that area now occupied by the Altiplano. These conclusions have been confirmed by more recent geological studies (e.g., Marinovic and Lahsen, 1984; Hartley, 1987; Hartley and others, 1988). The ultimate result was the development of an Early Tertiary regional erosion surface that is still locally preserved in the Coastal Cordillera and as the sub-alluvial floor of the Intermediate Depression. Mortimer (1980) also showed that the landscape and drainage style of the Antofagasta Region was largely established before the close of the Miocene. This view also has been confirmed by recent studies, which have obtained K-Ar dates ranging between 19 and 2.9 Ma for ash fall deposits intercalated with alluvial piedmont deposits in the Antofagasta segment of the Andes (Chavez, 1985; Naranjo, 1987; Herve, 1987; Alpers and Brimhall, 1988). These piedmont deposits were traditionally considered to be Pleistocene to Recent, and this erroneous assumption contributed to the persistence of the idea of very recent uplift of the Andes in the Antofagasta Region.

Miocene-Pleistocene sediments on the western side of the Salar de Atacama show minor *en echelon* open folds with northeast trending axes and Pliocene ignimbrites are affected by minor reverse faults in the easternmost section of the Antofagasta Region (Ramirez and Gardeweg, 1982). These features indicate only minor Pliocene-Pleistocene tectonic activity. The major regional faults of the Antofagasta Region do not show significant displacement since the Late Miocene. Thus tectonic activity and related uplift seem to have declined since that time in the western flank of the Andes. In contrast, important Pliocene to Recent reverse faulting and significant uplift have occurred in the easternmost Andes and Sub-Andean region of Argentina (Jordan and others, 1983; Lyon-Caen and others, 1985; Strecker and others, 1989). These areas are currently characterized by shallow crustal seismicity indicating active E-W horizontal compression. Earthquake locations closely correlate with major range-bounding fault trends (Eremchuk and others, 1981; Chinn and Isacks, 1983; Jordan and others, 1983; Triep and Cardinali, 1984; Strecker and

others, 1989). This compression may be accompanied by local extension (e.g., Dalmayrac and Molnar, 1981), but certainly the Pliocene to Recent has not exclusively been a period of extension as advocated by some authors for the Central Andes (e.g., Charrier, 1981; Aguirre, 1985; Frutos, 1981, 1982, 1985).

In summary the uplift of modern Andes was accomplished through the additive effects of at least three major compressive events. Significant uplift of the westernmost Andes was already achieved in the Late Cretaceous during the **Peruvian** compressive phase. Subsequent denudation resulted in a erosion surface preserved locally in the Coastal Cordillera and under the Early Tertiary volcanic cover of the Intermediate Depression, whereas an aggradational surface was formed to the east due to the filling of an extensive epicontinental sedimentary basin by terrestrial red beds and minor marine deposits. Even though most of the positive relief produced during the Late Cretaceous was probably eroded, most of the Antofagasta Region remained subaerial. Early Tertiary volcanic deposits partly covered both the erosional and aggradation surfaces. Differential uplift of major crustal blocks at about the Middle-Late Eocene (**Incaic** tectonic event) introduced major physiographic changes and established the major longitudinal relief units of the Antofagasta segment of the Andes. These conclusions, based on presently available geologic and geochronologic data, are further supported by new fission track data (see Chapter 5). The deposition of Oligocene terrestrial sedimentary sequences farther east in the Altiplano indicates that the main uplift of this zone probably post-dates the Oligocene (Jordan and Alonso, 1987). The main uplift of the Altiplano correlates with the **Quechua** Miocene and Pliocene compressive pulses. This tectonic event was also accompanied by reverse faulting along the Domeyko Cordillera increasing its uplift. Fission track data from the Eastern Cordillera of Bolivia imply important Late Miocene uplift in the easternmost section of the Central Andes (Crough, 1983; Benjamin and others, 1987).

There is a pattern of eastward migration of deformation with time, which correlates with the migration of the magmatic front in this Andean segment (Rutland, 1971); Mortimer and Saric, 1975) and in the Peruvian Andes (Megard, 1984).

Even though the geologic and geochronologic data published in the literature are consistent with a protracted, complex uplift history in this Andean segment, the concept that most of the uplift of the modern Andes was accomplished since the Miocene persists (e.g., Jordan and Gardeweg, 1989).

### 2.17.3 Causes of the uplift

The geosynclinal theory assumed that the continents were essentially fixed and oceanic basins permanent. Accordingly, the Andean Orogen was regarded as largely controlled by vertical forces; compressional movements were considered subordinate, and crustal shortening minimal. Even though the modern geological knowledge of the Andes shows an entirely different picture, these ideas are still advocated by some influential authors (e.g., Aguirre, 1985; Frutos, 1985).

The Central Andes are now regarded as a classic example of a simple orogen developed along a convergent plate margin (Dewey and Bird, 1970; James, 1971; Jordan and others, 1983; Jordan and Gardeweg, 1989). They represent a non-collisional mountain belt formed over a long-lived, currently active, subduction system.

One school of thought maintains that collision is a necessary prerequisite for mountain building (Nur and Ben-Avraham, 1977, 1981, 1982, 1983; Jones and others, 1982), and the concept that Andean orogenesis is caused by the subduction of "normal" oceanic lithosphere, has been questioned (Nur and Ben-Avraham, 1983). They would require the

collision (or subduction) of, at least, aseismic ridges to initiate tectonism. Others, however, (Dalziel and Forsythe, 1985); Dalziel, 1986; Megard, 1987; Jordan and Gardeweg, 1989) argue that the Andean orogenesis is not the result of collision of allochthonous "terranes" with the South American continent, but rather the result of tectonic and magmatic processes related to the subduction of "normal" oceanic lithosphere. Computer modelling has shown that substantial horizontal deviatoric compressive stresses may be generated in the trench-arc region as a result of the downpull of a dense oceanic slab (Bott and others, 1989).

The most remarkable aspect of the structure of the Central Andes is its crustal thickness, which varies from 30 km along the coast to more than 70 km beneath the Main Andean Cordillera (Western Andes) and western part of the Altiplano (Fig. 1.2). The crust thins rapidly eastward, and beneath the Eastern Cordillera (Bolivia and northwestern Argentina) is only about 50 to 55 km thick (James, 1971, 1971b; Goetze and others, 1988; Wigger, 1988). The crustal thickness of more 70 km beneath the Western Cordillera and Western Altiplano is among the greatest yet measured anywhere in the world. The deep crustal root provides the required isostatic support for the Andean Cordillera (e.g. Molnar, 1986).

The uplift of the Andes and formation of a crustal root has been ascribed to either magmatic or tectonic processes. Gough (1973) postulated that the uplift and isostatic compensation of the Andes, is the result of contamination of a column of the lithosphere and asthenosphere by andesitic magma originating from the subducted oceanic plate. He estimated that the known uplift of the Andes may be attained within a time scale of 63 Ma. The isostatic compensation by this model is dynamic and the uplift continuous. However, this is inconsistent with this study's evidence for continuous magmatism and episodic uplift. Alternatively, Baker and Francis (1978) and Thorpe and others (1981) postulated that the crustal thickening is the result of magmatic addition from the mantle since the Jurassic. However geologic evidence suggests that crustal thickening and related uplift occurred over a much shorter time span and

that this has certainly not been continuous. In fact the uplift is related to discrete, short compressive phases that, according to Megard (1984), may have lasted few hundred thousand years to few million years. The sedimentary record also suggests abrupt changes in the physiography of the region. Thickening by magmatic processes alone within few million years would require magmatic production rates at least one order of magnitude higher than average estimates of Reymer and Shubert (1984) for convergent margins.

Rutland (1971) postulated periodic loss of continental crustal material (subduction erosion) for explaining the orogenic history of northern Chile. This hypothesis assumes episodic tectonic removal of crustal blocks from the continental edge by the subducting slab. The crustal material is thought to be dragged under the continent, remobilized, and incorporated into the existing crust. The consequent advance of the arc-trench system accounts for the eastward migration of both the magmatic front and deformation. The present position of the Jurassic magmatic arc on the edge of the continental plate, immediately east of the Chile-Peru oceanic trench, suggests that at least part of the continental border has been removed and that the trench has advanced towards the continent. Moreover, the dragging of trench sediments under the continental border of Central Andes has been documented by geophysical data, and the erosion of the continental border has been postulated by several authors (e.g., Hilde, 1983; Coulbourn, 1981; Schweller and others, 1981; Wortel and Cloetingh, 1985). On the other hand, Stern (1988, 1989; and in print) argued that crustal contamination of Quaternary volcanic rocks at the northern end of the Southern Volcanic Zone of the Andes is inherited from a mantle source region contaminated by components derived from subducted terrigenous sediments and tectonically-eroded continental crust. Unfortunately, there is presently no known way to determine the real importance of subduction erosion, because the evidence is destroyed by the process. The removal of crustal strips from the continental border may also occur by lateral transport, and the dragging of light continental materials down into the mantle by subduction may be hampered by their buoyancy. In addition, both the crustal thickening and eastward shifts of

magmatic and structural processes of the Central Andes can be explained exclusively by crustal shortening. Consequently, even though subduction erosion of the continental border may have played a role in the tectonic evolution of the Central Andes, the significance of this process to Andean uplift cannot be evaluated.

Increasing evidence points to the importance of compressional crustal shortening in the uplift of the Central Andes (Mingramm and others, 1979; Allmendinger and others, 1983; Dalmayrac and others, 1980b; Buchfield and others, 1981; Jordan and others, 1983; Suarez and others, 1983; Megard, 1984; Lyon-Caen and others, 1985; Sheffels and others, 1986; Allmendinger, 1986; Roeder, 1988; Goetze, 1989). The magmatic addition has been estimated only to be 10% (Roeder, 1988). Several estimates suggest Late Cenozoic shortening in the Central Andes on the order of 100 km or more (Isacks, 1988).

The structural shortening may take place as distributed shortening, as advocated by Suarez and others (1983) for the northern part of the Altiplano, or by underthrusting of the Brazilian Shield beneath the orogenic belt (A-subduction of Balli, 1981), as suggested by Lyon-Caen and others (1985) and Molnar (1986). The study of Allmendinger (1986) of the southeastern border of the Altiplano (NW Argentina) showed that the regional structure in combination with the *en echelon* block structure precludes the underthrusting model as a structural mechanism for the southernmost Altiplano, whereas distributed shortening may account for some of the characteristics of the area.

Isacks (1988) has advanced an interesting model for the uplift of the Central Andean Altiplano. According to his hypothesis the Andean topography is largely a result of crustal shortening following thermal thinning of the lithosphere. The model proposes that thermal weakening caused by convective and magmatic processes in the wedge of asthenosphere located between the upper and subducted plates has allowed compressional failure of the overriding South American Plate. This model does not require collision or addition of enormous volumes of magma to the

crust, but instead calls upon plausible amounts of crustal shortening and lithospheric thinning.

The thermal weakening of the lithosphere by magmatic processes has been completely overlooked by previous tectonic models, but it has probably played a major role in locating the zone of crustal deformation (e.g., Moscoso and Mpodozis, 1988), because temperature is the leading factor controlling the ductile behaviour of the rocks. Advection of heat by the magmas rising from the asthenospheric mantle increases the geothermal gradient so that the brittle-ductile transition zone is closer to the surface, influencing both the location and structural style of deformation. For example Moscoso and Mpodozis (1988) estimated that the top of the brittle-ductile transition zone may have been as shallow as 5 km during thick-skinned deformation of the crystalline basement in the High Andes of northern Chile between latitudes 28°and 31° S. The eastward shift of structural events in the Central Andes can be attributed to migration of the thermally weakened zone following the inland advance of the magmatic front after crustal or lithospheric shortening events. The correlation of compression phases with major events of plate reorganization and reorientation that resulted in increased convergence rates (e.g., Pardo-Casas and Molnar, 1987), suggests that compressional failure of the thermally weakened zone on the continental border takes place during periods of increased horizontal deviatoric compressive stress within the continental border. This is further supported by the geological record of the Antofagasta Region that shows the persistence of extended periods of steady subduction, which were characterized by continuous magmatic processes, but without significant crustal tectonic activity. The compressive tectonic events have taken place during discrete, short periods of geological time with deformation largely concentrated in the region where active magmatism was taking place. Crustal shortening was often followed by the inland migration of the magmatic front.

## 2.18 CONCLUSIONS

This study shows that the geologic evolution of the western slope of the Central Andes between 21° and 26° S since the Late Carboniferous was characterized by the development of a series of magmatic arcs accompanied by coeval sedimentation mostly within ensialic back-arc basins. The magmatic front occupied different positions along the continental border and its development was accompanied by the deposition of volcanic strata that were intruded by almost coeval plutons, and marine or terrestrial sedimentation mostly immediately behind the arc. Shifts of the magmatic front were preceded by discrete tectonic events that resulted in deformation, uplift, and erosion represented by regional unconformities. During the Mesozoic-Cenozoic the position of the magmatic front shifted systematically east from the Coastal Cordillera to ca. 300 km inland. Thus different volcanic units were deposited along separate longitudinal belts. The compilation and reassessment of published radiometric ages of igneous rocks of the study area substantiate these conclusions and show that there is no evidence for recurrence of magmatism west of the front once post-Paleozoic eastward shifts occurred.

Two major trench-linked strike-slip fault systems dominate the structural make-up of the region. The sinistral Atacama Fault system developed along the Coastal Cordillera in the Late Jurassic-Early Cretaceous. The dextral Domeyko Fault System developed in the Late Eocene-Oligocene along the Domeyko Cordillera. Both major fault systems were generated along the position of the magmatic front during periods of oblique convergence between the oceanic plate and the South American continent. Minor reactivation of these structures occurred in the Neogene.

This study confirms that Andean uplift has been episodic, associated with three tectonic events since the Late Cretaceous, and not restricted to the Miocene and younger events as often implied.

# CHAPTER 3. MINERAL DEPOSITS

The most prominent metallic deposits of the Antofagasta Region are enormous porphyry copper deposits with subordinate molybdenum. Some of them are among the largest and highest grade deposits of this type in the world (e.g., Chuquicamata, La Escondida). Other important mineral deposits are stratabound and vein copper deposits, gold and silver-bearing epithermal veins, and lenticular volcanogenic iron deposits. In addition, many stratabound, and irregular sulphur deposits related genetically to solfataric activity of Miocene to Quaternary strato-volcanoes occur in the easternmost part of the region.

## 3.1 MINERAL DISTRIBUTION

The Antofagasta segment of the Central Andes includes more than 750 known metallic mineral deposits grouped into 90 local mining districts or camps (Fig. 3.1). The mineral deposits are regionally distributed within three north-south metallogenic belts spatially coincident with the major physiographic units of the Antofagasta Region: the Coastal Cordillera, the Domeyko Cordillera, and the Main Cordillera Metallogenic Belts. The term "Metallogenic Belt" is used in this study to designate an area characterized by a particular assemblage of mineral deposits, which may have had more than one episode of mineralization. Even though this is the definition of a "Metallogenic Province" (Bates and Jackson, 1980) the term Metallogenic Belt is preferred at this scale. Ericksen (1975, 1976) has previously defined the whole Andes as an "Andean Metallogenic Province" including northern Chile within a "Copper Metallogenic Sub-province."

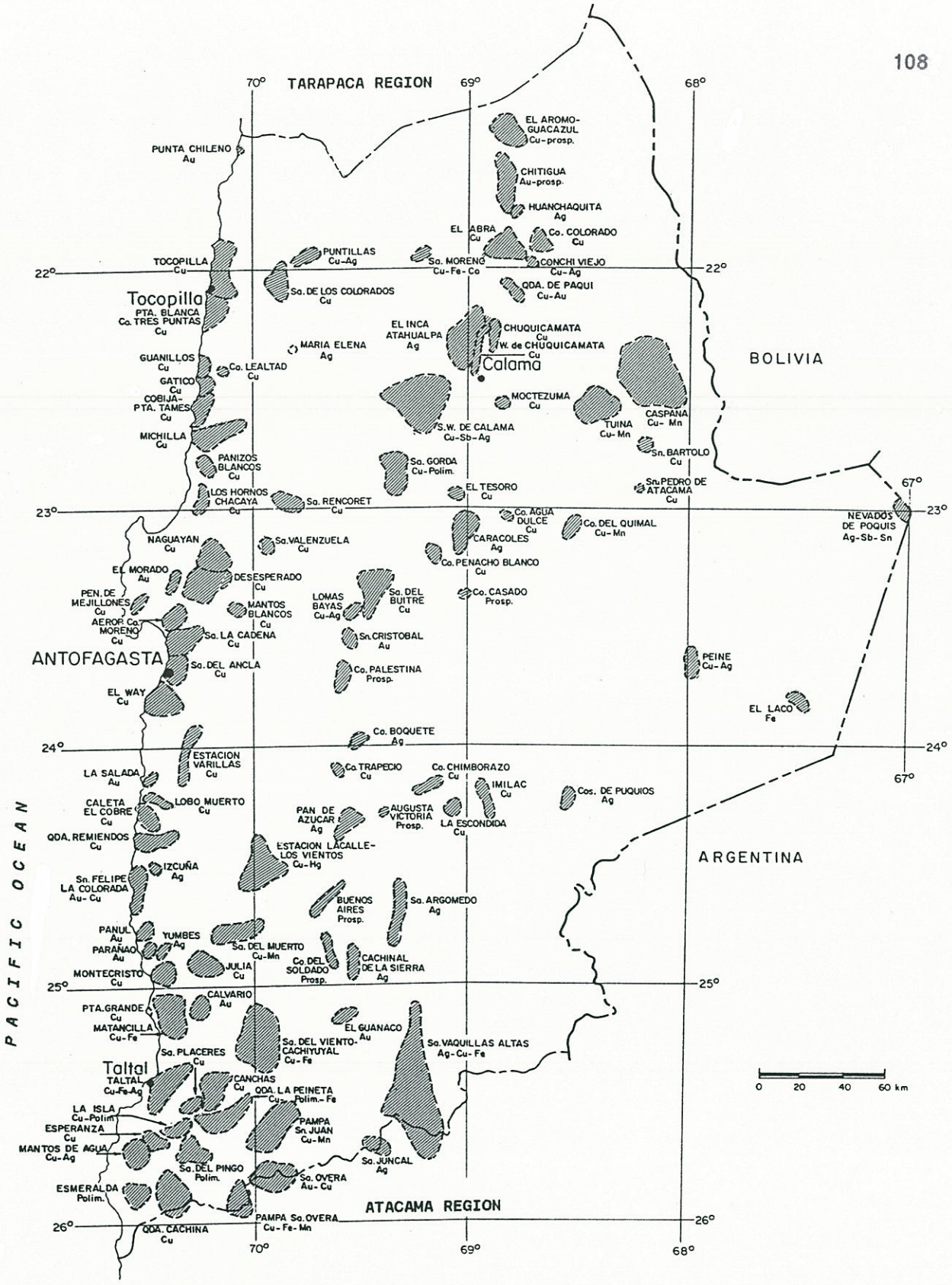


Figure 3.1. Mining districts of the Antofagasta Region.

### 3.1.1 Coastal Cordillera Metallogenic Belt

This metallogenic belt extends along the Coastal Cordillera in the westernmost section of the Antofagasta Region. It includes the highest number of individual metallic ore deposits, mostly of copper (more than 500; Fig. 3.2). The most important are stratabound copper deposits (with subordinate silver) hosted by Jurassic volcanic rocks (e.g., Mantos Blancos, Buena Esperanza, and Santo Domingo; Figs. 3.2, 3.4). Copper-bearing veins hosted by Middle to Late Jurassic batholiths have subordinated relevance (e.g., Tocopilla, Gatico, Naguayan, and Julia districts; Figs. 3.2, 3.4). In addition, there are many small veins bearing copper, gold, silver, iron, manganese, nickel-cobalt, and mercury. These minor deposits are hosted either by Jurassic or Early Cretaceous igneous rocks and lack economic significance.

### 3.1.2 Domeyko Cordillera Metallogenic Belt

This metallogenic belt extends along the Domeyko Cordillera and the eastern section of the Intermediate Depression. It contains fewer metallic ore deposits than the coastal area (close to 200), but includes the largest and most important ore deposits of this Andean segment: giant porphyry copper deposits. The most prominent is Chuquicamata. Since 1915 it has produced more than 15 million metric tons[1] of metallic copper, 126,000 tons of molybdenum, and a significant production of gold and silver. It still possesses proven and probable reserves of about $2.5 \times 10^9$ tons averaging 1.03% Cu (Ambrus, 1979). Chuquicamata, La Escondida, El Abra, Quebrada Blanca, Copaquire, El Salvador, and Potrerillos porphyry copper deposits (Fig. 3.7) are genetically related to the emplacement of Upper Eocene-Lower Oligocene stocks and collectively they constitute one of the largest copper concentrations in the world.

---

[1] All tonnage values are expressed in metric tons in this study.

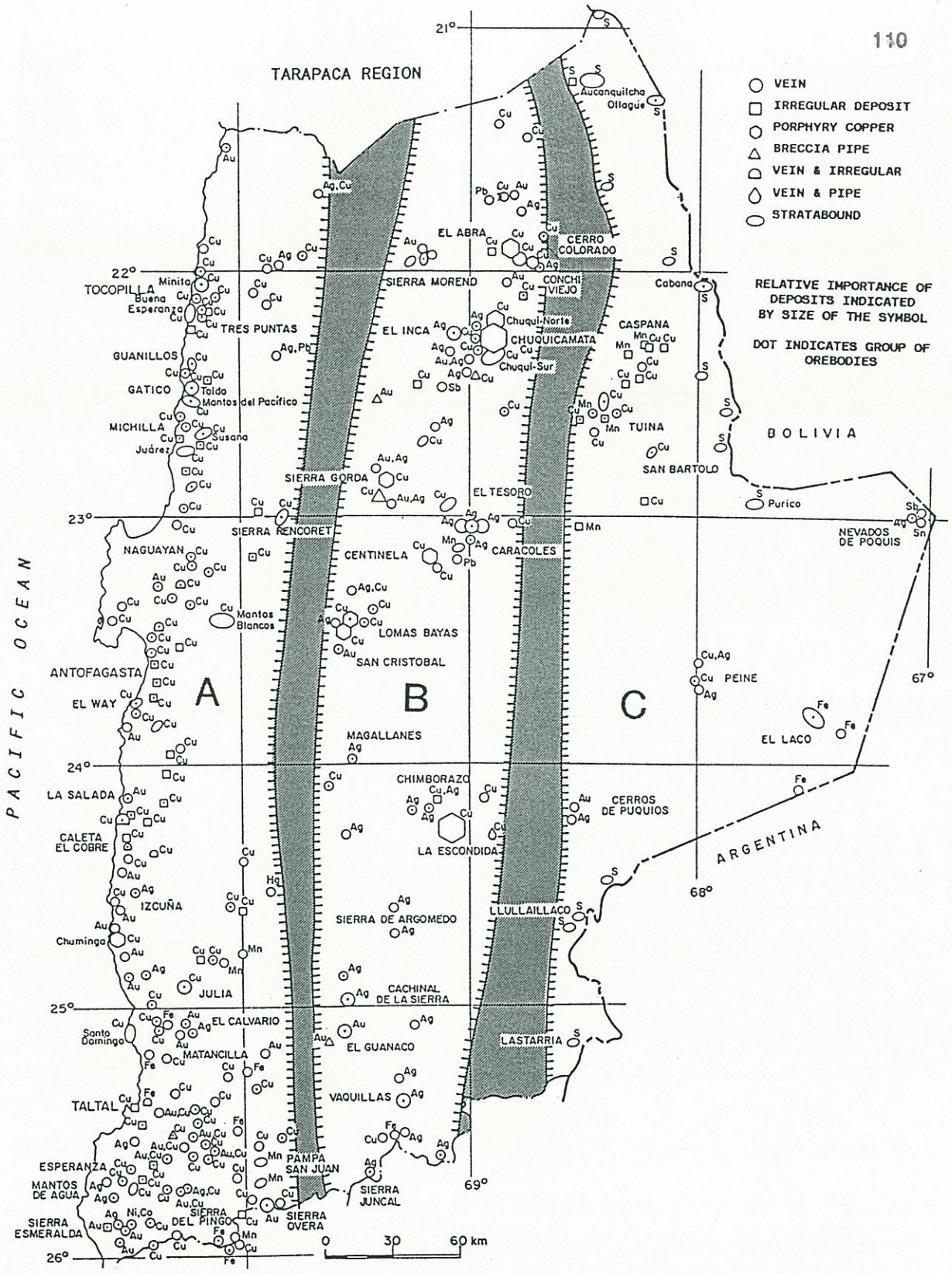


**Figure 3.2.** Metallogenic belts of the Antofagasta Region. (A) Coastal Cordillera Metallogenic Belt. (B) Domeyko Cordillera Metallogenic Belt. (C) Main Andean Cordillera Metallogenic Belt.

Other important deposits located within the Domeyko Cordillera Metallogenic Belt are epithermal veins bearing silver and gold (e.g., Caracoles, El Inca, Cachinal de la Sierra, Vaquillas, and El Guanaco districts; Figs. 3.2, 3.6) related genetically to Paleocene volcanic rocks and subvolcanic intrusive rocks, copper-bearing veins associated with Oligocene intrusives (e.g., El Abra district), copper-bearing breccia pipes (e.g., Sierra Gorda district), and sub-economic porphyry copper deposits (Sierra Gorda, Lomas Bayas-Fortuna, Centinela) that are related to Paleocene intrusive rocks. Small veins, stratiform and irregular deposits of copper, iron, manganese, lead-zinc, antimony, and copper-cobalt are also located within this metallogenic belt but lack economic significance. These are small deposits mostly hosted by Late Cretaceous to Paleogene igneous rocks, but also within Upper Carboniferous to Middle Triassic igneous rocks.

### 3.1.3 Main Andean Cordillera Metallogenic Belt

This metallogenic belt extends along the Main Andean Cordillera, and the Chilean segment of the Altiplano in the easternmost section of the Antofagasta Region. Relatively scarce known metallic ore deposits occur in this area (about 60; Figs. 3.2, 3.8). The most remarkable are magnetite lava flows and subvolcanic intrusive bodies that constitute the El Laco volcanogenic iron deposit associated genetically with Pliocene volcanic rocks. Another significant deposit is the Porvenir copper vein-stratabound orebody (Tuina district) hosted by Late Carboniferous to Middle Triassic rocks. Small vein and irregular deposits bearing copper and manganese are also hosted by Late Carboniferous to Middle Triassic volcanic and intrusive rocks and small veins bearing silver, antimony, or tin, which are hosted by Miocene-Holocene volcanic and subvolcanic rocks. In addition, the Main Cordillera Metallogenic Belt includes many solfataric native sulphur deposits associated with late Cenozoic volcanoes (e.g., Aucanquilcha, Ollagüe, Cabana, and Putana volcanoes; Fig. 3.8).

## 3.2 CHARACTERIZATION OF MINERAL DEPOSITS

The purpose of the present chapter is to provide a general description of the mineral deposits representative of the different periods of the geological history of the Antofagasta Region to depict the evolution of mineralizing processes through geologic time. A detailed description of individual mineral deposits is out of the scope of this thesis, and can be found elsewhere in the literature.

The Lower Paleozoic and pre-Paleozoic rocks of the Antofagasta Region lack known metallic ore deposits, whereas the Late Carboniferous to Middle Triassic rocks are sparsely mineralized, hosting veins and irregular bodies bearing copper and manganese, and small veins bearing silver, or gold (Fig. 3.3). Most metallic mineral deposits of the Antofagasta Region are hosted by Mesozoic and Cenozoic igneous rocks. These ore deposits are progressively younger from west to east concordant with the age of the host igneous units (see Chapters 2 and 4).

### 3.2.1 Mineral deposits in Upper Carboniferous to Middle Triassic rocks

The few mineral deposits hosted by Upper Carboniferous to Middle Triassic rocks occur chiefly in the eastern section of the study area within both the Domeyko Cordillera and Main Andean Cordillera Metallogenic belts. They are mostly sub-economic veins, bearing copper, silver, or gold, and irregular bodies of copper or manganese oxides primarily hosted by Upper Paleozoic intrusive and volcanic rocks. The largest deposits occur within a sedimentary intercalation (110 m thick) within the middle section of the Upper Carboniferous to Middle Triassic volcanic sequence at Tuina (Fig. 3.3). The Tuina district includes composite vein and stratiform orebodies formed of copper oxides impregnating sandstones along north-south trending reverse faults, and veins and irregular bodies bearing manganese within brecciated volcanic rocks.

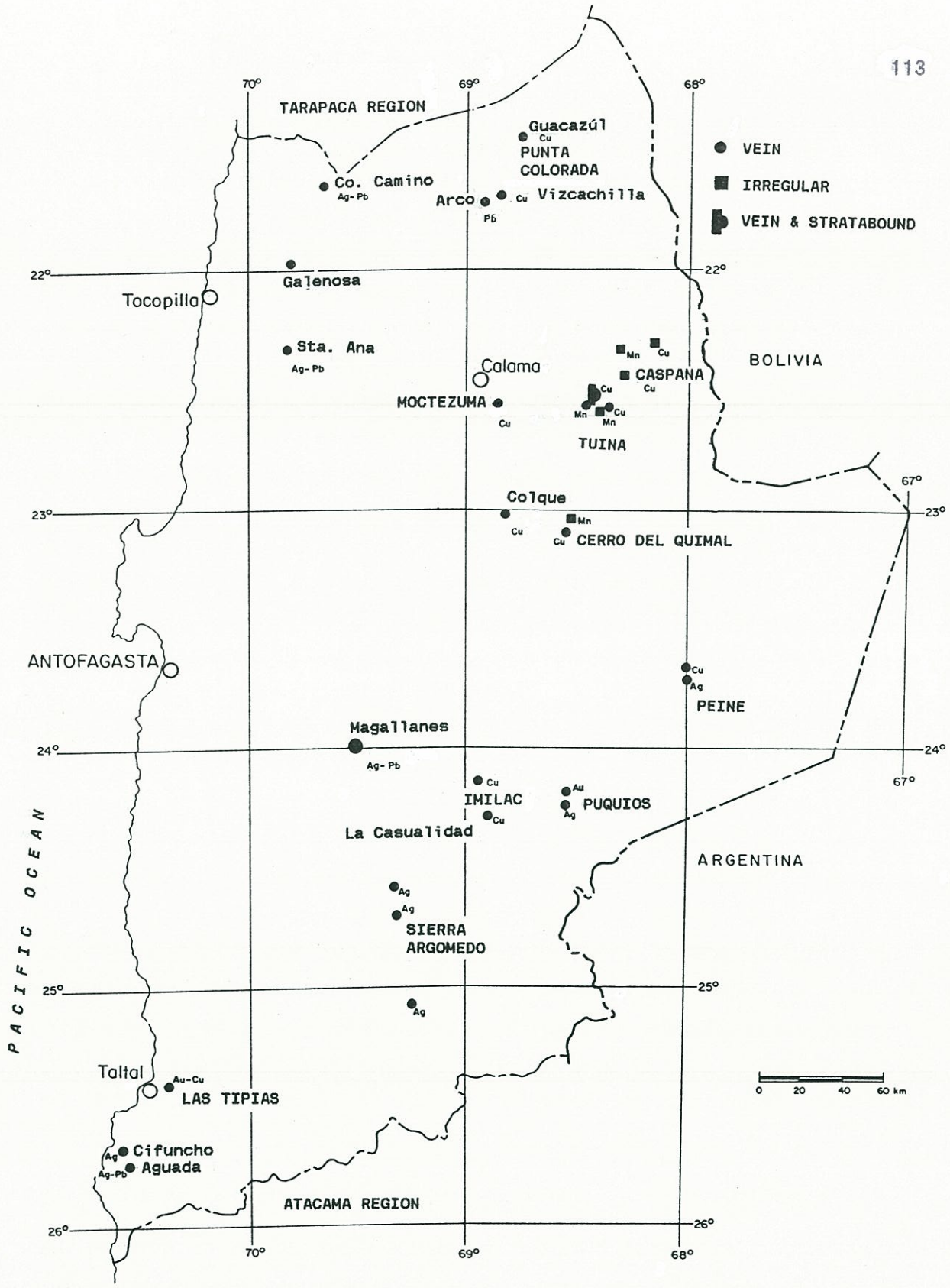


Figure 3.3. Metallic mineral deposits in Upper Carboniferous to Middle Triassic rocks.

Extensive and pervasive argillization (assemblage of clay minerals, sericite, chlorite, and rare calcite) is associated with copper ores (Raczynski, 1963). The Porvenir copper deposit is the largest of the Tuina District, the orebody is 370 m long, 20 to 50 m wide, and 25 to 80 m thick. The ore at Porvenir copper mine is mostly formed of secondary copper oxides and subordinate sulfides. The ore minerals occur as a fine dissemination and small irregular veinlets within folded sandstones and mudstones, immediately east of a north-south reverse fault (San Jose fault). At the surface the dominant ore minerals are colloform and fibrous silicate copper oxides (chrysocolla, dioptase, shattuckite, plancheite) accompanied by minor proportions of malachite, cuprite, tenorite, and native copper. However, the ore is mostly a mixture of copper oxides and sulfide minerals, and there is a progressive increase of copper sulfides with depth so that 40 m underground chalcopyrite, chalcocite, digenite, and minor bornite, constitute 80% of the ore minerals. Gangue minerals are quartz, chlorite, and calcite. The deposits at Tuina have been affected by supergene processes and higher copper grades occur 5 to 10 m beneath the surface, usually underlying leached rocks. The enriched zones have an average grade of 2.5% Cu, whereas primary grades are about 1% Cu (Raczynski, 1963).

Manganese deposits at Tuina consist of steeply dipping, north-northwesterly-trending veins, up to 200 m long and 0.5 to 2.0 m wide. These have been worked to depths of 25 m. The ore minerals are manganese oxides (braunite and minor psilomelane) and are either massive or cement brecciated volcanic rocks. Manganese ores at Tuina district also occur in series of small irregular and discontinuous braunite veinlets hosted by volcanic rocks forming extensive irregular low-grade bodies up to 2,000 $m^2$ in section and 30 m in thickness.

The age of the deposits of Tuina District is poorly constrained. A minimum age for the host volcanic sequence, with terrestrial sedimentary intercalations, is fixed by a biotite K-Ar age of 225 ± 7 Ma on a dacitic porphyry emplaced within the stratified sequence (Marinovic and Lahsen, 1984). The same minimum age is tentatively

ascribed for the primary mineralization. The economic copper orebodies were largely formed by supergene enrichment processes that probably took place in Tertiary times.

Small silver-bearing veins (e.g., Peine and Puquios areas; Fig. 3.3) and one gold vein (Mercedes mine; Puquios area) are hosted by Late Carboniferous-Permian granitoids in the Main Andean Cordillera. Most veins are less than 60 m long, 0.1 to 0.2 m wide, and 30 m downdip. The precise age of these minor silver deposits is unknown, but it is tentatively attributed to the Late Paleozoic.

The only dated Upper Paleozoic deposit in the Antofagasta Region is the La Casualidad copper-bearing vein of the Imilac district (Fig. 3.3), which is associated with a tourmaline breccia pipe. Sericite from the La Casualidad vein has given a K-Ar age of 298 ± 7 Ma (Late Carboniferous; Davidson and others, 1985). An alteration zone in the northern part of the Domeyko Cordillera containing minor copper oxides (Punta Colorada; Fig. 3.3) has yielded a whole rock K-Ar date of 232 ± 8 Ma (recalculated from Huete and others, 1977).

Few Upper Paleozoic ore deposits occur in the Antofagasta Region and most of them lack economic importance. Thus there is no record of a significant Late Paleozoic metallogenic epoch. However, during the Late Paleozoic (329 to 272 Ma), sub-economic porphyry copper deposits were formed in the Argentinean Andes (Sillitoe, 1977). One of those deposits (Taca-Taca) with a biotite K-Ar age of 329 ± 10 Ma (recalculated from Sillitoe *op. cit.*) is located in the Andes of northwestern Argentina, east of the Antofagasta Region. Although the Argentinean Upper Paleozoic porphyries are sub-economic, their occurrence suggests that significant metallic concentration processes did take place in the Late Paleozoic in the Andes at these latitudes. Thus the paucity of metallic mineral deposits within Late Paleozoic to Middle Triassic rocks in the Antofagasta Region may be the result of a relatively deep erosion level reached by older rock units with consequent removal of mineral deposits, rather than to the lack of mineralizing processes during

the Late Paleozoic. Sillitoe (1988) has suggested that the paucity of pre-Mesozoic copper deposits is probably due to a different magma chemistry of the Paleozoic intrusions. However, the petrochemical data of Brown (1989) from Late Paleozoic plutons of the Domeyko Cordillera do not substantiate Sillitoe's view. These plutons are calk-alkaline and have affinity to I-type granitoids, similar to Mesozoic-Cenozoic intrusions.

### 3.2.2 Mineral deposits in Jurassic rocks

The metallic ore deposits hosted by Jurassic rocks are largely restricted to a narrow belt along the coastal section of the Antofagasta Region (Fig. 3.4). There is a marked dominance of copper deposits. The largest and economically most important are stratabound copper deposits hosted by Jurassic volcanic rocks (they currently constitute the second source of copper in the region), secondary importance have copper-bearing veins hosted by Middle to Upper Jurassic plutons. In addition, small gold and silver-bearing veins are hosted by Jurassic plutons.

The coastal Jurassic igneous rocks are remarkably rich in copper deposits, but there is a conspicuous absence of known Jurassic porphyry copper deposits in northern Chile and Southern Peru. This suggests that conditions for the generation and/or preservation of porphyry copper deposits were lacking in the Central Andes during the Jurassic period.

#### 3.2.2.1 Copper stratabound deposits hosted by Jurassic volcanic rocks

The largest stratabound copper deposit is Mantos Blancos with production and reserves totalling 113 million tons of ore averaging 1.56% Cu and 6 g/ton Ag (Tobar, 1981). Other similar deposits are

significantly smaller, but some deposits contain several million tons of ore (production plus reserves) with average grades ranging between 1 and 3.8 % Cu and 8 to 25 g/ton Ag. The most relevant are: Buena Esperanza, Susana, Santo Domingo, Juarez, Mantos del Pacifico and Mantos de la Luna (Fig. 3.4). These stratabound deposits are hosted by Jurassic basaltic to andesitic porphyritic lavas, although at Mantos Blancos the sequence also includes dacitic and rhyolitic rocks. Most of the deposits occur near gabbroic, dioritic, or andesitic subvolcanic intrusive bodies, such as dikes, sills, stocks, or volcanic necks. These intrusive bodies have been interpreted as feeder conduits of the Jurassic volcanism (Palacios and Definis, 1981, 1981b; Espinoza, 1982). The intrusions are mostly barren and usually seem to post-date copper mineralization (e.g., Buena Esperanza, Susana, Santo Domingo). However, in Mantos Blancos and Mantos del Pacifico mineralized rhyodacitic and andesitic sills occur.

The stratabound copper deposits are restricted to the Jurassic volcanic sequence but they are typically composite and may include stratiform, lenticular, breccia pipe, and irregular orebodies. These are either concordant or discordant to the stratification. For example, Mantos Blancos includes five lenticular main orebodies forming an overall, slightly unconformable, irregular, tabular body (Chavez, 1985). In both the Buena Esperanza and Susana deposits, copper ore occurs within a central breccia pipe and in a series of conformable stratiform orebodies ("mantos") around the breccia pipe. The stratiform orebodies are restricted to amygdaloidal and brecciated portions of the lavas (Palacios and Definis, 1981, 1981b; Dreyer and Soto, 1985). In Santo Domingo and Mantos de la Luna deposits, conformable stratiform and unconformable irregular orebodies occur. Most of the stratabound deposits include small veins along fractures. Post-mineralization faulting has widely distorted the original shape of the orebodies.

The stratabound copper deposits usually have an upper zone of supergene copper oxides and a lower zone with hypogene copper sulfides. The degree of supergene oxidation is variable, some deposits include almost exclusively copper oxides (e.g., Mantos de la Luna,

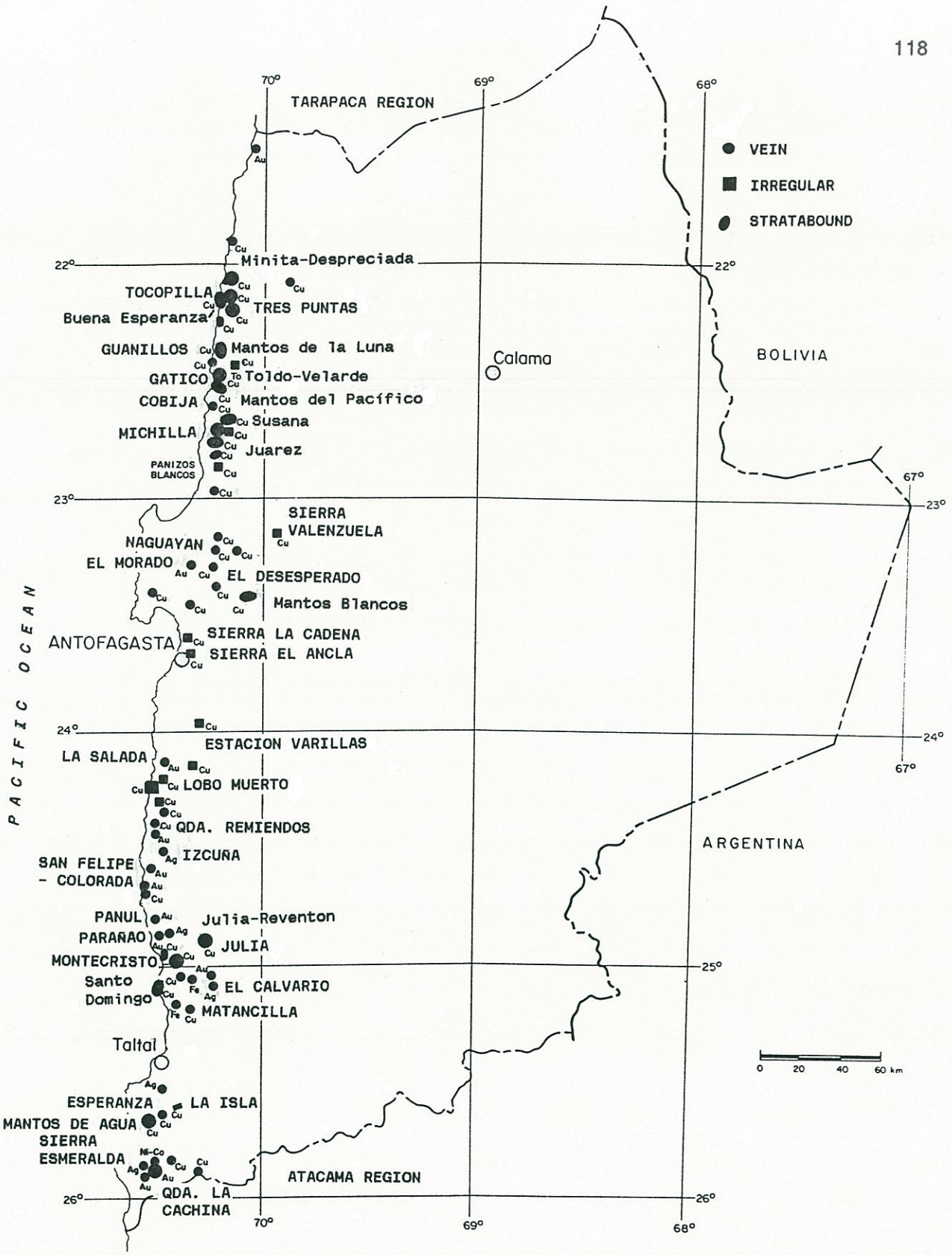


Figure 3.4. Metallic mineral deposits in Jurassic rocks.

Juarez), whereas others include only sulfides (e.g., Buena Esperanza). The boundary between the supergene and hypogene ores is gradational, so that some deposits include a zone with a mixture of copper sulfides and oxides (e.g., Susana, Santo Domingo).

The oxidized zone includes mainly atacamite, minor proportions of chrysocolla, malachite, copper sulphates, and rare cuprite and native copper. The gangue minerals are hematite, goethite, gypsum, and minor jarosite, natroalunite, and kaolinite. The maximum depth of this zone is 250 m in Mantos Blancos (Chavez, 1985). The hypogene ores contain chalcocite and bornite, with minor chalcopyrite. Some deposits also include covellite and digenite. Gangue minerals are quartz, hematite, pyrite, chlorite, and calcite.

The orebodies in Mantos Blancos and Santo Domingo have a lateral hypogene mineral zonation characterized by a copper-rich core with chalcocite-bornite and digenite, surrounded by a rim of bornite-chalcopyrite or chalcopyrite, and an external halo, usually uneconomic, of chalcopyrite-pyrite or just pyrite (Chavez, 1985; Definis, 1985). A weak to moderate hydrothermal alteration characterized by the assemblage albite-chlorite-hematite-quartz-sericite-calcite-epidote-sphene-scapolite-anatase is associated with ore minerals in the stratabound copper deposits (Losert, 1973; Chavez, 1984, 1985; Palacios, 1986). This local alteration is superposed upon the regional alteration-metamorphism (prehnite-pumpellyite facies) of the Jurassic volcanic sequence. The hydrothermal alteration is particularly pervasive in Mantos Blancos, where geochemical evidence shows important metasomatism of the host rocks with addition of sodium, iron and magnesium (Chavez, 1985).

Paragenetic studies of stratabound copper deposits have shown that usually the first deposited hypogene sulfides are pyrite-chalcopyrite-bornite followed by subordinate amounts of chalcocite-covellite-digenite. The paragenetic sequence indicates gradual increase of the proportion of copper in the sulfides, and decrease of the sulphur activity in the mineralizing fluids with time (Chavez, 1985; Losert,

1974). The successive replacement of iron-rich sulfides (pyrite, chalcopyrite) by copper-rich sulfides (bornite, chalcocite, covellite, digenite) resulted in the release of iron and the formation of profuse hematite within these deposits (e.g., Chavez, 1984).

The hypogene mineral assemblage (ore and gangue minerals) indicates that the stratabound copper deposits were formed at relatively low temperatures (Ruiz and others, 1965; Chavez, 1985). Fluid inclusions in calcite that contain copper sulfides at Buena Esperanza have yielded homogenization temperatures ranging between 65° and 195°C and minimum formation pressures of about 285-315 bars (Nisterenko and others, 1973). Sulphur isotopes from ores of Mantos Blancos, Buena Esperanza, and Susana deposits show a restricted range of $\delta^{34}S$ from -0.1 to -2.1 $^{0}/_{00}$ suggesting magmatic derivation of the sulphur (Sasaki and others, 1984).

The origin of the copper stratabound deposits of the Antofagasta Region has been a matter of long and still unresolved controversy. Detailed discussions about the origin of the Chilean copper stratabound deposits have been published by Sato (1984) and Camus (1985). Initially Ruiz and Ericksen (1962) considered that these ores were epigenetic and that hypogene minerals were deposited by cavity filling or replacement, but later Stoll (1965) and Ruiz and others (1965, 1971) adopted the view that they are syngenetic and volcanic exhalative in origin. Ruiz and others (1965) argued that the host volcanic rocks have an overall anomalously high copper content (200-300 ppm). However, subsequent studies have not substantiated those values but found mean copper contents from 66 to 168 ppm for the Jurassic volcanic rocks (Campano, 1978; Palacios, 1978; Buchelt and Zeil, 1986). An epigenetic origin for the stratabound copper deposits is now widely accepted, mostly because of the hydrothermal alteration associated with ores and the discovery, during the 1980s, of discordant orebodies such as breccia pipes (Palacios and Definis, 1981, 1981b; Dreyer and Soto, 1985; Orquera, 1987). Different genetic interpretations persist, which can be condensed in two basic hypothesis: (a) A diagenetic-metamorphic origin (Losert, 1973; Sato,

1984), and (b) hydrothermal derivation related to subvolcanic intrusive bodies (Espinoza, 1981, 1982; Chavez, 1985; Palacios, 1986).

The first hypothesis presumes the leaching of copper contained within the volcanic sequence, during low grade metamorphic processes, and subsequent concentration of metallic sulfides in favourable sites controlled by the presence of structures, porous strata and subvolcanic intrusives (Losert, 1973; Sato, 1984). The mineralizing fluids are believed to be metamorphic waters, generated by dehydration processes during burial metamorphism. The extensive propylitization of the Jurassic volcanic rocks has long been ascribed to burial metamorphism (see Chapter 2). However, a major objection to the diagenetic-metamorphic hypothesis is that all the reactions involved in the regional prehnite-pumpellyite facies alteration-metamorphism characterizing the Jurassic volcanic sequence are reactions of hydration, thus the volcanic rocks have probably absorbed water instead of liberating fluids to produce mineralization. Metamorphic grades higher than greenschist facies have never been observed in the Jurassic volcanic rocks. Losert (1973, 1974) envisaged an alternative dehydration of the volcanic rocks and fluid mobilization by emplacement of Jurassic batholiths within the volcanic sequence. These major intrusions could have also contributed part of the fluids, sulphur, and metals involved in the mineralization.

The second hypothesis postulates that the copper mineralization is directly associated with small subvolcanic intrusions (dikes, sills, necks) that constituted the feeder conduits for the Jurassic volcanism. A fluid phase separated from the intrusive magma account for the copper mineralization (Espinoza, 1981, 1982; Chavez, 1985; Palacios, 1986). Chavez (1985) also envisages the possible deposition of copper sulfides immediately after the accumulation of the lavas, due to fumarolic activity, and a later remobilization and concentration during the emplacement of subvolcanic intrusions. Even though hydrothermal mineralization genetically related to subvolcanic intrusives may account for the spatial relationship between the stratabound copper deposits and intrusive stocks and dikes, these intrusives are largely barren, and some

of them clearly crosscut orebodies. The mineral assemblage of these deposits (ore, gangue, and hydrothermal alteration) and the homogenization temperatures of fluid inclusions of calcite at Buena Esperanza indicate relatively low temperatures during mineralization, which are not consistent with a direct derivation of mineralizing fluids from the subvolcanic intrusions.

The stratabound copper deposits appear to be formed by low temperature fluids that produced moderate hydrothermal alteration of the host volcanic rocks. The replacement of pre-existent pyrite by copper rich sulfides described in Buena Esperanza (Losert, 1973) and Mantos Blancos (Chavez, 1985) suggests that the copper sulfides may have replaced previously pyritized areas around feeder conduits of the Jurassic volcanism. The idea advanced by Losert (1973) that the emplacement of Jurassic batholiths may have produced the dehydration of the volcanic rocks and contributed primary magmatic fluids for the mineralization is especially appealing. The isotopic data suggest a magmatic derivation of the sulphur, and the copper stratabound deposits usually occur not more than 2 to 6 km from extensive Middle to Upper Jurassic plutons emplaced within the volcanic succession. These intrusive bodies contain abundant copper deposits (actinolite-magnetite-chalcopyrite veins; see below). However, more detailed geological and isotopic studies are required to further constrain possible genetic models for the coastal stratabound copper deposits.

Jurassic volcanic rocks also host many small irregular copper deposits formed of copper oxides. These are concentrated in fracture zones, particularly in the Buena Esperanza-Tres Puntas, Michilla, Sierra Valenzuela, Sierra La Cadena, Sierra El Ancla, Estacion Varillas, and La Isla Districts (Fig. 3.4). These minor copper deposits have been exploited only during periods of higher copper prices, and appear to represent supergene remobilization of hypogene ore minerals contained within the volcanic sequence (Wendel, 1947; Burnol, 1966)

The Jurassic age of the stratabound copper deposits is now relatively well established by radiometric dating (see Chapter 4), but the precise position within the Jurassic period is not yet clear. The radiometric dates at Buena Esperanza (host volcanic rocks 186 ± 14; gabbroic stock 168 ± 5 Ma; see Chapter 4) suggest (but do not prove) a Middle to Late Jurassic mineralization for this deposit.

### 3.2.2.2 Copper-bearing veins hosted by Jurassic plutons

Many copper-bearing veins that occur along the Coastal Cordillera of the Antofagasta Region are hosted by dioritic to granodioritic Jurassic batholiths. The most important are located in the districts of Tocopilla, Gatico, Naguayan, Desesperado, Julia, and Montecristo (Fig. 3.4). These veins were of primary economic importance in the later half of the last century, when Chile was the world's major copper producer. At present they are mostly abandoned. The largest veins are: Minita-Despreciada (Tocopilla district), Toldo-Velarde (Gatico district), and Julia-Reventon (Julia district) (Fig. 3.4). The Minita-Despreciada deposit is composed of six, steeply dipping (60°N to 90°), N70°E trending, *en echelon* veins. Each one is as much as 750 m long, 1 to 2 m wide, and extends to depths of about 670 m (Flores and Hevia, 1952; Klohn, 1961; Alfaro, 1973). The Toldo-Velarde vein (N85°W/85°N-85°S) is 1,700 m long, 1 to 3 m wide, and 500 m in vertical extent. The Julia vein (NS-N10°E/80°E-90°) is 2,000 m long, 1 to 12 m wide, and 370 m in vertical extent. The other numerous copper veins of the Coastal Cordillera are significantly smaller. The copper orebodies along these structures are usually discontinuous: ores concentrate in rich pockets separated by low grade or barren sections along fault zones. Mafic dikes (dioritic, andesitic, lamprophyres) occur along the same fractures. These dikes are locally mineralized, but usually constitute one of the barren wall rocks of the copper-bearing veins.

The hypogene minerals of the veins fill fractures and openings either as irregular and discontinuous veinlets or massive pockets with banded textures and also as a fine dissemination. The hypogene paragenetic sequence of the largest veins is tourmaline-actinolite-quartz-magnetite-hematite-pyrite-chalcopyrite-bornite-calcite (Klohn, 1961; Muñoz, 1942; Ferraris and others, 1973). Strong hydrothermal alteration is associated with these copper deposits (silicification, argillization, chloritization) and is usually restricted to the veins but may extend some metres into the wall rocks.

The coastal copper-bearing veins have a marked vertical mineralogical zonation produced by supergene processes. Typically an upper zone of copper oxides occurs, followed by an intermediate zone of secondary copper sulfides and a lower zone of hypogene sulfides. These zones are well developed in the Minita-Despreciada deposit, where they have a vertical extent of 200, 140 and 330 m respectively. Most of the past exploitation of the veins concentrated in the two upper zones because they are significantly enriched (grades up to 12% Cu). The primary ores in depth have lower grades (2-4% Cu) and have only been mined in the largest veins.

The ore minerals in the oxidized zone are atacamite, chrysocolla, malachite, copper sulfates, cuprite, and minor native copper. The secondary sulfides in the intermediate zone are largely covellite and chalcocite, whereas the primary sulfides at depth are chalcopyrite, pyrite, bornite and locally arsenopyrite. Some of the major veins include also minor amounts of molybdenite and uraninite, as well as traces of nickeline, chloanthite, and cobaltite (e.g., Minita-Despreciada, Toldo-Velarde). Nickel and cobalt minerals also occur in two veins of the Sierra Esmeralda district (Don Rigoberto mine, Anonymous, 1947; Zentilli, 1974). Supergene gangue is composed of limonite, hematite, and gypsum, whereas the hypogene gangue minerals are quartz, amphibole (actinolite-tremolite), magnetite, hematite, apatite, calcite, tourmaline (dravite), and minor K-feldspar.

The characteristics of this type of copper-bearing vein indicate that they are high to moderate temperature hydrothermal deposits (Klohn, 1961; Ruiz and others, 1965; Ferraris and others, 1973), which are genetically associated with emplacement and cooling of Jurassic batholiths. Homogenization temperatures of fluid inclusions from minerals of veins of the Montecristo district range from 275° to 363°C and provide minimum temperature estimates for the mineralization (JICA-MMAJ-SERNAGEO-MIN, 1986). The K-Ar and $^{40}Ar$-$^{39}Ar$ ages of actinolite-tremolite gangue from several copper-bearing veins are mostly concordant with the K-Ar, Rb-Sr, and $^{40}Ar$-$^{39}Ar$ dates of the host granitoids, indicating therefore, that copper-bearing veins were formed during cooling of Middle to Upper Jurassic batholiths (see Chapter 4).

3.2.2.3 Small gold and silver vein deposits hosted by Jurassic plutons

Along the Coastal area south of the Mejillones Peninsula many small gold-bearing veins hosted by Jurassic gabbroic to dioritic plutons occur (e.g., La Salada, Panul, Parañao, and Sierra Esmeralda districts; Fig. 3.4). The veins are usually less than 350 m long, 0.5 m wide, and 100 m in vertical extent. They occur along faults and minor fractures and have a very irregular distribution of gold. These coastal gold-bearing veins have been only exploited in the upper oxidized zone where they have been enriched by supergene processes (grades >20 g/ton), which usually extends down dip no more than 50 m. This upper zone includes fine disseminations and stringers of native gold and minor copper oxides (chrysocolla, malachite, atacamite), with gangue of quartz, hematite, limonite, calcite, as well as rare magnetite, sericite, and tourmaline. The hypogene minerals at depth are chalcopyrite and auriferous pyrite.

The gold vein deposits of the Coastal Cordillera are largely restricted to gabbroic to dioritic plutons that have yielded K-Ar ages ranging from 164 to 115 Ma (Herve and Marinovic, 1989), whole rock

Rb-Sr isochron ages of 200 and 172 Ma (Diaz and others, 1985; Herve and Marinovic, 1989) and zircon U-Pb ages of 191 and 196 Ma (Damm and others, 1986). Thus a Jurassic age is tentatively ascribed to the gold deposits.

A low-grade irregular gold deposit (Gaviota-Maria) occurs in the Sierra Esmeralda district in the Coastal Cordillera south of Taltal. The gold deposit is hosted by silicified Upper Triassic and Lower Jurassic sedimentary rocks. A strongly altered dike from the mineralized area yielded a whole rock K-Ar age of 168 ± 7 Ma (see Chapter 4) suggesting a minimum Middle Jurassic age for the hydrothermal alteration and associated gold mineralization.

Several small, steeply dipping, silver-bearing veins, with diverse orientations occur along the Coastal Cordillera, south of Antofagasta. They are hosted by dioritic-granodioritic Jurassic plutons and by Lower Jurassic limestones (Sierra Esmeralda district). The maximum dimensions of these veins are 1,200 m long, 1.5 m wide and 400 m in vertical extent, but economic ores are very irregularly distributed and limited to discontinuous pockets. The mining of the silver-bearing veins has been restricted to the upper oxidized zone, which has produced ores with grades ranging between 100 to 250 g/ton Ag, and low grades of copper and lead. The oxidized zone contains iodargirite, chlorargirite, and native silver and minor copper oxides (chrysocolla, malachite, atacamite), and lead oxides (cerussite, anglesite). The hypogene minerals are argentiferous galena, pyrite, chalcopyrite, and scarce sphalerite. In addition, in the Sierra Esmeralda district pyrargirite, acanthite and arsenopyrite have been identified (Kuntz, 1928; Travisany, 1976).

### 3.2.3 Mineral deposits in Lower Cretaceous rocks

The Lower Cretaceous rocks of the Coastal Cordillera contain many small copper, gold, silver, manganese, iron and polymetallic (Cu-Ag-Au) deposits (Fig. 3.5). The copper deposits are largely veins

hosted by Lower Cretaceous granodioritic plutons in the southern part of the area. Many contain significant amounts of gold (Pampa Sierra Overa, Sierra Overa, and Pampa San Juan districts). Two copper-bearing breccia pipes hosted by a Lower Cretaceous (biotite K-Ar age 111 ± 2 Ma; Naranjo and Puig, 1984) granodioritic pluton occur in the Sierra Placeres district, and a sub-economic porphyry copper prospect in the Puntillas district (Fig. 3.5). This has yielded whole rock K-Ar ages of 118 ± 15 and 132 ± 8 Ma (see Chapter 4).

In the coastal area south of the port of Antofagasta stratiform copper deposits and veins occur within Upper Jurassic-Lower Cretaceous red beds (El Way district). These deposits constitute one of the few examples of mineralization associated with sedimentary processes in the Antofagasta Region. Concordant copper orebodies (dipping 10°-15° SE) occur at several horizons in clast-supported (permeable) conglomerates and fracture zones within the Caleta Coloso Formation (Espinoza, 1983; Flint and others, 1986). Copper is never found within matrix-rich debris flow deposits of the Caleta Coloso Formation (Flint and others *op. cit.*). The mineralized layers are 0.4 to 6 m thick, up to 110 m long, and extend up to 70 m downdip. The volumetrically most important ore mineral is atacamite, which occurs as an early matrix, rimming detrital grains, as veinlets through brecciated grains, and also as late pore-fillings associated with gypsum. The economic ores consist of sulfide mineral assemblage (chalcopyrite, bornite, chalcocite (djurleite), and covellite) and cuprite. Gangue is formed of hematite, quartz, calcite, dolomite, gypsum, potash feldspar, analcime, and illite. Espinoza (1983) suggested exogenic origin for the copper deposits of El Way district. According to the latter author the ore and gangue minerals were deposited from ground waters containing sulfates, chlorides, and copper ions. The source of the copper was ascribed to leaching of pre-existent copper deposits within the Jurassic volcanic rocks of the Coastal Cordillera. The studies of Flint (1985) and Flint and others (1986) suggested a more complex genesis involving the mixing of diagenetically derived copper-rich brines and sulphur-rich hydrothermal fluids. According to this interpretation uneconomic metal concentrations were transported from the Jurassic

volcanic rocks into the basin as detrital phases and released by diagenetic reactions (the Caleta Coloso red beds were deposited within a 10 by 15 km pull-apart basin formed during the Late Jurassic-Early Cretaceous sinistral strike-slip displacement of the Atacama Fault System; see Section 2.16.2). The precipitation of copper minerals (mainly atacamite) followed authigenic formation of quartz, potash-feldspar, analcime, and calcite and also some secondary porosity generation. The later influx of warm hydrothermal fluids along faults resulted in the precipitation of copper sulfides and the subsequent return to oxidizing conditions produced a second post-sulfide phase of deposition of atacamite.

The gold deposits in Lower Cretaceous rocks are largely small veins hosted by granodioritic plutons (district of Canchas, Quebrada la Peineta, La Isla, Sierra del Pingo, and Sierra Overa). The largest veins occur in the Sierra Overa district, where they are up to 600 to 1,500 m long (Flor mine), 0.5 m wide and 330 m in vertical extent (Overa mine). These are steeply dipping, northwesterly trending veins hosted either by a Lower Cretaceous granodiorite or volcanic rocks. These gold-bearing veins contain also up to 2% Cu and 70 g/ton Ag (e.g., Sierra Overa District). Small silver-bearing veins hosted by Lower Cretaceous intrusive and volcanic rocks occur in the districts of La Isla and Sierra del Pingo, south of Taltal.

Veins and stratabound deposits bearing manganese oxides occur in the southernmost part of the region. These are hosted by Lower Cretaceous volcanic rocks (Sierra del Muerto, Pampa San Juan, and Pampa Sierra Overa districts).

Magnetite vein and irregular deposits are hosted by Lower Cretaceous intrusive and volcanic rocks in the southernmost part of the region (Sierra del Viento, Cachiyuyal, Taltal, Quebrada la Peineta, and Pampa Sierra Overa districts). These iron deposits are small and lack economic significance, but they are the northern tip of an important belt

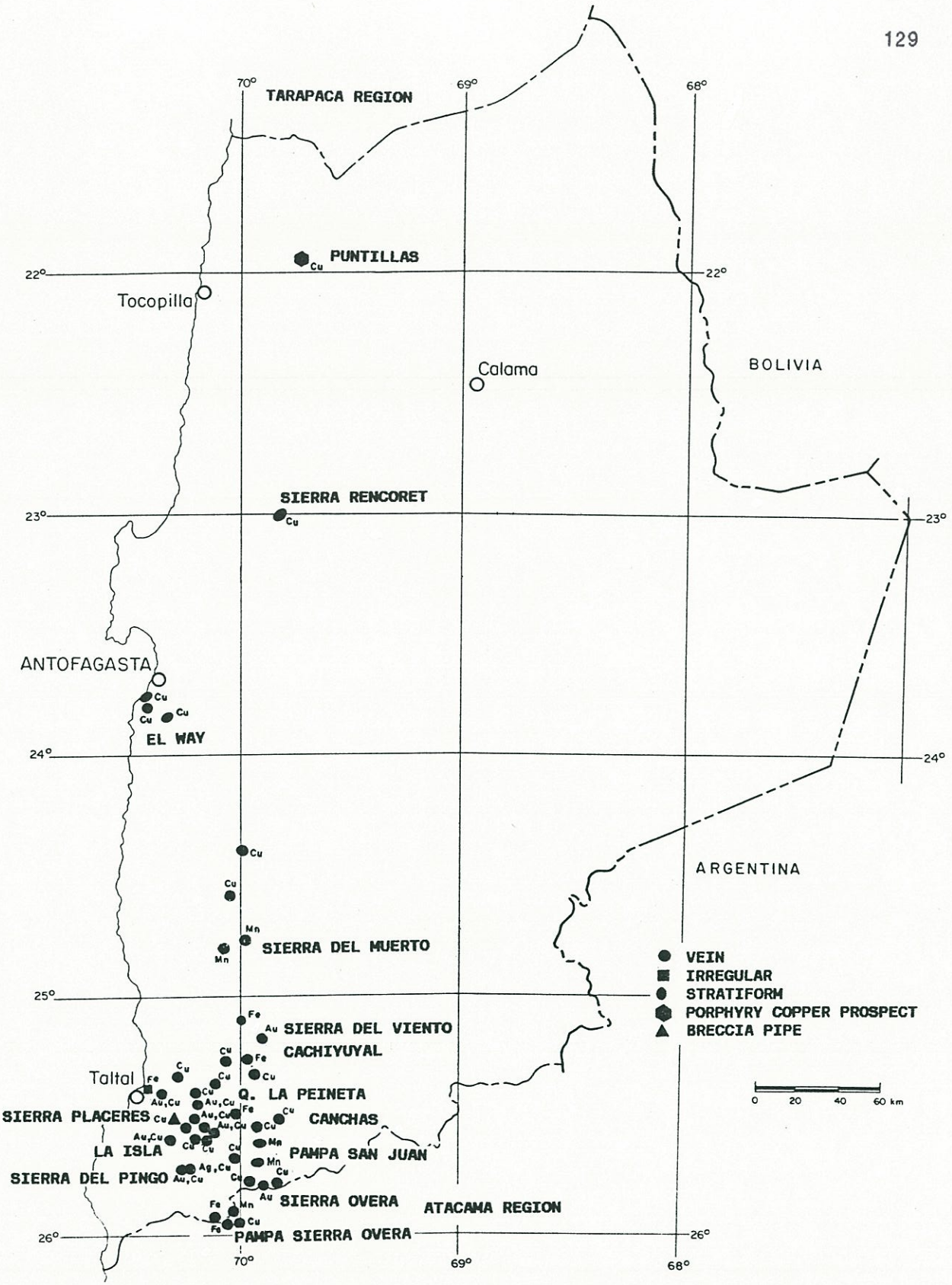


Figure 3.5. Metallic mineral deposits in Lower Cretaceous rocks.

of Cretaceous iron deposits that occur largely in the Atacama and Coquimbo Region, south of the study area (Ericksen, 1976; Sillitoe, 1976).

In spite of the apparent abundance and diversity of Lower Cretaceous metallic mineral deposits, particularly in the southern section of the Coastal Cordillera of the Antofagasta Region, these ore deposits have little economic significance. Therefore this period does not constitute an important metallogenic epoch in the Andean segment under study.

### 3.2.4 Mineral deposits in Upper Cretaceous rocks

The Late Cretaceous is an epoch of uplift and erosion in most of the Antofagasta Region (see Chapter 2), therefore scant Upper Cretaceous igneous rocks or associated metallic ore deposits were preserved. One remarkable exception is the Caracoles silver district, located 155 km northeast of the port of Antofagasta, and is the most important silver mineralization centre of the study area (Kuntz, 1928; Flores, 1976; Cabello, 1978). Silver ores occur in veins hosted by Jurassic limestones and by a stock of tonalitic porphyry, which has yielded a whole rock K-Ar age of 76 ± 4 Ma. The latter date, coupled with other K-Ar, $^{40}Ar$-$^{39}Ar$, and fission track data, suggests a Late Cretaceous silver mineralization (Campanian; see Chapter 4).

Three main steeply east-dipping or vertical, northerly-trending vein systems occur in Caracoles. They are 2,000 to 3,500 m long but are discontinuous due to the displacement by WNW post-mineralization faults. The average width of the veins varies from 1 to 2 m, increasing to 10 m both at intersections with secondary fractures and at places where the veins are hosted by permeable limestones or conglomerates. The richest silver ores occur within the Jurassic sedimentary sequence near the contact with the Upper Cretaceous tonalitic porphyry. The vertical extent of the mine works range from 100 to 200 m, but the Gran Corrida

Flor del Desierto vein system has been exploited in the Deseada shaft to a maximum depth of 310 m and reconnaissance workings extend to 750 m.

The rest of the veins of the Caracoles district are located in clusters 2 km northwest and 3 km southwest of the principal vein systems (Casa de Tablas and La Isla groups). They are hosted by Jurassic sedimentary rocks near to porphyritic intrusions. These veins have NW to WNW or less commonly NNE orientations, are up to 500 m long, 0.5 to 1 m wide, and workings extend to 150 m in depth.

The hypogene minerals at Caracoles are galena, sphalerite, pyrite, freibergite, acanthite, polybasite, pearceite, aramayoite, and minor chalcopyrite and arsenopyrite. These are preserved at depths of more than 150 m and occur both as disseminations and veinlets along the major structures. The gangue is composed of barite, quartz, and calcite. The upper 80 m of the veins are oxidized and include native silver, chlorargirite, iodargirite, bromargyrite, embolite, and both lead and zinc carbonates and sulfates. The zone between about 80 to 150 m in depth contains secondary sulfides such as acanthite, stephanite, and ruby silvers (pyrargirite, proustite). Strong to moderate silicification and argillization is associated with silver ores. This hydrothermal alteration is pervasive in the porphyritic stocks, whereas in the Jurassic sedimentary rocks it is restricted to a narrow band bordering the veins.

The characteristics of the silver-bearing veins and associated hydrothermal alteration indicate epithermal origin. The term "epithermal" was defined by Lindgren (1922, 1933) to include a broad range of precious metal, base metal, mercury, and stibnite deposits, which he believed formed from aqueous fluids charged with igneous emanations at low temperature (<200°C) and moderate pressure. It is now generally accepted that the fluids may be dominantly of meteoric origin at slightly higher temperatures (200°-350°C), and pressures of less than a few hundred bars are present during the formation of this type of deposits (e.g. Heald and others, 1987).

Some authors (Flores, 1976; Amstutz and others, 1985) have suggested that silver ores at Caracoles originated by the remobilization of silver contained within the Jurassic calcareous host rocks, as a result of convective circulation of meteoric fluids driven by the heat from subvolcanic stocks. Although this may be true, the epithermal silver deposits of the study area are directly associated with Upper Cretaceous to Paleocene volcanic rocks and subvolcanic stocks (see below) with many deposits completely unrelated to calcareous sequences suggesting instead a primary magmatic derivation of silver. Lead isotopic data reported by Puig (1988) for galenas from Caracoles show a very restricted variation from 18.586 to 18.592, 15.631 to 15.636, and 38.554 to 38.575 on $^{206}Pb/^{204}Pb$, $^{207}Pb/^{204}Pb$, and $^{208}Pb/^{204}Pb$ ratios respectively. These values are similar to those of mineral deposits from "mature arc volcanics" (Zartman, 1984) and are compatible with lead derivation from an enriched upper mantle with contribution of crustal leads. The association of primary silver mineralization with argentiferous galenas may suggest a similar source for the silver.

### 3.2.5 Mineral deposits in Paleocene-Eocene rocks

The ore deposits hosted by Paleocene-Eocene rocks are rich epithermal silver deposits (districts of Huanchaquita, El Inca, Chimborazo, Pan de Azucar, Cachinal de la Sierra, Vaquillas, and Sierra Juncal), gold vein deposits (San Cristobal, El Guanaco, and Sierra Gorda districts), sub-economic porphyry copper deposits (Sierra Gorda, Centinela, Lomas Bayas, Fortuna del Cobre), and copper-bearing breccia pipes (Quetena, Copucha). They occur along a NNE trending belt in the central part of the Antofagasta Region (Fig. 3.6) coinciding with the distribution of Lower Tertiary igneous rocks (see Chapter 2). Within this area there are several prospects, mostly Lower Tertiary hydrothermal alteration zones, which have preserved features characteristics of near surface environments, such as sinter deposits, "silica caps," and

hydrothermal breccias (Rivera and Stephens, 1988). Most of the dated deposits are Paleocene in age (see Chapter 4).

3.2.5.1 Epithermal silver vein deposits hosted by or associated with Paleocene igneous rocks

The epithermal silver vein deposits are largely hosted by Paleocene andesitic to dacitic volcanic rocks, or coeval porphyritic intrusive rocks. At Vaquillas district the host rocks are Lower Cretaceous sedimentary rocks, but the veins occur spatially associated with Late Cretaceous to Paleogene porphyritic intrusions. The maximum length of the veins is 1,500 m (Cachinal de la Sierra) and the average width 1 to 2 m, although at vein intersections pockets attain up to 20 m in width. The veins have been exploited down to 50 to 150 m and exceptionally down to 320 m (Arturo Prat mine of Cachinal de la Sierra District). The exploitation has largely been limited to ores enriched by supergene processes (oxidized ores and secondary sulfides and sulfosalts). The mineralogy of the veins is akin to that previously described for the Caracoles district. The oxidized ores include chlorargirite, iodargirite, bromargyrite, and native silver, which are disseminated within a mass of clay minerals, quartz, limonite, calcite, gypsum, barite, and minor copper, lead, and manganese oxides. The average grades of the oxidized ores range usually between 200 to 300 g/ton Ag. The zone between about 80 to 150 m in depth contain secondary sulfides such as acanthite and sulfosalts (e.g., pyrargirite, proustite). This zone has produced ores with grades up to 700 g/ton Ag. Primary ores occur at depths of more than 150 m and include argentiferous galena, sphalerite, minor pyrite, and chalcopyrite. The primary ore minerals occur in veinlets, massive bodies, and disseminated within a gangue of quartz, calcite, barite, hematite, manganese oxides, and adularia. The host rocks usually are affected by hydrothermal alteration around the veins including a strong silicification, sericitization, and argillization. Veinlets 1 to 2 mm thick composed of quartz with adularia and fluorite criss-cross the altered

rocks at Cachinal de la Sierra. Fluid inclusion data from Cachinal de la Sierra show homogenization temperatures ranging between 195° to 330°C and salinities from 0 to 4.8% $NaCl_{eq}$ (JICA-MMAJ-SERNAGEOMIN, 1986).

The silver-bearing veins have characteristics typical of epithermal origin (*cf.* Schmitt, 1950) and were formed during the Paleocene (K-Ar 60 to 50 Ma; see Chapter 4). They are genetically associated with andesitic-dacitic volcanic complexes and related subvolcanic intrusions. At Cachinal de la Sierra silver mineralization is related to two resurgent calderas whose associated volcanic and subvolcanic rocks have yielded K-Ar ages ranging from 62 to 55 Ma (Puig and others, 1988).

3.2.5.2 Epithermal gold vein deposits hosted by Paleocene igneous rocks

Gold epithermal vein deposits occur in the El Guanaco, San Cristobal, and Sierra Gorda districts (Fig. 3.6). The most important are those of the El Guanaco district, where 20 veins were intensively exploited from 1886 to 1928 producing about 30 ton of metallic gold. El Guanaco is the second largest Chilean gold deposit (after El Indio).

Gold-bearing veins are hosted by Paleocene rhyolitic ignimbrites (El Guanaco district) and Paleocene granodioritic to dioritic rocks (San Cristobal, Sierra Gorda districts). Some of the veins at Sierra Gorda are hosted by Lower Cretaceous volcanic rocks, but consistently near Paleocene intrusions. The veins occur along steeply-dipping local faults with different orientations in each district. At El Guanaco the largest veins are up to 1,000 m long, 0.5 to 2 m wide, and have been recognized down to 270 m. The veins of San Cristobal and Sierra Gorda are considerably smaller and ore is concentrated at fracture intersections and zones of strike or dip changes. This is particularly notable at San Cristobal, where numerous mineralized structures exist (Rivera, 1980) but

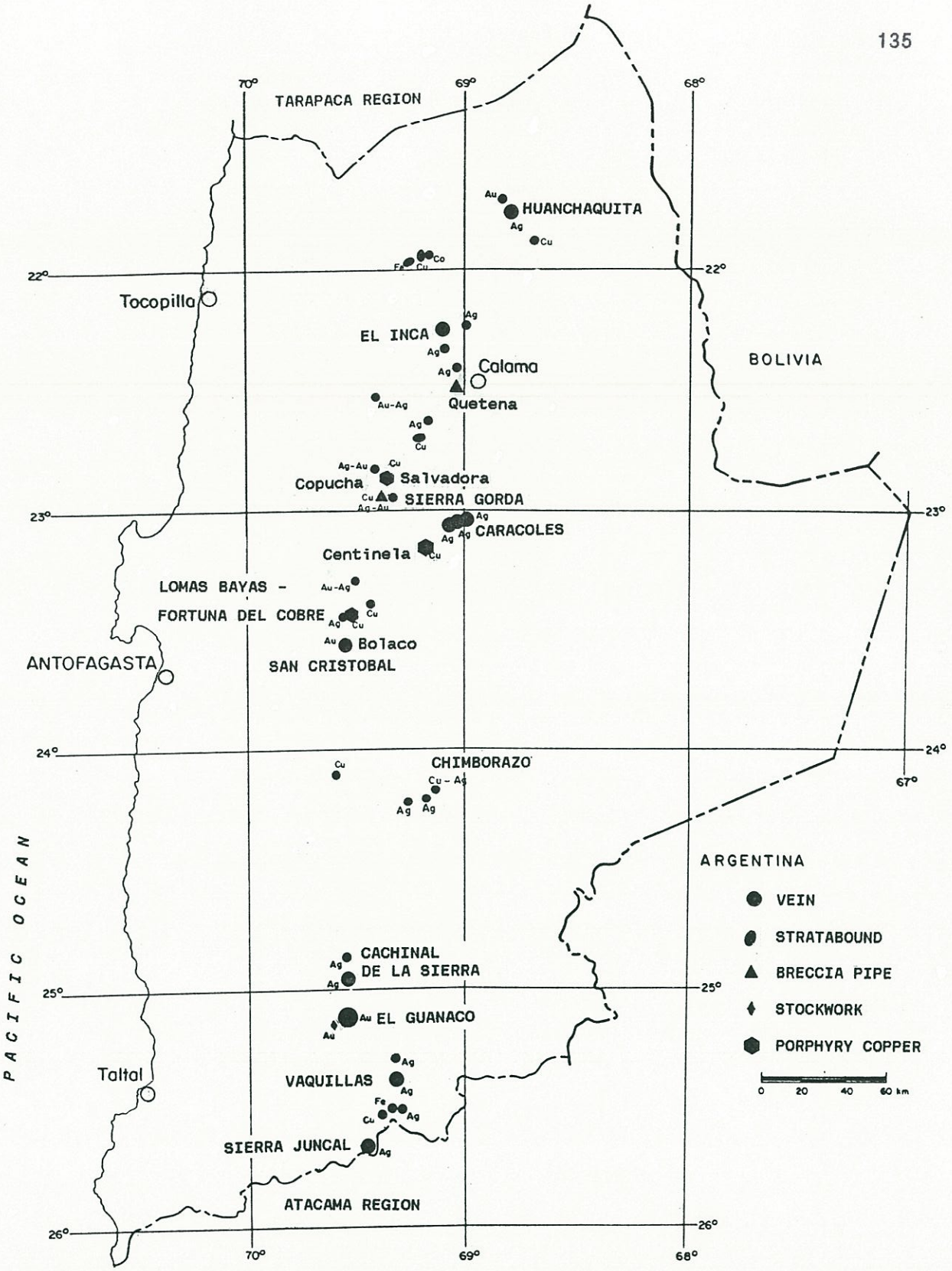


**Figure 3.6.** Metallic mineral deposits in Upper Cretaceous to Eocene rocks.

mining has concentrated on one pocket 80 m long, 0.7 m wide and 170 m in vertical extent (Bolaco mine). The San Cristobal district is now considered as an important gold prospect, which may contain a significant amount of low grade-ore amenable to bulk mining (Lowell, 1987).

Intense hydrothermal alteration is associated with gold-bearing veins. It is particularly extensive and pervasive at El Guanaco, where the rhyolitic tuffs have been affected by silicification, advanced argillic alteration, and chloritization. Extreme silicification is typically associated with mineralized veins accompanied by barite, alunite, natroalunite, anhydrite, and kaolinite. The veins are surrounded by haloes from 2 to 200 m wide, where alunite and barite have replaced pre-existent feldspar in the rocks, as well as kaolinite, pyrophyllite, and traces of dickite. The matrix of these rocks is strongly silicified and includes interstitial kaolinite. Propylitization (chlorite, epidote) occurs in external haloes (Puig and others, 1988). The hydrothermal alteration is more localized near the veins in the other districts, but is analogous to that described above.

The upper 100 m of the veins are oxidized and enriched by supergene processes. In this zone native gold (finely disseminated, flakes, small veinlets, films coating fractures, scales, and dendrites) occurs with quartz, and minor barite, calcite, opal-chalcedony, hematite, and limonite; and many copper, lead, silver, sodium and aluminium oxides. Particularly abundant are copper chlorides. The gold-bearing ores in the supergene oxidized zone occur filling fracture zones both in the primary veins and within the fractured and altered host rocks, thus forming economic orebodies 10 m or more in width (Pohl, 1985; Llaumet, 1979).

The exploitation of the gold vein deposits has mostly been restricted to the upper oxidized enriched zone, which has produced ores with more than 10 g/ton Au. A lower zone of secondary sulfides, or partly oxidized, has only been exploited in some mines producing ores up to 10 g/ton Au. The hypogene ores at depth have not been exploited because gold grades are significantly lower (0.5 to 2 g/ton). The

hypogene ores at El Guanaco include enargite, auriferous pyrite, and minor chalcopyrite, whereas at Sierra Gorda and San Cristobal auriferous pyrite is accompanied by subordinate amounts of galena, sphalerite, tetrahedrite, and chalcopyrite. A zone with secondary chalcocite and covellite exists at El Guanaco, whereas in the veins of the other districts only a zone of mixed oxides and primary sulfides developed (Kuntz, 1928; Llaumet, 1979; Rivera, 1980; Pohl, 1985).

The gold-bearing veins are typical epithermal deposits, which according to their ore and alteration mineralogy may be classified as "acid-sulfate" type of Hayba and others (1986) and Heald and others (1987). The gold mineralization of El Guanaco, Sierra San Cristobal and Sierra Gorda is primarily related to Paleocene igneous activity according to K-Ar and $^{40}Ar$-$^{39}Ar$ dating (see Chapter 4), but the formation of economic orebodies is a consequence of subsequent supergene processes.

In summary, precious-metal (Au and Ag) epithermal deposits constitute an important mineral belt in the Antofagasta Region. They were largely formed during the Paleocene based on geochronological data (see Chapter 4). The mineralization at Caracoles district seems have occurred somewhat earlier during the Late Cretaceous. The formation of economic orebodies is related to later supergene processes.

### 3.2.5.3 Paleocene porphyry copper and breccia pipe deposits

Sub-economic porphyry copper deposits occur in isolated mountainous ranges in the eastern section of the Intermediate Depression (western section of the Domeyko Metallogenic Belt). These are Sierra Gorda, Lomas Bayas, Fortuna del Cobre, and Centinela (Fig. 3.6). Copper-bearing breccia pipes (Copucha, Quetena, Centinela) are associated with the porphyry copper deposits.

The porphyry copper deposits at Sierra Gorda, Lomas Bayas and Fortuna del Cobre are associated with Paleocene granodioritic porphyries (64 to 59 Ma; see Chapter 4). The Centinela deposit is hosted by a tonalitic porphyry of Eocene minimum age (sericitized whole rock K-Ar age of 44.3 ± 1.5 Ma; Chapter 4). The copper ores are irregularly distributed, and occur within both the porphyritic stocks and the surrounding host rocks. The orebodies are irregular in shape, isolated, concentrated on fractured zones, and distributed within areas up to 3 by 1.5 $km^2$ (Sierra Gorda). Hydrothermal alteration associated with these porphyry copper deposits is silicification, sericitization, tourmalinization (brecciated bodies), and argillization. The latter is probably partly supergene in origin. The alteration is extensive and pervasive at Sierra Gorda, Fortuna del Cobre, and Centinela, whereas it is more restricted and less pervasive at Lomas Bayas. Potassic alteration is lacking in all these deposits.

Primary sulfide ore have only been recognized in drill cores. It is usually low grade (<1% Cu) and contains disseminated pyrite, chalcopyrite, and minor molybdenite. The upper portion of the deposits, down to 140-250 m, is partly leached and oxidized. Copper ores in this upper zone are erratic including mostly atacamite, malachite, cuprite, chalcanthite, and other subordinate mineral species. Gangue is composed of limonite, jarosite, quartz, tourmaline, hematite, sericite, and abundant clay minerals. These minerals are distributed within fractures, veinlets, and minor disseminations, and within the matrix of tourmaline breccias. Minor amounts of chalcocite and covellite occur mixed with the copper oxides. The overall copper content of the oxidized zone is low (0.1 to 0.4% Cu) and economic grades (2 to 4% Cu) are restricted to pockets within fractured zones. They have been exploited during periods of high copper prices down to 125 m (Kuntz, 1928; Serrano, 1960; Sepulveda, 1963; Sillitoe and Newmann, 1970; Quezada, 1967; Simic, 1971).

The Paleocene porphyry copper deposits have no significant enriched supergene zones, but the occurrence of relict supergene sulfides within the oxidation zone suggests that an early

cementation zone was oxidized due to lowering of the water table (see Section 3.3). The only exception is a body of tourmaline breccia at Sierra Gorda (Salvadora mine). Here, average grades of 0.97% Cu (between 140 and 340 m in depth) show enrichment, with supergene covellite and chalcocite, to grades of 1.15% Cu at shallow levels (between 140 and 270 m in depth) (Simic, 1971). At Sierra Gorda uranium minerals (metazeunerite and torbernite) occur within the oxidized zone related to aplitic and granitic facies of the porphyry. Uranium grades are erratic ranging from traces to a maximum 1% $U_3O_8$ in the area of the Catalina, Salvadora, and San Armando mines (Serrano, 1960).

The origin of these porphyry copper deposits is related to hydrothermal processes associated with emplacement of Paleocene porphyritic stocks. Subsequent supergene processes produced an upper leached-oxidized zone. The occurrence of minor chalcocite and covellite within the leached-oxidized zone suggests an earlier development of a zone with secondary sulfides that was subsequently oxidized due to lowering of the water table (Sepulveda, 1963).

The copper-bearing breccia pipes are cylindrical, steeply dipping bodies, with elliptical plan sections 230 to 250 m long, 65 to 70 m wide, and recognized down to 380 m (Copucha). They are composed of angular and strongly altered fragments of the host rocks (silicification, sericitization, and argillization). The breccia fragments usually range from 1 cm to 50 cm in size and are cemented by a network of veinlets of black tourmaline, quartz, copper oxides, and fine grained material as matrix. The Copucha breccia pipe is hosted by a 63 Ma granodiorite (see Chapter 4) and the Quetena breccia pipe is hosted by Lower Cretaceous andesites but near a Paleocene stock of andesitic porphyry (March and Zeihen, 1948; Marinovic and Lahsen, 1984). Tourmaline breccias also occur within the Sierra Gorda and Centinela porphyry copper deposits. The copper ores occur mostly within the tourmaline-rich matrix of the breccias and as minor dissemination within the breccia fragments. The Copucha and Quetena deposits include an upper leached-oxidized zone with copper sulfates, atacamite, and chrysocolla and gangue of quartz,

hematite, limonite, tourmaline, and iron sulfates. The oxidized zone extends down to 150 m at Quetena and 230 m at Copucha and the average grades are 2 and 1.4% Cu respectively (March and Zeihen, 1948; Anonymous 1967). At Copucha minor chalcocite occurs within the oxidized zone, suggesting that the oxidation of an earlier zone of secondary sulfides took place (Ortiz, 1969). Hypogene ores have only been reached by drilling and they include pyrite and chalcopyrite with low copper grades. No enrichment with secondary sulfides was recognized (Ortiz, 1969).

The copper-bearing breccia pipes are genetically related to late-stage hydrothermal processes associated with epizonal emplacement of porphyritic stocks during the Paleocene. The formation of these brecciated bodies correlates with the formation of numerous breccia pipe copper deposits in the Atacama Region, south of the study area (Sillitoe and Sawkins, 1971; Zentilli, 1974).

### 3.2.6 Mineral deposits in Upper Eocene to Lower Oligocene rocks

Upper Eocene to Lower Oligocene porphyritic stocks that occur along the Domeyko Cordillera are associated with the most important porphyry copper deposits of the study area. They host the Chuquicamata, La Escondida, El Abra, El Salvador, Potrerillos, Quebrada Blanca, and Copaquire porphyry copper deposits (Fig.3.7). Chuquicamata is a giant porphyry copper. The main orebody initially contained more than $3.9 \times 10^9$ tons of ore with an average grade of 1.16% Cu (Ambrus, 1979). More than $1 \times 10^9$ ton 1.6% Cu have been exploited since 1915 and remaining resources are about $2.5 \times 10^9$ tons 1.03 % Cu. The entire Chuquicamata system, including the orebodies of Chuqui Norte porphyry copper and the Chuqui Sur exotic copper deposit totals $8.85 \times 10^9$ tons of 0.46% Cu (Sisselman, 1978; Sillitoe, 1981). The more recently discovered La Escondida (Utah Mines Ltd. in 1981) contains $1.76 \times 10^9$ tons of ore with an average grade of 1.59% Cu (at a 0.7% Cu cutoff grade; Ojeda, 1986). El Abra includes $1.37 \times 10^9$ tons of 0.59% Cu (at 0.4% Cu cutoff grade; Ambrus, 1977). These

porphyry copper deposits are, at least, one order of magnitude larger than any other type of metallic deposits of the Antofagasta Region. They constitute one of the largest copper concentrations in the world and the outstanding metallogenic characteristic of the study area. A general description of these deposits follows and a detailed metallogenic examination is presented in Chapter 7.

The copper-bearing porphyries are mostly of granodioritic composition, but quartz-dioritic, quartz monzonitic, monzonitic, and granitic porphyries also occur (see Section 7.2.7). They were emplaced between 41 and 31 Ma (see Chapter 4). The copper ores are typically hosted by several porphyritic stocks with distinctive textures or diverse composition (quartz monzonite, granodiorite, granite), which represent separate intrusive pulses. Usually only one or two of these stocks host the copper ores (e.g., El Abra, Ambrus, 1977; El Salvador, Gustafson and Hunt, 1975; La Escondida, Ojeda, 1986). A granodioritic porphyry occurs at Chuquicamata with granitic to monzonitic facies that have been attributed by Ambrus (1979) to the widespread growth of potash-feldspar crystals during an intense phase of potassic alteration. Its textural variations were the result of uneven cooling conditions within a single pluton (14 km long, 1 to 2 km wide). The same view was advocated by Alvarez and others (1980) who distinguished three main textural variations within the granodioritic Chuquicamata porphyry: the "East," "West," and "Banco" porphyries. Alternatively Alvarez and Aracena (1985) suggested that these may represent distinct intrusive pulses. These porphyries do not show significant differences in major element petrochemical characteristics and their biotite K-Ar dates are concordant (ranging from 32.6 [2] to 33.8 Ma; Alvarez and Aracena, 1985).

The orebodies of the major porphyry copper deposits are essentially irregular stockworks. The largest one is the main orebody of

---

[2] Age recalculated with new constants (Steiger and Jäger, 1977); the original date of 31.8 ± 0.9 Ma reported by Alvarez and Aracena (1985) was obtained in 1968 and calculated with old constants.

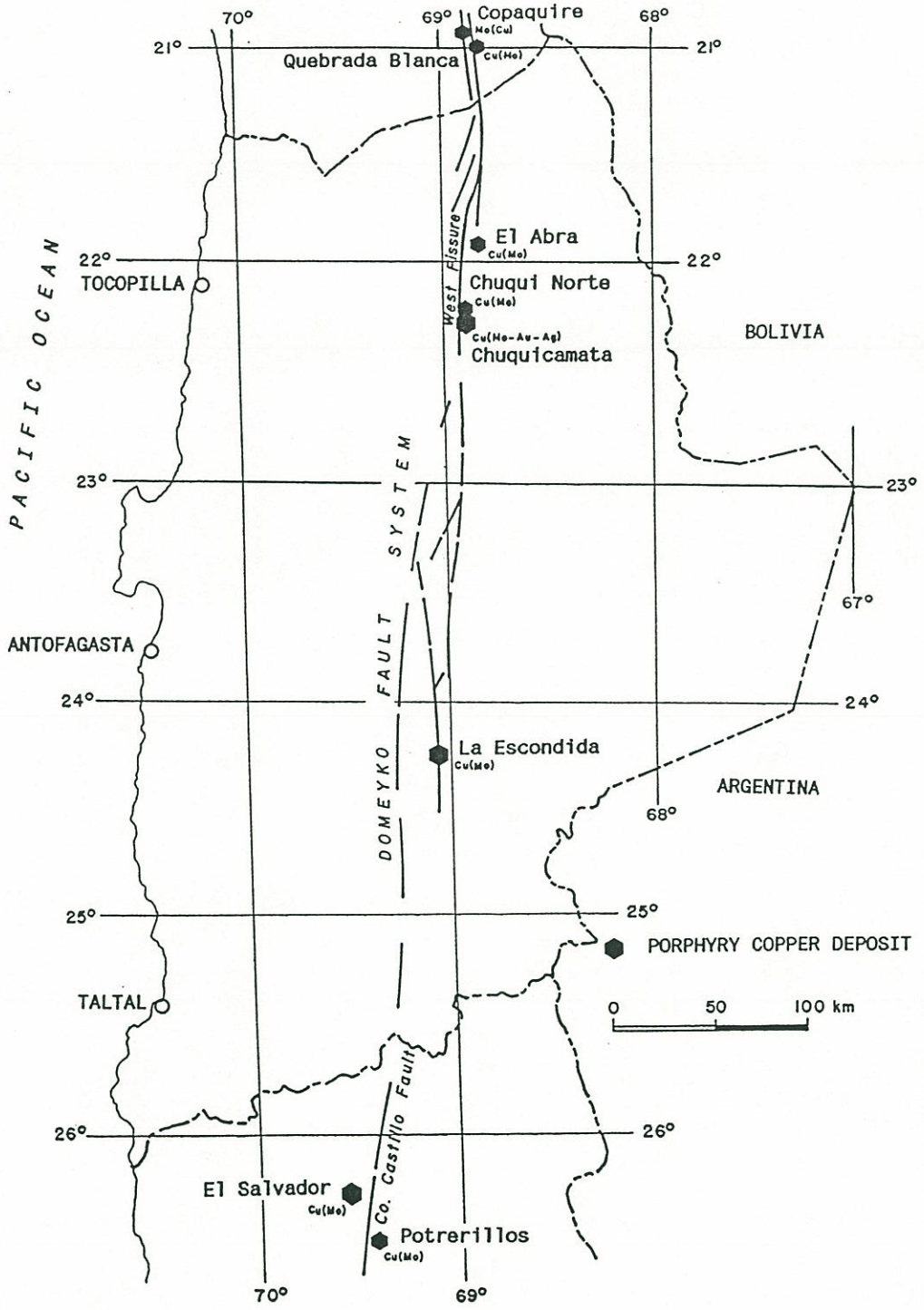


**Figure 3.7.** Upper Eocene - Lower Oligocene major porphyry copper deposits.

Chuquicamata: 3.5 km long, 1.0 km wide, and has been recognized down to 1.5 km. Commonly there is a core of hypogene chalcopyrite-bornite associated with potassic alteration surrounded by a zone of chalcopyrite-pyrite (with minor molybdenite) associated with phyllic alteration. The amount of hypogene sulfides decrease outwards, and usually the proportion of pyrite increases. Hypogene grades are lower than 1% Cu: mostly between 0.3 and 0.6%. The orebodies show a marked vertical mineralogical zonation produced by supergene processes including an upper leached-oxidized zone, followed by a zone of secondary sulfides and deepest hypogene sulfides. These zones are described in Section 3.3.2.

The major porphyry copper deposits are aligned conspicuously along the domain of the Domeyko Fault System (Fig. 3.7; see Chapter 7). Structural control is obvious at Chuquicamata (Lopez, 1939; 1942) where the emplacement of the porphyry appears to have taken place within a tensional site within an active right lateral strike-slip fault system (see Section 7.2.11). Consequently, several authors have suggested that the faults exerted a fundamental control on the emplacement of the porphyritic intrusions (Frutos, 1973, 1975, 1982; Hollister, 1978; Ambrus, 1979; Oyarzun and Frutos, 1980; Alvarez and others, 1980; Hunt and others, 1983; Ojeda, 1986; Olson, 1989). Accordingly, the prevalent view is that the faults were essential in originating these giant porphyry copper deposits. This study forwards instead the notion that the spatial association between the porphyries and the fault system is the result of the nucleation and development of strike-slip faults along the weak zone defined by the magmatic front itself (see Section 2.16.5). Tensile fractures at Chuquicamata have obviously provided openings for hydrothermal fluids and controlled the location of hydrothermal activity and sulfide deposition (see Section 7.2.11), but such a significant structural control is lacking in other porphyry copper deposits of this region (e.g., El Salvador, Gustafson and Hunt, 1975; El Abra, Ambrus, 1977). Neither is this control apparent in the major porphyry copper deposits of southern Peru or central Chile (Sillitoe, 1981). Thus the fault system does not seem essential to generate this type of copper deposit.

### 3.2.7 Mineral deposits in Miocene to Holocene rocks

Miocene to Holocene igneous rocks constitute a prominent volcanic chain in the easternmost section of the Antofagasta Region. It is part of the Central Volcanic Zone of the Andes (CVZ; Thorpe and others, 1984). Few metallic ore deposits have been discovered within the Antofagasta section of this volcanic belt (Fig. 3.8). The most prominent are the El Laco volcanogenic iron deposit and other considerably smaller iron deposits. Subordinate occurrences of silver, antimony and tin occur at Nevados de Poquis volcano, and minor concentrations of covellite exist within sulphur deposits at Aucanquilcha volcano. In addition, many solfataric sulphur deposits (>50) occur associated with strato-volcanoes. Two exogenous copper deposits (Chuqui Sur and Leonor) are hosted by Oligocene-Miocene gravels and red-bed copper deposits occur within a section of the Upper Oligocene - Lower Miocene sedimentary sequence at San Bartolo.

The paucity of metallic ore deposits associated with the Miocene to Recent volcanic chain is attributable to the virtual lack of erosion since the Middle Miocene in the Antofagasta Region. This is the result of a combination of geomorphologic and climatic factors (see Chapter 1 and 2) contributing to the almost intact preservation of Miocene volcanic forms. Sillitoe (1988) stated that copper deposits less than about 4 Ma old are generally absent in the Andes, because they are yet to be unroofed. In the desert Antofagasta segment of the Andes this is probably true for metallic deposits less than about 15 Ma old. Although significant underground hydrothermal mineralizing processes probably developed during the Miocene and Pliocene, as attested by covellite occurrences within solfataric sulphur deposits at Aucanquilcha volcano (Clark, 1970), and minor silver, antimony, and tin occurrences at Nevados de Poquis volcano, no important deposits have been exhumed. This view is further supported by the occurrence of rich epithermal gold and silver deposits within the volcanic chain farther south in the Atacama Region

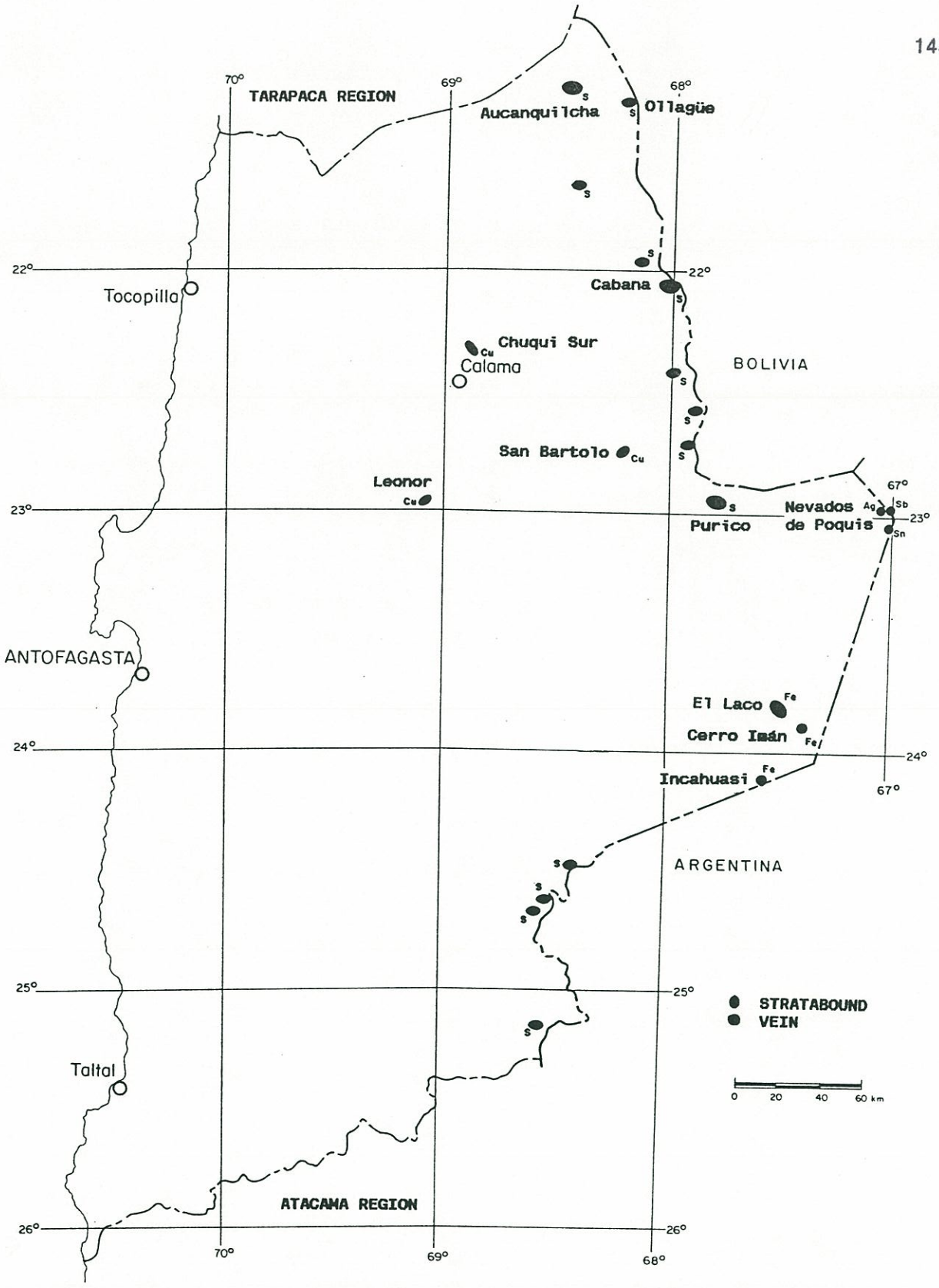


Figure 3.8. Mineral deposits in Miocene to Holocene rocks.

(26°30' to 28°00' S; Cabello, 1986). There Neogene erosive processes have been relatively more active due to relatively less arid conditions, and particularly because in sharp contrast with the endorheic drainage systems of the Antofagasta Region, the rivers crossing the southern desert (Atacama Region) have long been draining to the sea (Mortimer, 1973).

3.2.7.1 Iron deposits hosted by Miocene and Pliocene volcanic rocks

El Laco iron deposit is located in the Altiplano in the easternmost section of the Antofagasta Region at 4,500 to 5,100 m of altitude (Fig. 3.8). It is composed of four main stratabound orebodies (Laco Norte, Laco Sur, San Vicente Alto, Rodados Negros), three minor irregular orebodies (San Vicente Bajo), and three vein orebodies (Cristales Grandes, Laquito and part of Rodados Negros). The proven and probable reserves of these orebodies are 184.1 x $10^6$ tons averaging 63-64% Fe (information provided by Minera del Pacifico, 1985). The iron orebodies circle the Pliocene Pico El Laco volcano and are mostly composed of magnetite (partially martite) and minor hematite. The host rocks are calc-alkaline andesitic lavas and pyroclastic rocks that erupted from a central crater (Pico El Laco). These volcanic rocks are strongly altered by solfataric activity, they are bleached and typically show an assemblage of quartz, tridymite, alunite, natroalunite, limonite, sericite, chlorite, clay minerals, gypsum, and native sulphur.

The stratabound iron orebodies have textural and physical characteristics, such as the development of blocky flows, convolute laminations, ropy surfaces (typical of pahoehoe lavas), pyroclastic inclusions, and abundant vesicles, bubbles, and gas escape tubes that indicate their extrusive origin (Park, 1961; Haggerty, 1970; Henriquez and Martin, 1978). The bodies are lenticular or irregular with a maximum thickness of 60 m. Their shape at the surface is circular, ellipsoidal, or crescent-shaped, with diameters of 300 to 900 m. The magnetite shows spherulitic, dendritic, and idiomorphic textures

(Henriquez and Martin, 1978). Gangue minerals (apatite, quartz, alunite, rutile, plagioclase, and sanidine) constitute only a minor proportion by volume of the ore.

The irregular body (San Vicente Bajo) and the veins are composed of massive magnetite. They crosscut the host volcanic rocks and have been interpreted as subvolcanic intrusions (Henriquez and Martin, 1978). San Vicente Bajo is 350 m long, 250 m wide, and has been recognized down to 45 m. The veins are dike-like up to 300 m long, and 3 to 15 m thick. The gangue minerals are more prominent within the intrusive bodies and include apatite, diopsidic pyroxene, and scarce quartz and actinolite.

The characteristics of the iron deposits at El Laco indicate that they are both extrusive and subvolcanic intrusive bodies of magmatic magnetite, which are a remarkable example of iron deposits associated with volcanic activity (Park, 1961; Rogers, 1968; Henriquez and Martin, 1978). Fission track dating of apatite[3] from the El Laco magnetite bodies has given an age of 2.1 ± 0.2 Ma (see Chapter 5), which is concordant with the K-Ar whole rock age of 2.0 ± 0.3 Ma obtained by Gardeweg and Ramirez (1985) for an andesite from El Laco volcano, thus indicating that the iron bodies were emplaced during the volcanic activity that constructed the El Laco volcano. According to Wegner (1978) the magnetite rich magma was produced by fractional crystallization, whereas Henriquez (1981) postulated the segregation from a primary magma of two immiscible fractions one rich in magnetite and the other silicic. Some authors (Thomas, 1970; Oyarzun, 1974; Oyarzun and Frutos, 1974) have also suggested that the El Laco iron deposit was originated by the remobilization of iron from underlying Paleozoic ferruginous strata. There is no concrete geological evidence supporting such ideas and thus a deep origin associated with calk-alkaline El Laco volcano as suggested by Henriquez (1975; 1981) and Werner (1978) is now widely accepted.

---

[3] Apatite samples provided by Moyra Gardeweg.

Other minor iron deposits that occur within the volcanic chain are the Cerro Iman and Incahuasi deposits. Cerro Iman is located 15 km east of El Laco. It is formed by three main veins hosted by Miocene andesites and a Late Miocene monzonitic porphyry. These veins are composed of massive hematite and specularite and have north-south and northwest-southeast orientation, vertical dip, exposed lengths of 300 to 1,200 m, and widths to 4 m (Gardeweg and Ramirez, 1985).

Incahuasi, located 26 km south of El Laco (Fig. 3.8), includes two main veins hosted by a monzonitic porphyry ascribed to the Late Miocene. The veins have N35°W/60°E and N70°W/70°NW orientations, exposed lengths of 50 m, and widths of 3 m. The dominant ore mineral is massive magnetite, with minor specularite with gangue of apatite, and actinolite. The apatite[4] from this deposit has yielded a Late Miocene fission track date of 10.3 ± 1.6 Ma, which is concordant with whole rock K-Ar ages of 10.7 ± 0.5 and 10.5 ± 0.9 Ma obtained in the northern flank of Incahuasi volcano by Gardeweg and Ramirez (1985).

3.2.7.2 Silver, antimony and tin occurrences at Nevados de Poquis volcano

Several veins bearing silver, antimony, or tin occur at the Nevado de Poquis area. These are small deposits and occurrences that lack economic importance, but constitute further examples of metallic mineral deposits associated with Miocene-Pliocene igneous rocks of the Antofagasta Region. The silver and antimony deposits are hosted by a dacitic porphyry (Poquis Porphyry) that occurs in the easternmost section of the region, on the northern foothills of the Nevados de Poquis volcano. The veins range from 10 to 50 m in length, and 5 to 30 cm in thickness. Silver grades from 2 to 488 g/ton in veins composed largely of limonite and manganese oxides, which are surrounded by argillized haloes, and manganese veinlets (Anonymous, 1975; Travisany and Diaz, 1978). Antimony

---

[4] Apatite samples provided by Moyra Gardeweg.

occurs within 12 small veins hosted by the same porphyry within an area of 750 x 170 $m^2$. These veins are surrounded by silicified haloes of about 10 m wide (Wendell and Weissemborn, 1940). The ore mineral is stibnite, with gangue of quartz, and marcasite; the veins lack economic value due to their small dimensions (Travisany and Diaz, 1978). Both silver and antimony-bearing veins are epithermal deposits probably associated with emplacement of the Poquis Porphyry, which has been dated by Marinovic (1979) at 12.9 ± 0.5 Ma (biotite K-Ar age).

The only tin deposits in the Antofagasta Region occur on the southeast flank of the Nevado de Poquis volcano, 2 km west of the Chilean-Argentinean border. They are small cassiterite-hematite veins up to 10 m long, and 15 cm wide, developed along N50°W fractures (Wendell and Weissemborn, 1940). They are hosted by dacitic lavas ascribed to the Pliocene by Gardeweg and Ramirez (1985). These tin occurrences are uneconomic, but they constitute one of the rare examples of tin mineralization in the Chilean Andes.

### 3.2.7.3 Sulphur deposits in Miocene to Holocene volcanoes

Numerous deposits of native sulphur occur on Miocene and Pliocene volcanoes in the easternmost section of the area (Fig. 3.8). Although the sulphur is a nonmetallic element, its deposits are associated with igneous processes similar to most of the metallic deposits of the Antofagasta Region. Sulphur deposits occur at altitudes ranging from 4,500 to 6,150 m a.s.l. The largest deposit is Aucanquilcha, followed by Ollagüe, Cabana, and Purico (Fig. 3.8). The rest of the deposits are either small occurrences or have not been exploited.

The sulphur deposits occur on the flanks and tops of Miocene to Holocene andesitic and subordinate dacitic strato-volcanoes. The sulphur occurs as disseminations and veinlets that are mostly restricted to pyroclastic deposits of the volcanoes. Deposits are both

stratabound ("mantos de caliche") and irregular ("bolsonadas"). Only locally does sulphur occur filling fractures and vesicles of lava flows to form irregular deposits. Most of the native sulphur occurs as cement in pyroclastic deposits, along with clay minerals (kaolinite, montmorillonite) and aluminium and calcium sulfates (alunite, natroalunite, gypsum). Sulphur distribution is irregular, with grades ranging from 35 to 70% S. The higher grades occur within pyroclastic deposits with more homogeneous grain size. This has been attributed to the higher permeability of these deposits (Sanchez, 1968). At Ollagüe local replacement of primary minerals in the pyroclastic deposits resulted in crystalline sulphur concentrations with grades higher than 80% S (Ahlfeld, 1940; Sanchez, 1968). At Aucanquilcha small concretions of covellite within nuclei of native sulphur occur (Clark, 1970).

The sulphur orebodies are relatively parallel to the ground surface. They are commonly covered by a thin overburden of detrital or pyroclastic materials, but locally are covered by barren andesitic lavas 60 to 100 m thick (e.g., Aucanquilcha; Sanchez, 1968). The size of the orebodies is variable, their surfaces range from some hundred of square metres up to 2.75 $km^2$ at Aucanquilcha. The stratabound deposits are sub-horizontal (dips <30°), and range from 0.5 to 5 m in thickness, but at Aucanquilcha and Ollagüe they are more than 35 m thick (Sanchez, 1968).

Sulphur deposits are usually associated with strongly altered zones of the volcanoes. In these zones the volcanic rocks are usually bleached, and show kaolinization, limonitization, and pervasive silicification. Solfataric activity and deposition of native sulphur is now occurring at some deposits. This activity includes either the emission of gases ($H_2S$, $H_2O$ vapour, $CO_2$), or water-vapour hot springs, which emit sulphurous gases ($H_2S$, $SO_2$, S) and sulphuric, hydrochloric, and carbonic acids. Sulphur deposition is consequence of oxidation reactions of ascending sulphurous gases, particularly $H_2S$. Where these sulphurous gases interact with water they are oxidized to sulphuric acid solutions. The interaction of these sulphuric acid solutions with sulphurous gases

also results in the deposition of native sulphur. Hydrolytic reactions affecting minerals of pyroclastic materials that interact with acid solutions account for the pervasive alteration typically associated with sulphur deposits (hydrogen metasomatism of Hemley and Jones, 1964).

### 3.2.7.4 Copper deposits in Oligocene-Miocene sediments

Exogenous and diagenetic processes have produced a few copper deposits within Oligocene-Miocene sediments (Fig. 3.8). The most important is Chuqui Sur (former Exotica orebody): its probable reserves were estimated to be 180 x $10^6$ tons 1.42 % Cu (Trask, 1968). The Chuqui Sur deposit is located 2 km south of the Chuquicamata porphyry copper. The orebody is a sub-horizontal lens inclined at about 5° to the south, with a northwest-southeast axis 2.2 km long, and a short axis with a maximum length of 1.2 km. The maximum thickness of the orebody is 110 m with an average thickness of 53 m (Mortimer and others, 1977, 1978). The ore minerals consists of copper oxides impregnating Miocene gravels and underlying bedrock. About two thirds of the orebody are contained within the bedrock and the rest lies within the overlying Miocene sedimentary cover. The ore minerals are mainly chrysocolla, "copper wad" (amorphous mixture of Cu, Fe and Mn oxides), "copper pitch" (Mn and Fe-rich chrysocolla), and atacamite. Subordinate species include libethenite, devilite, leytonite, brochantite, antlerite, sampleite, conichalcite, marshite, chalcanthite, and plancheite (Mortimer and others, 1977).

The Chuqui Sur deposit was originated by leaching of copper from the Chuquicamata porphyry copper by exogenous processes and subsequent redeposition within alluvial gravels and underlying bedrock (Marin, 1973; Munchmeyer and Urqueta, 1974; Mortimer and others, 1977; Ambrus, 1979; Alvarez and others, 1980). According to Mortimer and others (1977) the emplacement of the Chuqui Sur orebody took place during the Early Miocene, and was partly coincident with the development of supergene enrichment processes of the Chuquicamata porphyry copper deposit that were

ascribed to the Upper Oligocene-Early Miocene. The latter authors indicate that all supergene activity had ceased by the Middle Miocene after extreme climate desiccation.

The Leonor deposit is another exogenous copper deposit hosted by Miocene-Pliocene gravels at El Tesoro mining camp (75 km south of Chuquicamata). The deposit is formed by three lenticular bodies of N42-60°E/15-20°NW orientation that are 150 to 600 m long, 1 to 4 m thick, and have been recognized 60 m downdip. The copper ores are very irregularly distributed and include colloform chrysocolla and black earthy masses of tenorite that occur as cement in the gravels, particularly within well sorted beds (Raczynski, 1966). The primary source of copper at Leonor deposit is unknown, but may be from the Marietta copper-bearing vein located 800 m northeast (Raczynski, 1966).

Pre-Upper Miocene stratabound red-bed copper deposits occur in the middle section of the Oligocene-Early Miocene San Pedro Formation at San Bartolo, north of the Salar de Atacama (Flint, 1986, 1987). The copper ores are hosted by up to 15 sandstone bodies that range in thickness from 0.5 to 2.5 m within a stratigraphic interval of 75 m and are exposed along strike for about 4 km. Mineralized sands show pervasive bleaching, and poor cementation at outcrop. This colour change contrasts strongly with the red, well-cemented unmineralized strata. Most of the ore minerals occur as matrix to detrital silicates replacing earlier carbonate and sulfate cements. They form conformable lenticular orebodies, but veinlets locally occur crosscutting the stratification. The important ore minerals in order of abundance are atacamite, tenorite, cuprite, and native copper. Minor galena is widespread, and native silver is associated with native copper and copper oxides, but both galena and silver contents are uneconomic. Some sections of the deposits include copper sulfides: chalcocite-group minerals are dominant along with covellite, but rarely chalcopyrite forms an earlier cement. The copper grades are erratic, and economic concentrations are restricted to localized sections of the sandstone bodies. Grades range from 0.7 to 3.0% Cu at the surface and average 1.2% Cu (Travisany, 1978). The origin of

the copper mineralization has been attributed by Flint (1986) to low temperature (<100°C) diagenetic processes with the involvement of chloride-rich ground water derived through related diagenesis of the abundant evaporites in the sedimentary succession. The ground water would have leached copper from the sediments and redeposited the metal within sandstones with favourable physico-chemical conditions.

Provenance studies of the host sediments and lead isotope data for the sulfides imply that both the sandstones and the lead were derived from an earlier volcano-plutonic complex. Sulphur isotope results for copper sulfides show very light $\delta^{34}S$ values ($-33^{0}/_{00}$), indicative of biogenic sulfate reduction under conditions of unrestricted sulfate supply (Flint, 1986). All the above sediment-hosted copper deposits seem to be originated by Early Miocene remobilization of earlier copper deposits associated with older igneous rocks.

## 3.3 SUPERGENE ENRICHMENT

### 3.3.1 Introduction

The primary sulfide assemblages of most of the metallic ore deposits are unstable at near-surface oxidizing conditions (above the water table). The resulting process of supergene alteration involves the release of metallic cations and sulfate anions through the oxidation of hypogene sulfides. The metallic cations descend, in solution, and may be redeposited on reaction with carbonate, hydroxyl, silicate, sulfate or sulfide ions. Copper and silver are precipitated under the water table level by hypogene sulfides to form sulfides richer in copper or silver respectively. Thus an ideal supergene alteration profile is composed of an oxidized zone, with its upper part leached, underlain by a supergene sulfide enrichment zone (cementation zone), and passing downwards into hypogene ore or protore. The profile may be significantly modified by the

superposition of successive cycles of supergene alteration and local conditions (Sillitoe, 1969; Sillitoe and Clark, 1969). In principle the zone of oxidation reaches the water table, thus its lower limit in many deposits has been controlled by water table positions and therefore is a function of the sequence of geomorphological events that have resulted in the present landscape of the region.

In the oxidized zone the hypogene minerals are destroyed and the mineralogy, structure, and chemical composition of the ores are profoundly modified. In the lower part of the oxidized zone, underlying leached rocks, new oxygen-bearing minerals are formed through reaction of metal cations in solution with anions such as carbonate and silicate. In the enriched or cementation zone immediately below the water table, where oxygen is essentially absent, metal sulfates react with hypogene sulfides to form supergene sulfides. This zone is generally of higher grade than the hypogene and oxidized ore in copper and silver deposits. In contrast, gold enrichment is largely restricted to the oxidized zone, where its enrichment is mainly residual by destruction of associated sulfides but some mobilization is possible in the presence of certain elements such as chlorine and bromine. Supergene gold only occurs as the native metal, which exhibits less tendency to be enriched in secondary sulfide zones.

Supergene processes have produced important enrichment of copper, silver, and gold ores of the Antofagasta Region. Indeed, past mining has largely been restricted to sections of mineral deposits enriched by supergene processes. Hypogene ores are mostly sub-economic, and only exceptionally have they been mined within some high-grade deposits: Buena Esperanza, Mantos Blancos, Santo Domingo, Caracoles, and Chuquicamata; Fig. 3.2; and the largest copper-bearing veins of the Coastal Cordillera (Tocopilla, Gatico, Julia, and Montecristo districts; Fig. 3.4). Despite the considerable contribution of supergene processes to the concentration of copper, silver, and gold ores of the Antofagasta Region, these processes have received very little attention. Only descriptions of the supergene zone of individual deposits exist, particularly of major porphyry copper deposits (e.g., Jarrell, 1944;

Flores, 1985; Hunt and others, 1983; Pohl, 1985, 1986; Alpers, 1986; Alpers and Brimhall, 1988, 1989;). The only comprehensive regional study of the supergene alteration of copper deposits of northern Chile is that by Sillitoe (1969; also Sillitoe and Clark, 1969), but he concentrated on copper deposits located south of the latitude of 26° S. (Atacama Region).

Supergene processes takes place within discrete periods of geological time (e.g., Ague and Brimhall, 1989) following exhumation of the ore deposits, and terminates when a new stable mineral assemblage is formed within the oxidation zone. The process may readily be reactivated by subsequent changes of the water table. Consequently the exhumation of the deposits is a pre-condition for the operation of supergene alteration-enrichment processes, and these processes are sensitive to the physiographic evolution of the region. Several other factors control the supergene processes such as climate, hypogene mineralogy (ore and gangue minerals), wallrock composition, structure, porosity, permeability, and position of the water table. These factors are interdependent, and their relative importance varies from one deposit to another. In the Antofagasta Region the development of supergene alteration profiles of many mineral deposits seems to have been favoured by the persistence of arid climate and low erosion rates.

### 3.3.2 Supergene enrichment of copper deposits

The stratabound copper deposits hosted by Jurassic lavas in the Coastal Cordillera show an upper oxidized zone that extends to a maximum 250 m in depth. The oxidized ores include chiefly atacamite, minor chrysocolla, malachite, copper sulfates, and rare cuprite and native copper. The oxidized zone directly overlies the hypogene zone, and both have similar copper grades. Only the largest deposits such as Mantos Blancos and Susana have enriched zones with supergene chalcocite group minerals and covellite (Astudillo, 1984; Chavez, 1985).

The poor development of secondary enrichment within the stratabound copper deposits may be due to the paucity of hypogene pyrite, and hypogene ores dominated by copper-rich sulfides (chalcocite, bornite). Pyrite is particularly important during oxidation processes, because it releases sulphuric acid, and ferric sulfate solutions that attack other hypogene sulfides. Another possible reason is the presence of profuse calcite gangue within these copper deposits, which may have readily neutralized supergene acid solutions and thus precluded the leaching of metallic cations from the oxidized zone.

The supergene paragenesis at Mantos Blancos according to Chavez (1985) indicates that secondary sulfides (chalcocite, covellite and digenite) were formed first followed by chrysocolla, atacamite, and finally gypsum, and natroalunite. This paragenetic sequence suggests the lowering of the water table during the supergene alteration processes. Chavez (1985) obtained a K-Ar age of 14 ± 7 Ma for the natroalunite from a vein of supergene atacamite-natroalunite of Mantos Blancos suggesting that the supergene processes occurred during the Neogene.

In contrast to the stratabound deposits, copper-bearing veins hosted by Jurassic plutons of the Coastal Cordillera show well developed supergene profiles similar to ideal supergene alteration profiles. Their upper oxidized zone extends down to about 200 m and includes atacamite, chrysocolla, malachite, copper sulfates, cuprite and minor native copper. From about 200 to 340 m depth lies an intermediate zone of supergene sulfides (mostly chalcocite and covellite) that passes downwards into hypogene ore. Both the oxidized and the cementation zones of the veins are copper enriched 3 to 6 times relative to the grades of the protore. This significant enrichment of the oxidized zone is a deviation from an ideal supergene profile, which should to be somewhat leached. Exploitation of the oxidized zone of the copper-bearing veins has concentrated on rich pockets containing red-brown to chocolate-brown mixtures of copper oxides known to the local miners as "almagre." Sillitoe (1969) studied in detail these high-grade mixtures of copper oxides from several copper deposits of northern Chile, showing that they

derive from the oxidation of supergene massive chalcocite. Therefore the supergene alteration profile, and related copper enrichment of the copper-bearing veins is the result of the superposition of successive cycles of supergene alteration rather than from a single-stage process.

The sub-economic Paleocene porphyry copper deposits and tourmaline breccia pipes of the western portion of the Intermediate Depression include an upper oxidized zone, which extends to 140 to 250 m in depth including atacamite, malachite, cuprite, chalcanthite and many other minor mineral species. The oxidized zone of these porphyry copper deposits (Sierra Gorda, Lomas Bayas, Centinela, Fortuna) is partly leached and shows overall low copper grades (0.1 to 0.4% Cu). However, local concentrations of copper oxides within highly fractured rocks constitute economic orebodies that have been mined. The overall copper grades of the oxidized zone of tourmaline breccia pipes are higher, ranging from 1.4% Cu at Quetena to 2.0% Cu at Copucha deposit. The oxidized zone in both types of copper deposit passes downward into hypogene ore and a zone of supergene sulfides is normally absent. However, minor chalcocite and covellite do occur within the oxidized zone suggesting an earlier development of a cementation zone, which was subsequently oxidized and leached due to a lowering of the water table level (Sepulveda, 1963; Ortiz, 1969).

The major Late Eocene - Early Oligocene porphyry copper deposits of the Domeyko Cordillera show well developed supergene alteration profiles, and several deposits include important copper enriched blankets with supergene sulfides (particularly Chuquicamata, La Escondida, Quebrada Blanca, El Salvador). These giant deposits usually show an upper leached-oxidized zone that normally extends down to 100 to 200 m. However, at La Escondida this zone is 400 m thick and at El Salvador it is 350 m thick. The ore minerals within this zone are atacamite, chrysocolla, brochantite, antlerite, chalcanthite, krohnkite, natrochalcite, bisbeeite, cornuite, rare cuprite, and native copper. Tiny veinlets and small masses of turquoise occur. The gangue minerals are

largely iron, magnesium, calcium, and sodium sulfates (blodite, coquimbite, melanterite, jarosite, fibroferrite, copiapite, mirabilite, pisanite, romerite, gypsum), halite, and limonite. Both ore and gangue minerals occur along fractures, disseminated through the rocks as replacement of primary sulfides, and as replacement of feldspars (Bandy, 1938; Jarrell, 1944; Alvarez and others, 1980; Ojeda, 1986). The copper grades of the oxidized zone are variable so that isolated orebodies of 1.00 to 1.65% Cu occur separated by almost barren strongly-leached rocks. The largest volume of oxidized ores occur at Chuquicamata (900 x $10^6$ tons and largely mined out) and El Abra (180 x $10^6$ tons) (Ambrus, 1979), whereas at La Escondida the oxidized zone is almost completely leached, leaving only a near-surface orebody containing 68 x $10^6$ tons of 1.22 % Cu (Ojeda, 1986).

The widespread oxychloride mineral **atacamite** ($Cu_2Cl(OH)_3$) within the oxidation zone of many copper deposits of the Antofagasta Region was probably formed by reaction between primary copper and chlorine in saline solutions of the weathering zone (at Chuquicamata the copper iodide mineral marshite also occurs). Groundwater analyses at Chuquicamata reported by Jarrell (1944) show abundant dissolved sulphate, with nitrate and chloride present in about equal amounts, and silica least abundant. The chlorides and nitrates were probably leached from extensive surficial salt deposits that are characteristic of this desert region (see below). These salt deposits commonly include soluble chlorides and nitrates (Stoertz and Ericksen, 1974; Ericksen, 1983).

Underlying the leached-oxidized zone of the porphyry copper deposits a zone with supergene sulfides usually occurs. The dominant sulfides are chalcocite (sooty and steely), djurleite, covellite and anilite. These secondary sulfides replace primary chalcopyrite, enargite, bornite and coat pyrite. The supergene sulfide zone is usually enriched about 3 to 4 times in copper relative to the protore, and its extent controls the economic value of these giant copper deposits. The

extent of secondary enrichment varies sharply from one porphyry copper deposit to another. This suggests that although regional factors such as geomorphological evolution and the climate constitute the primary control of the supergene processes, the extent of secondary enrichment is largely determined by local rather than regional factors. For example, despite Chuquicamata and Chuqui Norte orebodies being separated only by 4 km, hosted by the same granodioritic porphyry, having similar hypogene mineral assemblages, and probably experiencing synchronous supergene processes Chuquicamata has an important enriched zone with supergene sulfides up to 750 m thick (Alvarez and Flores, 1985) while at Chuqui Norte the enriched blanket averages only 20 m in thickness (Tufiño, 1973).

Important supergene enriched blankets occur also at El Salvador (Gustafson and Hunt, 1975), Quebrada Blanca (Hunt and others, 1983), and La Escondida (Alpers, 1986; Ojeda, 1986). The effects of the supergene processes are very well developed at La Escondida where a thick effectively leached capping zone (350-400 m) is followed downwards by a blanket 20 to 500 m thick with supergene sulfides that has an elongate northwest plan section of 1 x 4.5 $km^2$ and includes most of the 1.76 x $10^9$ tons of ore (averaging 1.59% Cu) of this deposit (Ojeda, 1986). In contrast, at El Abra only oxidation of primary sulfides took place. Here essentially *in situ* development of a copper-oxide blanket now covers an area of 800 x 400 $m^2$ and extends from 100 to 150 m depth (Ambrus, 1977; Alvarez and Aracena, 1982). At the base of the oxidized zone at El Abra a zone of mixed oxides and sulfides occurs, which varies from a few centimetres to 60 m in thickness with no increase of copper grades (Ambrus, 1977). This zone includes partly oxidized secondary chalcocite, suggesting the oxidation of an earlier cementation zone. Two stages of supergene enrichment are also seen at Chuquicamata (Taylor, 1935; Jarrell, 1944) with two distinct zones of chalcocite-bearing ore. The upper zone is extensively oxidized largely to sulphates, and the lower zone is little altered and attains a maximum depth of 585 m. In the central and eastern parts of the orebody, the two enriched zones are separated by up to 50 m of oxidized hypogene ore (Jarrell, 1944). At Potrerillos March (1935)

described a zone of strong enrichment (1.43% Cu) that terminates abruptly about 100 below the top of the sulfides and is followed by a zone of moderate enrichment. March (*op. cit.*) interpreted the highly enriched zone as the re-enriched root of an earlier, secondary sulfide zone. Remnant supergene sulfide minerals within the oxidized-leached zone at La Escondida (Ojeda, 1986), also suggests more than one stage of supergene enrichment.

The supergene processes took place subsequent to the formation of the major porphyry copper deposits and pre-date the deposition of Late Miocene gravels at Chuquicamata (Mortimer and others, 1977) and Quebrada Blanca (Hunt and others, 1983). At La Escondida Alpers and Brimhall (1988) reported 4 K-Ar dates on supergene alunites (see Appendix 2) ranging from 14.7 to 18 Ma, which were taken to indicate the minimum age of supergene processes within this deposit. At El Salvador Gustafson and Hunt (1975) reported K-Ar ages of supergene alunite of 36.9 ± 0.6 Ma and 36.8 ± 2.5 Ma (ages recalculated), and concluded that the supergene oxidation and enrichment probably followed no more than 5 Ma after hypogene mineralization. The regional geological data show that during the Oligocene the Domeyko Cordillera was subjected to significant erosion, but erosion rates decreased by the Miocene and virtually ceased since the Middle Miocene (see Chapters 2 and 5; also Alpers and Brimhall, 1988). Therefore, supergene processes in major porphyry copper deposits probably developed largely during the Late Oligocene and Early Miocene. The partial oxidation of supergene sulfides reported at Chuquicamata, La Escondida, and El Abra perhaps reflects a more recent lowering of the water table possibly related to geomorphologic changes introduced by the Late Miocene Quechua phase, or due to the Mid-Miocene climatic desiccation described by Alpers and Brimhall (1988), or a combination of these factors.

### 3.3.3 Supergene enrichment of silver deposits

The major silver deposits of the Antofagasta Region (Caracoles, Cachinal de la Sierra, El Inca) show an upper oxidized zone that extends down to about 80 m. It is characterized by the presence of silver halides (chlorargirite, iodargirite, bromargyrite, embolite), native silver, and lead carbonates and sulfates. Between about 80 to 150 m a zone of supergene sulfides occurs with acanthite, and silver sulfosalts. These have replaced primary galena, sphalerite, chalcopyrite, and only partially pyrite.

The available information about silver grades of these epithermal veins is sketchy, but it is clear that highest silver grades occurred within the supergene sulfide zone, where ores with grades ranging between 500-600 g/ton Ag have been exploited and rich pockets have produced ores with 1400 to 6000 g/ton Ag (see Sections 3.2.4, 3.2.5). The Caracoles silver district, from 1870 to 1902 produced 235,000 tons of hand-sorted ore averaging 6,000 g/ton Ag. The upper oxidized ores, in general, average 200 to 300 g/ton Ag, but rich pockets with considerably higher grades are common. The oxidized zone is enriched relative to the protore with grades usually lower than 200 g/ton Ag. Hypogene ores have been exploited only in the largest veins of Caracoles (Flores, 1976; Cabello, 1978). Silver enrichment of the oxidation zone of the veins appears to be the result of the availability of halogens that formed insoluble silver halides above the water table, as demonstrated by the presence of chlorargirite, iodargirite, bromargyrite, and embolite. Surficial soluble halides, sulfates, and nitrates are widespread within this desert. They occur as cement of soils, as impregnations, and as veins in bedrock, and mostly as salt-encrusted playas. The chief source of the ordinary salt constituents (sulfate, chloride, sodium, calcium, magnesium and potassium) are water-soluble minerals in the volcanic rocks of the Andes, which are leached by rain water, and carried into the desert chiefly by streams and groundwater; wind-transported particulate salts of

evaporated spray from the Pacific Ocean may also contribute (Ericksen, 1983). The source of iodine and bromine is less understood, but they are also commonly found within surficial saline deposits of the Antofagasta Region.

### 3.3.4 Supergene enrichment of gold deposits

The gold-bearing veins of the Antofagasta Region show an upper oxidized zone that extends to depths of 50 to 100 m with grades usually above 20 g/ton Au. The past exploitation of the gold deposits in this region has been almost entirely restricted to the supergene altered upper zone. Hypogene sulfide ores at depth have low gold grades (0.5 to 2 g/ton Au) and the width of orebodies is usually considerably reduced downwards. The oxidized ores include native gold, which occurs as fine disseminations, flakes, thin veinlets, films coating fractures, scales, and dendrites. Gold is commonly associated with copper oxychlorides, limonite, and hematite. Gold in the oxidized zone is not restricted to the primary veins but extends about 5 to 15 m into fractured wall rocks. For example, at El Guanaco veins 0.5 to 3 m in width have produced oxidized ores with 40-50 g/ton Au, but silicified haloes up to 30 m wide have gold grades ranging between 0.5 to 7 g/ton Au (Llaumet, 1979). Similarly at Sierra Gorda the fault-filling veins (0.1 to 1.0 m wide) grade 20 g/ton Au but gold-bearing rocks extend 5 m from these fractures forming orebodies 10 m wide averaging 8 g/ton Au, and 1,500 g/ton Ag within 40 m from the surface (Pohl, 1985). A cementation zone is lacking in the gold-bearing veins of the San Cristobal and Sierra Gorda districts, where only a zone of mixed oxides and hypogene sulfides occurs. The hypogene ore minerals at depth are auriferous pyrite, galena, sphalerite, tetrahedrite, and chalcopyrite (Kuntz, 1928, Rivera, 1980, Pohl, 1985, 1986). In contrast the veins of the El Guanaco district show a well developed zone of supergene sulfides (chalcocite, covellite) from 70 to 120 m in depth. The exploitation of this supergene sulfide zone has focused on ores with high copper grades (3-4% Cu) rather than gold, whose

grades range from 0.5 to 5.0 g/ton Au (Llaumet, 1979). The hypogene sulfides at El Guanaco are auriferous pyrite, enargite, luzonite, and chalcopyrite with less than 2.0 g/ton Au (Llaumet, 1979).

The only study of the supergene enrichment of gold-bearing veins of the Antofagasta Region was done by Pohl (1985, 1986) at Sierra Gorda. According to Pohl (*op. cit.*) the formation of the economic gold orebodies is the result of the exposure of the hypogene minerals, mostly of auriferous pyrite, to oxidizing conditions near the Earth's surface. Oxidation and chemical and physical leaching of the hypogene sulfides and gangue minerals released gold that migrated and was concentrated within the upper oxidized zone of the veins and fractured rocks in their vicinity. The ultimate result was a significant increase in both the gold grades (2-10 times) and the width of the mineralized bodies (10-30 times) from the near-surface to depths of about 40 to 80 m. The common copper oxychloride atacamite overgrown by native gold in the oxidized zone at Sierra Gorda suggests the involvement of descending chloride solutions in the gold enrichment processes. Pohl (1986) also showed that a significant role was played by bromine, important because Au-Br complexes are more stable than Au-Cl complexes. Minor amounts of bromine extend the Eh range under which gold is soluble, and increase total dissolved gold relative to chloro-complexes by two orders of magnitude (Pohl, 1986). Ground water at La Compañia mine of Sierra Gorda is essentially a Na-Cl-Br solution. The Br/Cl ratio of 0.3 is among the highest recorded from natural waters (Pohl, *op. cit.*). As previously mentioned bromine and chlorine are common within surficial salt deposits of the Antofagasta Region. Furthermore chlorargirite and bromargyrite commonly occur within the oxidized zone of silver-bearing veins, which strongly suggests that bromine and chlorine were involved in the transport, deposition, and supergene enrichment of gold in the majority of the gold-bearing veins of this desert region. According to Pohl (1985, 1986) texture and mineral relationships suggest that gold was precipitated from groundwater by evaporation and the breakdown of unstable aurous halide salts, rather than by reduction by ferrous iron.

The supergene alteration of epithermal silver and gold vein deposits of the Antofagasta Region followed the formation, mostly during the Paleocene, of the primary orebodies and their exposure to near-surface oxidizing conditions. Therefore it has probably taken place during the Late Paleocene or Early Eocene. Subsequent reactivation due to the geomorphologic changes introduced by the Incaic compressive phase in the Late Eocene is also plausible.

The preservation of the enriched zones of the copper, silver, and gold deposits is attributed to the meager regional erosion, which in turn is the result of a combination of geomorphologic peculiarities, and the remarkable persistence of an extremely arid climate in this section of the Atacama Desert since the Middle Miocene (Mortimer, 1980; Alpers and Brimhall, 1988; Abele, 1988, 1989).

The significant role of the supergene alteration processes in the formation of economic orebodies of copper, silver, and gold within the Antofagasta Region makes the period when major supergene alteration was active a "supergene metallogenic epoch" as previously proposed by Zentilli (1974). The most significant appears to be the Late Oligocene - Early Miocene interval. This was the time of formation of the enriched blankets of the major porphyry copper deposits. Enrichment processes were probably reactivated within older deposits at that time. The enrichment of older deposits may be the result of superposed cycles of supergene alteration but probably first developed in the deposits of the Intermediate Depression during the Late Paleocene - Early Eocene.

## 3.4 CONCLUSIONS

Metallic mineral deposits of the Antofagasta Region are distributed into three sub-parallel metallogenic belts coincident with the major mountain ranges. Copper deposits are common to these three metallogenic belts. In terms of copper concentration and economic

importance the porphyry copper deposits of Late Eocene - Early Oligocene age in the Domeyko Cordillera are the most important, followed by Jurassic stratabound copper deposits in the Coastal Cordillera.

Deposits of gold, silver, and iron are of subordinate importance. Sulphur deposits associated with Neogene and Recent solfataric activity are potentially significant. Supergene enrichment has been a fundamental factor in making many of the copper, silver and gold deposits economic.

# CHAPTER 4. POTASSIUM-ARGON GEOCHRONOLOGY

## 4.1 INTRODUCTION

In this chapter new geochronologic data and relevant previously published radiometric ages are reported. They are from mineralized areas and have implications for the metallogenic evolution of the Antofagasta segment of the Andes.

In recent decades the application of geochronological methods, based on nuclear decay of natural elements, has greatly contributed to a better understanding of the geological evolution of the Andes of Northern Chile. Radiometric dating has shown the occurrence of long-lasting igneous activity, and the eastward migration of the magmatic front since the Jurassic (e.g., Farrar and others, 1970; Zentilli, 1974, 1975; Boric and others, 1985; Rivano and others, 1985; Herve and Marinovic, 1989). Most Andean metallic ore deposits were produced by hydrothermal processes directly related to igneous activity that typifies this orogen. The dating of major ore deposits is essential to identify metallogenic epochs, and to correlate mineralizing events with Andean geological evolution. Consequently, in this thesis radiometric dating has been directed towards constraining the ages of major ore deposits and their host rocks. Conventional K-Ar, incremental heating $^{40}Ar$-$^{39}Ar$, and fission track dating methods were used. The rationale is that major ore deposits represent the product of efficient systems of metallic concentration. Therefore their formation and preservation are likely to occur during discrete periods of geological time following a sequence of favourable tectonic and geomorphologic conditions.

Dating of mineralized zones and/or mineralizing events by K-Ar methods is often complicated by the lack of suitable minerals. Potassium-bearing minerals are commonly destroyed or at least modified by the combined effects of hydrothermal alteration and supergene processes associated with the formation of metallic ore deposits, whereas newly formed minerals either lack potassium, or do not retain argon. Therefore host rocks were dated in order to obtain maximum values for the mineralization ages, or post-ore intrusive bodies with clear crosscutting relationships were dated in order to determine minimum ages. Nevertheless, the significant variations of potassium contents of minerals dated by K-Ar is the effect of hydrothermal alteration on some of the rocks and minerals dated.

Thirteen of the conventional K-Ar determinations were done on mineral separates, but another 10 K-Ar dates were obtained on whole rocks, and 5 on strongly altered minerals. Although the value of K-Ar ages on whole rock and altered minerals is debatable, they were done to obtain at least a rough age estimate for those mineralized rocks that lack suitable minerals for K-Ar dating. Five of these whole rock and strongly altered samples (Table 4.1; Appendix 4) gave K-Ar ages without geological significance because of their very low potassium content, whereas the rest produced reasonable K-Ar ages[1].

The $^{40}Ar$-$^{39}Ar$ dates were obtained exclusively on high purity mineral separates; only two samples of actinolite (II-562 and II-524; Tables A1.18, A1.22) have very low potassium content, but both released enough argon in two increments (850° to 900°C) to determine a reasonable $^{40}Ar$-$^{39}Ar$ age.

---

[1] Although "reasonable K-Ar ages" does not necessarily mean correct (accurate) ages, most of the obtained K-Ar ages are consistent with the geological setting of the samples.

### 4.1.1 K-Ar dating: basic theory and analytical procedure

The potassium-argon dating technique is a well-established and widely used geochronological method for determining ages of minerals and rocks, which was developed over 30 years ago. The method is based upon the occurrence in nature of the radioactive isotope of potassium $^{40}K$, which has a half-life of 1,250 Ma. This isotope of potassium has a dual decay to $^{40}Ca$ and to $^{40}Ar$, and the branch yielding radiogenic argon ($^{40}Ar*$) as daughter isotope provides the basis for the K-Ar dating technique through its accumulation over geological time (Dalrymple and Lanphere, 1969; McDougall and Harrison, 1988). In the conventional K-Ar dating method, the potassium and argon are measured on separate portions of the sample, and therefore possible errors from sample inhomogeneity are unavoidable. Potassium is measured as total potassium, and the amount of $^{40}K$ calculated from the known $^{40}K/K$ ratio in nature (0.01167). The conventional K-Ar method does not provide information about possible disturbances of the potassium-argon isotopic system in the sample, which may complicate the interpretation of K-Ar ages. Despite those limitations the K-Ar method is adequate for dating rocks in a regional scale study, and has been used here as a complement to the more refined $^{40}Ar$-$^{39}Ar$ method, which is described below.

The conventional K-Ar dating was done by Carlos Perez de Arce (Laboratory Technician) at the Geochronological Laboratory of the SERNAGEOMIN (Chilean Geological Survey) in Santiago, Chile. Argon extraction was achieved by fusing *in vacuo* individual samples (40 to 60 mesh) in a molybdenum crucible, by an external induction heater, in a Pyrex glass extraction line separate from the mass spectrometer. A known volume of a tracer enriched in $^{38}Ar$ was added during the fusion of the sample (isotope dilution technique). Gas was purified by copper oxide and titanium getters, and collected in a sample takeoff glass tube using liquid nitrogen around a small charcoal finger on the sample takeoff tube. Analyses were done by sequential scanning of masses 36, 38 and 40 using an AEI MS-10S mass spectrometer operating in static mode (isolated from its

pumping system) and adapted to automatically record digital data. $^{40}Ar/^{38}Ar$ and $^{36}Ar/^{38}Ar$ ratios calculated. Potassium analyses were done by triplicate using a Perkin Elmer 4000 atomic absorption spectrophotometer operating in emission mode with internal lithium standard in the Chemical Laboratory of the SERNAGEOMIN. K-Ar analytic uncertainties are expressed at 95% confidence level ($\pm 2\sigma$). The decay constants and potassium isotope abundance ratio used to compute the ages are those suggested by the Geochronological Subcommission of the IUGS (Steiger and Jäger, 1977).

### 4.1.2 $^{40}Ar$-$^{39}Ar$ dating method

The $^{40}Ar$-$^{39}Ar$ dating technique is an analytical variation of the conventional K-Ar dating method wherein a finite amount of $^{39}K$ in the sample is converted to $^{39}Ar$ by irradiation with fast neutrons. This induces the reaction $^{39}K(n,p)^{39}Ar$. This method is attributed to Merrihue (1965), even though it was first suggested in a paper in Icelandic by Sigurgeirsson (1962, *in* Dalrymple and Lanphere, 1971). The $^{40}Ar$-$^{39}Ar$ technique offers several important advantages over conventional K-Ar dating methods. First, both potassium and argon are determined simultaneously on the same sample, thus requiring a smaller amount of mineral for dating, and eliminating possible errors from sample inhomogeneity. Second, neither potassium nor argon absolute abundances are required. The age is calculated from the ratio $^{40}Ar^*/^{39}Ar$ ($^{40}Ar^*$ = radiogenic $^{40}Ar$) after the appropriate corrections for argon isotopes introduced from the atmosphere, and produced within the sample by certain undesirable neutron reactions with calcium and potassium (Dalrymple and Lanphere, 1971; Brereton, 1972). In practice, to avoid difficulties and the large errors involved in neutron flux measurement within the reactor, the age of a given sample is derived from its $^{40}Ar^*/^{39}Ar$ ratio by comparison with the $^{40}Ar^*/^{39}Ar$ ratio of a standard mineral of well-known age, which has been included in the same irradiation batch (for a detailed description see McDougall and Harrison, 1988). The Ar isotopic ratios can be measured more accurately by mass spectrometry than absolute abundances of either

potassium or argon, and thus $^{40}Ar$-$^{39}Ar$ analytical errors are lower compared with the conventional K-Ar technique. More important than these advantages of the $^{40}Ar$-$^{39}Ar$ method is the possibility of stepwise degassing of the mineral sample. This technique, also referred to as the incremental heating approach, was introduced by Merrihue and Turner (1966), and allows one to obtain a series of apparent ages for a single sample, an age spectrum. This spectrum is usually represented by plotting the data on a diagram with apparent age in the ordinate and cumulative per cent of $^{39}Ar$ released on the abscissa. The $^{40}Ar$-$^{39}Ar$ age spectrum may reveal such complications as partial argon loss and excess argon, which cannot be obtained by conventional K-Ar dating (Berger, 1975; Harrison and McDougall 1980, 1981).

The theoretical basis and advantages of the $^{40}Ar$-$^{39}Ar$ stepwise degassing technique were first described by Merrihue and Turner (1966), and have been further discussed in subsequent papers (Turner, 1968, 1969, 1970a, 1970b; Fitch and others, 1969; Dalrymple and Lanphere, 1971; Brereton, 1972). In short, if the sample contains no extraneous argon, and has been a closed system for both argon and potassium since the time of cooling below its closure temperature (temperature of an isotopic system at the time given by its apparent age; Dodson, 1973, 1975, 1976, 1979), then the ratio of radiogenic $^{40}Ar$ to neutron produced $^{39}Ar$ will be the same for each increment of gas released, and each increment will therefore have the same apparent $^{40}Ar$-$^{39}Ar$ age. The result will be an age spectrum that is essentially horizontal (a plateau). If because of a **physical** or **chemical** disturbance the sample has not been a closed system since formation, or because of $^{40}Ar$ not derived from *in situ* decay of $^{40}K$, then the apparent age of each gas increment may be different and the age spectrum be of a more complicated form. The cooling age of such a sample and perhaps part of its thermal story might be inferred from the spectrum pattern, even though its total gas $^{40}Ar$-$^{39}Ar$ age would be incorrect. The effect of partial argon loss usually is to decrease the ages of the lower temperature steps preferentially (e.g., Harrison, 1981). Excess argon in hornblende (extraneous $^{40}Ar$) appears to be characterized by saddle-shaped spectra in which both lowest and highest temperature steps yield

anomalously high ages (e.g., Harrison and McDougall, 1981; Richards and McDougall, 1990).

### 4.1.3 $^{40}Ar$-$^{39}Ar$ dating procedure

The $^{40}Ar$-$^{39}Ar$ dating was done in the Isotope Laboratory of the Geology Department of Dalhousie University by the author, but the preparation of irradiation packages, extraction line preparation, and radioactive sample handling were entirely done by Keith A. Taylor Laboratory Technician. High purity samples of biotite and hornblende were obtained from crushed rocks by conventional heavy liquid and magnetic separation techniques. Samples were wrapped in aluminium foil in the form of thin discs, which were stacked inside an aluminium canister lined with 1 mm of cadmium to absorb thermal neutrons during irradiation. Interspersed among the samples were six flux monitors (MMHb-1 hornblende standard; Alexander and others, 1978). Canisters were irradiated for 10 hours in position 5C of the McMaster University Reactor, Hamilton, Ontario. After irradiation, samples were stored for several weeks to allow the decay of short-lived isotopes generated during irradiation so that their radioactivity decreased to levels that permitted safer handling.

Each irradiated sample was loaded in a quartz boat and placed in a quartz tube connected to the argon extraction line. Next the complete glass extraction line was heated to 200°C, and the valves opened to the vacuum pumps. This "baking" procedure took at least 2 hours (usually done overnight), and was performed to ensure both the high vacuum, and cleanliness of the glass line during the subsequent argon extraction. The quartz tube was heated stepwise from 200° to 1150°C using an external resistance furnace (Lindberg type 59344) at 50°C increments for biotite, and variable temperature increments for hornblende. Each heating step was maintained for 1 hour. Temperature within the furnace was monitored by "Platinel" thermocouples, and controlled electronically.

Argon aliquots were extracted in 10 or 11 degassing steps, purified by a titanium sponge getter and, after passing through a cold trap (cooled by liquid nitrogen), injected directly into the chamber of an on-line, substantially modified AEI MS-10 mass spectrometer.

Analyses were done with the mass spectrometer operating in static mode by automated sequential scanning for masses 36, 37, 39 and 40. Mass 37 was omitted for biotites because of their low Ca/K ratios and mass 38 was not recorded for any sample. The peak detection procedure was executed automatically, controlled by a specifically adapted, on-line Apple IIe microcomputer. Each mass was measured 15 times in a period of about 45 minutes. The peak positions were relocated before the first, sixth and eleventh measurements.

Amplified signals from the mass spectrometer were digitized and the ratios $^{36}Ar/^{39}Ar$, $^{37}Ar/^{39}Ar$ and $^{40}Ar/^{39}Ar$ were calculated (the ratio $^{37}Ar/^{39}Ar$ was omitted for biotites). The measured isotopic ratios usually vary significantly over the 45 minutes of measurement. Thus, a linear extrapolation of ratios was made back to zero time (entry time to mass spectrometer). Once the argon extraction was completed, the $^{40}Ar/^{36}Ar$ ratio of a sample of air was measured for mass spectrometer discrimination calibration. After the determination of all above mentioned ratios, appropriate corrections for atmospheric argon and for interfering isotopes were made, and the partial and total gas $^{40}Ar$-$^{39}Ar$ ages calculated from the corrected isotopic ratios using the decay constants and isotopic abundance ratios suggested by the IUGS Subcommission on Geochronology (Steiger and Jäger, 1977). **Total gas ages** were computed for each sample by appropriate weighting of the age according to the $\%^{39}Ar$ released in each temperature increment. The same procedure was used to derive **plateau ages**, which are considered defined if the ages recorded by two or more contiguous gas fractions that together constitute more than 50% of the total gas released from a sample are mutually coincident at a 95% confidence level ($\pm 2\sigma$) (definition of Fleck and others, 1977). All the analytical uncertainties of geochronologic data are reported in this thesis at the 95% confidence level ($\pm 2\sigma$). The complete $^{40}Ar$-$^{39}Ar$ data sets,

summary sheets and age spectra were stored on diskettes and retained in the Isotope Laboratory. Summary tables of $^{40}Ar$-$^{39}Ar$ analytical data, and age spectra are included in Appendix 1.

Fifteen $^{40}Ar$-$^{39}Ar$ age spectra obtained in this study (Appendix 1) show a drop in apparent ages, and an increase in analytical errors, at heating steps above 900°-1000°C. The apparent age drop in all cases correlates with high proportions of atmospheric argon (74 to 99% Atm. Ar). This atmospheric gas at high temperature increments must come either from the degassing of the quartz tube and quartz boat holding the sample within the furnace, or from leakage at atomic level, of air through the quartz tube at temperatures above 900°-1000°C. This effect becomes relatively important when a significant fraction of the radiogenic argon from the sample is released at high temperatures, but has little effect on the total gas ages. The standard air correction assumes that all non-radiogenic argon has a $^{40}Ar/^{36}Ar$ ratio equal to 295.5 (the atmospheric value). However, the gas released from or through the quartz tube of the extraction line at high temperatures has inherently a lower argon ratio; therefore a significant air correction to high temperature increments tends to lower ages. In summary, the drop in apparent ages at the highest temperature increments is most probably an analytical artifact, which originates from the quartz tube used to heat the samples during the degassing procedure. This error has not been corrected (blank correction) because in this study it does not mask the pertinent information provided by the age spectra.

## 4.2 MINERALIZATION AGES

The main purpose of this section is to define periods of geological time during which the major ore deposits of this Andean segment were formed (metallogenic epochs) from consideration of new geochronologi-

cal data and previously published radiometric ages of the rocks associated with major ore deposits.

The reader should be warned that because of the regional nature of this study the K-Ar and $^{40}Ar-^{39}Ar$ ages have to be interpreted with somewhat flexible criteria, and that "preferred ages" are selected considering all geological and experimental constraints known to the writer. The data are discussed geographically from west to east.

### 4.2.1 Coastal Cordillera

The Coastal Cordillera includes a great number of metallic ore deposits, largely of copper. The most important are stratabound copper deposits hosted by Jurassic lavas (Fig. 4.1), which usually are irregular and stratiform composite ore bodies. The largest deposit of this type is Mantos Blancos (see Section 3.2.2). The minimum age of the copper mineralization at Mantos Blancos is determined by the hornblende K-Ar dates of 149 ± 13 and 147 ± 13 Ma obtained by Chavez (1983) for dikes crosscutting the ore bodies, whereas the Early Jurassic age that can be ascribed to the host volcanics may also be regarded as the maximum mineralizing age.

The rest of the stratabound copper deposits of the Coastal Cordillera are considerably smaller than Mantos Blancos, but they constitute an important source of copper and silver (see Section 3.2.2). At Buena Esperanza deposit (south of Tocopilla city; Fig. 4.1) a barren gabbroic stock that crosscuts the mineralized Jurassic volcanic strata yielded a plagioclase K-Ar age of 168 ± 5 Ma (II-RB-74; Table 4.1), a date that may be regarded as a minimum age for copper mineralization (if the gabbroic intrusion post-dates copper mineralization). The maximum age is given by the whole rock, 18 point Rb-Sr isochron of 186 ± 14 Ma (MSWD 4.2; Initial $^{87}Sr/^{86}Sr$ ratio 0.70315) obtained by Rogers (1985) for the host Jurassic lavas south of Tocopilla.

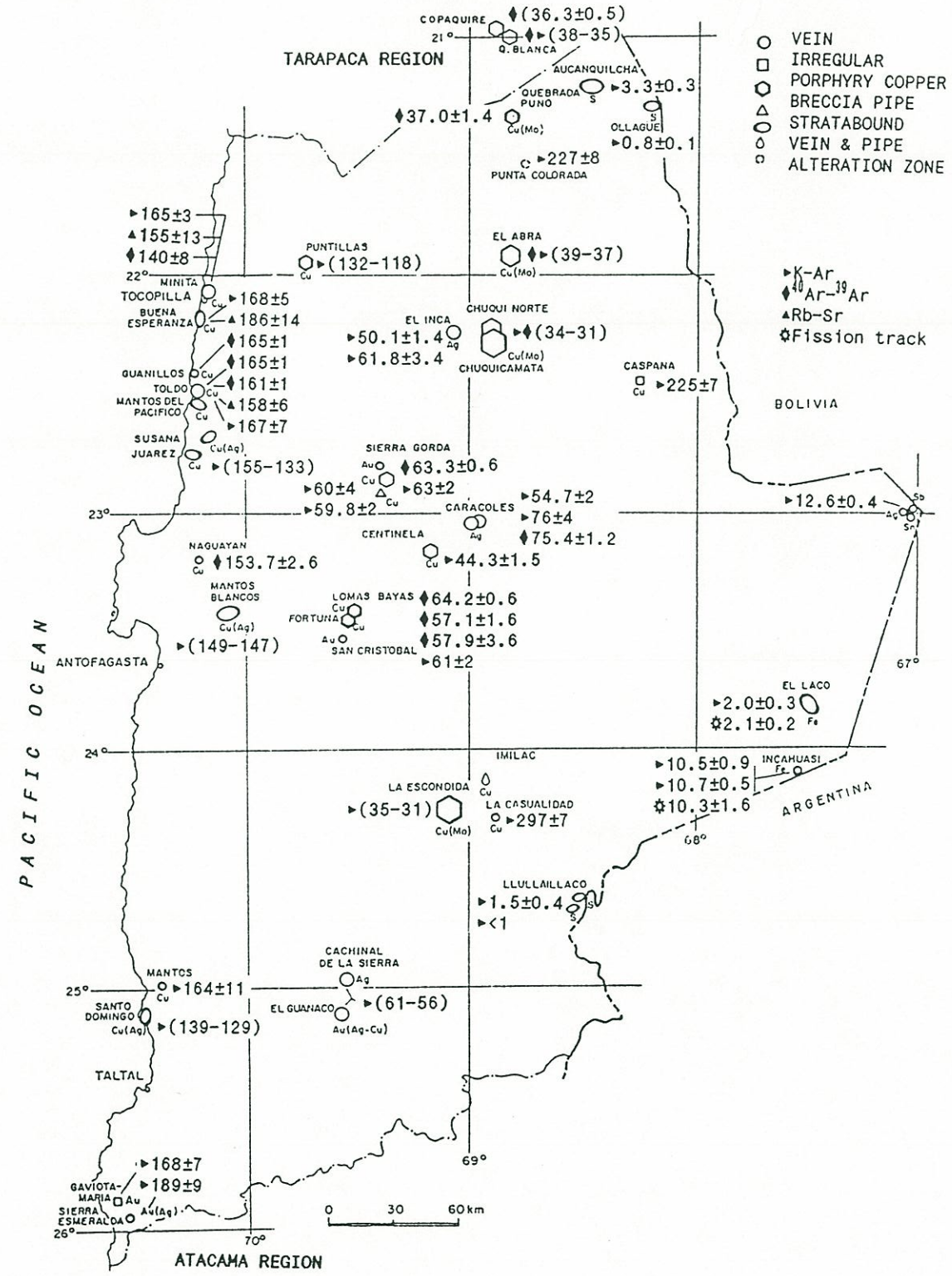


**Figure 4.1.** Main metallic ore deposits of the Antofagasta Region and radiometric dates of associated igneous rocks.

The minimum age of mineralization in the Susana deposit (Michilla District; Figs. 3.1, 4.1) is determined by the whole rock K-Ar ages of 149 ± 4 and 154 ± 8 Ma obtained by Astudillo (1984) for a barren gabbroic stock, and a dike of the same composition that crosscuts the mineralized volcanic rocks. Further south in the Santo Domingo deposit, the minimum mineralizing age is set by the plagioclase K-Ar ages of 133 ± 4 and 139 ± 5 Ma obtained during this study for barren dioritic dikes crosscutting ore bodies (II-RB-48 and II-RB-52, Table 4.1). An altered andesite from this deposit (II-RB-51) yielded a whole rock age of 129 ± 4 Ma, which is regarded as a minimum value for these Jurassic volcanics (Fig. 4.1).

The maximum mineralizing age for Susana and Santo Domingo stratabound copper deposits is determined by the Early Jurassic maximum age of the host volcanics.

The minimum age of mineralization in the Susana deposit (Michilla District; Figs. 3.1, 4.1) is determined by the whole rock K-Ar ages of 149 ± 4 and 154 ± 8 Ma obtained by Astudillo (1984) for a barren gabbroic stock, and a dike of the same composition that crosscuts the mineralized volcanic rocks. Further south in the Santo Domingo deposit, the minimum mineralizing age is set by the plagioclase K-Ar ages of 133 ± 4 and 139 ± 5 Ma obtained during this study for barren dioritic dikes crosscutting ore bodies (II-RB-48 and II-RB-52, Table 4.1). An altered andesite from this deposit (II-RB-51) yielded a whole rock age of 129 ± 4 Ma, which is regarded as a minimum value for these Jurassic volcanics (Fig. 4.1).

TABLE 4.1 K-Ar AGES

(Analytical data in Appendix 4)

| Sample Id. | Lat. S Long. W | Dated Mat. | AGE (Ma) (±2σ) | Observations |
|---|---|---|---|---|
| II-RB-74 | 22°09'54" 70°12'36" | Plg | 168 ± 5 | Altered gabbro; crosscuts Cu ore bodies at Buena Esperanza |
| Iquiqueña | 22°01'00" 70°11'35" | Bt | 165 ± 3 | Diorite; hosts Cu mineralization at Tocopilla district |
| LG 2 | 21°55'18" 69°43'30" | WR | 118 ± 15 | Altered dacitic porphyry, Puntillas prospect (Cu) |
| RB-1 | 22°23'30" 70°13'40" | A-T | 167 ± 7 | Gangue from Carmen-Florencia vein Guanillos district (Cu) |
| II-RB-43 | 24°41'06" 70°32'36" | Alt Plg | 116 ± 10 | Gabbro; host rock of Chuminga irregular copper deposit |
| II-RB-48 | 25°05'30" 70°29'06" | Plg | 133 ± 4 | Altered dioritic dike; crosscuts orebodies at Santo Domingo deposit |
| II-RB-51 | 25°05'30" 70°29'06" | WR | 129 ± 4 | Altered and mineralized andesite; Santo Domingo deposit (Cu) |
| II-RB-52 | 25°05'30" 70°29'06" | Plg | 139 ± 5 | Altered dioritic dike; Santo Domingo stratabound Cu deposit |
| II-RB-63 | 25°50'48" 70°36'00" | WR | 168 ± 7 | Altered dike; Gaviota-Maria metasomatic gold deposit |
| II-RB-9 | 22°15'24" 69°04'42" | WR | 50.1 ± 1.4 | Altered quartz porphyry; El Inca district (Ag) |
| II-RB-36 | 22°52'18" 69°21'12" | Bt | 64 ± 2 | Monzodiorite; host-rock Sierra Gorda district (Cu) |
| II-RB-37 | 22°54'48" 69°22'12" | Bt | 63 ± 2 | Granodiorite; host-rock, Sierra Gorda district (Cu) |
| II-RB-34 | 22°50'30" 69°20'36" | Plg | 60 ± 4 | Altered and mineralized porphyry; Sierra Gorda porphyry copper |
| II-RB-38 | 22°54'24" 68°22'12" | WR | 59.8 ± 2.0 | Fragment of granodiorite; Copucha breccia pipe, Sierra Gorda (Cu) |
| II-RB-19 | 23°02'10" 68°59'18" | WR | 76 ± 4 | Tonalitic porphyry; hosts Ag veins at Caracoles district |

| Sample Id. | Lat. S Long. W | Dated Mat. | AGE (Ma) (±2σ) | Observations |
|---|---|---|---|---|
| II-RB-22 | 23°00'36" 69°01'54" | WR | 54.7 ± 2.0 | Altered felsic porphyry; hosts Ag veins at Caracoles district (Ag) |
| II-RB-20 | 23°02'12" 68°58'18" | Hbl chl | 41.3 ± 4.4 | Tonalitic porphyry; Caracoles district (Ag) |
| II-RB-25 | 23°09'54" 69°09'42" | WR Ser | 43.8 ± 1.5 | Dacitic porphyry; Centinela (Cu) |
| II-RB-26 | 23°09'54" 69°09'42" | WR Ser | 44.3 ± 1.5 | Dacitic porphyry; Centinela (Cu) |
| II-RB-68 | 23°25'12" 69°33'42" | Bt | 61 ± 2 | Granodiorite; Lomas Bayas porphyry copper deposit |
| II-RB-65 | 23°25'12" 69°33'36" | Bt chl | 33.2 ± 7.3 | Granodioritic porphyry; Lomas Bayas porphyry copper deposit |
| II-473 | 24°05'30" 69°20'28" | WR | 42.1 ± 1.5 | Dacite; Augusta Victoria Fm. |
| II-147 | 24°01'20" 69°08'10" | Bt | 55.0 ± 1.4 | Rhyolitic ignimbrite; basal section Augusta Victoria Fm. |
| II-39 | 23°33'30" 69°16'55" | WR | 52 ± 2 | Rhyolite; Augusta Victoria Fm. |
| II-68 | 24°05'15" 69°23'05" | Bt | 59 ± 1 | Dacitic ignimbrite; Augusta Victoria Fm. |
| FT-67 | 20°55'30" 68°53'24" | Bt | 37.4 ± 3.1 | Granodioritic porphyry; Copaquire Mo-Cu porphyry |
| FT-67 | 20°55'30" 68°53'24" | Bt | 34.2 ± 1.8 | Granodioritic porphyry; Copaquire Mo-Cu porphyry |
| FT-66 | 20°59'30" 68°48'06" | Bt | 37.7 ± 0.9 | Quartz monzonitic porphyry; Quebrada Blanca porphyry copper |
| FT-66 | 20°59'30" 68°48'06" | WR | 35.9 ± 1.2 | Quartz monzonitic porphyry; Quebrada Blanca porphyry copper |
| FT-43 | 22°14'12" 68°55'30" | Bt | 39.5 ± 1.1 | Fortuna Granodiorite NW of Chuquicamata mine. |
| FT-23 | 22°20'48" 68°58'54" | Bt | 39.0 ± 1.2 | Fortuna Granodiorite SW of Chuquicamata mine. |

Abbreviations of dated materials (Table 4.1):

A-T : Actinolite - Tremolite
Alt : Altered
Bt : Biotite
chl : Chloritized
Hbl : Hornblende
Plg : Plagioclase
WR : Whole rock
ser : sericitized

---

The maximum mineralizing age for Susana and Santo Domingo stratabound copper deposits is determined by the Early Jurassic maximum age of the host volcanics. Other relatively important stratabound deposits are Juarez, Mantos del Pacifico and Mantos de la Luna. These still lack radiometric data; however, their stratigraphic position and geographic location close to the Susana deposit strongly suggest that they are also Jurassic in age.

Other deposits of considerable volume in the Coastal Cordillera are copper-bearing veins hosted by dioritic, and granodioritic Jurassic plutons (Tocopilla, Guanillos, Gatico, El Desesperado, Julia and Montecristo districts: Figs. 3.4, 4.1, 4.2). These copper-bearing veins appear to have been formed by a residual fluid phase from the same magmas that produced the Jurassic plutons (see Section 3.2.2.2); a view that is supported by the geochronological data discussed below. The largest deposit of this type is Minita-Despreciada of Tocopilla district (Figs. 3.4, 4.1), which is hosted by a large granodioritic intrusive body (Tocopilla Pluton, ca. 280 $km^2$). The intrusive host-rock has a biotite K-Ar age of 165 ± 3 Ma (Iquiqueña, Table 4.1). In addition, an actinolite sample (II-562) from a veinlet in the Barriles creek yielded a $^{40}Ar$-$^{39}Ar$ plateau age of 139.8 ± 7.7 Ma (66.3% of $^{39}Ar$ released; Fig. 4.2). However, only two steps (increments between 850 and 950°C) released sufficient argon to be measured by mass spectrometry (due to the low potassium content of actinolite). Therefore this age has to be regarded as a

minimum. Furthermore, Rogers (1985) obtained a whole rock, twelve point Rb-Sr errorchron of 155 ± 13 Ma (MSWD 9.5; Initial $^{87}Sr/^{86}Sr$ ratio 0.7033) for the host Tocopilla Pluton.

Dioritic intrusive bodies emplaced within a Jurassic volcanic sequence along the coastal area between Guanillos and Punta Tames area (22°20'-22°40' S) also host many copper-bearing veins (Guanillos, Gatico and Cobija districts; Fig. 4.2). Biotite samples from Guanillos (II-571), Gatico (II-537), and Cobija (II-539) yielded $^{40}Ar-^{39}Ar$ total gas ages of 158.5 ± 1.0, 158.8 ± 1.4, and 159.9 ± 1.4 Ma (Appendix 1; Fig. 4.2). The $^{40}Ar-^{39}Ar$ age spectra of these three samples are irregular, but an age of 165.5 Ma may be inferred from the first two (Samples II-571 and II-537; Figs. A1.19, A1.20), and an age of 161 Ma may be deduced from the third (Sample II-539; Figs. A1.21, 4.2). In addition, the actinolite-tremolite of the Carmen-Florencia vein of the Guanillos district yielded a K-Ar age of 167 ± 7 Ma (Table 4.1). On the other hand, Rogers (1985) obtained a whole rock, seven point Rb-Sr isochron of 158 ± 6 Ma (MSWD 0.8; Initial $^{87}Sr/^{86}Sr$ ratio 0.7039) at Gatico (Fig. 4.1). These geochronological data suggest a Callovian-Oxfordian[2] age range for both pluton emplacement and vein formation in these coastal districts.

The Naguayan copper district (23°10' S; Figs. 3.1, 4.1, 4.2) is hosted by an extensive dioritic to granodioritic composite intrusive body (ca. 900 $km^2$). Actinolite from the Angel de la Guarda vein (II-524) of the Naguayan district yielded a $^{40}Ar-^{39}Ar$ plateau age of 153.7 ± 5.2 Ma (two increments representing 60.4% of $^{39}Ar$ released). Samples of host rocks collected in Naguayan area were too altered to be dated by K-Ar methods (chlorite, epidote, calcite, clay minerals), but a sample (II-527) collected 5 km to the west of the mineralized area from a dioritic dike that crosscuts the same pluton (west of the Mititus fault) has yielded a hornblende $^{40}Ar-^{39}Ar$ plateau age of 148.5 ± 1.0 Ma, and a sample (II-526) of tonalite stock that crosscut both the pluton and dioritic dikes yielded

---

[2] Ages referred to the Geological Time Scale compiled by Palmer (1983), for the Geological Society of America.

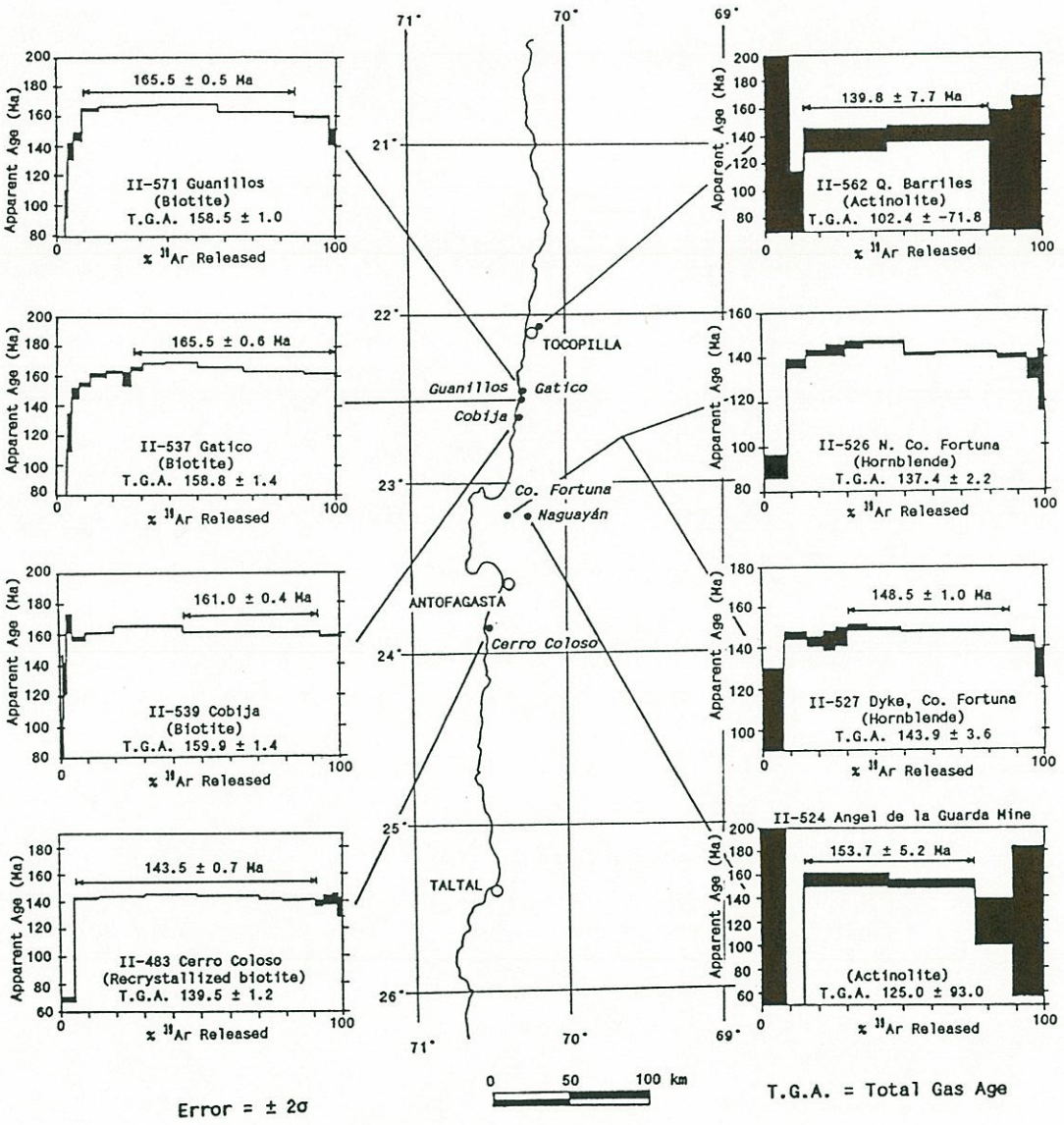


Figure 4.2. $^{40}Ar$-$^{39}Ar$ dates and age spectra of intrusive rocks and veins of the Coastal Cordillera. Analytical uncertainties (±2σ) are represented by vertical width of bars (See Appendix 1 for analytical data and detailed age spectra).

a hornblende $^{40}Ar$-$^{39}Ar$ total gas age of 137.4 ± 2.2 Ma. Its $^{40}Ar$-$^{39}Ar$ age spectrum shows a gradient from 137.6 to 146.6 Ma (Fig. 4.2; Appendix 1), but the last increments (representing the 43.5% of $^{39}Ar$ released) almost define a plateau at 141.5 ± 0.9 Ma. The radiometric data suggest that vein formation in the Naguayan district occurred during the Oxfordian, and was probably synchronous with that in the Guanillos, Gatico, Cobija, Punta Tames, and Tocopilla districts (Figs. 4.1, 4.2). A comparable age is also inferred for the veins of the Montecristo district (Fig. 4.1) from the actinolite-tremolite K-Ar age of 164 ± 11 Ma of the Mantos vein (JICA-MMAJ-SERNAGEOMIN, 1986). The Montecristo copper district is hosted by a Jurassic batholith in the southern coastal section of the area (25°S). A biotite K-Ar age of 159 ± 3 Ma has been published by Naranjo and Puig (1984) for this batholith, which has been referred to as the "Matancilla Plutonic Group." The more detailed geochronological study of Herve and Marinovic (1989) reported 10 biotite K-Ar ages for the same intrusive unit (but referred to as the "Paranal unit") ranging from 162 to 123 Ma, the older ones being 162 ± 4, 155 ± 4 and 151 ± 4 Ma. The latter authors also obtained a whole rock four point Rb-Sr isochron of 170 ± 28 Ma (MSWD 0.0; Initial $^{87}Sr/^{86}Sr$ ratio = 0.70315).

The only porphyry copper type deposit in the Coastal Cordillera is the Puntillas sub-economic prospect (Maksaev and Marinovic, 1980). A whole rock K-Ar age of 118 ± 15 Ma (LG-2, Table 4.1) has been obtained in this study for the altered and mineralized dacitic porphyry of this prospect. Previously Munizaga and others (1985) reported a whole rock K-Ar age of 132 ± 8 Ma for the same porphyry: both results suggest an Early Cretaceous age for the prospect (Fig. 4.1).

In the Coastal Cordillera an altered dike from the metasomatic irregular, low grade, gold deposit Gaviota-Maria was also dated. It gave a whole rock K-Ar age of 168 ± 7 Ma (II-RB-63, Table 4.1; Fig. 4.1). A gabbro that hosts the coastal Chuminga irregular copper deposit (24°41'06"-70°32'36") gave a K-Ar age of 116 ± 10 Ma (II-RB-43, Table 4.1) on argillized plagioclase. The coastal gabbroic plutons have yielded K-Ar ages ranging between 164 and 115 Ma (Herve and Marinovic,

1989), whole rock Rb-Sr isochron ages of 200 and 172 Ma (Diaz and others, 1985; Herve and Marinovic, 1989) and zircon U-Pb ages of 191 and 196 Ma (Damm and others, 1986). Therefore the 116 ± 10 Ma age obtained at Chuminga is probably partly reset. However, one cannot say whether this resetting is related to the copper mineralization event or just to the low argon retention of the argillized plagioclase.

In summary, the radiometric data of the Coastal Cordillera show that copper veins were formed in the Middle to Late Jurassic (Callovian to Oxfordian) during the cooling of plutons of batholitic dimensions emplaced within the coastal Jurassic volcanic sequence. The geochronological data are still insufficient to resolve whether the coastal stratabound copper deposits hosted by Jurassic volcanics represent a separate mineralizing event or were formed synchronously with the batholith emplacement and copper vein formation. The radiometric age range from 186 to 168 Ma shown above for the stratabound Buena Esperanza copper deposit may suggest that this deposit was formed during the emplacement of copper veins in the Coastal Cordillera. The possibility that the stratabound copper deposits hosted by Jurassic volcanics of the Coastal area were related to the same mineralizing event that produced the copper veins within the Jurassic batholiths emplaced within the Jurassic volcanic sequence is appealing, but the geochronological data are not sufficient to prove it.

### 4.2.2 Intermediate Depression and western foothills of the Domeyko Cordillera

The area comprising the Intermediate Depression and western foothills of the Domeyko Cordillera contains important districts of silver and gold-bearing epithermal veins (El Inca, Caracoles, Cachinal de la Sierra, Vaquillas, Sierra Juncal, Guanaco, and San Cristobal districts; Fig. 3.2, 4.1), as well as sub-economic porphyry copper

deposits (Sierra Gorda, Centinela, Lomas Bayas, and Fortuna del Cobre), and copper-bearing tourmaline breccia pipes (Copucha) (Fig. 3.6, 4.5).

The silver district of El Inca (March, 1931; Alvarez and Miranda, 1985) is located 20 km to the west of Chuquicamata (Fig. 4.1). A sample (II-RB-9) of an altered quartz porphyry collected near the Blanca Independencia vein in this district gave a whole rock K-Ar age of 50.1 ± 4 Ma, which may be regarded as a minimum age for the mineralization. The hornblende K-Ar age of 61.8 ± 3.4 Ma of a monzonite from the "Granitic-Monzonitic Complex" reported by Ambrus (1979) would be the maximum age, as the porphyry is emplaced within this intrusive complex.

In the district of Caracoles, epithermal silver-bearing veins are hosted by both Jurassic limestones and intrusive stocks (Kuntz, 1928; Flores, 1976; Cabello, 1978). One K-Ar age of 41.3 ± 4.4 Ma was obtained for chloritized hornblende (II-RB-20, Table 4.1) from a tonalitic porphyry. This age is thought to be incorrect because it is significantly younger than the rest of the dates obtained for stocks of this district. This suggests that there was significant argon loss from the chloritized hornblende dated. An altered tonalitic porphyry (II-RB-22) from the Casas de Tablas mining camp gave a whole rock K-Ar age of 54.7 ± 2.0 Ma, which must be regarded as a minimum value. In addition, the tonalitic porphyry that hosts two important silver vein systems (Gran Corrida del Desierto and Gran Corrida de Caracoles vein systems) yielded a whole rock age of 76 ± 4 Ma (II-RB-19, Table 4.1; Fig. 4.1). A sample (II-597) from a dioritic stock located 1.5 km to the NE of another vein group (La Isla) gave a biotite $^{40}Ar$-$^{39}Ar$ total gas age of 75.4 ± 1.4 Ma, its incremental-release $^{40}Ar$-$^{39}Ar$ age spectrum is somewhat irregular (Fig. 4.3; Appendix 1), but 81.9% of the $^{39}Ar$ released suggests an age of about 76.7 Ma. The apatite from this sample (II-597) yielded a fission track age of 77.9 ± 6.2 Ma, which is concordant (within error limits) with the $^{40}Ar$-$^{39}Ar$ age. The geochronological data obtained for Caracoles suggest a Late Cretaceous age

(Campanian[3]) for the emplacement, and cooling of intrusive stocks. A comparable age may be ascribed to the mineralization, as it seems to be related to these intrusives.

Puig and others (1988, 1989) published 26 new K-Ar dates from the area of the Cachinal de la Sierra silver district, and El Guanaco gold district (Fig. 4.1). These age determinations on minerals and whole rocks range from 61 to 56 Ma indicating that the epithermal silver and gold deposits in these districts are Paleocene in age.

Sub-economic porphyry copper deposits and copper-bearing breccia pipes located within the Intermediate Depression are related to granodioritic porphyries. The radiometric data obtained suggest a Paleocene formation age (Fig. 4.5); see discussion in Section 4.3.

The geochronological data suggest that the major metallic ore deposits in the Intermediate Depression and western foothills of the Domeyko Cordillera were formed during a Paleocene mineralizing event. The epithermal silver mineralization at Caracoles could be an exception, since it seems to be related to Late Cretaceous stocks.

In summary, a Paleocene mineralizing event in the Antofagasta Region formed important silver and gold epithermal deposits, as well as sub-economic porphyry copper deposits and breccia pipes. This Paleocene mineralizing event correlates with the formation of the major porphyry copper deposits of southern Peru (Vidal, 1985) and also with the formation of many copper tourmaline breccia pipes in the Atacama Region (26°-29°S; Sillitoe and Sawkins, 1971).

---

[3] Ages referred to the Geological Time Scale compiled by Palmer (1983) for the Geological Society of America.

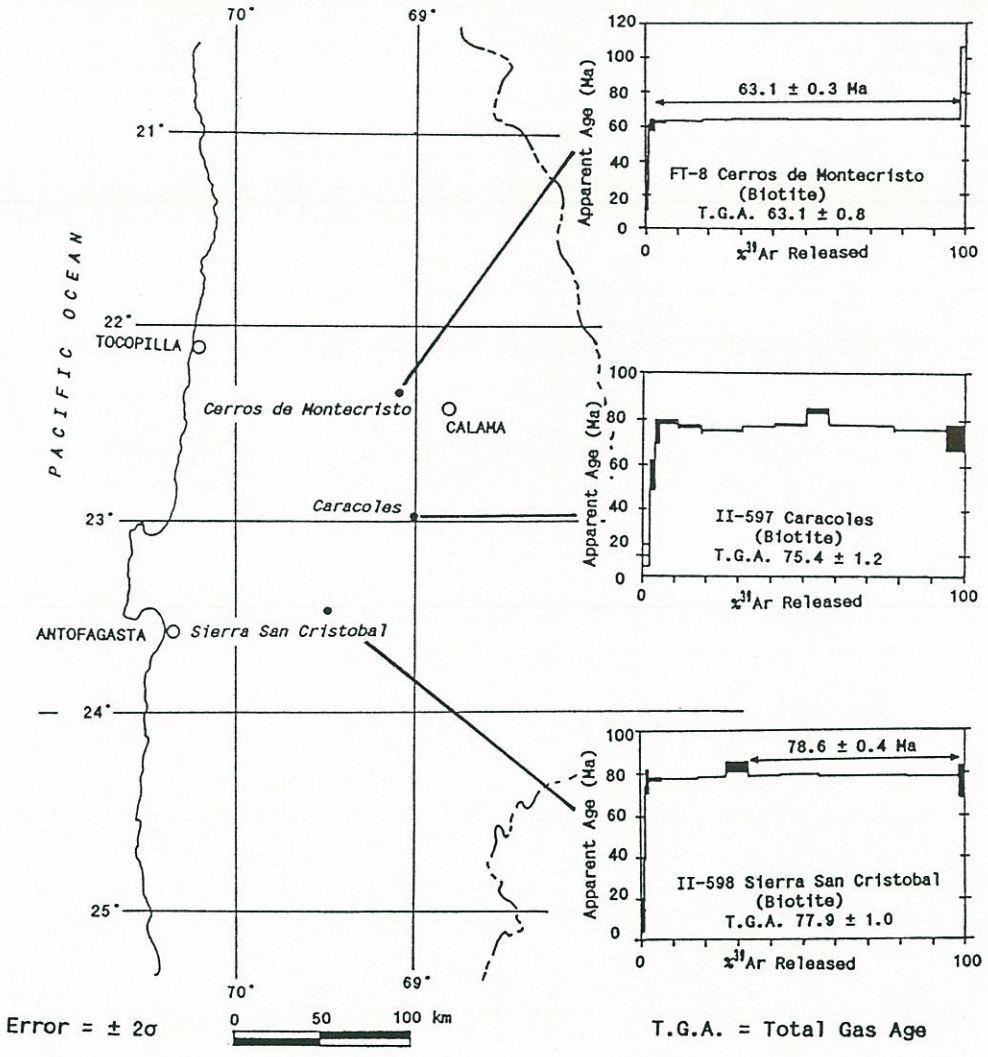


**Figure 4.3.** $^{40}Ar$-$^{39}Ar$ dates and age spectra of intrusive rocks of the Intermediate Depression. Analytical uncertainties (±2σ) are represented by vertical width of bars (See Appendix 1 for analytical data and detailed age spectra).

### 4.2.3 Domeyko Cordillera

The Domeyko Cordillera is the locus of the major porphyry copper deposits of this Andean segment (Figs. 3.7, 4.4). New biotite $^{40}Ar$–$^{39}Ar$ dates from Chuquicamata, El Abra, Quebrada Blanca, Copaquire, and the Quebrada Puno prospect range between 39 and 31 Ma (Fig. 4.4); these data are discussed in Section 4.3. The previously published radiometric dates (largely K-Ar) range between 41 and 28 Ma (Quirt and others, 1971; Hunt and others, 1983; Ambrus, 1977; Alvarez and others, 1980; Alvarez and Aracena, 1985; Alpers, 1986; Ojeda, 1986; Gustafson and Hunt, 1975; Olson, 1989). The radiometric data show that these porphyry copper deposits were formed during a discrete Late Eocene-Early Oligocene mineralizing event. This event is the most important metallogenic epoch in the history of the Antofagasta Region since it has produced one of the world's largest copper concentrations.

### 4.2.4 Neogene to Quaternary volcanic chain

Few metallic deposits occur in the Neogene to Quaternary volcanic chain of the easternmost section of the Antofagasta Region. The most important is the El Laco volcanogenic iron deposit (see Section 3.2.7; Fig. 3.8). Apatite crystals from this deposit gave a fission track age of 2.1 ± 0.2 Ma (Fig. 4.1), which appears to be the time of effusion of magnetite lavas from the El Laco volcanic complex (see Sections 3.2.7, and 5.2.6). Apatite crystals from magnetite bodies in the southern flank of the Incahuasi volcano (26 km south of El Laco; Fig. 4.1) yielded a fission track age of 10.3 ± 1.6 Ma, which is also thought to be the formation age of the iron deposit (see Section 3.2.7, and 5.2.6). Other minor veins of silver, antimony and tin are hosted by a rhyodacitic porphyry in the Nevados de Poquis volcanic complex. Marinovic (1979) dated the porphyry at 12.9 ± 0.5 Ma (biotite, K-Ar).

## 4.3 GEOCHRONOLOGY OF PORPHYRY COPPER DEPOSITS OF NORTHERN CHILE

### 4.3.1 Introduction

Porphyry copper deposits are unquestionably the most remarkable characteristic of Andean metallogeny. They were first ascribed to the Early Tertiary, primarily due to the belief that the "metallogenic cycle of the Andean Geosynclinal region was closed with the mineralization originated by the Early Tertiary intrusive phase" (Ruiz and others, 1965). This assumption appeared to be further supported by the K-Ar age determination of Laughlin and others (1968) of 60.1 ± 1.8 Ma (recalculated) for the Toquepala porphyry copper in southern Peru. Therefore the idea that all South American porphyry copper deposits were distributed along a single north-south belt formed in a "Laramide" metallogenic epoch persisted at least until the mid-seventies (e.g., Neumann, 1973; Frutos, 1973, 1975). Although Ruiz and others (1965) reported some imprecise Pb-α determinations on zircons from Chuquicamata, El Salvador, Potrerillos and Disputada ranging between 68 and 25 Ma, as well as an Oligocene K-Ar date for the Fortuna Granodiorite at Chuquicamata, and a Miocene K-Ar age for the Disputada porphyry copper in central Chile, these ages were dismissed as incorrect. A truer picture arose from the systematic K-Ar dating of Chilean porphyry copper deposits done by Quirt (1972; Quirt and others, 1971) using samples collected in part by R. Sillitoe. In addition, subsequent dates (mostly K-Ar) reported by various authors (Gustafson and Hunt, 1975; Ambrus, 1977, 1979; Alvarez and others, 1980; Alvarez y Aracena, 1985; Rogers, 1985; Alpers, 1986; Ojeda, 1986; Olson, 1989) further constrained the age of the porphyry copper deposits of northern Chile, and allowed the separation of different age belts (Sillitoe, 1981, 1988). These geochronological data (see compilation by Sillitoe, 1988) show that the major porphyry copper deposits of northern Chile were formed between 41 and 31 Ma. However, these data do not provide information on possible disturbances of the K-Ar isotopic systems,

nor on errors derived from sample inhomogeneity. The different ages cannot be easily compared because they were calculated using dissimilar decay constants, measured in various laboratories, and the analytical data are generally unavailable.

In this study the more precise $^{40}Ar-^{39}Ar$ dating method was used to acquire an internally consistent data set, and to investigate the behaviour of the K-Ar isotopic system for biotites from the major porphyry copper deposits of northern Chile, as well as biotites and hornblendes from host rocks of other minor deposits (Figs. 4.4, 4.5; Appendix 1). As an independent check, some samples were also dated by the conventional K-Ar method.

Samples were collected from major porphyry copper deposits in the Domeyko Cordillera, from Chuquicamata to the north (Fig. 4.4), specifically from biotite-bearing rocks with strong potassic alteration, and from fresh pre-mineralization intrusives. Also sampled were minor porphyry copper deposits that occur within the Intermediate Depression (Fig. 4.5), but $^{40}Ar-^{39}Ar$ dating was restricted to their intrusive host rocks, because of the absence of suitable minerals within the mineralized ones.

### 4.3.2 Biotite in porphyry copper deposits

The cores of most copper-bearing porphyries contain fresh biotite crystals 1 to 4 mm in size, which presumably are of primary igneous origin, but also fine biotite crystals disseminated within the porphyry, or forming veinlets together with quartz, and constituting aggregates (possibly replacing hornblende). This fine-grained biotite is obviously of secondary origin, and is thought to be formed during the potassic alteration that affected the porphyries. During the mineral separation no attempt was made to segregate the two types of biotites, first because such a segregation is very difficult, and second because the

closure temperature of biotite for the K-Ar isotopic system ranges from 280° to 345°C (Harrison and others, 1985), which is below the range from 350° to 550°C at which potassic alteration takes place (Rose and Burt, 1979). The latter temperature interval coincides with the equilibrium temperature range that Parada and others (1987) determined for the Chuquicamata porphyry using the two feldspar geothermometer of Stormer (1975). Consequently both the hydrothermal and igneous biotites theoretically record a K-Ar age only after cooling below 345°C (maximum closure temperature of biotite), when the potassic alteration has largely ceased. This fact makes it difficult to distinguish the K-Ar age of stock emplacement from the K-Ar age of hydrothermal alteration within porphyry copper deposits as was observed in practice by Sillitoe (1988) and Skewes (1985).

K-Ar or $^{40}Ar$-$^{39}Ar$ ages on magmatic, hydrothermal or on mixtures of both types of biotites are cooling ages. These cooling ages cannot be regarded as an average for magmatic and hydrothermal events, as asserted by Skewes (1985), nor do they necessarily represent accurately the age of an early phase of K-silicate alteration when exclusively secondary biotite is dated, as interpreted by Sillitoe (1981; 1988) for the Los Pelambres porphyry copper deposit further south.

Disturbance of the K-Ar isotopic system, and consequent irregularities of $^{40}Ar$-$^{39}Ar$ spectra of biotites from major porphyry copper deposits may result from their interaction with fluids of hydrothermal and supergene origin. Investigations of the geochemistry of biotites from various alteration assemblages in porphyry copper deposits (Jacobs and Parry, 1974, 1979; Taylor and Fryer, 1982) have shown that biotite continuously re-equilibrates with the changing hydrothermal fluids producing wall rock alteration. Furthermore, experimental work of Newman (1970) showed that potassium is readily replaced by hydrated cations in micas during circulation of saline aqueous solutions similar to those of supergene environments.

### 4.3.3 Thermal activity in porphyry systems

Previous studies have shown differences of about 2 to 4 Ma among conventional K-Ar ages obtained within individual deposits. For example, the difference between biotite and sericite K-Ar ages from Chuquicamata porphyry has been interpreted by Ambrus (1977) as "an age difference between the late magmatic processes and pure hydrothermal processes of about one to two million years" and a similar view has been supported by Sillitoe (1988) who stated "at Chuquicamata, a time difference of about 3 Ma is discernable between the mean ages of K-silicate and sericitic events." However, these conclusions are questionable, first, because as shown above the biotite closure temperature for the K-Ar isotopic system is significantly lower than the temperature of igneous processes, or at which the potassic alteration occurs. In fact it is well within the temperature of sericitic alteration. Therefore, biotite K-Ar dates of porphyry copper deposits may record the time of occurrence of sericitic alteration rather than that of late magmatic processes or potassic alteration. Second, a simple two-dimensional cooling model (Jaeger, 1968) was used to calculate the duration of cooling of an idealized dike-like intrusive body (representing Chuquicamata, the largest porphyry copper deposit of northern Chile). Parameters were infinite lateral dimension, 1,200 m thick, zero permeability and thermal diffusivity of 0.01 $cm^2/sec$. The model predicts that Chuquicamata would have cooled by conductive heat loss in less than 114,000 years. This is the time for the contrast in temperature between the intrusion and the host rocks, at an epizonal level, to drop to less than 18% of its initial value (roughly a temperature drop from 770° to 140°C assuming initially cool host rocks). An epizonal level of emplacement is warranted by the external halo of propylitic alteration that surrounds the porphyries, which indicates outward rapid temperature drop (e.g., Rose and Burt, 1979). The 114,000 years may be regarded as a **maximum** period required for cooling an epizonal intrusive body such as the Chuquicamata porphyry, which is 14 km long and 1 km average width, because the calculation assumes exclusively conductive heat loss restricted to two sides (e.g., a

rectangular body cools faster as it loses heat by its four sides). In addition, if the permeability of the same infinite dike-like intrusive body, and its host rocks is set to 0.25 mD, so that fluids could circulate in a convective system, the cooling time is reduced by one order of magnitude, and only about 20,000 years are required for accomplishing the same temperature drop. If the permeability is set at 1 mD it will be further reduced to only about 5,000 years. The average permeability measured in geothermal fields ranges from 3 to 100 mD, and in one porphyry copper an average of 0.25 mD has been measured, and a value of 400 mD has been obtained for fracture zones (Cathles and others, 1979). The implication is that most of the hydrothermal circulation and cooling occurs in the initial few tens of thousands of years after the intrusion of a porphyry as previously stressed by Cathles (1977, 1981), a period of time that is well below the resolution of common geochronological methods. For example, the minimum analytical error of the conventional K-Ar method is 1 to 2%, thus 300,000 to 600,000 years for samples 30 Ma old. The more precise $^{40}Ar$-$^{39}Ar$ method may achieve errors of a few tenths of a percent for samples irradiated together, but still error margins would be higher than 100,000 years for a sample 30 Ma old. The analytical error of the Rb-Sr method ranges from 0.5 to 1%, but the Rb/Sr method is not appropriate for such young rocks because of the long half-life of $^{87}Rb$ ($48.8 \times 10^9$ yrs), and the consequent infinitesimal amounts of radiogenic $^{87}Sr$ produced. A whole-rock eight-point Rb-Sr isochron of 34.2 ± 4.0 Ma has been obtained for the Chuquicamata porphyry (Zentilli and others, 1988), but because of its relatively large analytical error this age does not clarify the meaning of radiometric age variation in this copper deposit.

The range of K-Ar ages in Chuquicamata, and other porphyry copper deposits may well be just a result of analytical errors, or due to the variations in K/Ar ratios attributable to inhomogeneous composition of the dated minerals. Alternatively, it may be the result of different intrusive pulses (not obvious from the geology of Chuquicamata, but common in other deposits), or the consequence of the long-term supply of hot fluids from a deeper, larger intrusive body as suggested by Sillitoe (1973; 1981; 1988). To ascertain whether the age difference is

real or just an analytical artifact, would require a more detailed geochronological study using the $^{40}Ar$-$^{39}Ar$ and fission track dating methods combined with the application of a dating technique that has higher closure temperature (650°-750°C), such as Pb-U dating of zircons. Although this type of study probably is more appropriate for younger porphyry copper deposits such as those of central Chile (Late Miocene-Pliocene), since analytical errors would be less significant.

### 4.3.4 Chuquicamata

In this enormous copper deposit biotite and orthoclase from a sample (FT-19) of the East Porphyry (nomenclature after Alvarez and others, 1980) from the eastern section of the mine pit were dated. The rock is a medium-grained porphyry; it is mineralized (copper sulfides) and is strongly affected by potassic alteration (orthoclase, biotite). It is made up of plagioclase (slightly sericitized) and quartz phenocrysts, which coexist with zoned orthoclase megacrysts up to 5 cm in length. The groundmass is composed of a fine-grained aggregate of quartz and potassic-feldspar, which constitutes only about 10% of the rock. The East Porphyry shows evidence of ductile deformation on the microscopic scale. This evidence is occurrence of bent plagioclase crystals (with slipbands and deformation twinning), elongate quartz crystals with undulatory extinction, subgrains, serrate borders, or mortar texture, and bent and kinked biotites with undulatory extinction.

The incremental-release $^{40}Ar$-$^{39}Ar$ age spectrum obtained for the biotite from the East Porphyry of Chuquicamata defines a plateau at 31.7 ± 0.4 Ma (68% of $^{39}Ar$ released; Fig. 4.4). The age spectrum shows a significant drop in apparent ages from the 800°-850°C degassing step up, being particularly conspicuous at the degassing step 850°-900°C (apparent age 22.8 ± 4.2 Ma), but partially recovering higher apparent ages in the increments above 900°C, thus defining a saddle-shaped spectrum. This is a relatively common, but not well understood feature of $^{40}Ar$-$^{39}Ar$ age

spectra of biotites, which account in part for the discrepancy of 0.9 Ma between the total gas age of 30.8 ± 1.0 Ma and the above plateau date.

Orthoclase from megacrysts of the East Porphyry of Chuquicamata (FT-19) yielded a $^{40}Ar$-$^{39}Ar$ total gas age of 31.4 ± 0.8 Ma. The age spectrum is somewhat irregular at lower temperature increments, but high temperature steps define a plateau at 31.4 ± 0.2 Ma (57% $^{39}Ar$ released; Fig. 4.4), which is concordant within error limits with the total gas age, and also with the biotite plateau age. This concordance of ages implies a fast cooling of the porphyry, taking in consideration that K-feldspar closure temperature is about 150 ± 30°C (Harrison and McDougall, 1980). This conclusion is further supported by the concordant apatite fission track age of 30.2 ± 4.4 Ma that has been obtained for the same sample (FT-19). The closure temperature of apatite for fission tracks falls in the range 70°-125°C (Green and others, 1986). The fast cooling, at least from about 300° to 100°C, of the Chuquicamata porphyry is compatible with its epizonal (near surface) emplacement.

The $^{40}Ar$-$^{39}Ar$ plateau age of 31.7 ± 0.4 Ma obtained for the biotite of the Eastern Porphyry of Chuquicamata is younger than previously reported biotite K-Ar ages of 34.8 ± 1.8 Ma (Ambrus, 1979) and 34.4 ± 0.9 Ma (recalculated from Ambrus, 1977; original age 33.6 ± 0.9 Ma). The plateau $^{40}Ar$-$^{39}Ar$ age coincides with sericite K-Ar ages of 31.2 ± 1.3 Ma (Ambrus, 1979), 31.0 ± 1.3 Ma (recalculated from Ambrus, 1977) and 30.5 ± 0.9 Ma (recalculated from Quirt, 1972).

The Chuquicamata porphyry copper deposit is abruptly terminated to the west by a major fault, the West Fissure, beyond which outcrops the pre-mineral Fortuna Granodiorite. The dominant lithology is a medium-grained, largely equigranular granodiorite made up of plagioclase (dominant mineral), quartz, orthoclase, biotite, and hornblende. The biotite from a sample of Fortuna Granodiorite (FT-23), collected 10.5 km to the southwest of the Chuquicamata deposit was dated by the $^{40}Ar$-$^{39}Ar$ method. The incremental-release $^{40}Ar$-$^{39}Ar$ age spectrum obtained does not define a plateau, but suggests some degree of disturbance of the K-Ar

system, yielding a total gas age of 35.6 ± 1.0 Ma. However, four steps (not adjacent) suggest a cooling age of 37.1 ± 0.5 Ma (58% $^{39}Ar$ released; Fig. 4.4) for the granodiorite. The spectrum shows a drop in apparent age in the step 650°-700°C, and also from 750° to 900° (saddles). Biotite from the same sample (FT-23) was also dated by conventional K-Ar method in the Geochronological Laboratory of SERNAGEOMIN in Chile, yielding an age of 39.0 ± 1.2 Ma (Table 4.1). This K-Ar date is about 3 Ma older than the $^{40}Ar$-$^{39}Ar$ total gas age, which may be attributed either to a difference in laboratory calibration or the result of inhomogeneous distribution of either potassium or argon within the dated biotite. Another sample of the Fortuna Granodiorite collected 5 km to the northwest of the Chuquicamata deposit (FT-43) has given a biotite K-Ar age of 39.5 ± 1.1 Ma in the SERNAGEOMIN laboratory, thus further suggesting a calibration discrepancy between the geochronological laboratories.

Sample FT-24 is from a section where the Fortuna Granodiorite is conspicuously foliated. It was collected 9 km to the southwest of Chuquicamata, and 1.5 km eastward of the FT-23 sample (closest to the West Fissure). The marked foliation (N10°E/vertical) derives from a preferential orientation of micas, amphiboles and feldspars, as well as from stretching and recrystallization of quartz. The feldspars are often bent, show slipbands and deformation twinning; biotites are bent, have undulatory extinction, and some of them are fragmented or recrystallized; quartz crystals are stretched, have undulatory and banded extinction, show development of subgrains or have been recrystallized to a microcrystalline aggregate that tends to define bands; hornblende crystals are oriented preferentially and show some microfracturing. These characteristics are typical of ductile deformation dominated by dislocation slip and dynamic recrystallization (Vernon, 1974, Etheridge and Wilkie, 1979). The existence of ductile deformation of feldspars suggests that it occurred when the granodiorite was still hot, roughly within a range of temperature from 600° to 300°C according to studies of natural and experimental deformation of granitic rocks (Hanmer, 1982; Tullis and Yund, 1978, 1980; Simpson, 1985; Burg and Iglesias, 1985).

The incremental-release $^{40}Ar$-$^{39}Ar$ age spectrum obtained for the FT-24 biotite does not define a plateau, but 60.2 % of the $^{39}Ar$ released in non-contiguous steps coincides at 36.3 ± 0.6 Ma. A "saddle" at increments from 750° to 850°C separates two flat segments of the age spectrum (Fig. 4.4). The total gas age is 34.8 ± 1.6 Ma, which is concordant, within error limits, with the $^{40}Ar$-$^{39}Ar$ age obtained for the non-foliated granodiorite. The 36.3 ± 0.6 Ma is a minimum age for the dynamic ductile deformation of the eastern border of the Fortuna Granodiorite (near the West Fissure). The dynamic deformation is related to a stage of right-lateral strike-slip displacement along the West Fissure of Chuquicamata (see Section 2.16), which according to the above textural and geochronological data was active at the time of emplacement of this granodiorite.

### 4.3.5 El Abra

The El Abra porphyry copper deposit is located 42 km north of Chuquicamata. It is characterized by multiple intrusive phases that have been emplaced at about the same site (Ambrus (1977). This complicates dating, since successive thermal pulses have likely reset the K-Ar radiometric clock of biotites. The nomenclature for the rock units used in this section is that of Ambrus (1977).

Sample FT-47 is from the El Abra Diorite, which is the rock unit that contains most of the copper ore within this deposit. The sample includes copper sulfides and has been strongly affected by potassic alteration (biotite), it is a medium-grained quartz diorite made up of plagioclase (partly replaced by biotite), quartz of secondary appearance (crystal aggregates and veinlets), abundant biotite both medium-grained (presumably primary magmatic) and profuse fine-grained (hydrothermal). The larger biotite crystals are commonly bent and show undulatory extinction.

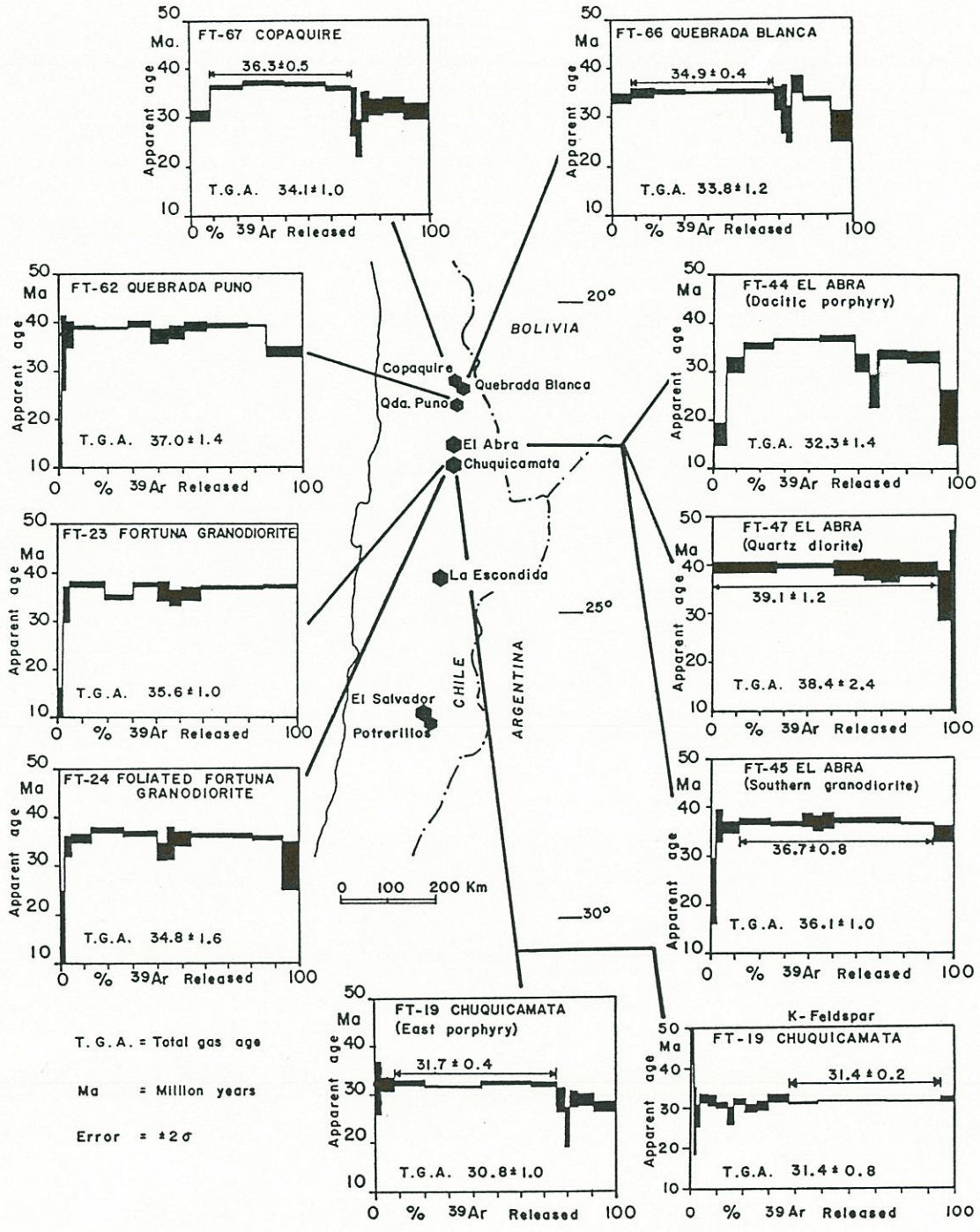


**Figure 4.4.** $^{40}Ar$–$^{39}Ar$ dates and age spectra of biotites (except when indicated otherwise) from major porphyry copper deposits and pre-mineral intrusions. Analytical uncertainties (±2σ) are represented by vertical width of bars (See Appendix 1 for analytical data and detailed age spectra).

The incremental-release $^{40}Ar$-$^{39}Ar$ age spectrum obtained for the FT-47 biotite is incomplete, because the first two increments were lost (faulty vacuum valve in the argon extraction line). However, the gas lost is non-essential for the age determination, because usually the first steps only release a very small amount of radiogenic argon and yield too low ages due to the degassing of non-retentive sites of the crystals, such as defects, dislocations, and inclusions. The $^{40}Ar$-$^{39}Ar$ age spectrum obtained defines a plateau at 39.1 ± 1.2 Ma (Fig. 4.4). Between the heating increments from 700° to 900° there is an increase of analytical error, and a slight decrease in apparent ages, which might imply a minor isotopic disturbance of the K-Ar system, but no significant argon loss is apparent.

The above 39.1 ± 1.2 Ma biotite $^{40}Ar$-$^{39}Ar$ plateau age is significantly older than the K-Ar range from 34.3 to 36.2 Ma[1] determined by Ambrus (1977) for the El Abra copper deposit. However, the age is compatible with the 36.8 ± 0.7 Ma biotite K-Ar age published by the same author (recalculated here) for the post-mineralization Pajonal Diorite. Thus the K-Ar ages obtained by Ambrus (1977) have probably been reset by thermal events associated with late (post-mineralization) intrusive pulses.

Sample FT-44 is from the El Abra Dacitic Porphyry, a mineralized rock and one affected by strong potassic alteration. This porphyry constitutes north-northeast trending dike-like intrusions that crosscut the previously described El Abra Diorite. Lithologically, it is a medium-grained porphyry with plagioclase, quartz and biotite phenocrysts. The groundmass is composed of a fine aggregate of quartz, plagioclase and biotite. The biotite phenocrysts are presumably primary, but the porphyry contains abundant, disseminated, hydrothermal, fine-grained biotite. The incremental-release $^{40}Ar$-$^{39}Ar$ age spectrum of the FT-

---

[1] Age range recalculated using new decay constants, original range reported by Ambrus (1977) was 33.5 to 35.4 Ma.

44 biotite is quite irregular (Fig. 4.4); it shows initially a gradient of ages from 17.1 to 36.8 Ma followed by a pronounced saddle, features that indicate a disturbance of the K-Ar system and argon loss. Thus the $^{40}Ar$-$^{39}Ar$ total gas age of 32.3 ± 1.4 Ma obtained is obviously incorrect. The higher apparent age of the gradient at 36.8 ± 0.6 Ma may represent the cooling age of this biotite sample. The apatite from the same sample (FT-44) yielded a fission track age of 37.6 ± 5.2 Ma, which is concordant (within error limits) with the highest apparent $^{40}Ar$-$^{39}Ar$ age of the gradient and the total gas age.

The higher step of the disturbed $^{40}Ar$-$^{39}Ar$ age spectrum of the FT-44 biotite at 36.8 ± 0.6 Ma (best estimate of the cooling age of the biotite) is only slightly older than the biotite K-Ar age of 35.0 ± 0.6 Ma obtained previously by Ambrus (1977) for the Dacitic Porphyry, and is identical to the biotite K-Ar age of 36.8 ± 0.7 Ma determined by the same author for the post-mineralization Pajonal Diorite. Therefore there is a chance that the K-Ar isotopic system of the FT-44 biotite has been disturbed by both a post-mineralization thermal event and alteration, which caused significant argon loss.

Sample FT-45 is from the Southern Granodiorite 2.5 km southwest of the El Abra porphyry copper deposit. The Southern Granodiorite forms a pluton located immediately south of the El Abra porphyry copper. It is an equigranular, medium-grained granodiorite made up of plagioclase, K-feldspar, quartz, biotite and hornblende. The rock shows some bent biotites, quartz with undulatory extinction, and plagioclase crystals are slightly curved, evidencing some minor ductile deformation. The incremental-release biotite $^{40}Ar$-$^{39}Ar$ age spectrum defines a plateau at 36.7 ± 0.8 Ma. This $^{40}Ar$-$^{39}Ar$ age plateau is concordant, within error limits, with a three point Rb-Sr isochron of 38.7 ± 2.2 Ma obtained by Rogers (1985) for the Southern Granodiorite. In addition, it is concordant with the $^{40}Ar$-$^{39}Ar$ age inferred above for the Dacitic Porphyry, which clearly intrudes granodiorite. It is also concordant with the biotite K-Ar age of 36.8 ± 0.7 Ma (recalculated) reported by Ambrus (1977) for the post-mineralization Pajonal Diorite. Furthermore,

considering the $^{40}Ar-^{39}Ar$ age of 39.1 ± 1.2 Ma determined above for the mineralized El Abra Diorite, there is a discrepancy with the apparent field relationships, which according to Ambrus (1977) show that the Southern Granodiorite is the oldest pluton of the El Abra Intrusive Complex. These considerations strongly suggest that the 36.7 ± 0.8 Ma biotite $^{40}Ar-^{39}Ar$ plateau is a reset age, and therefore does not represent the original cooling age of the Southern Granodiorite.

Apatite from the sample FT-45 of the Southern Granodiorite yielded a fission track age of 35.3 ± 4.4 Ma, whereas another sample collected east of El Abra (FT-48) gave an apatite fission track age of 37.7 ± 5.0 Ma. These dates are concordant with the biotite $^{40}Ar-^{39}Ar$ plateau age obtained for this pluton.

In summary, the biotite $^{40}Ar-^{39}Ar$ plateau age of 39.1 ± 1.2 Ma of the mineralized El Abra Diorite is the oldest radiometric age obtained so far within this porphyry copper deposit. The rest of the dates are essentially concordant at about 36 Ma. The latter seems to be the age of a post-mineralization thermal pulse, probably associated with the emplacement of the Pajonal Diorite, which probably reset the K-Ar isotopic system of most biotites in the area of this copper deposit.

### 4.3.6 Quebrada Puno

Quebrada Puno is an alteration zone located 104 km to the north of Chuquicamata. The prospect includes sub-economic copper-molybdenum ores at depth (Miranda, 1982, 1986). Sample FT-62 was collected from an intrusive apophysis that outcrops within the altered zone; it is a medium-grained quartz monzonite composed of abundant plagioclase, biotite, and minor chloritized hornblende. These minerals are embedded within a fine-grained aggregate, partly graphic, of anhedral quartz and K-feldspar with inclusions of tiny plagioclase crystals.

Besides chloritization of hornblende, this rock does not show significant effects of hydrothermal alteration and includes only a minor proportion of pyrite. The incremental-release biotite $^{40}Ar$-$^{39}Ar$ age spectrum does not define a plateau (Fig. 4.4); it shows a saddle at the increments between 750° and 900°C and a conspicuous drop[2] in apparent age for the increment 1000-1100°C. The $^{40}Ar$-$^{39}Ar$ total gas age, 37.0 ± 1.4 Ma, is regarded as a minimum date because of the irregular age spectrum. Five non-contiguous increments (57% $^{39}Ar$ released) suggest a cooling age of 38.9 ± 0.7 Ma for this biotite. Huete and others (1977) reported a younger whole rock K-Ar date of 32.4 ± 2.2 Ma[3] for the same quartz monzonite. A whole rock K-Ar date involves the integrated release of argon from retentive and non-retentive phases; thus a younger age is to be expected.

### 4.3.7 Quebrada Blanca

The Quebrada Blanca porphyry copper deposit is located at latitude 21°00'S (Fig. 4.4); a description of its geology has been published by Hunt and others (1983). Sample FT-66 of mineralized quartz monzonite porphyry from this deposit was collected. This rock has been affected by potassic alteration (biotite). The porphyry is composed of plagioclase, K-feldspar, quartz (anhedral and with embayments) and euhedral biotite phenocrysts. The groundmass is made up of a microcrystalline aggregate of quartz, feldspar, and abundant, secondary, fine-grained biotite. Aggregates of fine-grained biotite also replace pre-existing mafic minerals (probably hornblende). The incremental-release $^{40}Ar$-$^{39}Ar$ age spectrum obtained for the biotite defines a plateau at 34.9 ± 0.4 Ma (63% $^{39}Ar$ released; Fig. 4.4). The $^{40}Ar$-$^{39}Ar$ total gas age, 33.8 ± 1.2 Ma, is slightly younger because of a minor irregularity of the

---

[2] Effect of high blank at higher temperature.

[3] Recalculated using new decay constants.

age spectrum (saddle at higher temperature increments). The same sample (FT-66) was also dated by the conventional K-Ar method in the Geochronological Laboratory of the SERNAGEOMIN in Chile, where a biotite K-Ar age of 37.7 ± 0.9 Ma, and a whole rock K-Ar date of 35.9 ± 1.2 Ma were obtained. The biotite $^{40}Ar$-$^{39}Ar$ plateau age of 34.9 ± 0.4 Ma is thought to be a good estimate of the minimum age of copper mineralization at this deposit, even though it is somewhat younger than the biotite K-Ar date obtained in Chile, and also lower than the 38 ± 2 Ma K-Ar date[4] reported by Hunt and others (1983) for a quartz monzonite from this copper deposit and to the altered biotite K-Ar dates of 37.2 ± 1.4 Ma and 36.5 ± 1.4 Ma published by Vergara and Thomas (1984). The discrepancy with the $^{40}Ar$-$^{39}Ar$ date may reflect disparity in laboratory calibration, the effect of more than one thermal pulse within this deposit, or both.

### 4.3.8 Copaquire

Copaquire is a porphyry copper-molybdenum prospect located 10 km northwest of Quebrada Blanca and 160 km north of Chuquicamata (Hollister and Bernstein, 1975)(Fig. 4.4). It is the only Chilean porphyry type deposit where molybdenum mineralization dominates over copper. A sample (FT-67) of a granodioritic porphyry mineralized with molybdenite, and affected by potassic alteration (K-feldspar, biotite) from this deposit was dated. The porphyry is composed of medium-grained argillized plagioclase, K-feldspar, quartz and biotite, and a groundmass (<10%) made up of quartz and K-feldspar microcrystalline aggregate. The rock shows evidence of a partial argillization, probably of supergene origin, but except for some oxidation, the biotite is fresh. The incremental-release biotite $^{40}Ar$-$^{39}Ar$ spectrum strictly does not define a plateau, but shows a saddle over the 750°-900°C range of degassing temperature (Fig. 4.4). The $^{40}Ar$-$^{39}Ar$ total gas age is 34.1 ± 1.0 Ma.

---

[4] No indication of mineral dated nor analytical data are provided by these authors.

However 4 steps (60.4% of $^{39}Ar$ released), with only minor apparent age discrepancies, suggest a date of 36.3 ± 0.5 Ma. Biotite from the same sample was separated by density and the two splits dated by the conventional K-Ar age in the Geochronological Laboratory of the SERNAGEOMIN in Chile, where they produced ages of 37.4 ± 3.1 Ma and 34.0 ± 1.8 Ma. These K-Ar ages have large analytical errors, but they are roughly concordant with the $^{40}Ar$-$^{39}Ar$ date.

### 4.3.9 La Escondida

The rich porphyry copper deposit La Escondida is located 150 km WSW of the Antofagasta port. No $^{40}Ar$-$^{39}Ar$ dating was done at this deposit[5], but Alpers (1986; also Alpers and Brimhall, 1988) have recently reported several K-Ar ages ranging between 38.3 ± 1.5 to 31.0 ± 1.4 Ma. The latter authors ascribed biotite K-Ar ages ranging from 33.7 ± 1.3 to 32.8 ± 1.3 Ma, and a sericite K-Ar age of 33.7 ± 1.4 Ma to an "early hypogene alteration." In addition, sericite K-Ar ages ranging between 31.6 ± 1.6 and 31.0 ± 1.4 Ma were ascribed to a "late hypogene alteration." They considered unreliable the older dates on two hypogene alunite veins, and one on a biotitic whole rock. The hypogene alunites from La Escondida gave apparent K-Ar ages of 35.7 ± 1.8 and 38.3 ± 1.5 Ma, which were interpreted by Alpers (1986) as indicative of excess $^{40}Ar$ in the alunite crystals, particularly from abundant sub-micron size fluid inclusions. The whole rock sample of biotitized andesite from the wall rocks gave an apparent K-Ar age of 35.4 ± 1.8 Ma, this age was thought by Alpers (*op. cit.*) to be influenced by the possible presence of relict grains of potassium-bearing minerals that had not been completely reset at the time of biotitization. On the other hand, four samples of supergene alunites gave apparent K-Ar ages ranging from 18.0 ± 0.8 to 14.7 ± 0.7 Ma. These ages were taken by the above author to imply that supergene activity

---

[5] No sampling was allowed by Utah Minera de Chile Inc. at La Escondida in 1986.

occurred at least partly during the Early and Middle Miocene. Supergene alunite probably constantly re-equilibrates as it interacts with circulating fluids. Therefore it probably became effectively a closed system with respect to argon diffusion when the circulation of supergene solutions ceased. Consequently, K-Ar dates on supergene alunite represent a minimum age estimate of supergene alteration. A similar conclusion has been recently reached by Bird and others (1990) in a study of surficial alunites in Australia. Although these authors indicated that the early formation of supergene alunite in ore deposits may be a special case (e.g., Ashley and Silberman, 1976), they showed that supergene alunite usually does not crystallize synchronously with active weathering, but its formation, in many cases appear to be related to a late gradual desiccation.

Another set of whole rock and biotite K-Ar dates from La Escondida was reported by Ojeda (1986). These range from 34.6 ± 1.8 to 31.8 ± 1.2 Ma. An older biotite K-Ar age of 39.1 ± 1.1 Ma was obtained for a biotitized andesite collected from the deepest drill-hole. Ojeda (*op. cit.*) dismissed this older age as anomalous.

### 4.3.10 El Salvador

No new dating was done at El Salvador, but the detailed study of this porphyry copper deposit by Gustafson and Hunt (1975) reported several K-Ar and Rb-Sr dates, which range from 41.3 ± 1.4 to 39.1 ± 1.1 Ma (see Appendix 2). The volcanic host rocks yielded K-Ar ages ranging between 50.3 and 45.4 ± 1.4 Ma, whereas supergene alunites gave K-Ar ages of 36.1 ± 0.6 and 36.0 ± 2.5 Ma. The latter dates suggest that supergene processes developed no more than 5 Ma after the hypogene mineralization. Unfortunately, all these dates have to be taken only as indicative, because they were likely calculated using old decay constants, and no analytical data, nor dates considered anomalous were reported by Gustafson and Hunt (*op. cit.*).

### 4.3.11 Potrerillos

The mineralized Cobre Porphyry at Potrerillos was recently dated by Olson (1989) at 37.0 ± 0.5 Ma (biotite K-Ar). At the same district, an unmineralized plagioclase lamprophyre yielded a whole rock K-Ar age of 45.2 ± 1.0 Ma and a quartz-plagioclase porphyry a hornblende K-Ar age of 40.5 ± 4.2 Ma. Biotite from the Cerro El Hueso porphyry, which is an intrusion located 3 km east of the porphyry copper deposit that contain low-grade gold mineralization, gave K-Ar ages of 32.6 ± 0.5 and 31.8 ± 0.4 Ma (Olson, *op. cit.*). However, Colley and others (1989) indicated that mineralized samples of the Cerro El Hueso porphyry gave a Rb-Sr isochron at 37 ± 4 Ma. Therefore, they implied a cogenetic epithermal-gold and porphyry-copper mineralization at this district.

### 4.3.12 Sierra Gorda

Sierra Gorda is a sub-economic porphyry copper deposit located on the eastern section of the Intermediate Depression (Fig. 4.5). The biotite from a sample (II-592) of equigranular medium-grained granodiorite was dated by the $^{40}Ar$-$^{39}Ar$ method. This granodiorite constitutes the host-rock of the copper-bearing porphyry of Sierra Gorda, and it is composed of plagioclase, quartz, orthoclase, biotite and hornblende. The biotite is fresh, except for minor chloritization. The incremental-release $^{40}Ar$-$^{39}Ar$ age spectrum obtained for the II-592 biotite shows a well-defined age plateau at 63.3 ± 0.6 Ma (85.1% of $^{39}Ar$ released). Another sample (II-RB-36) of the same granodiorite dated by the conventional K-Ar method in the Geochronological Laboratory of SERNAGEOMIN in Chile gave a biotite K-Ar date of 64 ± 2 Ma concordant (within error limits) with the above biotite $^{40}Ar$-$^{39}Ar$ plateau age. Furthermore, a sample (II-RB-34) of the altered and mineralized porphyry that outcrops in the area of the mines San Armando and Salvadora of Sierra Gorda yielded a plagioclase K-Ar age of 60 ± 4 Ma. In the same mining district, but 8 km to the south, a

whole rock K-Ar age of 59.8 ± 2.0 Ma was obtained for a fragment of granodiorite from a breccia pipe with copper mineralization (Copucha mine). A biotite K-Ar age of 63 ± 2 Ma was obtained for the host granodiorite (II-RB-37) that outcrops in the Cerros de Bella Esperanza. These new $^{40}Ar$-$^{39}Ar$ and K-Ar dates show that the mineralization at Sierra Gorda very probably occurred within the range 60 to 64 Ma (Fig. 4.1). Quirt (1972) reported a K-Ar age of 44.9 ± 1.6 Ma (recalculated here) for a mixture of altered biotite and some hornblende from a breccia pipe at Sierra Gorda. This was regarded as a minimum age because of the altered nature of the biotite. His view is corroborated by the new data.

### 4.3.13 Lomas Bayas - Fortuna del Cobre

Lomas Bayas is a minor porphyry copper deposit located within the Intermediate Depression. A sample of medium-grained granodiorite (II-611), which constitutes the host rock of this copper deposit was dated by the $^{40}Ar$-$^{39}Ar$ method. The sample was collected 2 km to the northeast of the ore body, and it is composed of plagioclase, quartz, K-feldspar, chloritized biotite (variable degree), and hornblende with inclusions of biotite. The incremental-release $^{40}Ar$-$^{39}Ar$ age spectrum obtained for the biotite defines a plateau at 64.2 ± 0.6 Ma (Fig. 4.5), even though one gas increment was lost due to a mistake during the stepwise degassing. In contrast, the hornblende of the same sample (II-611) produced a particularly irregular age spectrum (Fig. 4.5), which shows a gradient from 46.7 to 59.9 Ma, evidence of significant argon loss. Although the second and third increments produced apparent ages of 57.6 and 59.9 Ma interrupting the mentioned gradient, these older ages are attributed to the degassing of biotite inclusions within the amphibole as these increments show particularly low $^{37}Ar/^{39}Ar$ ratios (Appendix 1). The 57.0 ± 7.8 Ma apatite fission track age obtained for the same sample (II-611) is concordant (within error limits) with the $^{40}Ar$-$^{39}Ar$ ages. The $^{40}Ar$-$^{39}Ar$ data suggest that the granodiorite has been affected by a process that produced partial argon loss from the amphiboles without affecting the

biotite K-Ar isotopic system, or signify excess argon in the biotite. The higher closure temperature of the hornblende (500 ± 25°C; Harrison, 1981) compared with that of biotite (310 ± 35°C; Harrison and others, 1985) rules out argon loss from the hornblende by a thermal event. The argon loss from the hornblende may be the result of circulating hydrothermal fluids, not sufficiently hot to reset the biotite, and probably in equilibrium with this mineral. These fluids probably circulated during the emplacement and mineralization of the neighbouring Lomas Bayas porphyry, and reacted with hornblende (minor alteration) producing a chemical perturbation of its K-Ar isotopic system. The alternative of excess argon in the biotite cannot be ruled out, however, but its well defined $^{40}Ar$-$^{39}Ar$ age plateau is compatible with undisturbed K-Ar system.

An attempt was made to date the mineralized granodioritic porphyry of the Lomas Bayas copper deposit by the conventional K-Ar method using chloritized biotite (II-RB-25). However, the K-Ar date of 33.2 ± 7.3 Ma obtained is thought to lack geological meaning, because this altered biotite has one order of magnitude less potassium than a common biotite (Appendix 4). On the other hand, a biotite K-Ar age of 61 ± 2 Ma was obtained for the host granodiorite 200 m from the contact with the mineralized porphyry, which agrees with the $^{40}Ar$-$^{39}Ar$ data.

The Fortuna del Cobre prospect is located 3 km to the southwest from the Lomas Bayas deposit, and is hosted by the same granodioritic pluton. The hornblende from a sample of the host granodiorite collected 3 km to the southwest of the Fortuna prospect (II-607) produced a rather irregular incremental-release $^{40}Ar$-$^{39}Ar$ age spectrum (Fig. 4.5); it shows a gradient from 48.1 to 63.4 Ma, which is interrupted by two steps with higher apparent ages (57.9 and 55.8 Ma) and low $^{37}Ar/^{39}Ar$ ratios. This spectrum suggests that the granodiorite cooling age is about 63.4 Ma, and shows evidence of significant argon loss from the amphibole resulting in the younger $^{40}Ar$-$^{39}Ar$ total gas age of 57.9 ± 3.6 Ma. These are characteristics comparable to those observed in the age spectrum of the above II-611 hornblende.

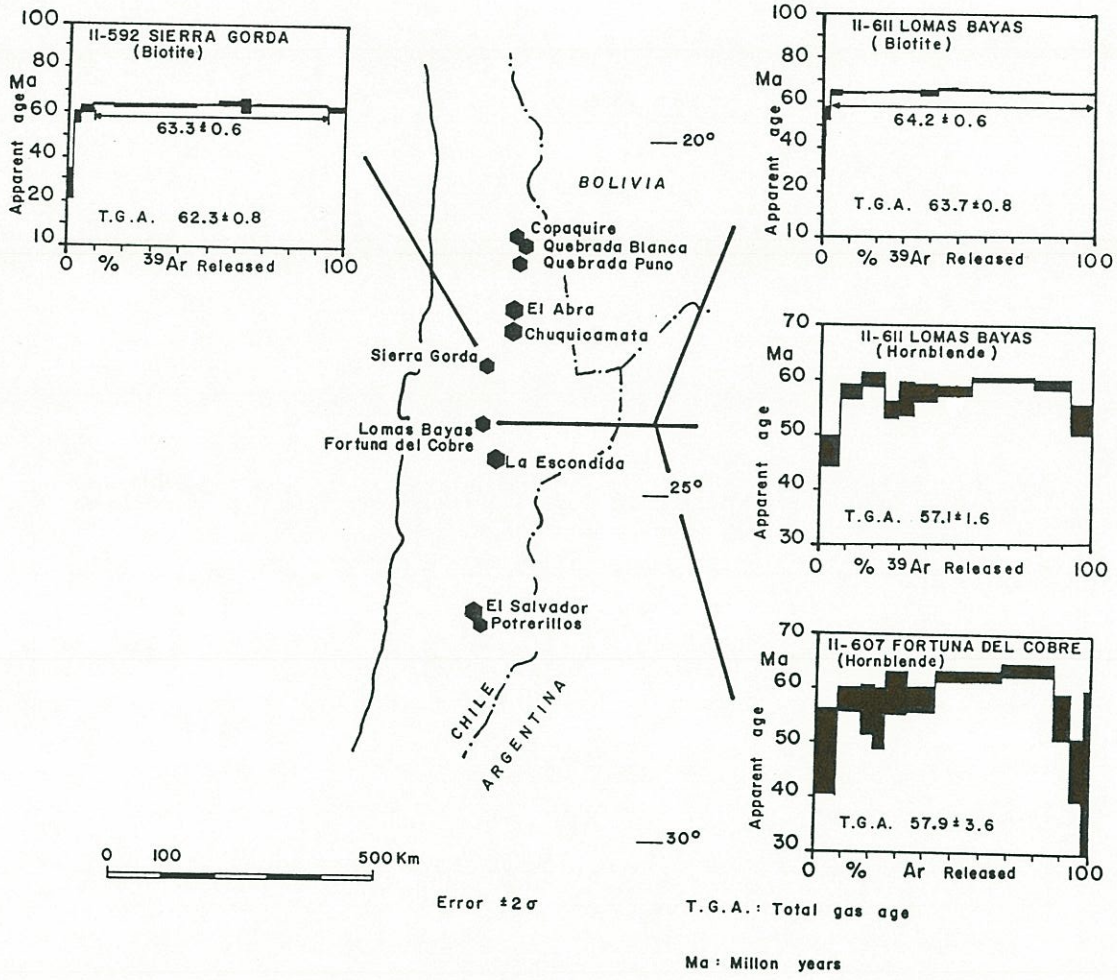


**Figure 4.5.** $^{40}Ar$–$^{39}Ar$ dates and age spectra of wallrocks of minor porphyry copper deposits. Analytical uncertainties (±2σ) are represented by vertical width of bars (See Appendix 1 for analytical data and detailed age spectra).

In summary, the biotite $^{40}Ar$-$^{39}Ar$ plateau age of 64.2 ± 0.6 Ma of the host granodiorite is the maximum age for the copper mineralization at Lomas Bayas - Fortuna del Cobre deposits. The minimum age is still not well constrained, but the emplacement of the porphyries probably took place in the Paleocene or Early Eocene if one takes into consideration the partial resetting of amphiboles, and the concordant fission track age of apatite. The hydrothermal activity related to copper mineralization is thought to account for the argon loss from the hornblende of the granodioritic pluton that hosts the Lomas Bayas and Fortuna deposits.

### 4.3.14 Centinela

Centinela is a porphyry type prospect located 15 km southwest of the Caracoles silver district (Fig. 4.1). Supergene copper oxides are hosted by a bleached dacitic porphyry that shows quartz eyes within a pervasively silicified, sericitized, and argillized mass. Two whole rock K-Ar age determinations on the altered porphyry gave values of 43.8 ± 1.5 and 44.3 ± 1.5 Ma. These must be regarded as minimum ages because of the altered nature of the porphyry and because only whole rock analyses were carried out.

## 4.4 CONCLUSIONS

Twenty-five new $^{40}Ar$-$^{39}Ar$ and thirty-one new K/Ar dates were produced in the course of this study to constrain the age of major metallic ore deposits. These data clearly indicate that the major metallic deposits of this Andean segment are not distributed randomly throughout geological time, but formed within discrete time intervals.

The main copper and gold deposits of the Coastal Cordillera were formed during a Middle to Late Jurassic mineralizing event, although the precise position of the stratabound copper mineralization within the Jurassic is still poorly defined. The silver, gold, and copper deposits of the Intermediate Depression and western foothills of the Domeyko Cordillera were formed during the Paleocene, except for the probably Late Cretaceous silver mineralization at Caracoles. The major porphyry copper deposits of the Domeyko Cordillera were formed during a period of 10 Ma during the Late Eocene - Early Oligocene.

The three main mineralizing events are markedly shorter than the long-lasting periods of igneous activity that characterize this Andean segment (see Chapter 2, and Fig. 6.1). These are considered the most important metallogenic epochs in the history of the Antofagasta segment of the Andes.

The post-Paleozoic ore deposits are older in the coastal area, and become progressively younger inland. Therefore there is a conspicuous eastward shift of the mineralizing centres since the Jurassic, which coincides with the migration of the magmatic front. This concurrence reflects the close genetic relationship between metallic mineralization and igneous activity in this Andean segment. However, special geological conditions, in addition to igneous activity, appears to be necessary to form anomalous metallic concentrations. These conditions are achieved only during relatively short intervals of geological time, and account for discrete metallogenic epochs that contrast with long-lasting intervals of magmatism. The identification of these particular geological conditions is essential for an understanding of the relationships between geological evolution and the metallic mineralization.

The metallogenic epochs inferred from the geochronological data, coupled with the knowledge of mineral distribution, may be used to direct mineral exploration since they roughly indicate which type and size of deposits may be located within the geological units or belts of different age in this region.

The geochronological data provide evidence for the recurrence of copper mineralization throughout the geological history of this Andean segment. This probably reflects a consistent system of magma generation, and probably a homogeneous source of copper, as previously concluded by Zentilli (1974) for the Atacama Region (26°-29°S).

The $^{40}Ar$-$^{39}Ar$ radiometric ages obtained in this study for the major porphyry copper deposits of the Antofagasta Region range from 39.1 ± 1.2 to 31.7 ± 0.4 Ma. Thus the $^{40}Ar$-$^{39}Ar$ data corroborate that the giant porphyry copper deposits of the Domeyko Cordillera were formed over about a 10 Ma interval during the Late Eocene to Early Oligocene[6]. On the other hand, minor porphyry copper deposits located within the Intermediate Depression are the result of a Paleocene mineralizing event, which correlates with the porphyry copper mineralization of southern Peru (Vidal, 1985), and copper mineralization of breccia pipe deposits of the Atacama Region (Sillitoe and Sawkins, 1971).

The incremental-release $^{40}Ar$-$^{39}Ar$ age spectra obtained for biotites collected from major Late Eocene - Oligocene porphyry copper deposits commonly show a decrease of apparent ages for the increments between 750° and 900°C, defining saddle-shaped spectra. The meaning of these saddles is uncertain, but they partly account for the 0.7 to 2.2 Ma difference between the $^{40}Ar$-$^{39}Ar$ plateau ages and the total gas ages on biotites. Furthermore, higher differences (1.3 to 4.5 Ma) are shown by samples with irregular $^{40}Ar$-$^{39}Ar$ age spectra. These differences may suggest that the conventional biotite K-Ar ages of porphyry copper deposits (which are essentially total gas ages) may be somewhat inaccurate, even beyond the precision of the method. This gives support to the idea that K-Ar age variation within individual deposits is an analytical artifact rather than the persistence of long periods of thermal activity within the copper deposits.

---

[6] Ages referred to the Geological Society of America Geological Time Scale (Palmer, 1983).

At least three of the dated biotites (Chuquicamata, El Abra) have $^{40}Ar$-$^{39}Ar$ ages concordant (within error limits) with apatite fission track ages from the same rocks; a concordant K-feldspar age was also obtained at Chuquicamata. This concordance of radiometric dates is consistent with abrupt temperature drop from about 300° to less than 100°C, implying fast cooling of the copper-bearing intrusions.

The biotites from the host rocks of minor Paleocene porphyry copper deposits produced well-defined incremental-release $^{40}Ar$-$^{39}Ar$ age plateaus. In contrast, hornblendes from the granodiorite that hosts the Lomas Bayas - Fortuna altered copper-bearing porphyries yielded irregular $^{40}Ar$-$^{39}Ar$ age spectra and younger ages than the biotite from the same rock. This suggests that hornblende may readily lose argon during low temperature hydrothermal events, but alternatively excess argon in the dated biotite may also account for its older age plateau.

The stepwise heating $^{40}Ar$-$^{39}Ar$ method has shown to be very useful in dating porphyry copper deposits, because it effectively reveals disturbances of the K-Ar isotopic system, which cannot be detected by the conventional K-Ar system. Also it has inherently lower analytical errors. However, in order to determine the thermal history of individual porphyry copper deposits, more detailed study is required, preferably employing several of the geochronological methods.

Estimates of the duration of hydrothermal activity within individual porphyry copper deposits based on K-Ar radiometric ages (e.g., Chuquicamata 2 to 3 Ma, Ambrus, 1977; Sillitoe, 1988) may be incorrect, because such age ranges can be artifacts of errors involved in the conventional K-Ar dating. The possibility of separated thermal pulses cannot be ruled out particularly within deposits where successive intrusive pulses occurred. Notwithstanding, the cooling interval of individual porphyritic intrusions probably took only a few tens of thousands of years, which is well below the resolution of common geochronological methods for rocks between 41 and 31 Ma.

# CHAPTER 5. FISSION TRACK THERMOCHRONOLOGY

## 5.1 INTRODUCTION

This study explores the potential genetic relationship between porphyry copper magma generation and Middle-Late Eocene crustal thickening (Chapter 7). Furthermore, it is known that both supergene enrichment and the preservation of these copper deposits depend on a balance between erosion and uplift (see Section 3.3). Apatite fission track dating appears to be a suitable method to evaluate these hypotheses. In this section the results of fission track dating, and track length analysis of apatite separates from the Paleozoic crystalline basement of the Domeyko Cordillera, intrusive rocks in the Coastal Cordillera and Intermediate Depression, and porphyry copper deposits are reported. The constraints these analyses place on tectonic and metallogenic models are also discussed.

### 5.1.1 Fission track dating

The technique for cooling age determination based on fission tracks in minerals was developed in the 1960s by the work of Price and Walker (1963), Fleischer and Price (1964), Fleischer and others (1965, 1965b, 1975), Naeser (1967), Wagner (1968) and Aumento (1969). The method is based on the natural fission decay of $^{238}U$, the most abundant uranium isotope. Uranium-238 decays by two schemes: $\alpha$-decay that ends with a lead isotope, and the less frequent spontaneous fission, which produces various lighter elements, whose masses centre around 95 and 135 (Naeser, 1967). Each fission event of a $^{238}U$ atom releases about 200 MeV

of energy, therefore two nuclei of approximately equivalent mass are forcefully thrown in opposite directions, thereby disrupting the crystalline structure of the host mineral along their path.

The physical nature of fission tracks is not well understood, but the prevailing explanation is the "ion explosion spike" mechanism of Fleischer and others (1965, 1965b), which implies that a damaged zone is created by ionization of atoms along the path followed by highly charged positive fission fragments. The secondary cations mutually repel, and are forced into the crystalline structure away from the path of the fission fragment, thus creating a damaged zone of less than 50 angstroms in diameter and 10 to 20 microns long. The accumulation of fission tracks through time within a host mineral constitutes the geochronological basis of the method. Apatite, zircon and sphene are the minerals most commonly dated by this method, because they have an adequate, and evenly distributed uranium content. General descriptions of the fission track method have been presented by Fleischer and others (1965b, 1975), Wagner (1968), McDougall (1976), Naeser (1976), and Hurford (1986).

Similar to other isotopic methods the fission track age equation (1) centres on the ratio of the remaining parent atoms relative to those that have radioactively decayed, here by spontaneous fission (Price and Walker, 1963; Naeser, 1967; Hurford, 1986).

$$T = \frac{1}{\lambda_D} \ln\left[1 + \frac{\lambda_D \phi \sigma I \rho_s}{\lambda_f \rho_i}\right] \qquad (1)$$

$\lambda_D$ = $1.55125 \times 10^{-10} yr^{-1}$, total decay constant for $^{238}U$ (Jaffey and others, 1971; Hurford, 1990).

$\lambda_f$ = spontaneous fission decay constant for $^{238}U$.

$I$ = $7.2527 \times 10^{-3}$, $^{235}U/^{238}U$ isotope abundance ratio (Cowan and Adler, 1976; Hurford, 1990).

$\sigma$ = $580.2 \times 10^{-24}$ $cm^2$, thermal neutron fission cross section for $^{235}U$ (Hannah and others, 1969; Hurford, 1990)

$\phi$ = thermal neutron fluence

$\rho_s/\rho_i$ = spontaneous/induced fission track density ratio in the sample (after Price and Walker, 1963, and Naeser, 1967).

Since the values for the constants $\lambda_g$, $\sigma$, and $I$ are widely accepted (Hurford, 1990), the determination of the track density $\rho_s/\rho_i$ ratio, the measure of the neutron fluence in the reactor, and the value of the $\lambda_f$ are required to calculate an age. Unfortunately there is a 20% variation on the calculated values of $\lambda_f$ , with results mostly grouped around $8.46 \times 10^{-17}$ $yr^{-1}$ and $7.00 \times 10^{-17}$ $yr^{-1}$ (Thiel and Herr, 1976; Bigazzi, 1981). In addition, the determination of absolute values for the neutron fluence in a reactor is complex (Green and Hurford, 1984). For fission track it may be monitored by the inclusion of standard glasses, which produce an induced track density in an external mica detector attached to the standard during irradiation. The flux $\phi$ is related to this track density $\rho_d$ by:

$$\phi = B \rho_d \qquad (2)$$

Where B is a fluence calibration factor, which can be determined by inducing gamma ray emission by neutron irradiation of gold, copper or cobalt foils surrounded by cadmium (Green and Hurford, 1984). However, there is no consistency between different methods of flux dosimetry, which coupled with the uncertainty of the $\lambda_f$ value makes the ages calculated by equation (1) unreliable (Hurford, 1986).

An alternative approach suggested by Fleischer and Hart (1972) avoids the use of $\lambda_f$, and the absolute dosimetry of neutron flux. Substituting equation (2) into (1), gives:

$$T = \frac{1}{\lambda_D} \ln\left[1 + \frac{\rho_s}{\rho_i} \sigma I \lambda_D \left(\frac{B \rho_d}{\lambda_f}\right)\right] \qquad (3)$$

All the constants, except for $\lambda_D$, can be grouped as a single calibration constant zeta ($\zeta$):

$$T = \frac{1}{\lambda_D} \ln\left[1 + \lambda_D \zeta \frac{\rho_s}{\rho_i} \rho_d\right] \qquad (4)$$

Zeta represents a calibration baseline (Zeta calibration; Hurford and Green, 1983) for the specific dosimeter glass in which $\rho_d$ is counted, and can be evaluated from a series of mineral age standards by:

$$\zeta = \frac{(e^{\lambda_D T_{STD}} - 1)}{\lambda_D (\rho_s / \rho_i)_{STD} g \rho_d} \qquad (5)$$

$T_{STD}$ = Age of standard mineral[1]

$(\rho_s/\rho_i)_{STD}$ = Spontaneous/induced track density ratio of a standard.

$\rho_d$ = Induced track density of a standard glass with known uranium content.

$g$ = Geometry factor = 0.5 for external detector method (Gleadow and Lovering, 1977)

The zeta approach is analogous to that used in $^{40}Ar$-$^{39}Ar$ dating, in the sense that the age of a given sample is derived from its $\rho_s/\rho_i$ ratio by comparison with the $\rho_s/\rho_i$ ratio of a standard mineral of well known age, except that $\zeta$ is evaluated over a series of calibration runs, as compared with the J-factor in $^{40}Ar$-$^{39}Ar$ dating, which is irradiation specific (Hurford, 1990).

The error estimation in fission track dating makes the assumption that track counts follow a Poisson distribution. The analysis of errors of Green (1981), used in this study, assumes that there is no

---

[1] 27.8 ± 0.2 Ma for Fish Canyon apatite (Hurford and Hammerschmidt, 1985), and 31.4 ± 0.5 Ma for Durango apatite (Green, 1985).

additional source of variation in measurement of track densities. For a Poisson distribution the standard deviation ($\sigma$) of a track count is provided by the square root of the number of tracks counted N:

$$\sigma = \sqrt{N} \qquad (6)$$

To calculate the standard deviation of the fission track age, $\sigma$ (T), the errors on each track density are combined with some estimate of error for the system calibration:

$$(\sigma)T = T\sqrt{\frac{1}{N_s} + \frac{1}{N_i} + \frac{1}{N_d} + \sigma\ (\zeta)^2} \qquad (7)$$

where $N_s$, $N_i$ and $N_d$ are, respectively, the total numbers of spontaneous, induced and dosimeter tracks counted, and $\sigma$ ($\zeta$) represents the reproducibility of zeta determination.

5.1.2 Analytical procedures

Standard heavy liquid and magnetic separation procedures were used to obtain apatite concentrates from previously crushed, sieved, washed and dried samples. Final apatite separates were obtained usually by hand-picking with the aid of a binocular microscope. The dating procedure was done using the external detector method (Gleadow, 1981). Apatites were mounted in epoxy resin by the Naeser (1976) method, polished to expose internal surfaces, etched, and covered with low-uranium mica fission track detectors. Etching conditions were: 40 seconds in 7% $HNO_3$ for apatite, 14 minutes in 48% HF for mica detectors, 40 minutes in 48% HF for glass dosimeter mica, all at about 25°C (room temperature). The dosimeter micas were etched longer because of the low track density, so that counting could be done at lower magnification. Irradiations were

carried out at the McMaster University Nuclear Reactor (550 seconds in site 9D). After irradiation samples were stored to "cool down" for two or three weeks, and the analytical procedure continued only when the radioactivity level was low enough for safe sample handling. The neutron fluence in the reactor was monitored using 4 pieces of dosimeter glass SRM614 interspersed among the samples in each irradiated canister. Dosimeter glass SRM614 together with Fish Canyon apatite age standard, from four separate irradiations, were used to make 16 zeta determinations, and the same glass with Durango apatite age standards provided other 3 values of this calibration parameter. The overall baseline or personal zeta calibration factor of 11515.8 ± 421.4 was established (Table 5.1; Fig. 5.1), which was used for age calculations. Counting of tracks was done with a Leitz transmitted/incident light microscope at 1250X dry magnification for apatite and mica, and 625X dry for the glass dosimeter mica. Between 16 and 57 grains were counted for each sample. Clean grains, oriented parallel to c-axes, were selected for counting. Fission track lengths were measured at 1562.5X dry magnification on horizontal, confined tracks, using a drawing tube fitted to the microscope, and a digitizing tablet.

Count data were subjected to a Chi-squared ($\chi^2$) test (at 95% cutoff) to test for variation beyond that predicted by Poissonian statistics (Galbraith, 1981; Green, 1981). Most analyses passed this $\chi^2$ test; in such cases zeta factors, fission track ages, and analytical uncertainties were calculated using pooled track density ratios. Ages and error estimates for those analyses that failed the Chi-squared test were calculated using mean ratios.

The confined etchable track lengths were measured, grouped into length intervals, and distribution histograms were generated. In addition statistical parameters such as mean, standard deviation, skewness, kurtosis, and standard error of the mean calculated. The standard error of the mean is given by:

$\sigma/\sqrt{N-1}$ :where $\sigma$ = standard deviation; $N$ = number of measured tracks.

TABLE 5.1 ZETA DETERMINATIONS FOR STANDARD GLASS SRM-614

| Apatite standard | ζ | Two standard deviations | Date of analysis |
|---|---|---|---|
| Fish Canyon | 11,107.6 | 2,177.0 | 08/15/1987 |
| Fish Canyon | 9,002.6 | 1,528.4 | 08/18/1987 |
| Fish Canyon | 12,917.1 | 2,676.0 | 08/21/1987 |
| Fish Canyon | 12,194.7 | 3,087.8 | 08/24/1987 |
| Fish Canyon | 11,851.2 | 1,777.6 | 10/16/1987 |
| Fish Canyon | 11,848.7 | 1,536.0 | 10/25/1987 |
| Fish Canyon | 13,298.2 | 2,208.6 | 10/27/1987 |
| Fish Canyon | 11,338.7 | 1,680.8 | 10/30/1987 |
| Fish Canyon | 11,265.9 | 1,802.6 | 04/24/1988 |
| Fish Canyon | 10,621.1 | 1,783.4 | 04/25/1988 |
| Fish Canyon | 10,695.0 | 1,793.0 | 04/25/1988 |
| Fish Canyon | 10,987.3 | 1,841.2 | 04/26/1988 |
| Durango | 12,910.1 | 1,864.8 | 04/28/1988 |
| Durango | 12,181.1 | 1,913.2 | 04/29/1988 |
| Durango | 11,044.0 | 1,368.6 | 04/29/1988 |
| Fish Canyon | 11,437.0 | 2,056.8 | 05/25/1988 |
| Fish Canyon | 11,483.0 | 2,169.0 | 05/26/1988 |
| Fish Canyon | 11,935.0 | 1,909.8 | 05/27/1988 |
| Fish Canyon | 10,041.9 | 1,997.2 | 05/31/1988 |

**Overall weighted mean ζ ± 2σ= 11,515.7 ± 421.4**

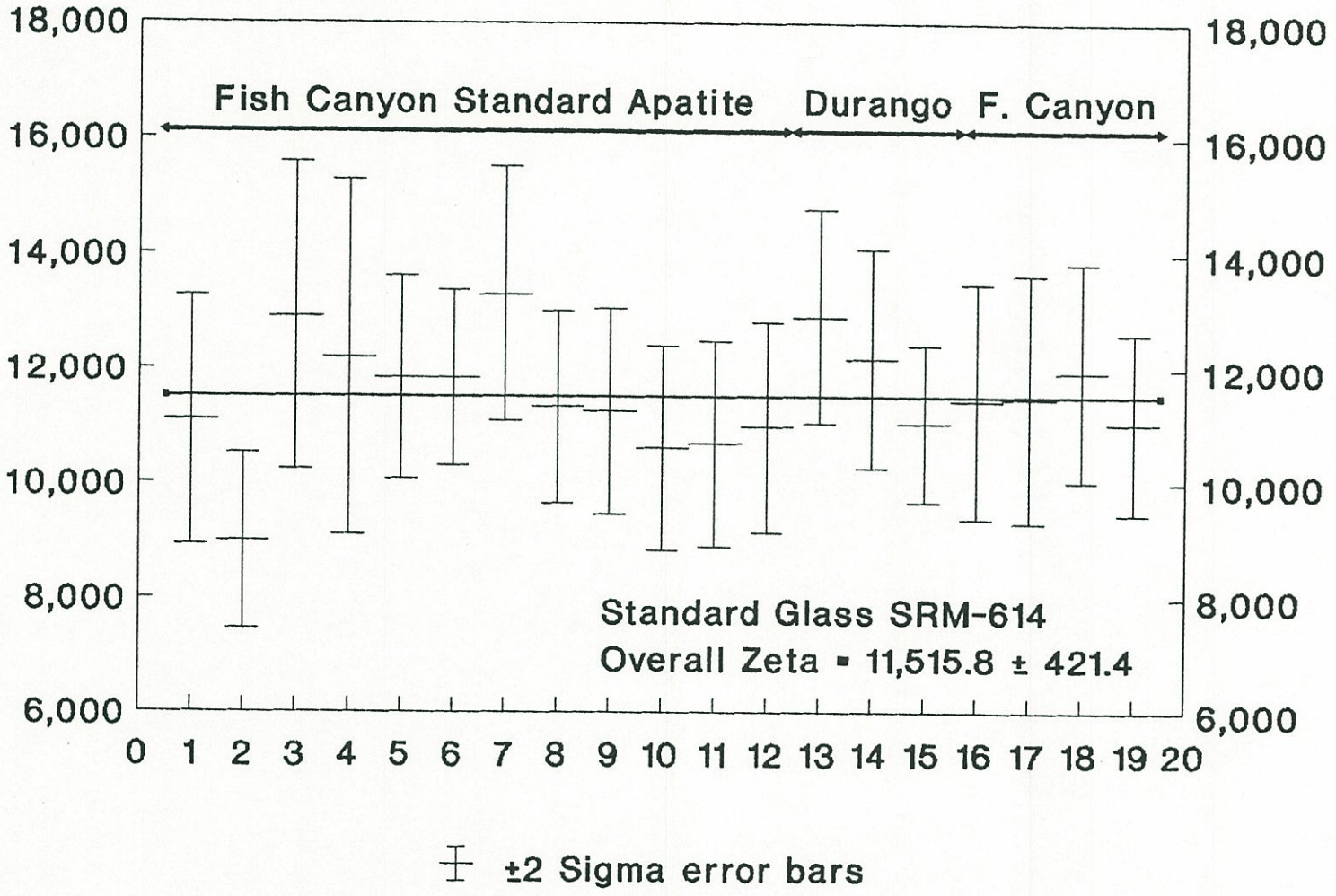


Figure 5.1. Personal zeta calibration for standard glass SRM-614.

### 5.1.3 Thermochronological application

Isotopic clocks are based on the retention of radiogenic daughter products within certain rock-forming minerals under geological conditions. This is attained when a sample cools below a certain threshold temperature, or **closure temperature.** Thus isotopic dating of minerals is also a measure of paleo-temperatures. The concept of closure temperature was defined by Dodson (1973, 1975, 1976, 1979) as "the temperature of an isotopic system at the time given by its apparent age." Limited closure temperature variation also results from different cooling rates: higher cooling rates signifying higher closure temperatures. Fission track annealing does not involve the retention of radiogenic atoms, but the concept of closure temperature nevertheless applies to track annealing (Dodson, 1979).

The annealing temperature for fission track in apatite ranges between 70 - 125°C for cooling rates from 1 to 100°C/Ma (Naeser and Faul, 1969; Wagner and Reimer, 1972; Naeser and Forbes, 1978; Zimmermann and Gaines, 1978; Gleadow and Duddy, 1981; Green and others, 1986). Because of this low temperature threshold, apatite fission track dating, unlike other geochronological techniques, may record cooling of rocks as they are exhumed by erosion in the upper several kilometres of the earth. Cooling is recorded in two ways:

First, different minerals of individual rock samples will have a variety of apparent ages, recorded by isotopic systems with distinct closure temperatures.

Second, where topographic relief is sufficient, ages of a sensitive isotopic system (e.g., apatite fission track) will be elevation dependent, with younger ages at low altitudes and older ones at higher elevations.

The age variation with altitude results from earlier cooling of samples at higher elevation, provided that the set of samples passed through an essentially horizontal stable isotherm during exhumation, and no further heating events occurred. Although fission track ages in strict sense provide only a measure of past thermal variations, regional cooling result usually from erosion activated by uplift. Therefore the dynamic interpretation of cooling ages is possible (e.g., Wagner and Reimer, 1972). Closure temperature can be converted into depth by assuming a paleo-geothermal gradient. Thus, for any pair of ages of different minerals, erosion (uplift) rate is the ratio between the difference in their depths of closure and the difference in their apparent ages (Mineral-pair method; Wagner, and others, 1977; Parrish, 1983; Zeitler and others, 1982; Zeitler, 1983). When a suite of samples showing elevation-dependent ages is available, erosion (uplift) rate is given by the ratio between variation of elevation and difference in age, provided the ages have geological meaning (Relief method; Wagner and others, 1977; Parrish, 1983; Zeitler and others, 1982; Zeitler, 1983). Such a straightforward approach has been used in several studies of orogenic belts (e.g., Wagner and others, 1977; Zimmermann and others, 1975; Parrish, 1983; Zeitler, 1983; Benjamin and others, 1987).

Recent developments indicate that fission track ages are a reflection of both the time over which tracks have been retained, and the distribution of etchable track lengths. The reduction of fission track length in apatite (annealing) occurs even at Earth's surface temperatures (e.g., Donelick, 1988). Therefore shortening of apatite fission tracks, and consequent reduction of track density (hence reduction of apparent age), is the norm rather than the exception. This led Green (1988) to conclude that **"an apatite fission track age must be understood as a reflection of both time over which tracks have been retained and the amount of shortening (annealing) that has taken place during that time."** Thus apatite fission track ages can only be interpreted as representing a geologically meaningful event provided that the samples have had a simple history, with all tracks accumulating at low temperatures (ca. < 50°C) leading to mean confined track lengths of ca. 14-15 μm (comparable to the

track lengths in apatite standards), and a standard deviation of the distribution of confined track lengths of ca. 1 µm (Green *op. cit.*). These recent developments do not invalidate the conventional approach described above, but imply that track length data are essential for accurate tectonic interpretations of fission track ages.

## 5.2 RESULTS AND DISCUSSION

### 5.2.1 Paleozoic crystalline basement of the Domeyko Cordillera

In the Domeyko Cordillera the Paleozoic basement, which according to the stratigraphic evidence remained under the sea during the Jurassic, and part of the Early Cretaceous (see Chapter 2), has been uplifted to 4,000 to 4,500 m a.s.l. Paleozoic intrusive rocks outcropping along the Domeyko Cordillera block between 21°00' and 22°30' S were sampled for fission track dating (Figs. 5.2, 5.7). Previously published biotite K/Ar ages (closure temperature between 280 - 345°C; Harrison and others, 1985) of these granitoids range from 324 to 202 Ma (Huete and others, 1977; Maksaev, 1978; Vega and Bordones, 1981), whereas two potassium-feldspar K-Ar ages (closure temperature about 150 ± 30°C; Harrison and McDougall, 1980) from basement rocks from the same area have yielded ages of 116 ± 3 and 111 ± 2 Ma (recalculated from Huete and others, 1977). Apatite fission track ages obtained in this study range between 45.2 and 35.3 Ma, and show a regular variation with altitude (Fig. 5.3; Table 5.2). Comparable dates (43.6 to 45.9 Ma; Table 5.3) were obtained on apatites from Upper Paleozoic granitoids at Salar de Pedernales area, east of Potrerillos mining district (26°S). However, as shown above, no unambiguous interpretations of this fission track age information are possible without consideration of track length data.

Samples from the areas of Quehuita, Cerros de Paqui and East of Chuquicamata come from three separate Upper Paleozoic plutons

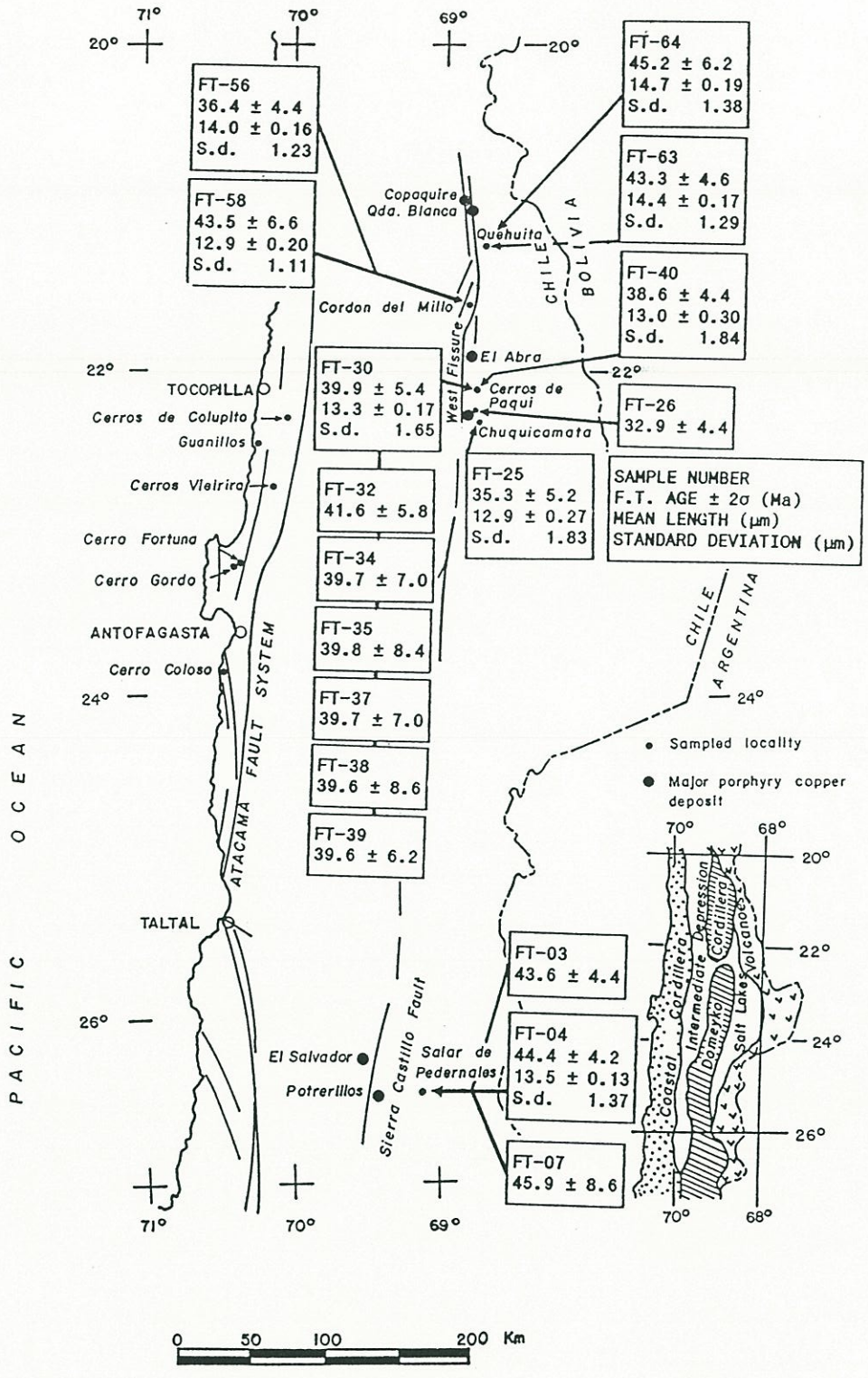


Figure 5.2. Apatite fission track data from basement rocks of the Domeyko Cordillera block. See figure 5.7 for detailed location of samples from Cerros de Paqui area.

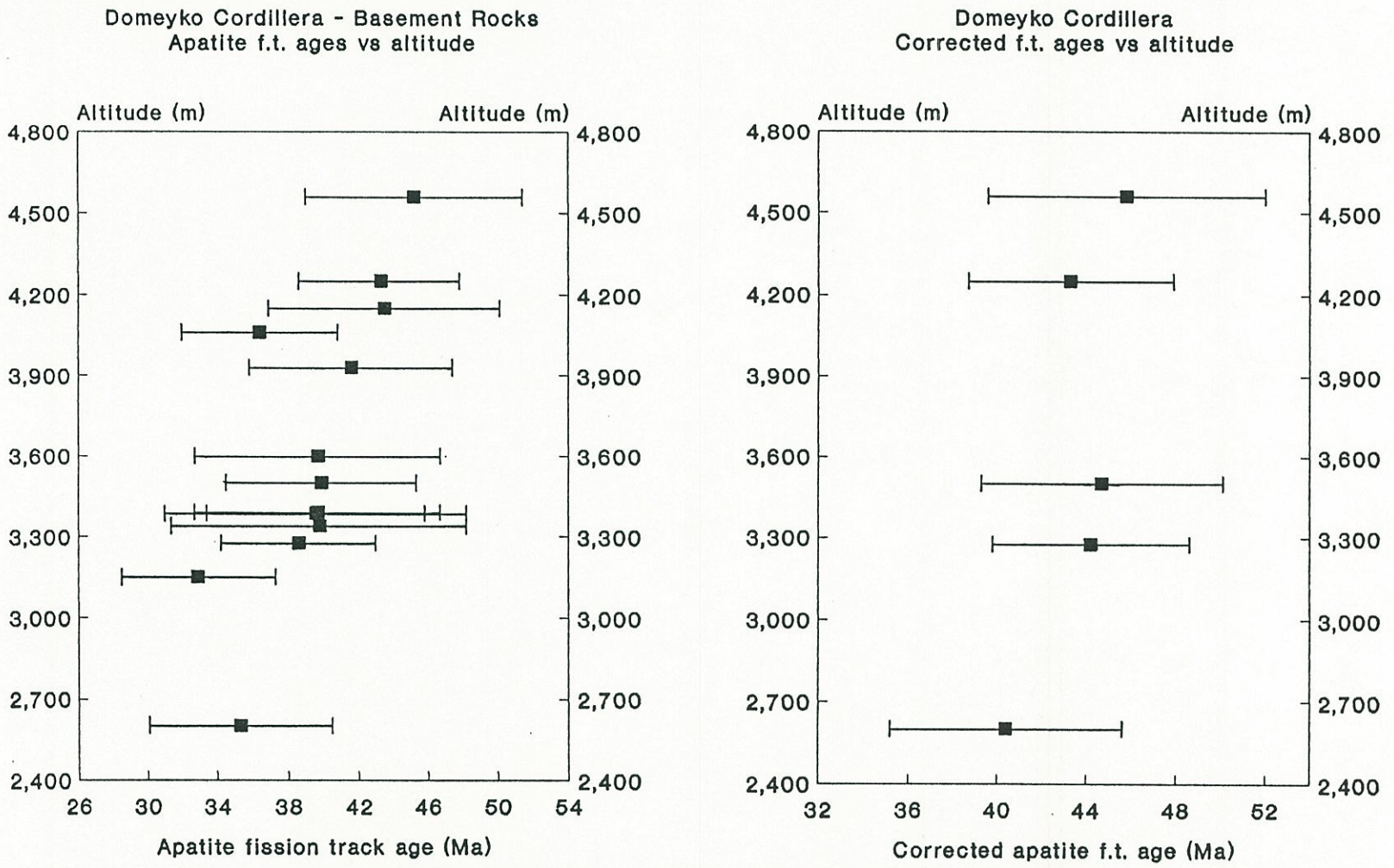


**Figure 5.3.** Apatite fission track ages from basement rocks of the Domeyko Cordillera versus altitude. Left graph show original fission track ages. Right graph show corrected ages according to the track length of the sample (only samples located east of the West Fissure are included).

within the uplifted Domeyko block east of the West Fissure (Fig. 5.2). Samples FT-30 and FT-32 come from the same block, but from a 68 Ma dioritic stock emplaced within basement rocks at Cerros de Paqui (Fig. 5.7). The Cordon del Millo samples come from a block of Paleozoic intrusives west of the West Fissure (Fig 5.2).

TABLE 5.2 APATITE FISSION TRACK AGES FROM UPPER PALEOZOIC GRANITOIDS OF THE DOMEYKO CORDILLERA
(Analytical data in Appendix 5)

| Sample | Alt. (m) | Locality | Age (Ma) and error (± 2σ) |
|---|---|---|---|
| FT-64 | 4560 | Quehuita | 45.2 ± 6.2 |
| FT-63 | 4250 | Quehuita | 43.3 ± 4.6 |
| FT-58 | 4150 | Cordon del Millo | 43.5 ± 6.6 |
| RECOUNT | | | 41.2 ± 9.4 |
| FT-56 | 4060 | Cordon del Millo | 36.4 ± 4.4 |
| RECOUNT | | | 38.2 ± 4.8 |
| FT-32 | 3930 | Cerros de Paqui | 41.6 ± 5.8 |
| FT-34 | 3600 | Cerros de Paqui | 39.7 ± 7.0 |
| FT-30 | 3500 | Cerros de Paqui | 39.9 ± 5.4 |
| FT-37 | 3390 | Cerros de Paqui | 39.7 ± 7.0 |
| FT-38 | 3385 | Cerros de Paqui | 39.6 ± 8.6 |
| FT-39 | 3385 | Cerros de Paqui | 39.6 ± 6.2 |
| FT-35 | 3340 | Cerros de Paqui | 39.8 ± 8.4 |
| FT-40 | 3275 | Cerros de Paqui | 38.6 ± 4.4 |
| RECOUNT | | | 38.3 ± 5.0 |
| FT-26 | 3150 | 0.5 km E of Chuquicamata | 32.9 ± 4.4[2] |
| FT-25 | 2600 | 5 km E of Chuquicamata | 35.3 ± 5.2 |

[2] Sample from the Elena Granodiorite at Chuquicamata obtained 500 m east of the porphyry copper deposit. The apatite age is identical to the radiometric dates of the porphyry intrusion (see Chapter 4) and is inferred to be reset by it.

The measured mean etchable lengths of horizontal, confined tracks in apatites from basement rocks range from 12.9 to 14.7 μm, with a standard deviations from 1.11 to 1.84 μm (Table 5.4). The track length distributions are consistently unimodal, and negatively skewed (Figs. 5.4, 5.5; Table 5.4). For these track length distributions a correction for observational bias according to the geometrical arguments of Laslett and others (1982) would be minimal. Therefore such a correction has been disregarded in the analysis of the fission track ages, but corrected distributions are used for modelling time-temperature paths in Section 5.3. The low track density and consequent absence of tracks in tracks (TINTS), or tracks in cleavages (TINCLES) precluded the measure of confined track lengths in several apatite samples.

TABLE 5.3 APATITE FISSION TRACK AGES FROM UPPER PALEOZOIC GRANITOIDS OF SALAR DE PEDERNALES AREA
(Analytical data in Appendix 5)

| Sample | Alt. (m) | Locality | Age (Ma) and error (± 2σ) |
|---|---|---|---|
| FT-07 | 3650 | Salar de Pedernales | 45.9 ± 8.6 |
| FT-04 | 3425 | Salar de Pedernales | 44.4 ± 4.2 |
| FT-03 | 3370 | Salar de Pedernales | 43.6 ± 4.4 |

The distributions of etchable track lengths in apatites from basement rocks of the Domeyko Cordillera compare to those of apatites from "undisturbed basement" rocks (Fig. 5.6) of Gleadow and others (1986). This type of etchable track length distribution is consistent with a "simple" cooling history (i.e., temperature decreased progressively with time).

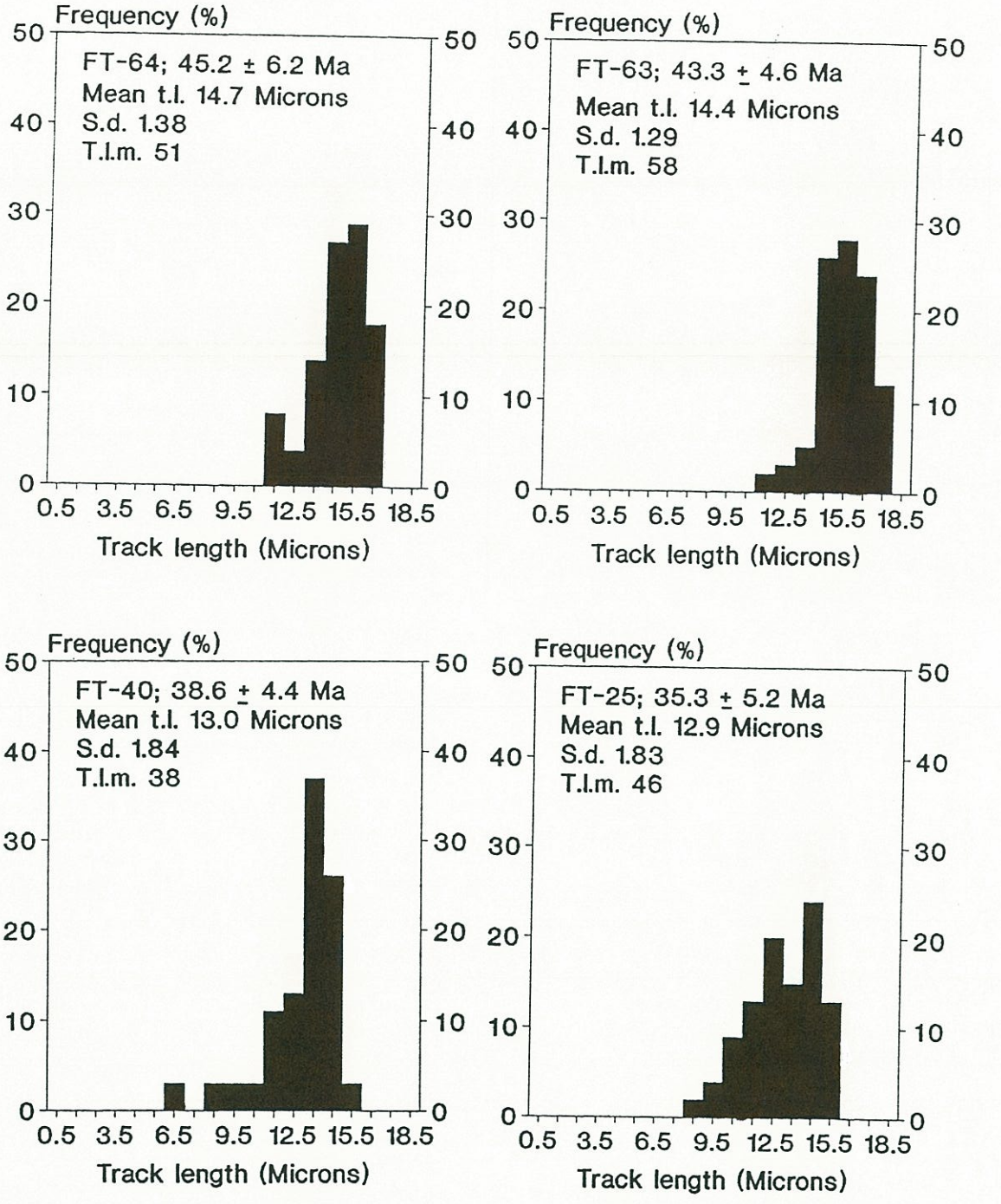


**Figure 5.4.** Distributions of confined fission track lengths of apatites from basement rocks of the Domeyko Cordillera. The altitude of the samples decrease in the order FT-64, FT-63, FT-40, FT-25: the decrease in altitude is reflected by progressive reduction in mean track lengths.

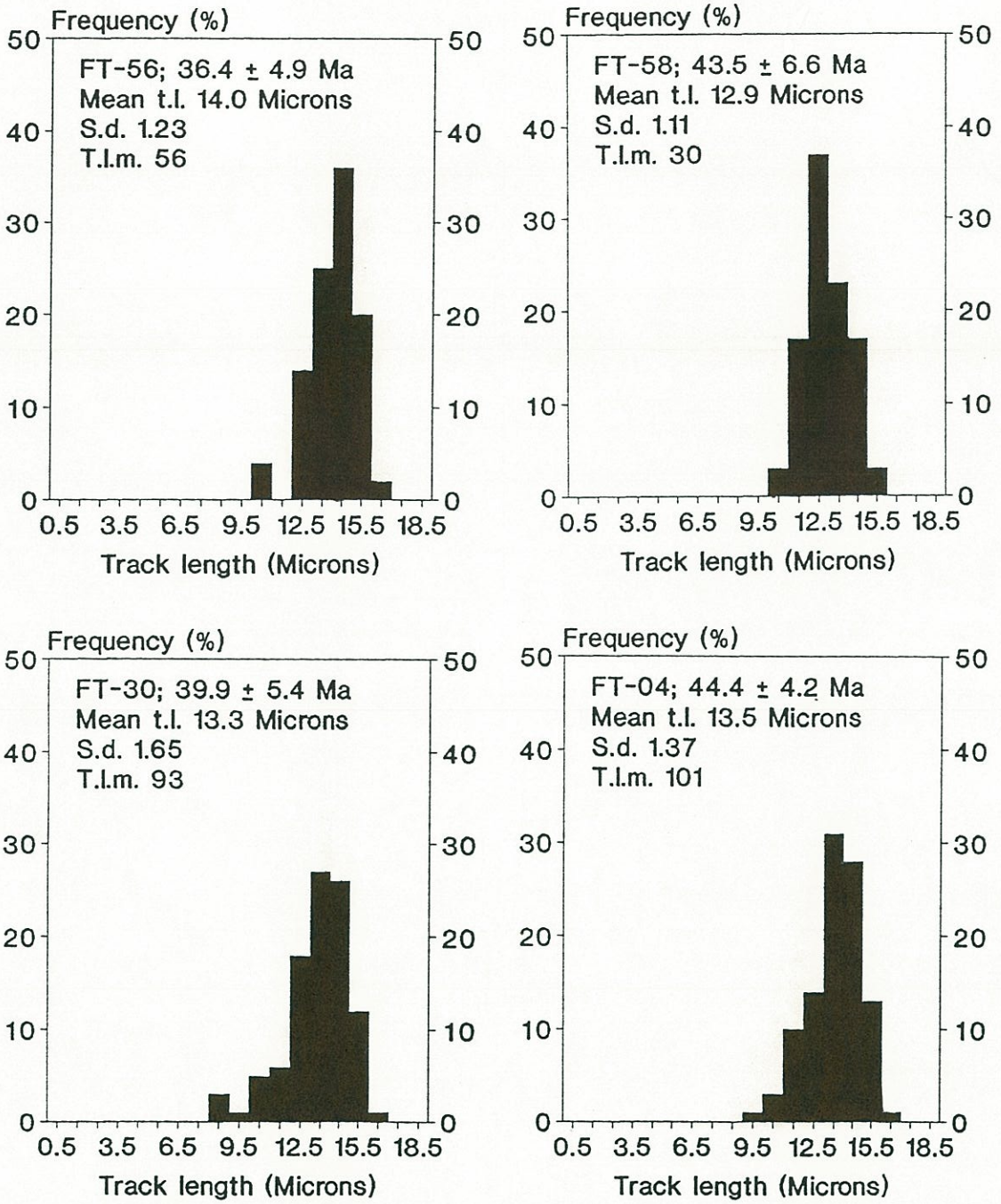


**Figure 5.5.** Distributions of confined fission track length of apatites from the Domeyko Cordillera. FT-56 and FT-58 basement Upper Paleozoic granitoids from Cordon del Millo (west of the West Fissure); FT-30 from a 68 Ma dioritic stock at Cerros de Paqui; FT-04 Upper Paleozoic granite from Salar de Pedernales area (26°S).

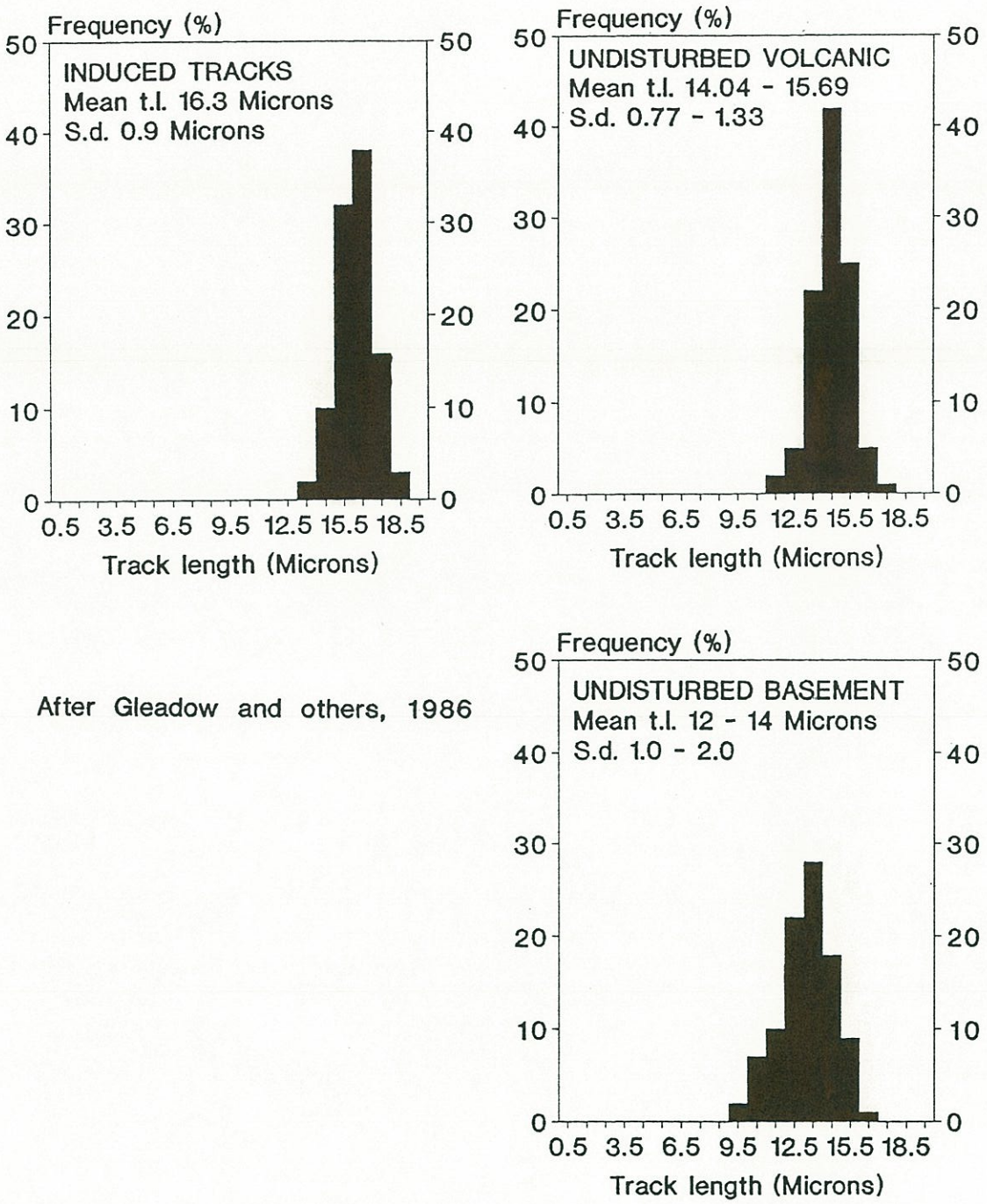


After Gleadow and others, 1986

**Figure 5.6.** Representative distributions of apatite confined fission tracks: neutron induced tracks, natural "undisturbed volcanic", and "undisturbed basement" types after Gleadow and others (1986).

Etchable mean track lengths in basement apatites range from 12.9 to 14.7 μm, but only samples obtained at highest elevations (4,250-4,560 m) have mean track lengths longer than 14 μm (Table 5.4). Samples collected below 4,250 m of altitude have mean track lengths shorter than 14 μm, and their standard deviations are larger than 1 μm, thus they fall below the range of "confidence" suggested by Green (1988). These apatites probably spent more time at temperatures above ca. 50°C, therefore their track length and track density have been significantly reduced: hence their ages would be younger than any geologically meaningful event. Therefore a mean length reduction correction has to be applied to the calculated apatite fission track ages.

Green (1988) demonstrated that the relationship between track length reduction ($L/L_0$) and track density reduction ($\rho/\rho_0$) in apatite is a direct 1:1 for $L/L_0$ from 1.0 to 0.65. Thus for apatite samples that have a track reduction within this range, which is the case of the above samples, a corrected age is given by:

**"Corrected" fission track age = Apparent age x** $L_0/L$ (for $L/L_0$ >0.65)

According to measurements of Green (in Gleadow and others, 1986) standard Fish Canyon apatites have an etchable mean track length of 15.0 μm, and Durango apatites of 14.2 μm. These are shorter than those of freshly produced induced fission track that have a mean track length of 16.3 μm (Gleadow and others, *op. cit.*). Since the fission track ages are derived relative to the apatite standards a value of 14.9 μm for $L_0$ has been selected here, which is the weighted mean of 16 Fish Canyon and 3 Durango standards used to derive the zeta baseline calibration in this study.

The corrected ages range between 50 and 40 Ma (Table 5.4), which is consistent with the range of Middle to Late Eocene ages inferred from K-Ar dating of tuffs overlying the Incaic erosional surface in the Andes of Southern Peru (Noble and others, 1978, 1979; Megard, 1987; see Section 2.17.2). The corrected ages from Upper Paleozoic rocks

outcropping east of the West Fissure, although obtained from three isolated plutons, show a regular increase of age with altitude from 40.7 to 45.8 Ma (Fig. 5.3), which could be argued suggest a rate of exhumation of about 0.4 mm/yr during that period of time. However, the ± 5 Ma analytical error of the ages (at 2σ level) does not warrant any determination of exhumation rates, since all dates can be considered identical within error limits.

TABLE 5.4 SUMMARY OF TRACK LENGTH DATA AND CORRECTED AGES

| Sample | No tracks | Mean length (μm) | Standard deviation (μm) | Skewness | Corrected age ± error (Ma) |
|---|---|---|---|---|---|
| FT-64 | 51 | 14.7 | 1.38 | -0.76 | 45.8 ± 6.2 |
| FT-63 | 58 | 14.4 | 1.29 | -0.55 | 44.8 ± 5.2 |
| FT-30 | 93 | 13.3 | 1.65 | -0.92 | 44.7 ± 5.4 |
| FT-40 | 38 | 13.0 | 1.84 | -1.67 | 44.2 ± 4.4 |
| FT-25 | 46 | 12.9 | 1.83 | -0.47 | 40.4 ± 5.2 |
| FT-58 | 30 | 12.9 | 1.11 | 0.24 | 50.0 ± 4.6 |
| FT-56 | 56 | 14.0 | 1.23 | -0.60 | 38.7 ± 4.4 |
| FT-04 | 101 | 13.5 | 1.37 | -0.55 | 49.0 ± 4.2 |

In conclusion, the corrected fission track apatite ages from Upper Paleozoic Rocks from a vast area along the Domeyko Cordillera are compatible with a Mid-Late Eocene regional cooling event. This cooling event is attributed to active erosion resulting from the Incaic uplift (see Section 2.17.2). The fission track data do not preclude, however, the possible effect of a regional thermal pulse of the same age, but such regional heating is unlikely since apatite fission track ages of 63 and 78 Ma have been preserved at Cerros de Montecristo (20 km west of Chuquicamata), and at Caracoles (75 km south of Chuquicamata) respectively (see below).

### 5.2.2 Tertiary plutons west of Chuquicamata

The Cerros de Montecristo granodioritic pluton, located 20 km west of Chuquicamata porphyry copper deposit (Fig. 5.7), has a biotite $^{40}Ar$-$^{39}Ar$ plateau age of 63.1 ± 0.3 Ma (Fig. 4.3). The apatite fission track age of 62.4 ± 7.4 yielded by sample FT-14 collected at highest altitude (2,880 m) is concordant with the above $^{40}Ar$-$^{39}Ar$ age obtained from sample FT-8. the rest of the apatite fission track ages decrease steadily with elevation down to 47.4 Ma at 1,990 m (Fig. 5.8; Table 5.5). The concordance between the biotite $^{40}Ar$-$^{39}Ar$ and the apatite fission track ages is taken to suggest that the sample from the highest elevation of the Cerros de Montecristo Pluton has remained under ca. 50°C since pluton cooling, hence no significant age reduction occurred. This is consistent with permanence at a level very close to the surface (< 2,000 m in depth assuming a 30°C/km paleo-geothermal gradient). The younger ages at lower altitude representing a progressively longer stay of the samples at slightly higher temperatures (deeper), but probably well below the closure temperature of apatite. Thus those apatites are partially annealed and their younger ages have no geological meaning, except for the residence of the samples at some depth corresponding to temperatures probably higher than ca. 50°C and lower than ca. 100°C.

TABLE 5.5 APATITE FISSION TRACK AGES FROM CERROS DE MONTECRISTO PLUTON
(Analytical data in Appendix 5)

| Sample | Alt. (m) | Locality | Age and error (Ma) |
|---|---|---|---|
| FT-14 | 2880 | Cerros de Montecristo | 62.4 ± 7.4 |
| RECOUNT | | | 64.7 ± 7.4 |
| FT-13 | 2690 | do | 58.9 ± 6.0 |
| FT-12 | 2440 | do | 58.2 ± 5.6 |
| FT-11 | 2435 | do | 53.4 ± 5.6 |
| FT-9 | 2100 | do | 55.6 ± 6.0 |
| FT-8 | 1990 | do | 47.4 ± 5.4 |
| RECOUNT | | | 47.5 ± 5.6 |

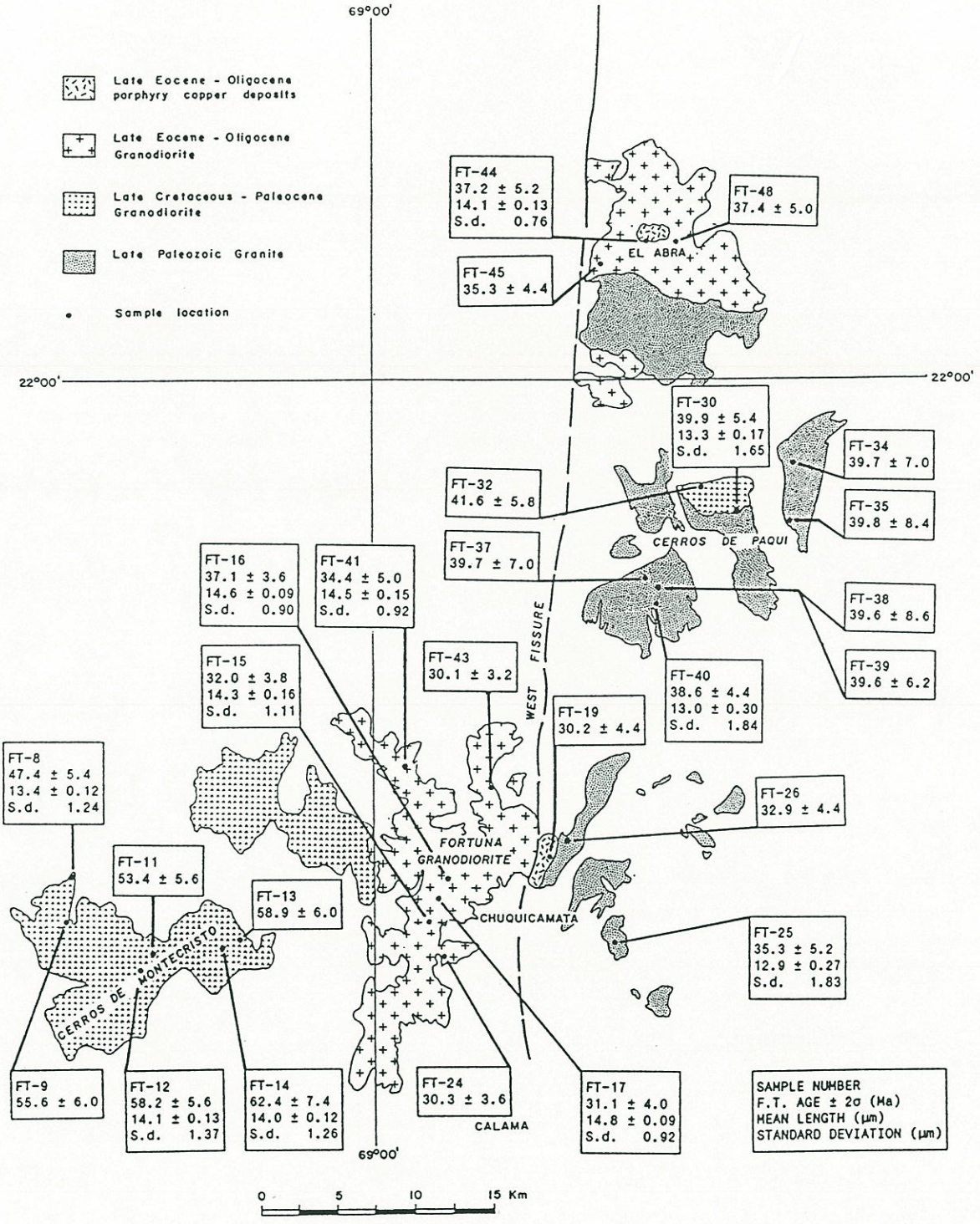


Figure 5.7. Apatite fission track data from the Chuquicamata area.

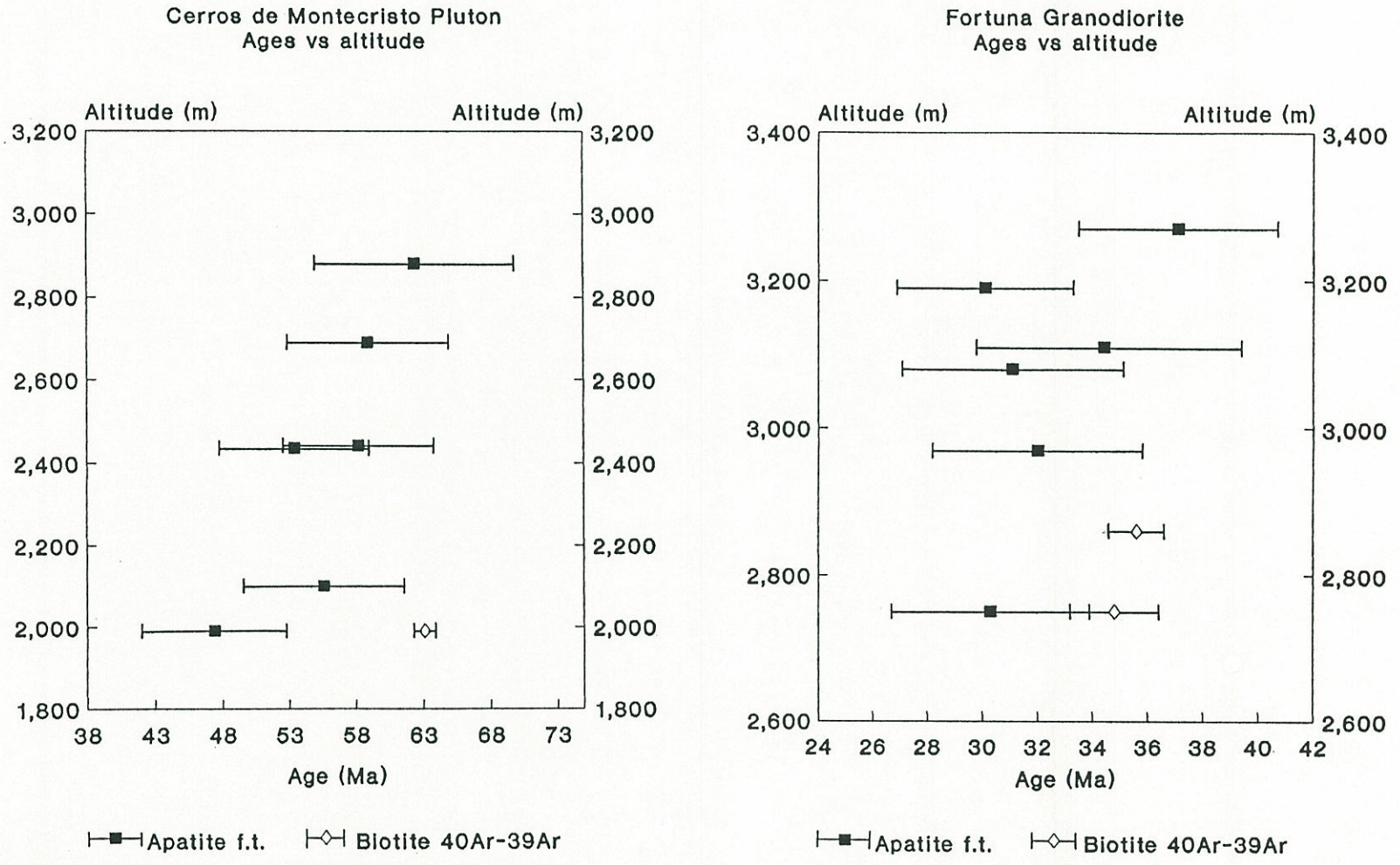


**Figure 5.8.** Apatite fission track ages and biotite $^{40}Ar$-$^{39}Ar$ dates versus altitude of samples from the Cerros de Montecristo pluton (left graph) and Fortuna Granodiorite (right graph).

TABLE 5.6 SUMMARY OF TRACK LENGTH DATA AND CORRECTED AGES

| Sample | No tracks | Mean length (μm) | Standard deviation (μm) | Skewness | Corrected age ± error (Ma) |
|---|---|---|---|---|---|
| FT-14 | 100 | 14.0 | 1.26 | -0.49 | 66.4 ± 7.4 |
| FT-14 | 63 | 14.1 | 0.99 | -0.37 | 65.9 ± 7.4 |
| FT-12 | 101 | 14.1 | 1.37 | -1.06 | 61.5 ± 5.6 |
| FT-12 | 105 | 14.4 | 1.09 | -0.28 | 60.2 ± 5.6 |
| FT-8 | 102 | 13.4 | 1.24 | -0.67 | 52.8 ± 5.4 |

The measured mean confined track lengths in apatites from the Cerros de Montecristo pluton range between 13.4 and 14.4 μm, with standard deviations from 0.99 to 1.37 (Table 5.6; Fig. 5.9). The distributions of track lengths are narrow and unimodal, and except for the sample at lowest altitude, compare to "undisturbed volcanic" apatites (Fig. 5.6) of Gleadow and others (1986). This type of confined track length distribution is that of apatite standards. These because of their volcanic origin cooled immediately after deposition and have not been thermally disturbed since formation, therefore give concordant ages in all isotopic systems (Gleadow and others, 1986). The apatite fission track age of sample FT-14 is concordant with a biotite $^{40}Ar$-$^{39}Ar$ plateau age of the Cerros de Montecristo pluton, and the apatite fission track age of sample FT-12 is only slightly younger than the $^{40}Ar$-$^{39}Ar$ age (Table 5.5). Thus the fission track data indicate abrupt cooling following the emplacement of the Cerros de Montecristo pluton, compatible with either intrusion at a very shallow level within cool wallrocks (about 2-3 km in depth, assuming a 30°C/km paleo-geothermal gradient), or with an exceedingly rapid exhumation of the pluton after intrusion. The preservation of the original cooling age of the pluton in the apatites from sample FT-14 collected at highest altitude indicates that the denudation at the top of the Cerros de Montecristo mountain range has progressed probably no more than about 2 km (depending on the paleo-geothermal gradient) since about 63 Ma.

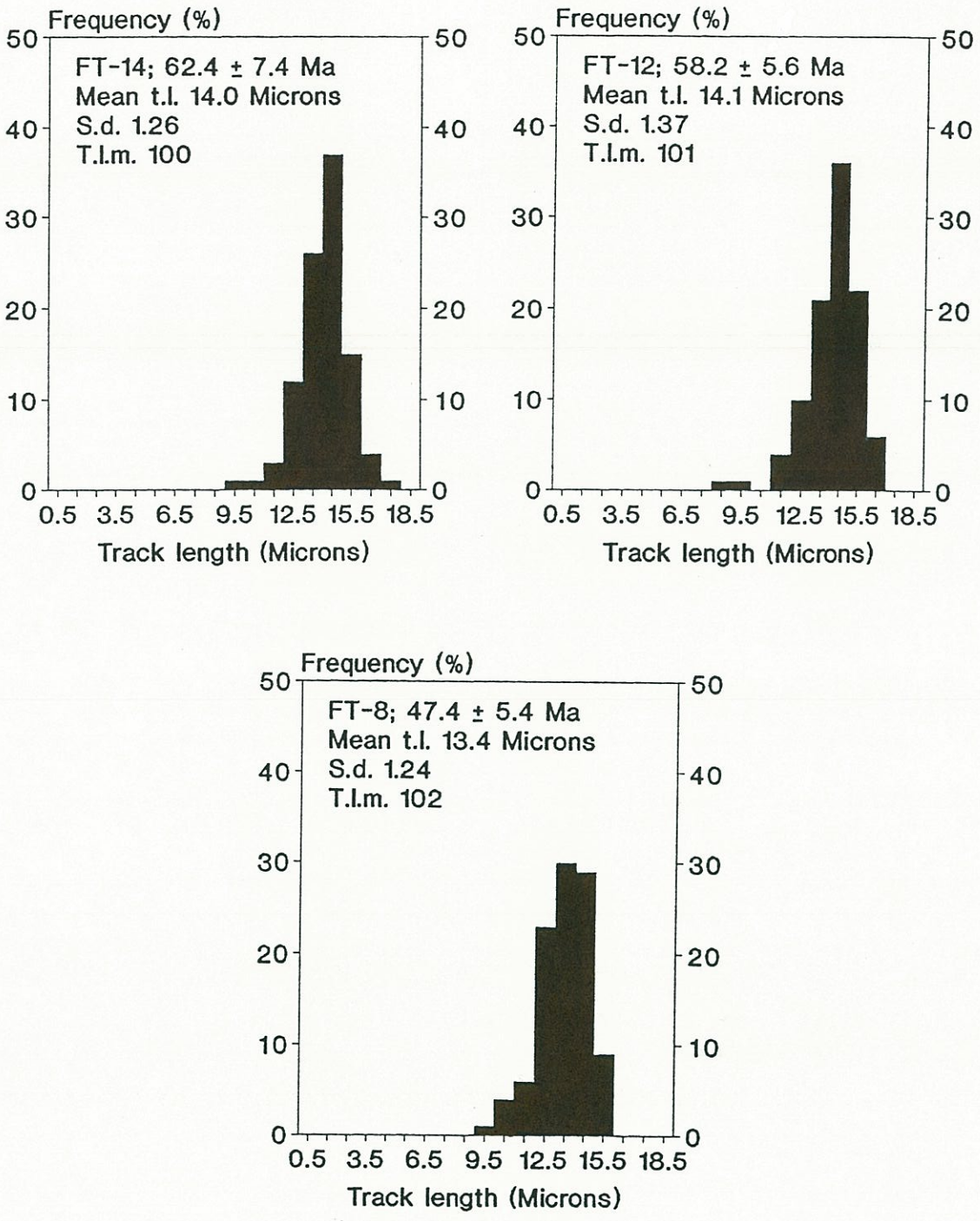


**Figure 5.9.** Distributions of confined fission track lengths of apatites from the Cerros de Montecristo Pluton: distributions of apatite from samples FT-14 and FT-12 collected at higher altitude, compare well to the "undisturbed volcanic" type of figure 5.6.

TABLE 5.7 APATITE FISSION TRACK AGES FROM THE FORTUNA GRANODIORITE
(Analytical data in Appendix 5)

| Sample | Alt. (m) | Locality | Age (Ma) and error (± 2σ) |
|---|---|---|---|
| FT-16 | 3270 | W of Chuquicamata | 37.1 ± 3.6 |
| FT-43 | 3190 | do | 30.1 ± 3.2 |
| FT-41 | 3110 | do | 34.4 ± 5.0 |
| FT-17 | 3080 | do | 31.1 ± 4.0 |
| FT-15 | 2970 | do | 32.0 ± 3.8 |
| FT-24 | 2750 | do | 30.3 ± 3.6 |

TABLE 5.8 SUMMARY OF TRACK LENGTH DATA

| Sample | No tracks | Mean length (μm) | Standard deviation (μm) | Skewness |
|---|---|---|---|---|
| FT-16 | 100 | 14.6 | 0.90 | -0.08 |
| FT-41 | 36 | 14.5 | 0.92 | -0.19 |
| FT-17 | 100 | 14.8 | 0.92 | -0.18 |
| FT-15 | 46 | 14.3 | 1.11 | -0.57 |

The Fortuna Granodiorite is a pluton located immediately west of Chuquicamata of about 37 Ma (see Section 4.3.4). Sample FT-16 at highest elevation has given an apatite fission track date of 37.1 ± 3.6 Ma concordant with biotite $^{40}Ar$-$^{39}Ar$, and K-Ar ages of the granodiorite (see Section 4.3.4). The rest of the samples at lower elevations yielded younger dates concordant, within error limits, with the age of the neighbouring Chuquicamata porphyry copper deposit (about 31 Ma; see Section 4.3.4). The Fortuna Granodiorite hosts several copper veins, which probably were formed by hydrothermal activity coeval with the emplacement of the Chuquicamata porphyry, and therefore local resetting of apatite fission track ages during this thermal event likely occurred.

However, except for sample FT-43, there is a regular variation with altitude (Fig. 5.8), which may suggest that the apatites are partially annealed similarly to those of the Cerros de Montecristo pluton.

The measured confined mean track lengths of apatites from the Fortuna Granodiorite range from 14.3 to 14.8 μm, with a standard deviation from 0.92 to 1.11 μm (Table 5.8). The distributions of track lengths are unimodal, and very narrow (Fig. 5.10). They are similar to those of apatite standards or "undisturbed volcanic" rocks of Gleadow and others (1986). These distributions of track length, along with the above age data, indicate that samples from the Fortuna Granodiorite cooled very rapidly, and therefore either have remained close to the Earth's surface (probably no more than 2 km in depth) since the emplacement of the Chuquicamata porphyry at about 31 Ma, or were very rapidly exhumed at that time. The concordant apatite fission track age of sample FT-16 collected at highest altitude with the $^{40}Ar$–$^{39}Ar$ age of the granodiorite suggests, that denudation has not progressed more than about 2 km on the top of the pluton since 37 Ma. Sillitoe (1973) postulated that the Fortuna Granodiorite was the batholithic root of the Chuquicamata porphyry copper deposit; therefore he cited this pluton as an example of the bottom of a porphyry copper system. However, Sillitoe's hypothesis is not substantiated by the above fission track data, unless the granodiorite cooled very rapidly at the time of porphyry copper emplacement. Furthermore, the geochronological data of Section 4.3.4 demonstrate that the intrusion of the Fortuna Granodiorite pre-dates the porphyry copper emplacement by at least 4 Ma. Thus it is more likely that the Fortuna Granodiorite was already at a near-surface level at the time of the emplacement of the Chuquicamata porphyry.

### 5.2.3 Chuquicamata and El Abra

The apatite from a sample (FT-19) of the Chuquicamata porphyry, obtained from the mine pit, 400 m below the natural (pre-mine)

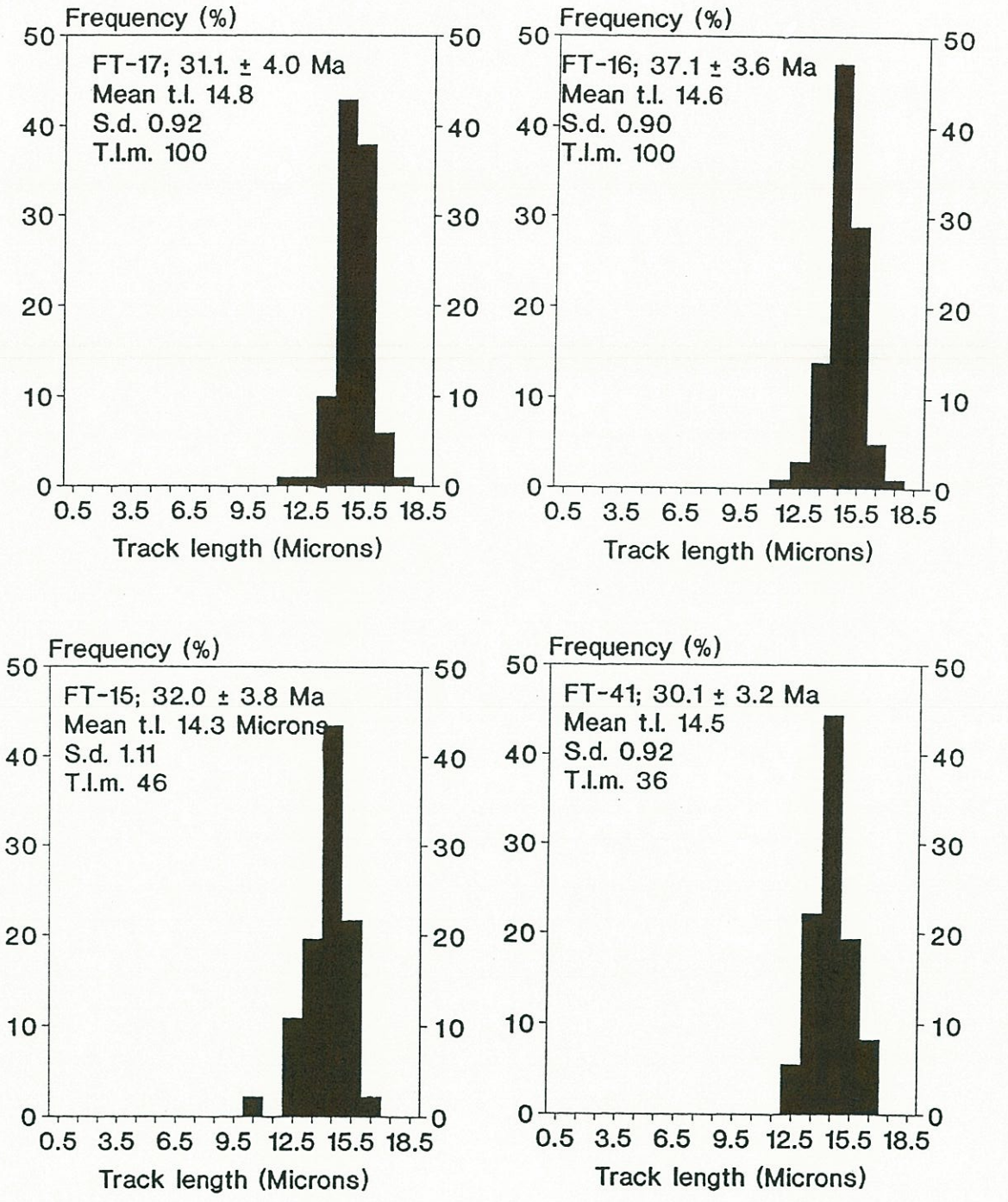


**Figure 5.10.** Distributions of confined fission track lengths of apatites from the Fortuna Granodiorite. The distributions are identical to "undisturbed volcanic" type (Fig. 5.6) suggesting fast cooling and long-term near-surface residence of the rocks.

surface, gave a fission track age of 30.2 ± 4.4 Ma (Table 5.9), which is concordant with a K-feldspar $^{40}Ar$-$^{39}Ar$ plateau age of 31.4 ± 0.2 Ma, and also with a biotite $^{40}Ar$-$^{39}Ar$ plateau age of 31.7 ± 0.4 Ma obtained from the same sample (see Section 4.3.4). The concordance of these three ages, from minerals with significantly different closure temperatures, indicates fast cooling of the porphyry, at least within the temperature range from about 300° to 100°C. Such rapid cooling is consistent either with epizonal emplacement, or rapid exhumation of the intrusive body. The first alternative is more probable since the development of secondary boiling in porphyry systems is inversely dependent upon depth (Burnham, 1985).

TABLE 5.9 APATITE FISSION TRACK AGES FROM CHUQUICAMATA AND EL ABRA
(Analytical data in Appendix 5)

| Sample | Alt. (m) | Locality | Age |
|---|---|---|---|
| FT-19 | 2580 | Chuquicamata porphyry | 30.2 ± 4.4 |
| FT-44 | 3860 | Dacitic Porphyry El Abra | 37.2 ± 5.2 |
| FT-45 | 3835 | Southern Granodiorite El Abra | 35.3 ± 4.4 |
| FT-48 | 4050 | Southern Granodiorite El Abra | 37.4 ± 5.0 |

TRACK LENGTH DATA

| Sample | No tracks | Mean length (μm) | Standard deviation (μm) | Skewness |
|---|---|---|---|---|
| FT-44 | 32 | 14.1 | 0.76 | -0.13 |

Sample FT-44 from the Dacitic porphyry of El Abra yielded an apatite fission track age of 37.2 ± 5.2 Ma (Table 5.9), which is concordant with the 38.6 Ma age inferred from the $^{40}Ar$-$^{39}Ar$ of the biotite from the same sample (see Section 4.3.2). The confined mean track length of this apatite separate is 14.1 μm with a standard deviation of

0.76 μm. The distribution is narrow and unimodal (Fig. 5.16) comparable to "undisturbed volcanic" rocks of Gleadow and others (1986). Apatite fission track ages of the pre-mineral Southern Granodiorite of El Abra of 35.3 ± 4.4 (FT-45), and 37.4 ± 5.0 Ma (FT-48) are also concordant with the biotite $^{40}Ar$-$^{39}Ar$ plateau age of 36.7 ± 0.8 Ma (FT-45; see Section 4.3.2). Fission track counts of apatite samples from El Abra area failed the $\chi^2$ test for Poissonian distribution (Appendix 5), due to abundant dislocations in the apatites that made accurate track counting difficult. However, the obtained apatite fission track ages are concordant with biotite $^{40}Ar$-$^{39}Ar$ dates. Therefore, although these fission track ages have to be considered with caution, they are consistent with fast cooling of El Abra porphyry copper deposit at about 37-36 Ma, and its residence since that time at temperatures under about 50°C.

### 5.2.4 Intrusions of the Intermediate Depression

An apatite fission track age of 53.2 ± 6.2 Ma (II-592; Fig. 5.11) was obtained for the granodioritic pluton that hosts a copper-bearing porphyry at Sierra Gorda. This age is younger than the biotite $^{40}Ar$-$^{39}Ar$ plateau age of 63.3 ± 0.6 Ma obtained for the same sample.

An apatite fission track date of 57.0 ± 7.8 Ma (II-611) was obtained for the granodioritic wallrock of the Lomas Bayas copper-bearing porphyry (Fig. 5.11). This age is concordant, within error limits, with a biotite $^{40}Ar$-$^{39}Ar$ plateau age of 64.2 ± 0.6 Ma, and a hornblende $^{40}Ar$-$^{39}Ar$ total gas age of 57.1 ± 1.6 obtained for the same sample (see Section 4.3.10). Sample II-607 from the same area (Fig. 5.11) gave an apatite fission track age of 50.8 ± 6.4 concordant, within error limits, with a hornblende $^{40}Ar$-$^{39}Ar$ total gas age of 57.9 ± 3.6. Sample II-598 yielded an apatite fission track age of 49.5 ± 5.0 Ma that is younger than the biotite $^{40}Ar$-$^{39}Ar$ plateau age of 78.6 ± 1.0 Ma of the same rock sample.

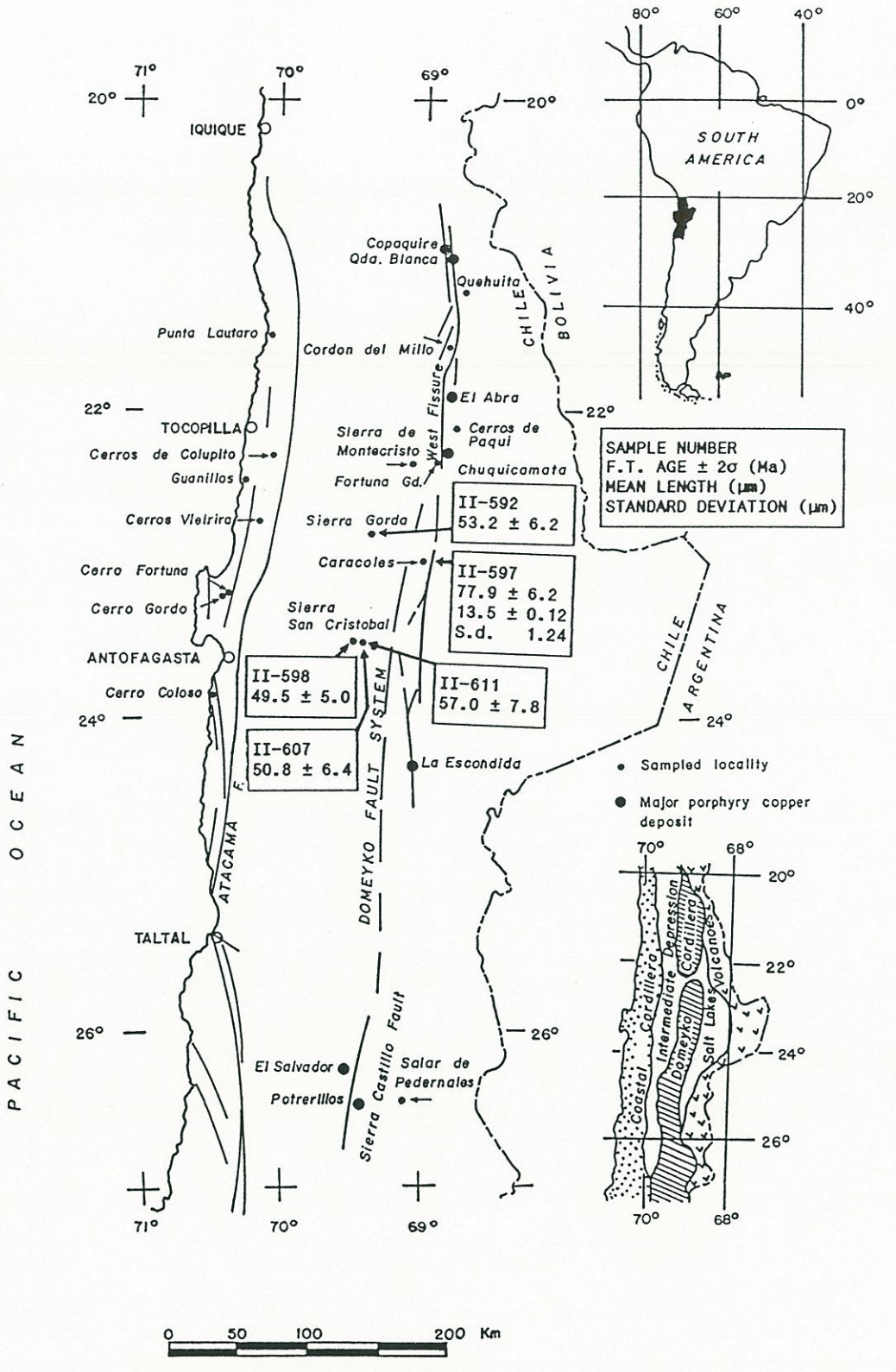


**Figure 5.11.** Apatite fission track data from intrusive rocks of the Intermediate Depression.

TABLE 5.10 APATITE FISSION TRACK AGES FROM THE INTERMEDIATE DEPRESSION
(Analytical data in Appendix 5)

| Sample | Alt. (m) | Locality | Age (Ma) and error (± 2σ) |
|---|---|---|---|
| II-592 | 1730 | Sierra Gorda | 53.2 ± 6.2 |
| II-611 | 1600 | Sierra San Cristobal | 57.0 ± 7.8 |
| II-607 | 1750 | Sierra San Cristobal | 50.8 ± 6.4 |
| II-598 | 1550 | Sierra San Cristobal | 49.5 ± 5.0 |
| II-597 | 2600 | Caracoles | 77.9 ± 6.2 |

TRACK LENGTH DATA

| Sample | No tracks | Mean length (μm) | Standard deviation (μm) | Skewness |
|---|---|---|---|---|
| II-597 | 100 | 13.5 | 1.24 | -0.49 |

As shown above apatite fission track ages are either concordant, within error limits, with biotite, and hornblende $^{40}Ar$-$^{39}Ar$ dates or slightly younger, and there is no regular variation of ages with altitude (Fig. 5.13). The younger apatite fission track ages are interpreted as partially annealed, analogous to the case of the Cerros de Montecristo pluton, which itself is located on the western boundary of the Intermediate Depression.

Sample II-597 from a diorite stock of the Caracoles epithermal silver district (Fig. 5.11, Table 5.10) yielded a fission track age of 77.9 ± 6.2 Ma, which is concordant with the age of 76.7 Ma inferred from the $^{40}Ar$-$^{39}Ar$ spectrum of the biotite from the same rock. The mean confined track length is 13.5 μm with a standard deviation of 1.24 μm. The track length distribution is narrow and unimodal (Fig. 5.16), which is comparable to that of "undisturbed volcanic" rocks of Gleadow and others (1986). It is now generally accepted that epithermal veins are formed at pressures of less than a few hundred bars (e.g., Schmitt, 1950; Heald and

others, 1987), which corresponds to the upper ca. 1,000 m of the Earth's crust. Therefore the concordance of the apatite fission track age with the biotite $^{40}Ar$-$^{39}Ar$ date very probably reflects the shallow emplacement of the subvolcanic intrusion, and implies that the epithermal systems have remained at low temperature (near surface) since the Late Cretaceous. Although this conclusion may appear surprising, it can be demonstrated that in the Intermediate Depression (between the Coastal Cordillera and the Domeyko Cordillera; Fig. 1.3) of this Andean segment, hydrothermal alteration features characteristic of near surface environments (sinter deposits, "silica caps" and hydrothermal breccias) are preserved within several sub-volcanic epithermal mineral deposits and prospects of early Tertiary age (Rivera and Stephens, 1988).

In summary although the degree of denudation may be locally variable, the apatite fission track data from mountainous ranges located within the Intermediate Depression are compatible with an overall limited extent of erosion since the Early Tertiary (maximum ca. 1 - 3 km assuming 30°C/km paleo-geothermal gradient).

### 5.2.5 Coastal Cordillera Mesozoic Rocks

In the Coastal Cordillera, a preliminary study of samples from different Jurassic intrusives from near sea level to 1500 m elevation, gives Cretaceous apatite fission track ages ranging between 123 and 70 Ma (Table 5.11; Fig. 5.12). The lack of systematic variation with altitude (Fig. 5.13) precludes estimations of denudation rates by the topographic method. However, the Cretaceous age of samples at sea level implies that the coastal area has not been greatly buried since the Mesozoic.

TABLE 5.11 APATITE FISSION TRACK AGES FROM THE COASTAL CORDILLERA
(Analytical data in Appendix 5)

| Sample | Alt. (m) | Locality | Age (Ma) and error (± 2σ) |
|---|---|---|---|
| II-565 | 1500 | Cerros de Colupito | 103 ± 14.0 |
| II-547 | 1420 | Cerros Vieirira | 92.2 ± 12.6 |
| II-571 | 550 | Guanillos | 122 ± 12.4 |
| II-527 | 430 | Cerro Fortuna | 98.8 ± 11.6 |
| II-528 | 200 | Cerro Gordo | 86.1 ± 8.0 |
| II-558 | 150 | Punta Lautaro | 115 ± 14.4 |
| II-483 | 100 | Cerro Coloso | 70.9 ± 5.8 |
| II-536 | 20 | Guanillos | 129 ± 12.6 |

TABLE 5.12 SUMMARY OF APATITE TRACK LENGTH DATA FROM THE COASTAL CORDILLERA

| Sample | No tracks | Mean length (μm) | Standard deviation (μm) | Skewness |
|---|---|---|---|---|
| II-565 | 81 | 14.4 | 1.24 | -1.18 |
| II-571 | 100 | 14.6 | 1.09 | -0.12 |
| II-558 | 100 | 14.0 | 1.13 | -0.28 |
| II-483 | 101 | 13.1 | 1.12 | -0.55 |
| | 101 | 13.2 | 1.22 | -0.94 |
| II-536 | 93 | 14.4 | 1.48 | -0.62 |

Mean confined track lengths in apatites from plutons of the Coastal Cordillera range from 14.0 to 14.6 μm, except for sample II-483 that has a mean track length of 13.1 μm (Table 5.12). The standard deviations range from 1.09 to 1.48 μm. The distributions of track lengths are narrow, and unimodal (Fig. 5.14), typical of samples that have remained near-surface since cooling, such as "undisturbed volcanic" rocks

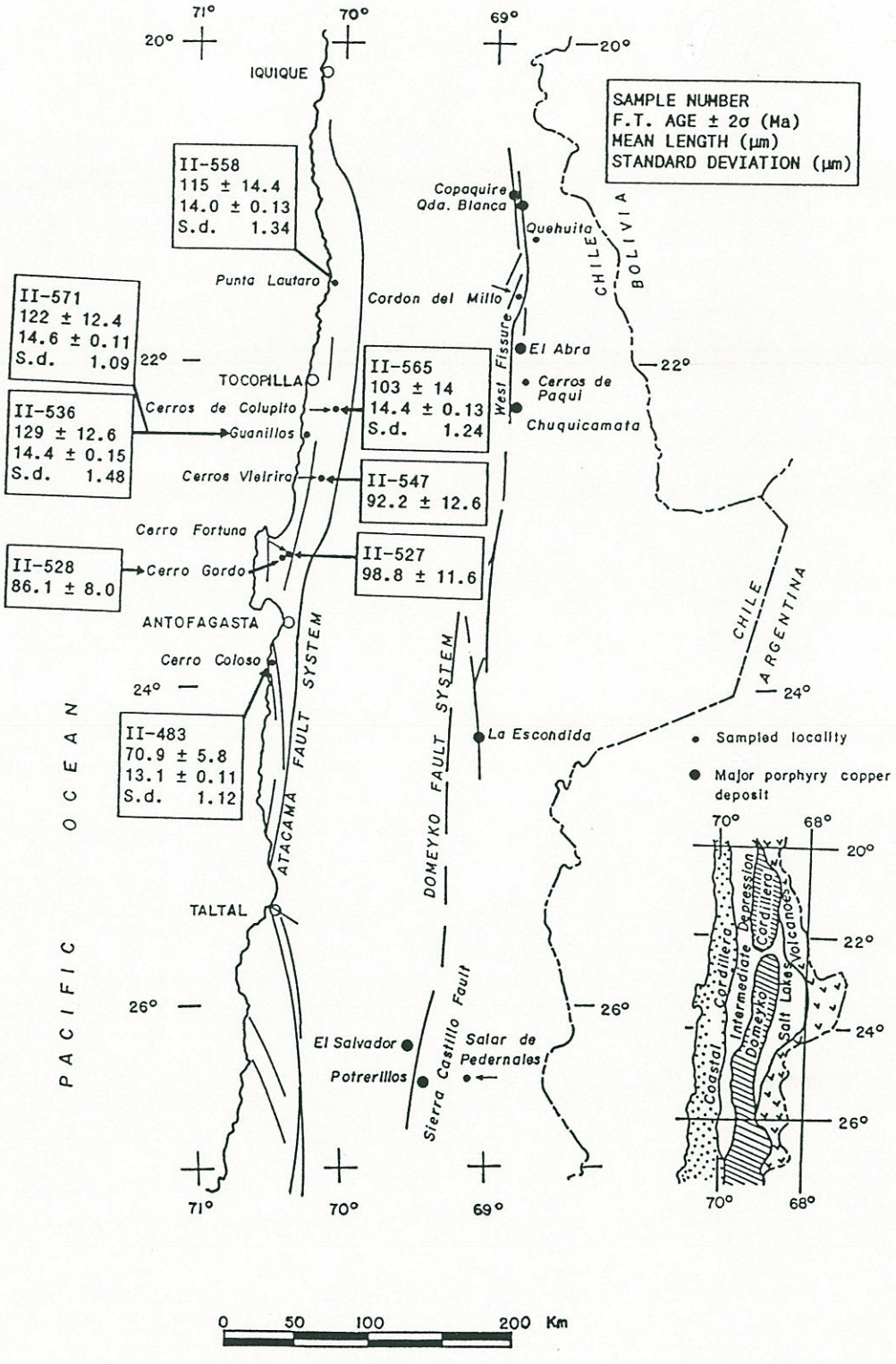


Figure 5.12. Apatite fission track data from Jurassic plutons of the Coastal Cordillera.

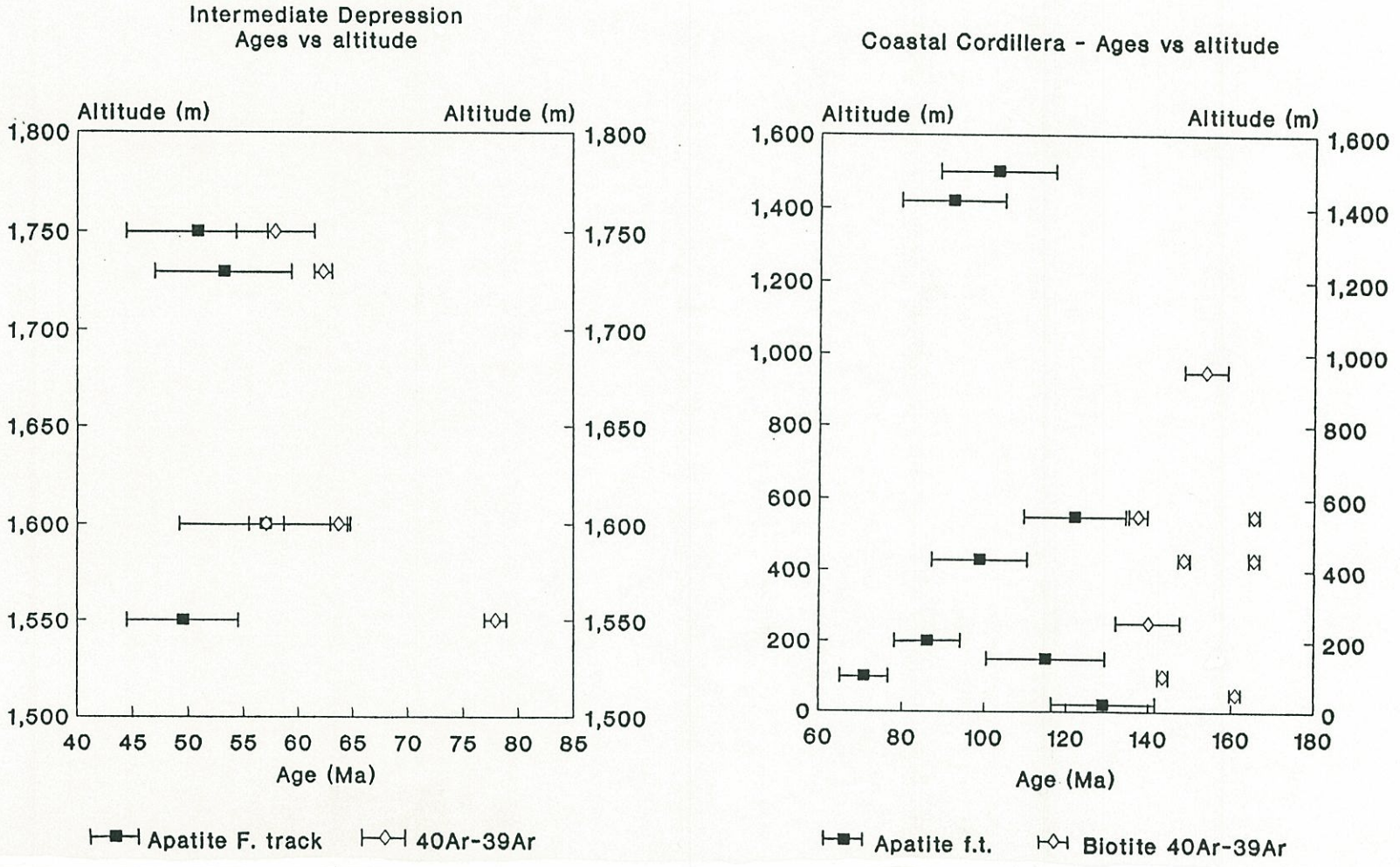


**Figure 5.13.** Apatite fission track ages and $^{40}Ar$-$^{39}Ar$ dates versus altitude. Left graph shows data from the Intermediate Depression. Right graph includes data from the Coastal Cordillera. No regular variation of fission track ages with altitude is apparent.

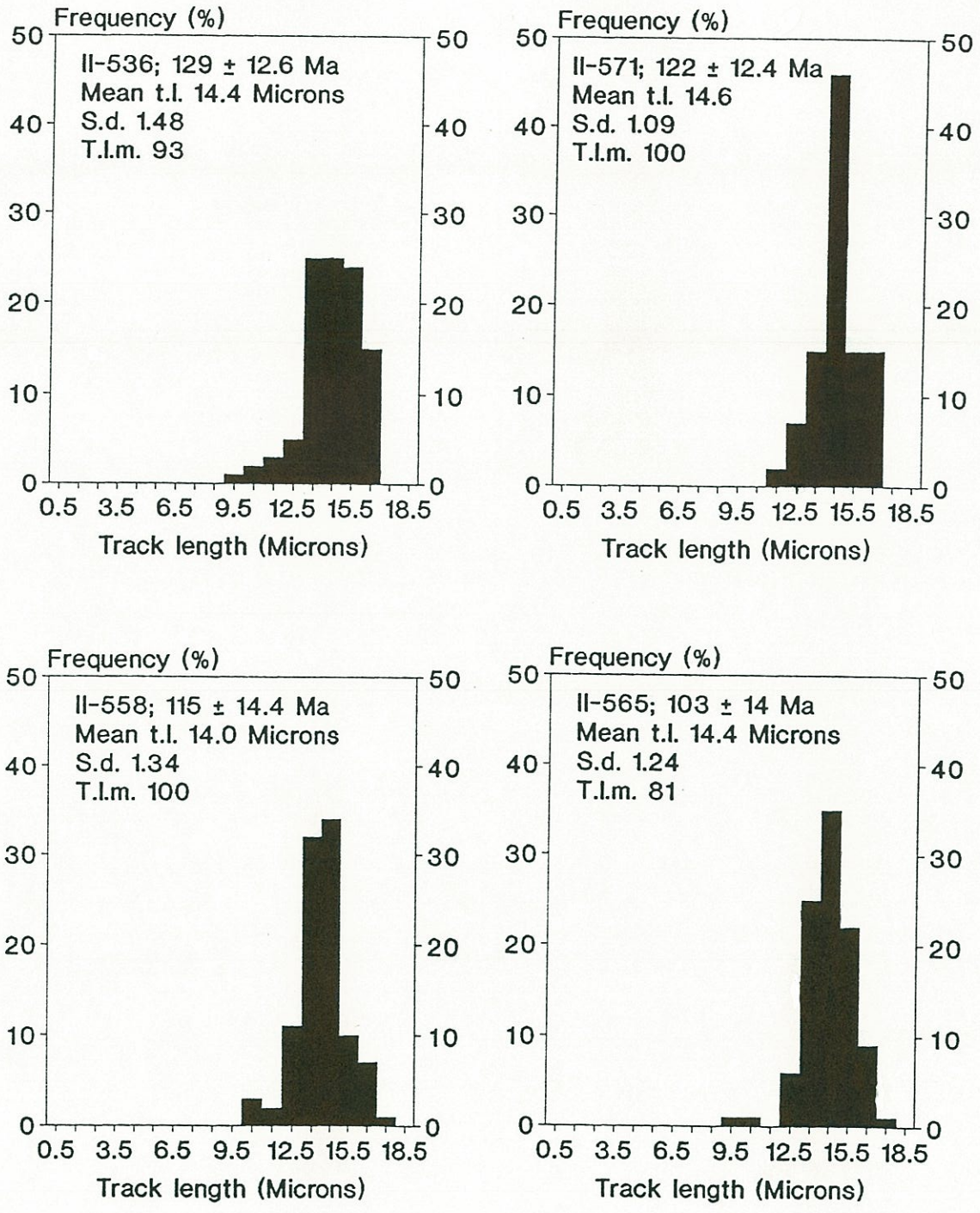


Figure 5.14. Distributions of confined fission track lengths of apatites from the Coastal Cordillera. These distributions compare to the "undisturbed volcanic" type (Fig. 5.6) implying a long-term near-surface residence of the samples.

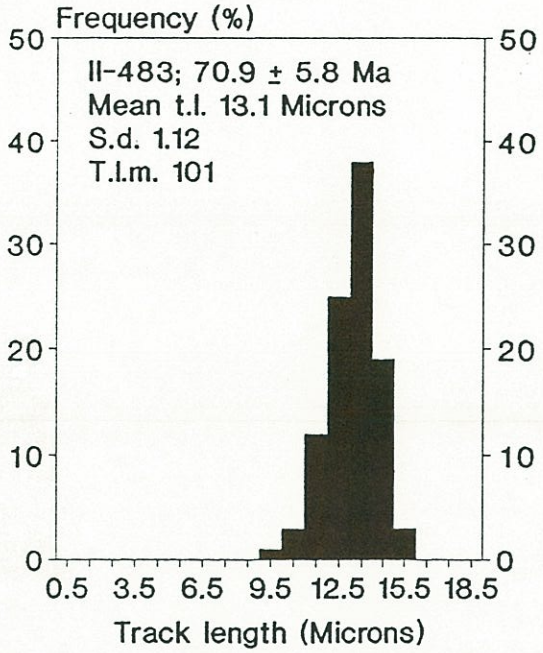


**Figure 5.15.** Distribution of track lengths of apatites from sample II-483: a foliated Jurassic gabbro from the Coastal Area.

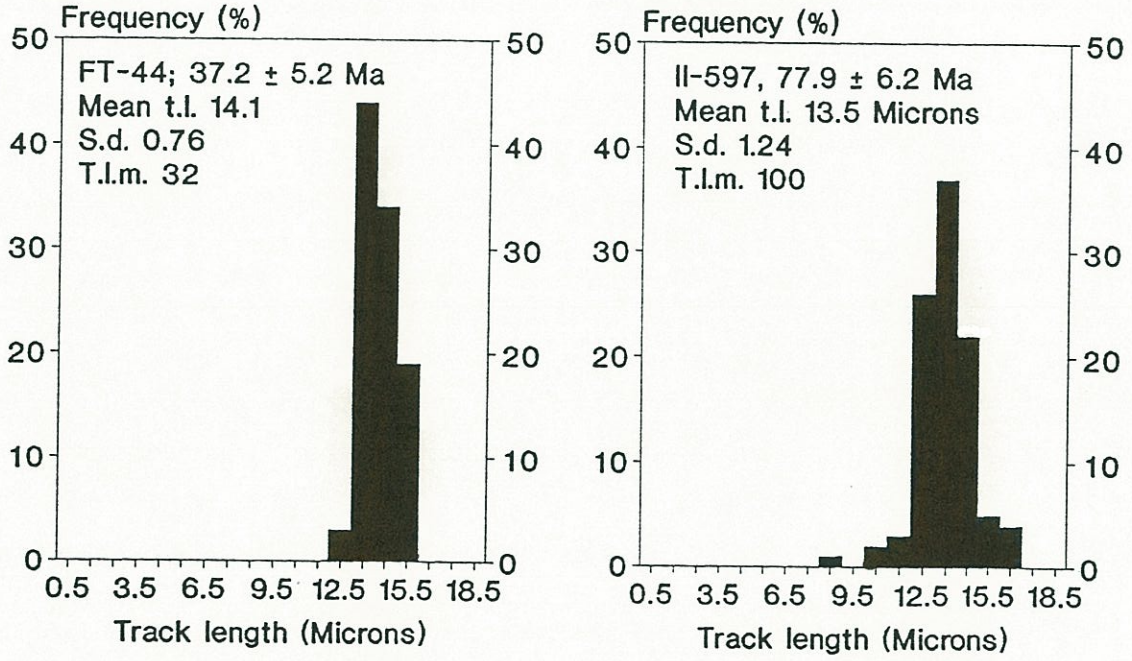


**Figure 5.16.** Distributions of confined track lengths of apatites from sample FT-44 a dacitic porphyry from El Abra porphyry copper, and II-597 a dioritic stock from the Caracoles silver district.

of Gleadow and others (1986). The Early Cretaceous apatite fission track ages and track lengths above 14 µm, represent cooling under the 70-125°C range (apatite annealing temperature) of the Mid-Late Jurassic coastal plutons, and are consistent with their permanence since that time at a near-surface level (temperatures below ca. 50°C). The lack of variation of apatite fission track ages or track lengths with altitude may indicate that an Early Cretaceous uplift-erosion episode is not the direct cause of cooling, although later faulting may have distorted the fission track record. The compiled geochronological data (Appendix 2) show that during the Early Cretaceous pluton emplacement was active along the Coastal Cordillera (see Section 2.8.6). Therefore it seems likely that the apatite fission track ages of Jurassic plutons reflect the thermal effect of the emplacement along the Coastal Cordillera of the Early Cretaceous plutons. This may account for the lack of regular variation with altitude of the apatite fission track ages and relatively long mean track lengths if the Jurassic rocks were near-surface in the Early Cretaceous (less than about 2 km depending on the paleo-geothermal gradient).

In summary, the fission track data from the Coastal Cordillera show that this area has not been deeply buried since the Early Cretaceous, and are compatible with a permanence of the rocks probably not deeper than 2 km since that time (assuming 30°C/km paleo-geothermal gradient). Therefore a limited extent of erosion of this mountain range since the Early Cretaceous is implied.

Scheuber and Andriessen (1989) inferred a post-Jurassic displacement of 12.5 km along the WNW-ESE El Way fault to account for the exposure at the surface of foliated Jurassic gabbros in the Coastal Cordillera south of El Way (Fig. 2.10), which according to these authors were deformed under amphibolite facies (pressure <3 Kb, temperature about 500°C). The El Way fault is interpreted in this study as the southern boundary of the pull-apart basin that contains the Lower Cretaceous limestones of the El Way Formation (see Section 2.16.2). Local relative displacements of that magnitude are not rare in this type of tectonic depression (e.g., Christie-Blick and Biddle, 1985; Sawyer and others,

1987; Pitman and Andrews, 1985). Scheuber and Andriessen (*op. cit.*) obtained an amphibole K-Ar age of 163 ± 14 Ma for a foliated gabbro 30 km south of Antofagasta, a biotite K-Ar age of 138 ± 9 Ma, a zircon fission track age of 119 ± 22 Ma, and an apatite fission track age of 118 ± 13 Ma. The concordance of apatite and zircon fission track ages, within error limits, with the biotite K-Ar age indicates an Early Cretaceous rapid cooling, and subsequent permanence at low temperatures of these rocks. This is consistent with uplift of the coastal Jurassic foliated gabbros south of Antofagasta during latest Jurassic to Early Cretaceous as inferred by Scheuber and Andriessen (1989) and Reutter and others (1988). A foliated gabbro was also dated during this study at Cerro Coloso (20 km north of the locality dated by Scheuber and Andriessen, 1990). Recrystallized biotite yielded a $^{40}Ar$-$^{39}Ar$ plateau age of 143.5 ± 0.7 Ma (II-483; see Chapter 2), concordant within error limits with the biotite K-Ar age obtained by the above authors. The apatite from this rock yielded an age of 70.9 ± 5.8, with a mean confined track length of 13.1 μm, and standard deviation of 1.12 μm (Table 5.12, Fig. 5.15). This particular sample appears to have remained somewhat deeper relative to the rest of the samples of the coastal area, and cooled below the annealing temperature of apatite in the Late Cretaceous.

In summary, fission track data from the Coastal Cordillera are consistent with the permanence of most dated rocks below ca. 50°C (near surface) since the Early Cretaceous, without either deep burial or significant erosion since that time. The geomorphological studies of Mortimer and Saric (1975) and Mortimer (1980) have shown that the Coastal Cordillera block has been a barrier for the drainage to the sea in northern Chile at least since the Oligocene. These observations have been corroborated by the recent studies of Abele (1988, 1989). Therefore the coastal crustal block controlled the regional erosion baselevel at least during part of the Tertiary, thereby inhibiting the erosion of this entire Andean segment. The other major factor controlling erosion has been the perennial arid climate that has characterized the Antofagasta region at least since the Cretaceous (see Chapter 1).

### 5.2.6. Dating of magnetite deposits of the Altiplano

The volcanogenic magnetite bodies of El Laco and Incahuasi iron deposits contain large fluorapatite crystals (0.5 - 2 cm long), which have been used in this study for the direct dating of the magnetite orebodies. The fluorapatite samples were provided by Moyra Gardeweg (geologist of SERNAGEOMIN working in that area). Apatite sections parallel to the c-axis were cut, and four of them from different crystals were mounted in epoxy for fission track analysis. Because of the large size of the fluorapatite sections, in each crystal the tracks within 36 to 85 microscope fields (2,500 $\mu m^2$ each) were counted, as well as their respective image on the external mica detector. The counts were all at 100 microscope fields for the Incahuasi apatites. The apatite from El Laco has a mean uranium content of 35 ppm, and a track density of $3.48 \times 10^4$ $tr/cm^2$, whereas the apatites from Incahuasi have only 3 ppm of uranium and a spontaneous track density of only $1.37 \times 10^4$ $tr/cm^2$: hence more fields were required in the latter. As a test, an additional checking recount of 100 fields was done for one of the El Laco crystals. This produced the same $\rho_s/\rho_i$ that the initial count of 85 fields did ($0.019 \pm 0.002$). Since the recount was done only to determine the reproducibility of the track count, it was not used in the age calculation. The results are summarized on Table 5.13.

An apatite fission track age of $2.1 \pm 0.2$ Ma was obtained for El Laco, which is concordant with a whole rock K-Ar age of $2.0 \pm 0.3$ Ma obtained by Gardeweg and Ramirez (1985) for the El Laco volcano. The low track density of this young apatite limited the measurement of confined track lengths. Mounted apatite sections were fractured by bending the epoxy mount and etched; 17 track in fractures were measured ranging between 15.2 and 16.7 µm, with a mean at 15.8 µm, and a standard deviation of 0.59 µm. These values are not very reliable, they are

TABLE 5.13 APATITE FISSION TRACK AGES OF EL LACO AND INCAHUASI

EL LACO (23°50.1'-67°28.8'): INDIVIDUAL GRAIN DATA

| Crystal | $N_s$ | $N_i$ | Fs. | $\rho_s/\rho_i$ | $\rho_s$ | $\rho_i$ | U ppm | Age Ma |
|---|---|---|---|---|---|---|---|---|
| 1 | 145 | 7451 | 85 | 0.019 | 4.37E+04 | 2.24E+06 | 37 | 2.3 ± 0.2 |
| 2 | 81 | 4474 | 81 | 0.018 | 2.56E+04 | 1.41E+06 | 24 | 2.1 ± 0.2 |
| 3 | 50 | 3016 | 36 | 0.017 | 3.56E+04 | 2.14E+06 | 36 | 1.9 ± 0.3 |
| 4 | 49 | 2801 | 37 | 0.017 | 3.39E+04 | 1.94E+06 | 32 | 2.0 ± 0.3 |
| | 325 | 17742 | | | 3.48E+04 | 1.90E+06 | 32 | |

Checking recount

| Crystal | $N_s$ | $N_i$ | Fs. | $\rho_s/\rho_i$ | $\rho_s$ | $\rho_i$ | U ppm | Age Ma |
|---|---|---|---|---|---|---|---|---|
| 1 | 149 | 7980 | 100 | 0.019 | 3.81E+04 | 2.04E+06 | 34 | 2.2 ± 0.2 |

EL LACO APATITE FISSION TRACK DATE = 2.1 ± 0.2 Ma

INCAHUASI (24°05.5'-67°32.0'): INDIVIDUAL GRAIN DATA

| Crystal | $N_s$ | $N_i$ | Fs. | $\rho_s/\rho_i$ | $\rho_s$ | $\rho_i$ | U ppm | Age Ma |
|---|---|---|---|---|---|---|---|---|
| 1 | 49 | 645 | 2500 | 0.076 | 1.25E+04 | 1.65E+05 | 3 | 8.7 ± 1.3 |
| 2 | 61 | 616 | 2500 | 0.099 | 1.56E+04 | 1.58E+05 | 3 | 11.4 ± 1.5 |
| 3 | 47 | 567 | 2500 | 0.083 | 1.20E+04 | 1.45E+05 | 2 | 9.5 ± 1.4 |
| 4 | 57 | 563 | 2500 | 0.101 | 1.46E+04 | 1.44E+05 | 2 | 11.6 ± 1.6 |
| | 214 | 2391 | | | 1.37E+04 | 1.54E+05 | 3 | |

INCAHUASI APATITE FISSION TRACK AGE = 10,3 ± 1.6 Ma

similar to those of recent induced tracks but the track lengths include the opening of the fractures, and the sample was somewhat overetched. However the narrow distribution of track lengths is consistent with the volcanic nature of the deposit.

The apatites from Incahuasi iron deposit (located at the southern foothills of the Incahuasi volcano) yielded a fission track age of 10.3 ± 1.6 Ma, which is concordant with whole rock K-Ar dates of 10.7 ± 0.5 and 10.5 ± 0.9 Ma obtained by Gardeweg and Ramirez (1985) in the northern foothills of the Incahuasi volcano. Although a similar procedure to the one described above was tried, the extremely low track density of these low-uranium, young apatites precluded the measurement of track lengths.

The apatite fission track ages of the volcanogenic magnetite bodies of the Altiplano substantiate the hypothesis that they were emplaced during the volcanic activity of their respective centres. This constitutes an application of the fission track method to direct dating of volcanogenic mineralization.

## 5.3 MODEL TIME-TEMPERATURE PATHS FROM FISSION TRACK DATA

### 5.3.1 Introduction

The apatite fission track age and the distribution of etchable confined track lengths reflect the time-temperature history of the mineral since formation of the oldest fission track. Recent advances in fission track analysis (Laslett and others, 1982, 1984, 1987; Duddy and others, 1988; Green, 1988; Donelick, 1988; Green and others, 1989) enable

one to estimate the time-temperature (t-T) path experienced by an apatite sample, provided that the fission track age and track length distribution have been measured. Such estimation is based on the extrapolation to geological timescales of the empirical calibration of the annealing process in Durango apatite done by Laslett and others (1987). In practice, the rate of annealing depends on the composition, specifically on the Cl/(F+Cl) ratio, with fluorapatites being more easily annealed than chlorapatites (Green and others, 1985, 1986, 1989; Green, 1989). Consequently, the model t-T paths must be regarded with some caution when applied to geological evolution, because inaccuracy may arise from possible compositional variation of apatites, and from the extrapolation to geological timescales of laboratory observations of apatite annealing lasting up to 500 days. Green and others (1989) indicated that the precision in predicted track length values is of the order of 0.25 - 0.5 μm, which is equivalent to an uncertainty in the absolute paleo-temperature estimates of ca. ± 10°C. The accuracy of the method is more difficult to estimate, but Green and others (1989) obtained consistent predictions of fission track parameters for a number of geological situations in which the thermal history is known, or can be inferred with some confidence. Thus the latter authors implied that extrapolation of annealing data from laboratory to geologic timescales is valid.

The computer program AFTAMTTP developed by Donelick (1988) was used in this study to generate synthetic stepped t-T paths from the measured apatite fission track age and track length data. This program provides a preliminary answer that serves as a starting point for forward modelling. Therefore a t-T path was inferred from the stepped one and used (input data) to derive a model age and track length distribution using the program CALCTLD (Donelick, 1988). Successive attempts by trial and error were necessary to match the measured fission track data. The model t-T paths and the inferences that may arise from them are discussed within the geological context of the samples.

### 5.3.2 The AFTAMTTP and CALCTLD computer modelling programs

The AFTAMTTP software developed by Donelick (1988) generates model t-T paths, provided that two conditions are met by the samples. First, the apatite crystals must show a narrow range in chemical composition. In a strict sense the composition must equal that of the Durango apatite, but more importantly the apatites must be monocompositional. The apatites analyzed in this study all come from intrusive bodies, and no significant variation in degree of etching was observed within each mount, which is compatible with limited or no compositional variation within each sample. Second, the apatite cannot have experienced an episode of significant heating since formation of the oldest track, because mean track length in apatite depends more on temperature than on time (Green and others, 1989; Donelick, 1988).

The model t-T path is generated by following sequential steps (after Donelick, 1988):

1) Generation of a measured track distribution by allocating the measured track lengths into several length intervals characterized by distinct interval size and known mid-points.

2) Correction of observational bias from measured track length distribution according to the geometrical arguments of Laslett and others (1982).

3) Resolution of the model track length distribution obtained in (2) into a best-fit sum of weighted component track length distributions.

4) Calculation of the age of the oldest fission track using the fission track age and the weighted component distributions obtained in (3).

5) Assignation of time intervals to each of the component distributions obtained in (3) so that the sum of the time intervals equals the age of

the oldest fission track and the duration of each time interval is proportional to the weight of its associated component distribution.

6) Calculation of average temperatures for each time interval as a function of the mean length of the associated component distribution and temperatures calculated for all subsequent time intervals. This is done by numerical solution of the empirical calibration of track length reduction of Laslett and others (1987) and using the concept of equivalent time of Duddy and others (1988). The latter assumes that at any moment a track that has been annealed to a certain degree behaves during further annealing in a manner that is independent of the conditions that caused the prior annealing, but which depends only on the degree of annealing that has occurred, and the prevailing conditions of temperature and time.

The methods used by the AFTAMTTP program to solve each step and the basic equations are detailed by Donelick (1988) and are not included here. This program provides a rough estimate of model average paleo-temperatures, without estimating precision levels.

The CALCTLD program (Donelick, 1988) allows forward modelling from a given time-temperature path. The recent advances in the understanding of fission track annealing in apatite allow one to predict the hypothetical length of a fission track that has followed a given time-temperature path. Thus the CALCTLD program generates a number of synthetic fission tracks through time, which are shortened according to the time-temperature path selected by the user. The track length reduction is based on the empirical calibration of Laslett and others (1987) and the concept of equivalent time of Duddy and others (1988). The synthetic track lengths are subsequently grouped into length intervals and a model distribution histogram generated. The statistical parameters of the model distribution are also calculated, and the model age determined according to the reduction of the track density.

For the sake of comparison, figure 5.17 shows the model t-T paths for the Fish Canyon and Durango apatite standards (after Donelick,

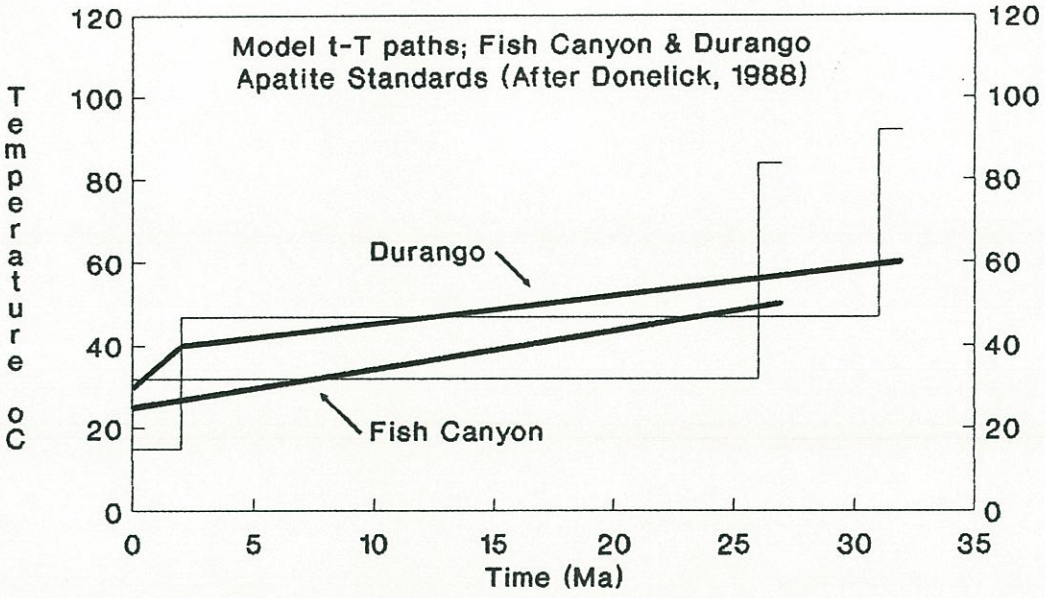


| | |
|---|---|
| **Fish Canyon** | **Measured** |
| Age | 28 ± 2 Ma |
| Mean t.l. | 15.00–15.60 µm |
| Std. dev. | 0.91–1.14 µm |
| | **Modelled** |
| Age | 27.5 Ma |
| Mean t.l. | 15.19 ± 0.08 µm |
| Std. dev. | 0.83 µm |
| **Durango** | **Measured** |
| Age | 31 ±3 Ma |
| Mean t.l. | 14.24–14.80 µm |
| Std. dev. | 0.64–1.25 µm |
| | **Modelled** |
| Age | 31.5 Ma |
| Mean t.l. | 14.67 ± 0.09 µm |
| Std. dev. | 0.89 µm |

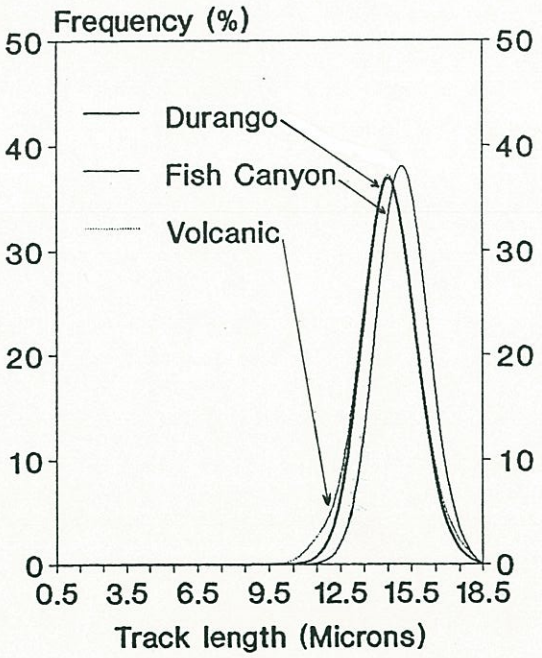


**Figure 5.17.** Model time-temperature paths for the Fish Canyon and Durango apatite standards. Step lines (after Donelick, 1988) were generated by AFTAMTTP inverting the fission track age and confined length distribution. Solid lines are t-T paths inferred from these step histories. Model track length distributions generated by CALCTLD based on the inferred model t-T paths are shown in the inset. The distribution of apatite track lengths from "undisturbed volcanic" rocks and measured lengths after Gleadow and others (1986) are included for the sake of comparison.

1988). The flat t-T paths inferred for these standard apatites reflect their long-term residence at near-surface levels of the Earth. The figure also shows the model fission track length distributions calculated using the CALCTLD program for the above t-T paths. The track length distribution of apatites from "undisturbed volcanic" rocks of Gleadow and others (1986) has been included for comparison. This is an average from measured track length distributions of apatite standards (Fish Canyon and Durango), which coincides almost exactly with the model track length distribution calculated for the Durango apatite (Fig. 5.17).

## 5.4 RESULTS OF MODELLING

### 5.4.1 Paleozoic crystalline basement of the Domeyko Cordillera

The samples from the Quehuita Late Paleozoic pluton (biotite K-Ar 252 ± 18 Ma; Appendix 1) collected at highest altitude on the Cordillera de Domeyko block (FT-64, 4,560 m; FT-63, 4,250), have the longest mean confined track lengths in basement apatites, and also older fission track ages compared with those obtained at lower altitudes. The model t-T paths obtained for these samples (Figs. 5.18, 5.19) are consistent with rapid cooling during the Mid-Late Eocene and subsequent limited cooling. The relatively flat segments at lower temperatures, which are similar to those of the apatite standards (Fig. 5.17) suggest a near-surface residence of the samples since about the end of the Eocene.

Samples FT-30 and FT-40, collected at 3,275 - 3,500 m altitude from the Cerros de Paqui area show comparable model t-T paths to the above (Fig. 5.20, 5.21). However, the initial cooling is slightly delayed and the flat segments occur at higher temperature, which is consistent with the lower altitudes relative to FT-64 and FT-63. Even higher temperatures characterize the model t-T path for sample FT-25, collected at 2,660 m of altitude 5 km east of Chuquicamata (Fig. 5.22).

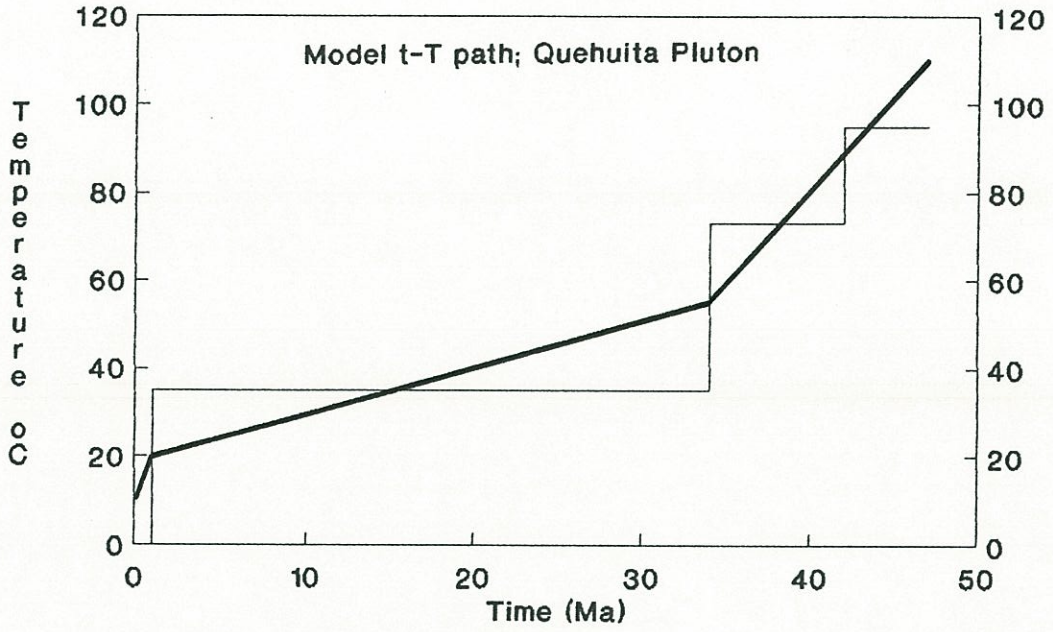


| Sample FT-64 | Measured |
|---|---|
| Age | 45.2 ± 6.2 Ma |
| Mean t.l. | 14.57 ± 0.14 µm |
| Std. dev. | 0.99 µm |
| Skewness | 1.08 |
| Kurtosis | -1.39 |
| | **Modelled** |
| Age | 45.7 Ma |
| Mean t.l. | 14.56 ± 0.15 µm |
| Std. dev. | 1.54µm |
| Skewness | -1.20 |
| Kurtosis | 1.79 |

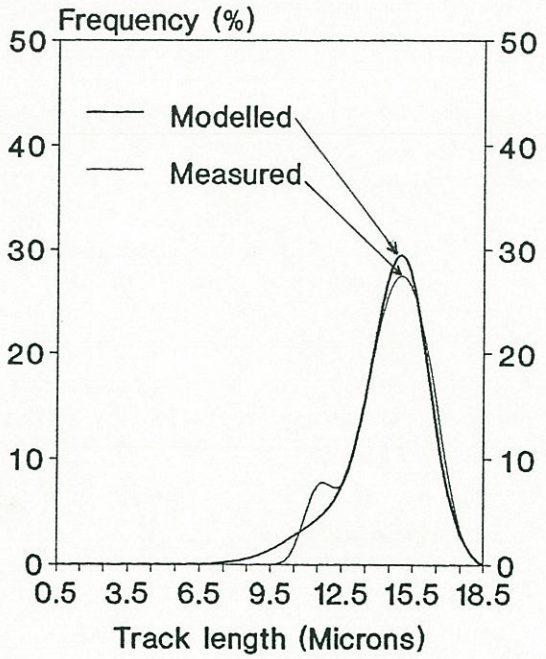


**Figure 5.18.** Model t-T path for the sample FT-64 (h = 4,560 m) from the Quehuita Pluton. Step history calculated by AFTAMTTP program. Solid line is the inferred t-T path. Model track length distribution generated by CALCTLD, and measured one are shown in the inset. The measured track length distribution in this, and subsequent diagrams, has been corrected for observational bias according to geometrical arguments of Laslett and others (1982).

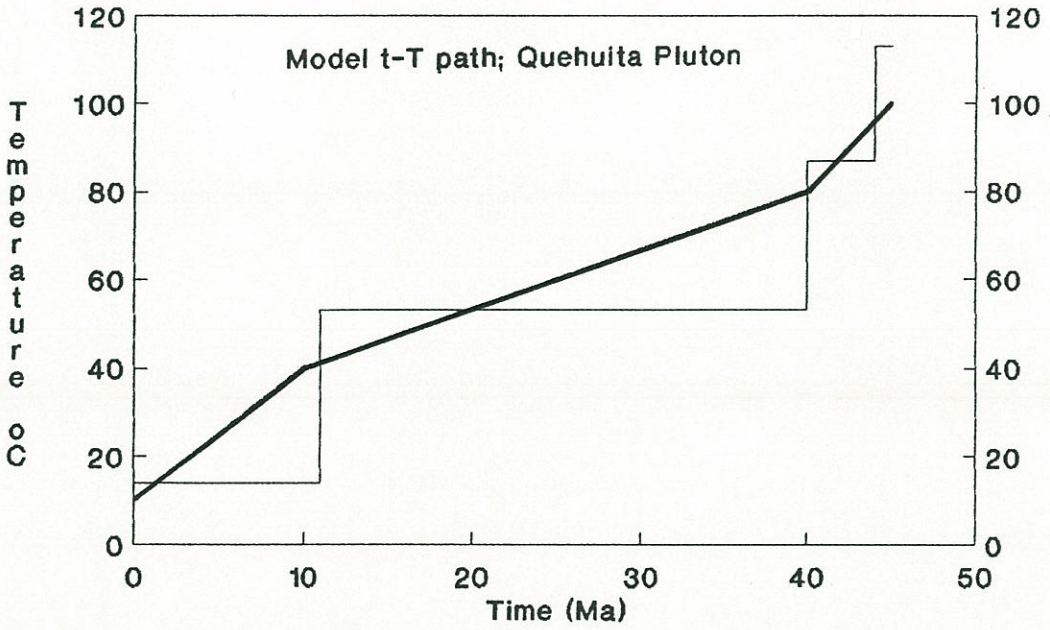


| Sample FT-63 | Measured |
|---|---|
| Age | 43.3 ± 4.6 Ma |
| Mean t.l. | 14.31 ± 0.21 µm |
| Std. dev. | 1.61 µm |
| Skewness | 1.24 |
| Kurtosis | -1.35 |
| | **Modelled** |
| Age | 43.1 Ma |
| Mean t.l. | 14.31 ± 0.14 µm |
| Std. dev. | 1.38 µm |
| Skewness | -0.33 |
| Kurtosis | -0.15 |

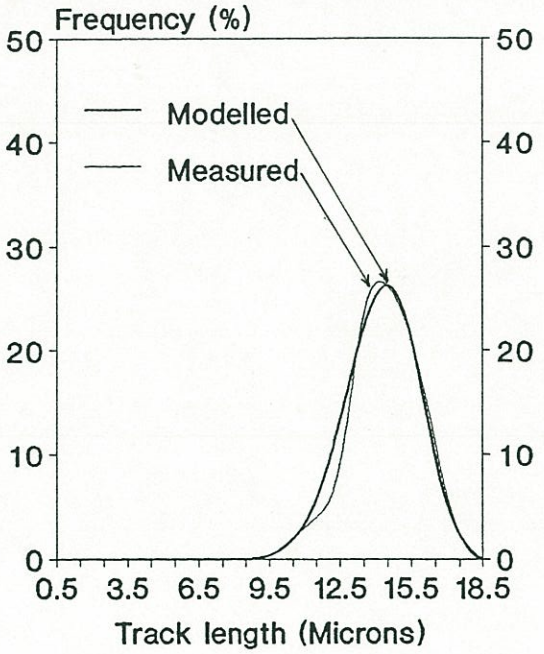


Figure 5.19. Model time-temperature path for the sample FT-63 (h = 4,250 m) from the Quehuita Pluton. Step history calculated by AFTAMTTP program. Solid line is the inferred t-T path. Model track length distribution generated by CALCTLD, and measured one are shown in the inset.

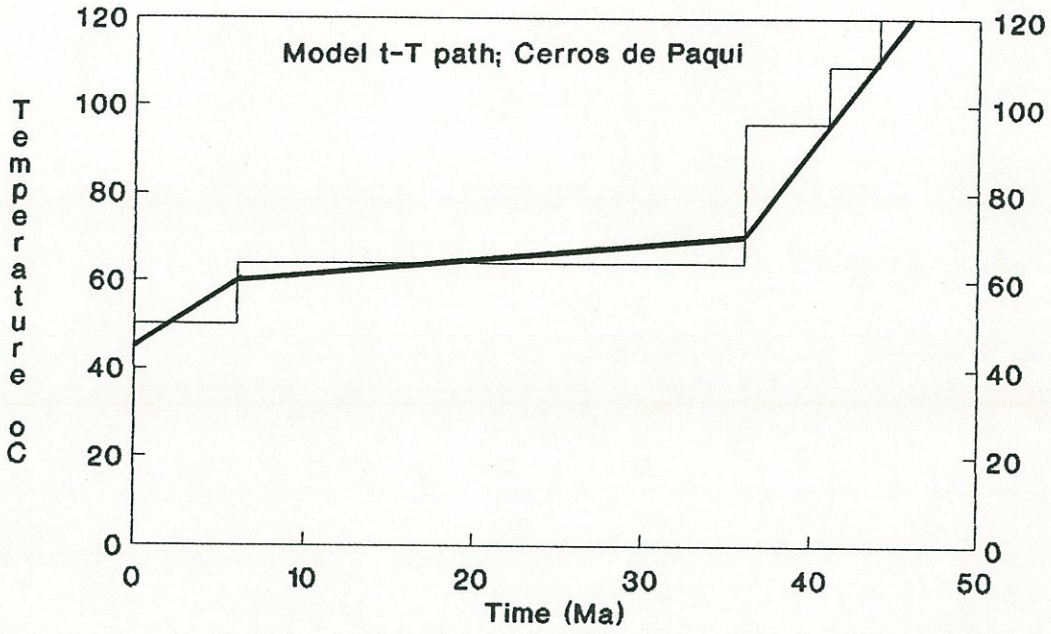


| Sample FT-40 | Measured |
|---|---|
| Age | 38.6 ± 4.4 Ma |
| Mean t.l. | 12.67 ± 0.23 µm |
| Std. dev. | 1.42 µm |
| Skewness | 0.17 |
| Kurtosis | -1.19 |
| | Modelled |
| Age | 40.5 Ma |
| Mean t.l. | 13.26 ± 0.16 µm |
| Std. dev. | 1.63 µm |
| Skewness | -1.43 |
| Kurtosis | 3.54 |

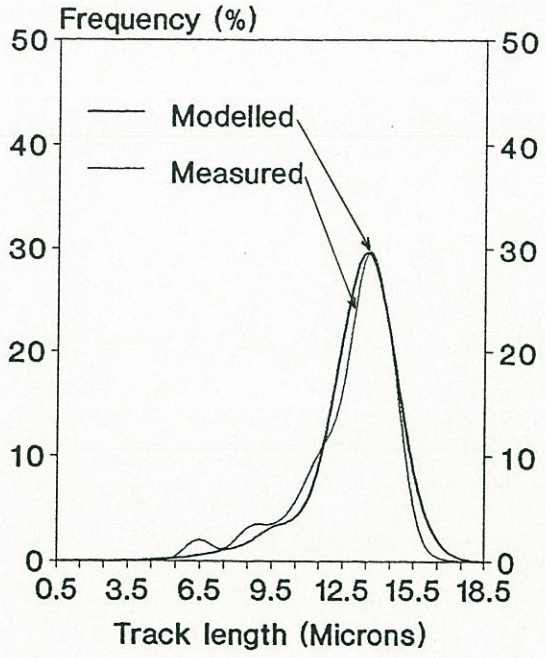


Figure 5.20. Model t-T path for the sample FT-40 (h = 3,275 m) from the Cerros de Paqui area. Step history calculated by AFTAMTTP program. Solid line is the inferred t-T path. Model track length distribution generated by CALCTLD, and measured one are shown in the inset.

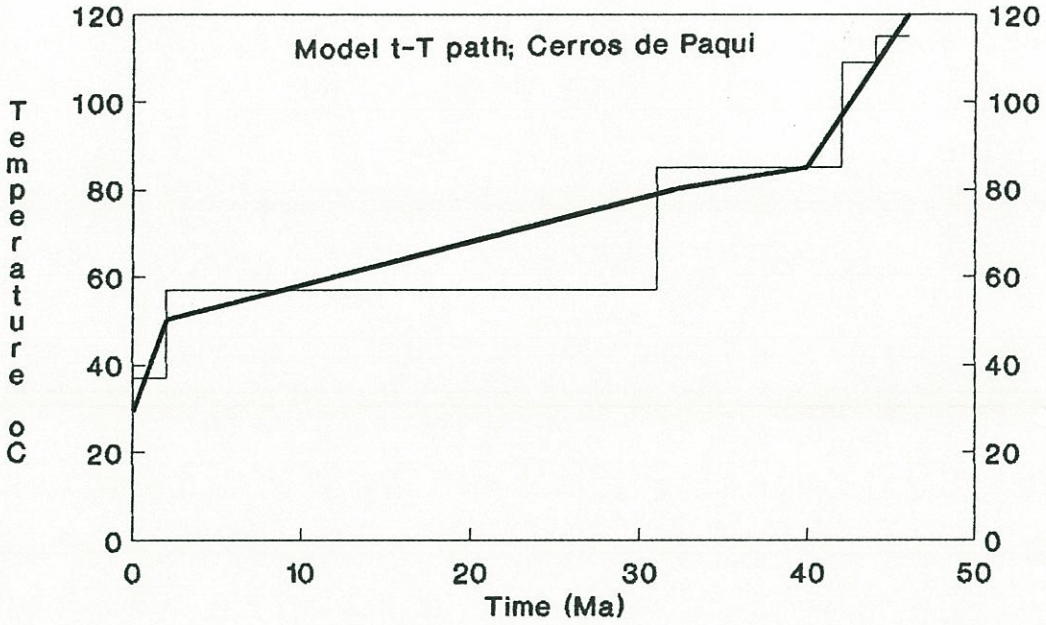


| Sample FT-30 | Measured |
|---|---|
| Age | 39.9 ± 5.4 Ma |
| Mean t.l. | 13.15 ± 0.17 µm |
| Std. dev. | 1.71 µm |
| Skewness | -1.16 |
| Kurtosis | -1.31 |
| | **Modelled** |
| Age | 40.3 Ma |
| Mean t.l. | 13.20 ± 0.17 µm |
| Std. dev. | 1.67 µm |
| Skewness | -0.92 |
| Kurtosis | 1.85 |

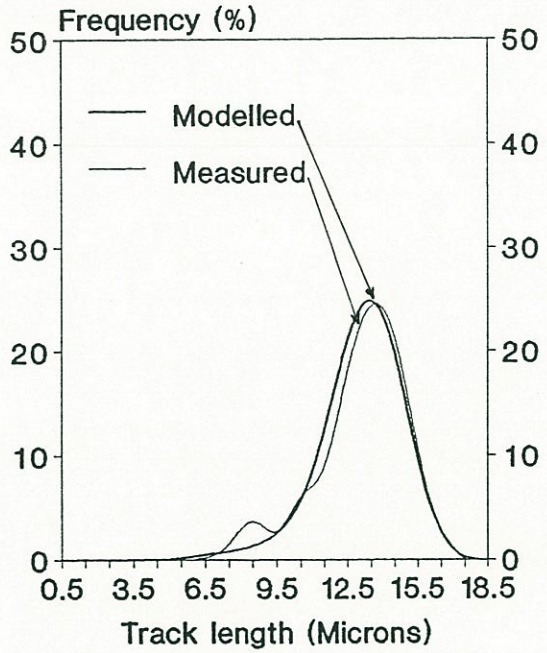


Figure 5.21. Model t-T path for the sample FT-30 (h = 3,500 m) from the Cerros de Paqui area. Step history calculated by AFTAMTTP program. Solid line is the inferred t-T path. Model track length distribution generated by CALCTLD, and measured one are shown in the inset.

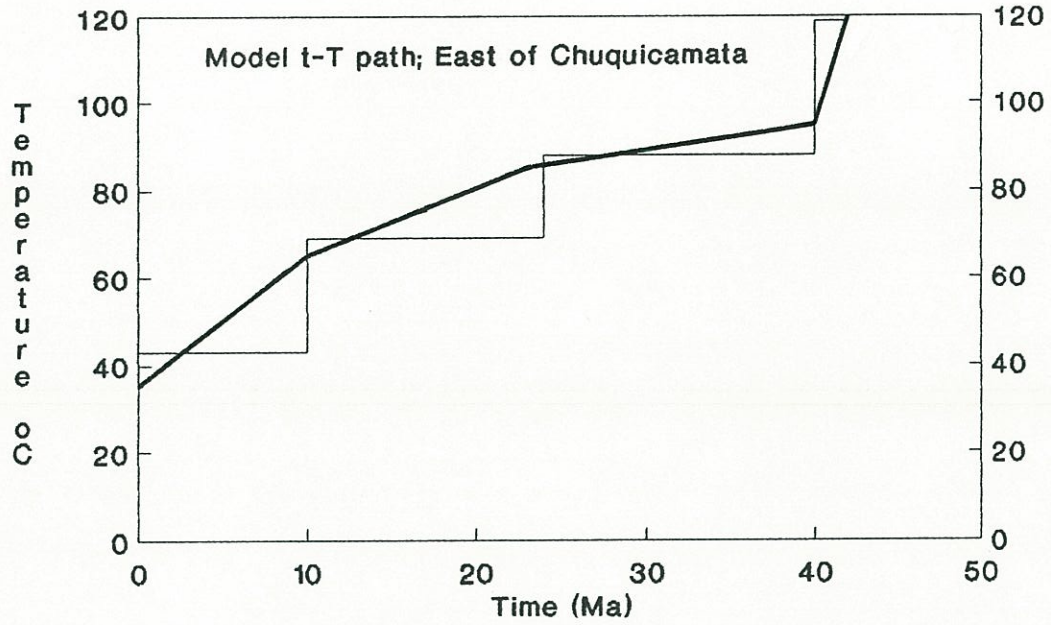


| Sample FT-25 | Measured |
|---|---|
| Age | 35.3 ± 5.2 Ma |
| Mean t.l. | 12.65 ± 0.22 µm |
| Std. dev. | 1.51 µm |
| Skewness | 0.71 |
| Kurtosis | -1.40 |
| | Modelled |
| Age | 36.9 Ma |
| Mean t.l. | 13.21 ± 0.18 µm |
| Std. dev. | 1.81 µm |
| Skewness | -0.24 |
| Kurtosis | -0.61 |

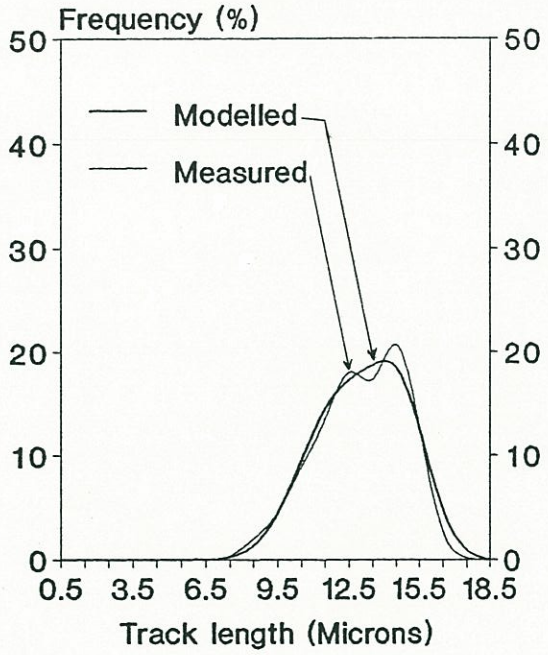


Figure 5.22. Model t-T path for the sample FT-25 (h = 2,600 m) collected east of Chuquicamata. Step history calculated by AFTAMTTP program. Solid line is the inferred t-T path. Model track length distribution generated by CALCTLD, and measured one are shown in the inset.

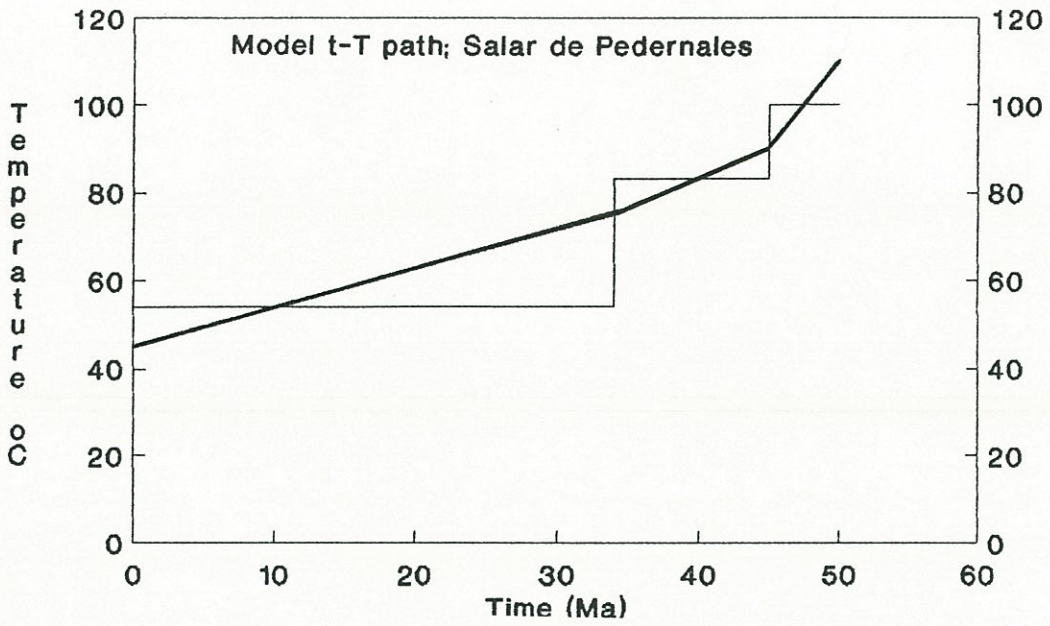


| Sample FT-04 | Measured |
|---|---|
| Age | 44.4 ± 4.2 Ma |
| Mean t.l. | 13.42 ± 0.15 µm |
| Std. dev. | 1.59 µm |
| Skewness | 0.40 |
| Kurtosis | -1.61 |
| | Modelled |
| Age | 44.8 Ma |
| Mean t.l. | 13.44 ± 0.15 µm |
| Std. dev. | 1.46 µm |
| Skewness | -0.61 |
| Kurtosis | 0.50 |

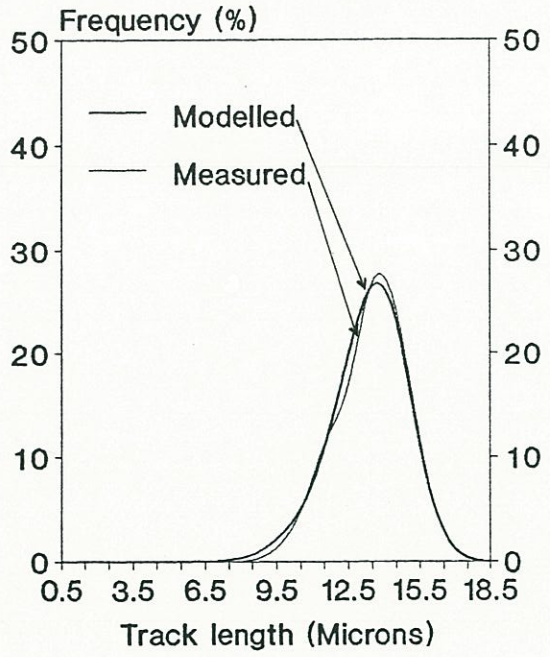


Figure 5.23. Model t-T path for the sample FT-04 (h = 3,425 m) from Salar de Pedernales area (26°S). Step history calculated by AFTAMTTP program. Solid line is the inferred t-T path. Model track length distribution generated by CALCTLD, and measured one are shown in the inset.

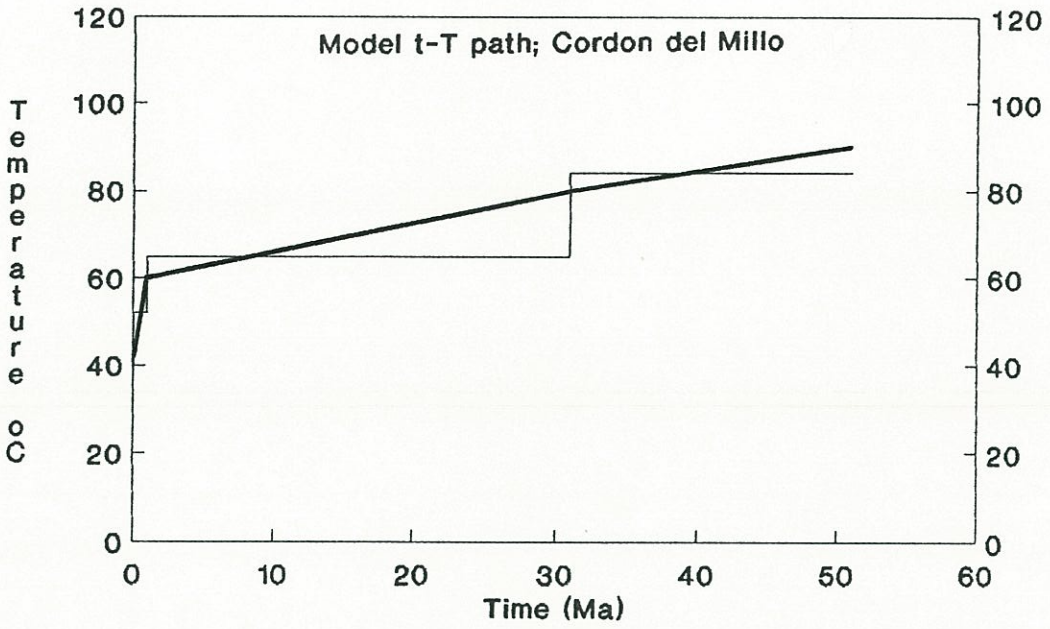


| Sample FT-58 | Measured |
|---|---|
| Age | 43.5 ± 6.6 Ma |
| Mean t.l. | 12.84 ± 0.17 µm |
| Std. dev. | 0.91 µm |
| Skewness | -0.63 |
| Kurtosis | -1.41 |
| | **Modelled** |
| Age | 43.7 Ma |
| Mean t.l. | 12.83 ± 0.13 µm |
| Std. dev. | 1.30 µm |
| Skewness | -0.03 |
| Kurtosis | -0.22 |

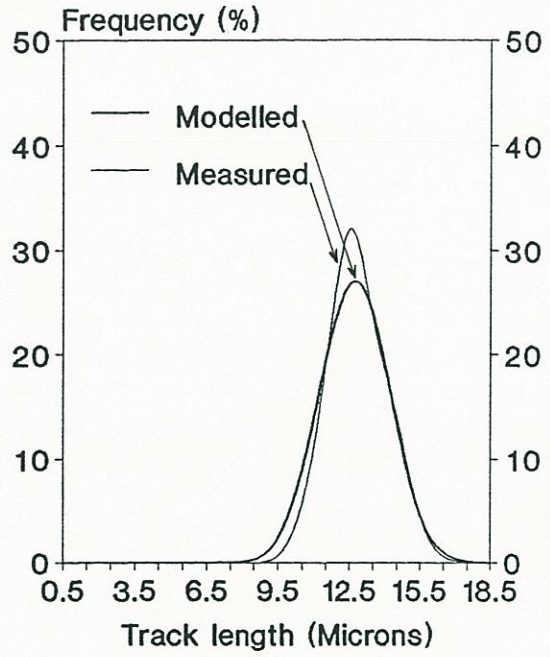


Figure 5.24. Model t-T path for the sample FT-58 (h = 4,150 m) from the Cordon del Millo area. Step history calculated by AFTAMTTP program. Solid line is the inferred t-T path. Model track length distribution generated by CALCTLD, and measured one are shown in the inset.

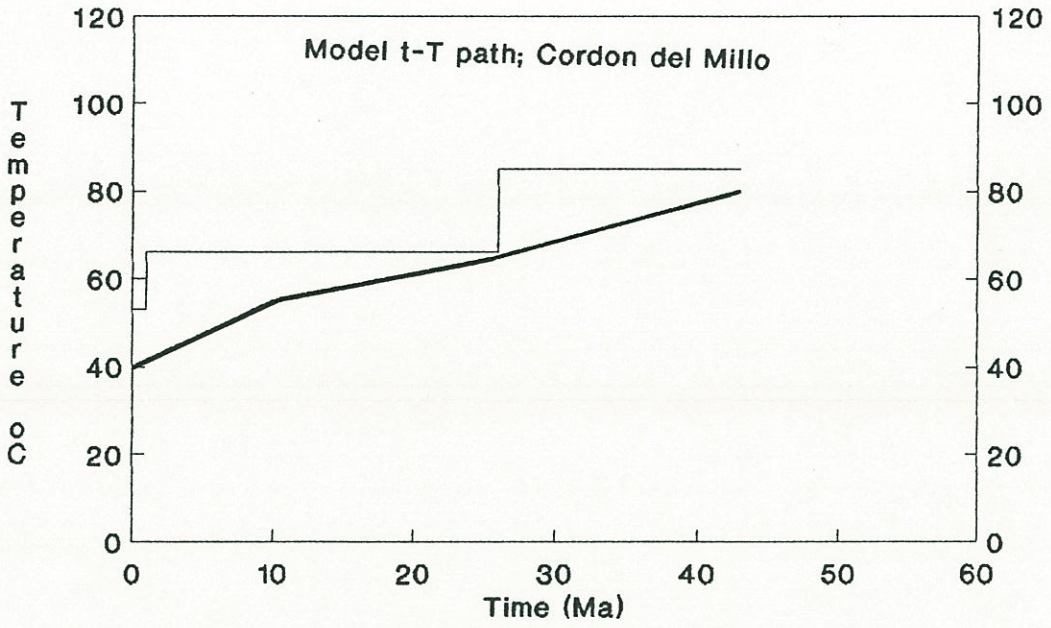


| Sample FT-56 | Measured |
|---|---|
| Age | 36.4 ± 4.4 Ma |
| Mean t.l. | 13.94 ± 0.14 µm |
| Std. dev. | 1.09 µm |
| Skewness | 1.63 |
| Kurtosis | -0.13 |
| | **Modelled** |
| Age | 40.1 Ma |
| Mean t.l. | 13.94 ± 0.11 µm |
| Std. dev. | 1.09 µm |
| Skewness | -0.01 |
| Kurtosis | -0.20 |

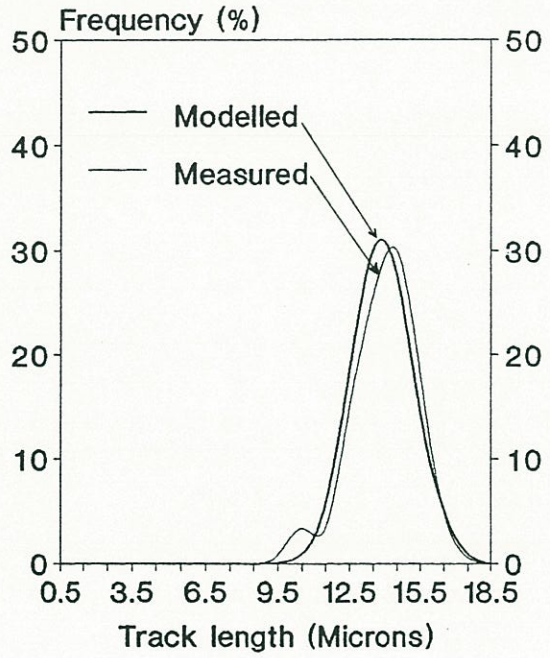


**Figure 5.25.** Model t-T path for the sample FT-56 (h = 4,060 m) from the Cordon del Millo area. Step history calculated by AFTAMTTP program. Solid line is the inferred t-T path. Model track length distribution generated by CALCTLD, and measured one are shown in the inset.

The model t-T pattern of this sample also suggests relatively rapid cooling from Miocene to recent times. All these samples were collected from different plutons along the same crustal block located east of the West Fissure between 21°00' and 22°30' S. The progressive increase of model temperatures with lower sample altitude, is compatible with a deeper past position of the samples now at lower topographic altitudes. This gives further support for the postulated Mid-Late Eocene rapid cooling being related to a period of increased erosion of the Domeyko Cordillera following the Incaic uplift, as inferred from apatite fission track ages and geological evidence. An additional rapid cooling during the Miocene is suggested by the model t-T path of sample FT-25. This may reflect reactivation of erosion associated with the Miocene Quechua tectonic event (see Section 2.17).

The model t-T inferred for sample FT-04 collected in the Domeyko Cordillera at Salar de Pedernales area (26°S), shows Mid-Late Eocene relatively rapid cooling followed by a flat segment compatible with near surface residence (Fig. 5.23). The pattern is similar to those obtained for Paleozoic plutons between 21°00' and 22°30'S. This suggests coherent uplift and erosion of the Domeyko Cordillera crustal block during the Mid-Late Eocene.

Samples FT-58 and FT-56 from the Cordon del Millo are from an uplifted block located immediately west of the West fissure (Fig. 5.7). The track length distribution of both samples is consistent, with similar model t-T paths (Figs. 5.24, 5.25) that are essentially flat at synthetic temperatures of the order of 60-80°C since Eocene times. These patterns differ markedly from those of samples from the eastern block of the West fissure and suggest a long-term residence of the samples at temperatures (depths) that allowed significant annealing to occur.

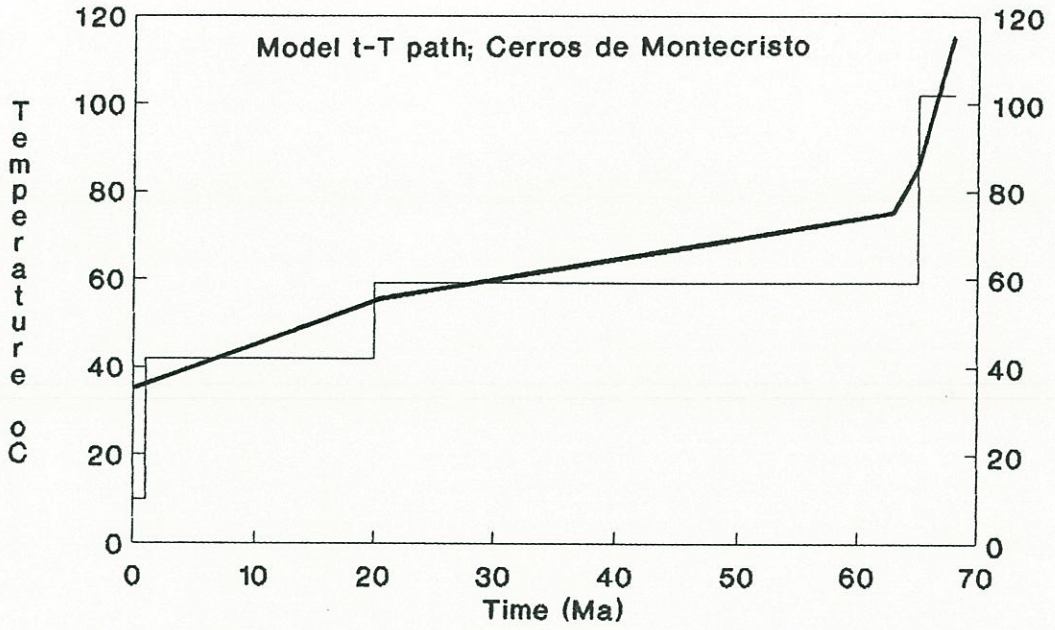


| Sample FT-14 | Measured |
|---|---|
| Age | 62.4 ± 7.4 Ma |
| Mean t.l. | 13.95 ± 0.12 µm |
| Std. dev. | 1.33 µm |
| Skewness | -0.57 |
| Kurtosis | 1.17 |
| | **Modelled** |
| Age | 63.0 Ma |
| Mean t.l. | 13.86 ± 0.13 µm |
| Std. dev. | 1.25 µm |
| Skewness | -0.43 |
| Kurtosis | 0.87 |

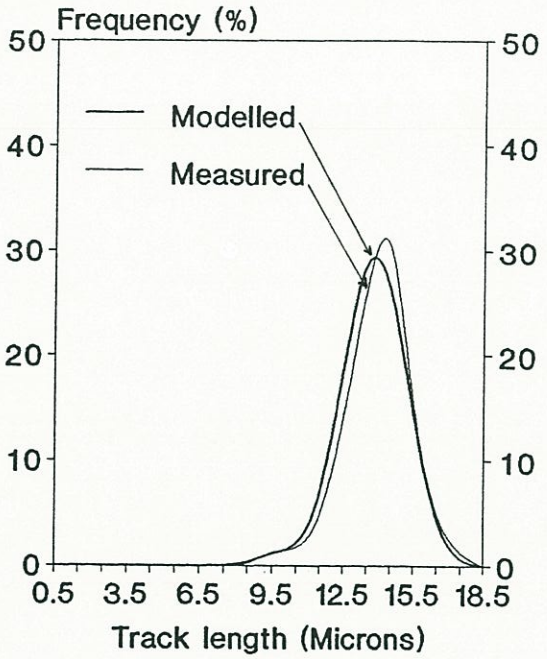


**Figure 5.26.** Model t-T path for the sample FT-14 (h = 2,880 m) from Cerros de Montecristo. Step history calculated by AFTAMTTP program. Solid line is the inferred t-T path. Model track length distribution generated by CALCTLD, and measured one are shown in the inset.

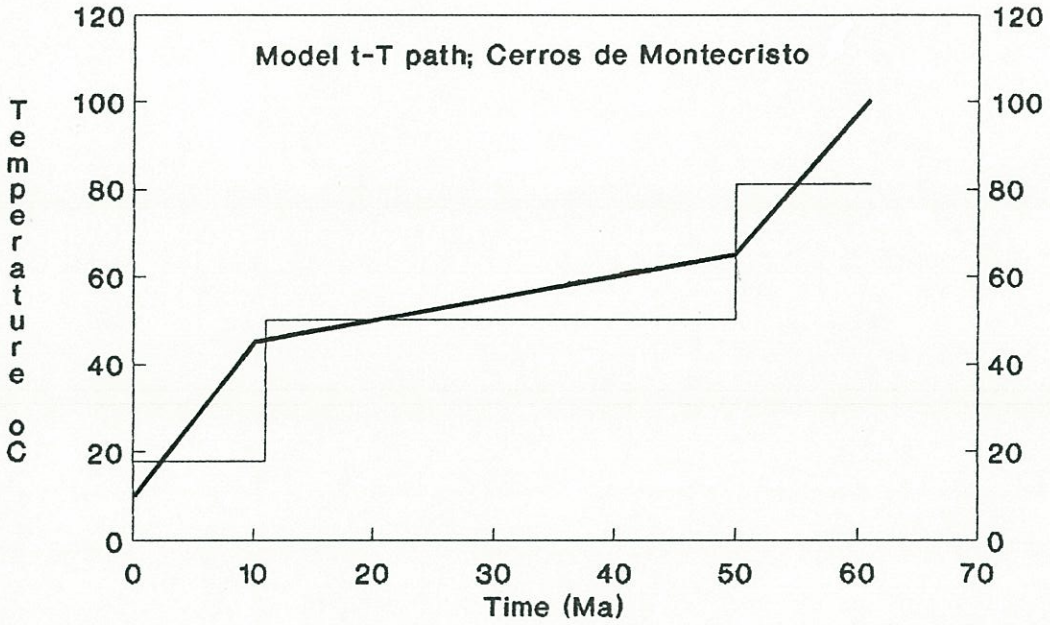


| Sample FT-12 | Measured |
|---|---|
| Age | 58.2 ± 5.6 Ma |
| Mean t.l. | 14.04 ± 0.13 µm |
| Std. dev. | 1.50 µm |
| Skewness | -1.17 |
| Kurtosis | 2.30 |
| | Modelled |
| Age | 58.1 Ma |
| Mean t.l. | 14.23 ± 0.13 µm |
| Std. dev. | 1.50 µm |
| Skewness | -0.35 |
| Kurtosis | 0.38 |

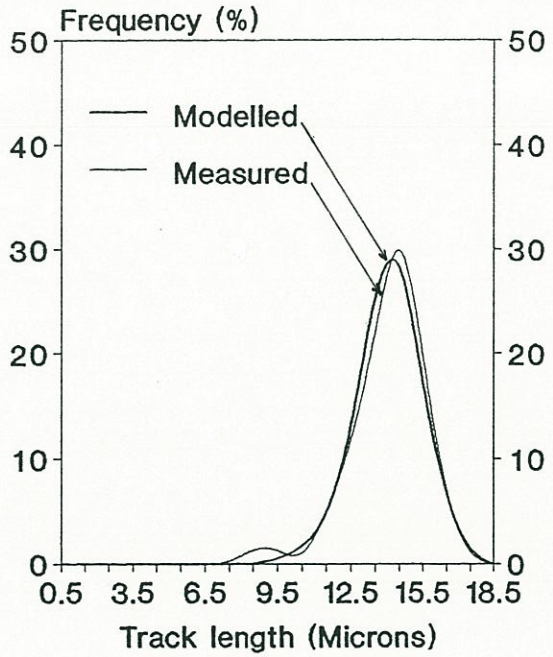


Figure 5.27. Model t-T path for the sample FT-12 (h = 2,440 m) from Cerros de Montecristo. Step history calculated by AFTAMTTP program. Solid line is the inferred t-T path. Model track length distribution generated by CALCTLD, and measured one are shown in the inset.

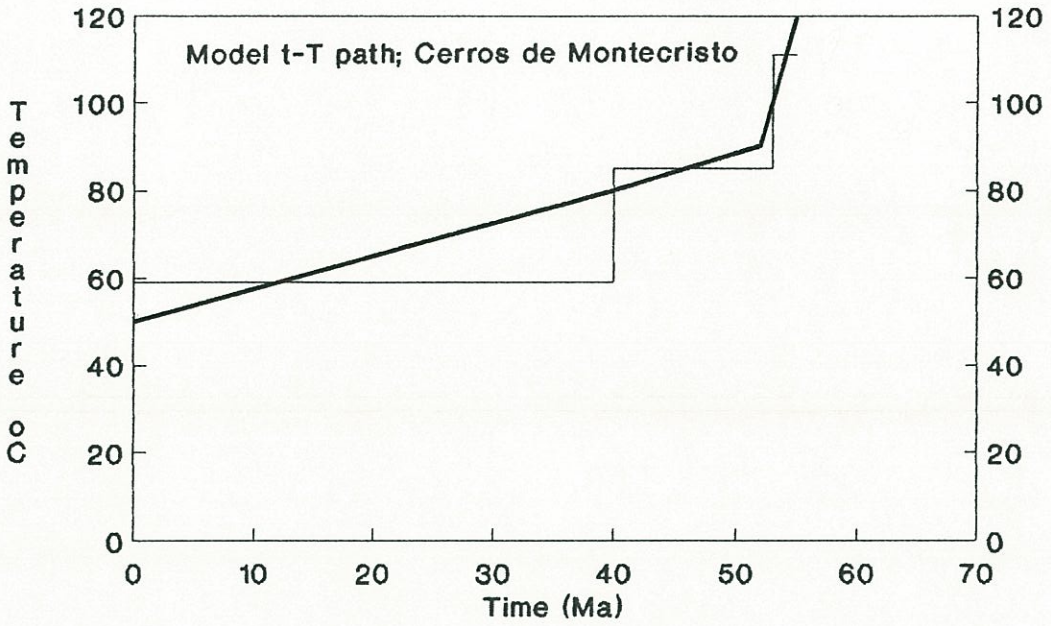


| Sample FT-8 | Measured |
|---|---|
| Age | 47.4 ± 5.4 Ma |
| Mean t.l. | 13.33 ± 0.11 µm |
| Std. dev. | 1.31 µm |
| Skewness | -0.55 |
| Kurtosis | 0.07 |
| | Modelled |
| Age | 48.4 Ma |
| Mean t.l. | 13.19 ± 0.14 µm |
| Std. dev. | 1.43 µm |
| Skewness | -0.60 |
| Kurtosis | 0.95 |

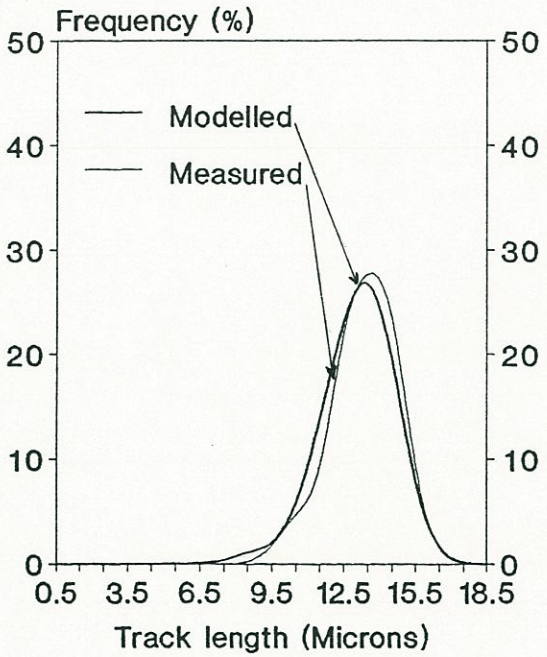


**Figure 5.28.** Model t-T path for the sample FT-8 (h = 1,570 m) from Cerros de Montecristo. Step history calculated by AFTAMTTP program. Solid line is the inferred t-T path. Model track length distribution generated by CALCTLD, and measured one are shown in the inset.

### 5.4.2 Tertiary plutons west of Chuquicamata

Samples from two Tertiary plutons that outcrop west of Chuquicamata (Fig. 5.7) were analyzed: the Cerros de Montecristo pluton with a biotite $^{40}Ar$-$^{39}Ar$ plateau age of 63.1 ± 0.3 Ma (FT-8) and the Fortuna Granodiorite with a $^{40}Ar$-$^{39}Ar$ age of about 37.1 ± 0.5 Ma (FT-23; see Chapter 4).

The model t-T path that matches the track length distribution of sample FT-14 collected at the top of the Cerros de Montecristo mountain range (2,880 m altitude) is very similar to those of apatite standards (Fig. 5.26). It is consistent with abrupt cooling after pluton emplacement at about 63 Ma, and subsequent near surface residence (temperatures < 70°C). This account for the apatite fission track age of sample FT-14 concordant with a biotite $^{40}Ar$-$^{39}Ar$ date of the pluton (see Section 5.2.2). These characteristics are consistent with exceedingly rapid cooling of the pluton, which may be the result of either very shallow emplacement or rapid exhumation following emplacement at depth. The track length distributions of samples FT-12, and FT-8, are compatible with rapid Eocene cooling but well after intrusion, followed by a flat section similar to that of apatite standards. These samples were collected at lower altitude (2440 and 1990 m) and their t-T paths are consistent with a deeper position relative to sample FT-14. The relatively rapid Eocene cooling may reflect erosion related to the Incaic uplift. The model t-T paths are consistent with the conclusion of section 5.2.2 that these samples remained at a relatively shallow level since pluton emplacement (about 2,000 to 3,000 m in depth assuming 30°C/km geothermal gradient).

Sample FT-16 obtained at highest altitude (3,270 m) from the Fortuna Granodiorite yielded a fission track date concordant with biotite $^{40}Ar$-$^{39}Ar$ and K-Ar ages of this granodiorite. The model t-T path inferred for this sample is identical to those of apatite standards, which implies a long-term residence virtually at a near-surface level (<2,000 m assuming 30°C/km geothermal gradient). This further indicates that the Fortuna

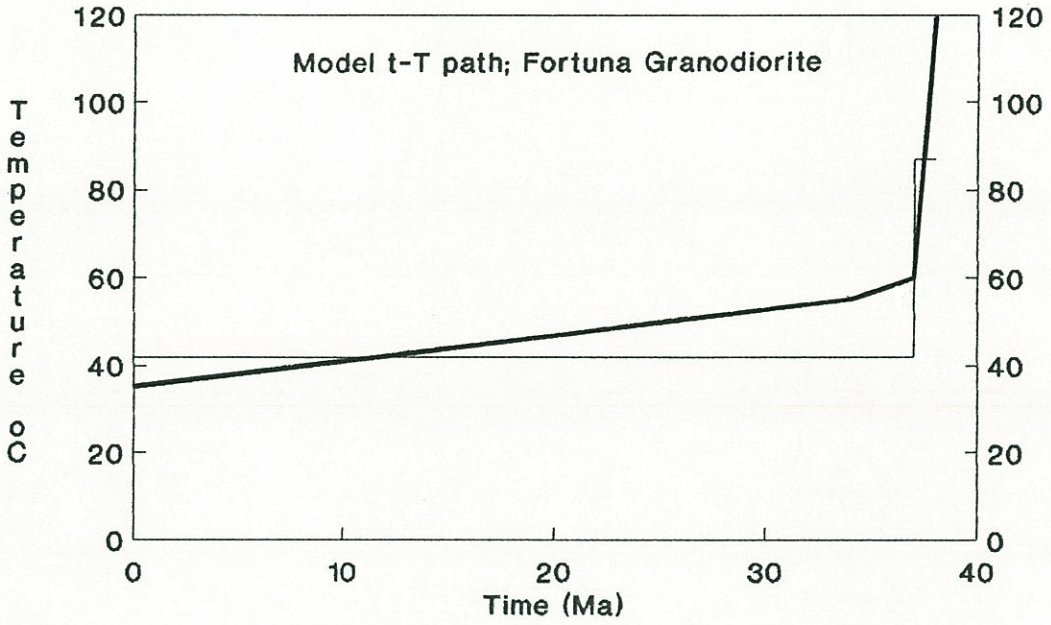


| Sample FT-16 | Measured |
|---|---|
| Age | 37.1 ± 3.6 Ma |
| Mean t.l. | 14.64 ± 0.05 µm |
| Std. dev. | 0.56 µm |
| Skewness | 1.50 |
| Kurtosis | 1.37 |
| | **Modelled** |
| Age | 37.5 Ma |
| Mean t.l. | 14.73 ± 0.09 µm |
| Std. dev. | 0.93 µm |
| Skewness | -0.46 |
| Kurtosis | 1.52 |

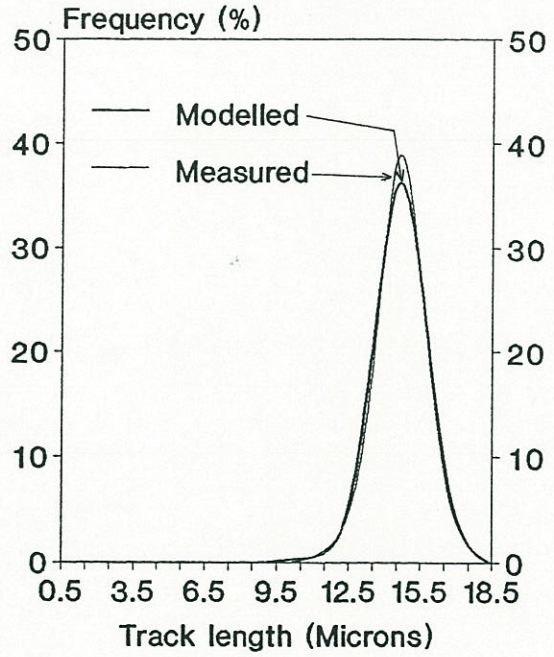


**Figure 5.29.** Model t-T path for the sample FT-16 (h = 3,270 m) from the Fortuna Granodiorite. Step history calculated by AFTAMTTP program. Solid line is the inferred t-T path. Model track length distribution generated by CALCTLD, and measured one are shown in the inset.

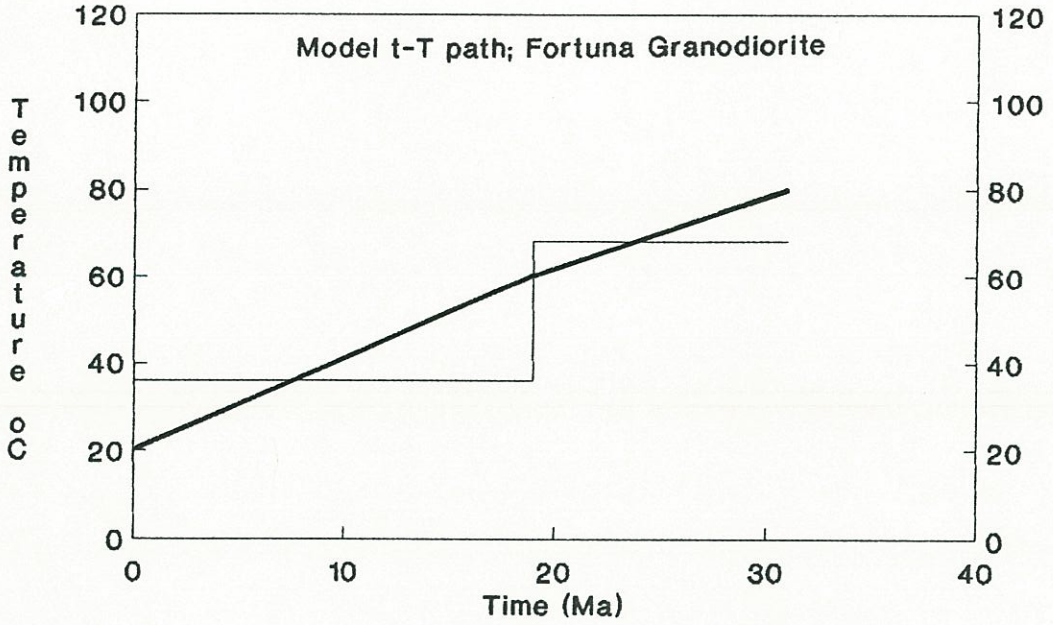


| Sample FT-41 | Measured |
|---|---|
| Age | 30.1 ± 3.2 Ma |
| Mean t.l. | 14.46 ± 0.15 µm |
| Std. dev. | 0.99 µm |
| Skewness | 0.12 |
| Kurtosis | -0.32 |
| | Modelled |
| Age | 30.3 Ma |
| Mean t.l. | 14.62 ± 0.12 µm |
| Std. dev. | 1.16 µm |
| Skewness | -0.19 |
| Kurtosis | -0.32 |

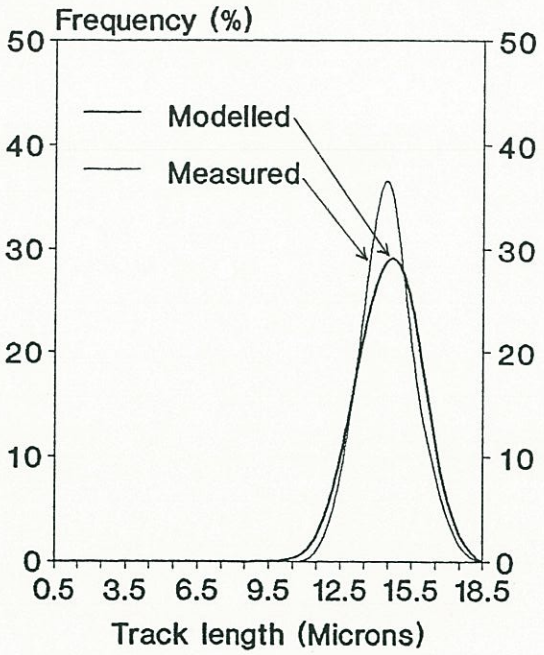


Figure 5.30. Model t-T path for the sample FT-41 (h = 3,190 m) from the Fortuna Granodiorite. Step history calculated by AFTAMTTP program. Solid line is the inferred t-T path. Model track length distribution generated by CALCTLD, and measured one are shown in the inset.

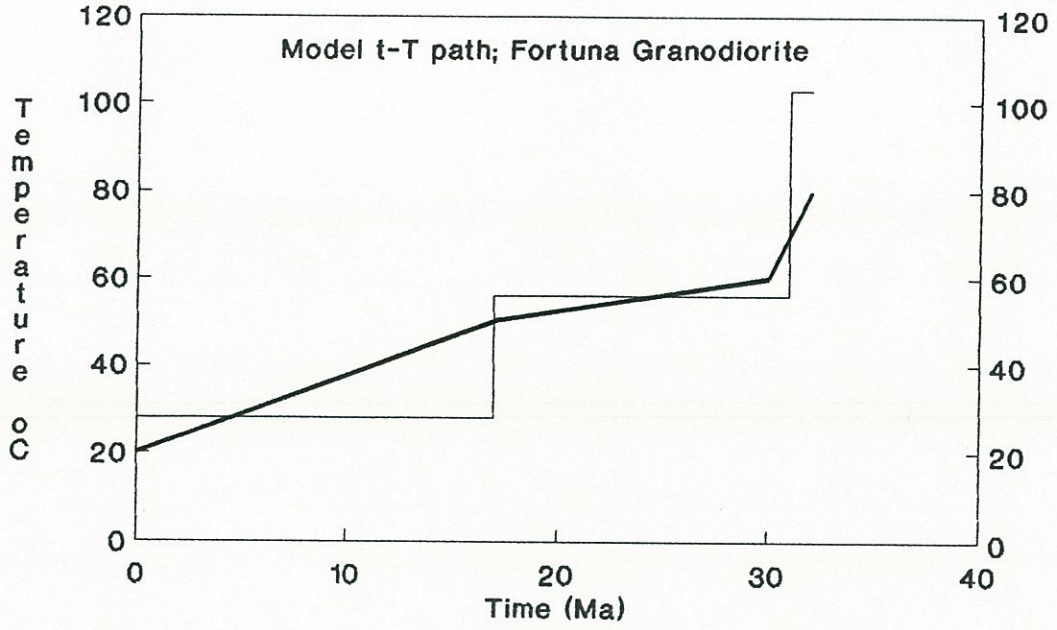


| Sample FT-17 | Measured |
|---|---|
| Age | 31.1 ± 4.0 Ma |
| Mean t.l. | 14.82 ± 0.08 µm |
| Std. dev. | 0.91 µm |
| Skewness | -0.48 |
| Kurtosis | 1.63 |
| | **Modelled** |
| Age | 31.9 Ma |
| Mean t.l. | 14.89 ± 0.10 µm |
| Std. dev. | 0.97 µm |
| Skewness | -0.06 |
| Kurtosis | -0.17 |

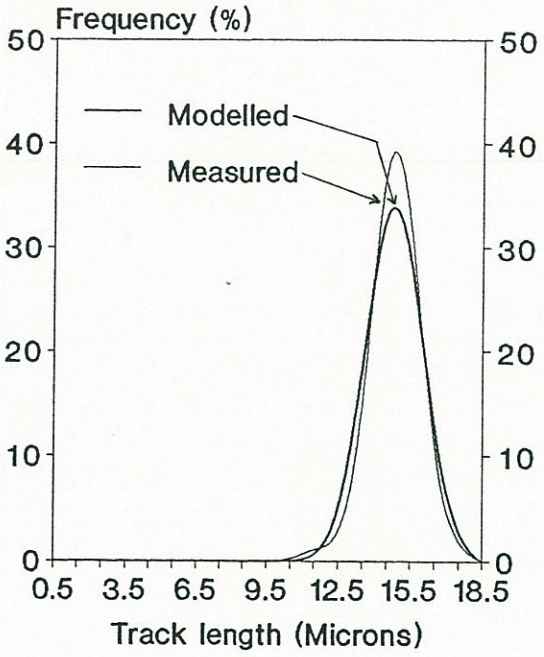


Figure 5.31. Model t-T path for the sample FT-17 (h = 3,080 m) from the Fortuna Granodiorite. Step history calculated by AFTAMTTP program. Solid line is the inferred t-T path. Model track length distribution generated by CALCTLD, and measured one are shown in the inset.

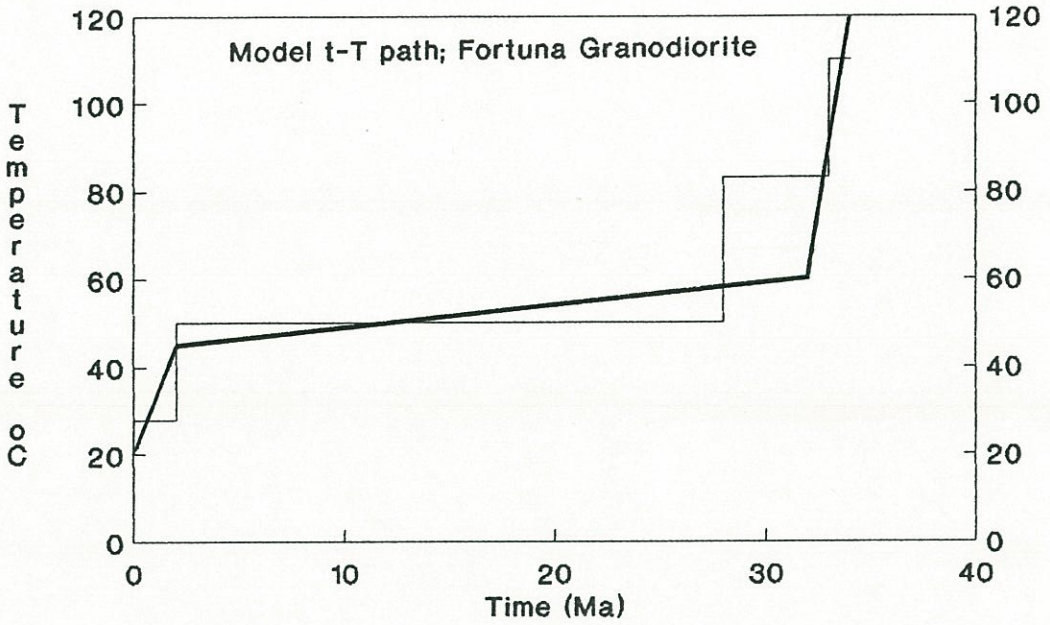


| Sample FT-15 | Measured |
|---|---|
| Age | 32.0 ± 3.8 Ma |
| Mean t.l. | 14.16 ± 0.16 µm |
| Std. dev. | 1.16 µm |
| Skewness | -0.85 |
| Kurtosis | 1.07 |
| | **Modelled** |
| Age | 32.9 Ma |
| Mean t.l. | 14.43 ± 0.10 µm |
| Std. dev. | 1.04 µm |
| Skewness | -0.70 |
| Kurtosis | 2.55 |

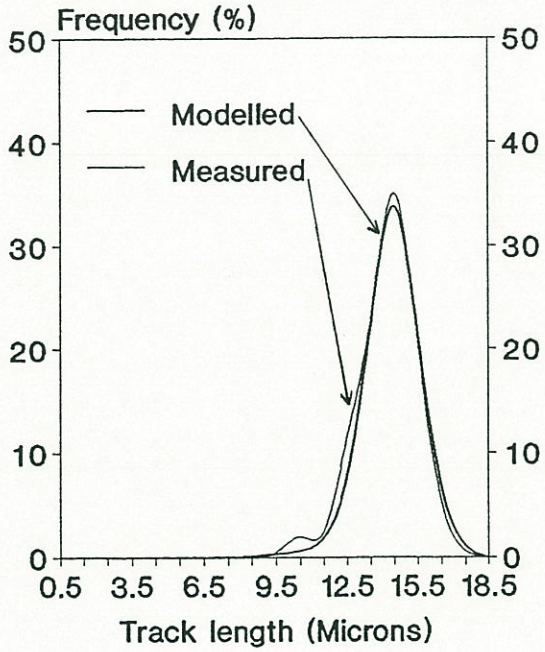


Figure 5.32. Model t-T path for the sample FT-15 (h = 2,970 m) from the Fortuna Granodiorite. Step history calculated by AFTAMTTP program. Solid line is the inferred t-T path. Model track length distribution generated by CALCTLD, and measured one are shown in the inset.

Granodiorite was either emplaced at a very shallow level or exhumed almost immediately after emplacement at 37 Ma, its higher section remaining close to the surface since that time. The model t-T paths for samples from the Fortuna Granodiorite collected at altitudes under 3,200 m are also consistent with their permanence at (cool) shallow levels, but all of them started to accumulate tracks at about 31 Ma which is the age of the neighbouring Chuquicamata porphyry. Therefore a total resetting of apatites by the thermal event related to the emplacement of the Chuquicamata porphyry is probable.

### 5.4.3 El Abra

A remarkably flat model t-T path matches the track length distribution of apatites from sample FT-44 of the mineralized Dacitic Porphyry of El Abra (Fig. 5.33), which is compatible with cooling immediately after intrusion and position of this porphyry copper deposit near the present-day surface level since about 37 Ma. This is further consistent with the concordance of apatite fission track and biotite $^{40}Ar$-$^{39}Ar$ ages and may reflect the very shallow emplacement of the porphyry, or its rapid denudation after intrusion.

### 5.4.4 Caracoles

Sample II-597 is from a diorite of the Caracoles silver district, located on the western flank of the Domeyko Cordillera 80 km south of Chuquicamata. This sample yielded an apatite fission track age of 77.9 ± 6.2 Ma concordant with its biotite $^{40}Ar$-$^{39}Ar$ date. The model t-T path determined for this sample (Fig. 5.34) is consistent with abrupt cooling after emplacement of the stock followed by a relatively flat segment, suggesting near-surface residence since the Late Cretaceous. The model t-T pattern is also compatible with the epithermal nature of the

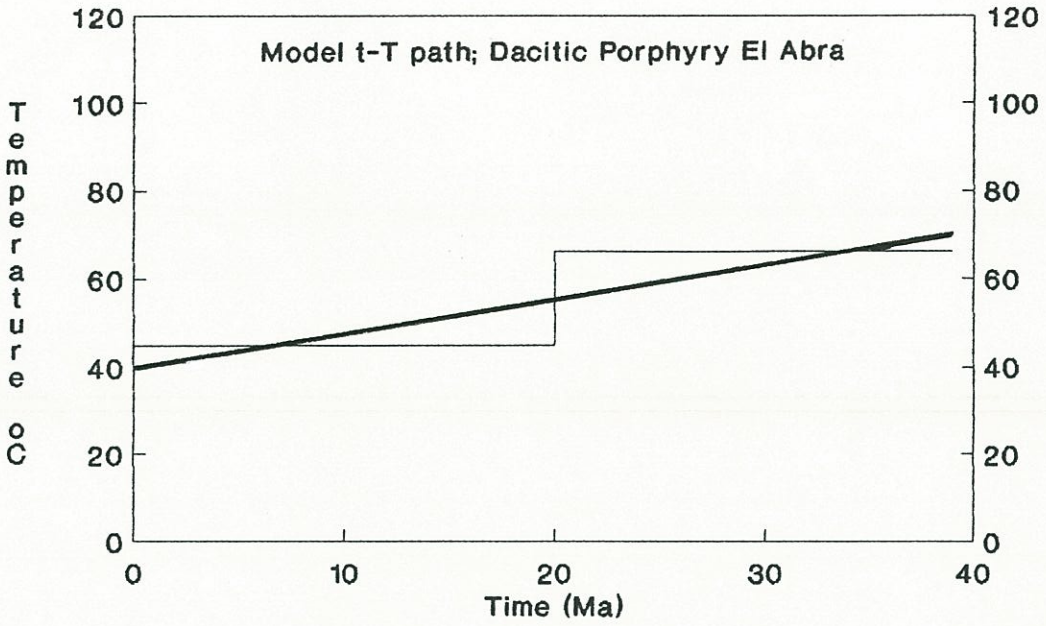


| Sample FT-44 | Measured |
|---|---|
| Age | 37.2 ± 5.2 Ma |
| Mean t.l. | 14.13 ± 0.09 µm |
| Std. dev. | 0.52 µm |
| Skewness | -0.28 |
| Kurtosis | -1.11 |
| | Modelled |
| Age | 37.5 Ma |
| Mean t.l. | 14.35 ± 0.10 µm |
| Std. dev. | 0.96 µm |
| Skewness | -0.03 |
| Kurtosis | -0.11 |

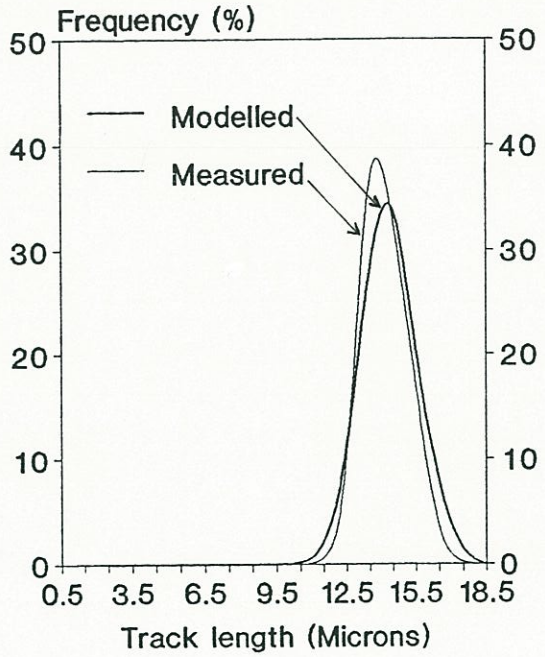


**Figure 5.33.** Model t-T path for the sample FT-44 (h = 3,860 m) from the Dacitic Porphyry of El Abra. Step history calculated by AFTAMTTP program. Solid line is the inferred t-T path. Model track length distribution generated by CALCTLD, and measured one are shown in the inset.

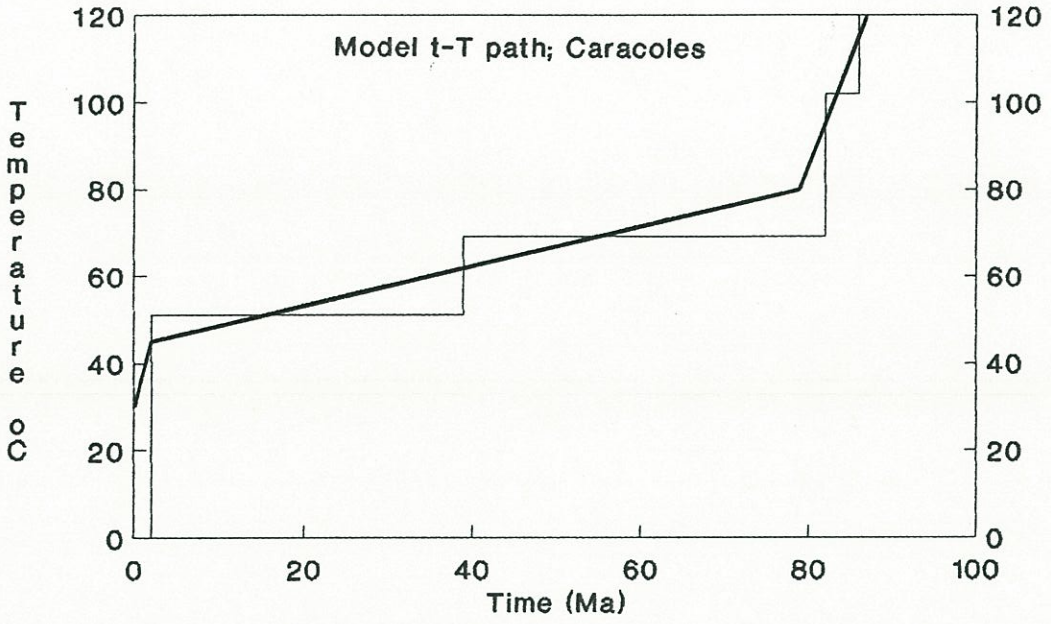


| Sample II-597 | Measured |
|---|---|
| Age | 77.9 ± 6.2 Ma |
| Mean t.l. | 13.42 ± 0.08 µm |
| Std. dev. | 0.85 µm |
| Skewness | -0.05 |
| Kurtosis | 0.00 |
| | Modelled |
| Age | 77.8 Ma |
| Mean t.l. | 13.43 ± 0.16 µm |
| Std. dev. | 1.54 µm |
| Skewness | -1.21 |
| Kurtosis | 3.46 |

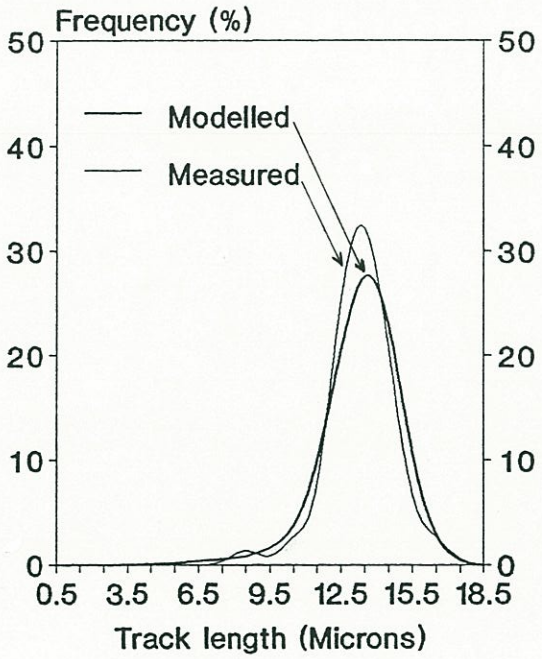


**Figure 5.34.** Model t-T path for the sample II-597 (h = 2,600 m) from the Caracoles silver district. Step history calculated by AFTAMTTP program. Solid line is the inferred t-T path. Model track length distribution generated by CALCTLD, and measured one are shown in the inset.

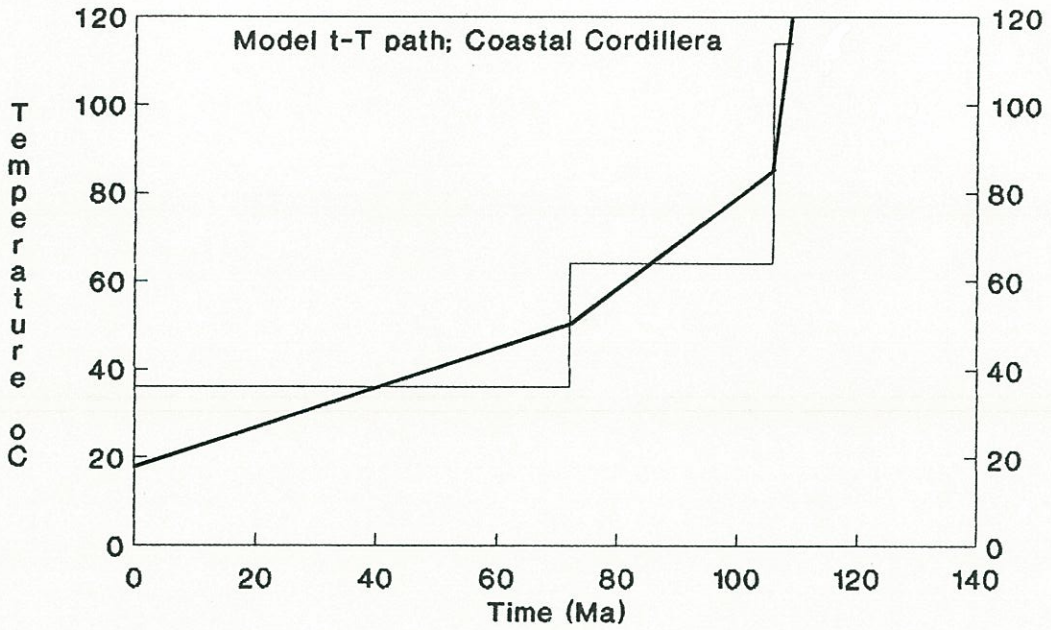


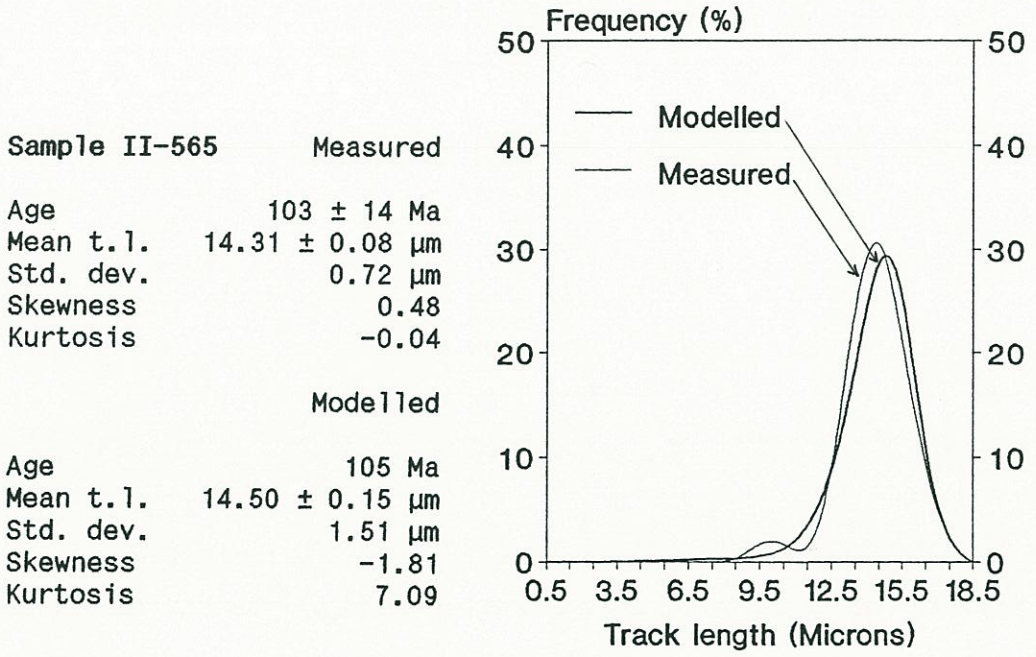


| Sample II-565 | Measured |
|---|---|
| Age | 103 ± 14 Ma |
| Mean t.l. | 14.31 ± 0.08 µm |
| Std. dev. | 0.72 µm |
| Skewness | 0.48 |
| Kurtosis | -0.04 |
| | Modelled |
| Age | 105 Ma |
| Mean t.l. | 14.50 ± 0.15 µm |
| Std. dev. | 1.51 µm |
| Skewness | -1.81 |
| Kurtosis | 7.09 |

**Figure 5.35.** Model t-T path for the sample II-565 (h = 1,500 m) from the Coastal Cordillera. Step history calculated by AFTAMTTP program. Solid line is the inferred t-T path. Model track length distribution generated by CALCTLD, and measured one are shown in the inset.

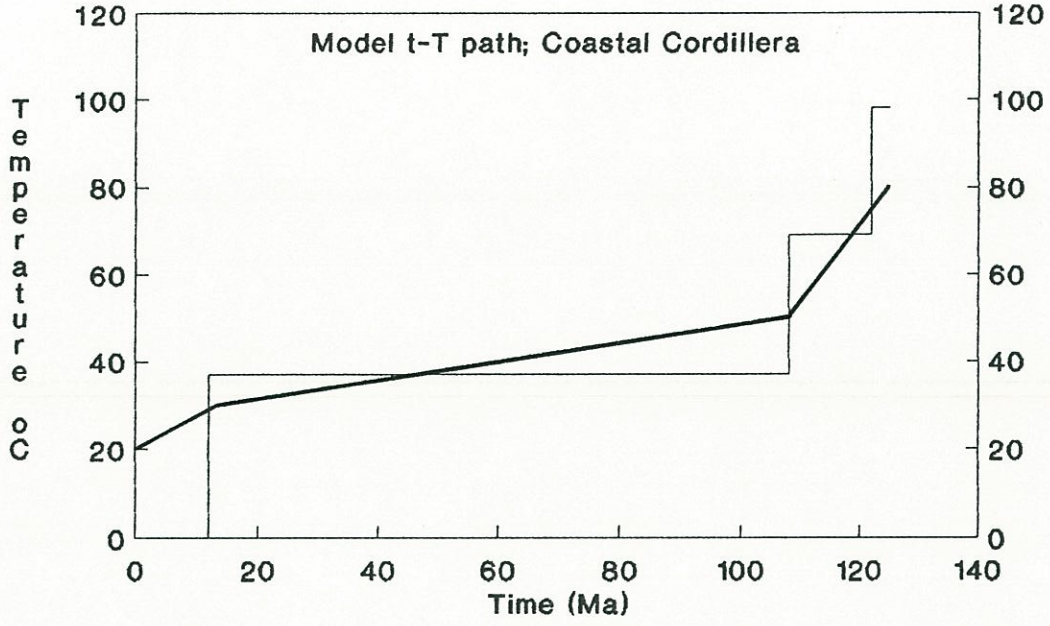


| Sample II-571 | Measured |
|---|---|
| Age | 122 ± 12 Ma |
| Mean t.l. | 14.53 ± 0.12 µm |
| Std. dev. | 1.16 µm |
| Skewness | 1.17 |
| Kurtosis | -1.48 |
| | Modelled |
| Age | 123 Ma |
| Mean t.l. | 14.74 ± 0.10 µm |
| Std. dev. | 0.96 µm |
| Skewness | -0.17 |
| Kurtosis | 0.11 |

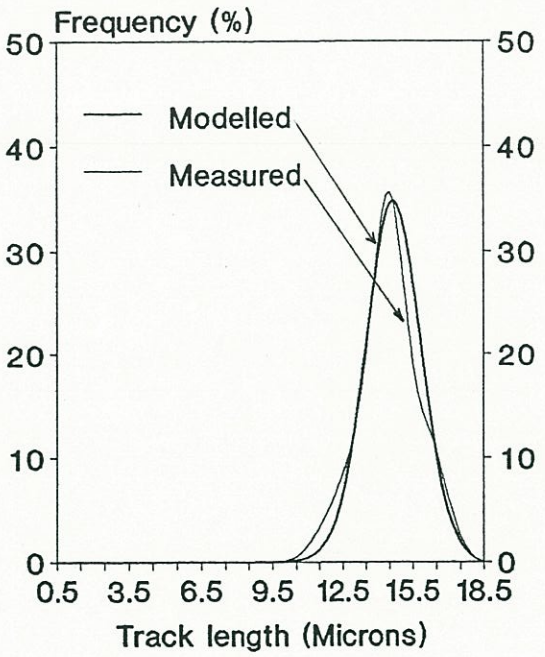


Figure 5.36. Model t-T path for the sample II-571 (h = 550 m) from the Coastal Cordillera. Step history calculated by AFTAMTTP program. Solid line is the inferred t-T path. Model track length distribution generated by CALCTLD, and measured one are shown in the inset.

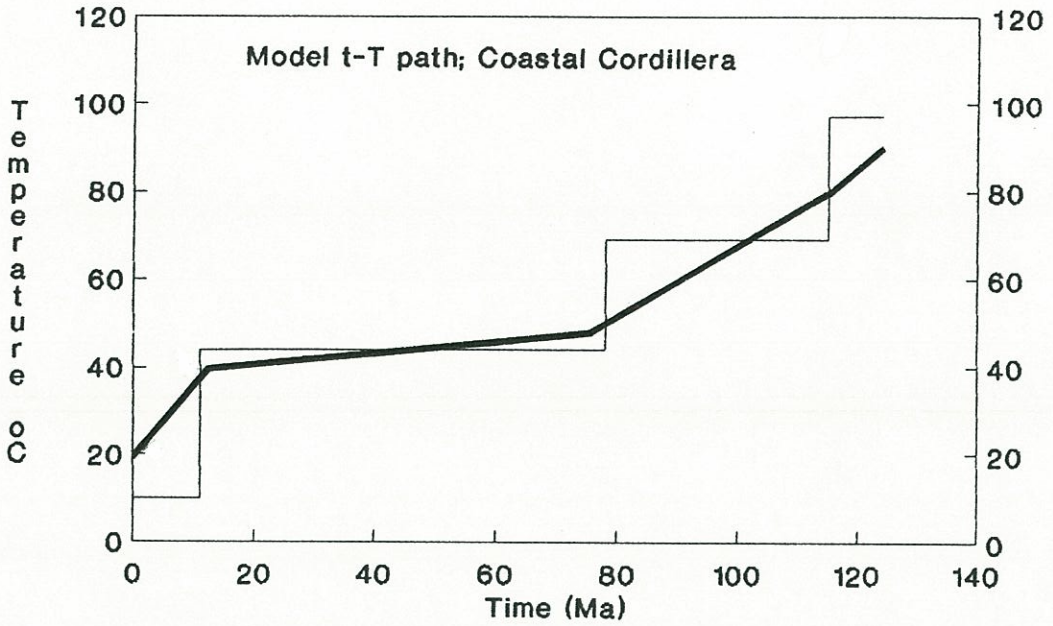


| Sample II-558 | Measured |
|---|---|
| Age | 115 ± 14 Ma |
| Mean t.l. | 13.93 ± 0.10 µm |
| Std. dev. | 1.01 µm |
| Skewness | 1.21 |
| Kurtosis | -1.25 |
| | Modelled |
| Age | 117 Ma |
| Mean t.l. | 14.16 ± 0.13 µm |
| Std. dev. | 1.27 µm |
| Skewness | -0.56 |
| Kurtosis | 0.37 |

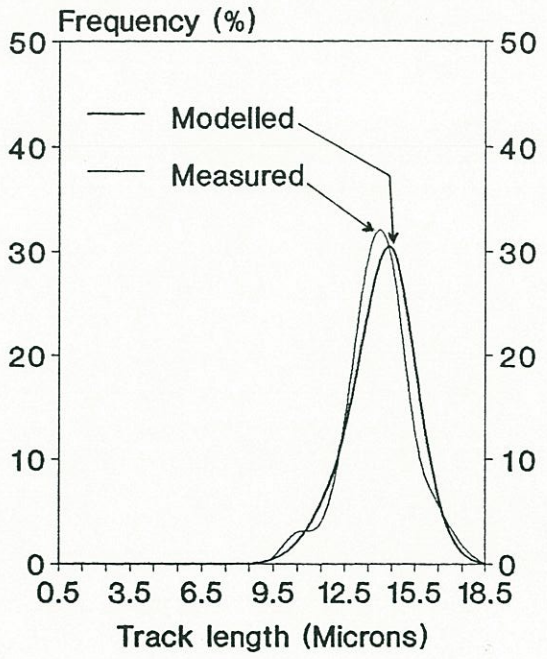


**Figure 5.37.** Model t-T path for the sample II-558 (h = 150 m) from the Coastal Cordillera. Step history calculated by AFTAMTTP program. Solid line is the inferred t-T path. Model track length distribution generated by CALCTLD, and measured one are shown in the inset.

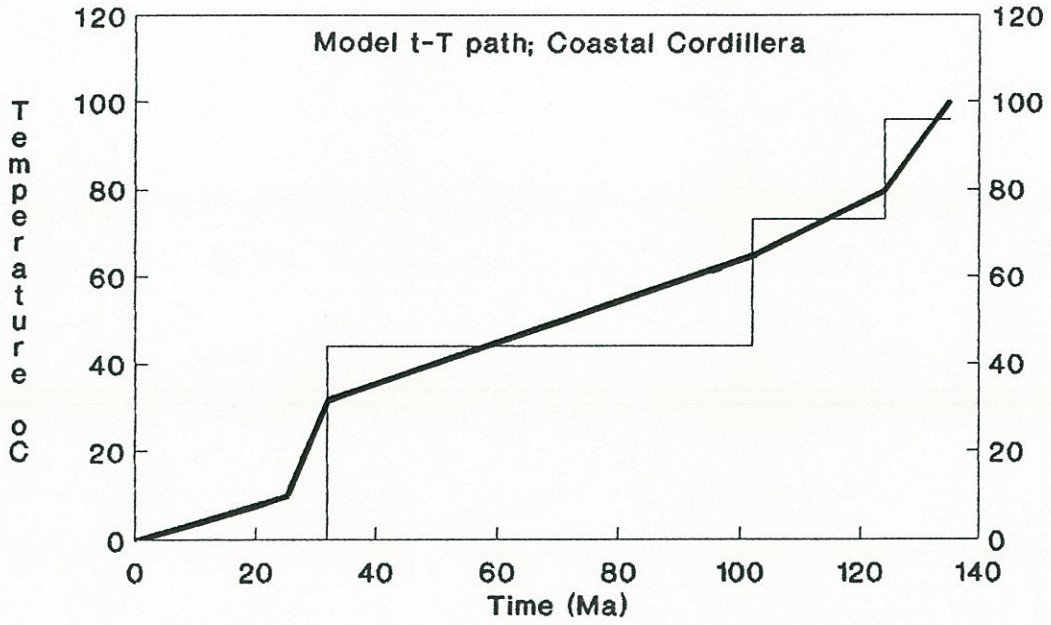


| Sample II-536 | Measured |
|---|---|
| Age | 129 ± 13 Ma |
| Mean t.l. | 14.27 ± 0.14 µm |
| Std. dev. | 1.36 µm |
| Skewness | -1.41 |
| Kurtosis | -0.41 |
| | Modelled |
| Age | 130 Ma |
| Mean t.l. | 14.41 ± 0.15 µm |
| Std. dev. | 1.51 µm |
| Skewness | -0.50 |
| Kurtosis | 0.08 |

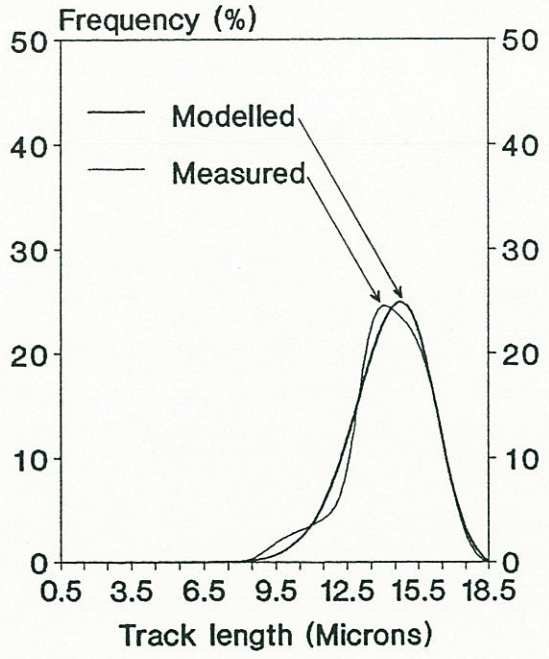


Figure 5.38. Model t-T path for the sample II-536 (h = 20 m) from the Coastal Cordillera. Step history calculated by AFTAMTTP program. Solid line is the inferred t-T path. Model track length distribution generated by CALCTLD, and measured one are shown in the inset.

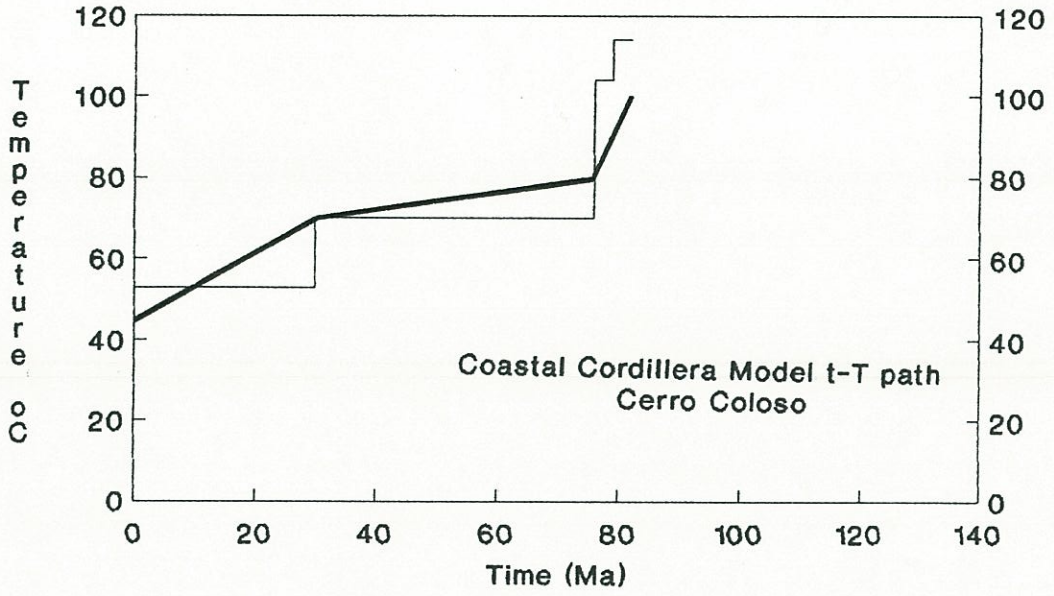


| Sample II-483 | Measured |
|---|---|
| Age | 70.9 ± 5.8 Ma |
| Mean t.l. | 13.05 ± 0.08 µm |
| Std. dev. | 0.81 µm |
| Skewness | 1.02 |
| Kurtosis | -0.73 |
| | Modelled |
| Age | 71.9 Ma |
| Mean t.l. | 13.12 ± 0.13 µm |
| Std. dev. | 1.32 µm |
| Skewness | 0.04 |
| Kurtosis | -0.34 |

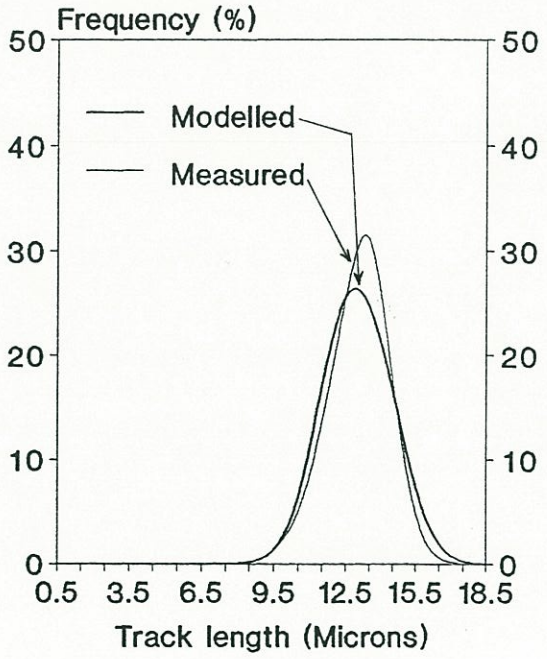


Figure 5.39. Model t-T path for the sample II-483 (h = 100 m) from the Coastal Cordillera. Step history calculated by AFTAMTTP program. Solid line is the inferred t-T path. Model track length distribution generated by CALCTLD, and measured one are shown in the inset.

silver veins of this district, and corroborates the interpretation that the remarkable preservation of the Late Cretaceous epithermal silver mineralization is the result of limited extent of denudation since the Late Cretaceous.

### 5.4.5 Coastal Cordillera Mesozoic Rocks

The model t-T patterns for apatites from Jurassic plutons of the Coastal Cordillera (Figs. 5.35, 5.36, 5.37, 5.38) show essentially rapid cooling by the end of the Early Cretaceous, and a subsequent near-surface residence since that time. This is consistent with the limited extent of erosion of this crustal block as concluded in Section 5.2.5. The model t-T path determined for sample II-483, which has shorter mean track lengths, is consistent with the position of this sample at higher temperatures (depths), and cooling in the Late Cretaceous below the closure temperature of apatite for fission tracks. Although a single sample does not warrant any conclusion, Late Cretaceous uplift-erosion of the Coastal Cordillera is likely since during that period the erosion of the Coastal and Intermediate depression areas provided volcanic materials that form the bulk sedimentary deposits of the eastern Late Cretaceous Purilactis Basin (see Chapter 2).

## 5.5 DISCUSSION

Model t-T paths based on apatite fission track ages and track length distributions provide a means to get insight on the cooling history of samples at temperatures between about 120° and 20°C, with a precision of about ± 10°C. The model t-T paths obtained in this study are consistent with thermal histories that can be inferred from geological grounds, and therefore may be regarded as relatively accurate estimates of the low temperature history of the samples.

No apatite fission track ages younger than Eocene were obtained in this study, despite obvious uplift of crustal blocks at that time related to major reverse faults (see Section 2.17). Most of the model t-T paths show relatively flat post-Eocene segments consistent with limited denudation. Thus, the fission track data support the suggested limited post-Eocene denudation in the region that Mortimer (1980) inferred on geomorphological grounds.

Apatite fission track data provide only estimates of paleotemperatures below ca. 120°C but depths may be estimated assuming a paleogeothermal gradient and that no other heat source is involved.

## 5.6 CONCLUSIONS

This study provides the first thermochronological investigation using apatite fission track dating on the western flank of the Central Andes. Forty-eight new apatite fission track ages and 25 samples studied for etchable track-length distributions complement the $^{40}Ar$-$^{39}Ar$ and K/Ar data and provide a detailed thermal history below ca. 120°C for rocks of the region. Apatite fission track data from basement rocks of the Domeyko Cordillera are compatible with rapid cooling during Mid-Late Eocene times (45-40 Ma), which may be related to the erosion and uplift of this crustal block during the Incaic tectonic event (see Section 2.17). The major porphyry copper deposits of the Andean segment between 21° and 26° S are related to the emplacement of Upper Eocene - Lower Oligocene epizonal porphyritic stocks (see Chapter 7). Thus apatite fission track data are compatible with porphyry copper mineralization following important Mid-Late Eocene uplift of the Domeyko Cordillera crustal block in the high Andes. The fission track data are also consistent with the shallow emplacement of these copper-bearing porphyries. Thus the thermochronological data support the hypothesis of a genetic relationship between the anomalous copper concentration and crustal thickening in the studied Andean segment.

The apatite fission track data are consistent with an overall paucity of post-Eocene erosion in the study area. The fission track data from the Intermediate Depression indicate limited denudation since the Late Cretaceous (less than 2,000 - 3,000 m assuming a 30°C/km geothermal gradient). The data from the Coastal Cordillera also are compatible with similar limited erosion but since the Early Cretaceous.

Apatite fission track thermochronology corroborates the control exerted by tectonic processes from the Late Cretaceous to the present in this entire Andean segment; while the erosion has been largely unable to keep pace with growth of topography (Mortimer and Saric, 1975; Mortimer, 1980; Abele, 1988, 1989).

# CHAPTER 6. METALLOGENY

This chapter summarizes the most significant relationships between metallic mineralization of the Antofagasta Region and its geological evolution. Previous interpretations, and the fundamental processes that determine the metallogenic characteristics of active continental margins are reviewed first. Finally the conclusions that arise from the present study of the regional metallogeny of the Antofagasta segment of the Andes are presented.

## 6.1 PREVIOUS STUDIES

The first comprehensive metallogenic studies of the Chilean Andes were published in the mid-sixties (Ruiz and others, 1965; Stoll, 1964, 1965). The metallogenic interpretations of these early investigations were strongly influenced by the deterministic "geotectonic cycle" and geosynclinal evolution theory. Thus they placed metallic mineralization processes within phases of classic geotectonic cycles rather than analyzing their primary origin.

Ruiz and Ericksen (1962) advanced one of the first analyses of the distribution and type of metallic mineralization in Chile. They recognized six metallogenic provinces: Copper, Gold, Iron, Lead-zinc-copper, Silver, and Manganese. These mostly mono-metallic provinces overlap one another, and contain "poly-paragenetic" deposits. The cited authors proposed a genetic-paragenetic classification of the metallic deposits, but did not address the question of age of mineralization.

A subsequent study of the Chilean metallogeny by Ruiz and others (1965) showed a rather different approach defining an "Andean Geosyncline Metallogenic Province" that includes poly-paragenetic deposits of various metals and several sub-provinces, belts, or alignments of mono-paragenetic metallic deposits. Ruiz and others (1965) ascribed ages to the main metallic mineralization of the Chilean Andes, relating mineralizing events to periods in the evolution of the "Andean Geosyncline." They recognized the minor importance of Paleozoic and pre-Paleozoic mineralization in the Chilean Andes, and correctly ascribed to the Jurassic the stratabound copper deposits and copper veins of the Coastal Cordillera of the Antofagasta Region. However, the Late Cretaceous age attributed to the gold and silver veins of the same region, and the Early Tertiary age imputed to the major porphyry copper deposits of northern Chile, were equivocal. The major porphyry copper deposits were regarded as Early Tertiary because the evolution of the "Andean Geosyncline" was thought to have ended with an Early Tertiary tectonism and intrusive phase. They stated: "the metallogenic cycle of the Andean Geosyncline came to a close with the mineralization formed during the Early Tertiary intrusive phase."

Stoll (1964; 1965) analyzed the distribution of Andean mineral deposits and identified several metallogenic belts including a "Chilean Copper Belt" dominated by copper, but containing also deposits of iron, gold, silver, and other metals. This belt was thus poly-paragenetic and polymetallic, and comparable to the Andean Geosyncline Metallogenic Province of Ruiz and others (1965). The formation of the Chilean Copper Belt was ascribed by Stoll (*op. cit.*) to the second and third phases in the evolution of the "Andean Geosynclinal Cycle" (which was ideally separated into five periods), suggesting a general Jurassic to Eocene age range for the mineralization but stressing a "Laramide" age (Late Cretaceous to Eocene) for the main mineralization of the Chilean Andes.

Petersen (1970) reviewed the regional distribution of South American ore deposits, but although his paper is entitled "Metallogenic Provinces of South America," he did not define metallogenic

provinces, nor address the issue of mineralization ages. His major contribution was to describe a regional mineral zonation of ore deposits into longitudinal belts, which came to be considered typical of the Central Andes. These belts, from the coast inland, are: Iron, Copper, Lead-zinc, and Tin. The longitudinal discontinuity of these belts along the Andes was attributed to different erosion levels exposed within distinct sections of this mountain chain, whereas the fundamental control determining the type of mineralization was attributed to crustal processes. Petersen (1970) speculated that the metallic content of mineralizing fluids was determined by the amount of metals as trace elements within the host rocks of the ore deposits.

Plate tectonics stimulated the search for new explanations of the Andean metal zonation described by Petersen (1970). One metallogenic model that became popular, due to its inherent simplicity, was the "**geostill concept.**" This model envisages (a) selective extraction of metals from seawater-saturated oceanic crust by partial melting under conditions of increasing pressure and temperature during descent of oceanic lithosphere along a Benioff zone, (b) upward transport of the metals in fluid and gaseous phases, (c) addition of other metals during flow through overlying mantle and continental lithosphere, and (d) concentration of the metals as deposits in volcanic island arcs and mountain chains by primary processes at the time of solidification of the volcanic rocks and by secondary processes following their solidification (Sawkins, 1972, Sillitoe, 1972b, Guild, 1972; Field and Dasch, 1981). According to this idea, the zoning of metallic deposits relative to the plate margin (Fe, Cu, Pb-Zn, Sn) described by Petersen (1970) is the result of liberation of specific metals at different depths during the subduction of oceanic lithosphere under the continental edge. The same general concept was used by the metallogenic models of Mitchell and Garson (1972) and Oyarzun and Frutos (1974), but they attributed the regional mineral zonation to the release, at different depths in the subduction zone, of halogen elements (Cl, F) or sulphur respectively. Thus these models are variations of the basic geostill concept.

Subsequent studies (Clark and others, 1970; Clark and Zentilli, 1972; Quirt, 1972) showed that the metallic ore deposits that define the regional mineral zonation in the Central Andes are diachronous, that the zoning of metallic deposits described by Petersen (1970) in the Andes of southern Peru is not observed in other Andean sections, and that this difference cannot be attributed solely to differential erosion (e.g., Clark and others, 1976). Advances in the petrological knowledge that point to asthenospheric mantle as the main source of magmas at subduction zones (e.g., Pearce, 1983) and physico-chemical considerations about the role of fluids under magmatic conditions (Burnham, 1979; 1981) show that the geostill concept is not a valid metallogenic model for the Central Andes. It is apparent that the geostill concept is an over-simplification of complex metallogenic processes.

Zentilli (1974; 1975), in a comprehensive regional metallogenic study of the Atacama Region (26°-29° S), showed the distribution of the mineral deposits into longitudinal belts, whose age decreases eastward from the coast. These belts were called "metallogenetic sub-provinces" and, citing K-Ar dates, a chronology was ascribed to them. These sub-provinces get younger from west to east:

(1) The Jurassic Metallogenetic Sub-Province encompasses copper-bearing veins hosted by plutons and copper stratabound deposits hosted by volcanic rocks.

(2) The Cretaceous Metallogenetic Sub-Province contains vein deposits of copper, iron, apatite, gold, silver, and manganese, as well as copper-bearing skarns, major irregular iron deposits, and manganese, copper, silver and iron stratabound deposits.

(3) The Paleocene Metallogenetic Sub-Province encompasses vein deposits of gold, silver, and copper and copper-bearing tourmaline breccia pipes.

(4) The Late Eocene - Early Oligocene Metallogenetic Sub-Province includes the major porphyry copper deposits.

(5) Neogene Metallogenetic Sub-Province and Centres contain gold-silver-copper epithermal deposits and solfataric native sulphur deposits.

Zentilli (1974) stressed the importance of supergene enrichment processes, which were ascribed to an Eocene-Oligocene "supergene metallogenetic epoch." He also showed that the Atacama Region is characterized by recurrent copper specialization, and that the zoning of economic metallic deposits relative to the plate margin, as described by Petersen (1970), and stressed by various authors, is poorly represented. He further noted that the recurrence of copper mineralization cannot be satisfactorily explained by the erosion level or by selective distillation from the subducted oceanic plate. Thus the mineral zonation into longitudinal metallogenetic belts was regarded as the result of the magmatic, tectonic, and geomorphologic evolution of the region. These were characterized by a sequence of longitudinal magmatic fronts related to the subduction of oceanic crust under the South American continental border. The magmatic front and associated mineralization systematically migrated eastward from the beginning of the Mesozoic to the Pliocene. These conclusions are consistent with those derived from the present study of the Antofagasta Region located immediately north of the area studied by Zentilli (*op. cit.*).

Ericksen (1975, 1976) defined an "**Andean Metallogenic Province**" encompassing all the Andes and was divided into five longitudinal sub-provinces of Iron, Copper, Polymetallic Base Metals, Tin, and Gold. The regional distribution of these sub-provinces roughly coincides with the mineral zonation of Petersen (1970). The Chilean Andes were included within the **copper sub-province**, except for a section of the Coastal Cordillera of northern Chile, which was incorporated into the iron sub-province. Ericksen stressed the spatial and genetic relationship of the metallic deposits to plutons, subvolcanic intrusions, and calc-alkaline volcanic rocks. The position and chronological distribution of the igneous rocks were taken to indicate the persistence of a subduction zone, at least since the Triassic. He proposes that the eastward decrease in age of igneous rocks and metallic deposits may be due to either the slow eastward migration of the subduction zone, the progressive deepening of the zone of magma generation, the decrease of the angle of subduction, or to a combination of these phenomena.

Sillitoe (1976) recognized five "metallogenic belts" in the Central Andes (from west to east): Fe, Cu-(Mo-Au), Cu-Pb-Zn-Ag, Cu-Fe, and Sn-(W-Ag-Bi). He indicated that these longitudinal metallogenic belts terminate or change in characteristics at transverse tectonic boundaries described by Sillitoe (1974). Northern Chile was included by Sillitoe (1976) within the Cu-(Mo-Au) metallogenic belt, except for a section of the Coastal Cordillera between the latitudes of 26° and 30° S, which was included within the Fe metallogenic belt. The distribution of the ore deposits within longitudinal belts was attributed to the progressive increase of the depth of metal release within a "stable," low angle subduction zone.

Oyarzun (1985), in an extended review of the Andean geology and metallogeny, identified four "metallogenic provinces," these are: (Fe (P), Cu (Mo-Cu), Cu-Pb-Zn-Ag, and Sn (W-Ag-Bi)). These are essentially the same as those that Sillitoe (1976) called metallogenic belts. Oyarzun (*op. cit.*) stressed the direct relationship that exists between the Andean mineralization and subduction-related calc-alkaline magmatism. He attributed the transverse mineral zonation to a hypothetical distinct oxidation conditions ($fO_2$) of magmas generated at different distances from the oceanic trench. Thus he conjectured that there is a regional distribution of "anionic" elements (S, Cl, F), or complexes, which ultimately determine the type of associated metals. He author also envisaged a role for the paleogeographic evolution, particularly for explaining the Pb, Zn, and Ag mineralization. This together with recycling of igneous materials accounted for a theoretical metallogenic "maturation" of the Andes, a phenomena that would have culminated in the Tertiary. The metallogenic maturation is seen as the superimposition of multiple stages of concentration or reconcentration of metallic elements within the crust as proposed by Routhier (1980).

Frutos and Pincheira (1985), in a special publication about Chilean geology and mineral deposits, maintain that Andean

metallogeny was controlled by the "relative emplacement of the geosynclinal trough and its associated magmatic activity." They related copper mineralization to "eugeosynclinal facies" and polymetallic ores to "miogeosynclinal environments." These ideas, still strongly influenced by geosynclinal theory, cannot be considered valid in the light of the present geological knowledge of the Andes. In addition, these authors claim that there are two types of mineral zoning in the Andes: one transverse resulting from "the degree of evolution of the chain, the crustal thickness, and the depth of magma generation" and the other longitudinal reflecting "the degree of geological evolution of the orogen and the (metallogenic) heritage of each section."

Ruiz and Peebles (1988), in a description of the main Chilean mineral deposits, maintain the division of metallogenic provinces of Ruiz and others (1965), and include northern Chile within the "Andean Geosyncline Metallogenic Province." This is not appropriate considering present-day geotectonic ideas.

This review of previous metallogenic studies of the Andes of northern Chile shows that different authors used very dissimilar criteria to define basic spatial and temporal metallogenic units. Consequently, metallogenic epochs and provinces defined in various studies are usually not comparable. A general evolution from metallogenic models relating metallic mineralization to phases of orogenic cycles of a geosyncline, towards models that consider Andean mineralization to be genetically related to magmatism associated with subduction of oceanic lithosphere under the active plate edge of South America, is apparent. The latter concept is consistent with the data presented in this thesis and is used in the following discussion of the metallogeny of the Antofagasta Region.

## 6.2 FUNDAMENTAL PROCESSES THAT DETERMINE THE METALLOGENY OF ACTIVE CONTINENTAL MARGINS: A REVIEW

Mineralization in regions of plate convergence is typically of the hydrothermal type, and is associated, spatially and temporally, with calc-alkaline intrusive or extrusive igneous activity. There are a series of physical and chemical processes that determine the relationship between igneous rocks generated at convergent plate margins and hydrothermal mineralization. They operate in near-surface environments and at deeper levels in the zone of magma generation. There is a continuum between **orthomagmatic processes**, which involve silicate melts, and **hydrothermal processes** that involve aqueous fluids and solid phases (wallrocks and hydrothermal minerals) (Burnham and Ohmoto, 1980). Between these lies an ill-defined and poorly understood group of **transitional processes**, for which Burnham and Ohmoto (op. cit.) arbitrarily have set an upper limit at the stage where the operation of orthomagmatic processes leads to formation of a separate magmatic aqueous phase, and the lower limit at the $H_2O$-saturated solidus of the magma, i.e., the temperature, for a given pressure, below which hydrous silicate melt is not thermodynamically stable.

Many investigators, based on the petrochemistry and isotopic characteristics of igneous rocks agree that felsic magmas at active continental margins such as the Andes are chiefly derived from fractional crystallization of basaltic parent magmas generated by partial melting of the asthenospheric mantle (James and others, 1975; Dostal and others, 1977; Hawkesworth and others, 1979; Pearce, 1983; Harmon and others, 1984; Thorpe and others, 1984). Partial melting is thought to be induced by the flux of fluids into asthenospheric rocks at high pressures and temperatures from dehydration of the underlying oceanic lithosphere during subduction.

A distinct characteristic of granitoid magmas generated at subduction zones is that they contain several per cent "water" from

early stages of their development (Burnham and Ohmoto, 1980; Burnham, 1981; Ishihara, 1985; Whitney, 1988). Water greatly increases the solubility of metal compounds in melts relative to water-free magmas of the same composition. Burnham (1981) stressed that this may be the primary reason that many metal deposits are associated with granitoids in orogenic belts formed at convergent margins.

Burnham (1979, 1981, 1981a) showed that the water content of felsic magmas is critical to their capacity for generating hydrothermal metallic deposits. Magmas that contain less than about 2 wt% $H_2O$ are relatively inefficient at concentrating of metals and sulphur from their source rocks, and at exsolving a fluid phase producing significant hydrothermal processes at the place of emplacement. On the other hand, magmas with more than about 3-4 wt% $H_2O$ in the mantle, or 6 wt% $H_2O$ in the lower crust, are incapable of reaching the near-surface environment before crystallizing completely. Consequently the optimum range of initial water content of felsic magmas, in order to generate **major** hydrothermal deposits, is rather restricted. This may be the main reason that **major** metallic deposits are anomalous features, despite the common association of metal deposits with granitoids in orogenic belts formed at convergent margins (Burnham, 1981).

Some authors (Hollister, 1978; Titley, 1981) have suggested that major faults in the basement, activated by uplift, are important for mineralization in order to allow the necessary rapid access for porphyry magmas to shallow crustal levels. Magma ascent, however, is a complex, poorly-understood process, not necessarily dependent on the existence of brittle fractures in the crust (see section 7.3).

The formation of mineral deposits by hydrothermal fluids of magmatic parentage requires the separation of a fluid phase from the magma. Water solubility in magmas is only weakly temperature-dependent and very strongly regulated by pressure, decreasing rapidly at pressures below 3 kb (Burnham, 1979; Burnham and Ohmoto, 1980). Thus the release of fluids of magmatic parentage, and the development of hydrothermal

processes conducive to the formation of economic ore deposits is more likely to occur within the uppermost 10 km of the crust (Burnham, 1979). In addition, the amount of volatiles in the magma also determines the physical processes that occur during crystallization at near-surface environment. The volume change and the energy released during retrograde boiling produce different degrees of rock fracturing aiding in the development of hydrothermal circulation and mineralization (Burnham, 1979, 1985; Burnham and Ohmoto, 1980).

Copper and molybdenum are metals that are typically associated with calc-alkaline magmas generated at subduction zones. These chalcophile elements are trace constituents of the rocks, and therefore must be highly concentrated to form economic ore deposits. The concentration is achieved only when the metals and sulphur are favourably partitioned in a fluid phase, instead of the silicate melt phase of the magma. The partitioning is determined by the physico-chemical conditions in the magma, and an important role is played by the oxygen fugacity (see below).

Meteoric water also takes part in hydrothermal systems associated with emplacement of igneous masses, as demonstrated by oxygen and hydrogen isotopic studies. The role of meteoric water is particularly important in the formation of epithermal silver and gold deposits (e.g., Taylor, 1979). Sheppard and Gustafson (1976) show that hydrothermal biotites from El Salvador porphyry copper deposits appear to have formed from $H_2O$ with oxygen and hydrogen isotopic composition that coincides with the hypothetical field of primary magmatic waters, whereas clay minerals and sericite appear to have been formed from heated meteoric waters. Similar conclusions have been reached by Taylor (1979) for North American porphyry copper deposits. Thus main mineralization stages of porphyry copper systems appear to be dominated by magmatic fluids, while the participation of meteoric water is prominent at late stages.

One school of thought maintains that the formation of ore deposits requires source rocks anomalously enriched in certain metals

and/or poly-cyclic concentration of metals in the crust (e.g., Routhier, 1980; Oyarzun, 1985b). However, Krauskopf (1979), Burnham (1981), and Cline and Bodnar (1989) showed that major metallic deposits can be formed from igneous rocks with normal content of metals as trace elements. Thus hypothetical anomalous metallic concentrations at the source of magmas or within the crust appear to be unimportant. The convincing arguments of Burnham (1979, 1981) and Gustafson (1979) further suggest that the capacity of magmas to concentrate metals and sulphur from their source rocks and transport these elements to epizonal levels of the crust is strongly conditioned by their initial fluid contents, particularly a restricted optimum range of $H_2O$ content (see above).

The metals associated with igneous rocks at near-surface or surficial levels in the crust may be determined by the nature of the magma source. For example, the content of base and precious metals is generally higher in mafic rocks so that their partial melting may produce magmas enriched in these elements, whereas felsic metasedimentary rocks may tend to form magmas enriched in Sn, alkaline metals, Be, Ta, Nb, and rare earth elements (Ishihara, 1985). Nevertheless, distinctive groups of metals are associated with granitoids according to the oxygen fugacity of the magma during its solidification. Ishihara (1980, 1981, 1985) has stressed that an oxidized magma (magnetite-series; high magnetic susceptibility) seems to have higher capacity to dissolve and transport Cu, Mo, Pb, Zn, Ag, Au, and S occurring mainly as sulfides. As mentioned above the content of these metals is normally higher in mafic rocks, which constitute the source of the magnetite-series magmas. In contrast a reduced magma (ilmenite-series; low magnetic susceptibility) has commonly associated Sn, W, Be, Nb, Ta, and Th mainly as oxides.

According to Burnham (1979) and Ishihara (1985) the oxygen fugacity ($fO_2$) regulates the partitioning of dissolved sulphur in a melt-aqueous solution system. Sulphur is dissolved in water-bearing melts bonded in the silica tetrahedron as bisulfide ion ($SH^-$), and is present as $H_2S$ or $SO_2$ in aqueous solution (Burnham, 1979; Burnham and Ohmoto, 1980). As $SO_2$ is much less soluble than $H_2S$ in magmas, if the

oxygen fugacity rises (at a given pressure) then the amount of $SO_2$ increases relative to $H_2S$. Thus the $SO_2/H_2S$ ratio increases, and the partition coefficient for sulphur ($\Sigma S^{VI}/\Sigma S^{-II}$) rises. An opposite effect results from an increase in the fugacity of $H_2O$ ($fH_2O$, hence $fH_2$), but a water dissociation and preferential diffusive loss of hydrogen from the system is likely to occur, the result may be a net increase of $fO_2$ in the magma. In addition, Burnham and Ohmoto (1980) suggested that $fO_2$ in granitoid magmas produced from non-carbon-containing igneous rocks is higher than the quartz-fayalite-magnetite (QFM) buffer (Carmichael and others, 1974) and that $fSO_2/fH_2S$ for aqueous solutions in equilibrium with such a magma is 0.1-10 with an average of almost 1. In contrast, in magmas generated from sedimentary rocks containing carbon, because $fO_2$ is lower than the QFM buffer and $fCO_2/fCH_4$ is close to unity (Ohmoto and Kerrick, 1977), $fSO_2/fH_2S$ is probably less than 0.01 (one to two order of magnitude lower than in carbon-free rocks). Consequently, sulphur is strongly fractionated in the aqueous phase and has probably greater tendency to form sulfide deposits after separating from magmas with high $fO_2$ (magnetite-series magmas; Ishihara, 1977, 1980) rather than from magmas with low $fO_2$ (ilmenite-series), where a great proportion of the sulphur is partitioned toward the silicate melt increasing the tendency of the fluid phases to form oxide deposits of non-chalcophile metals. Thus $fO_2$ is strongly dependent on the carbon content of the magma. Furthermore, Ishihara and Sasaki (1989) have suggested that the assimilation of sedimentary wall rocks at the site of magma emplacement may result in the introduction of organic carbon to the magmatic system, thereby significantly decreasing $fO_2$. Thus a magnetite-series magma may be transformed to give rise to an ilmenite-series granitoid. According to this idea, contamination with organic carbon may also define the associated metallic mineralization.

Magnetite-series magmas (Ishihara, 1977, 1980) are commonly associated with large-scale tectonic processes such as subduction because this setting provides favourable conditions for vast zonal melting or partial fusion of mafic material at depth.

The metals associated with magnetite-series granitoids, may be dissolved in magmas as sulfides, but it is thought that they occur mostly as chloride complexes. The volatile element, chlorine, is dissolved in melts mainly as chloride ion ($Cl^-$) and is highly concentrated in aqueous solutions exsolved from magmas (Klinic and Burnham, 1972; Candela and Holland, 1986; Cline and Bodnar, 1989). This is because chloride minerals are not stable in magmas of intermediate to felsic compositions, and highly stable, neutral chloride complexes are formed with hydrogen, alkali metals, alkaline earths, and heavy metals in aqueous solutions at magmatic temperatures and low to moderate pressures (Burnham and Ohmoto, 1980). Fluorine also forms stable neutral fluoride complexes in magmatic fluids, but high solubilities of fluorine in silicate melts, coupled with high thermal stabilities of minerals such as fluorite, topaz, and micas cause fluorine to be partitioned largely towards the condensed phases. Therefore fluorine plays a secondary role in mineralizing processes. Carbon dioxide, dissolved sparingly in felsic melts as $CO_2$ and partitioned strongly toward the volatile phase, appears to play only a minor chemical role in transitional processes (Burnham and Ohmoto, 1980).

The fractional crystallization of magmas at crustal levels is commonly regarded as being of secondary importance for defining the character of the mineralization associated with igneous rocks. However, it is thought to be very important in higher-level intrusive bodies of metal sulfide-bearing magmas, where fractional crystallization concentrates the ore metals, sulphur, and chlorine in the more hydrous residual melt. Furthermore, the early crystallization of sodium-bearing hornblende in granodioritic magmas causes NaCl/KCl to decrease markedly; therefore the high ratio of potassium to sodium in aqueous chloride solutions coexisting with hornblende-bearing magmas may provide a possible explanation for the extensive potassium metasomatism (potassic alteration) that is characteristically associated even with potassium-poor dioritic porphyry copper deposits (Burnham and Ohmoto, 1980). In the study area plagioclase fractionation has played a significant role in the evolution of unmineralized calc-alkaline igneous rocks of the Antofagasta Region, but this fractionation is not apparent in the evolution of copper-bearing

porphyries with plagioclase phenocrysts (see Section 7.2.7). This suggests that plagioclase fractionation at depth is a negative factor for copper concentration in felsic magmas.

The final metallic concentrations as economic ore deposits are achieved by near-surface hydrothermal processes. The character of individual ore deposits may be modified by local conditions; i.e., the water-rock interaction at the site of ore deposition, wall rock composition, structure, geomorphology, etc.

## 6.3 METALLOGENY OF THE ANTOFAGASTA REGION

Most of the rich metallic ore deposits of the Antofagasta Region are of hydrothermal type. They are genetically related to calc-alkaline plutonism and volcanism consistent with the geotectonic setting of the area on the active continental margin of South America.

### 6.3.1 Geologic considerations

The geologic data for the Antofagasta Region show that since the Late Carboniferous calc-alkaline plutonism and volcanism developed for extended periods along longitudinal magmatic fronts parallel to the continental margin. There are five major periods of magmatic activity established from new and compiled geochronological data: (a) Late Carboniferous to Early Triassic, (b) Jurassic to Early Cretaceous, (c) Late Cretaceous to Middle Eocene, (d) Late Eocene to Oligocene, and (e) Miocene to Holocene.

A plot of radiometric dates versus distance to the present-day axis of the oceanic trench (Fig. 6.1) shows that during each period the magmatic front was essentially stationary, but that the position of the front changed from one magmatic period to another. A

systematic eastward shift of the magmatic front since the Jurassic has occurred. This compares well to the post-Paleozoic migration of granitic foci described by Farrar and others (1970) in the Atacama Region immediately south of the study area, and by Rivano and others (1985) farther south in Central Chile. The eastward migration of the magmatic front attains its maximum extent inland, about 300 km, at the latitude of Antofagasta (23°S). Therefore in this region, unlike other sections of the Andes, post-Paleozoic magmatic arcs were developed in separate areas with limited or no overlap.

The eastward migration of the magmatic front in the study area does not appear to have been a continuous phenomenon. Instead stepwise shifts occurred following phases of crustal deformation (Fig. 6.1). These compressive deformative phases correlate with periods of increased convergence rate associated with major plate reorganization events and with reorientation of the spreading system in the East Pacific ocean (see Chapter 2).

The petrochemical and isotopic characteristics of igneous rocks of the Central Andes are consistent with derivation by fractional crystallization of basaltic parent magmas formed by partial melting of an asthenospheric mantle wedge containing components from subducted oceanic lithosphere (James and others, 1975; Dostal and others, 1977; Hawkesworth and others, 1979; Thorpe and others, 1984; Rogers and Hawkesworth, 1989). Thus I-type granitoids (classification of Chappel and White, 1974) or magnetite-series granitoids (*cf.* Ishihara, 1977, 1980; Ishihara and others, 1984) typically occur and are associated with Cu, Mo, Ag, Au, Fe, and S mineralization.

Removal by deep erosion may account for the absence of important deposits in pre-Mesozoic rocks. The overall erosion of the Antofagasta Region has been limited during the Tertiary. This is substantiated by the apatite fission-track data presented in this study (see Chapter 5). Denudation virtually ceased since the Middle Miocene

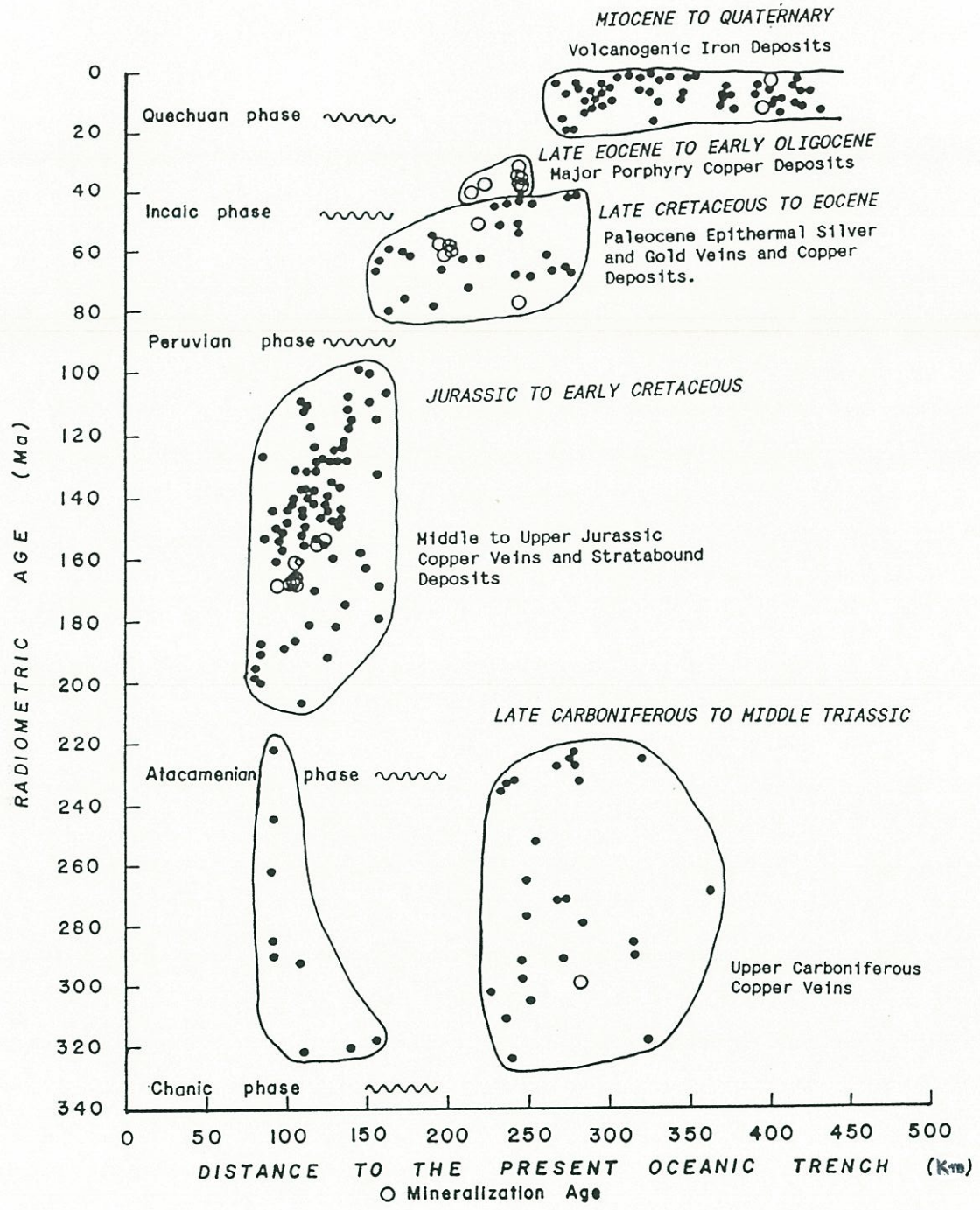


Figure 6.1. Radiometric dates of igneous rocks versus distance to the present oceanic trench. Igneous activity periods and position changes of the magmatic front are apparent, as well as the discrete periods of mineralization. Temporal position of deformative phases are also shown.

(see Chapter 2). Any metallic deposits formed in Neogene-Quaternary rocks have yet to be exposed due to this extremely low rate of erosion.

### 6.3.2 Metallogenic characteristics

Ore deposits of the Antofagasta Region are distributed within three longitudinal metallogenic belts of about 50 to 100 km in width, which coincide with the major physiographic units of the region: Coastal Cordillera, Domeyko Cordillera, and Main Andean Cordillera Metallogenic Belts. The major ore deposits were generated during three discrete metallogenic epochs: (I) Middle to Late Jurassic, (II) Paleocene, and (III) Late Eocene to Early Oligocene (Fig. 6.1). The eastward shift of the mineralizing centres since the Jurassic, following the migration of the magmatic front, is apparent but metallogenic epochs were distinctly shorter than the periods of active magmatism.

The regional mineral zonation in the Antofagasta segment of the Andes includes a Coastal Cordillera Metallogenic Belt dominated by copper; followed inland by the Domeyko Cordillera Metallogenic Belt that includes copper (-molybdenum), silver, and gold deposits; and the Main Andean Cordillera Metallogenic Belt with iron and sulphur deposits. Farther inland, in the Andes of Bolivia, a tin-tungsten-bismuth belt exists. This mineral distribution compares to the zonation described by Zentilli (1974) for the Atacama Region (26°-29° S) except that major iron deposits that occur in the Coastal Cordillera of the Atacama region are absent in Antofagasta. However, there are significant differences with the zonation (Fe, Pb-Zn, Cu, Sn) described by Petersen (1970) in the Andes of Peru.

Significant copper mineralization in the Antofagasta Region developed in the Jurassic, Paleocene, and Late Eocene to Early Oligocene metallogenic epochs related to intrusive or volcanic rocks. In addition, pre-Mesozoic copper deposits exist in the area, and covellite

occurrences in the sulphur deposits of the Pliocene Aucanquilcha volcano (Clark, 1970) suggest also a younger episode of copper concentration. The most important of these copper deposits are major porphyry copper deposits formed during the Late Eocene to Early Oligocene metallogenic epoch.

Supergene processes have produced important secondary enrichment within copper, silver, and gold deposits of the Antofagasta Region, following their exhumation in the early Tertiary. The virtual lack of erosion since the Middle Miocene contributed to the preservation of the enriched sections of the deposits that constitute the main source of the regional metallic mining production.

### 6.3.3 Discussion

The extended periods of active calc-alkaline magmatism in the Antofagasta Region are thought to reflect intervals of steady subduction under the South American continental margin. This is consistent with the characteristics of the igneous rocks, and also with the geochronological data that show that volcanism and plutonism developed synchronously.

Recent tectonic-structural studies of the Central Andes indicate that most of the crustal thickening, and consequent uplift is the result of a structural shortening. Only about 10% of the crustal volume can be ascribed to magmatic addition (see Section 2.17). Tectonic processes have resulted in the remarkable Puna or Altiplano continental high plateau, which is about 300 km in width, and is underlain by a crust up to 70 km thick (James, 1971b; Isacks, 1988; Götze and others, 1988). The amount of crustal shortening required for producing the continental high plateau is, by itself, probably sufficient to account for the 250-300 km total eastward relative advance of the subduction zone since the Jurassic. Thus it appears unnecessary to postulate either a hypothetical subduction erosion of the continental border (Rutland, 1971), the

variation of the subduction angle through time (Mitchell, 1973) or the progressively deeper generation of magmas within a stable subduction zone (Zentilli, 1974; Sillitoe, 1976).

The eastward shift of the magmatic front since the Jurassic appears to be the aftermath of major reorganization in plate interactions during which compressive stress was increased within the continental edge of South America and crustal shortening occurred. This is consistent with the stationary position of the magmatic front and its change of position following deformative phases that correlate with periods of increased convergence rates and major plate reorganizations. The westward shift of the magmatic front during the Triassic was also preceded by crustal movements (possibly extensional tectonics), but the subduction zone probably retreated relative to the continent. The exact reason is still unknown (see Chapter 2), but it produced major paleogeographic change that has been traditionally regarded as the beginning of the "Andean Geotectonic Cycle."

The occurrence of three discrete metallogenic epochs, distinctly shorter than that of the more extended periods of igneous activity, implies that the formation of major (economically significant) mineral deposits is limited to periods of geologic time when several unique geological conditions concur, which favour the anomalous concentration of metals in the crust. For example, variations of the convergence rates, subduction angle, crustal thickness, tectonic deformation, etc., may modify conditions of magma generation at convergent plate margins. These variations may affect the initial content of volatiles in the magma and may also determine its capacity to form metallic ore deposits at near-surface levels. Longitudinal variations in the nature of metallogenic belts in the Andes, therefore, may reflect past differences in plate interaction along the convergent margin and may account for the tectonic segmentation of the Andes described by Sillitoe (1974).

The recurrence of copper mineralization in the different magmatic arcs developed on the continental border suggests a

similar source for the magmas and metals. The copper specialization suggests a rather homogeneous source or the operation of a homogenizing mechanism involving contributions from more than one source. This does not support the idea of a metallogenic maturation as envisaged by Oyarzun (1985b) and Frutos and Pincheira (1985). These authors envisage the metallogenic evolution in the Chilean Andes as related to the progressive thickening of the crust with progressively more interaction of juvenile magmas with the crust, and/or involving recycling of igneous materials and associated mineralization. However, such increasing magma interaction with the crust is not warranted by the chemical and isotopic characteristics of the Mesozoic and Paleogene igneous rocks that host most of the economic mineral deposits in the Andes of northern Chile (e.g., Rogers and Hawkesworth, 1989; Miller and Harris, 1989).

The close relationship between the hydrothermal metallic mineralization of the Antofagasta Region and the igneous rocks, makes the latter a first-order **metallotect**. This term applies to any geologic feature (tectonic, lithologic, geochemical, etc.) considered to have influenced the concentration of elements to form mineral deposits. It implies ore control, but without the implication of economic value. In this context, the Jurassic igneous rocks of the Coastal Cordillera constitute a copper metallotect. The Paleocene igneous rocks of the Intermediate Depression and Domeyko Cordillera make a silver, gold and copper metallotect. The Late Eocene - Early Oligocene porphyritic intrusive rocks of the Domeyko Cordillera form an important copper and molybdenum metallotect. The Miocene to Holocene igneous rocks of the Main Andean Cordillera and the Altiplano comprise an iron and sulphur metallotect. Structural control is important at the scale of individual orebodies but is not apparent at a regional scale with the significant exception of the domain of the Domeyko Fault System along which the major porphyry copper deposits are located. Therefore this fault system also constitutes a copper and molybdenum regional metallotect.

### 6.3.2 Conclusions

Metallic mineral deposits of the Antofagasta Region were chiefly generated by hydrothermal processes associated with calc-alkaline magmatism along a longitudinal magmatic front that shifted its position following deformation phases. Copper, molybdenum, silver, gold, and iron were preferentially concentrated, mostly as sulfides. The dominance and recurrence of copper mineralization is apparent. Porphyry copper deposits with subordinate molybdenum are the most important metallogenic characteristic of the study area. Their metallogeny is examined in Chapter 7.

The metal assemblage associated with each position of the magmatic front and particular types of ore deposits appear to be controlled by the specific geologic, tectonic, and geomorphologic conditions under which calc-alkaline magmatism and associated hydrothermal processes operated. Major deposits were generated during discrete metallogenic epochs reflecting periods when particularly favourable conditions concurred to concentrate metallic elements in the upper levels of the crust. This coupled with the shifting position of the magmatic front account for the regional distribution of ore deposits.

Longitudinal variations in the nature of metallogenic belts in the Andes are related to the tectonic segmentation of this mountain belt. They are thought to reflect past differences in plate interactions along this convergent plate margin.

Limited erosion, due to prevalence of arid climate and morphologic factors, has allowed the development of important supergene enrichment processes in copper, silver, and gold deposits, as well as contributed to their preservation.

# CHAPTER 7. UPPER EOCENE - LOWER OLIGOCENE PORPHYRY COPPER DEPOSITS: IN SEARCH OF A GENETIC MODEL.

## 7.1 INTRODUCTION

The Upper Eocene - Lower Oligocene porphyry copper deposits of northern Chile are among the largest and highest grade porphyry copper deposits of the Andes. They are undoubtedly the outstanding metallogenic characteristic of the Antofagasta Region. This chapter examines the geologic, geochronological, thermochronological, petrochemical, and isotopic data that constrain the genesis of this group of porphyry copper deposits. A conceptual model for explaining the origin of this remarkable copper mineralization is advanced.

Porphyry type deposits are the principal source of copper in the Andes. They have largely contributed to the early recognition of this orogen as a metallogenic province dominated by copper (e.g., Ruiz and Ericksen, 1962; Stoll, 1965). Although porphyry copper deposits are distributed along the whole length of the Andean orogen (Petersen, 1977; Hollister, 1978; Sillitoe, 1981, 1988), economic deposits are restricted to three sections of the Andes: (1) The Paleocene - Lower Eocene deposits of southern Peru (Cerro Verde-Santa Rosa, Cuajone, Quellaveco, and Toquepala), (2) The Upper Eocene -Lower Oligocene deposits of northern Chile (Quebrada Blanca, Copaquire, El Abra, Chuquicamata, La Escondida, El Salvador, and Potrerillos), and (3) The Upper Miocene - Pliocene deposits of central Chile (Los Pelambres, Rio Blanco-Disputada, and El Teniente) (Fig. 7.1).

The conspicuous spatial association of porphyry copper deposits with Andean calc-alkaline igneous rocks led various authors to

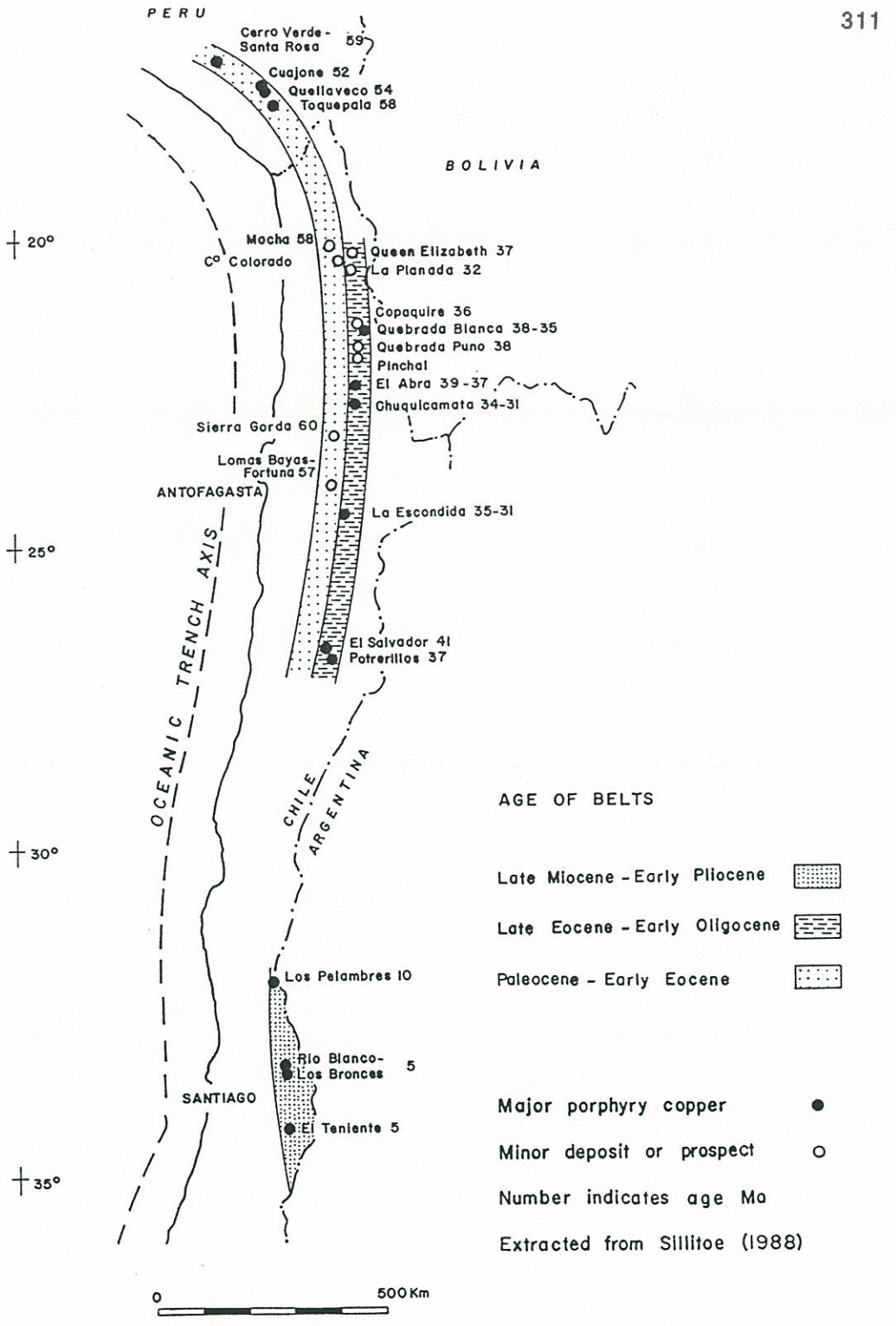


**Figure 7.1.** Distribution of the major (economic) porphyry copper deposits of the Central Andes (Extracted from Sillitoe, 1988; dates modified according to new data of the present study).

propose a genetic relationship with the long-lived, currently active, subduction zone over which the post-Paleozoic Andean orogen has developed (e.g., Sillitoe, 1972, 1981, 1988; Mitchell and Garson, 1972; Oyarzun and Frutos, 1974, 1980; Gustafson, 1979). Even though a genetic connection between porphyry copper deposits and calc-alkaline magmatism on the active South American plate margin seems certain, the specific mechanisms are still obscure. This section offers insight into the processes that contributed to the origin of a very important group of porphyry copper deposits of the Central Andes, the Upper Eocene - Lower Oligocene deposits of the Antofagasta Region.

### 7.1.1 Porphyry copper deposits: what are they?

The term porphyry copper has been in use since the early 1920's (Parsons, 1933; 1957), but no definition of porphyry copper has been universally accepted. Mining geologists prefer to emphasize that porphyry copper deposits are large, low-grade copper deposits, which are amenable to mass mining methods regardless of their genesis and host rock type (Guilbert and Park, 1986). The Glossary of Geology of the American Geological Institute (Gary and others, 1972) defines a porphyry copper as a low-grade disseminated copper deposit that is always in close association with a quartz-bearing igneous rock, but may be also in schist, silicated limestone, and volcanic rock. Copper-bearing minerals occur typically in disseminated grains and/or in veinlets through a large volume of rock. One distinctive feature that is missing from the above definition is the typical pervasive hydrothermal alteration associated with copper mineralization. The large size of the intrusive-related porphyry copper hydrothermal system is possibly their most impressive feature (e.g., McMillan and Panteleyev, 1980). Furthermore, Hunt (1977) defined porphyry copper deposits as "large crustal sulphur anomalies containing copper and other metals" and stressed that much of the sulphur in these deposits is in an oxidized state. The anomalous sulphur concentration has also been stressed by Gustafson (1979). Thus the most

distinctive feature of porphyry copper deposits is the close association of the hypogene sulfide copper mineralization with intrusive rocks, commonly porphyritic stocks, and pervasive hydrothermal alteration. However, the adjectives "large" and "low" used in these definitions are subjective, and therefore the general term porphyry copper applies to deposits ranging from tens of thousand tons of ore grading from 0.3 to 0.7% Cu, such as most of the Philippine porphyries (Sutulov, 1974; Gilmour, 1982; Sillitoe and Gappe, 1984), up to giant deposits of more than 3 billion tons of ore grading from 1.0 to 1.85 % Cu, such as the Chilean deposits of Chuquicamata and El Teniente (Ambrus, 1979; Gilmour, 1982). It becomes apparent on close inspection that porphyry copper deposits are a diverse suite of copper deposits whose common denominator is the close association with stocklike porphyritic intrusions and related hydrothermal alteration.

The major copper deposits of the Antofagasta Region fall into a "classic" porphyry copper deposit type defined by McMillan and Panteleyev (1980). These are associated with chiefly granodioritic stocks intruding unrelated host rocks, whereas co-magmatic volcanic piles, if they ever existed, are not preserved. The plutonic complexes are commonly characterized by successive, small (0.5 to 2 $km^2$), cylindrical porphyritic intrusions, and include numerous pre-, intra-, and post-mineralization porphyry dykes or stocks emplaced at shallow depth. Copper- and molybdenum-bearing minerals typically occur in disseminated grains, and/or in a network of veinlets throughout a large volume of rock (stockwork) indicating significant fracturing and volume increase of the igneous rock mass during mineralizing processes (e.g., Burnham, 1985). Pervasive hydrothermal alteration zones of the potassic, phyllic, propylitic, and argillic types in general form annular shells around intrusions similar to the model of Lowell and Guilbert (1970) but distortions due to local conditions or multiple intrusive pulses do occur (e.g., El Abra; Ambrus, 1977). The hypogene mineralization of chalcopyrite, bornite, pyrite, molybdenite, and locally enargite is chiefly associated with the potassic and phyllic alteration zones. The orebodies conform to irregular but roughly domal cappings, which are restricted to the apical section of the

intrusive bodies. The hypogene shape of the orebodies has been almost in all cases modified by supergene processes, therefore the richest copper ores commonly underlie partially leached, oxidized rocks forming irregular "blankets" containing supergene sulfides (chalcocite, djurleite, covellite and anilite) that replaced hypogene minerals. Chuquicamata shows several characteristics that deviate from the above general description, due to the strong influence of local factors (see below), but this giant copper deposit may certainly be included in the classic porphyry copper group of McMillan and Panteleyev (1980).

## 7.2 CONSTRAINTS ON THE GENESIS OF THE MAJOR PORPHYRY COPPER DEPOSITS

The geologic, isotopic and petrochemical constraints on the genesis of the major porphyry copper deposits of the region are examined in this section. The implications they pose on the genesis of the copper deposits are discussed.

### 7.2.1 Geological setting of the major porphyry copper deposits of northern Chile

The major porphyry copper deposits of Northern Chile have a marked linear distribution within the domain of the Domeyko Fault System (Fig. 7.2), which roughly coincides with the western limit of uplifted crustal blocks cored by Late Paleozoic rocks (Domeyko Cordillera; altitude 4,000 to 4,500 m). The copper bearing stocks are located either along the strike of faults belonging to this regional system (i.e., Copaquire, Quebrada Blanca, Chuquicamata, Chuqui Norte and la Escondida; Fig. 7.2), or close to these structures such as El Abra (3 km to the east of the West Fissure; Ambrus, 1977), El Salvador and Potrerillos (9 km to the west and 7 km to the east respectively from the Cerro Castillo Fault;

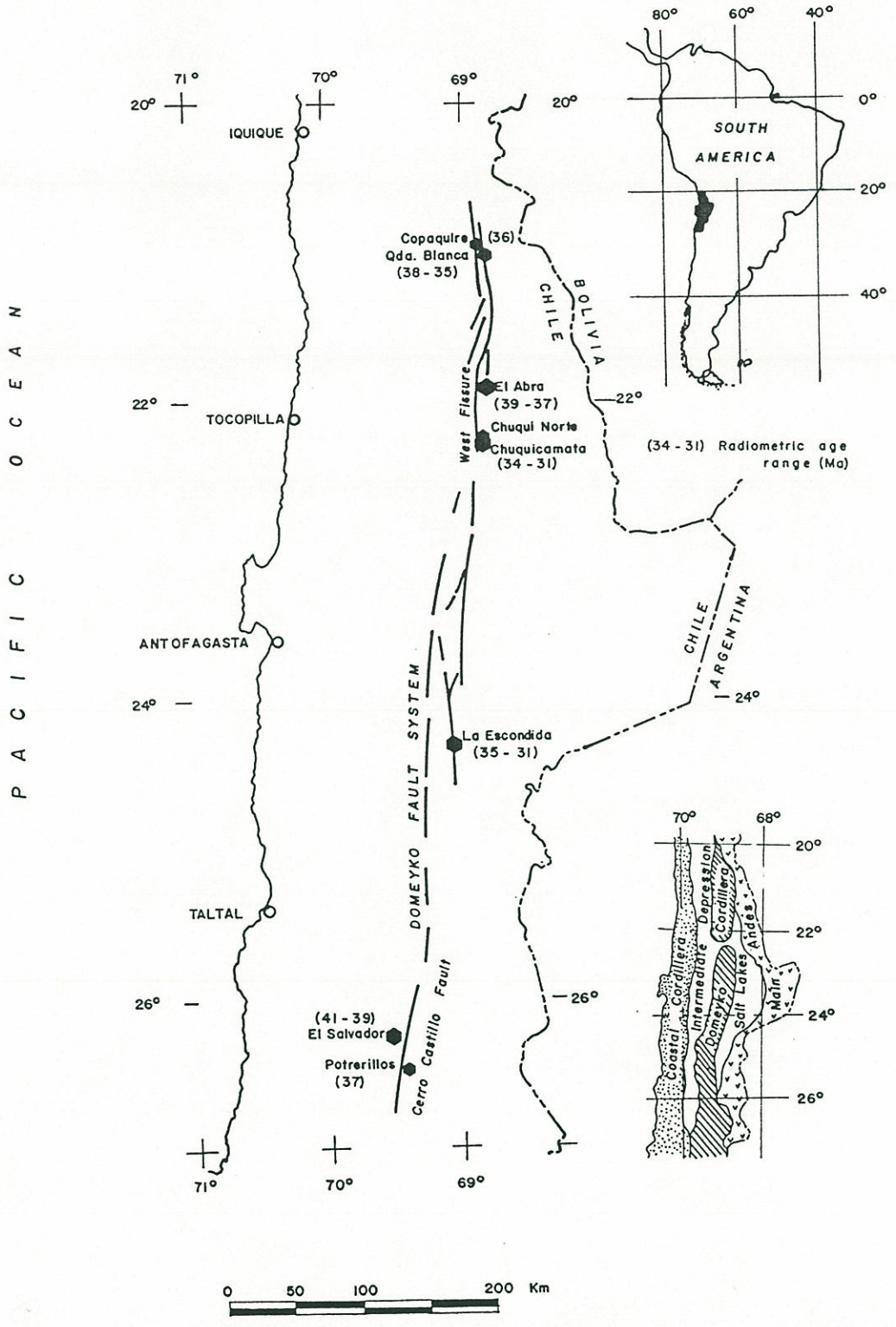


**Figure 7.2.** Distribution of major porphyry copper deposits of northern Chile within the domain of the Domeyko Fault System.

Tobar, 1977). The spatial relationship with a regional fault system is the most distinctive geological characteristic shared by this group of porphyry copper deposits. Several authors have suggested a direct genetic relationship between the fault system and copper mineralization (e.g., Sillitoe, 1981, Hunt et al., 1983, Baker and Guilbert, 1987).

The location of the copper-bearing stocks also coincides with Upper Eocene-Lower Oligocene pre-mineralization equigranular granodioritic plutons ("plutonic precursors" of Sillitoe, 1988). Some of these unmineralized plutons have yielded radiometric ages that are very close to the age of mineralized rocks (see Section 4.3) and constitute the country rocks of porphyritic mineralized stocks; e.g., the Southern Granodiorite at El Abra (Ambrus, 1977) and the Fortuna Granodiorite at Chuquicamata (Sillitoe, 1988). Post-mineralization intrusions (usually minor dikes and stocks) are also common, which according to the geochronologic data available, were emplaced very shortly after the mineralization. The concurrence of the locus of unmineralized and mineralized Late Eocene-Early Oligocene plutons suggests that several batches of magma followed a similar ascent path. The mineralized stocks and minor associated post-mineralization intrusions represent the final 10 Ma of magmatic activity within the Domeyko Cordillera. Subsequent magmatic activity occurred along a longitudinal belt 100 to 150 km to the east in the High Andes and Altiplano.

The composition of mineralized stocks varies from quartz diorite to granite but granodiorite (dacite) dominates. The host rocks are of diverse nature and age (Table 7.1), therefore there is no obvious association of copper-bearing intrusions with a particular lithology or age of host rocks.

The porphyry copper mineralization developed during a period of reactivated erosion of the uplifted Domeyko Cordillera block and sedimentation of terrestrial sequences 1.3 to 2.2 km thick on the periphery of this Cordillera (Sichal, San Pedro, Tambores and Pampa Mulas Formations; see Chapter 2).

**TABLE 7.1 MINERALIZED AND COUNTRY ROCKS OF THE PORPHYRY COPPER DEPOSITS OF NORTHERN CHILE.**

(Arranged from north to south)

| | |
|---|---|
| Copaquire: | Granodioritic porphyry (36 Ma[1]) emplaced within a sequence of Upper Jurassic marine sedimentary rocks and Lower Cretaceous volcanics (Hollister and Bernstein, 1975). |
| Quebrada Blanca: | Quartz monzonite and quartz monzonitic porphyry (38-35 Ma) emplaced within a Permian granodiorite and a sequence of Carboniferous to Permian rhyolites and andesites (Hunt and others, 1983). |
| El Abra: | Quartz diorite and dacitic porphyry (39-37 Ma) emplaced within a Paleozoic granodiorite and Paleocene-Eocene andesites (Ambrus, 1977). |
| Chuquicamata: | Granodioritic porphyry (34-31 Ma) emplaced within an Upper Paleozoic granodiorite and Carboniferous to Permian volcanic rocks (Alvarez and others, 1980; Alvarez and Aracena, 1985). |
| La Escondida: | Quartz monzonitic and quartz dioritic porphyries (35-31 Ma) emplaced within a sequence of Paleocene-Eocene volcanics and Upper Jurassic-Lower Cretaceous sedimentary rocks (Ojeda, 1986; Alpers, 1986; Alpers and Brimhall, 1988). |
| El Salvador: | Granodioritic and rhyolitic porphyries (41-39 Ma) emplaced within a sequence of Paleocene-Eocene volcanic rocks (Gustafson and Hunt, 1975). |

[1] See Section 4.3 for the actual dates and their discussion.

Potrerillos: Quartz dioritic porphyry (37 Ma) emplaced within a sequence of Jurassic marine limestones (Olson, 1989; March, 1935).

A dacitic ignimbrite intercalated in the Sichal Formation with a biotite K-Ar age of 35.5 ± 0.8 Ma (Huete et al., 1977) and intercalations of tuffs within the San Pedro Formation with K-Ar ages of 28.6 ± 6.0 and 24.9 ± 1.0 (Marinovic and Lahsen, 1984), indicate that terrestrial sedimentation persisted during the Oligocene with infrequent volcanic activity. Erosion virtually ceased by the Early Miocene. The exhumation of the porphyry copper deposits was produced by Late Eocene - Early Oligocene erosion leading to the development of supergene enrichment processes. These processes developed only 5 Ma after hypogene mineralization at El Salvador (Gustafson and Hunt, 1975). Reduction of denudation rates during Oligocene, and subsequent virtual cessation of erosion contributed to the preservation of the porphyry copper deposits and their enriched blankets (Mortimer, 1980; Alpers and Brimhall, 1988, 1989).

### 7.2.2 Geochronological constraints

Many radiometric ages, chiefly K-Ar, from porphyry copper deposits of northern Chile have been reported in several previous studies (Quirt, 1972; Hunt et al., 1983; Ambrus, 1977, 1979; Alvarez and others, 1980; Alvarez and Aracena, 1985; Alpers, 1986; Ojeda, 1986; Gustafson and Hunt, 1975; Olson, 1989): a compilation has been published by Sillitoe, (1988). These ages demonstrate that the copper mineralization developed within a discrete interval of geological time from 41 to 31 Ma.

During the present study, biotites of mineralized porphyritic stocks at Chuquicamata, El Abra, Quebrada Puno, Quebrada Blanca and Copaquire deposits have been dated using the more precise $^{40}Ar/^{39}Ar$ step heating technique (see Section 4.3). Ages ranging from 39.2

to 31.8 Ma were obtained confirming that copper mineralization developed within a discrete interval of geologic time. In addition, the $^{40}Ar$-$^{39}Ar$ dating suggests that the variation in conventional biotite K-Ar dates of individual porphyry copper deposits may be an analytical artifact rather than the persistence of long periods of thermal activity (see Sections 4.3.3, 4.4). Simple thermal modelling indicates that the porphyritic stocks cooled within a few tens of thousands of years after intrusion (see Section 4.3.3). This modelling does not support interpretations based on K-Ar dating that ascribe periods of hydrothermal activity lasting 1 to 3 Ma in porphyry copper systems (e.g., Ambrus, 1977, Alpers, 1986; Sillitoe, 1988).

The concordance of $^{40}Ar$-$^{39}Ar$ dates of biotite (31.7 ± 0.4 Ma) and potassium-feldspar (31.4 ± 0.2 Ma) with the apatite fission track age (30.2 ± 4.4 Ma) at Chuquicamata and biotite $^{40}Ar$-$^{39}Ar$ dates (36.8 ± 0.6 and 36.7 ± 0.8 Ma) with apatite fission track ages at El Abra (37.6 ± 5.2, 35.3 ± 4.4, and 37.7 ± 5.0 Ma) are consistent with fast cooling of the copper-bearing porphyritic stocks (see Chapters 4 and 5). This concordance is also consistent with their epizonal emplacement and indicates the absence of subsequent heating events.

### 7.2.3 Relation of the porphyry copper deposits to the magmatic history of the Andes of northern Chile

Volcanic and plutonic processes were virtually continuous in the Andean segment between 21°-26° S during the Late Cretaceous and Paleogene (78 to 31 Ma). They took place along a longitudinal belt of about 50 to 100 km wide located about 100 km east of the present Pacific coast (see Chapter 2). This belt includes a great number of stocks, which have variable composition from gabbro to monzogranite and radiometric ages ranging from 78 to 43 Ma. Furthermore, a volcanic sequence of variable thickness (0 to 4,900 m) occurs along the same belt. This unit includes rocks ranging in composition from basalt to

rhyolite but dominated by andesites and dacites. Radiometric dates of the volcanics vary from 75 to 40 Ma with most in the range 65 to 40 Ma (see Appendix 2).

The extensive Paleocene and Early Eocene volcanic activity virtually vanished in the Late Eocene. From 41 to 31 Ma magmatism was essentially restricted to the emplacement of major porphyry copper deposits within a narrow belt along the Domeyko Cordillera. The only volcanic rock of similar age to the porphyry copper deposits is a dacitic ignimbrite (biotite K-Ar age is 35.5 ± 0.8 Ma; recalculated from Maksaev, 1978) intercalated in the mid-section of the Oligocene-Lower Miocene terrestrial sedimentary sequence deposited on the west foothills of the Domeyko Cordillera. No other coeval volcanic rocks have been recognized in the whole Andean segment between 21° and 26° S. Sillitoe (1988) emphasized that intrusion-related copper mineralization in the Andes was the culmination of extended periods of subaerial volcanism, which lasted for at least 5 to 9 Ma, mentioning El Salvador as an example. Although this is true if Paleocene-Early Eocene volcanism of the Antofagasta Region is considered, the copper mineralization at El Salvador as well as that in the other porphyry copper deposits of northern Chile apparently took place during a period of volcanic quiescence. It is also possible that the extrusive equivalents of the copper-bearing intrusions were not preserved due to strong erosion, but even so, this hypothetical volcanism was considerably reduced compared with that of the Paleocene-Eocene.

As shown above, porphyry copper emplacement was spatially and temporally more restricted than the early Tertiary volcano-plutonic processes. Sillitoe (1988) showed that the generation of Cenozoic porphyry copper deposits in the Andes took place during three distinct epochs of copper mineralization that lasted for 10 to 14 Ma and were separated by quiescent intervals of about the same duration. Each porphyry mineralization epoch developed in different segments of the Andes. Thus the generation of porphyry copper deposits in the Central Andes is an episodic phenomenon, which is significantly restricted in time

and space compared with the virtually continuous magmatic activity in this convergent plate margin.

### 7.2.4 Tectonic setting of the porphyry copper deposits

The Andean segment between 21° and 26° S is located on the active plate margin of the South American continent. The Late Cretaceous to Paleogene calc-alkaline (see Section 7.2.7) volcano-plutonic activity represents an ancient magmatic arc developed on the continental margin. Different plate reconstructions, based on the paleomagnetic record of the ocean floor, show relatively steady convergence between the oceanic lithosphere and continental South American since the time of anomaly 18 (Pilger, 1983, 1984; Cande, 1983, Pardo-Casas and Molnar, 1987). From anomaly 18 to 7 (ca. 42 to 26 Ma) the paleomagnetic record shows southwest-northeast oblique convergence. During that period oceanic expansion occurred along a northwest-trending oceanic ridge separating the Pacific and Farallon oceanic plates (Mammerickx et al., 1980). In contrast, since the time of anomaly 7 the convergence has been perpendicular following the establishment of the northeast trending East Pacific Rise and fragmentation of the Farallon plate in the Nazca and Cocos plates. Two periods of high convergence rates (about 12 cm $yr^{-1}$) have been determined, one from anomaly 18 to 13 (ca. 42 to 35.5 Ma), and the other from anomaly 7 to 5 (ca. 26 to 10 Ma) (Cande, 1983). These periods of increased convergence rates coincide with major re-organization in plate boundaries identified by various authors (Cande and others, 1982, Mammerickx and others, 1980, Rona and Richardson, 1978, Schwan, 1985), and correlate with the compressive **Incaic** and **Quechua** tectonic events and related uplift in northern Chile (see Chapter 2 and Section 2.17).

The major porphyry copper deposits of the Andes of northern Chile between 21° and 26° S were formed during a period of northeast-southwest oblique convergence between the Nazca and South American plates. During oblique convergence a horizontal component of the

total displacement exists at the plate boundary. Shear stresses are generated within the continental plate, and trench-linked strike-slip faults (see Section 2.16) develop along the section of lithosphere thermally weakened by active magmatism, i.e. the magmatic front (Dewey, 1980; Beck, 1983, 1986; Woodcock, 1986; Sylvester, 1988; Busby-Spera and Saleeby, 1990). These faults are likely to be discontinuous and arranged en echelon (Segall and Pollard, 1980). Therefore, the spatial relationship of the major porphyry copper deposits of northern Chile with the Domeyko Fault System can be adequately explained as a consequence of the dextral shear produced on the continental edge, due to Late Eocene-Early Oligocene oblique convergence. This led to the development of a trench-linked strike-slip fault system along the position of the magmatic front. This is consistent with the field observations (see Chapter 2) and biotite $^{40}Ar$-$^{39}Ar$ date of 36.3 ± 0.6 inferred for the ductile deformation of the Fortuna Granodiorite next to the West Fissure at Chuquicamata, and the biotite $^{40}Ar$-$^{39}Ar$ age of 31.7 ± 0.4 Ma for the Chuquicamata porphyry, which also shows some ductile deformation (see Section 4.3.4).

Sillitoe (1981) suggested that faults associated with the porphyry copper systems acted as zones of weakness and were perhaps active during emplacement, thereby aiding ascent and localization of porphyry copper-bearing stocks and plutons. Several other authors have expressed a similar view, implying a direct genetic link between faulting and generation of porphyry copper deposits (Hollister and Bernstein, 1975; Ambrus, 1979; Alvarez and others, 1980; Hunt and others, 1983; Baker and Guilbert, 1987; Davies, 1989). The above $^{40}Ar$-$^{39}Ar$ ages for rocks that display ductile deformation indicate that strike-slip faulting was, in fact, active during the emplacement of the copper-bearing stocks. Chuquicamata in particular constitutes a notable example of a synkinematic intrusion within a tensile zone associated with a strike-slip fault system (see Section 7.2.11). Nonetheless, important porphyry copper deposits, such as El Salvador and El Abra and the porphyry copper deposits of southern Peru or central Chile lack apparent structural control. Therefore although local extensional zones associated with fault development may provide favourable sites for the epizonal emplacement of

intrusive stocks, this is not regarded as essential for the generation of porphyry copper deposits. The position of the magmatic front itself (warm lithosphere) may have controlled the position of the faults and fluid pressure exerted by magmas may significantly facilitate subsequent fault movement by reducing effective stresses[2].

The ascent of magmas is conditioned by the stress conditions within the asthenosphere and lithosphere, magmas following the path of least resistance, but the strong reduction of effective stresses due to the fluid nature of magmas may promote tensile fracturing. In fact, extensional (hydraulic) fracture mechanisms are thought to play a significant role in magma transport (Weertman, 1971; Yoder, 1976; Anderson and Grew, 1977; Shaw, 1980; Spera, 1980) and critical tensile stresses necessary for the propagation of cracks are smallest in materials with reduced rigidities (Spera, 1980). Therefore magmas may open their own conduits upwards, particularly through rocks that have been warmed by previous igneous activity. Decoupling of the magma ascent routes from a shear zone in the uppermost brittle levels of the crust may be expected. This may account for the occurrence of porphyry copper deposits such as El Abra and El Salvador located 3 and 9 km respectively from a regional fault, and for the characteristic successive intrusions within the same site (pre-mineralization plutons, mineralized porphyries and post-mineralization intrusions).

### 7.2.5 Strontium and neodymium isotopic constraints

Isotopes of Sr and Nd give some insight into the source and evolution of the porphyry magmas. Sr and Nd isotope abundances were determined on samples from deep drill holes at Chuquicamata (650-950 m under the pit-floor), and from the deep section (Inca level) of the El

---

[2] Effective stress is the rock stress at a point minus the fluid pressure acting at that point.

Salvador mineralized porphyry. Initial $^{87}Sr/^{86}Sr$ ratios vary between 0.70380 and 0.70465 ($\epsilon^{i}_{Sr}$ = -12.09 to -0.7; Table 7.2) and initial $^{143}Nd/^{144}Nd$ ratios range between 0.512685 and 0.512856 ($\epsilon^{i}_{Nd}$ = +1.33 to +4.48)[3]. All these isotopic ratios plot in a tight cluster on the "mantle array" in the depleted quadrant of an $\epsilon_{Sr(t)}$ versus $\epsilon_{Nd(t)}$ diagram (Fig. 7.3). The isotopic data for the pre-mineralization Southern Granodiorite of El Abra reported by Rogers (1985) show initial $^{87}Sr/^{86}Sr$ values between 0.70447 and 0.70457 ($\epsilon^{i}_{Sr}$ = -2.7 to -1.2) and initial $^{143}Nd/^{144}Nd$ ratios from 0.512659 to 0.512683 ($\epsilon^{i}_{Nd}$ = +1.34 to +1.81), which are identical to the values from Chuquicamata. Previously published initial $^{87}Sr/^{86}Sr$ ratios for copper-bearing porphyries of El Salvador porphyry copper deposit range from 0.7031 to 0.7045 (Halpern, 1978; Gustafson, 1979; Shibata and others, 1984), which are essentially concordant with the data presented in this study. Identical values (0.70436 - 0.70464) have been published for the pre-mineral Fortuna Granodiorite at Chuquicamata by Shibata and others (1984) and the Late Miocene-Pliocene Rio Blanco-Disputada and Pliocene El Teniente porphyry copper deposits of central Chile (0.7037 - 0.7044; Halpern, 1979). In addition, Lopez-Escobar (1984) indicated that the rocks from the Rio Blanco-Disputada porphyry copper deposit exhibit $^{143}Nd/^{144}Nd$ ratios in the range 0.512860 - 0.512890.

Older pre-porphyry intrusions such as the 63 Ma Cerros de Montecristo granodiorite cropping out 20 km east of Chuquicamata have initial $^{87}Sr/^{86}Sr$ ratios from 0.70384 to 0.70451 ($\epsilon^{i}_{Sr}$ = -10.4 to -1.0) and initial $^{143}Nd/^{144}Nd$ ratios from 0.512597 to 0.512611 ($\epsilon^{i}_{Nd}$ = +1.71 to +1.99) (Rogers, 1985). The same parameters for the 65 Ma Cerro Colorado gabbroic pluton, located 20 km east of El Abra, are 0.70372 to 0.70397 ($\epsilon^{i}_{Sr}$ = -12.8 to -9.3) and 0.512742 to 0.512779 ($\epsilon^{i}_{Nd}$ = +3.63 to +4.36). These Sr and Nd isotopic data from pre-porphyry intrusions also plot within the mantle array in the depleted quadrant of a $\epsilon_{Sr(t)}$-$\epsilon_{Nd(t)}$ diagram (Fig. 7.4, after Rogers, 1985). Initial $^{87}Sr/^{86}Sr$ of early Tertiary pre-porphyry volcanic rocks at El Salvador (Indio Muerto rhyolite and rhyolitic domes; ca. 50 Ma) range between 0.7039 and 0.7042 (Gustafson, 1979), similar to those of

---

[3] $\epsilon^{i}_{Nd}$ determined using $^{147}Nd/^{144}Nd$ = 0.6 x Sm/Nd (see **Appendix 6**).

## TABLE 7.2 STRONTIUM ISOTOPIC DATA

**CHUQUICAMATA**

| Sample | Rb (ppm) | Sr (ppm) | $\frac{^{87}Rb}{^{86}Sr}$ | $\frac{^{87}Sr}{^{86}Sr}$ | $\frac{^{87}Sr}{^{86}Sr(i)}$ | $\epsilon^{i}_{Sr}$ |
|---|---|---|---|---|---|---|
| ZCH1 | 91.6 | 408.3 | 0.6493 | 0.70461 | 0.70432 | -4.80 |
| ZCH2 | 75.4 | 691.9 | 0.3152 | 0.70470 | 0.70456 | -1.44 |
| ZCH3 | 161.6 | 248.2 | 1.8844 | 0.70532 | 0.70449 | -2.44 |
| ZCH4 | 187.2 | 298.9 | 1.8125 | 0.70532 | 0.70452 | -1.99 |
| ZCH5 | 156.3 | 553.9 | 0.8165 | 0.70489 | 0.70453 | -1.87 |
| ZCH7 | 116.4 | 461.3 | 0.7303 | 0.70489 | 0.70456 | -1.33 |
| ZCH9 | 70.9 | 205.3 | 0.9994 | 0.70495 | 0.70451 | -2.16 |
| ZCH10 | 149.2 | 208.9 | 2.0667 | 0.70556 | 0.70465 | -0.17 |

**EL SALVADOR**

| Sample | Rb (ppm) | Sr (ppm) | $\frac{^{87}Rb}{^{86}Sr}$ | $\frac{^{87}Sr}{^{86}Sr}$ | $\frac{^{87}Sr}{^{86}Sr(i)}$ | $\epsilon^{i}_{Sr}$ |
|---|---|---|---|---|---|---|
| ES1548 | 42.5 | 409.5 | 0.3000 | 0.70397 | 0.70380 | -12.09 |
| ES5262 | 29.8 | 304.6 | 0.2826 | 0.70429 | 0.70413 | -7.41 |
| ES10178 | 51.0 | 572.5 | 0.2578 | 0.70432 | 0.70417 | -6.78 |

The analytical uncertainty of $^{87}Sr/^{86}Sr$ ratios, at 2σ level, is ± 0.00003; Rb and Sr concentrations were measured by X ray fluorescence with a precision between 5-10 %.

**EL ABRA** (Southern Granodiorite; Rogers, 1985)

| Sample | Rb (ppm) | Sr (ppm) | $\frac{^{87}Rb}{^{86}Sr}$ | $\frac{^{87}Sr}{^{86}Sr}$ | $\frac{^{87}Sr}{^{86}Sr(i)}$ | $\epsilon^{i}_{Sr}$ |
|---|---|---|---|---|---|---|
| 80103 | 200.2 | 93.9 | | 0.70790 | 0.70451 | -2.0 |
| 80104 | 141.4 | 486.0 | | 0.70503 | 0.70457 | -1.2 |
| 80107 | 65.2 | 748.1 | | 0.70460 | 0.70447 | -2.7 |

## TABLE 7.3 NEODYMIUM ISOTOPIC DATA

**CHUQUICAMATA**

| Sample | Sm (ppm) | Nd (ppm) | $^{143}Nd/^{144}Nd \pm 2\sigma \times 10^{-6}$ | $^{143}Nd/^{144}Nd_{(i)}$ | $\epsilon^{i}_{Nd}$ |
|---|---|---|---|---|---|
| ZCH1 | 1.63 | 10.9 | 0.512690 ± 11 | 0.512672 | +1.40 |
| ZCH2 | 1.63 | 10.4 | 0.512685 ± 12 | 0.512666 | +1.28 |
| ZCH4 | 1.90 | 12.2 | 0.512691 ± 11 | 0.512672 | +1.40 |
| ZCH10 | 1.72 | 10.3 | 0.512689 ± 12 | 0.512669 | +1.33 |

**EL SALVADOR**

| Sample | Sm (ppm) | Nd (ppm) | $^{143}Nd/^{144}Nd \pm 2\sigma \times 10^{-6}$ | $^{143}Nd/^{144}Nd_{(i)}$ | $\epsilon^{i}_{Nd}$ |
|---|---|---|---|---|---|
| ES4785 | 4.47 | 29.6 | 0.512716 ± 14 | 0.512692 | +2.02 |
| ES5262 | 2.99 | 15.7 | 0.512737 ± 12 | 0.512706 | +2.29 |
| ES10178 | 3.47 | 18.3 | 0.512740 ± 12 | 0.512710 | +2.37 |
| ES1548 | 2.77 | 11.6 | 0.512856 ± 11 | 0.512818 | +4.48 |

Nd isotopic ratios determined by Dr. Alan Dickin at McMaster University by mass spectrometry. Sm and Nd concentrations determined by neutron activation technique.

**EL ABRA** (Southern Granodiorite; Rogers, 1985)

| Sample | Sm (ppm) | Nd (ppm) | $^{143}Nd/^{144}Nd \pm 2\sigma \times 10^{-6}$ | $^{143}Nd/^{144}Nd_{(i)}$ | $\epsilon^{i}_{Nd}$ |
|---|---|---|---|---|---|
| 80103 | 3.431 | 20.89 | 0.512708 ± 14 | 0.512683 | +1.81 |
| 80104 | 4.485 | 24.12 | 0.512687 ± 12 | 0.512659 | +1.34 |
| 80107 | 3.183 | 18.46 | 0.512689 ± 18 | 0.512663 | +1.42 |

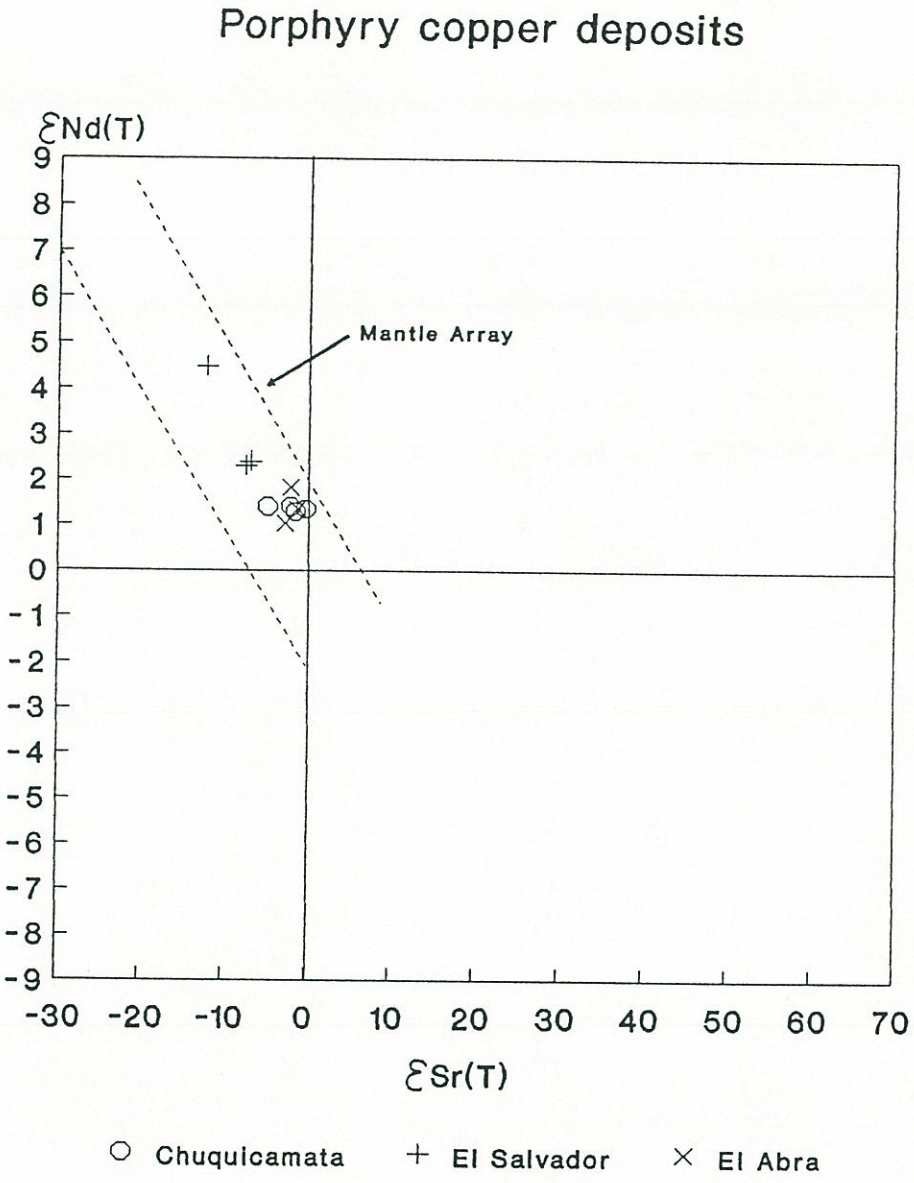


**Figure 7.3.** $\epsilon^{i}_{Sr}$ versus $\epsilon^{i}_{Nd}$ plot of the data from Chuquicamata, El Salvador and El Abra porphyry copper deposits. Data from Southern Granodiorite of El Abra after Rogers (1985).

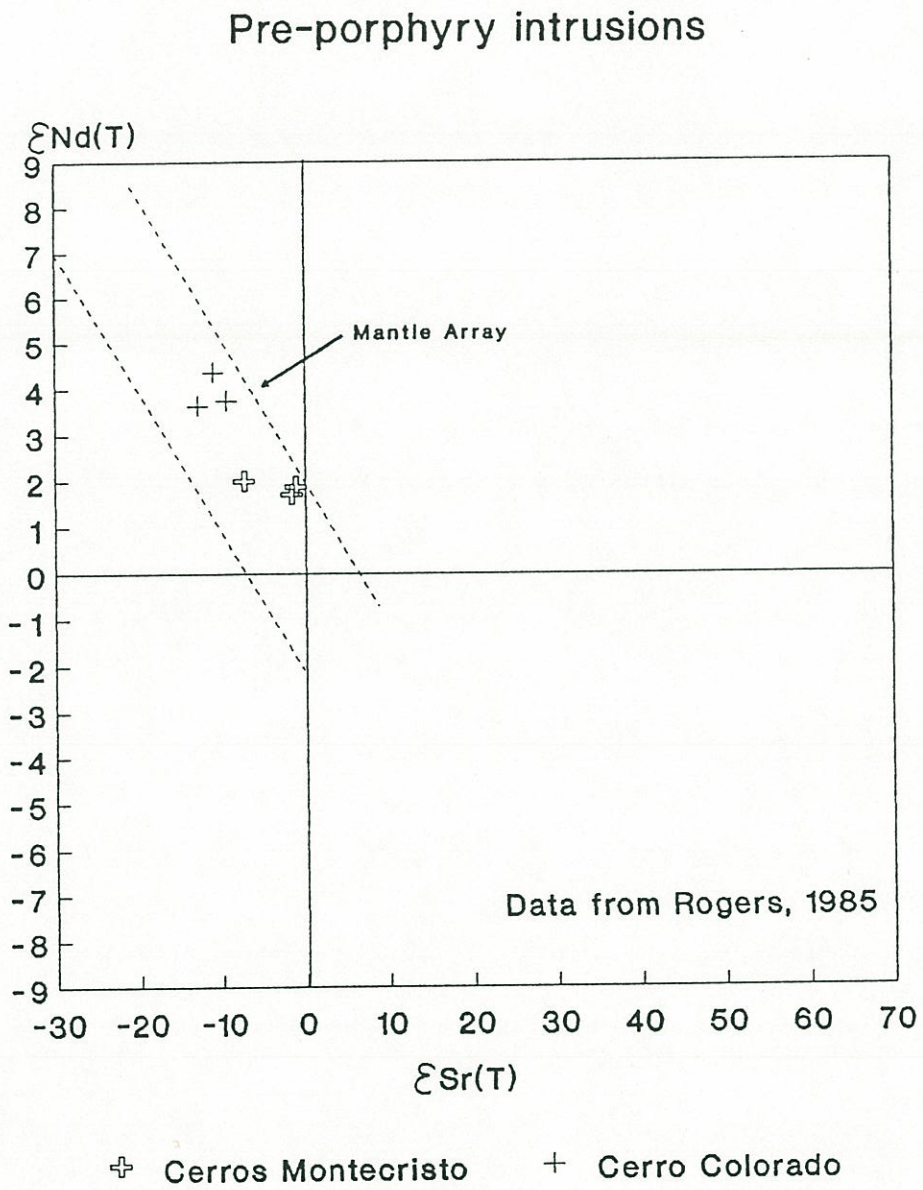


**Figure 7.4.** $\epsilon^{i}_{Sr}$ versus $\epsilon^{i}_{Nd}$ plot of the data from the 63 Ma Cerros de Montecristo granodioritic pluton and the 66 Ma Cerro Colorado gabbroic intrusion; data after Rogers (1985).

the copper-bearing porphyries and pre-mineral intrusions. However, Halpern (1978) reported higher initial $^{87}Sr/^{86}Sr$ ratios ranging between 0.7106 and 0.7114 for Lower Tertiary rhyolites west of La Escondida.

As shown above, the Sr and Nd isotopic data from the Chuquicamata, El Salvador, and El Abra porphyry copper deposits indicate magma derivation from a source with time-integrated isotopic depletion relative to "bulk Earth," compatible with a source region within the sub-crustal asthenospheric wedge. There is no obvious evidence to indicate contamination with upper crustal materials during the ascent and crystallization of the magmas. Basement rocks 45 km south of Chuquicamata analyzed by Rogers (1985) yielded $^{87}Sr/^{86}Sr_{(251)}$ ratios ranging from 0.70120 to 0.71022 ($\epsilon^{251}_{Sr}$ = -45 to +82). These rocks are schists and amphibolites that suffered a partial isotopic homogenization during the Late Paleozoic. The $^{143}Nd/^{144}Nd_{(251)}$ ratios of the same metamorphic basement varies between 0.512186 and 0.512646: $\epsilon_{Nd}$ at 251 Ma ranges from +1.67 to -6.63, with metavolcanic rocks having higher values ($\epsilon^{251}_{Nd}$ = +1.67 to -1.01) than the metasedimentary rocks ($\epsilon^{251}_{Nd}$ = -4.38 to -6.63). The same author reported initial $^{87}Sr/^{86}Sr$ ratios from 0.70600 to 0.70649 for the Late Carboniferous Limon Verde granitic pluton ($\epsilon^{i}_{Sr}$ = +23 to + 30.0); initial $^{143}Nd/^{144}Nd$ ratios are from 0.512195 to 0.512229 ($\epsilon^{i}_{Nd}$ = -2.0 to -1.3). Since basement rocks appear to have overall higher $^{87}Sr/^{86}Sr$ and lower $^{143}Nd/^{144}Nd$ ratios than the copper-bearing porphyries contamination with this upper crustal basement is unlikely. In addition, the relatively restricted variation of isotopic ratios, and lack of correlation of initial $^{87}Sr/^{86}Sr$ ratios of copper-bearing porphyries with increasing $SiO_2$ or Sr content, further support the lack of upper crustal contamination. Compared with lavas from recent volcanoes of the southern volcanic zone (SVZ) of the Andes the copper-bearing porphyries have initial Sr and Nd ratios intermediate between those of volcanoes of the southern section of the SVZ, which developed over a crust about 30-40 km thick, and those of volcanoes of the northern section of the SVZ, which occur over a crust 50-60 km thick (Harmon and others, 1984; Futa and Stern, 1988; Hildreth and Moorbath, 1988; McMillan and others, 1989). The isotopic ratios of the southern section of the SVZ are similar to those of intra-oceanic island arcs (Harmon and others,

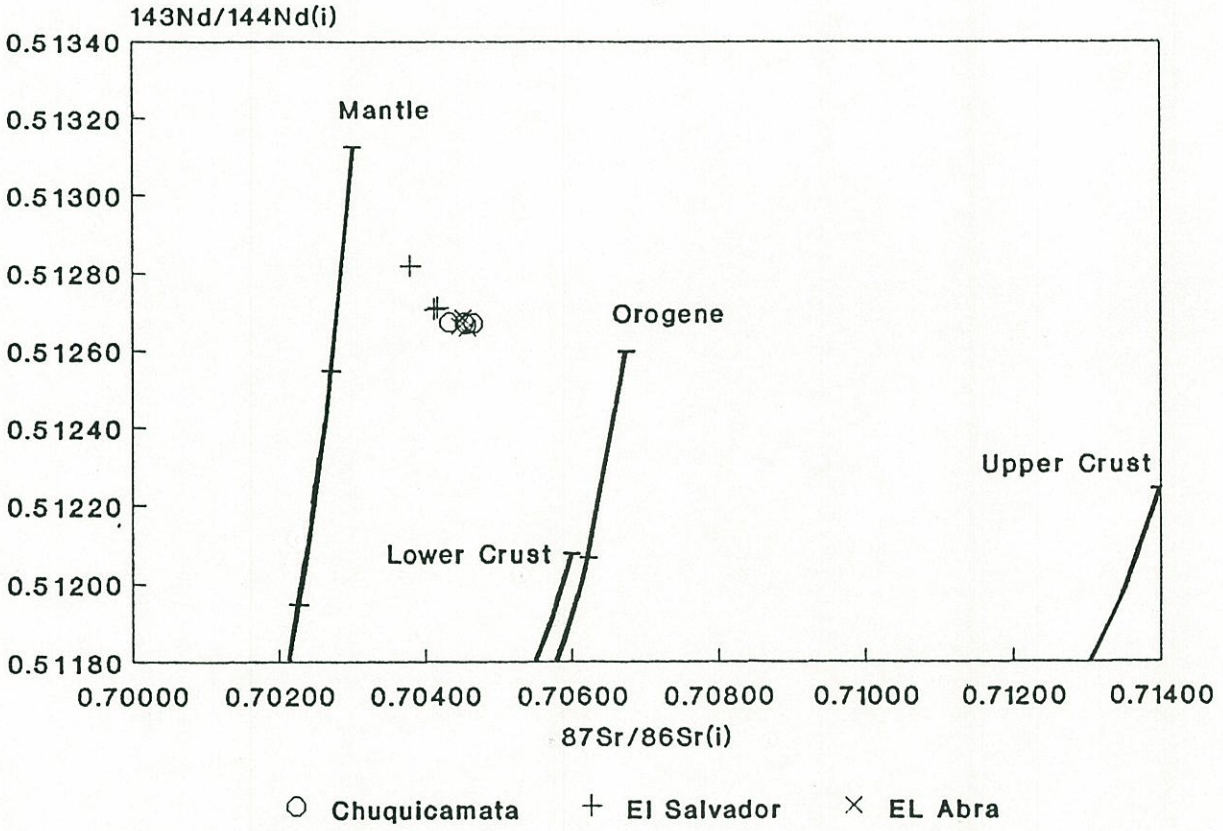


Figure 7.5. Initial $^{87}Sr/^{86}Sr$ ratios versus initial $^{143}Nd/^{144}Nd$ ratios of Chuquicamata, El Salvador and El Abra porphyry copper deposits. Evolution curves of isotopic reservoirs according to the model of Zartman (1984).

1984; Hickey and others, 1986) leading many workers to conclude that SVZ lavas are mostly uncontaminated by continental crust. This may suggest that porphyry copper magmas are derived from the mantle and uncontaminated by continental crust. However, recent work in the SVZ suggests instead that crustal contamination is an integral process in the production of magmas in the Andes and that restricted ranges of isotopic composition result when parental basalts and crustal contaminants have similar isotopic signatures (e.g., McMillan and others, 1989). Alternatively, Stern (1988, 1989, in press) suggested source region contamination by subduction erosion of terrigenous sediments and/or crustal materials. Thus crustal contamination by lower crust, or source region contamination cannot be ruled out in porphyry copper magma genesis.

Initial Nd and Sr isotopic ratios of porphyry copper deposits plot in a compact cluster (Fig. 7.5) between the lower crust and mantle curves of the expanded "plumbotectonic" model of Zartman (1984). According to this model, this position may suggest magma derivation from a mantle reservoir with some influx from the lower crust.

The relatively low Sr and high Nd isotopic ratios of copper-bearing porphyries of northern Chile are similar to those of other significantly younger Chilean porphyry copper deposits and to the available isotopic data of most pre-mineralization intrusive and volcanic rocks of the Antofagasta Region. This suggests that, irrespective of age, petrogenetic processes that generate porphyry copper magmas are fairly uniform. Alternatively, the narrow isotopic variation may reflect a very homogeneous magma source or effective homogenizing processes in the source region: e.g., active asthenospheric convection, (Hoffman and McKenzie, 1985) and/or MASH process[4] at the mantle-lower crust interface (Hildreth and Moorbath, 1988).

---

[4] MASH = melting, assimilation, storage, and homogenization.

### 7.2.6 Lead isotopic constraints

Rocks and sulfides from Chuquicamata and El Salvador porphyry copper deposits show a very restricted range of lead isotope ratios ($^{206}Pb/^{204}Pb$ = 18.493-18.592; $^{207}Pb/^{204}Pb$ = 15.593-15.624; $^{208}Pb/^{204}Pb$ = 38.429-38.586; Table 7.4), almost indistinguishable within experimental error. These values are virtually identical to those published by Puig (1988) for galena from La Escondida porphyry copper and the same values occur 1,000 km south in galenas of Late Miocene to Pliocene El Teniente and Disputada porphyry copper deposits of central Chile (Table 7.4). Furthermore, identical values of Pb isotopic ratios have been published for the Paleocene Toquepala porphyry copper deposit in Southern Peru, about 1,000 km north (Tilton and others, 1981; Barreiro and Clark, 1984), although one sample from the latter deposit is slightly more radiogenic. Thus despite different ages and geographic locations, Andean porphyry copper deposits have an identical lead isotopic signatures, implying either a very homogeneous source of lead or the operation of an effective homogenizing mechanism during magma genesis/mineralization.

The Pb isotopic ratios of galenas from older vein deposits of the Antofagasta Region (Puig, 1988) fall within a slightly wider range, but still within 1% of variation ($^{206}Pb/^{204}Pb$ = 18.557-18.692, $^{207}Pb/^{204}Pb$ = 15.593-15.654, $^{208}Pb/^{204}Pb$ = 38.496-38.724). The Pb isotope ratios of porphyry copper deposits overlap with the least radiogenic values. This is compatible with less magma interaction with the upper crust as concluded above from Sr and Nd isotopic data.

In conventional Pb-Pb diagrams (Fig. 7.6) the data from the study area plot in a tight cluster well above values of MORB and oceanic basalts of the Nazca plate (Unruh and Tatsumoto, 1976; Sun, 1980; Vidal and Clauer, 1981; Tilton, 1983). In contrast with sets of Pb isotope data published for the Aleutians, Cascades and Marianas arc (Kay and others, 1978; Church, 1973, 1976; Meijer, 1976; Hawkesworth, 1982), there is no evidence for a steep mixing line between MORB-type Pb and that

of a $^{207}Pb$-rich reservoir. If Pb derived from subducted oceanic lithosphere makes any contribution to the Pb of the mineral deposits, it can only be small relative to a contribution from a very homogeneous reservoir having elevated values of $^{207}Pb/^{204}Pb$ and $^{208}Pb/^{204}Pb$. The data do not necessarily imply a single Pb reservoir, but if the Pb-isotope signature results from the mixing of several reservoirs, a very special homogenizing mechanism is required to explain virtually identical Pb isotopic ratios of porphyries of different ages and locations.

**TABLE 7.4 LEAD ISOTOPIC DATA**

| | | | | | |
|---|---|---|---|---|---|
| Z-OAC | Galena | 18.592 | 15.624 | 38.586 | Chuquicamata |
| ZCH4 | Whole rock | 18.591 | 15.604 | 38.538 | do |
| | Corrected | 18.567 | 15.603 | 38.517 | |
| ZCH9 | Whole rock | 18.621 | 15.600 | 38.585 | do |
| | Corrected | 18.566 | 15.597 | 38.500 | |
| ES9960 | Galena | 18.516 | 15.600 | 38.482 | El Salvador |
| ES-ETF | Bornite | 18.514 | 15.596 | 38.434 | do |
| ES4785 | Whole rock | 18.557 | 15.616 | 38.567 | do |
| | Corrected | 18.514 | 15.614 | 38.492 | |
| ES1548 | Whole rock | 18.558 | 15.606 | 38.549 | do |
| | Corrected | 18.493 | 15.603 | 38.460 | |
| ES10178 | Whole rock | 18.571 | 15.602 | 38.511 | do |
| | Corrected | 18.503 | 15.599 | 38.429 | |
| Z-AA1 | Galena | 18.627 | 15.593 | 38.458 | Disputada |
| BRD-ET | Galena | 18.565 | 15.605 | 38.493 | El Teniente |
| | | | | | |
| Z-713 | Whole rock | 18.802 | 15.663 | 39.006 | Basement |
| | Cor. 40 Ma | 18.771 | 15.662 | 38.939 | Coastal area. |
| | Cor. 260 Ma | 18.603 | 15.653 | 38.578 | |

These lead isotopic ratios were obtained by Dr. Marcos Zentilli at the USGS in Denver Colorado. The chemical procedures used for isolating Pb,

U and Th from the samples and for determining their concentration by isotope dilution are those of Doe and Delevaux (1980). The isotopic ratios were measured by solid source mass spectrometry using the silica-gel emitter technique. The analytical uncertainty at 2σ level is lower than ± 0.15 %. Corrections for whole rock samples have been made to account for subsequent decay of U and Th. Sulfide samples do not require such a correction because of their negligible U and Th content.

**TABLE 7.5 LEAD ISOTOPE DATA FROM PREVIOUS STUDIES**

Puig (1988)

| Sample | Mineral | $^{206}Pb/^{204}Pb$ | $^{207}Pb/^{204}Pb$ | $^{208}Pb/^{204}Pb$ | |
|---|---|---|---|---|---|
| DDH-235 | Galena | 18.598 | 15.616 | 38.566 | La Escondida |
| 10857 | Galena | 18.512 | 15.598 | 39.449 | El Salvador |
| La Galenosa | Galena | 18.510 | 15.618 | 38.499 | Ag-Pb vein[5] |
| C. Bayos 1 | Galena | 18.680 | 15.654 | 38.720 | Ag-Pb vein |
| Caracoles | Galena | 18.592 | 15.636 | 38.575 | Ag-Pb vein |
| Caracoles | Galena | 18.587 | 15.631 | 38.554 | Ag-Pb vein |
| Caracoles | Galena | 18.586 | 15.636 | 38.564 | Ag-Pb vein |
| Jardin | Galena | 18.684 | 15.626 | 38.624 | Ag-Pb vein |
| Alicia | Galena | 18.672 | 15.654 | 38.743 | Ag-Pb vein |
| S. Imilac | Galena | 18.605 | 15.644 | 38.623 | Ag-Pb vein |
| S. Argomedo | Galena | 18.680 | 15.633 | 38.710 | Ag-Pb vein |
| S. Argomedo | Galena | 18.692 | 15.626 | 38.724 | Ag-Pb vein |

Tilton (1979)

| Sample | Mineral | $^{206}Pb/^{204}Pb$ | $^{207}Pb/^{204}Pb$ | $^{208}Pb/^{204}Pb$ | |
|---|---|---|---|---|---|
| Disputada | Pyrite | 18.611 | 15.615 | 38.510 | Disputada |

[5] Silver-lead vein deposits older than the porphyry copper deposits.

Tilton and others (1981)

| Sample | Mineral | $\frac{^{206}Pb}{^{204}Pb}$ | $\frac{^{207}Pb}{^{204}Pb}$ | $\frac{^{208}Pb}{^{204}Pb}$ | |
|---|---|---|---|---|---|
| ES-35 | Pyrite | 18.511 | 15.593 | 38.444 | El Salvador |
| Z-350 | Pyrite | 18.529 | 15.620 | 38.523 | El Salvador |
| S. Peru | Chalcopy. | 18.519 | 15.629 | 38.533 | Toquepala |
| S. Peru | Chalcopy. | 18.716 | 15.664 | 38.617 | Toquepala |

Barreiro and Clark (1984)

| Sample | Mineral | $\frac{^{206}Pb}{^{204}Pb}$ | $\frac{^{207}Pb}{^{204}Pb}$ | $\frac{^{208}Pb}{^{204}Pb}$ | |
|---|---|---|---|---|---|
| SP 137 | Diorite | 18.521 | 15.628 | 38.614 | Toquepala |
| SP 138 | Diorite | 18.609 | 15.576 | 38.581 | Toquepala |
| SP 77 | Volcanics | 18.616 | 15.582 | 38.637 | Toquepala |

The major porphyry copper deposits of the Central Andes are more enriched in $^{207}Pb/^{204}Pb$ than are pelagic sediments on the downgoing plate (Fig. 7.6). In addition, the Pb isotopic composition of sediments and sulfides from the Nazca plate is more varied compared with the porphyry copper deposits and define a mixing trend between typical low-radiogenic MORB leads and more radiogenic lead of oceanic manganese nodules (Dasch, 1981; Vidal and Clauer, 1981; Reynolds and Dasch, 1971). If Pb from subducted pelagic sediments is incorporated into the Andean porphyry copper deposits an additional component enriched in $^{207}Pb$ still is required to account completely for all the data. Therefore it is considered unlikely that the Pb of the porphyry copper deposits is dominated by a contribution from subducted pelagic sediments.

Volcanic rocks of the southern volcanic zone (SVZ) of the Andes in central and southern Chile show identical Pb isotope ratios

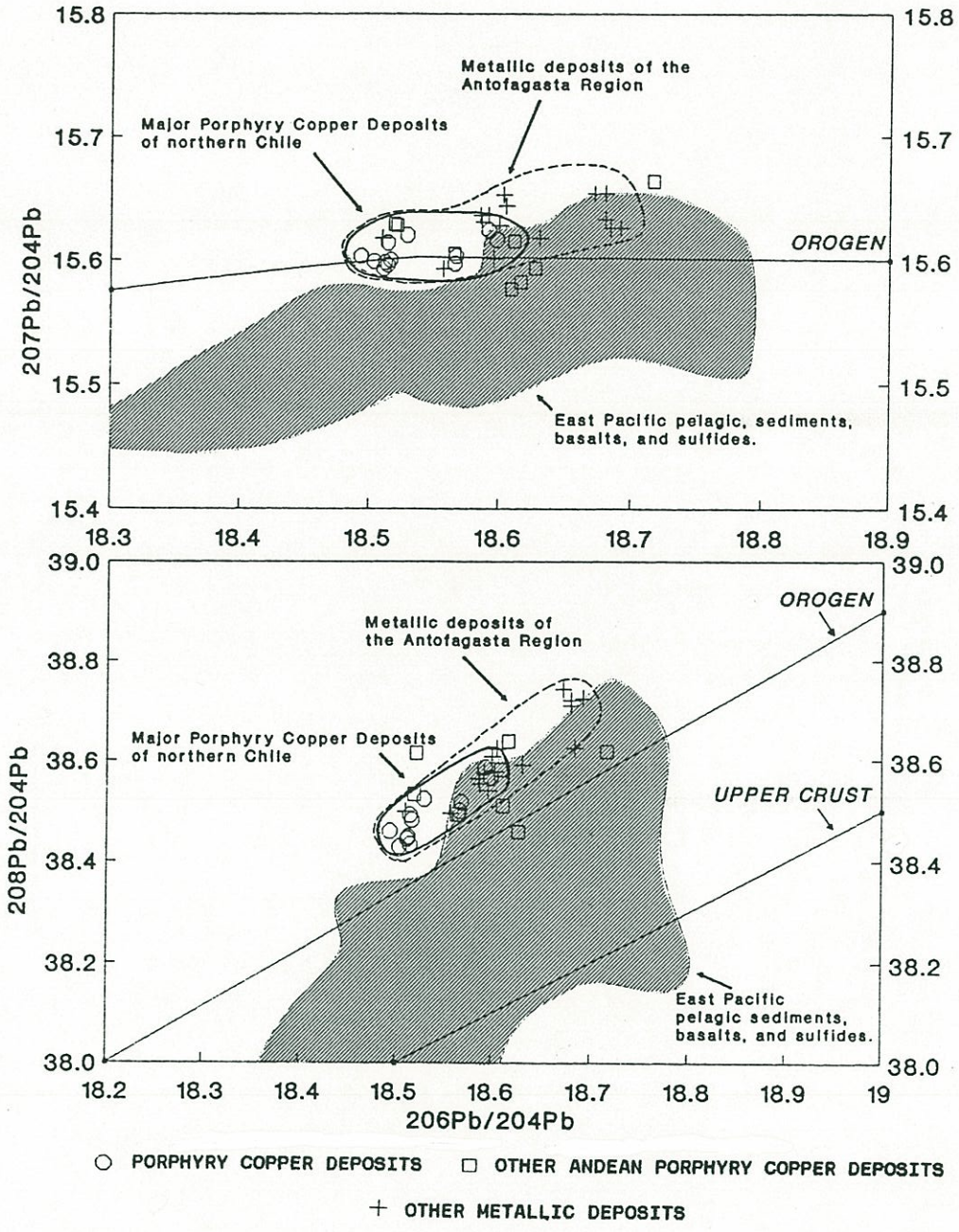


**Figure 7.6.** Lead isotopic composition of Chuquicamata and El Salvador porphyry copper deposits, and other Andean porphyry copper deposits and galena-bearing veins from the Antofagasta Region. Compared with the field of pelagic sediments, oceanic basalts and sulfides from the East Pacific sea floor. Pb-isotope model evolution curves after Zartman and Doe (1981). Sources of ocean floor data cited in text.

and range of variation to those of the deposits of the Antofagasta Region (Tilton, 1979; Barreiro, 1984; Harmon and others, 1984; Hildreth and Moorbath, 1988; McMillan and others, 1989). From these Pb isotopic data, coupled with petrochemical data, was initially inferred an isotopically homogeneous reservoir as the source of magmas, which was ascribed to an "enriched" subcontinental mantle (Tilton and Barreiro, 1980; Barreiro and Stern, 1982; Mukasa, 1986). An old enriched mantle is still advocated as the source of magmas in the Chilean Andes (e.g., Rogers and Hawkesworth, 1988) but the source of lead has been more frequently attributed to a mixture of sediments and altered igneous rocks of the subducted slab (Tilton and others, 1981; Hawkesworth, 1982; Barreiro, 1984; Sillitoe and Hart, 1984; Hickey and others, 1986). Recent studies (Hildreth and Moorbath, 1988; Puig, 1988) ascribe the highly radiogenic character of the Pb of Andean igneous rocks and mineral deposits to a crustal contribution. Puig (1988) envisaged a combination of crust and mantle sources, suggesting a very thorough mixture of reservoirs. This explanation may appear reasonable without focusing attention on the porphyry copper deposits. However, the extremely restricted variation of Sr, Nd and Pb isotopic ratios and lack of correlation of these ratios with $SiO_2$ within copper-bearing porphyries of different ages and locations rules out upper crustal contamination as the source of radiogenic lead. Thus if the crustal reservoir dominates the Pb isotope variability (Hildreth and Moorbath, 1988) the contribution has to be through the subduction of continental materials. Consequently, subducted terrigenous sediments are most likely candidate as source of Pb. Hildreth and Moorbath (1988) indicated that the downgoing sediments in the Andean subduction zone are strongly dominated by trench-filling terrigenous turbidites, largely of Andean provenance. Terrigenous sediments are likely to have an average of the isotopic ratios of extensive sections of the surface of the crust. Analyses of river mouth sediments from several rivers of central Chile done by Hildreth and Moorbath (1988) show a restricted variation of Pb isotopic ratios coincident with those of arc rocks ($^{206}Pb/^{204}Pb$ = 18.535-18.678, $^{207}Pb/^{204}Pb$ = 15.591-15.620, $^{208}Pb/^{204}Pb$ = 38.404-38.588). These values are remarkably similar to the restricted range shown by the porphyry copper deposits.

Sediment subduction has been documented by geophysical studies of the Chile-Peru trench (e.g., Kulm and others, 1977; Schweller and others, 1981; Hilde, 1983) and by studies of $^{10}Be$ in recent arc lavas (Brown and others, 1982; Tera and others, 1986; Morris and others, 1987). This is considered an essential part of the subduction process according to modern models of convergent margins (e.g., Cloos and Shreve, 1988). Estimates of sediment incorporation are model-dependant but limiting case calculations of Morris and Tera (1989) suggest less than 4% sediment in models of bulk incorporation and larger amounts if a Be-poor fluid is involved. The average lead concentration in crustal materials is about 20 ppm, whereas estimates for the mantle suggest less than 0.5 ppm (Zartman, 1984). Therefore, although the terrigenous sediments are probably a volumetrically minor component of arc magmas, the Pb of the porphyry copper deposits and other deposits of the study area may well be dominated by a contribution from subducted terrigenous sediments.

### 7.2.7 Petrochemical constraints

The petrochemical characteristics of the copper-bearing intrusive rocks are examined in this section, and compared with those of the Upper Cretaceous - Eocene volcanic and intrusive rocks. No petrochemical modelling is included, but analogies with other Andean igneous units are made to illustrate possible magma evolution schemes. Variable degree of alteration of the rocks analyzed account for the spread of alkalies content. Chemical analyses and description of analytical methods used are presented in Appendix 3.

The igneous rocks associated with the porphyry copper deposits are sub-alkaline and calc-alkaline according to the AFM and alkalies versus silica diagrams, comparable to the earlier Late Cretaceous-Eocene volcanic and intrusive rocks (Figs. 7.7, 7.8). The silica content of the analyzed Upper Eocene - Lower Oligocene intrusive rocks, including pre-mineralization plutons, ranges from 59 to 80 % $SiO_2$

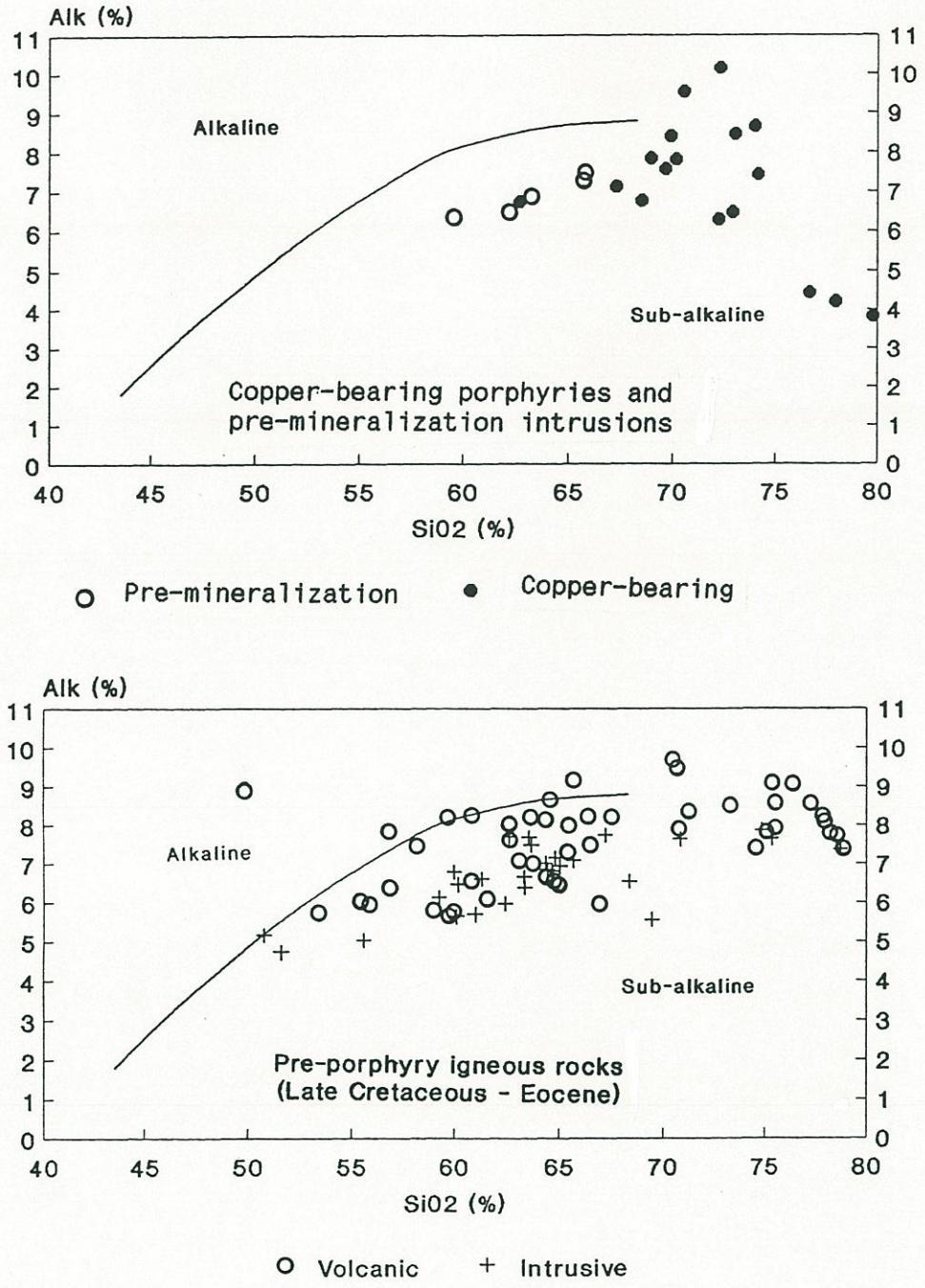


**Figure 7.7.** Alkalies versus silica diagrams for the copper-bearing porphyries and associated pre-mineralization granodiorites, and for the Upper Cretaceous to Eocene volcanic and intrusive rocks.

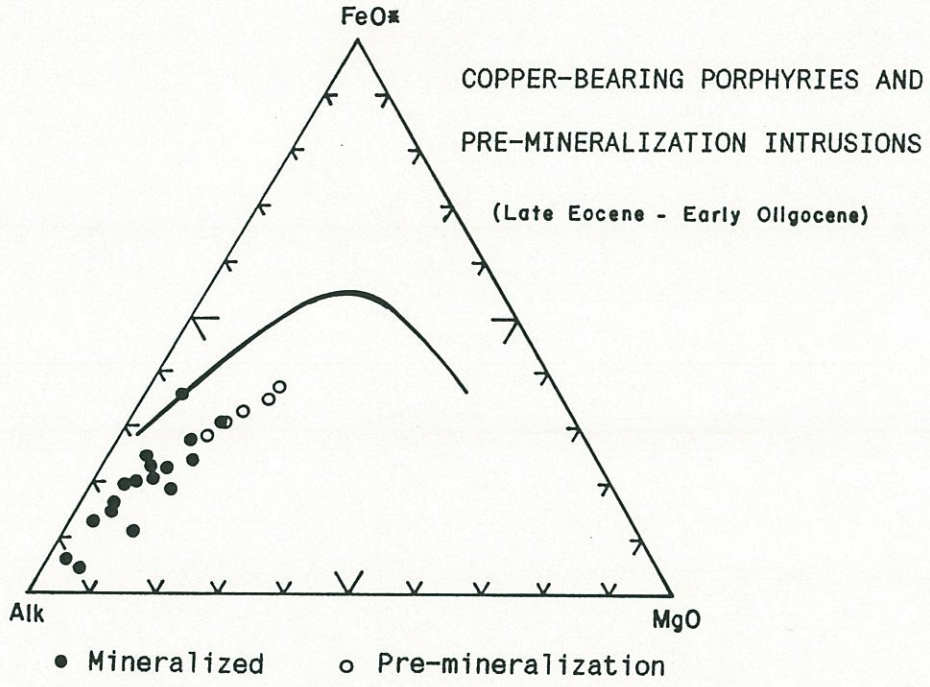


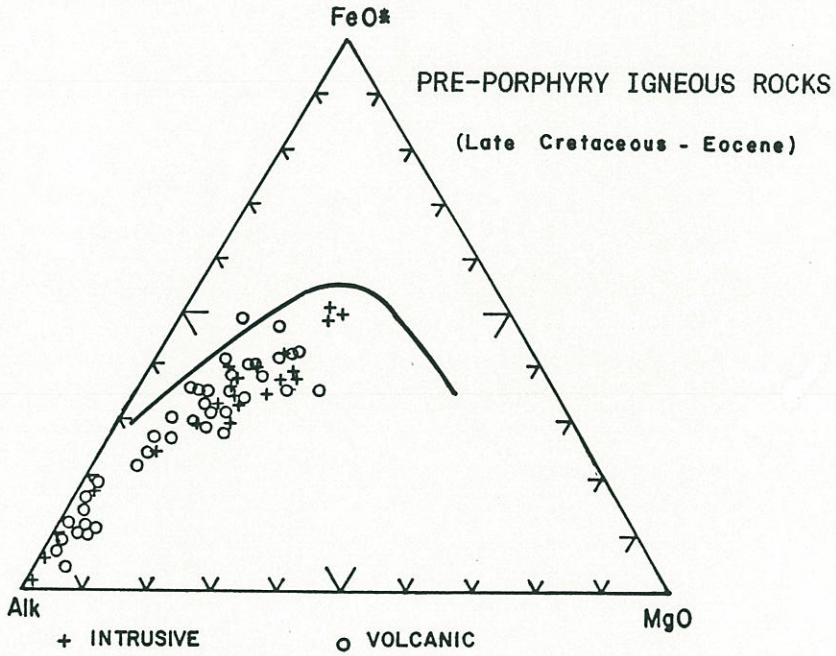


**Figure 7.8.** AFM diagrams for the copper-bearing porphyries and associated pre-mineralization granodiorites, and for the pre-porphyry Upper Cretaceous to Eocene volcanic and intrusive rocks.

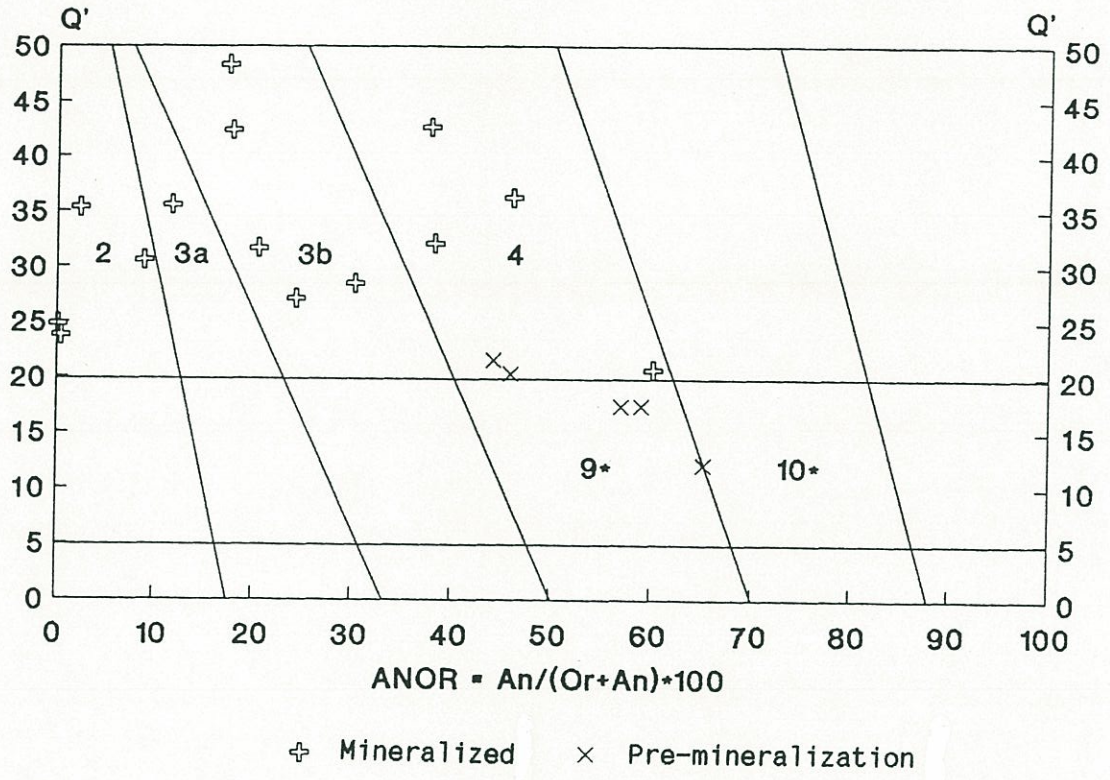


**Figure 7.9.** Chemical classification of copper-bearing rocks and associated Upper Eocene pre-mineralization intrusions (Fortuna Granodiorite and Southern Granodiorite of El Abra) on normative Q'-ANOR Diagram (after Streckeisen and Le Maître, 1979). Mineralized samples are enriched in $SiO_2$ and $K_2O$ due to potassic alteration. (2) Alkali-feldspar granite, (3a) Syenogranite, (3b) Monzogranite, (4) Granodiorite, (9*) Quartz monzodiorite, (10*) Quartz diorite. Q'= Q/(Q+Or+Ab+An)*100.

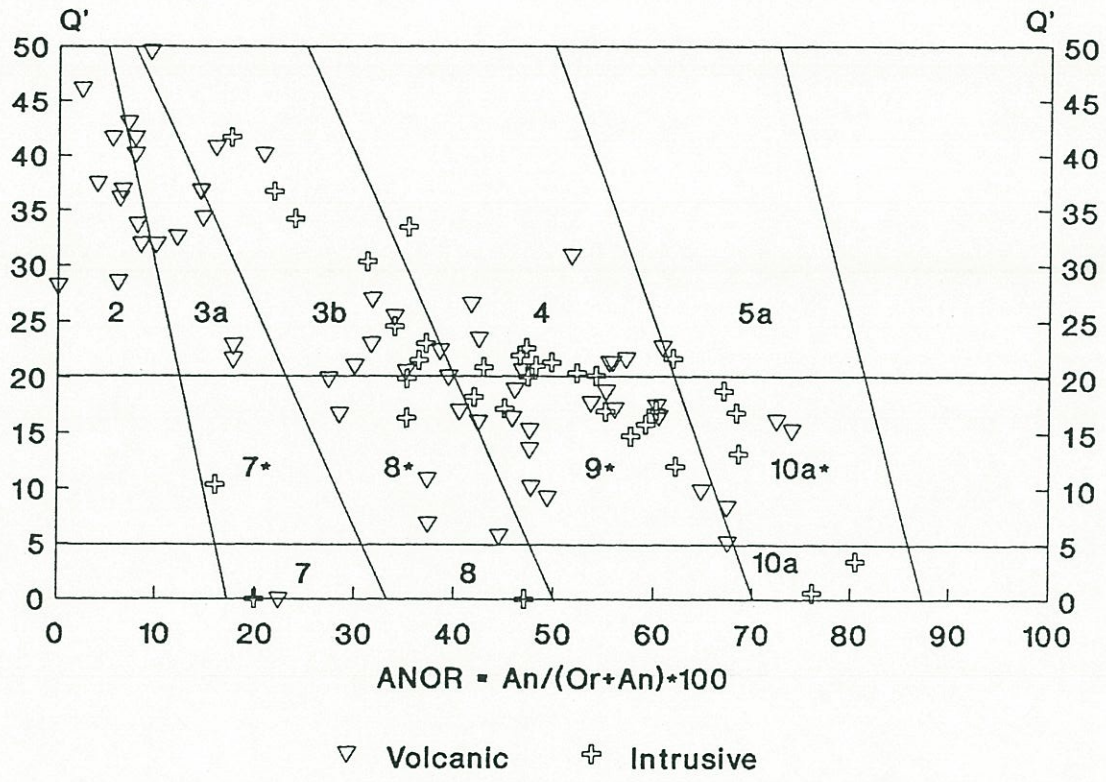


**Figure 7.10.** Chemical classification of the Upper Cretaceous to Eocene igneous rocks on normative Q'-ANOR diagram (after Streckeisen and Le Maître, 1979). (2) Alkali-feldspar granite - alkali-feldspar rhyolite, (3a) Syenogranite - rhyolite, (3b) Monzogranite - Rhyolite, (4) Granodiorite - Dacite, (5a) Tonalite - Dacite, (7*) Quartz syenite - quartz trachyte, (8*) Quartz monzonite - quartz latite, (9*) Quartz monzodiorite - andesite, (10a*) Quartz diorite - basaltic andesite, (10a) Gabbro - basalt. Q'= Q/(Q+Or+Ab+An)*100.

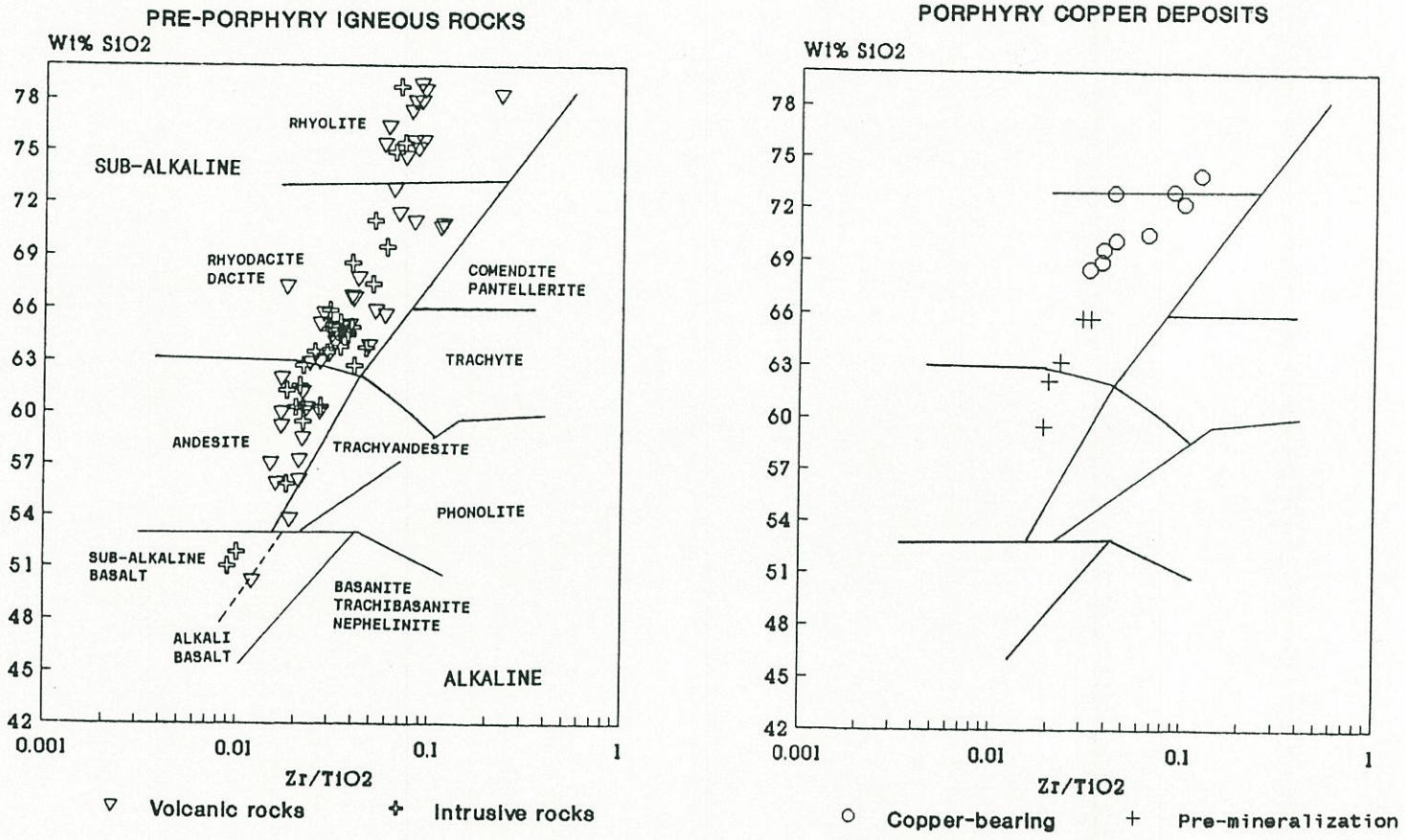


**Figure 7.11.** Classification of the igneous rocks associated to porphyry copper deposits and pre-porphyry magmatism using the diagrams of Winchester and Floyd (1977). The restricted compositional range of copper-bearing rocks is apparent, despite their high silica content due to potassic alteration.

(volatile-free basis), but the mineralized rocks from Chuquicamata, El Abra, Quebrada Blanca, Copaquire, and El Salvador fall in a more restricted range between 67 and 80 % $SiO_2$. The analyzed copper-bearing porphyries have pervasive potassic alteration that produced in Chuquicamata an increase of $SiO_2$ and $K_2O$, and decrease of $Fe_2O_3$, FeO, $Na_2O$, $MnO_2$, and MgO with $TiO_2$ largely unchanged (Alvarez and Aracena, 1985). Variations of major elements due to hydrothermal alteration complicate comparisons with unmineralized rocks, and account for the higher silica content of the mineralized rocks. The copper-bearing stocks are dominantly evolved biotite-bearing granodioritic and monzodioritic porphyries, but secondary hydrothermal K-feldspar, which is particularly prominent in Chuquicamata, shifts the chemical composition to granite (Fig. 7.9). In contrast, the silica content of the earlier Upper Cretaceous to Eocene volcanic rocks shows a broad range from 50 to 79 % $SiO_2$, and the coeval intrusive rocks from 51 to 79 % $SiO_2$ (Fig. 7.10). Consequently, a significant reduction in the compositional range of the igneous rocks occurred during the period of copper mineralization compared with the preceding igneous activity. The contrasting ranges of compositions are also illustrated using a classification diagram after Winchester and Floyd (1977) and Floyd and Winchester (1978) based on "immobile elements" (Zr, Ti) and $SiO_2$ (Fig. 7.11). Despite alteration most rocks fall in the field for rocks classified as "sub-alkaline," and show a trend characteristic of calk-alkaline igneous rocks (Fig. 7.11).

Upper Cretaceous to Eocene volcanic rocks (Augusta Victoria Formation) range from pyroxene-bearing basalts and basaltic andesites to rhyolites. These volcanics are characterized by high Ba/La (23.2-31.0) and La/Ta (21.0-30.9) ratios (alkaline earth/LREE and LREE/HFSE), which are typical of arc rocks (e.g., Kay and others, 1987, 1988). The trace element contents of the least siliceous Upper Cretaceous - Eocene igneous rocks (volcanic: II-34: 53.81 % $SiO_2$, II-27: 58.53 % $SiO_2$; intrusive: II-86: 51.88 % $SiO_2$, II-597: 51.05 % $SiO_2$; volatile-free basis) normalized to the average tholeiitic MORB of Pearce (1983) suggest significant enrichment of "large ion lithophile elements" (LILE) Sr, K, Rb, Ba, Th over "high field strength elements" (HFSE) Nb, Zr, P, Ti and Y

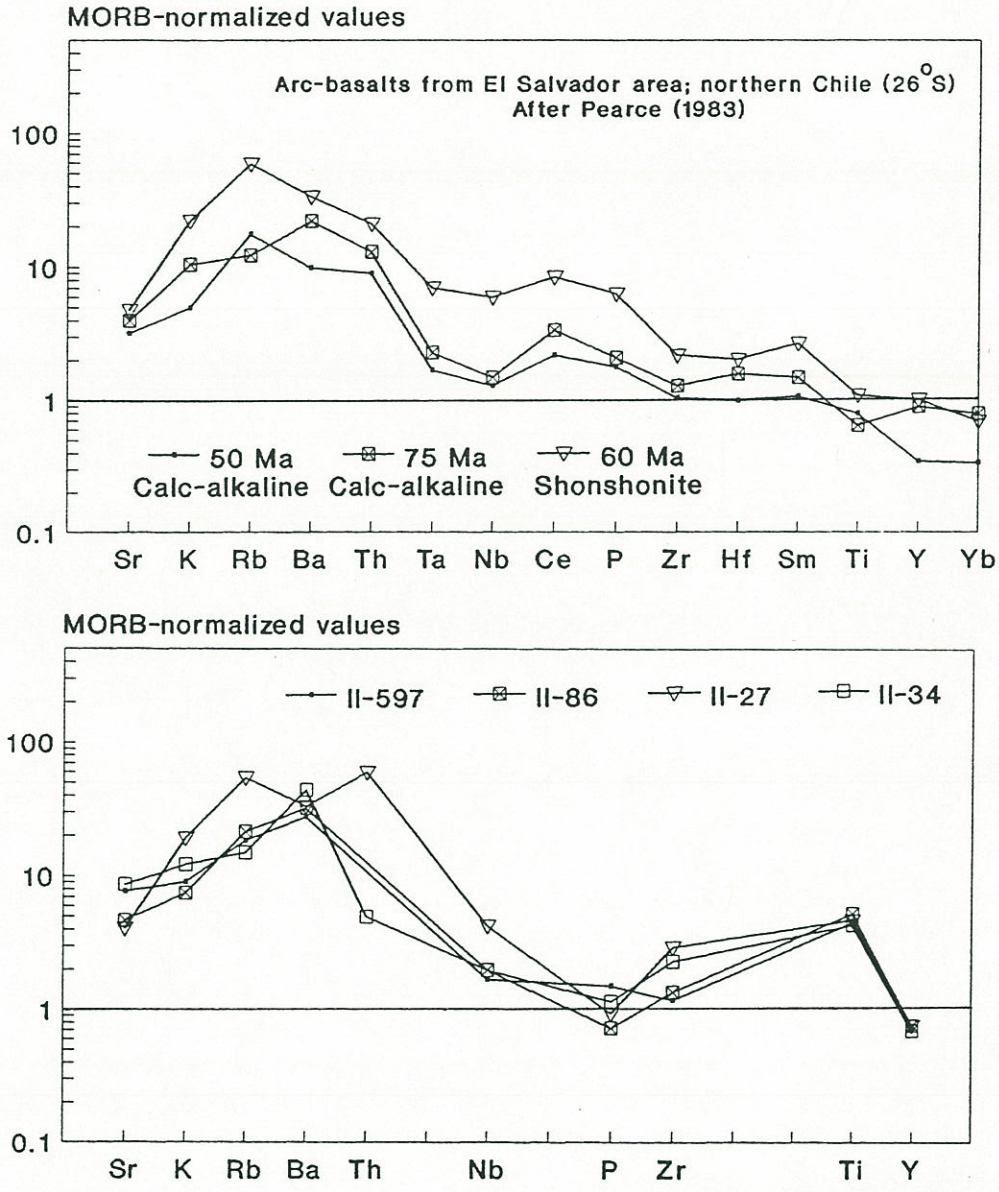


**Figure 7.12.** MORB-normalized diagrams of arc-basalts of northern Chile after Pearce (1983), and Upper Cretaceous to Eocene mafic intrusive and volcanic rocks. Normalization factors are from the average tholeiitic MORB of Pearce (1983): Sr 120, K 1500, Rb 2, Ba 20, Th 0.2, Ta 0.18, Nb 3.5, Ce 10, P 1200, Zr 90, Hf 2.4, Sm 3.3, Ti 1500, Y 30, Yb 3.4.

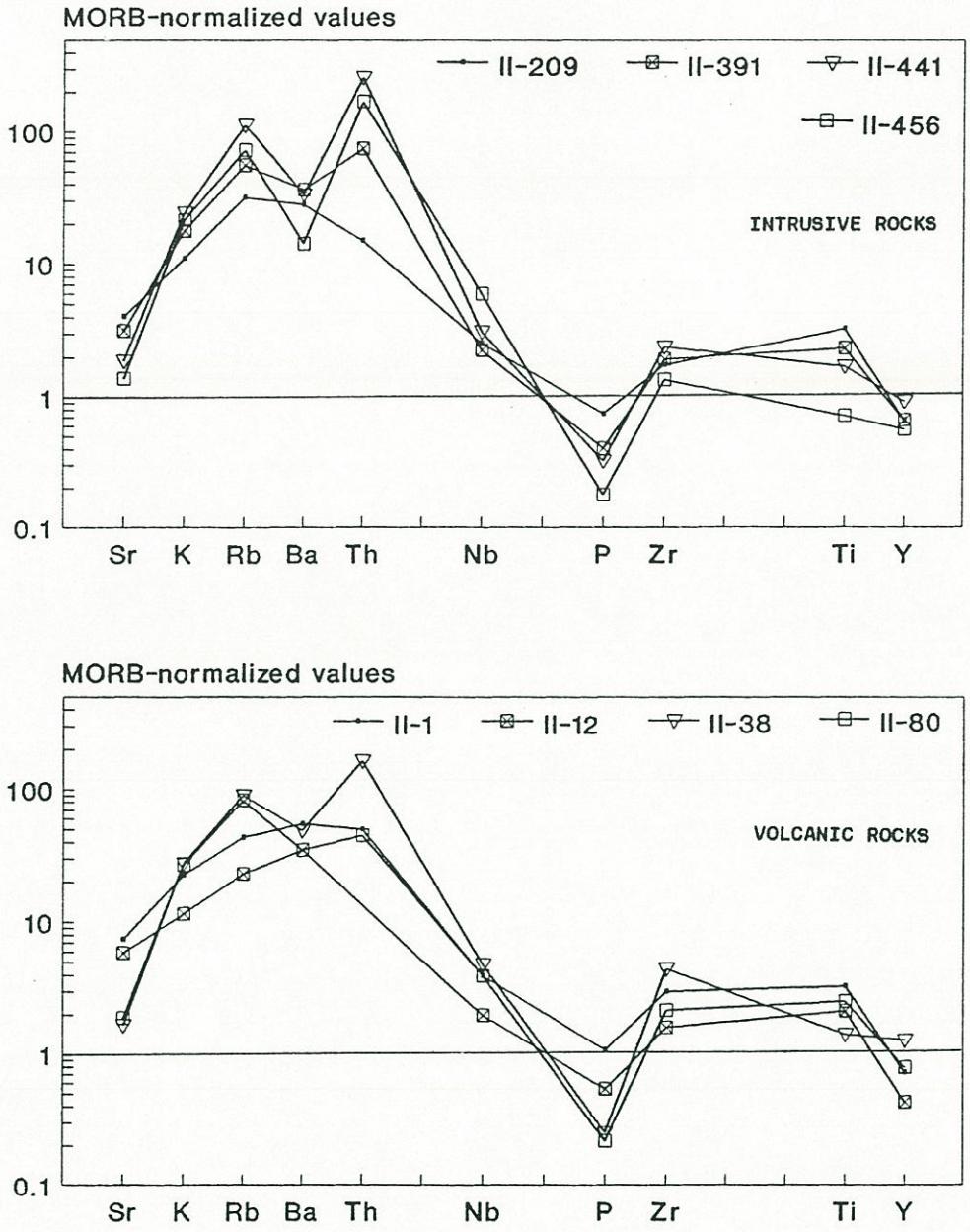


**Figure 7.13.** MORB-normalized diagrams of Upper Cretaceous to Eocene felsic intrusive and volcanic rocks.

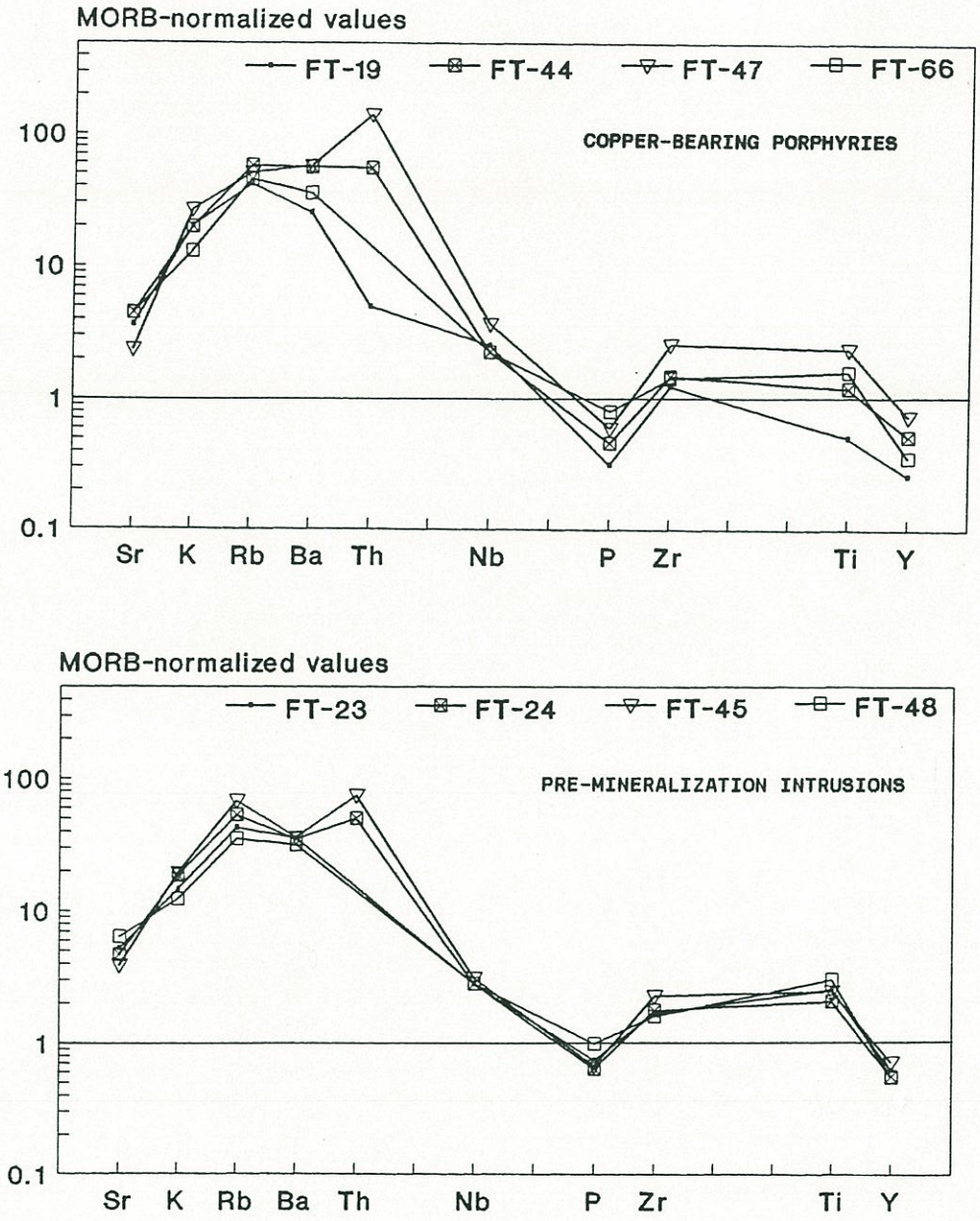


Figure 7.14. MORB-normalized diagrams of samples from copper-bearing porphyries and associated pre-mineralization granodioritic intrusions.

(Fig. 7.12) and enrichment of Nb, Zr, Ti and P (HFSE) relative to Y. The trace element pattern obtained for these rocks is closely comparable to those obtained by Pearce (1983) for arc basalts from the area of the El Salvador porphyry copper deposit in northern Chile (Fig. 7.12), and arc basalts from the Southern Volcanic Zone (37°-46°) of the Andes (Hickey and others, 1986). Thus, the trace element patterns of these rocks are compatible with sub-crustally derived, calc-alkaline arc magmas. LILE enrichment over HFSE is typical of subduction-related magmas (Hawkesworth, 1982; Pearce, 1983; Hole and others, 1984). Most investigators ascribe such enrichment to a "subduction component" (e.g., Pearce, 1983; Kay, 1980), because similar enrichment commonly occurs in basalts of intra-oceanic islands arcs, where there is little chance for magma interaction with continental crust. The enrichment of Nb, Zr, and Ti relative to Y is common in within plate oceanic and continental basalts (ocean island and continental plateau basalts), but it is not observed in basalts of oceanic island arcs. The latter, in contrast, show typically the depletion of HFSE relative to MORB. Enrichment of Nb, Zr, and Ti relative to Y is relatively common in Andean arc igneous rocks (e.g., Pearce, 1983, Atherton and others, 1983, Rogers, 1985; Buchelt and Tellez, 1988). As shown above, such HFSE enrichment could not be a subduction component, nor is it compatible with crustal interaction (e.g., Pearce, 1983). The latter author attributed the relative enrichment of Nb, Zr, P and Ti to a contribution from trace element enriched, metasomatized sub-continental lithosphere, which may act as a reservoir for incompatible elements over a long period of time. Pearce's argument is based on evidence from mantle xenoliths and basaltic magmas erupted in continental within plate settings that indicate that the sub-continental lithosphere has been variably enriched in incompatible elements by fluid metasomatism. Other authors (e.g., Morris and Hart, 1983; Hickey and others, 1986; Arculus and Powell, 1986) have favoured an oceanic island basalt (OIB, *cf.* Thompson and others, 1984) mantle source for arc magmas. However, Perfit and Kay (1986) have contended that incompatible element ratios in evolved rocks bear no information of source characteristics because they may be significantly modified by shallow-level fractionation. Unfortunately, primitive basalts are lacking in the Upper Cretaceous to Eocene volcanics,

and the rocks associated with the porphyry copper deposits are typically evolved intermediate to felsic rocks.

The intermediate to felsic Upper Cretaceous-Eocene intrusive and extrusive rocks display enrichment of K, Rb, Th, Nb and Zr relative to their basic counterparts. Sr remains either unchanged or declines, and a significant decrease of P is apparent (Fig. 7.13). The mineralized porphyries show trace element patterns closely comparable to those of the older felsic rocks (REE excluded), although a marked decrease in Y and also of Ti is evident in some samples (Fig. 7.14). Pre-mineral Upper Eocene intrusions show a similar pattern, but the drop of P is less pronounced relative to the mineralized rocks and older igneous rocks (Fig. 7.14). Thus both the older igneous rocks and those associated with the porphyry copper mineralization have similar trace elements content (REE excluded), which are compatible with sub-crustal calc-alkaline magmas generated at an active continental margin setting. The only apparent difference is the lower content of Y in copper-bearing stocks relative to unmineralized rocks. Baldwin and Pearce (1982) showed, based on rock analyses from the El Salvador - Potrerillos district, that mineralized intrusions show a significant depletion of Mn, Y, Yb and P compared with unmineralized intrusive rocks. They proposed a Y versus $MnO_2$ diagram for discriminating between productive (copper-bearing) and non-productive intrusive rocks. This diagram shows a significant split between the chemical data from unmineralized intrusive rocks and from porphyry copper deposits of the Antofagasta Region (Fig. 7.15). However, the distribution of the data points does not fit the boundaries proposed by Baldwin and Pearce (1982). In addition, two unmineralized altered quartz porphyries (from Cerro Buenos Aires and Anillo alteration zones) plot in the mineralized field. The diagram would appear to discriminate between **altered** and **unaltered** rocks, rather than mineralized versus unmineralized ones. Alternatively, it may suggest that these zones, which have been sites of (so far) unsuccessful exploration, may be promising prospects.

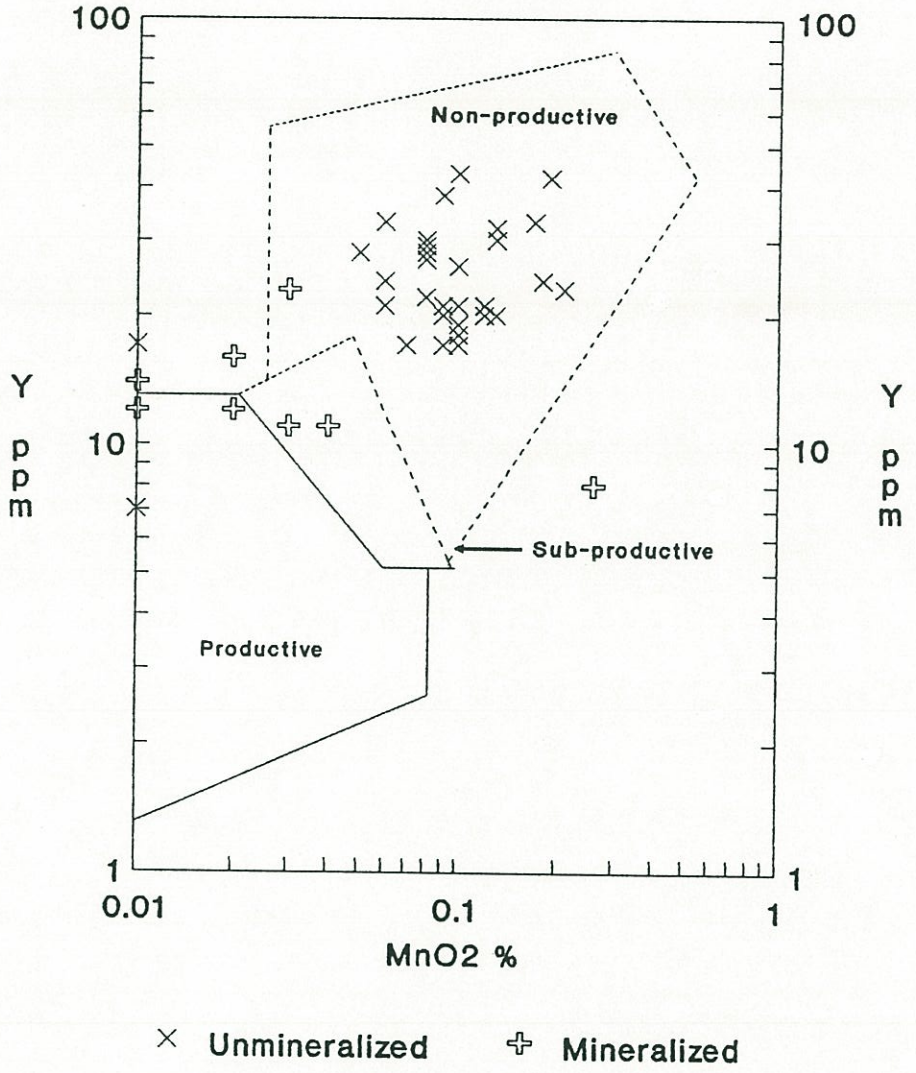


Figure 7.15. Discriminant diagram of Baldwin and Pearce (1983) between productive and non-productive intrusions. There is obvious segregation of the mineralized and unmineralized samples, although they do not fit the boundaries proposed by Baldwin and Pearce (1983). Two altered unmineralized samples plot in the productive field, suggesting that the diagram discriminates based on alteration rather than mineralization.

Chondrite-normalized[6] rare earth patterns of mineralized rocks from Chuquicamata and El Salvador show significant enrichment in light rare earth elements (LREE) (La 30 to 120 times chondrite) and conspicuously low contents of heavy rare earth elements (HREE) (Yb 2.4 to 2.8 times chondrite; Fig. 7.16). This implies strong REE fractionation between melt and a residual mineral phase that retained HREE's during magma genesis (e.g., garnet or amphibole). The La/Yb ratios are high, ranging between 15 and 35, in contrast to the significantly lower La/Yb ratios (less steep REE patterns; Figs. 7.18) of the Early Tertiary andesites and dacites of the Augusta Victoria Formation (9.5 to 14.5) and the 63 Ma Cerros de Montecristo and 65 Ma Cerro Colorado plutons (4.5 to 10.3; Rogers, 1985) (Fig. 7.20). The rhyolites of the Augusta Victoria Formation show moderate La/Yb ratios (17.1-19.2) but they are significantly more enriched in HREE's (Yb 5.4 to 8.6 times chondrite) compared with the copper-bearing stocks, and show conspicuous negative Eu anomalies (Eu/Eu* 0.49-0.68; Fig. 7.19), which are lacking in the latter (Figs. 7.16, 7.17). This suggests that their REE patterns are partially, if not wholly, attributable to relatively low pressure crystal fractionation of phases that selectively removed the middle and heavy REE (plagioclase, amphibole, clinopyroxene, apatite). These characteristics are similar to those of Oligocene to Lower Miocene rhyolites of the Tilito Member of the Doña Ana Formation (Chilean Andes 29° to 30°30' S; Kay and others, 1987, 1988). Therefore they may have evolved in a similar way by fractional crystallization from their more mafic counterparts.

The presence of garnet as a stable phase in the source region of magmas may significantly steepen REE patterns as this mineral effectively retains HREE (Nichols and Harris, 1980). Retention of amphibole in the source region or fractionation of amphibole can also steepen the REE patterns. However, without garnet even extreme amphibole fractionation results in La/Yb ratios of only 14-15, as observed in

---

[6] Normalization factors from the Leedy Chondrite: La 0.378, Ce 0.976, Nd 0.716, Sm 0.23, Eu 0.866, Tb 0.0589, Yb 0.249, and Lu 0.0387.

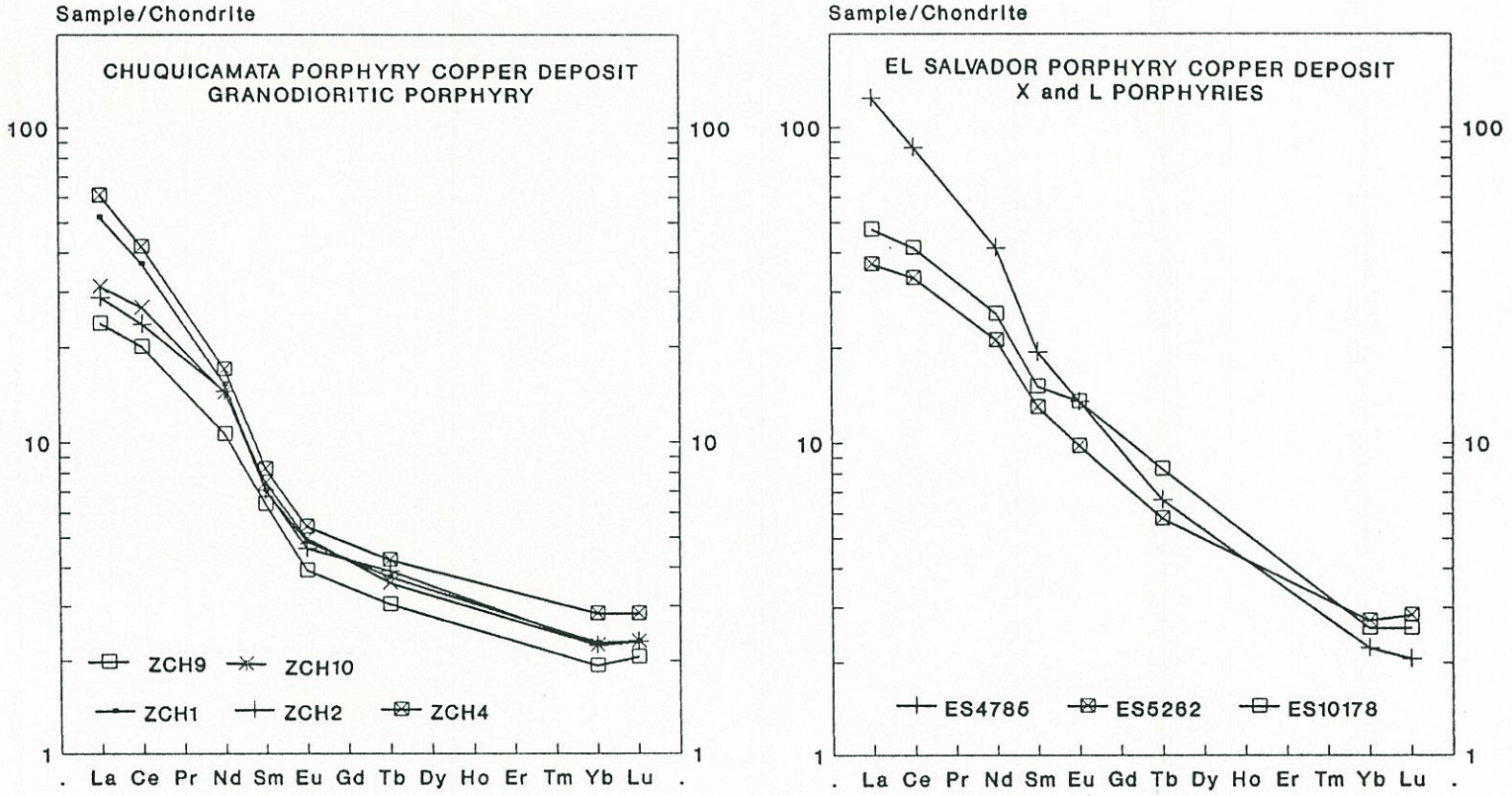


**Figure 7.16.** Chondrite-normalized REE patterns of copper-bearing porphyries from Chuquicamata and El Salvador porphyry copper deposits. Normalization factors from the Leedy Chondrite: La 0.378, Ce 0.976, Nd 0.716, Sm 0.23, Eu 0.866, Tb 0.0589, Yb 0.249, and Lu 0.0387.

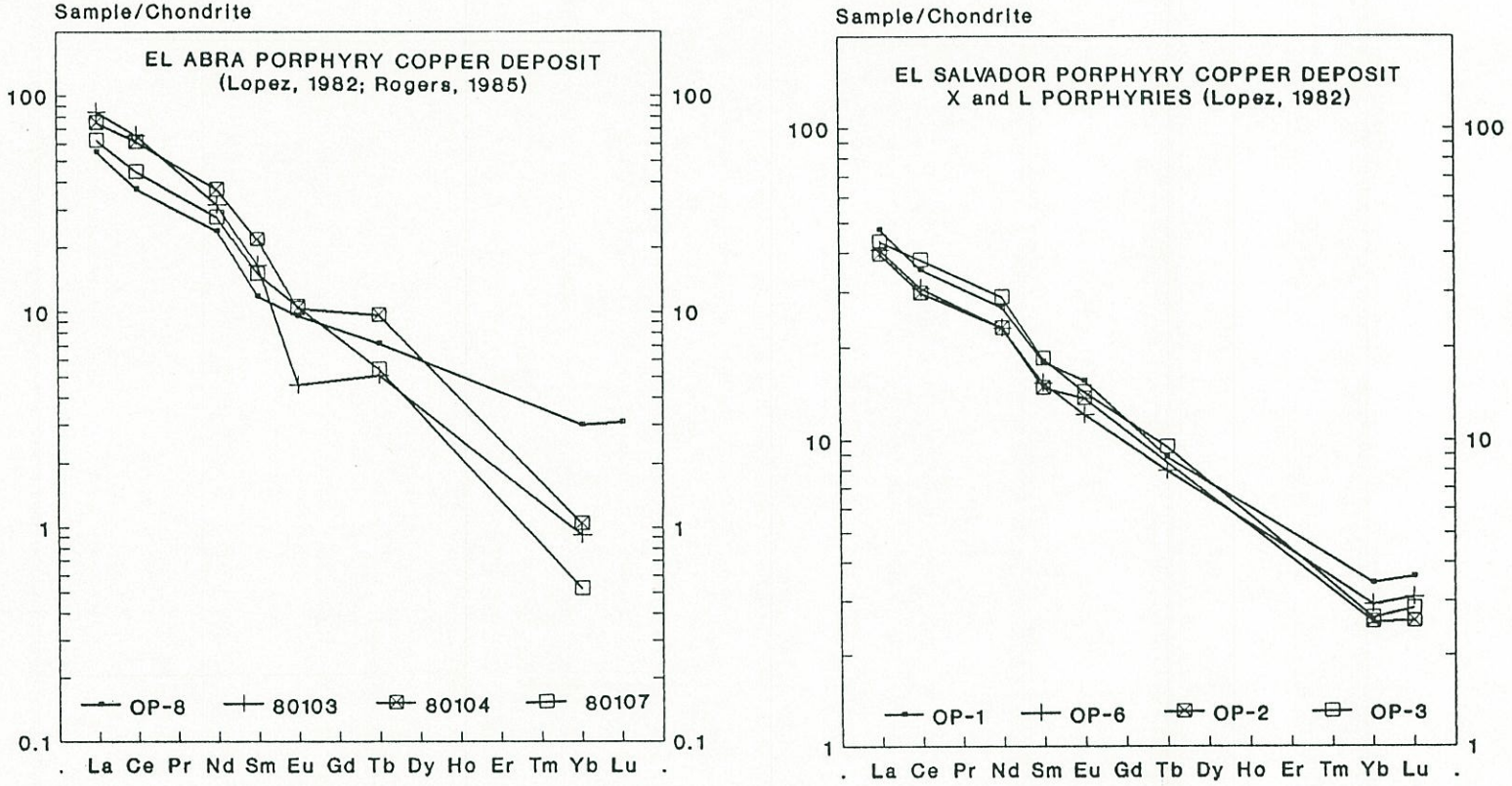


**Figure 7.17.** Chondrite-normalized REE patterns from El Abra and El Salvador porphyry copper deposits, based on data of Rogers (1985) and Lopez-Escobar (1982). The samples 80103, 80104, and 80107 are from the pre-mineral Southern Granodiorite of El Abra (Rogers, 1985).

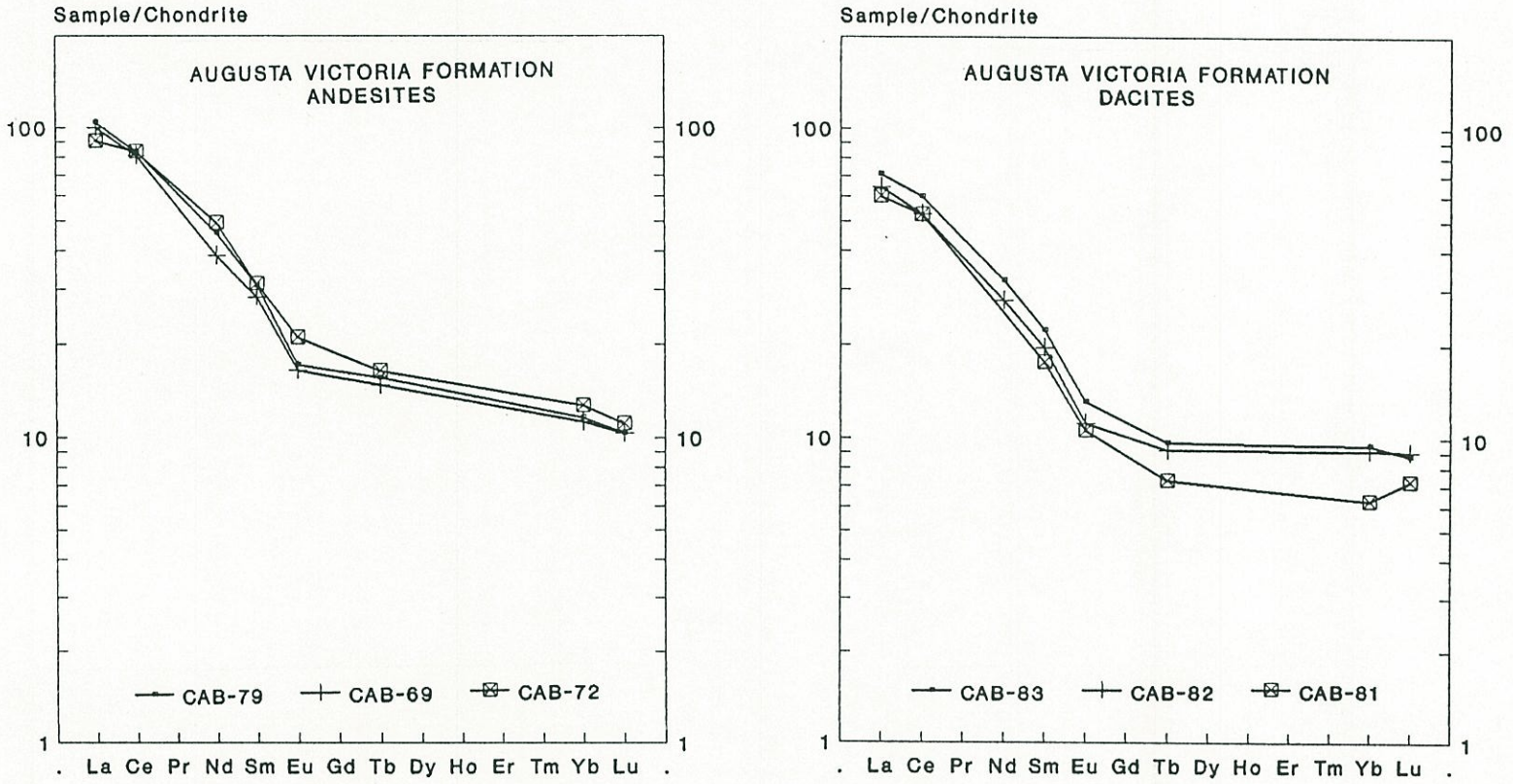


Figure 7.18. Chondrite-normalized REE patterns of andesites and dacites of the Augusta Victoria Formation (pre-porphyry volcanism; Late Cretaceous - Eocene).

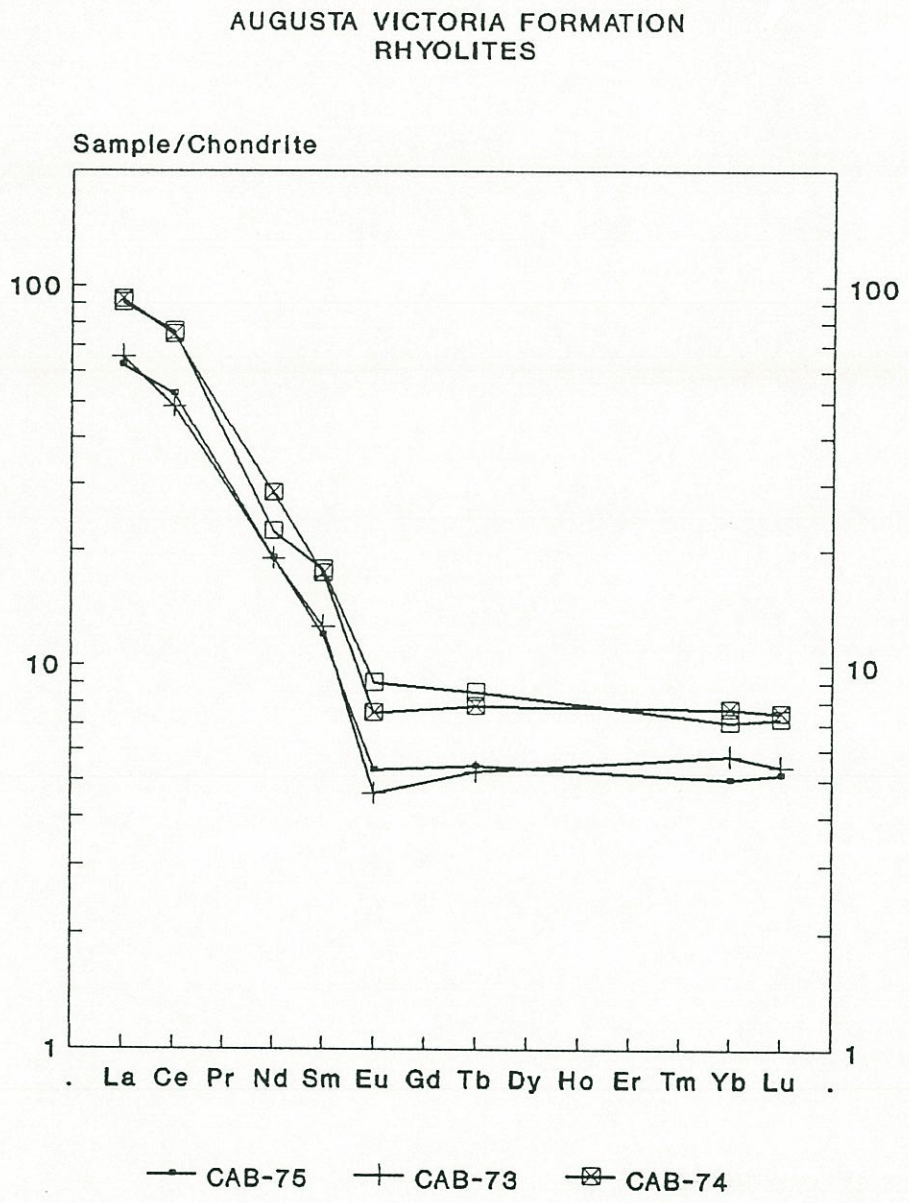


**Figure 7.19.** Chondrite-normalized REE patterns of rhyolites of Augusta Victoria Formation (pre-porphyry volcanism; Late Cretaceous - Eocene): note the marked Eu negative anomalies of these siliceous volcanic rocks, compatible with increased role of plagioclase fractionation.

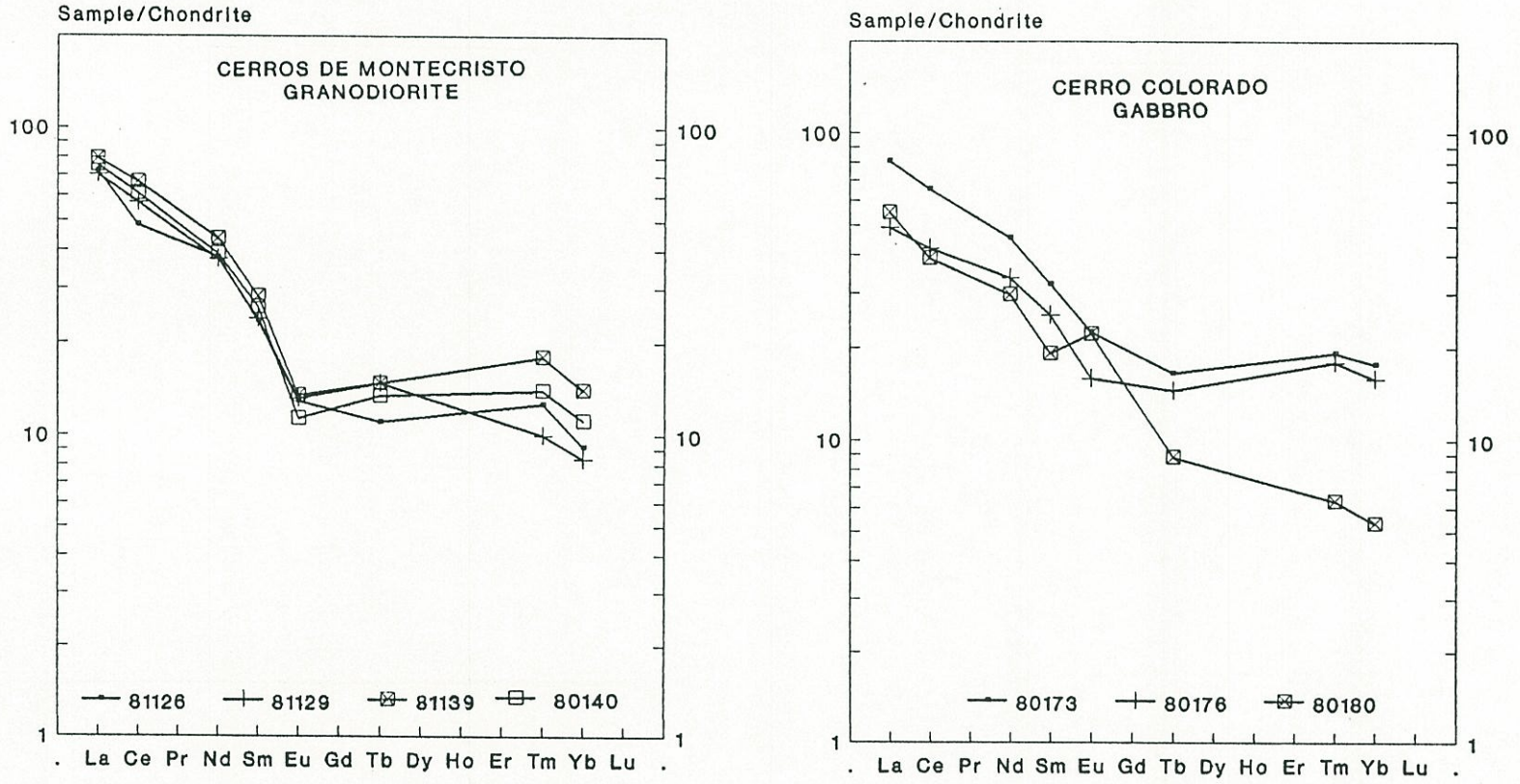


**Figure 7.20.** Chondrite-normalized REE patterns of the 63 Ma Cerros de Montecristo granodioritic pluton and 66 Ma Cerro Colorado gabbroic intrusion (pre-porphyry plutonism); Data after Rogers (1985).

Aleutian plutonic rocks (e.g., Kay and Kay, 1989). The fractional crystallization of hornblende in granodioritic magmas is thought to produce a marked decrease in the NaCl/KCl ratio, which would account for the extensive potassic alteration associated with porphyry copper deposits (Burnham and Ohmoto, 1980). Therefore fractionation of amphibole probably took place during evolution of magmas associated with porphyry copper deposits. Amphibole fractionation produces the relative depletion in the middle REE (Nichols and Harris, 1980). The concave upwards REE patterns of Chuquicamata (Fig. 7.16) may be partly attributable to the effect of amphibole fractionation, whereas REE patterns of El Salvador and El Abra are essentially straight (Lopez-Escobar, 1982, 1984; Rogers, 1985) suggesting a dominant role for garnet (Figs. 7.16, 7.17). Zircon is another phase which preferentially takes HREE and can steepen the REE pattern, but zircon fractionation is unlikely because the Th content of copper-bearing porphyries is not depleted (Fig. 7.14).

Another factor that may have influenced the REE patterns is the hydrothermal alteration associated with porphyry copper deposits. The effect of alteration on REE patterns has not been extensively investigated, although Taylor and Fryer (1982) showed that a potassically altered granodiorite porphyry from Bakirkay, northern Turkey has increased light and intermediate REE and depleted HREE relative to the unaltered rock. However, the question of whether the overall steep REE pattern (hence high La/Yb ratio) is intrinsic to the mineralized rocks or just a combination of amphibole fractionation and alteration overprint remains open. The REE patterns of the unaltered pre-mineral Upper Eocene Southern Granodiorite of El Abra are steep with a particularly marked depletion of HREE (Yb 0.13 to 3.01 times chondrite; Rogers, 1985) (Fig. 7.17) and La/Yb ratios ranging between 15 and 26.4. This suggests that steep REE patterns are intrinsic to Late Eocene-Early Oligocene intrusions rather than an alteration overprint.

Several authors have used steep REE patterns of Andean volcanic rocks to infer garnet in the source region (e.g., Lopez-Escobar and others, 1977; Lopez-Escobar, 1982, 1984; Kay and others, 1987, 1988;

Hildreth and Moorbath, 1988; Stern, 1988, 1989). In addition, Lopez-Escobar (1982, 1984) showed that irrespective of their age rocks from the El Abra, El Salvador, and Rio Blanco-Disputada porphyry copper deposits show typically steep REE patterns similar to andesites of the northernmost section of the Southern Volcanic Zone of the Andes (33°-34°S). This author also implied that garnet had been in equilibrium with melts at high pressure. The same inference was made by Rogers (1985) from REE patterns of the southern Granodiorite of El Abra (Fig. 7.17).

The incompatible trace element signatures (e.g., La/Sm, La/Yb ratios) of the andesites and dacites of the pre-porphyry Augusta Victoria Formation and the gabbroic and granodioritic intrusions of the Cerro Colorado and Cerros de Montecristo (Rogers, 1985), are similar to andesites of many other convergent margins particularly the SVZ (e.g., Lopez-Escobar, 1984; Hickey and others, 1986) and the Oligocene-Early Miocene volcanic rocks of the Andes between 29° and 30°30' S. (Doña Ana Formation; Kay and others, 1987, 1988). The composition of basaltic rocks of the southern section of the SVZ (37°-46°S) is consistent with a petrogenetic model involving partial melting of garnet-free peridotite followed by 10-20% crystal fractionation of olivine ± pyroxene (Lopez-Escobar, 1984). Low pressure fractionation accounts for the more felsic varieties. Generalized fractionation models for the Doña Ana volcanics are also consistent with magmatic evolution in a relatively garnet-free crust and asthenospheric mantle (Kay and others, 1987, 1988). Similar processes may account for the generation of pre-porphyry igneous rocks.

The higher La/Yb and La/Sm ratios of copper-bearing porphyries (Figs. 7.21, 7.22) compare to those of Andean Miocene volcanics of 29°-30°30'S (Kay and others, 1987, 1988), the lavas of the northernmost section of the SVZ (33°S) (Lopez-Escobar, 1982, 1984; Kay and others, 1990), and Neogene volcanic rocks of the CVZ (Dostal and others, 1977). Lopez-Escobar (1984) demonstrated that a single-stage petrological model involving the partial melting of oceanic basalts (eclogite) is incompatible with the petrochemical data of andesites of the northernmost section of the SVZ. He developed a model involving less than 5% fractional

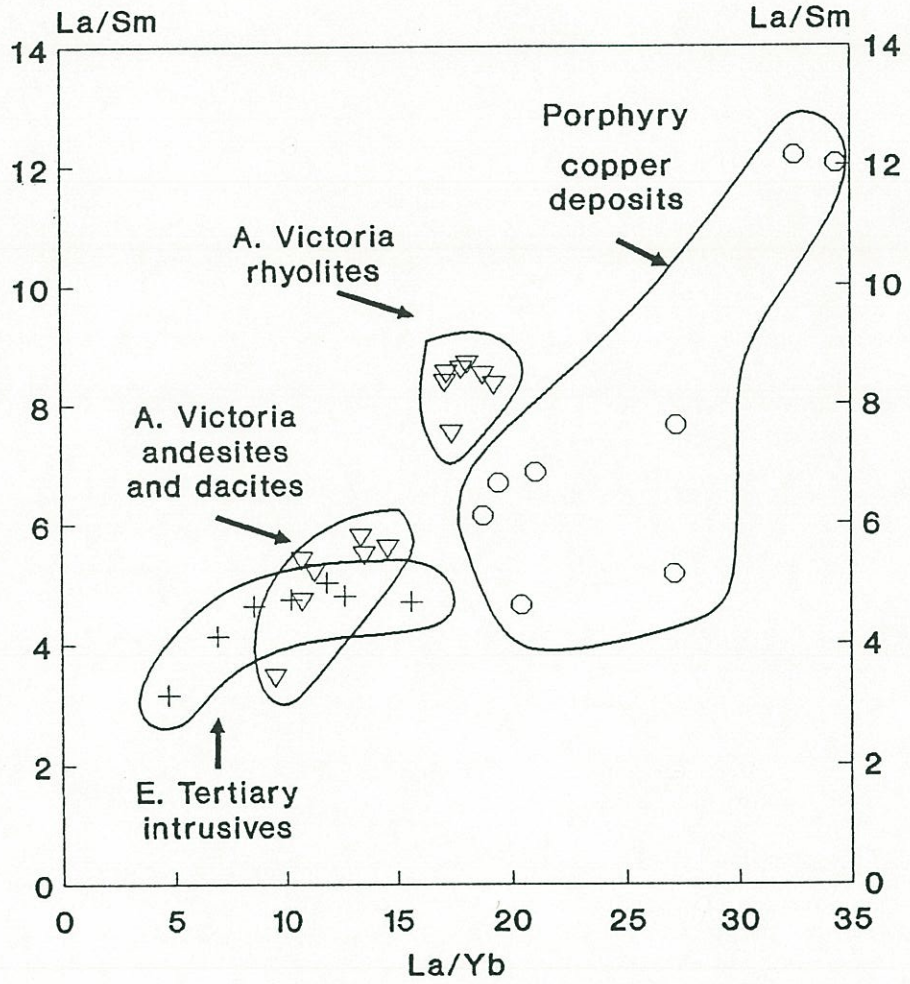


Figure 7.21. La/Sm versus La/Yb ratios of samples from copper bearing porphyries and pre-porphyry igneous rocks.

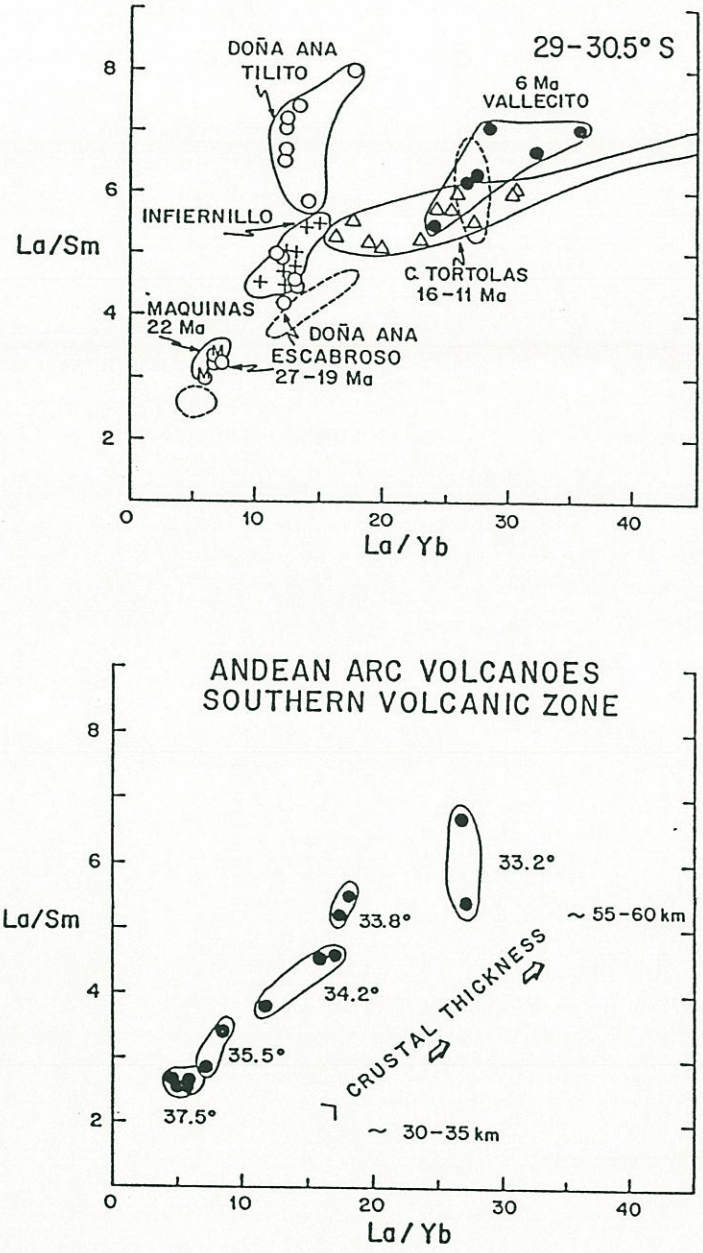


**Figure 7.22.** La/Sm versus La/Yb ratios for Oligocene-Miocene samples from the Andes between 29°-30.5° S, showing the overall increase of La/Yb and La/Sm ratios following a Miocene crustal thickening and flattening of the subduction zone (after Kay and others, 1987, 1988, 1990), and the northward increase of La/Yb and La/Sm ratios along the Southern Volcanic Zone of the Andes after Kay and others (1990) based on data of Hickey and others (1986) and Futa and Stern (1988). Crustal thicknesses are estimated by Hildreth and Moorbath (1988).

melting of garnet peridotite (about 5% residual garnet) at more than 70 km in depth (where garnet is a stable phase) followed by 20% fractional crystallization of olivine ± clinopyroxene, suggesting a similar origin for igneous rocks associated with Chilean porphyry copper deposits. The high LILE and LREE's imply a contribution from the subducted slab, which could be either fluids derived from the dewatering of oceanic crust or melts generated by low degrees of partial melting of eclogite (less than or equal to 5% according to Lopez-Escobar, 1984). An important role for garnet was also implied by Kay and others (1987, 1988) for the origin of the Miocene volcanics of 29°-30°30' S. and for the Neogene volcanics of the CVZ by Dostal and others (1977). Thus, despite the possible influence of amphibole fractionation and potassic alteration, the REE patterns of copper-bearing porphyries are consistent with their derivation as fractionation products of andesitic or basaltic magmas having originated by partial melting of garnet peridotites. Although, partial melting of eclogite, garnet granulite or other garnet-bearing rock in the lower crust cannot be ruled out. Hildreth and Moorbath (1988) contended that the sink of HREE is more likely to lie within a thicker crust rather than in the mantle wedge. These authors argued that garnet-bearing granulites, gabbros and eclogites are expected to be stable under thickened crust (such as the northernmost SVZ) and that garnet could even be a phenocryst in basaltic and andesitic magmas under the 12-17 kb pressures of deep crust. Accordingly they envisage that the main role of garnet may lie in the environment of lower-crustal mixing and homogenization, where LREE-rich crustal partial melts strongly depleted in HREE are mixed with basaltic magmas evolving toward andesitic ones.

The origin of porphyry copper magmas is obviously similar to that of other andesitic-dacitic arc magmas in the Andes. However, there is yet no consensus about the origin of the latter. Studies of volcanic rocks from the southern volcanic zone of the Andes (33°-42°S) have shown that SVZ magmas are compositionally very similar to those of intra-oceanic island arcs (Harmon and others, 1984; Hickey and others, 1984, 1986). These similarities led many workers to conclude that SVZ lavas are mostly uncontaminated by continental crust. Although most

investigators still agree that mantle-derived basaltic magmas are modified at crustal pressures by fractional crystallization and, perhaps magma mixing, for generating intermediate to felsic arc rocks (Frey and others, 1984; Gerlach and others, 1988; Hickey and others, 1984; Lopez-Escobar, 1984; Lopez-Escobar and others, 1977, 1981; McMillan and others, 1989), there has been an intense debate upon the extent of crustal contamination during the evolution of dacites and andesites of the SVZ, and the relative contributions of oceanic crust, mantle wedge, and continental crustal sources to parental mafic magmas (Davidson and others, 1987, 1988; Grunder, 1987; Frey and others, 1984; Harmon and others, 1984; Hickey and others, 1984, 1986; Hildreth and Moorbath, 1988; Lopez-Escobar, 1984; Lopez-Escobar and others, 1977, 1981). Recent work based on trace-element and O isotopic data in the northern SVZ (Davidson and others, 1987, 1988; Grunder, 1987; Hildreth and Moorbath, 1988) indicates that crustal contamination is an integral process in the production of arc magmas of the SVZ and that restricted ranges of isotopic composition occur when parental basalts and crustal contaminants have similar isotopic signatures (McMillan and others, 1989). Hildreth and Moorbath (1988) and Davidson and others (1987, 1988) stressed the importance of continental crust in a deep-seated assimilation process, named MASH (melting, assimilation, storage, and homogenization) by Hildreth and Moorbath (1988). These authors envisage that deep beneath each large magmatic centre, basaltic magmas ascending from the mantle wedge become neutrally buoyant at the interface mantle-crust or lowermost crust. Therefore, these magmas accumulate there inducing local melting, assimilation and extensive mixing. The magmas either crystallize completely or fractionate to the degree necessary to re-establish magma ascent. Magmas ascending from such zones may range from evolved basalts to dacites, but all will have acquired a base-level isotopic and trace-element signature characteristic of that particular MASH domain. By the MASH process Hildreth and Moorbath (1988) mean not simple contamination of basalts in the lower crust but true magma generation there (thermally induced by intrusion and crystallization of basalt) on a scale large enough that tens of percent of subsequently ascending mixtures can be of deep crustal derivation. The evolved character of the intrusive rocks associated with porphyry copper

deposits, their remarkable isotopic homogeneity, and no obvious interaction with the upper crust makes the MASH process particularly appealing for explaining such characteristics. The question is whether the MASH process has the capacity to produce identical isotopic signatures in copper-bearing porphyries of different ages and separated by thousands of kilometres along the Andes.

Stern (1988; 1989; in press) argues that the flattening of the subduction zone is ultimately accountable for more crustal participation in magma genesis in the northern SVZ, due to a decrease in the volume of sub-arc mantle and increased subduction of sediments and subduction erosion of the continental edge. Stern (*op. cit.*) suggested that these processes are significant, not only in the generation of the distinctive characteristics of magmas erupted along the present volcanic front between 33° and 34° S., but also in the genesis of the Late Miocene - Pliocene porphyry copper deposits of Los Pelambres, Rio Blanco-Disputada, and El Teniente located between 32 and 34° S. Stern (*op. cit.*) further proposed that those are key processes in generating the magmas of major porphyry copper deposits in northern Chile. Unfortunately, it is very difficult to evaluate the angle of subduction during the formation of the porphyry copper deposits of northern Chile or elsewhere. On the other hand, the alternative generation of magmas of porphyry copper deposits of central Chile following the crustal thickening related to the Miocene Quechua compressive phase cannot be ruled out, and therefore their origin may be unrelated to the flattening of the subduction zone, which took place in the segment between 28°-33° S. (Kay and others, 1987, 1988). In fact, the giant El Teniente deposit is located south of the present zone of "flat-slab" subduction. The probable result of subduction erosion of continental materials, as suggested by Stern (1988, 1989), is larger variations of isotopic ratios and compositional ranges of magmas, such as those observed in the CVZ (e.g., Thorpe and others, 1982). The porphyry copper deposits appear to have the same restricted Sr, Nd and Pb isotopic signature irrespective the nature of their basement or age.

In summary, intrusive rocks associated with porphyry copper deposits are petrochemically similar to other intermediate to felsic calc-alkaline volcanic and intrusive rocks of the Andes. Thus their origin is similar to other andesitic-dacitic arc magmas. However, there is still intense debate on the processes involved in the genesis of the latter. The main petrochemical difference between pre-porphyry igneous rocks and the copper-bearing stocks is the strong depletion of HREE in the latter. This suggest that the copper-bearing stocks crystallized from melts that had been in equilibrium with garnet at high pressures. This is compatible with a deeper magma generation (higher pressure) or cooling of the source region (evolution at lower temperatures) or both.

### 7.2.8 Mantle versus crustal REE fractionation in porphyry copper magma genesis

Trace element relations may provide some indication whether the characteristics of the REE patterns discussed above were primarily generated in the mantle or in the crust. The relations between Sr and REE's (particularly Eu) are important because they are concentrated in feldspar, a mineral common in the crust, but rare or absent in the mantle, so that they may record the role of minerals at high pressure that may not be present in the dominantly low pressure mineralogy. The range of variation of the REE and Sr is shown in plots of normalized ratios of La/Sr versus La/Yb and Eu/Eu*[7] (Fig. 7.23). The La/Yb versus La/Sr plot shows two trends, one with increasing La/Sr ratio and limited variation of La/Yb and other with increasing La/Yb ratio and limited variation of La/Sr ratio. The first extreme is defined by the silicic rhyolites of the pre-porphyry Augusta Victoria Formation and the second by the silicic copper-

[7] Eu* is the expected Eu concentration obtained by interpolating between Sm and Gd as though there were no anomaly, so that Eu/Eu* is less than 1 for negative anomalies.

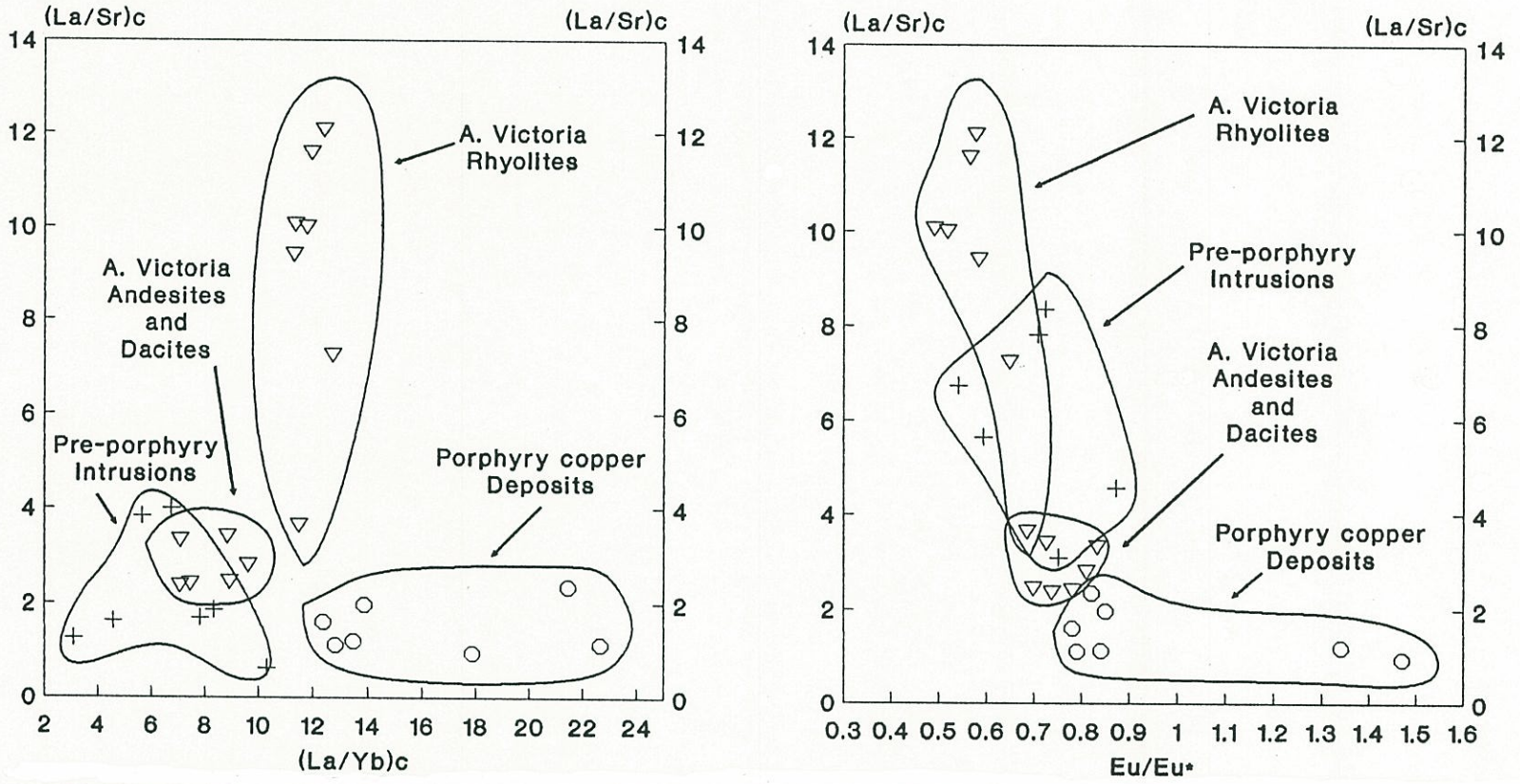


**Figure 7.23.** (La/Sr)c versus (La/Yb)c, and versus Eu/Eu* for samples of copper-bearing porphyries and pre-porphyry igneous rocks (c = chondrite normalized). The pre-porphyry igneous rocks with relatively low La/Yb ratios show a big increase of La/Sr ratio and have increasingly larger Eu anomalies with increasing $SiO_2$ as expected from plagioclase fractionation, consistent with low pressure crystal fractionation. In contrast copper-bearing porphyries with higher La/Yb ratios show no increase of La/Sr ratios with increasing $SiO_2$ and have no Eu anomalies consistent with a lesser role for plagioclase, and high pressure fractionation. Normaliza-tion for Sr = 14, La = 0.378 and Yb = 0.249.

bearing intrusions (Fig. 7.23). Comparison with the La/Sr versus Eu/Eu* plot shows that silicic rocks with high La/Sr ratios (Lower Tertiary rhyolites) have large negative Eu anomalies, while silicic copper-bearing porphyries with relatively low La/Sr ratios have little or no Eu anomaly (Fig. 7.23). These relations demonstrate the importance of feldspar fractionation in the Early Tertiary silicic rocks as expected for rocks fractionated at low pressures within the crust. In contrast, Upper Eocene - Lower Oligocene copper-bearing porphyries with high La/Yb ratios and relatively low La/Sr ratios have little o no Eu anomaly consistent with less plagioclase fractionation. According to Kay and others (1990) the correlation of relatively low La/Sr ratios (high Sr contents) with small Eu anomalies is important as small Eu anomalies alone can also result from fractionation of a phase (e.g., amphibole, titanite) with a negative Eu anomaly offsetting the positive Eu anomaly of plagioclase or from oxidizing conditions in which case Eu anomalies are not produced due to low $Eu_{+2}/Eu_{+3}$ ratios, and the same correlation is also important as fractionation of REE bearing phases can lower La concentrations. The correlation of high La/Yb ratios, which signify the presence of a high pressure phase (garnet and/or amphibole) with low La/Sr ratios and small Eu anomalies corroborates a lesser role for plagioclase in the petrogenesis of the copper-bearing porphyries, and probably an overall lesser role of low pressure fractionation processes. The lesser role of plagioclase fractionation in the genesis of igneous rocks associated with porphyry copper deposits, which typically include plagioclase phenocrysts, suggests that an early crystal fractionation of plagioclase may either impede the transport or contribute to dispersal of copper content of felsic magmas at depth, whereas plagioclase crystallization at shallow level during emplacement of a felsic stock probably results in a significant enrichment of residual phases in copper, because this metal is not accommodated in the crystalline structure of plagioclase, thus making copper readily available for subsequent concentration by hydrothermal processes at near-surface levels. Plagioclase crystallization at epizonal level may also contribute to the saturation of the residual melt in volatiles, therefore triggering the separation of an aqueous phase from the magma, and subsequent development of hydrothermal activity.

### 7.2.9 Crustal thickness and REE fractionation in Andean arc magmas: implications for the origin of porphyry copper magmas

La/Yb ratios (or Ce/Yb) ratios have been inferred to correlate with increasing crustal thicknesses through time in the zone with flat subduction ("flat slab," 29°00'-30°30' S) by Kay and others (1987, 1988, 1990) and along-strike in the Southern Volcanic Zone of the Andes by Hildreth and Moorbath (1988) (Fig. 7.22). The La/Yb and La/Sm ratios of the Late Cretaceous to Eocene igneous rocks are consistent with arc magmas generated under a normal crustal thickness of about 30-35 km, whereas the higher ratios of the Upper Eocene - Lower Oligocene stocks are compatible with a crustal thickness of about 50 km (Figs. 7.21, 7.22). A Late Eocene crustal thickening event is consistent with the geological evidence that suggest uplift related to the Incaic compression at that time (see Section 2.17), and also with a regional cooling event detected by fission-track dating of apatites from the basement of the Domeyko Cordillera (see Chapter 5).

As shown above, the intrusive rocks associated with porphyry copper deposits are essentially comparable to other volcanic and intrusive calc-alkaline arc rocks of the Andes. However, the REE data reveal that Upper Cretaceous to Eocene igneous rocks are similar to Oligocene-Lower Miocene volcanics of the Andes between 29° and 30°30' S., and those erupting in the central and southern SVZ, where the crust is relatively thin (ca. 35 km). Otherwise, magmas generated during Late Eocene-Early Oligocene (during porphyry copper formation) are similar to those erupting in the northern SVZ today, where crust is thicker (50-60 km) and asthenosphere thinner than in the southern SVZ. The REE patterns of igneous rocks suggest little or no role for garnet in the evolution of Late Cretaceous to Early Eocene magmas and the subsequent occurrence of garnet as a stable phase in the mantle or lower-crust during the Late Eocene-Early Oligocene when major porphyry copper deposits were generated. This change in the source region followed the occurrence of the Incaic

deformation and uplift (hence crustal thickening). A very similar scenario has been described by Kay and others (1987, 1988) for the Oligocene-Miocene petrogenetic evolution of the segment of the Andes between 29° and 30°30' S, where crustal thickening associated with the Miocene Quechua compressive phase, and the flattening of the subduction zone correlate with changes in the source region of magmas leading to an increasing role of garnet and amphibole during magma genesis, increased crustal involvement, as well as to a reduction of volume, and compositional range of Upper Miocene volcanics. Moreover, the steep REE patterns published by Lopez-Escobar (1984) for the Late Miocene Rio Blanco-Los Bronces porphyry copper deposit strongly suggest that the formation of Late Miocene-Pliocene major porphyry copper deposits in the Andean segment between 32° and 34° S. also followed a tectonically induced change of the source region of the magmas by the Miocene (Quechua) compression. Thus it is concluded that magmas associated with porphyry copper deposits were generated following the emergence of garnet in the source region induced by tectonic crustal thickening. The growth of garnet may have taken place due to an adiabatic transformation of spinel to garnet peridotite in the mantle following the complementary reduction of volume and extent of convection within the asthenospheric wedge or due to increase of pressure within the lower crust leading to stability of garnet granulites or both (e.g. Kay and others, 1987, 1988; Hildreth and Moorbath, 1988).

The reduction of the volume and extent of convection within the asthenospheric wedge may have resulted in further cooling of the source region and consequent cessation of magmatic activity in the Domeyko Cordillera leading to the eastward shift of the magmatic front after the formation of the porphyry copper deposits.

### 7.2.10 Sulphur isotopic constraints

No new sulphur isotopic analyses have been done during this study, but a short review of the data published by Field and

Gustafson (1976), and the sulphur isotope reconnaissance study of porphyry copper deposits by Sasaki and others (1984) is pertinent. The analyses of sulphur isotopes of monomineral samples from ores of El Salvador porphyry copper deposit by Field and Gustafson (1976) showed that hypogene sulfates range from +7.3 to +17.0 $\delta^{34}S^{0}/_{00}$ (mean +10.7 $\delta^{34}S^{0}/_{00}$), enriched in $^{34}S$ relative to hypogene sulfides that range from -10.1 to -0.3 $\delta^{34}S^{0}/_{00}$ (mean -3.0 $\delta^{34}S^{0}/_{00}$). Sasaki and others (1984) showed that the rock sulphur of the L Porphyry of El Salvador is also enriched in the heavier $^{34}S$ isotope (+5.9 $\delta^{34}S^{0}/_{00}$) relative to the hypogene sulfides. Similarly rock sulphur from the pre-mineral Fortuna Granodiorite with a value of +4.0 $\delta^{34}S^{0}/_{00}$ is enriched in the heavier $^{34}S$ compared with an analysis of mill concentrate from Chuquicamata deposit with a value of -4.7 $\delta^{34}S^{0}/_{00}$. Copper concentrates from the deposits of Rio Blanco, and El Teniente of central Chile yielded values ranging from -3.1 to -1.3, whereas rock sulphur from the same deposits ranges between +5.9 and +6.1 $\delta^{34}S^{0}/_{00}$. Thus according to Sasaki and others (1984) the sulphur of sulfide ores is consistently enriched in the lighter $^{32}S$ giving $\delta^{34}S_{rock} > \delta^{34}S_{ore}$. This relationship is similar to the trend observed in Japan, and can be interpreted as the result of isotopic partitioning between oxidized and reduced sulphur species in the magma-ore-fluid system, and subsequent deposition of the reduced species as sulfide ores. The relatively high difference between rock and ore sulfide $\delta^{34}S^{0}/_{00}$ in Chilean porphyry copper deposits may mean high $fO_2$ conditions during mineralization, therefore more sulphur fractionated towards oxidized sulphur species. This is consistent with the common presence of hypogene sulfates (e.g., anhydrite) in most of the porphyry copper deposits. Field and Gustafson (1976) stressed that mass balance calculations for El Salvador indicate a value probably significantly heavier than 0.0 $\delta^{34}S^{0}/_{00}$ for the entire deposit. The investigation of Sasaki and others (1984) suggested that the source sulphur is better represented by the host granitoid sulphur of Chilean porphyry copper deposits, which is much heavier than the ore sulphur having an average $\delta^{34}S$ of about $+5^{0}/_{00}$. The enrichment of the "rock sulphur" in $^{34}S$ may well be due to the presence of hypogene anhydrite in the rocks.

### 7.2.11 Oxygen and Hydrogen isotopic constraints

The only study of oxygen and hydrogen isotopes of a porphyry copper deposit of northern Chile is that of Sheppard and Gustafson (1976) at El Salvador. They have shown that biotites associated with the main mineralization stage of this deposit fall within the well-defined $\delta D$-$\delta^{18}O$ range of biotites from North American porphyry copper deposits at Santa Rita, Bingham and Ely. This supports the geologic arguments presented by Gustafson and Hunt (1975) that hydrothermal solutions responsible for early potassium alteration were derived from the porphyry melt and its underlying magma chamber. A trend to $^{18}O$ depleted water in pyrite-sericite-forming environments indicates that there was a significant component of meteoric water in the hydrothermal fluids associated with sericitization following potassic alteration (Sheppard and others, 1971). This is also typical in North American porphyry copper deposits (Taylor, 1974, 1979, 1984). The range of $\delta D$ values for advanced argillic assemblages is similar to that calculated for fluids responsible for the earlier sericitization events, but higher than the values calculated for later supergene water. Oxygen isotope geothermometry indicates temperatures continuously declining from about 700° to 300°.

According to K-Ar dates (36.9 Ma recalculated) on supergene alunite obtained by Gustafson and Hunt (1975) the supergene alteration at El Salvador followed within about 5 Ma after hypogene mineralization, but the water involved in the supergene process is slightly less deuterium rich than the meteoric water involved in the late hydrothermal alteration. According to Sheppard and Gustafson (1976) this implies that uplift of the Andes at the 26° S had begun by late Eocene, which is consistent with the geologic and thermochronologic data presented in this thesis.

### 7.2.12 Physico-chemical constraints

The physico-chemical constraints on porphyry copper mineralization have been reviewed by Burnham (1981a), who regarded their formation as a natural consequence of cooling and crystallization of certain hydrous felsic magmas in shallow crustal (epizonal) environments (Burnham, 1979, 1981, 1985; Burnham and Ohmoto, 1980). Thus his view follows a "magmatic hypothesis"[8] for the origin of porphyry copper deposits, like those based on extensive geological studies of this type of deposit by Lowell and Guilbert (1970), Gustafson and Hunt (1975), as well as on thermodynamic considerations by Burnham (1979). In fact, the magmatic origin for virtually all the essential components of porphyry copper deposits can be considered to be firmly demonstrated, from the data presented above and many other studies and by thermochemical studies (Candella and Holland, 1984, 1986) and various isotope studies (Sheppard and Gustafson, 1976; Field and Gustafson, 1976; Taylor, 1979; 1984; Farmer and De Paolo, 1987). A review of the ideas of Burnham (1981a) is presented below, whereas the alternative "convection hypothesis" (e.g., Anderson, 1980) is discussed later.

The major physico-chemical constraints on porphyry copper mineralization according to Burnham (1981a) are: (1) $H_2O$ content, (2) temperature or heat content, (3) metal content, (4) chlorine content, (5) sulphur content, and (6) oxidation state ($fO_2$).

(1) The water content of magmas that cause porphyry mineralization must be such that the mechanical energy released during crystallization and exsolution of aqueous fluids ("second boiling") is sufficient to produce extensive fracture systems over a depth interval between about 2 to 8 km (Phillips, 1973; Burnham, 1979, 1985). The $H_2O$ content also must be sufficient to stabilize hornblende and hydroxyl-rich biotite as phenocryst

---

[8] The magmatic hypothesis maintains that metals are carried with the magma from its origin to point of crystallization (Anderson, 1980).

phases at depths greater than about 2 km. Magmas that contain less than 2 wt.% $H_2O$ release insufficient mechanical energy through second boiling to produce extensive fracture systems (stockwork) and neither hornblende nor hydroxyl-rich biotite generally occurs as phenocrysts (Naney, 1983). On the other hand, felsic magmas containing more than 5 wt.% of $H_2O$ become saturated with water at depths greater than about 6 km, owing to their low liquidus temperatures and are therefore incapable of ascending to shallower levels without becoming completely crystalline.

(2) The temperatures of porphyry magmas, which are inversely related to their $H_2O$ contents, must be high enough to carry them to depths of 4 km or less in a largely liquid state. Burnham (1979) estimated that to fulfil this condition, temperatures in the source region must be 800°C or higher.

(3) The metal content of porphyry magmas must be sufficient to yield economic mineralization. The metal content is dependent upon many factors, and therefore no meaningful minimum can be established, although one cubic kilometre of magma containing 200 ppm Cu may form a 100 million ton orebody averaging 0.5 % Cu (assuming total removal of copper from the magma to form a deposit).

(4) The chlorine content of porphyry magmas must be sufficient to provide the magmatic aqueous fluids that are exsolved during second boiling with the capacity to transport both metals and reduced sulphur to form sulfide-rich porphyry mineralization and to effect extensive hydrothermal wallrock alteration (Candela and Holland, 1984, 1986). Burnham (1981a) estimated that at least 0.05 wt.% Cl is required to be effective in typical copper-molybdenum and copper-gold mineralization and alteration processes.

(5) Porphyry copper deposits are primarily large crustal sulphur anomalies (e.g., Hunt, 1977), and therefore parent magmas must have as much as 0.2 wt.% S.

(6) The oxidation state or oxygen fugacity ($fO_2$) of magmas that cause sulfide and sulfate-rich (anhydrite, alunite) porphyry mineralization

must be high enough for the hydrothermal fluids exsolved from them to transport large quantities of sulphur (see Metallogeny Chapter), together with metal chlorides (chiefly of Fe), and to localize sulfide and sulfate deposition in part by hydrolysis of $SO_2$.

Most of the physico-chemical conditions required to generate porphyry copper deposits probably are present during arc magmatism, except for the restricted range from 2 to 4 wt.% of $H_2O$ content in the mantle estimated by Burnham (1981) as optimum to generate porphyry copper deposits. The latter author stressed that this may be the main reason that major metallic ore deposits are not more common at convergent margins. Gustafson (1979) proposed a model for porphyry copper magma genesis involving deep magma generation to account for the relatively low initial $H_2O$ content. He envisaged variable $H_2O$ contents to result from inhomogeneities in the source region and variations in the degree of partial melting. However, in this study it is suggested that the deep magma generation and consequent low initial $H_2O$ are the effect of tectonic crustal thickening.

### 7.2.12 Chuquicamata porphyry copper deposit: a case for stock emplacement and mineralization within an extensional strike-slip duplex.

In the introductory remarks of the description of the Chuquicamata orebody Perry (1952) stated "nature appears to have resorted to little fanfare, either geographical or geological, in creating a setting for this greatest concentration of metallic wealth." Chuquicamata is indeed an outstanding deposit; its production and potential reserves add to more than $8 \times 10^9$ metric tons of ore averaging 0.46% Cu (Sillitoe, 1981; Gilmour, 1982), and it is substantially larger than the rest of the porphyry copper deposits of northern Chile and southern Peru. In fact, it is the largest copper deposit in the world (Gilmour, 1982). The hypogene grades of large parts of this giant deposit are also far above the hypogene grades of porphyry copper deposits elsewhere (>1% and even >2% in

portions of the deposit; Sillitoe, 1981). The aim of this section is to elucidate some of the unique conditions that favoured the concentration of copper, associated metals, and sulphur within this unusually large and rich deposit.

The Chuquicamata deposit is hosted by a ca. 31 Ma old dike-like granodiorite porphyry stock (Chuqui porphyry) 14 km long and 1 km wide (Alvarez and others, 1980). The porphyry is elongated in a N10°E direction, and the main Chuquicamata orebody occupies an area of about 3 x 1.5 km in the southern end of the porphyritic intrusion (three other orebodies occur within 5 km to the north, which collectively are known as Chuqui Norte; Tufiño, 1973; Alvarez and Guzman, 1985). To the east the mineralized porphyry intrudes an equigranular Upper Paleozoic granodiorite (Elena Granodiorite) and older gneissic rocks, but in the northeastern section of the deposit the boundary is a shear zone referred to as the Mesabi fault by Alvarez and Flores (1985), which does not extend to the southern section of the deposit. To the west the porphyritic stock and orebody are abruptly terminated by a major fault, the West Fissure, beyond which outcrops the pre-mineral Fortuna Granodiorite (Taylor, 1935; Lopez, 1939, 1942; Perry, 1952; Sillitoe, 1973; Alvarez and others, 1980). One of the distinctive characteristics of Chuquicamata orebody is the occurrence of innumerable criss-cross veins with intense mineralization and hydrothermal alteration (Perry, 1952). In fact, the anomalously high frequency of copper-bearing veins within a ubiquitously mineralized porphyry (disseminated and stockwork sulfide mineralization) is the main reason for overall high hypogene grades within this deposit. The section from the West Fissure to the centre of the deposit shows a pervasive phyllic (quartz-sericite-kaolinite) alteration, which is partly surrounded on the east side by a zone of potassic alteration (potassium-feldspar-biotite-quartz), and an easternmost belt of propylitic alteration (chlorite-specularite-quartz) (Fig. 7.25). This arrangement is partly reversed compared with the alteration pattern of the classic model of Lowell and Guilbert (1970). The fracture and vein pattern of the orebody (Lopez, 1939; 1942; Perry, 1952) is characterized by a series of NNE trending shear zones (Zaragosa, C-2, and Americana faults) and NE faults

(Portezuelo, El Negro, Balmaceda and Estanques Blancos faults), which separate distinct blocks within the deposit (Alvarez and Flores, 1985), and innumerable NE-trending veins and fractures as well as conjugate WNW and NW fractures (Lopez, 1942) (Fig. 7.24). According to Perry (1952) "Although on a much larger scale, the structural pattern here shows a striking similarity to the Leonard vein at Butte." This pattern is compatible with a dextral shear as suggested by Lopez (1939, 1942), Hollister (1978), and Sibson (1987). In fact, the pattern of fractures and mineralized veins within the Chuquicamata porphyry copper deposit (Lopez, 1939, 1942; Perry, 1952) is similar to natural and experimental (clay box experiments) fracture patterns produced within extensional strike-slip duplexes (Woodcock and Fisher, 1986; Swanson, 1988), also known as right-stepping *en echelon* strike-slip faults (Rodgers, 1980; Reading, 1980; Hempton and Neher, 1986) or dilational jogs (Sibson, 1985, 1986, 1987). The knowledge of the mechanics of discontinuous strike-slip faults, the fracture pattern of the extensional zones associated with right-stepping faults, and related formation of pull-apart basins has significantly increased in the last decade (Segall and Pollard, 1980, 1983; Aydin and Nur, 1982, 1985; Mann and others, 1983; Woodcock, 1986; Sylvester, 1988; Sibson, 1985, 1986, 1987; Woodcock and Fisher, 1986). Several authors have demonstrated the synkinematic intrusion of plutons into pull-apart structures along major transform fault zones, which provide a domain of extension for the intrusions (Davies, 1982; Hutton, 1982, 1988; Castro, 1985; Gapais and Barbarin, 1986; Guineberteau and others, 1987). In addition, arc volcanoes such as Mount St. Helens occur in tensile zones above deep shear zones that are preferentially oriented to accommodate horizontal strike-slip within the magmatic arc (Weaver and others, 1987). In Section 4.3.1 it was shown that ductile deformation of the pre-mineral Fortuna Granodiorite occurred at about 36 Ma and of the Chuqui porphyry at about 31 Ma, implying active dextral shearing along the West Fissure (Domeyko Fault System) during the emplacement of the Chuqui porphyry. Thus the fracture pattern, coupled with the ductile deformation of the Chuqui porphyry, indicates that the emplacement of the porphyritic stock took place within a zone of extension developed during active right-lateral displacement of the Domeyko Fault System. The master faults of

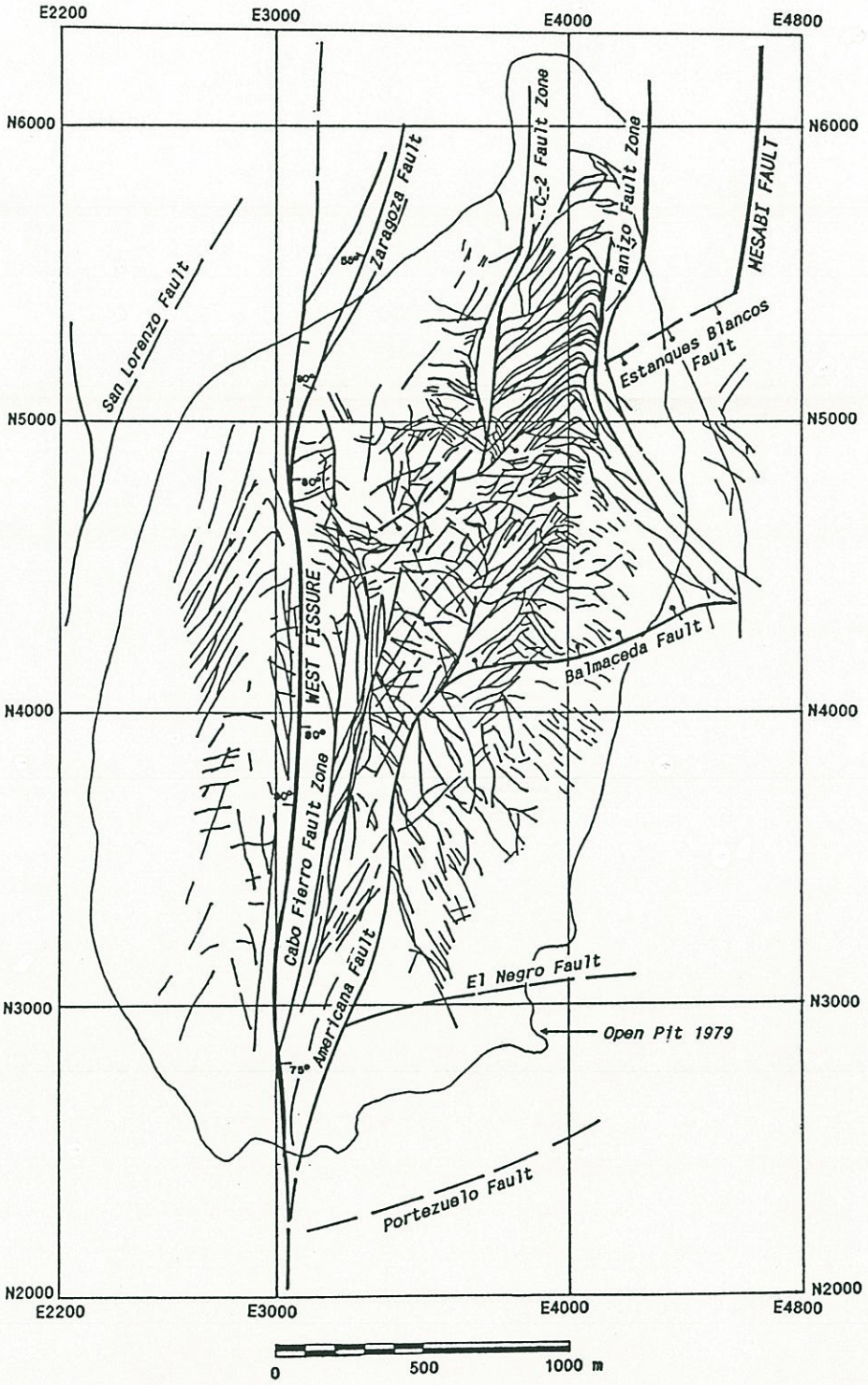


**Figure 7.24.** Fracture pattern of the porphyry copper deposit at Chuquicamata (compiled from Taylor, 1935; Lopez, 1942; Perry, 1952; Alvarez and others, 1980; and Alvarez and Flores, 1985).

the extensional strike-slip duplex were the West Fissure and the Mesabi fault, and innumerable fractures within the deposit accommodated the strike-slip displacement of the master faults (Fig. 7.24).

The structural setting of Chuquicamata has important implications for the development of mineralizing and alteration processes. First an extensional strike-slip duplex may have provided the path of least resistance for magma ascent. In this setting the "seismic pumping" mechanism (*cf.* Sibson and others, 1975; Sibson, 1985, 1986, 1987) may even have contributed to magma ascent. Second, the abrupt decompression of the magma column due to the added effect of near-surface retrograde boiling (cf. Burnham, 1979) and extension (dilation) might have contributed to the quenching (hence porphyritic texture) and the segregation of an aqueous phase from the magma. Thus, it is plausible that the initial ductile deformation of the porphyry was probably soon replaced by brittle repetitive opening of extensional fractures, due to hydraulic gradients generated during strike-slip fault displacements (Sibson and others, 1975; Sibson, 1985, 1986, 1987). This may have contributed to the seismic pumping of aqueous fluids from great depths, possibly from a larger magma chamber but primarily provided a path for **focusing** hydrothermal solutions with the fortunate effect that a myriad of mineralized fractures enriched the porphyry in copper, and other metals, far more than in other porphyry copper deposits. This fracture controlled, focused hydrothermal circulation may account also for the development of the phyllic alteration in the central part of the deposit (Fig. 7.25), resulting in the reversed pattern relative to the model of Lowell and Guilbert (1970). Perry (1952) stressed the contrast between the unmineralized surroundings of Chuquicamata pit and the extraordinary size and grade of the ore deposit, concluding that "there is an evident focus within the porphyry mass where effects of end-stage magmatic processes, complex fracturing and hydrothermal mineralization of the highest intensity, coincide and culminate to form an extraordinary concentration of metal." Another possible factor may have been the crystallization at depth due to decompression within the extensional strike-slip duplex so

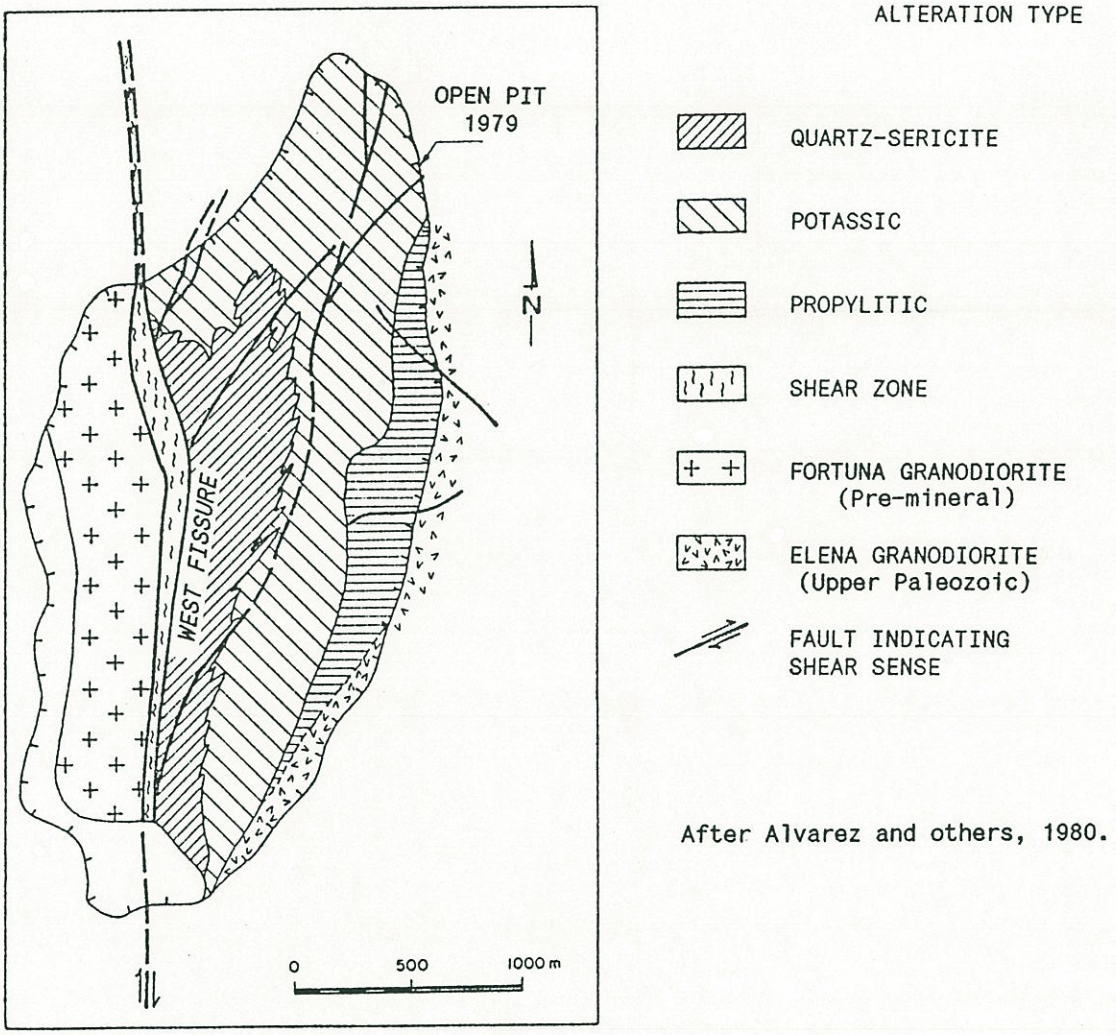


After Alvarez and others, 1980.

**Figure 7.25.** Alteration zoning within the porphyry copper deposit at Chuquicamata (After Alvarez and others, 1980).

that no significant post-mineralization intrusions, that could dilute the overall copper grades, occurred at Chuquicamata.

The formation of pull-apart basins (Rodgers, 1980; Aydin and Nur, 1982; Mann and others, 1983; Hempton and Neher, 1986) is the normal result of the development an extensional strike-slip duplex, so that the central section of the Chuquicamata orebody probably subsided forming a small depression at the surface. Alvarez and Flores (1985) stressed that the central section of the deposit, limited by the northeastern trending Estanques Blancos and Balmaceda faults, descended relative to the rest of the orebody, and particularly relative to the northern orebodies of Chuqui Norte. The likely formation of a small pull-apart basin could have controlled the local circulation of meteoric and ground water concentrating supergene enrichment within the highly fractured rocks underlying the depression. This is a satisfactory explanation for the contrasting thickness of the supergene enriched zone in Chuquicamata (up to 800 m thick) and the neighbouring Chuqui Norte deposit (20 to 40 m thick), despite analogous lithology and hypogene mineralogy (see Section 3.3). The orebodies at Chuqui Norte were probably at a higher topographic level relative to the main orebody at Chuquicamata. In fact, supergene enrichment at Chuquicamata may partly have occurred at Chuqui Norte's expense by leaching copper from the meteoric water recharge areas to the north.

A post-mineralization upthrow of the western block of the Western Fissure, evident from drag sulfides (Perry, 1952; Sillitoe, 1973) accounts for the abrupt western limit of the Chuquicamata orebody and related hydrothermal alteration. This late displacement took place probably during the Miocene associated with the Quechua compression.

It is thus proposed that Chuquicamata is a unique example of synkinematic emplacement of a porphyry copper deposit within an extensional zone associated with an active strike-slip fault. The effective focusing of hydrothermal and supergene processes by extensional

fractures probably played a leading role in the formation of one of the largest and richest copper deposits in the world.

## 7.3 TECTONICS AND PORPHYRY COPPER MINERALIZATION: A POSSIBLE CONNECTION

Increasing evidence reveals the importance of compressional crustal shortening in the uplift of the Central Andes (see Section 2.17). According to Megard (1984) compressive tectonic phases may have lasted from some hundred thousand to several million years.

The major porphyry copper deposits of northern Chile were formed following the crustal thickening and consequent uplift of the Domeyko Cordillera block produced by the Incaic compressive tectonic event in the Mid-Late Eocene. A thicker crust during porphyry copper mineralization is compatible with the geologic data that show the reactivation of erosion of the Domeyko Cordillera during the Late Eocene - Early Oligocene leading to terrestrial sedimentation on its flanks (see Chapter 2). Petrochemical evidence also suggests that magmas associated with porphyry copper deposits were generated following the emergence of garnet in the source region induced by tectonic crustal thickening. Furthermore the ca. 40 - 45 Ma regional cooling event detected by apatite fission-track dating of basement rocks of the Domeyko Cordillera (Chapter 5) is consistent with a period of enhanced erosion due to crustal thickening.

The Late Miocene - Pliocene porphyry copper mineralization of central Chile took place after Miocene crustal thickening associated with Quechua compressive tectonic event. The Paleogene to Early Eocene formation of major porphyry copper deposits in southern Peru followed the generalized emergence of Cretaceous marine sedimentary basins. This regression was attributed by Vidal (1985) to a crustal thickening event. Although, in Peru appear to be a time-lag between uplift and copper concentration, porphyry copper mineralization

following crustal thickening events is common to the three Cenozoic epochs of porphyry copper mineralization of the Central Andes. In addition, the North American porphyry copper deposits of the southern Cordillera (Nevada, Utah, Arizona, New Mexico and contiguous Mexico) also were formed following the Laramide uplift (e.g., Titley, 1981). This has been interpreted to indicate activation by uplift of crustal structures that allowed a rapid access of porphyry magmas to shallow levels (Titley, *op. cit.*).

The pattern of porphyry copper mineralization following uplift events is unlikely to be accidental, nor does it necessarily represent just the rapid ascent of magmas through crustal fractures, because the relationship between magma ascent and crustal structures is complex (see below). This pattern is interpreted in this study as indicative of a direct genetic relationship between crustal thickening and generation of 'anomalous' magmas appropriate for generating porphyry copper deposits during discrete metallogenic epochs at active continental margins.

The generation of magmas at convergent plate margins is the result of the particular tectonic conditions of the subduction system. Therefore changes of the tectonic regime, such as rapid crustal shortening and thickening must affect the conditions of magma generation (e.g. Kay and others, 1987, 1989, in press; Hildreth and Moorbath, 1988).

There are two important consequences of crustal thickening at convergent margins: (1) Decrease of the volume of the asthenospheric mantle wedge. (2) Overall decrease of geothermal gradients.

(1) The increase in the thickness of the crust probably produces an equivalent decrease in the volume of the asthenospheric wedge between the subducted oceanic and overlying continental plate (assuming that the subducting slab is not significantly affected). The aftermath may be the reduction of the extent of asthenospheric convection under the region of thickened crust. For example, crustal thickening from 30 to 60 km at an

active continental margin may result in a complementary reduction of the mantle wedge from 50 - 60 km to only 30 km, and a more significant reduction is possible if the whole lithosphere is shortened. However, the model of Isacks (1988) implies lithospheric thinning preceding crustal shortening events in the Andes. Reduced convection in the asthenosphere (reduced inflow of hot asthenospheric material) may lead to the subsequent cooling of the asthenospheric wedge, because the subducted oceanic plate is a heat sink due to its inherent cool nature and endothermic metamorphic reactions during subduction. The pronounced regional decrease in magma supply during the formation of porphyry copper deposits (volcanic quiescence, and localized plutonism) is consistent with a cooler and less actively convecting sub-arc asthenosphere.

(2) An overall decrease of geothermal gradients is the normal result of a rapid crustal shortening at a constant heat flow (e.g., England and Thompson, 1984). Thus a rapid thickening of the crust results in the descent of isotherms and consequent deepening of the source region of magmas. This is consistent with the emergence of refractory garnet in the mineralogy of the source region of porphyry copper magmas, as inferred from the depletion of heavy REE in copper-bearing intrusive rocks. According to computer models of England and Thompson (1984) the deepening of isotherms for regions of thickened crust is maximum for the case of homogeneous shortening of the whole lithosphere, as possibly occurs in the Andes (e.g., Isacks, 1988).

The thermal reequilibration following a disturbance of isotherms introduced by fast crustal or lithospheric shortening at a subduction system may take tens to hundreds millions of years. Its duration is controlled by the thermal diffusivity of the rocks, erosion rates (e.g., England and Richardson, 1977, 1980; England and Thompson, 1984), and rates of advective heat transfer by magmas. Plutonism associated with porphyry copper mineralization took place within a period of 10 Ma in the study area and similar duration is apparent in other Andean segments (Sillitoe, 1988).

Temperature may gradually decrease under the thickened crust as the asthenospheric wedge cools and further magmatism is likely to migrate inland, where hot asthenospheric mantle wedge remains. This is consistent with the copper-bearing stocks representing the last 10 Ma of magmatic activity before a major eastward shift of the magmatic front in the region.

The alternative hypothesis proposed by Stern (1989) involving the flattening of the Benioff zone may also provide the reduction of volume of the asthenospheric wedge with the gradual reduction and cessation of magmatic activity (e.g., Kay and others, 1987, 1988). The generation of porphyry copper magmas under this setting as implied by Stern (*op. cit.*) cannot be ruled out, but the present angle of the subduction in the studied Andean segment is about 30° (Barazangi and Isacks, 1976; Jordan and others, 1983), and its past variations are difficult to asses.

## 7.4 ANALYSIS OF PREVIOUS IDEAS AND MODELS OF PORPHYRY COPPER MINERALIZATION

The porphyry copper deposits of northern Chile and elsewhere show spatial and temporal association with epizonal calc-alkaline stocks, as recognized a long time ago leading to suggestions of a genetic link between intrusion and mineralization (Emmons, 1927; Lindgren, 1933; Sales, 1954). Two basic models for explaining the presence of metals in porphyry copper systems are current: the most favoured "magmatic hypothesis" maintains that metals are carried with the magma from its source rocks to the place of crystallization (Lowell and Guilbert, 1970; Rose, 1970; Gustafson and Hunt, 1975), while the "convection hypothesis" argues that the metals are leached from low concentrations in wall rocks and brought to the porphyritic stock to be deposited in higher concentrations (Norton, 1978; Anderson, 1980; McMillan and Panteleyev, 1980).

Some authors contest the capacity of magmas to transport and concentrate metals (e.g., Banks and Page, 1980). Furthermore, the extent to which superimposed meteoric-hydrothermal activity is a necessary and/or integral part of orebody formation in porphyry copper genesis is really unknown (e.g., Norton, 1978; Henley and McNabb, 1978; Eastoe, 1982; Sawkins, 1990). Notwithstanding, the distinct time and space distribution of porphyry copper deposits of the Antofagasta Region does not correlate with time or space disposition of the host rocks, as would be expected for a case of convective mineral concentration by circulating heated meteoric waters, but coincides with the porphyritic stocks. Thus apparently there is something unique about the magmas emplaced during the Late Eocene - Early Oligocene that caused the copper mineralization, which is consistent with the "magmatic hypothesis" for the origin of the porphyry copper deposits.

In early interpretations the Chilean porphyry copper mineralization was regarded as related to late phases (orogenic stage) of the evolution of a classic geosynclinal orogenic cycle (Stoll, 1964, 1965; Ruiz and others, 1965). Frutos (1973, 1975) proposed that a fundamental control for the location of porphyry copper deposits in the Andes of northern Chile was the position of a hypothetical "mioliminar" ridge, which according to this author separated an "euliminar zone" from a "mioliminar zone" during the Jurassic (*cf.* Aubouin and Borrello, 1966 and Aubouin and others, 1973). This was regarded as a zone of crustal weakness controlling the location of the copper-bearing intrusions. This idea has been discredited by subsequent studies (Zentilli, 1975; Sillitoe, 1981), because this alleged control does not exist if all porphyry copper deposits of the Central Andes are considered. Although Frutos (1982) maintained his early interpretation, there is no geologic evidence to support it. Besides, it fails to explain how the putative control was exerted, and why it was restricted only to the copper-bearing stocks. Frutos (1979) also proposed that the characteristics of porphyry copper deposits and their Cu/Mo ratios are determined by the degree of crustal evolution. However, the detailed compilation of Sillitoe (1986) showed no systematic variation of Cu/Mo ratios among the three Andean Cenozoic belts

of porphyry copper deposits and the lack of correlation of Cu/Mo ratios with lithology or age of known basement rocks, nor of crustal thickness, consistent with a subcrustal derivation of the metals. In fact, Candela and Holland (1986) have shown that Cu/Mo ratio is dependant on the depth of crystallization of water saturated melts, the chlorine content of the magma, and initial water concentration, factors that are unrelated to crustal evolution.

Routhier (1980) envisaged the Andean porphyry copper mineralization as resulting from increasing interaction of magmas with a progressively thicker andesitic pile anomalously enriched in copper. Routhier's key idea is the operation of multi-stage mineralization processes evolving throughout the re-concentration of metallic elements within the crust. However, some major porphyry copper deposits (i.e. Chuquicamata, Quebrada Blanca) were emplaced within basement rocks, and Sr, Nd and Pb isotopic data do not support such hypothetical crustal interaction of porphyry copper magmas.

The distinct association of porphyry copper deposits with convergent plate margins led Sillitoe (1972) to propose a model relating porphyry copper deposits to plate tectonics. The key idea of his proposal was that the metals contained in porphyry ore deposits were derived from the mantle at divergent plate margins, transported laterally to subduction zones as oceanic crust and overlying pelagic sediments, and incorporated in arc magmas through partial melting of the upper layers of the subducted oceanic lithosphere, consistent with the "Geostill" concept (Sillitoe, 1972b; see Chapter 6). According to paleomagnetic reconstructions (Pilger, 1983, 1984; Pardo Casas and Molnar, 1987) about 5,000 km of oceanic plate have been subducted under the South American continent during the Cenozoic (3,000 km after the formation of the major porphyry coper deposits of northern Chile); therefore the subducted plate may have provided a significant supply of copper. However, there is no convincing geologic evidence for copper derivation from the subducted oceanic plate, and the present writer agrees with the considerations of Burnham (1979) and Burnham and Ohmoto (1980) who suggested that a source enriched in

metals is not an essential requirement for generating magmas of porphyry copper deposits.

Sillitoe (1972) suggested that the accumulation of copper and molybdenum in high-level felsic stocks was a **normal** part of calc-alkaline magmatism in post-Paleozoic subduction-related orogenic belts. However, the geochronologic constraints, and the very restricted Sr, Nd, and Pb isotopic signature of the porphyry copper deposits, clearly show that this type of mineralization is highly **anomalous** within the long magmatic history of the Andean convergent margin, as recognized by the same author (Sillitoe, 1981, 1985, 1988).

The Geostill concept (Sillitoe, 1972b) and variations of the same idea, such as the models of Mitchell and Garson (1972), Oyarzun and Frutos (1974, 1980) and Frutos (1975, 1982) associate the spatial distribution of deposits relative to the continental margin with depth of partial melting or release of certain elements from the oceanic plate during subduction. However, those models fail to explain the distinct short time intervals (metallogenic epochs) of porphyry copper mineralization in the Andes, and are inconsistent with the physico-chemical conditions within the subduction zone (Burnham, 1979, 1981).

More recently Uyeda and Nishiwaki (1980) and Uyeda (1987) have shown that porphyry copper deposits tend to form in compressional arc systems ("Chilean type of subduction"), and appear to be notably scarce in extensional arcs ("Mariana type of subduction"), where Kuroko-type massive sulfide deposits dominate. This idea originated from the comparison of the distribution of circum-Pacific post-Mesozoic copper deposits, which demonstrated a correlation of the above copper deposits with distinctive types of plate interaction at subduction zones.

The inferred stress conditions in the lithosphere were used by Sillitoe (1980) to suggest that Kuroko-type massive sulfide deposits and porphyry copper mineralization are incompatible. The latter would be associated with development of andesitic-dacitic stratovolcanoes

in compressive environments, whereas the predominance of the former in resurgent calderas is due to the near-surface emplacement of large magma chambers in extensional tectonic regimes. The tectonic conditions in the lithosphere were also invoked by Olson (1989) to explain the porphyry copper mineralization at Potrerillos in northern Chile. This author indicated that Paleocene-Eocene volcanism was characterized by a bimodal assemblage of basaltic-andesite and rhyolite indicative of an extensional regime, whereas a compressive deformation took place during the porphyry copper formation. However, compressive conditions in the Chilean Andes began with the rapid opening of the south Atlantic at about 100 Ma (Larson and Pitman, 1972) and pre-porphyry volcanism is not bimodal but typical calc-alkaline dominated by andesites and dacites, with some basaltic andesites and rhyolites.

The notable absence of Jurassic porphyry copper deposits in the Central Andes, contrasting with an abundance of Jurassic strata-bound copper deposits in lavas, has been explained by the existence of a Mariana type of subduction (extensional regime) at that time (Munizaga and others, 1985; Boric and others, 1985), which is still the best explanation available. However, the compressive Chilean type of subduction has prevailed since the Late Cretaceous, following the opening of the south Atlantic Ocean, and porphyry copper mineralization has taken place only during restricted periods of time, thus implying that compressive stress regime is perhaps necessary but not sufficient, for generating porphyry copper mineralization.

The relations between magmatism and stress conditions in the lithosphere are equivocal, because actual rates of magma ascent and the effect on them of stress conditions, are largely unknown, being essentially a matter of speculation. If buoyant magma blobs 1 to 10 km in radius effectively ascend as diapirs, they would ascend at rates of 1000 to 10 cm/yr ($10^{-7}$ to $10^{-9}$ m/s), thereby creating "conduits" or warmed paths (Fedotov, 1976; Marsh, 1976, 1978; Spera, 1980; Gill, 1981). According to Marsh (1978) magmas could remain molten at these slow ascent rates even if they convect, especially the second or subsequent time a pre-warmed

pathway is used. Because the ascent of viscous diapirs is proportional to the density/viscosity ratio of magma, felsic magmas would ascend more slowly than basic ones. If, instead, magma ascends by elastic crack propagation or "magmafracturing" (Weertman, 1971; Yoder, 1976; Anderson and Grew, 1977; Shaw, 1980), rates can be $>10^6$ times faster ($10^{-2}$ to $10^{-1}$ cm/s) and according to Marsh (1978) must be $10^4$ times faster to prevent solidification. A possible but unlikely test of these models comes from earthquake precursors to volcanic eruptions. For example, earthquake foci preceding the 1959 eruption of tholeiitic basalt at Kilauea, Hawaii, first appeared at about 60 km depths and then ascended at about 1 km/day ($10^{-2}$ m/s). Eruption occurred when the earthquake foci reached the surface (Eaton, 1962). The observations of Blot (1972, 1976) indicate that some eruptions of andesites are preceded by patterns of earthquakes that "ascend" at 0.5 to 1.8 km/day (0.5 to 1.8 x $10^{-2}$ m/s), reaching the surface at the time of eruption. If the earthquake foci migration patterns accompany simultaneous magma movement, then magmas associated with volcanic eruptions ascend rapidly (Gill, 1981).

The magma-filled propagating fractures ("magmafracturing") and viscous diapir hypothesis are not mutually exclusive. In fact critical tensile stresses necessary for the propagation of cracks are smallest in materials with reduced rigidities (Spera, 1980). Therefore cracks could most easily nucleate and grow around the partially-fused rind surrounding a viscous (mostly-liquid) blob of ascending melt, and by inference along the warm path followed by a previous batch of magma. Earthquakes preceding and accompanying volcanic eruptions suggest that magmafracturing takes place even for magma ascent through weak, ductile asthenosphere. The orientation of the regional stress or the convection within the asthenospheric wedge may affect ascent paths and eventually may slow ascent rates by controlling crack distribution. Stress conditions and magma ascent are interdependent factors since the increase of regional stress produces the elevation of fluid pressure of magmas in the lithosphere and reduction of effective stress, thus probably enhancing magmafracturing and contributing to the faster ascent of magmas. Stress

magnitudes and orientations change with time and position, as batches of magma ascend episodically (Shaw, 1980). Periods during which extensional (hydraulic) failure conditions are not met account for the fact that magma chambers can form in the crust; these conditions are more likely to develop in an extensional regime due to relatively lower fluid pressures of magma.

Damon (1986) proposed a model coupling batholith emplacement with the formation of porphyry copper deposits of Mexico by density controlled "dome-in-dome" structures. This model does not seem to apply in the Central Andes, because no relationship between copper-bearing stocks and penecontemporanous batholith rocks, nor a regular spacing between porphyry copper deposits, are observed in the Andes. Instead the copper-bearing stocks intrude mostly unrelated older rocks at irregular distances from one to another. Even though Sillitoe (1973) suggested that the Fortuna Granodiorite is an example of a batholithic bottom of a porphyry copper deposit, the present evidence indicates that this intrusion is at least 4 Ma older than the Chuquicamata porphyry, and the fission-track data show that this pre-mineralization granodiorite has been at near-surface at least since the emplacement of the Chuquicamata porphyry (see Section 5.2.2). The existence of batholitic masses at depth cannot be ruled out, but the isotopic evidence implies that the porphyritic magmas have not interacted with the upper crust, and therefore probably ascended rapidly from a deep source in the mantle or lower crust.

Parada and others (1987), based on the observation that biotite crystals grew later than quartz and the extrapolation of experimental data of Maaloe and Willie (1975), concluded that the porphyry at Chuquicamata had less than 1.2 wt.% $H_2O$, and speculated that hydrothermal alteration resulted from the presence of meteoric water. However, the porphyry at Chuquicamata includes biotite phenocrysts and biotite pseudomorphs after hornblende phenocrysts. Naney and Swanson (1980) and Naney (1983) showed that biotite and hornblende are not stable

as phenocryst phases at epizonal levels unless the magma is saturated in $H_2O$ (>2 wt.% $H_2O$). These authors reported that a minimum initial water content of 4 wt.% is necessary to stabilize hornblende as a hypersolidus phase in an intermediate rock crystallizing at 2 kb pressure. The porphyry at Chuquicamata (likewise most of the porphyry copper deposits of northern Chile) includes two types of biotites: primary biotite phenocrysts and 'late' hydrothermal biotite. The latter grew after magma crystallization, due to the presence of alkali-rich fluids at almost igneous temperatures. These fluids probably were exsolved from a water-saturated magma after crystallization of Na-rich hornblende (Burnham, 1979; Burnham and Ohmoto, 1980). In fact, the microprobe analyses of biotites from Chuquicamata reported by Parada and others (1987) are similar to the composition of hydrothermal biotites at Bingham (Garret, 1972).

The present study tends to agree with the conclusions of the classic detailed geological study of the porphyry copper deposit at El Salvador in northern Chile by Gustafson and Hunt (1975), and isotopic investigations of the same deposit (Field and Gustafson, 1976; Sheppard and Gustafson, 1976), which indicate that copper and associated metals in this deposit have been precipitated from hydrothermal fluids of direct magmatic parentage during late-stage processes of felsic plutonism, although some meteoric water entered the system in the late alteration phases. This is comparable to North American porphyry copper deposits (Taylor, 1974, 1979).

The initial water content appears to be one of the critical factors determining the capacity of magmas to dissolve, transport and release a fluid phase with the capacity of concentrating metals at epizonal levels in the crust (Burnham, 1979; 1981). The model of Gustafson (1979) requires a deep magma source to account for the required relatively low initial water content. His suggestion of variations of $H_2O$ due to inhomogeneities of the source region appears to be untenable, because of the very homogeneous isotopic characteristics of the copper-

bearing porphyritic rocks, which suggest either a uniform source or coherent magmatic generation. On the other hand, variation of degrees of partial melting may account for some of the chemical characteristics of the porphyry copper deposits, since Hickey and others (1986), Futa and Stern (1988), Muñoz and Stern (1988) and Stern (1988) have suggested that lower degrees of partial melting in the mantle may account for increasing La/Yb and $K_2O$ from west to east across the SVZ. The model of Gustafson (1979) does not provide a mechanism for such potential decrease in partial melting. The present study has proposed possible link between tectonics and arc magmatism to account for the generation of magmas with the adequate initial $H_2O$ to generate porphyry copper deposits (see below).

## 7.5 A CONCEPTUAL MODEL FOR THE ORIGIN OF PORPHYRY COPPER DEPOSITS

The isotopic, petrochemical, and geologic data currently available are consistent with the "magmatic hypothesis" for the origin of the major "classic" porphyry copper deposits of northern Chile. Therefore their formation by shallow emplacement and solidification of hydrous magmas as previously proposed by Burnham (1979, 1981a, 1985), Gustafson (1979), and Burnham and Ohmoto (1980) is favoured here. Isotopic dating and thermochronology indicate that the generation of these 'anomalous' magmas occurred during a discrete interval of geological time following a crustal thickening event associated with the **Incaic** compressive phase.

Tectonic uplift originating from rapid crustal shortening may provide an adequate mechanism for deepening of the zone of magma generation at active continental margins (see section 7.3). Deepening of the source region during porphyry copper magma generation is compatible with the strong depletion of HREE of the copper bearing intrusions that contrast with less steep REE patterns of pre-porphyry igneous rocks (see Section 7.2.7). Deeply generated magmas have more chances of having an adequate initial water content to concentrate metals and sulphur from their source rocks, and to reach shallow levels in the

crust, developing active hydrothermal processes and mineralization typical of porphyry copper deposits (e.g., Gustafson, 1979; Burnham, 1979; 1981a).

The Late Eocene -Early Oligocene epoch of major porphyry copper mineralization is consequently attributed to a period of anomalously deep magma generation following tectonic crustal or lithospheric thickening on the active continental margin of South America.

The proposed mechanism only increases the likelihood of generation of magmas with the optimum volatile content for generating porphyry copper mineralization under the region of thickened crust, but several other physico-chemical conditions, besides the content of volatiles, have to be met for the actual formation of porphyry copper deposits (see Section 7.2.10). This is consistent with the typical occurrence of multiple phases of intrusion at sites of porphyry copper deposits with usually only one or two hosting the sulfide ore minerals.

Structural conditions in the upper crust may be important, as in the Chuquicamata example, in providing effective focusing of the hydrothermal mineralization, but are not regarded essential for the genesis of the porphyry copper magmas. Compressive stress conditions are required for producing the structural shortening of the lithosphere, and may also contribute to increase magmafracturing and the consequent faster ascent of porphyry copper magmas. This may be the reason for the association of porphyry copper deposits with compressive Chilean type convergent margins.

In conclusion, a genetic relationship between tectonics and porphyry copper magma generation is consistent with the presented geologic, geochronological, thermochronological and petrochemical data of the Andean segment under investigation, and probably also applies to other segments of the Andes or active continental margins elsewhere.

Differences in plate interactions along the convergent margin, similar to the present tectonic segmentation of the Andes related

to different angles of subduction of the Nazca plate (e.g., Barazangi and Isacks, 1976; Jordan and others, 1983), may account for the occurrence of this type of copper mineralization within distinct segments of the Andes. The possibility of a decrease of the angle of subduction as proposed by Stern (1989) leading to porphyry copper mineralization cannot be ruled out, but this model cannot be yet evaluated.

## 7.6 CONCLUSIONS

The origin of the major, "classic" porphyry copper deposits of northern Chile is now constrained by a significant geochronological, isotopic, petrochemical, and geologic database. These porphyry copper deposits were formed within a distinct period that lasted about 10 Ma during the Late Eocene - Early Oligocene. Therefore these intrusion-related copper deposits clearly represent an anomaly in the long-lasting magmatic history of the studied Andean segment.

The conspicuous spatial relationship between major porphyry copper deposits and the domain of the trench-linked Domeyko Fault System is attributed to the nucleation and development of strike-slip faults along the Oligocene magmatic front, as an effect of oblique convergence between the Farallon oceanic plate and the South American continent. The role of the fault is important at Chuquicamata in providing an extensional domain for focusing hydrothermal and supergene processes leading to the formation of the largest copper deposit of the world. However, this fault system is considered as non-essential for the origin of the porphyry copper magmas.

The restricted variation of Sr, Nd, and Pb isotopes in the porphyry copper deposits of the study area, as well as other copper-bearing porphyries of different ages and various locations along the Andes indicates either an homogeneous sub-crustal source, or an effective homogenizing mechanism during porphyry copper magma genesis. Limited S,

O, and H isotopic data are compatible with magmatic derivation of sulphur and water involved in the early stages of copper mineralization. Meteoric water appears to dominate in the late stages.

The overall petrochemical characteristics of the copper-bearing stocks are not very different from other Andean arc-related calc-alkaline igneous rocks, although a reduced range of composition and a significant depletion of heavy REE are apparent. The latter suggests a change within the source region of magmas involving the emergence of garnet control and/or reduction in the degree of partial melting. This implies an increase of pressure or decrease in temperature of the source region, compatible with a thicker crust during the generation of porphyry copper magmas relative to that of pre-porphyry igneous rocks. Thus, the origin of porphyry copper mineralization is thought to be related to a period of 'anomalous' deep magma generation during the Late Eocene - Early Oligocene following crustal thickening produced by the Mid-Late Eocene Incaic compression.

The discrete period of porphyry copper mineralization representing the last magmatic activity along the Domeyko Cordillera block implies that major tectonic processes that ultimately resulted in the eastward shift of the magmatic front were also related to the generation of magmas with the optimum volatile content to generate porphyry copper deposits.

The erosion activated by tectonic uplift contributed to the rapid exhumation of deposits and concomitant subsequent development of supergene enriched blankets. The virtual cessation of the denudation since the Miocene in the Andean segment from 21° to 26° S due to the dominance of a hyper-arid climate explains the remarkable preservation of the shallow porphyry copper systems and supergene enriched blankets.

# CHAPTER 8. MAIN CONTRIBUTIONS OF THE PRESENT STUDY

This thesis has attempted to integrate new data with previous work by the author, and with a revised database originating in work by others. I consider the following to be the main contributions of the thesis:

8.1 This study is an updated review or memoir of the state of geological understanding of the Antofagasta region, in particular of what is relevant to its metallogenic evolution. Together with its adjacent (Atacama Region) area to the south, which previous studies suggest has a comparable geologic history, the study applies to over 1,000 km along the Pacific flank of the Central Andean belt. Because this segment is richly mineralized, this study should be useful in interpreting Andean-type converging plate tectonic margins elsewhere.

8.2 The study documents, and unequivocally confirms the systematic migration of the magmatic front from near the coast in the Jurassic to its present location 300 km inland. This migration is fully supported by field data and new geochronological data.

8.3 The study has confirmed and documented the direct association of hydrothermal mineral deposit genesis with essentially coeval intrusive and volcanic activity over 200 Ma of Andean evolution. Since ore deposits go hand in hand with magmatism, the migration of the magmatic front implies the migration of metallogenic belts with time. This relationship, which associates particular types of mineral deposits with rocks that have a restricted range in age, has important implications for mineral exploration and resource evaluation along the Andean belt.

8.4 This is one of the first geochronological studies of the Central Andes using the $^{40}Ar-^{39}Ar$ technique. Within the limitations of the method the $^{40}Ar-^{39}Ar$ technique is considerably more precise and accurate than the conventional K-Ar technique. The results complement and amplify previous knowledge, but also document the fact that conventional K-Ar dates should not be taken at face value. The K-Ar dating of minerals within the alteration aureoles of mineral deposits has highlighted the problems inherent in dating hydrothermal systems. Nevertheless, they: (i) confirm the temporal link between magmatism and mineralization processes; (ii) indicate that the preserved mineral deposits were formed during discrete metallogenic events that are much shorter than the long-lasting periods of magmatic activity; and (iii) specifically restrict the ages of giant porphyry copper deposits to a 10 Ma period in the Late Eocene-Early Oligocene.

8.5 The study provides the first thermochronological apatite fission track analysis in the Andes of northern Chile. The use of apatite etchable length distribution measurements and modelling of time-temperature paths complement fission track ages. Together with other observations the fission track data are compatible with the shallow emplacement and rapid cooling of porphyry copper systems, in particular Chuquicamata and El Abra. Fission track data on the Paleozoic crystalline basement of the Domeyko Cordillera are compatible with erosion/cooling of that block in the Middle-Late Eocene. Fission track data on intrusive rocks of the Coastal Cordillera indicate that its presently exposed rocks have not been buried or reheated since the Early Cretaceous implying limited extent of erosion of this area. The first apatite fission track dates of magnetite flows associated with Neogene volcanoes of the High Andes indicate that the formation of these iron deposits was not limited to one isolated event but occurred at different times in several areas of the volcanic chain.

8.6 This study has provided the first integrated Nd, Sr, and Pb isotopic data for Chuquicamata and other porphyry copper deposits. It indicates that the isotopic composition of porphyry magmas is remarkably restricted,

and the data are in strong support of the "magmatic hypothesis" for the origin of porphyry copper deposits.

8.7 The thesis is one of the few recent studies attempting to relate the genesis of Andean porphyry copper deposits to tectonic processes. It suggests that porphyry copper deposits were formed following uplift resulting from crustal thickening. It proposes that oblique subduction has had a major influence in the association of major porphyry coppers with the Domeyko Fault System. The intrusion of a porphyry stock and the development of a hydrothermal system into a domain of shear-related trans-tension and dilation is advanced to explain the giant size of the Chuquicamata orebody, and also invoked as an agent in the development of an anomalously thick supergene blanket at Chuquicamata.

8.8 The study proposes that Cretaceous sedimentary strata found at El Way in the coastal area south of Antofagasta are not erosional remnants of a more extensive Cretaceous succession, but the result of sedimentation in a restricted pull-apart basin related to the evolution of the Atacama Fault System. This interpretation has implications for the interpretation of Atacama Fault tectonics and for metallogeny, since stratiform Cu deposits developed (El Way district) within this restricted basin.

8.9 This study clarifies the stratigraphic position and correlation of the Late Cretaceous to Eocene volcanic sequence (Augusta Victoria Formation), which has posed many problems to previous workers in the area. It represents arc-related calc-alkaline volcanism that predates the porphyry copper mineralization in the area.

# APPENDIX 1. SUMMARY OF ANALYTICAL $^{40}Ar$–$^{39}Ar$ DATA AND AGE SPECTRA

Table A1.1. $^{40}Ar$-$^{39}Ar$ data summary of FT-19 biotite; granodioritic Eastern Porphyry, CHUQUICAMATA (22°16'45" Lat.S - 69°53'45" Long.W).

| TEMP.(°C) | mV $^{39}Ar$ | % $^{39}Ar$ | % Atm. Ar | % I.I.C. | APPARENT AGE (Ma) (Error ± 2σ) |
|---|---|---|---|---|---|
| 200-550 | 16.5 | 2.8 | 91.7 | 0.2 | 31.1 ± 5.6 |
| 550-600 | 29.2 | 4.9 | 70.8 | 0.2 | 31.9 ± 1.6 |
| 600-650 | 73.8 | 12.5 | 47.3 | 0.2 | 32.2 ± 0.6 |
| 650-700 | 132.7 | 22.6 | 33.8 | 0.2 | 31.4 ± 0.2 |
| 700-750 | 130.0 | 22.1 | 34.8 | 0.2 | 31.9 ± 0.4 |
| 750-800 | 63.5 | 10.8 | 59.1 | 0.2 | 31.5 ± 0.6 |
| 800-850 | 19.5 | 3.3 | 74.8 | 0.2 | 28.6 ± 2.6 |
| 850-900 | 8.9 | 1.5 | 92.9 | 0.3 | 22.8 ± 4.2 |
| 900-950 | 20.6 | 3.5 | 88.7 | 0.2 | 28.6 ± 1.8 |
| 950-1000 | 38.0 | 6.4 | 87.0 | 0.2 | 28.6 ± 1.4 |
| 1000-1100 | 53.2 | 9.0 | 90.7 | 0.2 | 27.0 ± 1.2 |

J = 0.00248 TOTAL GAS AGE = 30.8 ± 1.0 Ma

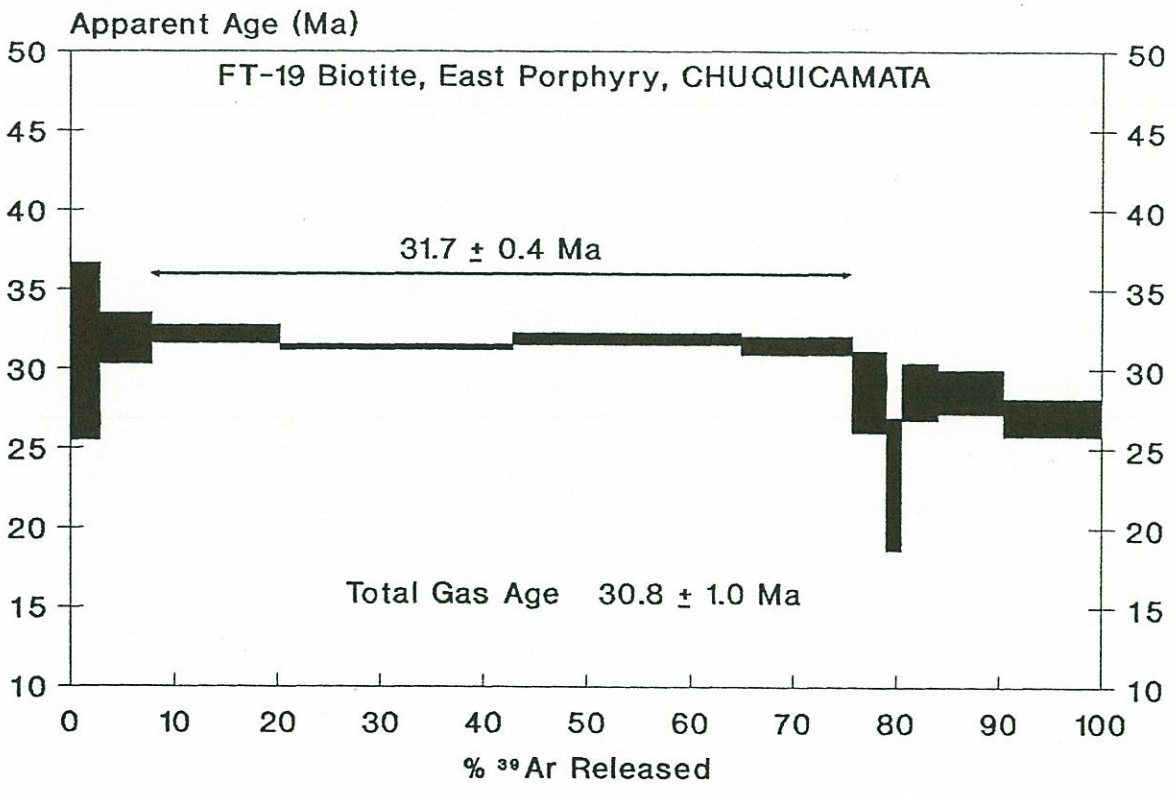


Figure A1.1. $^{40}Ar$-$^{39}Ar$ incremental-release age spectrum of biotite FT-19 from Chuquicamata porphyry copper deposit. Analytical uncertainties (± 2σ) are represented by vertical width of bars.

Table A1.2. $^{40}Ar$-$^{39}Ar$ data summary of FT-19 Orthoclase; granodioritic Eastern Porphyry, CHUQUICAMATA (22°16'45" Lat.S - 69°53'45" Long.W).

| TEMP.(°C) | mV $^{39}Ar$ | % $^{39}Ar$ | %Atm.Ar | % I.I.C. | APPARENT AGE (Ma) (Error ± 2σ) |
|---|---|---|---|---|---|
| 200-500 | 7.2 | 1.2 | 82.0 | 0.1 | 46.2 ± 5.2 |
| 500-550 | 5.2 | 0.8 | 61.9 | 0.2 | 26.8 ± 8.4 |
| 550-600 | 8.6 | 1.4 | 46.4 | 0.2 | 28.0 ± 2.8 |
| 600-650 | 18.8 | 3.1 | 28.8 | 0.2 | 32.2 ± 1.2 |
| 650-700 | 19.4 | 3.2 | 36.4 | 0.2 | 31.8 ± 1.4 |
| 700-750 | 27.4 | 4.6 | 33.0 | 0.2 | 30.6 ± 0.8 |
| 750-800 | 14.0 | 2.3 | 39.8 | 0.2 | 27.9 ± 2.2 |
| 800-900 | 28.0 | 4.7 | 35.9 | 0.2 | 31.5 ± 0.8 |
| 900-950 | 24.6 | 4.1 | 47.3 | 0.2 | 29.7 ± 1.0 |
| 950-1000 | 26.0 | 4.3 | 47.6 | 0.2 | 30.5 ± 1.2 |
| 1000-1050 | 47.4 | 8.0 | 38.2 | 0.2 | 32.2 ± 1.0 |
| 1050-1100 | 64.3 | 10.8 | 33.2 | 0.2 | 31.0 ± 0.4 |
| 1100-1150 | 151.9 | 25.6 | 19.6 | 0.2 | 31.5 ± 0.2 |
| 1150-1200 | 122.1 | 20.6 | 20.2 | 0.2 | 31.4 ± 0.2 |
| 1200-1250 | 26.0 | 4.3 | 36.0 | 0.2 | 31.8 ± 0.8 |

J = 0.00248 TOTAL GAS AGE = 31.4 ± 0.8 Ma

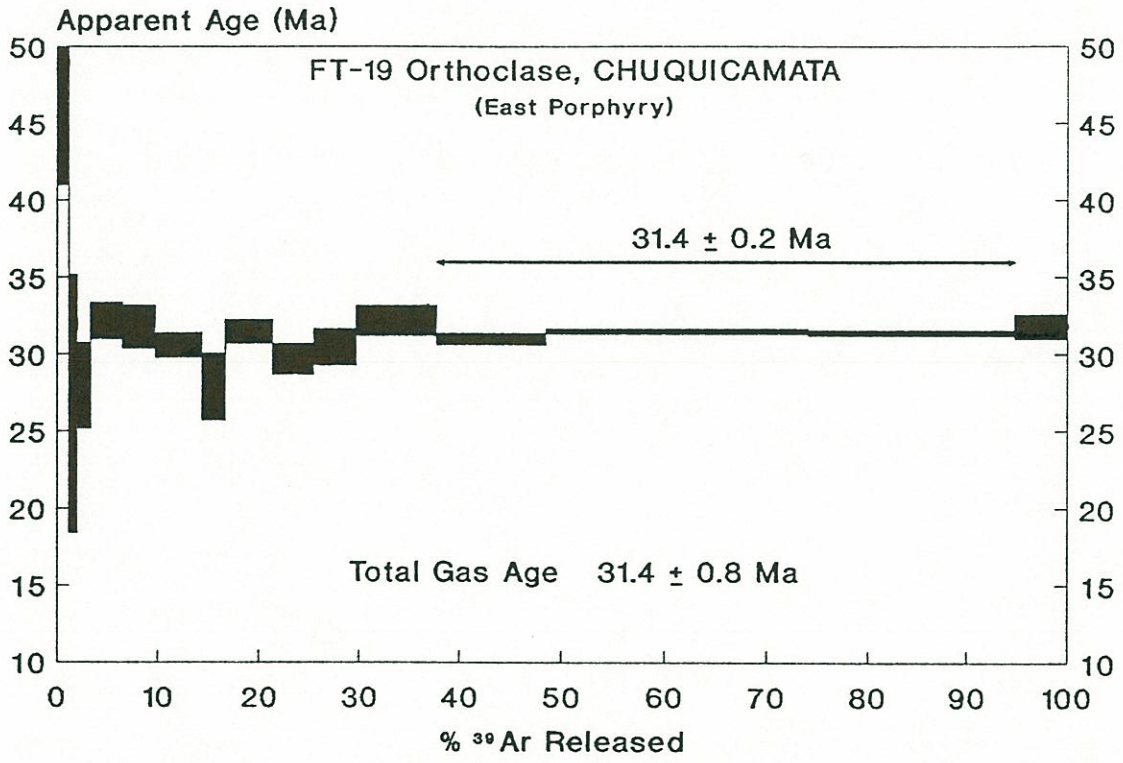


Figure A1.2. $^{40}Ar$-$^{39}Ar$ incremental-release age spectrum of orthoclase FT-19 from Chuquicamata porphyry copper deposit. Analytical uncertainties (±2σ) are represented by width of bars.

Table A1.3. $^{40}Ar$-$^{39}Ar$ data summary of FT-23 biotite; Fortuna Granodiorite, CHUQUICAMATA (22°20'53" Lat.S - 69°58'52" Long.W).

| TEMP.(°C) | mV $^{39}Ar$ | % $^{39}Ar$ | %Atm.Ar | % I.I.C. | APPARENT AGE (Ma) (Error ± 2σ) |
|---|---|---|---|---|---|
| 500-550 | 11.5 | 2.7 | 96.1 | 0.5 | 12.2 ± 4.4 |
| 550-600 | 12.8 | 3.1 | 85.7 | 0.2 | 33.3 ± 3.8 |
| 600-650 | 68.2 | 16.4 | 69.9 | 0.1 | 37.6 ± 0.6 |
| 650-700 | 54.5 | 13.1 | 60.3 | 0.1 | 34.9 ± 0.6 |
| 700-750 | 50.3 | 12.1 | 70.1 | 0.1 | 37.4 ± 0.6 |
| 750-800 | 23.4 | 5.6 | 85.4 | 0.1 | 35.9 ± 2.2 |
| 800-850 | 27.5 | 6.6 | 89.6 | 0.1 | 34.6 ± 1.6 |
| 850-900 | 40.6 | 9.8 | 87.7 | 0.1 | 35.4 ± 1.6 |
| 900-950 | 86.5 | 20.9 | 74.1 | 0.1 | 36.8 ± 0.4 |
| 950-1000 | 38.0 | 9.1 | 72.1 | 0.1 | 36.9 ± 0.4 |

J = 0.00248 TOTAL GAS AGE = 35.6 ± 1.0 Ma

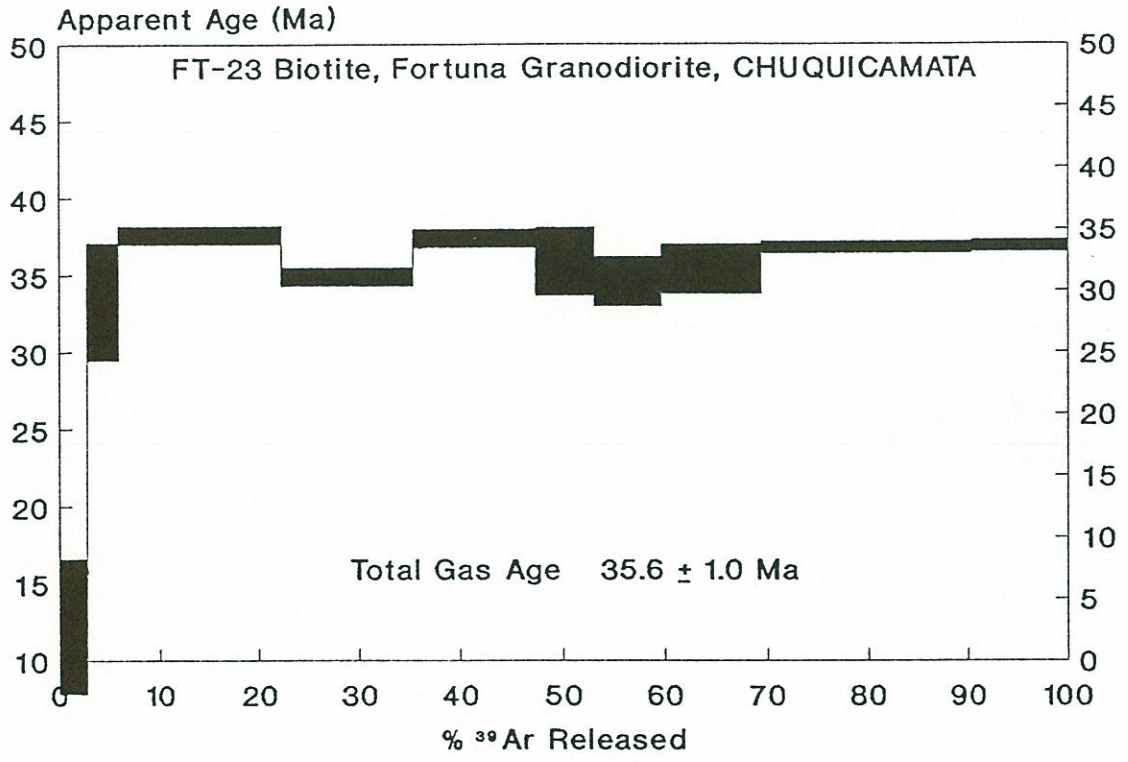


Figure A1.3. $^{40}Ar$-$^{39}Ar$ incremental-release age spectrum of biotite FT-23 from the Fortuna Granodiorite, Chuquicamata district. Analytical uncertainties (±2σ) are represented by width of bars.

Table A1.4. $^{40}Ar$-$^{39}Ar$ data summary of FT-24 biotite; foliated Fortuna Granodiorite, CHUQUICAMATA (22°20'47" Lat.S - 69°58'00" Long.W).

| TEMP.(°C) | mV $^{39}Ar$ | % $^{39}Ar$ | % Atm. Ar | % I.I.C. | APPARENT AGE (Ma) (Error ± 2σ) |
|---|---|---|---|---|---|
| 200-550 | 11.5 | 2.4 | 96.0 | 0.4 | 16.0 ± 8.0 |
| 550-600 | 17.7 | 3.8 | 77.7 | 0.2 | 33.7 ± 3.0 |
| 600-650 | 43.6 | 9.3 | 58.8 | 0.1 | 35.4 ± 1.0 |
| 650-700 | 70.4 | 15.1 | 47.1 | 0.1 | 37.1 ± 0.6 |
| 700-750 | 72.6 | 15.6 | 54.8 | 0.1 | 36.3 ± 0.6 |
| 750-800 | 21.1 | 4.5 | 81.1 | 0.2 | 32.6 ± 2.4 |
| 800-850 | 15.5 | 3.3 | 87.5 | 0.2 | 34.5 ± 4.2 |
| 850-900 | 38.6 | 8.3 | 84.3 | 0.1 | 35.4 ± 2.2 |
| 900-950 | 99.8 | 21.4 | 62.6 | 0.1 | 36.1 ± 0.6 |
| 950-1000 | 38.0 | 8.1 | 65.0 | 0.1 | 35.5 ± 0.6 |
| 1000-1100 | 36.1 | 7.7 | 95.0 | 0.2 | 29.0 ± 5.6 |

J = 0.00248 TOTAL GAS AGE = 34.8 ± 1.6 Ma

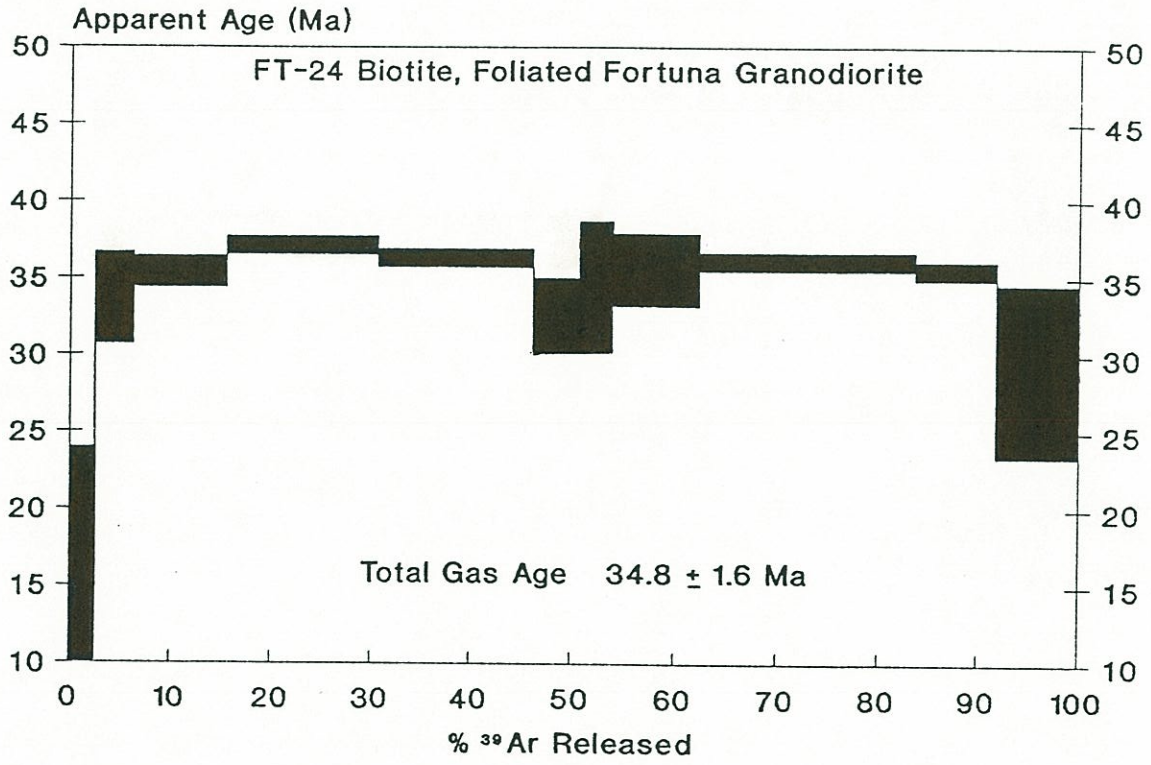


Figure A1.4. $^{40}Ar$-$^{39}Ar$ incremental-release age spectrum of biotite FT-24 from a foliated section of the Fortuna Granodiorite, Chuquicamata district. Analytical uncertainties (±2σ) are represented by width of bars.

Table A1.5. $^{40}Ar$-$^{39}Ar$ data summary of FT-47 biotite, quartz diorite, EL ABRA, East wall of the Ojo de Gallo quarry (21°55'02" Lat.S - 68°49'42" Long.W).

| TEMP.(°C) | mV $^{39}Ar$ | % $^{39}Ar$ | % Atm. Ar | % I.I.C. | APPARENT AGE (Ma) (Error ± 2σ) |
|---|---|---|---|---|---|
| 600-650 | 61.9 | 26.5 | 85.7 | 0.1 | 39.3 ± 1.4 |
| 650-700 | 55.6 | 23.7 | 62.0 | 0.1 | 39.7 ± 0.8 |
| 700-750 | 29.0 | 12.4 | 80.2 | 0.1 | 39.2 ± 1.8 |
| 750-800 | 17.3 | 7.4 | 84.3 | 0.1 | 38.7 ± 2.4 |
| 800-850 | 17.2 | 7.3 | 87.8 | 0.1 | 38.3 ± 2.6 |
| 850-900 | 36.5 | 15.6 | 81.8 | 0.1 | 38.7 ± 1.4 |
| 900-950 | 12.3 | 5.2 | 92.3 | 0.2 | 33.3 ± 5.0 |
| 950-1000 | 3.6 | 1.5 | 99.3 | 0.6 | 10.1 ± 47.4 |

J = 0.00248 TOTAL GAS AGE[1] = 38.4 ± 2.4 Ma

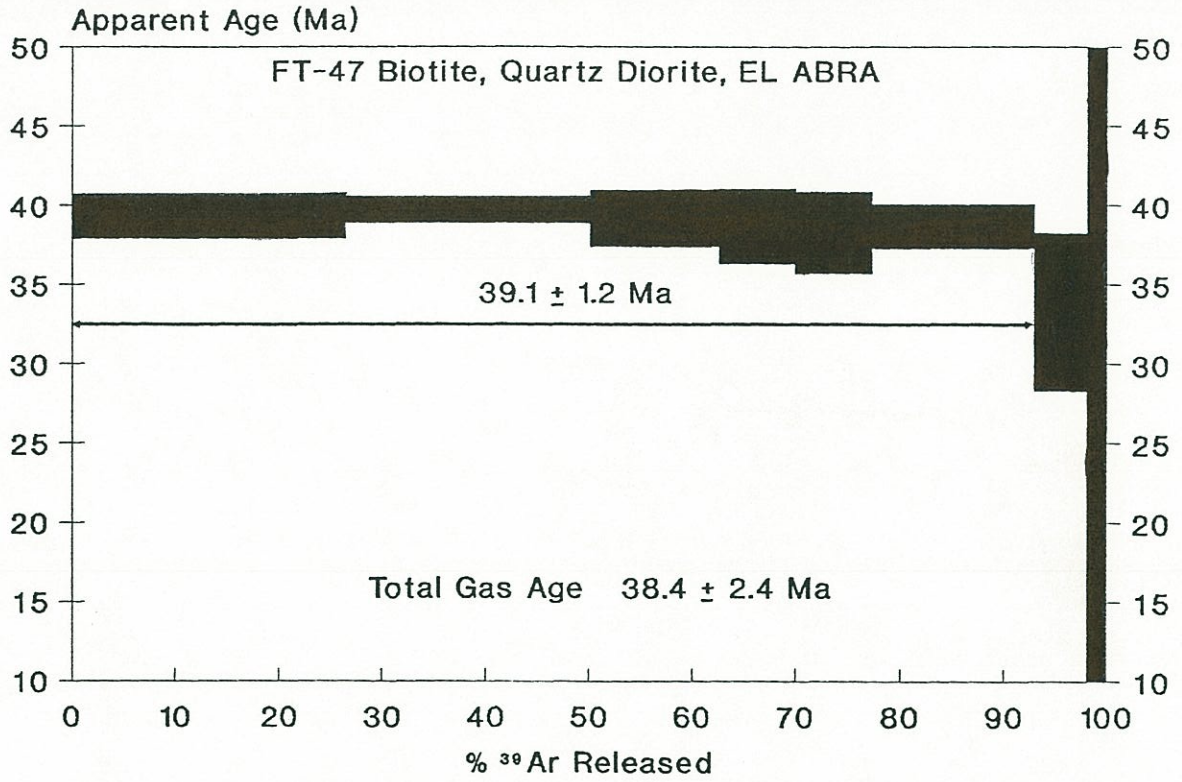


Figure A1.5. $^{40}Ar$-$^{39}Ar$ incremental-release age spectrum of biotite FT-47 from El Abra porphyry copper deposit (El Abra Diorite). Analytical uncertainties (±2σ) are represented by width of bars.

[1] The gas from the two first degassing steps was lost due to failure of a vacuum valve in the extraction line. Therefore this is not strictly the true total gas age.

Table A1.6. $^{40}Ar$-$^{39}Ar$ data summary of FT-44 biotite, dacitic porphyry, EL ABRA (21°55'06" Lat.S - 68°50'00" Long.W).

| TEMP.(°C) | mV $^{39}Ar$ | % $^{39}Ar$ | % Atm. Ar | % I.I.C. | APPARENT AGE (Ma) (Error ± 2σ) |
|---|---|---|---|---|---|
| 200-550 | 30.3 | 5.6 | 95.6 | 0.4 | 17.1 ± 2.4 |
| 550-600 | 39.2 | 7.3 | 84.2 | 0.2 | 31.4 ± 1.4 |
| 600-650 | 66.2 | 12.4 | 70.2 | 0.1 | 35.3 ± 0.8 |
| 650-700 | 98.4 | 18.4 | 68.0 | 0.1 | 36.6 ± 0.2 |
| 700-750 | 77.2 | 14.4 | 73.4 | 0.1 | 36.8 ± 0.6 |
| 750-800 | 31.6 | 5.9 | 90.0 | 0.2 | 31.8 ± 1.6 |
| 800-850 | 20.5 | 3.8 | 95.3 | 0.2 | 26.0 ± 3.2 |
| 850-900 | 63.0 | 11.8 | 89.5 | 0.2 | 33.5 ± 1.2 |
| 900-950 | 68.9 | 12.9 | 85.6 | 0.2 | 33.0 ± 0.8 |
| 950-1000 | 38.0 | 7.1 | 97.8 | 0.3 | 20.5 ± 5.4 |

J = 0.00248 TOTAL GAS AGE = 32.3 ± 1.4 Ma

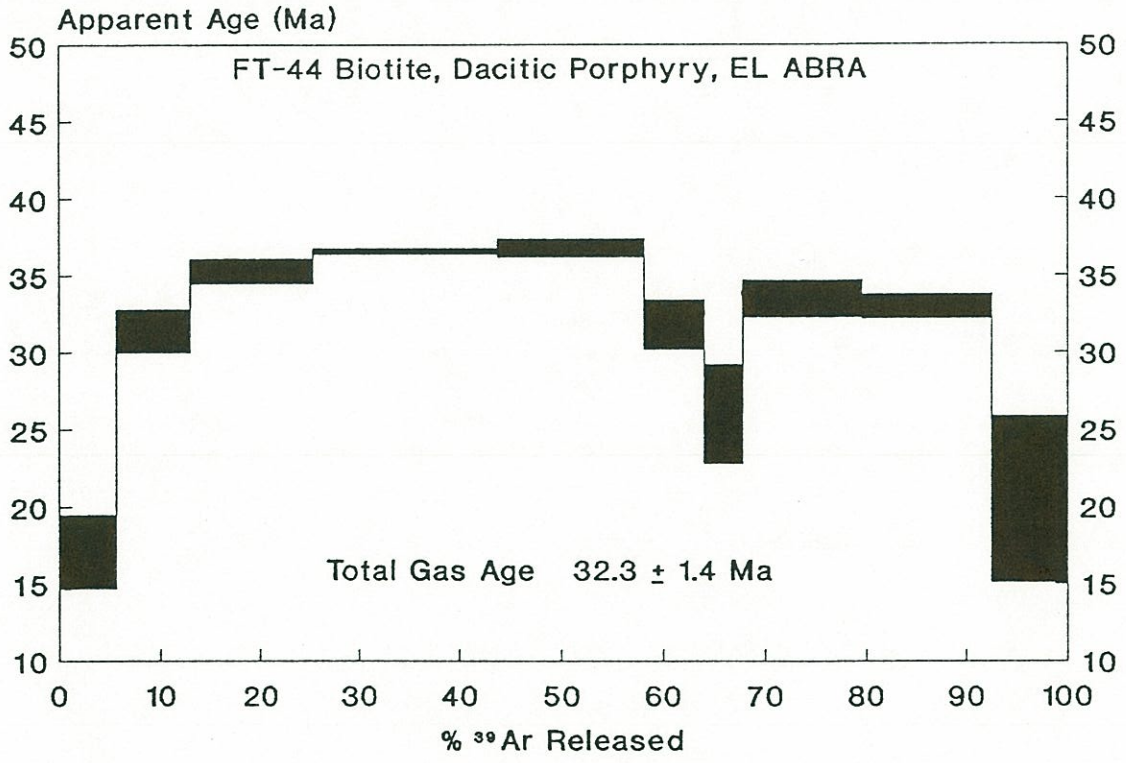


Figure A1.6. $^{40}Ar$-$^{39}Ar$ incremental-release age spectrum of biotite FT-44 from El Abra porphyry copper deposit (Dacitic Porphyry). Analytical uncertainties (±2σ) are represented by width of bars.

**Table A1.7.** $^{40}Ar$-$^{39}Ar$ data summary of FT-45 biotite, Southern Granodiorite, EL ABRA (21°55'45" Lat.S - 68°51'05" Long.W).

| TEMP.(°C) | mV $^{39}Ar$ | % $^{39}Ar$ | % Atm. Ar | % I.I.C. | APPARENT AGE (Ma) (Error ± 2σ) |
|---|---|---|---|---|---|
| 200-550 | 11.6 | 2.3 | 96.1 | 0.3 | 23.0 ± 6.6 |
| 550-600 | 18.0 | 3.7 | 87.7 | 0.1 | 35.8 ± 2.8 |
| 600-650 | 40.7 | 8.4 | 75.5 | 0.1 | 35.8 ± 1.0 |
| 650-700 | 75.1 | 15.5 | 60.1 | 0.1 | 36.8 ± 0.6 |
| 700-750 | 72.8 | 15.0 | 58.0 | 0.1 | 36.3 ± 0.4 |
| 750-800 | 29.2 | 6.0 | 77.1 | 0.1 | 37.0 ± 1.4 |
| 800-850 | 22.4 | 4.6 | 83.0 | 0.1 | 35.9 ± 2.2 |
| 850-900 | 28.9 | 5.9 | 80.5 | 0.1 | 36.7 ± 1.8 |
| 900-950 | 101.8 | 21.0 | 68.3 | 0.1 | 37.0 ± 0.6 |
| 950-1000 | 38.0 | 7.8 | 46.7 | 0.1 | 36.4 ± 0.2 |
| 1000-1100 | 45.4 | 9.3 | 86.7 | 0.2 | 34.2 ± 1.6 |

J = 0.00248 TOTAL GAS AGE = 36.1 ± 1.0 Ma

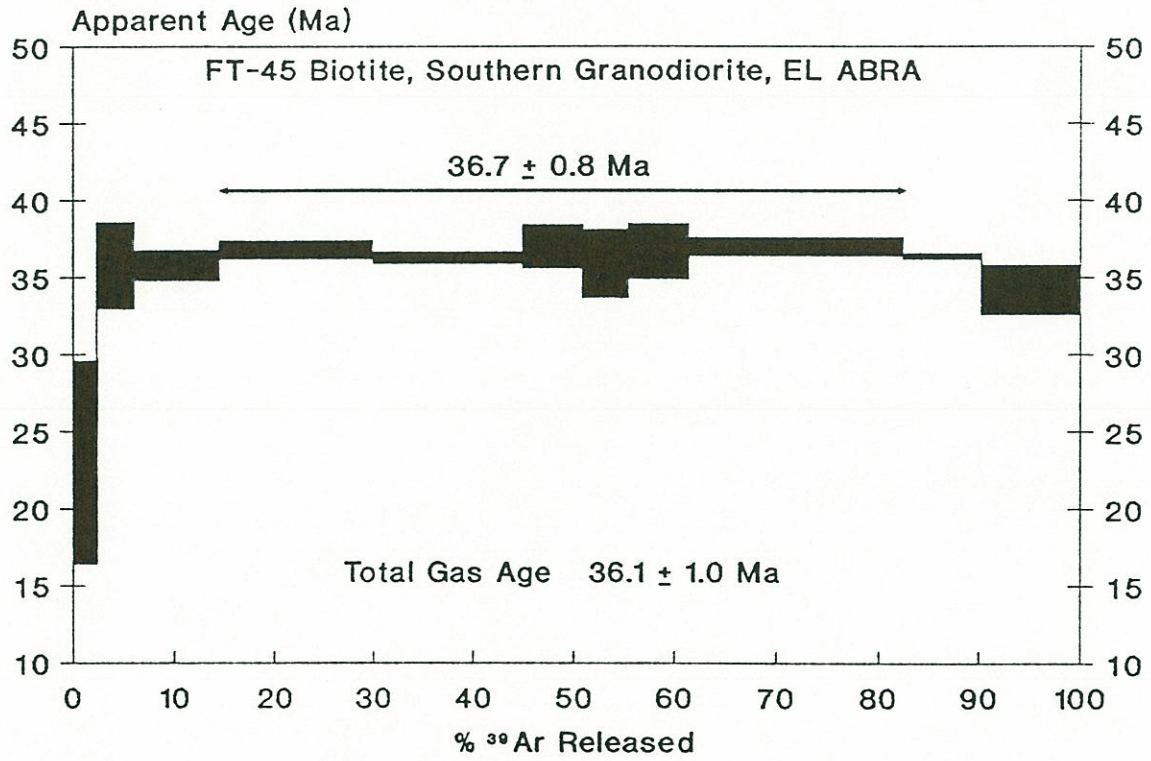


**Figure A1.7.** $^{40}Ar$-$^{39}Ar$ incremental-release age spectrum of biotite FT-45 from the Southern Granodiorite of El Abra. Analytical uncertainties (±2σ) are represented by width of bars.

**Table A1.8.** $^{40}Ar$-$^{39}Ar$ data summary of FT-62 biotite, quartz monzonite, QUEBRADA PUNO (21°21'00" Lat.S - 68°49'20" Long.W).

| TEMP.(°C) | mV $^{39}Ar$ | % $^{39}Ar$ | % Atm. Ar | % I.I.C. | APPARENT AGE (Ma) (Error ± 2σ) |
|---|---|---|---|---|---|
| 200-550 | 8.9 | 2.1 | 98.2 | 0.6 | 11.1 ± 8.2 |
| 550-600 | 7.5 | 1.7 | 93.2 | 0.2 | 34.0 ± 7.6 |
| 600-650 | 16.4 | 3.9 | 85.5 | 0.1 | 37.4 ± 3.2 |
| 650-700 | 43.8 | 10.4 | 71.7 | 0.1 | 39.0 ± 0.8 |
| 700-750 | 66.5 | 15.8 | 65.0 | 0.1 | 38.8 ± 0.6 |
| 750-800 | 42.5 | 10.1 | 73.3 | 0.1 | 39.6 ± 0.8 |
| 800-850 | 36.7 | 8.7 | 84.3 | 0.1 | 36.9 ± 1.2 |
| 850-900 | 34.1 | 8.1 | 85.2 | 0.1 | 37.7 ± 1.4 |
| 900-950 | 49.5 | 11.7 | 78.9 | 0.1 | 38.7 ± 1.0 |
| 950-1000 | 38.0 | 9.0 | 68.2 | 0.1 | 38.9 ± 0.4 |
| 1000-1100 | 76.5 | 18.1 | 90.1 | 0.2 | 33.6 ± 1.2 |

J = 0.00248 TOTAL GAS AGE = 37.0 ± 1.4 Ma

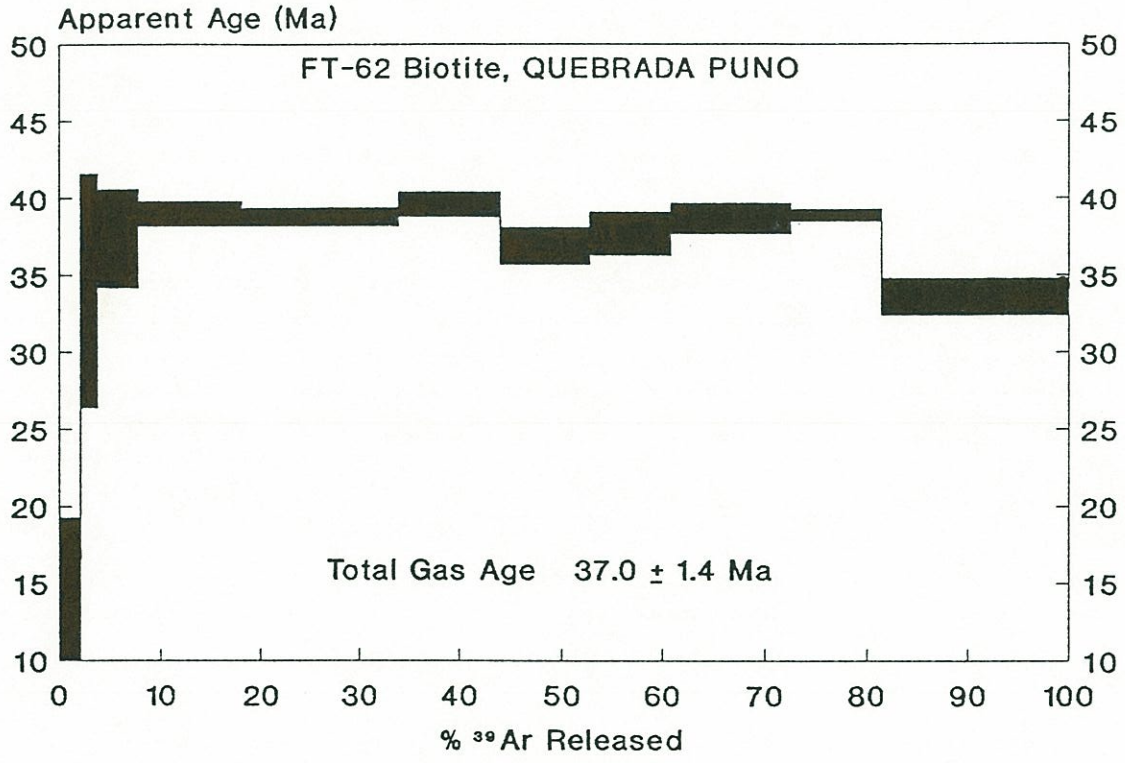


**Figure A1.8.** $^{40}Ar$-$^{39}Ar$ incremental-release age spectrum of biotite FT-62 from Quebrada Puno prospect (quartz monzonite). Analytical uncertainties (±2σ) are represented by width of bars.

Table A1.9. $^{40}Ar$-$^{39}Ar$ data summary of FT-66 biotite, quartz monzonitic porphyry, QUEBRADA BLANCA (20°59'20" Lat.S - 68°48'40" Long.W).

| TEMP.(°C) | mV $^{39}Ar$ | % $^{39}Ar$ | % Atm. Ar | % I.I.C. | APPARENT AGE (Ma) (Error ± 2σ) |
|---|---|---|---|---|---|
| 200-550 | 46.4 | 8.6 | 77.4 | 0.2 | 33.6 ± 0.8 |
| 550-600 | 51.7 | 9.6 | 51.3 | 0.1 | 34.5 ± 0.8 |
| 600-650 | 74.0 | 13.8 | 43.3 | 0.1 | 34.9 ± 0.4 |
| 650-700 | 72.6 | 13.5 | 35.6 | 0.1 | 34.8 ± 0.2 |
| 700-750 | 139.7 | 26.1 | 40.8 | 0.1 | 35.1 ± 0.4 |
| 750-800 | 16.8 | 3.1 | 87.2 | 0.2 | 33.0 ± 2.6 |
| 800-850 | 12.1 | 2.2 | 91.9 | 0.2 | 30.9 ± 5.0 |
| 850-900 | 10.5 | 1.9 | 92.1 | 0.2 | 26.8 ± 5.0 |
| 900-950 | 25.3 | 4.7 | 82.8 | 0.1 | 36.2 ± 3.6 |
| 950-1000 | 38.0 | 7.0 | 80.1 | 0.1 | 33.2 ± 0.8 |
| 1000-1100 | 47.7 | 8.9 | 94.4 | 0.2 | 27.8 ± 3.0 |

J = 0.00248 TOTAL GAS AGE = 33.8 ± 1.2 Ma

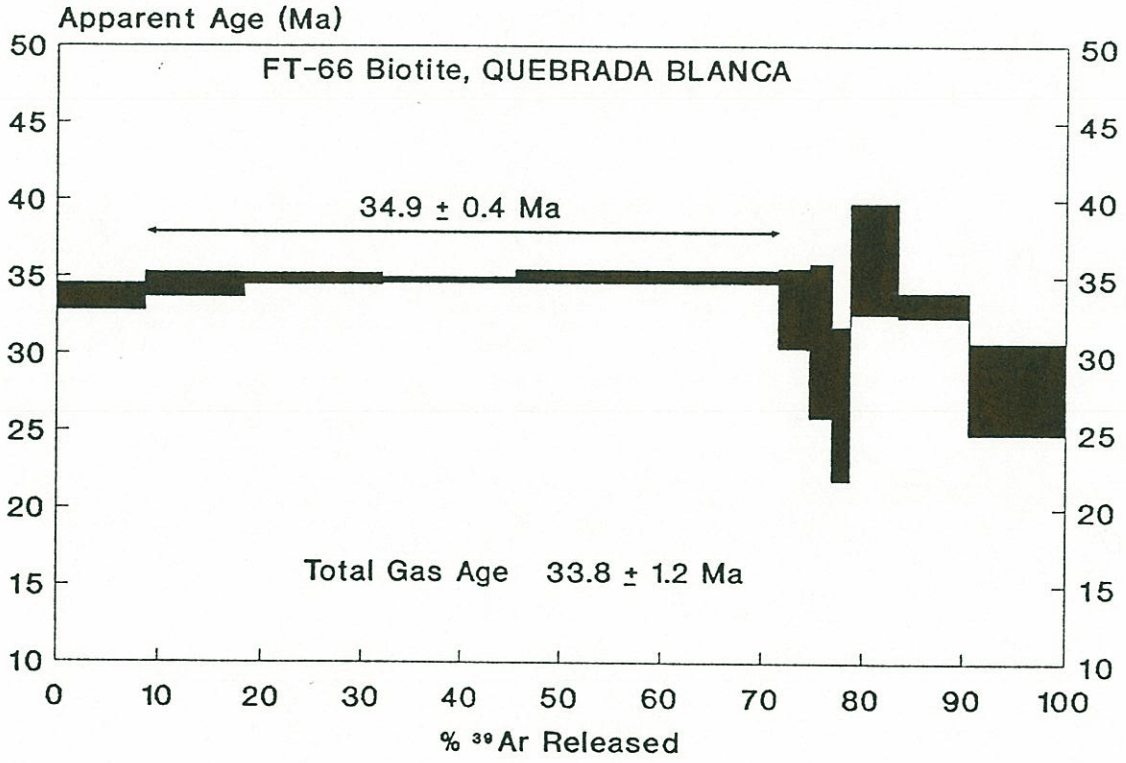


Figure A1.9. $^{40}Ar$-$^{39}Ar$ incremental-release age spectrum of biotite FT-66 from Quebrada Blanca porphyry copper deposit (quartz monzonite porphyry). Analytical uncertainties (±2σ) are represented by width of bars.

Table A1.10. $^{40}Ar$-$^{39}Ar$ data summary of FT-67 biotite, granodioritic porphyry, COPAQUIRE (20°55'16" Lat.S - 68°52'50").

| TEMP.(°C) | mV $^{39}Ar$ | % $^{39}Ar$ | % Atm. Ar | % I.I.C. | APPARENT AGE (Ma) (Error ± 2σ) |
|---|---|---|---|---|---|
| 200-550 | 46.3 | 9.1 | 83.0 | 0.2 | 30.2 ± 0.8 |
| 550-600 | 70.4 | 13.8 | 62.2 | 0.1 | 36.0 ± 0.6 |
| 600-650 | 88.5 | 17.4 | 52.4 | 0.1 | 36.8 ± 0.4 |
| 650-700 | 92.2 | 18.2 | 50.1 | 0.1 | 36.5 ± 0.4 |
| 700-750 | 56.1 | 11.0 | 65.4 | 0.1 | 35.5 ± 0.6 |
| 750-800 | 10.4 | 2.0 | 92.9 | 0.2 | 30.8 ± 5.0 |
| 800-850 | 11.1 | 2.1 | 94.1 | 0.2 | 25.2 ± 3.4 |
| 850-900 | 13.3 | 2.6 | 92.6 | 0.2 | 31.8 ± 3.8 |
| 900-950 | 30.9 | 6.1 | 89.2 | 0.2 | 31.6 ± 1.6 |
| 950-1000 | 38.0 | 7.4 | 87.4 | 0.2 | 32.0 ± 1.2 |
| 1000-1100 | 49.1 | 9.7 | 93.5 | 0.2 | 30.6 ± 1.8 |

J = 0.00248 TOTAL GAS AGE = 34.1 ± 1.0 Ma

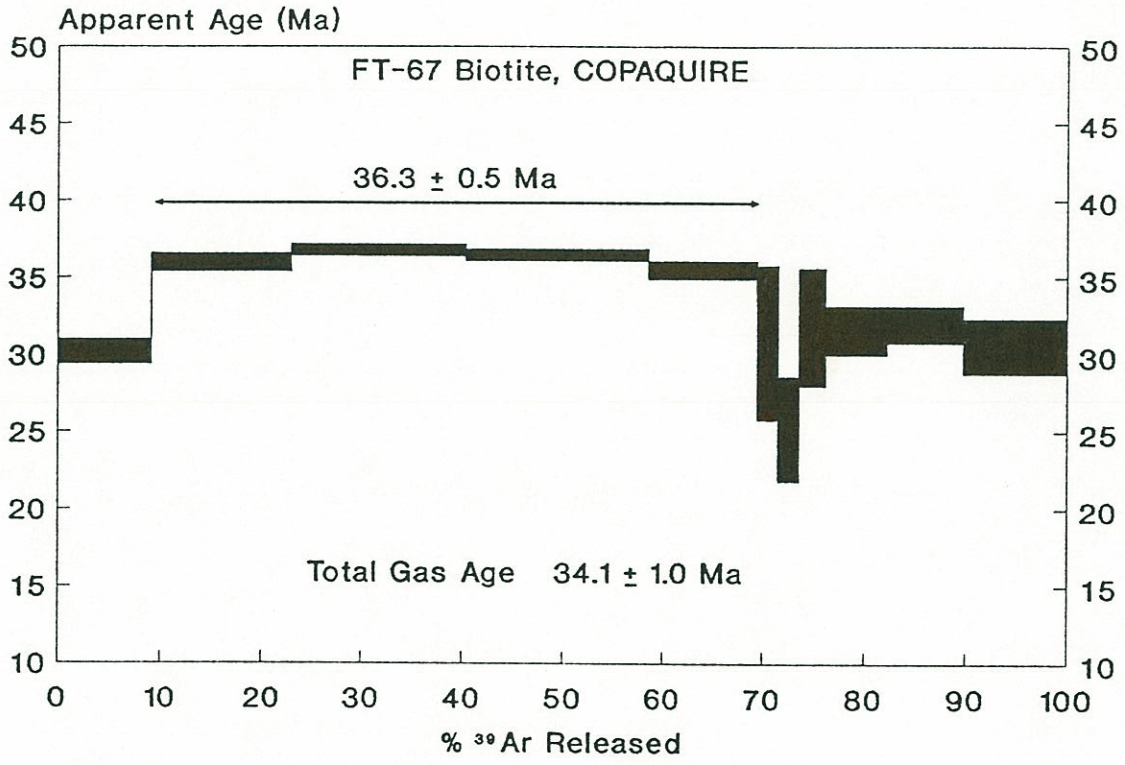


Figure A1.10. $^{40}Ar$-$^{39}Ar$ incremental-release age spectrum of biotite FT-67 from Copaquire porphyry molybdenum deposit (granodioritic porphyry). Analytical uncertainties (±2σ) are represented by width of bars.

Table A1.11. $^{40}Ar$-$^{39}Ar$ data summary of II-592 biotite, granodiorite, SIERRA GORDA (22°53'15" Lat.S - 69°21'20" Long.W).

| TEMP.(°C) | mV $^{39}Ar$ | % $^{39}Ar$ | % Atm. Ar | % I.I.C. | APPARENT AGE (Ma) (Error ± 2σ) |
|---|---|---|---|---|---|
| 200-550 | 14.2 | 2.1 | 95.4 | 0.2 | 27.0 ± 6.8 |
| 550-600 | 12.2 | 1.8 | 83.4 | 0.1 | 58.1 ± 2.4 |
| 600-650 | 26.3 | 4.0 | 67.3 | 0.1 | 61.4 ± 1.8 |
| 650-700 | 53.8 | 8.2 | 45.4 | 0.1 | 63.7 ± 0.6 |
| 700-750 | 99.8 | 15.3 | 43.3 | 0.1 | 62.8 ± 0.8 |
| 750-800 | 90.6 | 13.9 | 40.1 | 0.1 | 62.8 ± 0.4 |
| 800-850 | 53.3 | 8.2 | 54.7 | 0.1 | 63.0 ± 0.6 |
| 850-900 | 48.7 | 7.5 | 58.1 | 0.1 | 64.2 ± 1.0 |
| 900-950 | 21.4 | 3.3 | 51.2 | 0.1 | 63.9 ± 2.6 |
| 950-1000 | 186.8 | 28.7 | 30.8 | 0.0 | 63.5 ± 0.2 |
| 1000-1050 | 41.8 | 6.4 | 69.5 | 0.1 | 62.2 ± 1.0 |

J = 0.0240 TOTAL GAS AGE = 62.3 ± 0.8 Ma

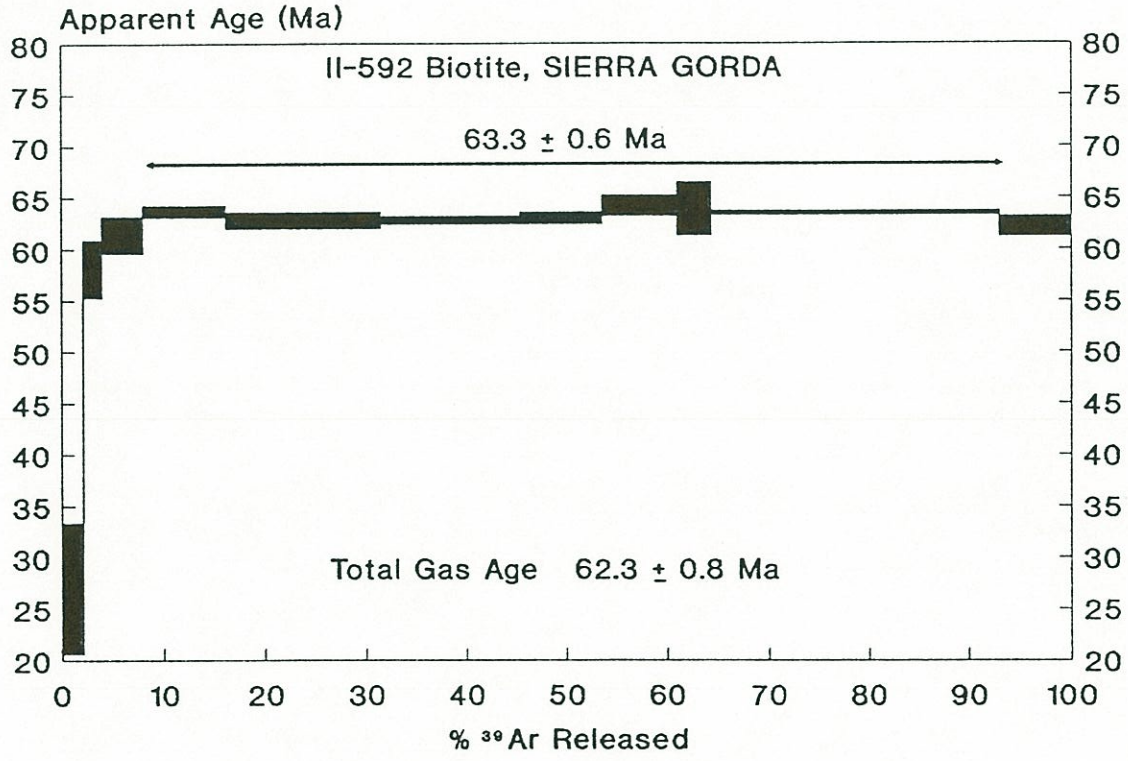


Figure A1.11. $^{40}Ar$-$^{39}Ar$ incremental-release age spectrum of biotite II-592 from host granodiorite of Sierra Gorda porphyry copper deposit. Analytical uncertainties (±2σ) are represented by width of bars.

Table A1.12. $^{40}Ar$-$^{39}Ar$ data summary of II-611 biotite, granodiorite, LOMAS BAYAS (23°25'25" Lat.S - 69°29'40" Long.W).

| TEMP.(°C) | mV $^{39}Ar$ | % $^{39}Ar$ | % Atm. Ar | % I.I.C. | APPARENT AGE (Ma) (Error ± 2σ) |
|---|---|---|---|---|---|
| 200-550 | 6.1 | 0.9 | 83.4 | 0.1 | 33.6 ± 8.6 |
| 550-600 | 13.7 | 2.1 | 70.7 | 0.1 | 55.0 ± 3.0 |
| 600-650 | 25.3 | 3.9 | 48.2 | 0.1 | 63.7 ± 1.6 |
| 650-700 | 56.3 | 8.8 | 33.3 | 0.1 | 63.8 ± 0.8 |
| 700-750 | | Gas lost during extraction | | | |
| 750-800 | 74.4 | 11.6 | 16.1 | 0.1 | 64.3 ± 0.4 |
| 800-850 | 37.8 | 5.9 | 47.7 | 0.1 | 63.7 ± 1.2 |
| 850-900 | 44.2 | 6.9 | 50.0 | 0.1 | 65.6 ± 1.0 |
| 900-950 | 77.7 | 12.1 | 45.3 | 0.0 | 65.4 ± 0.8 |
| 950-1000 | 154.2 | 24.1 | 25.7 | 0.1 | 64.0 ± 0.4 |
| 1000-1050 | 89.5 | 13.9 | 25.7 | 0.1 | 63.6 ± 0.4 |

J = 0.00240 TOTAL GAS AGE = 63.7 ± 0.8 Ma

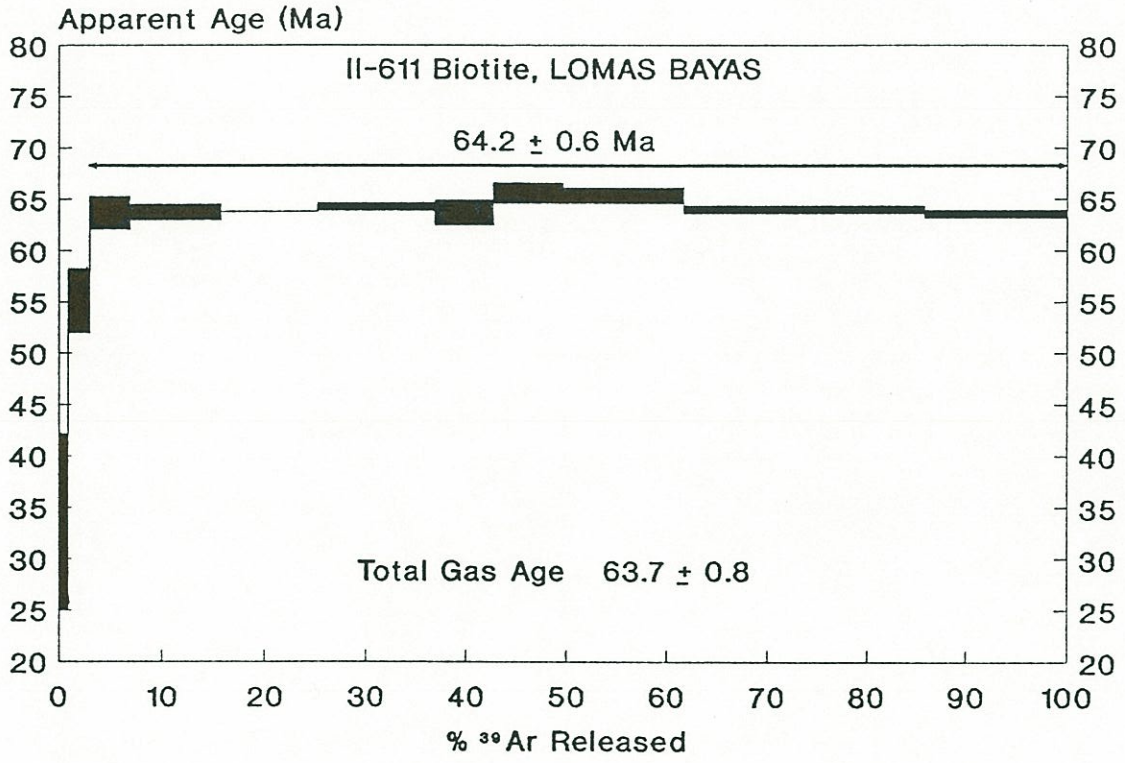


Figure A1.12. $^{40}Ar$-$^{39}Ar$ incremental-release age spectrum of biotite II-611 from host granodiorite of Lomas Bayas porphyry copper deposit. Analytical uncertainties (±2σ) are represented by width of bars.

**Table A1.13.** $^{40}Ar$-$^{39}Ar$ data summary of II-611 hornblende, granodiorite, LOMAS BAYAS (23°25'25" Lat.S - 69°29'40" Long.W).

| TEMP.(°C) | mV $^{39}Ar$ | % $^{39}Ar$ | %Atm.Ar | %I.I.C. | $^{37}Ar/^{39}Ar$ | APP. AGE (Ma) Error ± 2σ |
|---|---|---|---|---|---|---|
| 200-650 | 2.7 | 7.4 | 88.5 | 1.7 | 2.4 | 46.7 ± 2.6 |
| 650-725 | 3.0 | 7.9 | 59.8 | 0.1 | 0.3 | 57.6 ± 1.6 |
| 725-800 | 3.0 | 8.1 | 58.6 | 0.1 | 0.4 | 59.9 ± 1.2 |
| 800-870 | 1.9 | 5.2 | 78.5 | 1.5 | 2.6 | 54.4 ± 1.8 |
| 870-920 | 2.0 | 5.4 | 81.5 | 4.8 | 7.9 | 56.4 ± 3.6 |
| 920-950 | 3.3 | 8.8 | 73.8 | 7.3 | 12.0 | 57.5 ± 1.8 |
| 950-980 | 4.7 | 12.7 | 60.1 | 5.8 | 9.6 | 57.9 ± 1.0 |
| 980-1010 | 8.5 | 22.8 | 46.4 | 4.6 | 7.9 | 59.9 ± 0.4 |
| 1010-1050 | 5.0 | 13.3 | 60.8 | 3.4 | 5.8 | 59.0 ± 1.2 |
| 1050-1150 | 3.0 | 8.0 | 87.2 | 9.1 | 13.8 | 52.8 ± 2.6 |

J = 0.00240 TOTAL GAS AGE = 57.1 ± 1.6 Ma

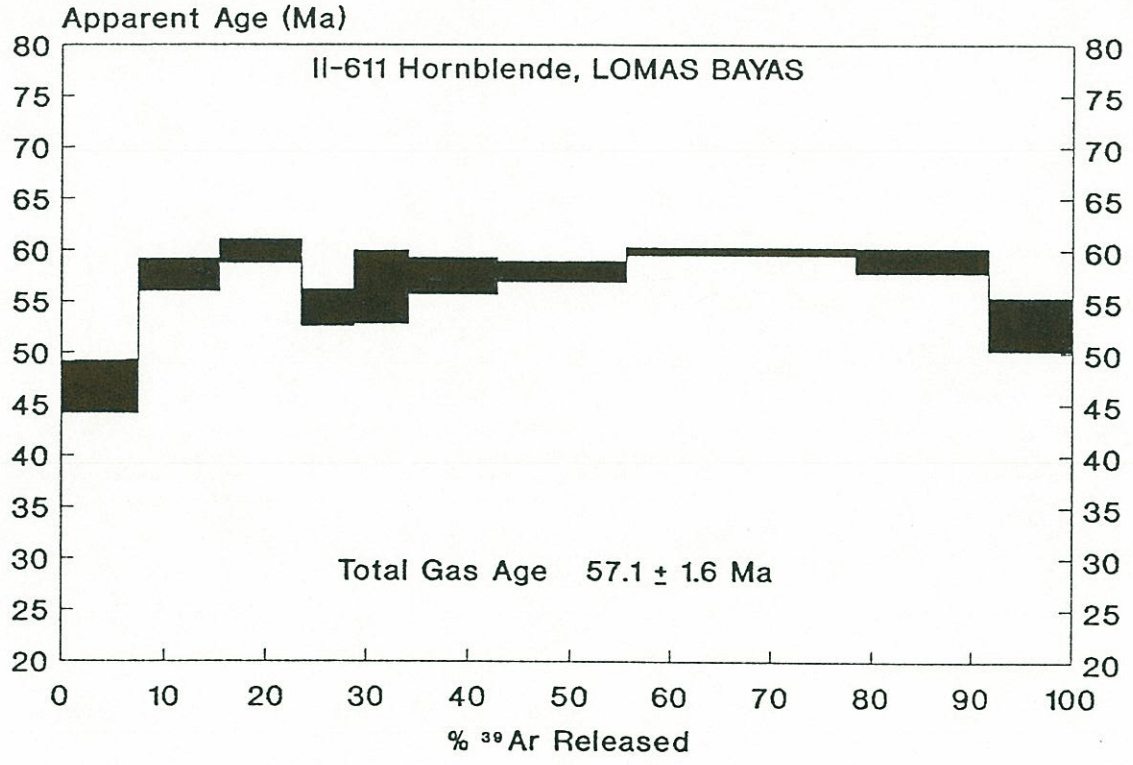


**Figure A1.13.** $^{40}Ar$-$^{39}Ar$ incremental-release age spectrum of hornblende II-611 from host granodiorite of Lomas Bayas porphyry copper deposit. Analytical uncertainties (±2σ) are represented by width of bars.

**Table A1.14.** $^{40}Ar$-$^{39}Ar$ data summary of II-607 hornblende, granodiorite, FORTUNA DEL COBRE (23°28'20" Lat.S - 69°33'10" Long.W).

| TEMP.(°C) | mV $^{39}Ar$ | % $^{39}Ar$ | %Atm.Ar | %I.I.C. | $^{37}Ar/^{39}Ar$ | APP. AGE (Ma) Error ± 2σ |
|---|---|---|---|---|---|---|
| 200-650 | 2.7 | 8.0 | 93.7 | 0.6 | 1.1 | 48.1 ± 8.0 |
| 650-725 | 2.9 | 8.7 | 83.0 | 0.1 | 0.3 | 57.9 ± 2.6 |
| 725-800 | 1.4 | 4.2 | 84.0 | 0.5 | 1.0 | 55.8 ± 5.2 |
| 800-850 | 1.3 | 3.9 | 87.4 | 1.9 | 3.0 | 53.7 ± 6.6 |
| 850-900 | 2.6 | 7.7 | 86.3 | 3.8 | 6.4 | 59.1 ± 4.4 |
| 900-950 | 3.6 | 10.7 | 78.0 | 6.8 | 11.2 | 58.0 ± 2.6 |
| 950-980 | 7.8 | 23.2 | 67.6 | 5.3 | 9.4 | 62.0 ± 1.2 |
| 980-1010 | 6.6 | 19.7 | 64.9 | 4.2 | 7.6 | 63.4 ± 1.4 |
| 1010-1050 | 2.2 | 6.7 | 86.1 | 4.7 | 7.5 | 54.8 ± 4.0 |
| 1050-1100 | 1.5 | 4.4 | 92.6 | 9.0 | 11.7 | 45.0 ± 7.0 |
| 1100-1140 | 0.7 | 2.2 | 95.9 | 14.5 | 17.8 | 42.2 ± 17.0 |

J = 0.00240 TOTAL GAS AGE = 57.9 ± 3.6 Ma

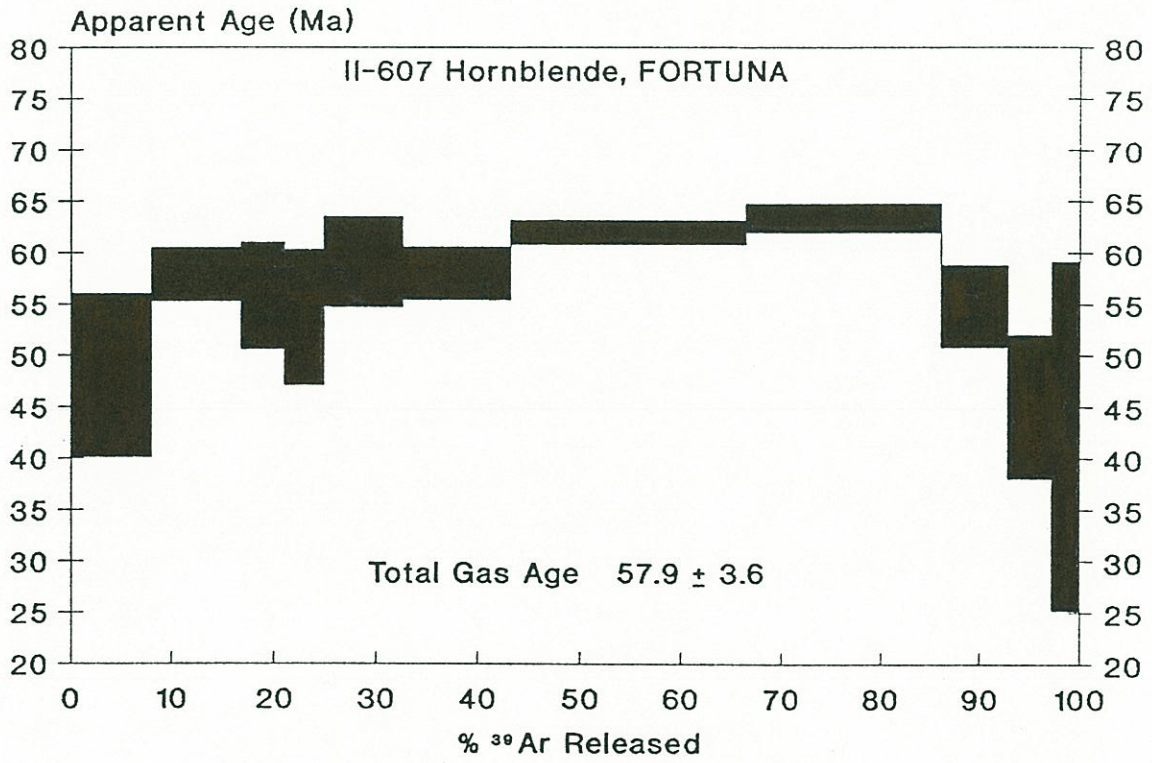


**Figure A1.14.** $^{40}Ar$-$^{39}Ar$ incremental-release age spectrum of hornblende II-607 from host granodiorite of Fortuna del Cobre porphyry copper deposit. Analytical uncertainties (±2σ) are represented by width of bars.

Table A1.15. $^{40}Ar$-$^{39}Ar$ data summary of II-598 biotite, granodiorite, Sierra San Cristobal (23°23'20" Lat.S - 69°35'50" Long.W).

| TEMP.(°C) | mV $^{39}Ar$ | % $^{39}Ar$ | % Atm. Ar | % I.I.C. | APPARENT AGE (Ma) (Error ±2σ) |
|---|---|---|---|---|---|
| 200-550 | 6.7 | 1.0 | 97.3 | 0.5 | 12.9 ± 8.4 |
| 550-600 | 3.6 | 0.5 | 89.7 | 0.1 | 57.1 ± 17.8 |
| 600-650 | 8.2 | 1.2 | 77.0 | 0.0 | 76.8 ± 6.0 |
| 650-700 | 25.9 | 4.0 | 55.7 | 0.0 | 77.3 ± 1.2 |
| 700-750 | 71.8 | 11.1 | 39.4 | 0.0 | 77.5 ± 0.6 |
| 750-800 | 57.0 | 8.8 | 39.3 | 0.0 | 78.6 ± 0.6 |
| 800-850 | 45.6 | 7.0 | 37.0 | 0.0 | 83.5 ± 2.6 |
| 850-900 | 61.5 | 9.5 | 35.8 | 0.0 | 78.7 ± 0.6 |
| 900-950 | 79.3 | 12.5 | 34.9 | 0.0 | 79.4 ± 0.4 |
| 950-1000 | 175.1 | 27.2 | 20.6 | 0.0 | 78.5 ± 0.2 |
| 1000-1050 | 99.4 | 15.4 | 29.1 | 0.0 | 78.0 ± 0.4 |
| 1050-1100 | 9.5 | 1.4 | 88.9 | 0.0 | 75.6 ± 7.8 |

J = 0.00240 TOTAL GAS AGE = 77.9 ± 1.0 Ma

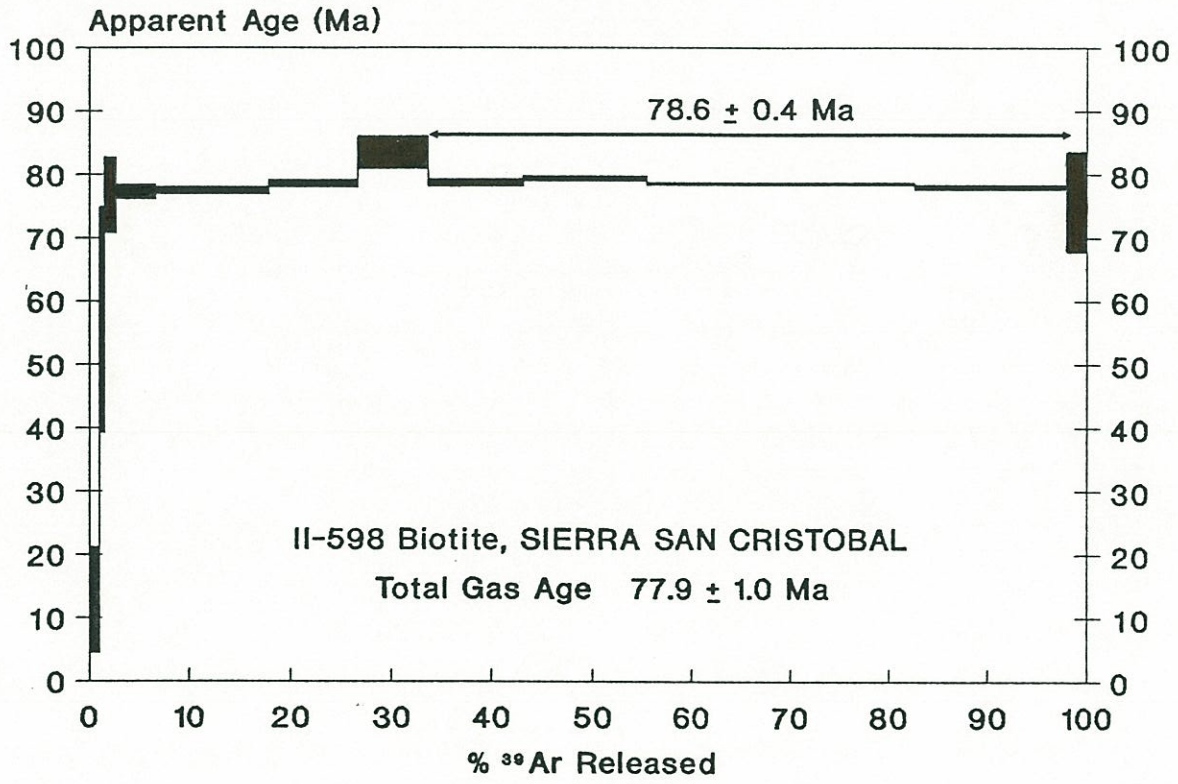


Figure A1.15. $^{40}Ar$-$^{39}Ar$ incremental-release age spectrum of biotite II-598 from a granodiorite of the Sierra San Cristobal. Analytical uncertainties (±2σ) are represented by width of bars.

Table A1.16. $^{40}Ar$-$^{39}Ar$ data summary of II-597 biotite, dioritic stock, Caracoles Silver District (23°03'20" Lat.S - 69°01'35" Long.W).

| TEMP.(°C) | mV $^{39}Ar$ | % $^{39}Ar$ | % Atm. Ar | % I.I.C. | APPARENT AGE (Ma) (Error ± 2σ) |
|---|---|---|---|---|---|
| 200-550 | 13.5 | 2.2 | 95.6 | 0.3 | 19.2 ± 5.0 |
| 550-600 | 8.8 | 1.4 | 91.0 | 0.1 | 55.3 ± 6.8 |
| 600-650 | 10.2 | 1.6 | 82.1 | 0.0 | 74.5 ± 5.4 |
| 650-700 | 35.7 | 5.9 | 61.5 | 0.0 | 78.5 ± 1.4 |
| 700-750 | 44.6 | 7.4 | 47.2 | 0.0 | 76.8 ± 1.0 |
| 750-800 | 76.3 | 12.6 | 36.0 | 0.0 | 74.9 ± 0.6 |
| 800-850 | 58.6 | 9.7 | 15.8 | 0.0 | 76.6 ± 0.6 |
| 850-900 | 60.0 | 9.9 | 44.5 | 0.0 | 77.7 ± 1.0 |
| 900-950 | 43.2 | 7.1 | 50.8 | 0.0 | 84.0 ± 1.2 |
| 950-1000 | 122.1 | 20.3 | 33.9 | 0.0 | 77.7 ± 0.4 |
| 1000-1050 | 97.1 | 16.1 | 31.9 | 0.0 | 75.7 ± 0.4 |
| 1050-1100 | 30.8 | 5.1 | 63.6 | 0.0 | 72.5 ± 6.0 |

J = 0.00240 TOTAL GAS AGE = 75.4 ± 1.2 Ma

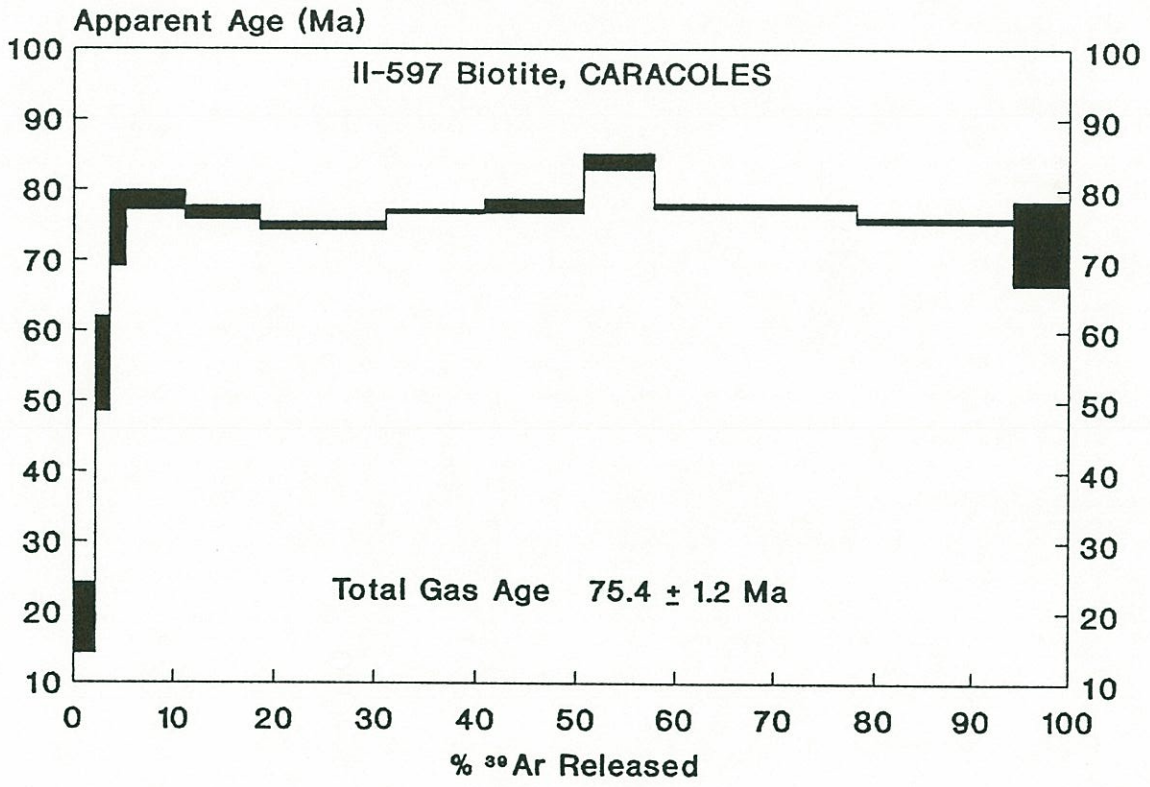


Figure A1.16. $^{40}Ar$-$^{39}Ar$ incremental-release age spectrum of biotite II-597 from a dioritic stock of the Caracoles silver district. Analytical uncertainties (±2σ) are represented by width of bars.

Table A1.17. $^{40}Ar$-$^{39}Ar$ data summary of FT-8 biotite, granodiorite, Cerros de Montecristo (22°17'10" Lat.S - 69°11'30" Long.W).

| TEMP.(°C) | mV $^{39}Ar$ | % $^{39}Ar$ | % Atm. Ar | % I.I.C. | APPARENT AGE (Ma) (Error ± 2σ) |
|---|---|---|---|---|---|
| 200-550 | 5.8 | 0.7 | 95.1 | 0.3 | 18.2 ± 8.4 |
| 550-600 | 5.2 | 0.6 | 85.7 | 0.1 | 51.8 ± 9.2 |
| 600-650 | 12.0 | 1.4 | 69.7 | 0.1 | 60.4 ± 3.8 |
| 650-700 | 30.1 | 3.6 | 48.5 | 0.1 | 62.1 ± 1.6 |
| 700-750 | 53.2 | 6.4 | 37.3 | 0.1 | 62.6 ± 0.6 |
| 750-800 | 43.0 | 5.2 | 45.8 | 0.1 | 62.2 ± 0.6 |
| 800-850 | 74.9 | 9.1 | 29.8 | 0.1 | 63.4 ± 0.4 |
| 850-900 | 138.8 | 16.9 | 22.4 | 0.1 | 63.6 ± 0.4 |
| 900-950 | 142.4 | 17.3 | 22.5 | 0.1 | 63.3 ± 0.2 |
| 950-1000 | 226.2 | 27.5 | 19.1 | 0.1 | 63.1 ± 0.0 |
| 1000-1050 | 77.1 | 9.4 | 38.5 | 0.1 | 63.3 ± 0.4 |
| 1050-1100 | 10.5 | 1.2 | 76.3 | 0.0 | 92.6 ± 13.8 |

J = 0.00240

TOTAL GAS AGE = 63.1 ± 0.8 Ma

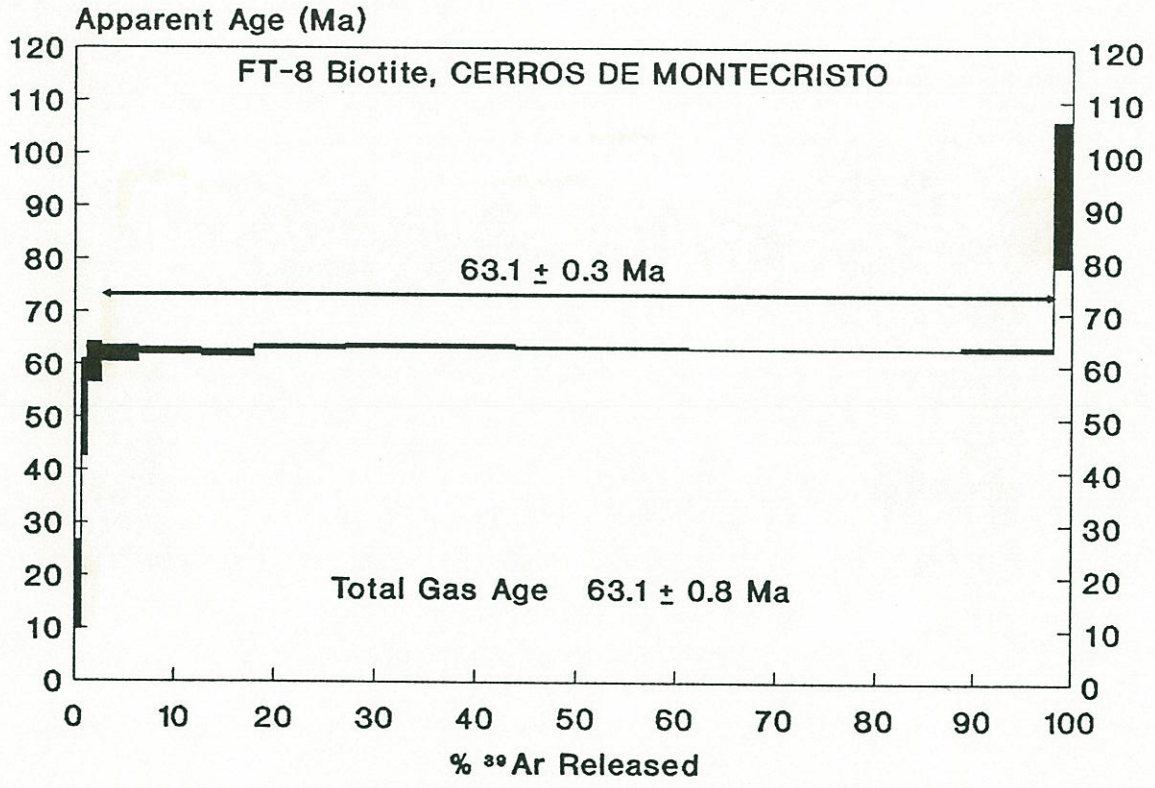


Figure A1.17. $^{40}Ar$-$^{39}Ar$ incremental-release age spectrum of biotite FT-8 from a granodiorite of the Cerros de Montecristo pluton. Analytical uncertainties (±2σ) are represented by width of bars.

Table A1.18. $^{40}Ar$-$^{39}Ar$ data summary of II-562 Actinolite, veinlet within granodiorite, Tocopilla District (22°04'45" Lat.S - 70°09'55" Long.W).

| TEMP.(°C) | mV $^{39}Ar$ | % $^{39}Ar$ | %Atm.Ar | %I.I.C. | $^{37}Ar/^{39}Ar$ | APP. AGE (Ma) Error ± 2σ |
|---|---|---|---|---|---|---|
| 200-650 | 0.3 | 6.2 | 100.7 | 2.9 | 6.8 | -65.2 ± -339.8 |
| 650-725 | 0.0 | 1.2 | 100.8 | 1.6 | 11.1 | -153.4 ± -6792 |
| 725-800 | 0.1 | 2.0 | 102.4 | 4.3 | 25.6 | -142.1 ± -669.2 |
| 800-850 | 0.2 | 5.1 | 98.0 | 51.2 | 56.1 | 37.7 ± 77.4 |
| 850-900 | 1.6 | 29.3 | 82.4 | 15.1 | 52.0 | 137.4 ± 9.0 |
| 900-950 | 2.1 | 37.0 | 78.4 | 14.9 | 52.4 | 141.7 ± 6.6 |
| 950-980 | 0.4 | 8.1 | 95.0 | 20.9 | 50.3 | 89.7 ± 69.8 |
| 980-1010 | 0.2 | 5.0 | 98.7 | 39.6 | 44.5 | 38.7 ± 172.0 |
| 1010-1080 | 0.3 | 5.7 | 97.7 | 16.4 | 43.7 | 101.0 ± 224.8 |

J = 0.00240

TOTAL GAS AGE = 102.4 ± -71.8 Ma[2]

PLATEAU AGE = 139.8 ± 7.7 Ma

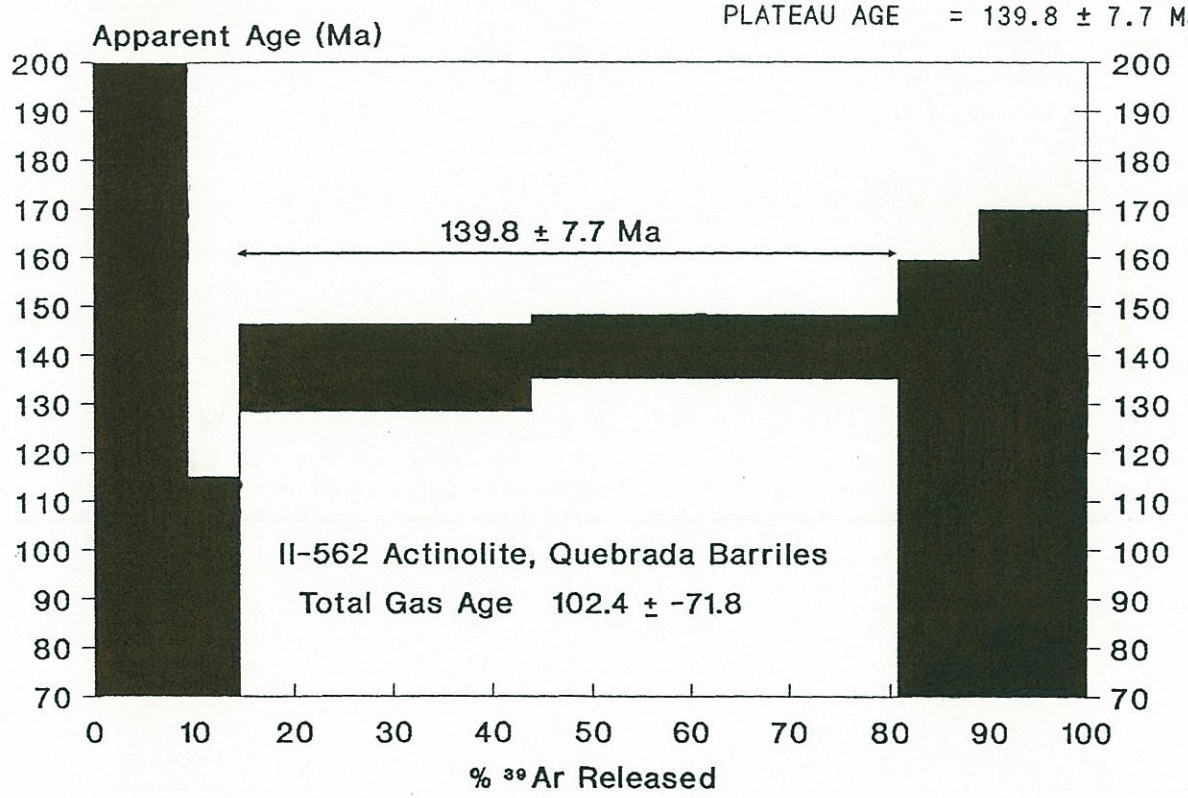


Figure A1.18. $^{40}Ar$-$^{39}Ar$ incremental-release age spectrum of actinolite II-562 from a veinlet in the Barriles creek, Tocopilla district. Analytical uncertainties (±2σ) are represented by width of bars.

[2] The total gas is incorrect because of only two steps released enough Ar to be properly measured.

Table A1.19. $^{40}Ar$-$^{39}Ar$ data summary of II-571 biotite, diorite, Guanillos District (22°23'55" Lat.S - 70°13'30" Long.W).

| TEMP.(°C) | mV $^{39}Ar$ | % $^{39}Ar$ | % Atm. Ar | % I.I.C. | APPARENT AGE (Ma) (Error ± 2σ) |
|---|---|---|---|---|---|
| 200-550 | 16.7 | 3.0 | 93.3 | 0.2 | 25.5 ± 3.8 |
| 550-600 | 5.3 | 0.9 | 79.6 | 0.0 | 101.7 ± 9.2 |
| 600-650 | 10.2 | 1.8 | 57.7 | 0.0 | 137.0 ± 5.8 |
| 650-700 | 16.6 | 3.0 | 42.7 | 0.0 | 146.7 ± 2.6 |
| 700-750 | 33.0 | 6.0 | 25.9 | 0.0 | 164.8 ± 1.4 |
| 750-800 | 56.6 | 10.3 | 19.5 | 0.0 | 166.6 ± 0.8 |
| 800-850 | 56.2 | 10.3 | 7.9 | 0.0 | 167.4 ± 0.4 |
| 850-900 | 117.2 | 21.5 | 10.2 | 0.0 | 168.0 ± 0.4 |
| 900-950 | 152.0 | 27.9 | 13.5 | 0.0 | 162.8 ± 0.4 |
| 950-1000 | 69.1 | 12.7 | 25.0 | 0.0 | 159.8 ± 1.0 |
| 1000-1050 | 11.4 | 2.0 | 74.0 | 0.0 | 146.2 ± 5.4 |

J = 0.00240

TOTAL GAS AGE = 158.5 ± 1.0 Ma

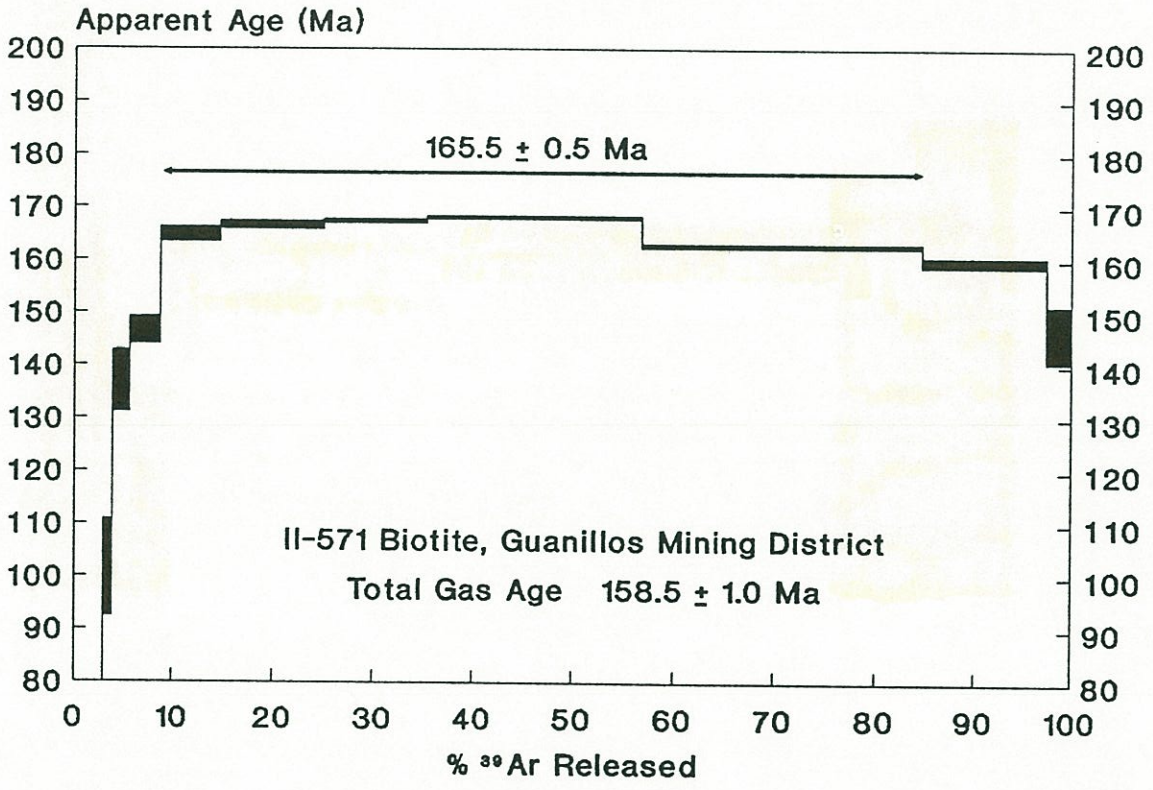


Figure A1.19. $^{40}Ar$-$^{39}Ar$ incremental-release age spectrum of biotite II-571 from a diorite of the Guanillos district. Analytical uncertainties (±2σ) are represented by width of bars.

Table A1.20. $^{40}Ar$-$^{39}Ar$ data summary of II-537 biotite, diorite, Gatico District (22°28'10" Lat.S - 70°13'30" Long.W).

| TEMP.(°C) | mV $^{39}Ar$ | % $^{39}Ar$ | % Atm. Ar | % I.I.C. | APPARENT AGE (Ma) (Error ± 2σ) |
|---|---|---|---|---|---|
| 200-550 | 16.9 | 3.5 | 91.2 | 0.2 | 26.7 ± 2.4 |
| 550-600 | 6.4 | 1.3 | 64.6 | 0.0 | 122.5 ± 12.8 |
| 600-650 | 11.7 | 2.4 | 40.0 | 0.0 | 148.5 ± 4.0 |
| 650-700 | 21.1 | 4.3 | 25.4 | 0.0 | 155.0 ± 1.6 |
| 700-750 | 27.1 | 5.6 | 18.5 | 0.0 | 161.2 ± 1.4 |
| 750-800 | 29.2 | 6.0 | 16.2 | 0.0 | 163.1 ± 1.2 |
| 800-840 | 13.7 | 2.8 | 27.0 | 0.0 | 158.6 ± 5.2 |
| 840-870 | 20.5 | 4.2 | 10.4 | 0.0 | 165.2 ± 1.8 |
| 870-900 | 37.2 | 7.7 | 9.8 | 0.0 | 168.9 ± 0.8 |
| 900-930 | 56.0 | 11.6 | 9.3 | 0.0 | 169.6 ± 0.6 |
| 930-960 | 80.2 | 16.6 | 6.8 | 0.0 | 166.4 ± 0.6 |
| 960-1000 | 106.9 | 22.1 | 8.1 | 0.0 | 163.2 ± 0.4 |
| 1000-1050 | 54.6 | 11.3 | 18.8 | 0.0 | 162.0 ± 0.8 |

J = 0.00240 TOTAL GAS AGE = 158.8 ± 1.4 Ma

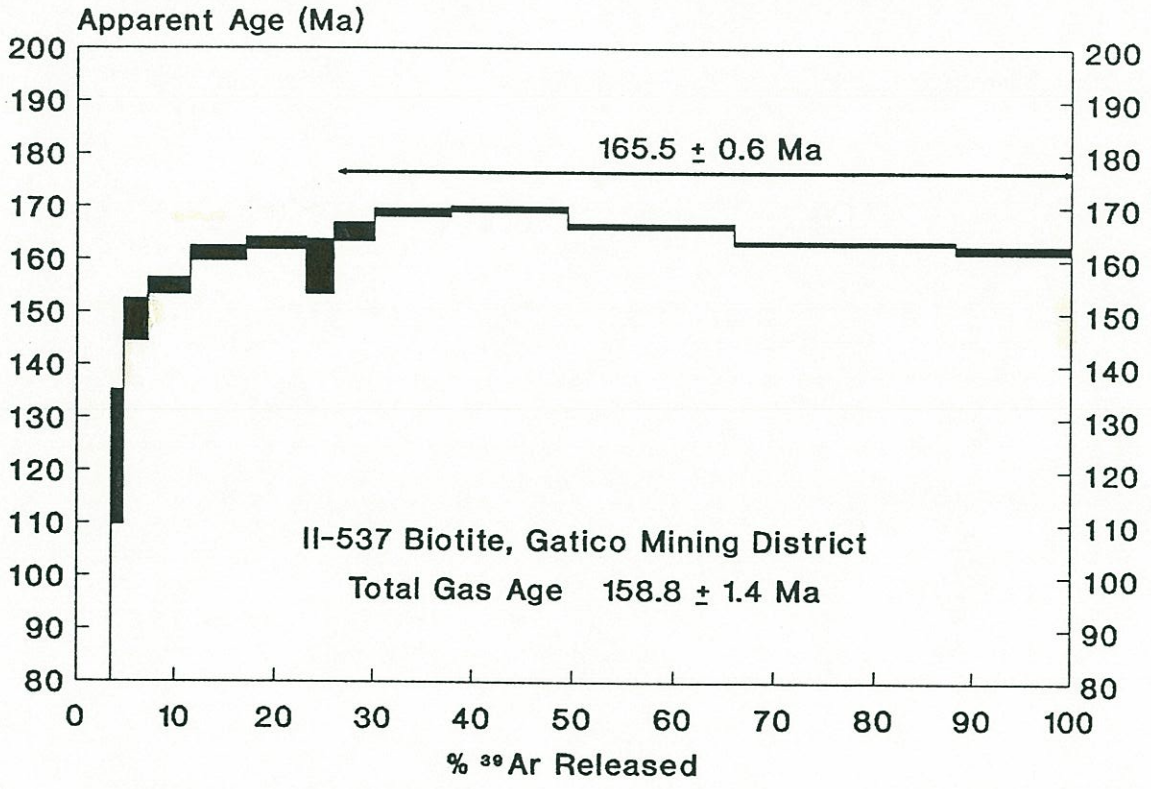


Figure A1.20. $^{40}Ar$-$^{39}Ar$ incremental-release age spectrum of biotite II-537 from a diorite of the Gatico district. Analytical uncertainties (±2σ) are represented by width of bars.

Table A1.21. $^{40}Ar$-$^{39}Ar$ data summary of II-539 biotite, diorite, Punta Tames, Cobija- Punta Tames district (22°31'45" Lat.S - 70°14'50" Long.W).

| TEMP.(°C) | mV $^{39}Ar$ | % $^{39}Ar$ | % Atm. Ar | % I.I.C. | APPARENT AGE (Ma) (Error ± 2σ) |
|---|---|---|---|---|---|
| 200-550 | 4.0 | 0.7 | 98.1 | 0.7 | 8.8 ± 21.8 |
| 550-600 | 1.5 | 0.3 | 89.5 | 0.0 | 67.7 ± 42.8 |
| 600-650 | 2.7 | 0.5 | 74.4 | 0.0 | 126.9 ± 21.4 |
| 650-700 | 4.9 | 0.9 | 67.9 | 0.0 | 132.8 ± 10.0 |
| 700-750 | 8.6 | 1.6 | 43.3 | 0.0 | 167.8 ± 6.2 |
| 750-800 | 26.4 | 5.0 | 26.1 | 0.0 | 157.7 ± 2.0 |
| 800-850 | 53.7 | 10.3 | 15.9 | 0.0 | 161.1 ± 0.8 |
| 850-900 | 122.4 | 23.4 | 7.1 | 0.0 | 165.0 ± 0.8 |
| 900-950 | 163.5 | 31.3 | 8.5 | 0.0 | 161.3 ± 0.4 |
| 950-1000 | 94.4 | 18.1 | 12.8 | 0.0 | 160.7 ± 0.4 |
| 1000-1050 | 38.5 | 7.3 | 35.8 | 0.0 | 158.0 ± 1.4 |

J = 0.00240

TOTAL GAS AGE = 159.9 ± 1.4 Ma

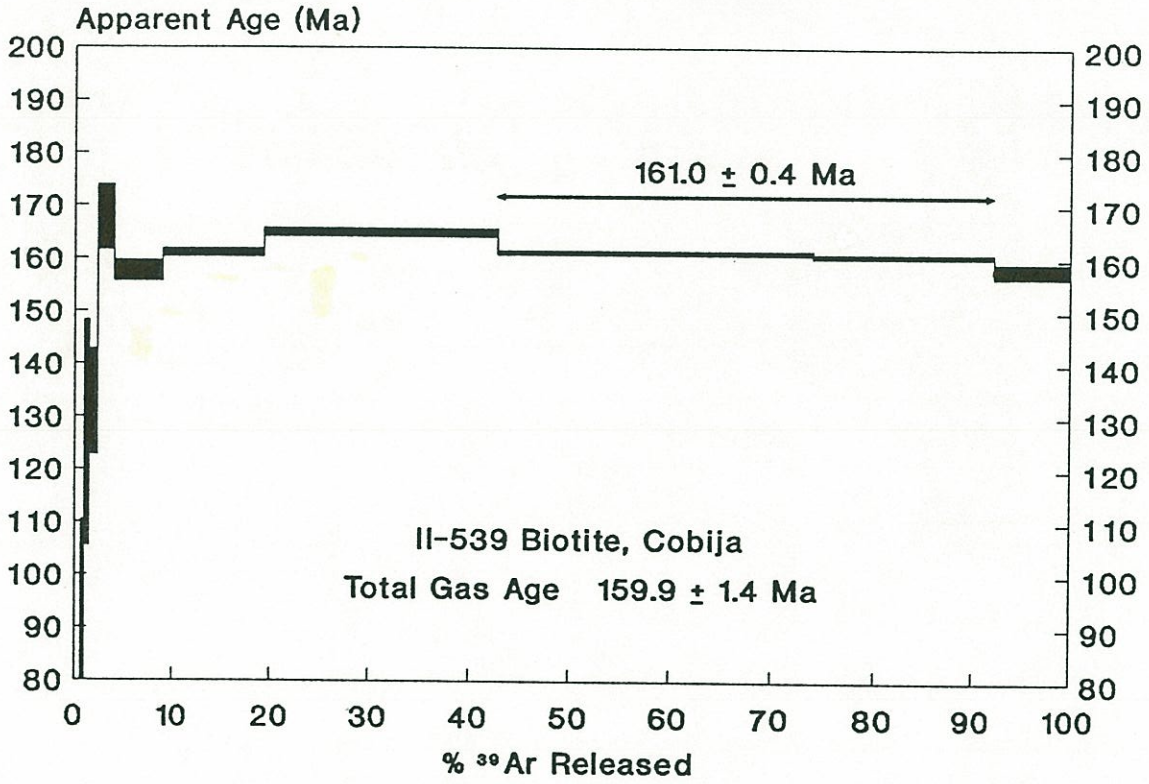


Figure A1.21. $^{40}Ar$-$^{39}Ar$ incremental-release age spectrum of biotite II-539 from Punta Tames, Cobija-Punta Tames district. Analytical uncertainties (±2σ) are represented by width of bars.

Table A1.22. $^{40}Ar$-$^{39}Ar$ data summary of II-524 actinolite, Angel de la Guarda Vein, Naguayan district (23°13'05" Lat.S - 70°14'15" Long.W).

| TEMP.(°C) | mV $^{39}Ar$ | % $^{39}Ar$ | %Atm.Ar | %I.I.C. | $^{37}Ar/^{39}Ar$ | APP. AGE (Ma) (Error ± 2σ) |
|---|---|---|---|---|---|---|
| 200-725 | 0.3 | 5.8 | 99.6 | 144.8 | 127.7 | 30.1 ± 1165.6 |
| 725-800 | 0.1 | 3.0 | 98.9 | 28.8 | 28.8 | 45.8 ± 487.4 |
| 800-850 | 0.3 | 6.3 | 101.2 | 107.0 | 53.9 | -15.9 ± -63.0 |
| 850-900 | 1.7 | 29.9 | 76.2 | 13.8 | 52.4 | 155.3 ± 6.6 |
| 900-950 | 1.8 | 30.5 | 52.9 | 12.9 | 48.1 | 152.2 ± 4.0 |
| 950-1050 | 0.8 | 13.4 | 84.8 | 12.4 | 38.2 | 119.5 ± 20.0 |
| 1050-1150 | 0.6 | 10.8 | 95.9 | 15.6 | 48.1 | 120.3 ± 64.0 |

J = 0.00240

TOTAL GAS AGE = 125.0 ± 93.0 Ma[3]

PLATEAU AGE = 153.7 ± 5.2 Ma

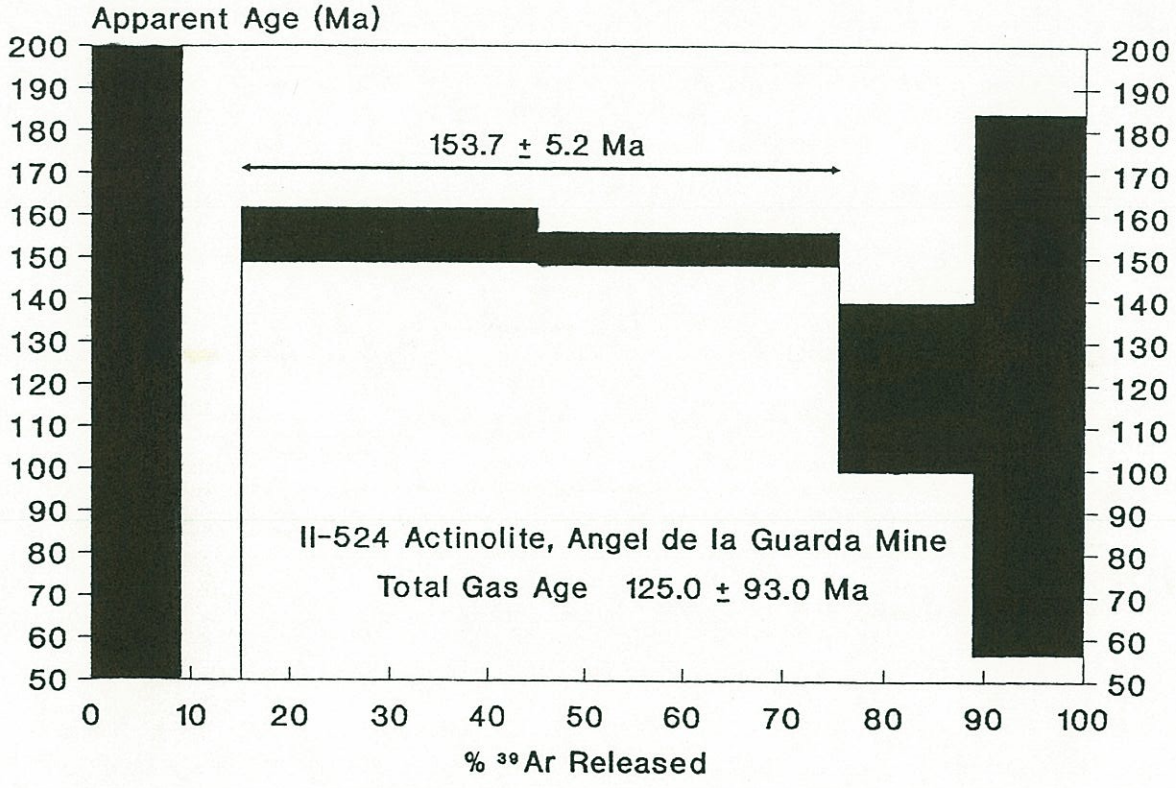


**Figure A1.22.** $^{40}Ar$-$^{39}Ar$ incremental-release age spectrum of actinolite II-524 from Angel de la Guarda vein, Naguayan district. Analytical uncertainties (±2σ) are represented by width of bars.

[3] Only 2 degassing steps yield a significant amount Ar to be measured. So that the total gas age of this sample is meaningless.

Table A1.23. $^{40}Ar$-$^{39}Ar$ data summary of II-527 hornblende, dioritic dike within the Cerro Fortuna Pluton (23°14'40" Lat.S - 70°18'45" Long.W)

| TEMP.(°C) | mV $^{39}Ar$ | % $^{39}Ar$ | %Atm.Ar | %I.I.C. | $^{37}Ar/^{39}Ar$ | APP. AGE (Ma) (Error ± 2σ) |
|---|---|---|---|---|---|---|
| 200-650 | 4.8 | 7.8 | 77.3 | 0.1 | 0.6 | 110.4 ± 20.2 |
| 650-725 | 5.0 | 8.1 | 53.8 | 0.0 | 0.2 | 146.3 ± 2.2 |
| 725-800 | 3.6 | 5.9 | 58.3 | 0.0 | 0.3 | 143.4 ± 2.6 |
| 800-850 | 2.5 | 4.1 | 67.1 | 0.1 | 0.8 | 143.7 ± 5.0 |
| 850-900 | 2.7 | 4.4 | 61.5 | 0.3 | 1.2 | 145.9 ± 4.8 |
| 900-950 | 4.4 | 7.3 | 45.7 | 0.5 | 2.2 | 149.9 ± 1.8 |
| 950-980 | 6.9 | 11.3 | 26.6 | 1.3 | 4.9 | 149.2 ± 1.2 |
| 980-1010 | 23.9 | 38.9 | 21.4 | 1.7 | 6.6 | 148.1 ± 0.8 |
| 1010-1050 | 5.6 | 9.1 | 44.4 | 1.1 | 4.3 | 144.0 ± 1.8 |
| 1050-1100 | 1.6 | 2.7 | 79.5 | 3.5 | 12.0 | 132.1 ± 7.2 |

J = 0.00240 TOTAL GAS AGE = 143.9 ± 3.6 Ma

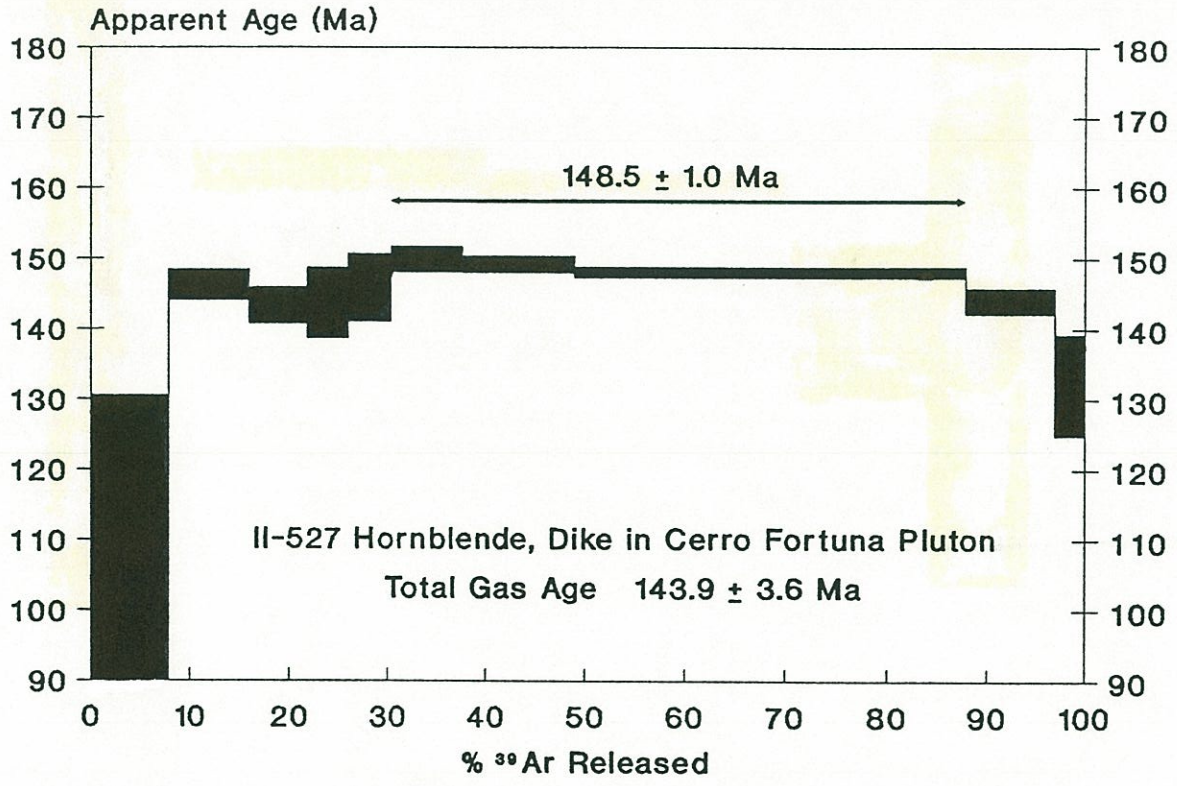


Figure A1.23. $^{40}Ar$-$^{39}Ar$ incremental-release age spectrum of hornblende II-527 from a dike that crosscutt Cerro Fortuna pluton (W of Naguayan district). Analytical uncertainties (±2σ) are represented by width of bars.

Table A1.24. $^{40}Ar$-$^{39}Ar$ data summary of II-526 hornblende, tonalitic stock within the Cerro Fortuna Pluton (23°14'05" Lat.S - 70°17'30" Long.W)

| TEMP.(°C) | mV $^{39}Ar$ | % $^{39}Ar$ | %Atm.Ar | %I.I.C. | $^{37}Ar/^{39}Ar$ | APP. AGE (Ma) Error ± 2σ |
|---|---|---|---|---|---|---|
| 200-650 | 4.7 | 8.7 | 91.7 | 0.4 | 1.2 | 91.3 ± 5.4 |
| 650-725 | 4.0 | 7.3 | 65.4 | 0.0 | 0.2 | 137.6 ± 2.4 |
| 725-800 | 3.7 | 6.8 | 57.5 | 0.0 | 0.4 | 142.2 ± 1.4 |
| 800-850 | 3.8 | 6.9 | 72.6 | 0.3 | 1.2 | 143.5 ± 2.6 |
| 850-900 | 3.6 | 6.5 | 54.6 | 0.6 | 2.4 | 145.6 ± 2.0 |
| 900-950 | 7.7 | 14.1 | 43.2 | 1.6 | 6.0 | 146.6 ± 0.8 |
| 950-980 | 6.0 | 11.0 | 29.7 | 2.6 | 9.3 | 141.3 ± 1.0 |
| 980-1010 | 11.8 | 21.6 | 33.5 | 3.0 | 10.8 | 141.8 ± 0.6 |
| 1010-1050 | 5.9 | 10.9 | 60.9 | 3.0 | 10.6 | 140.1 ± 1.4 |
| 1050-1100 | 2.0 | 3.7 | 80.2 | 3.7 | 12.7 | 134.1 ± 4.6 |
| 1100-1140 | 1.0 | 1.8 | 91.1 | 4.6 | 15.2 | 129.3 ± 13.8 |

J = 0.00240

TOTAL GAS AGE = 137.4 ± 2.2 Ma

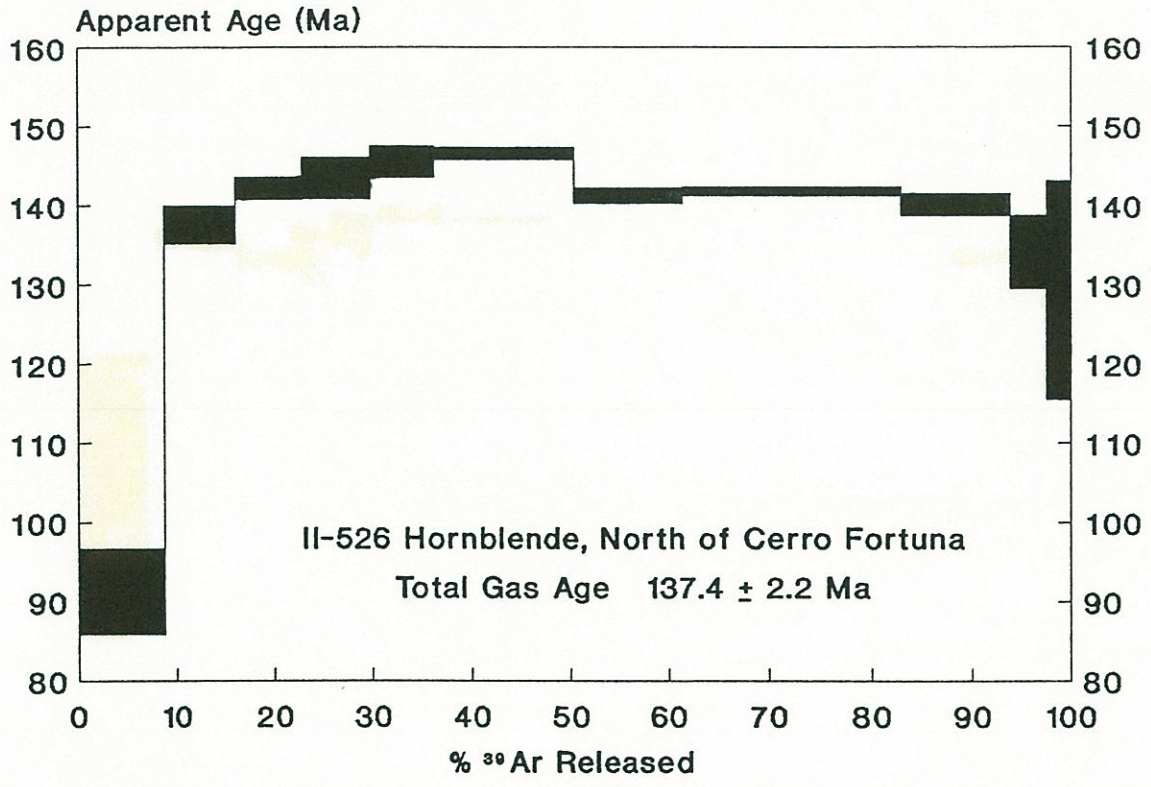


Figure A1.24. $^{40}Ar$-$^{39}Ar$ incremental-release age spectrum of hornblende II-526 from a tonalitic stock (W of Naguayan district). Analytical uncertainties (±2σ) are represented by width of bars.

Table A1.25. $^{40}Ar$-$^{39}Ar$ data summary of II-483 biotite, foliated gabbro, Cerro Coloso (23°47'00" Lat.S - 70°29'10" Long.W).

| TEMP.(°C) | mV $^{39}Ar$ | % $^{39}Ar$ | % Atm. Ar | % I.I.C. | APPARENT AGE (Ma) (Error ± 2σ) |
|---|---|---|---|---|---|
| 200-550 | 28.9 | 5.0 | 74.5 | 0.0 | 69.3 ± 1.8 |
| 550-650 | 50.1 | 8.6 | 24.8 | 0.0 | 142.7 ± 1.0 |
| 650-750 | 94.4 | 16.3 | 16.9 | 0.0 | 144.1 ± 0.6 |
| 750-800 | 106.5 | 18.4 | 15.4 | 0.0 | 145.2 ± 0.6 |
| 800-850 | 125.2 | 21.6 | 15.7 | 0.0 | 144.2 ± 0.4 |
| 850-875 | 46.4 | 8.0 | 25.6 | 0.0 | 142.0 ± 1.0 |
| 875-900 | 37.2 | 6.4 | 28.8 | 0.0 | 140.8 ± 1.0 |
| 900-925 | 33.5 | 5.7 | 34.3 | 0.0 | 141.1 ± 1.0 |
| 925-950 | 16.0 | 2.7 | 24.4 | 0.0 | 138.4 ± 2.4 |
| 950-975 | 16.3 | 2.8 | 58.1 | 0.0 | 141.0 ± 3.8 |
| 975-1000 | 13.0 | 2.2 | 66.7 | 0.0 | 141.6 ± 4.6 |
| 1000-1050 | 10.6 | 1.8 | 78.2 | 0.0 | 135.5 ± 7.4 |

J = 0.00240 TOTAL GAS AGE = 139.5 ± 1.2 Ma

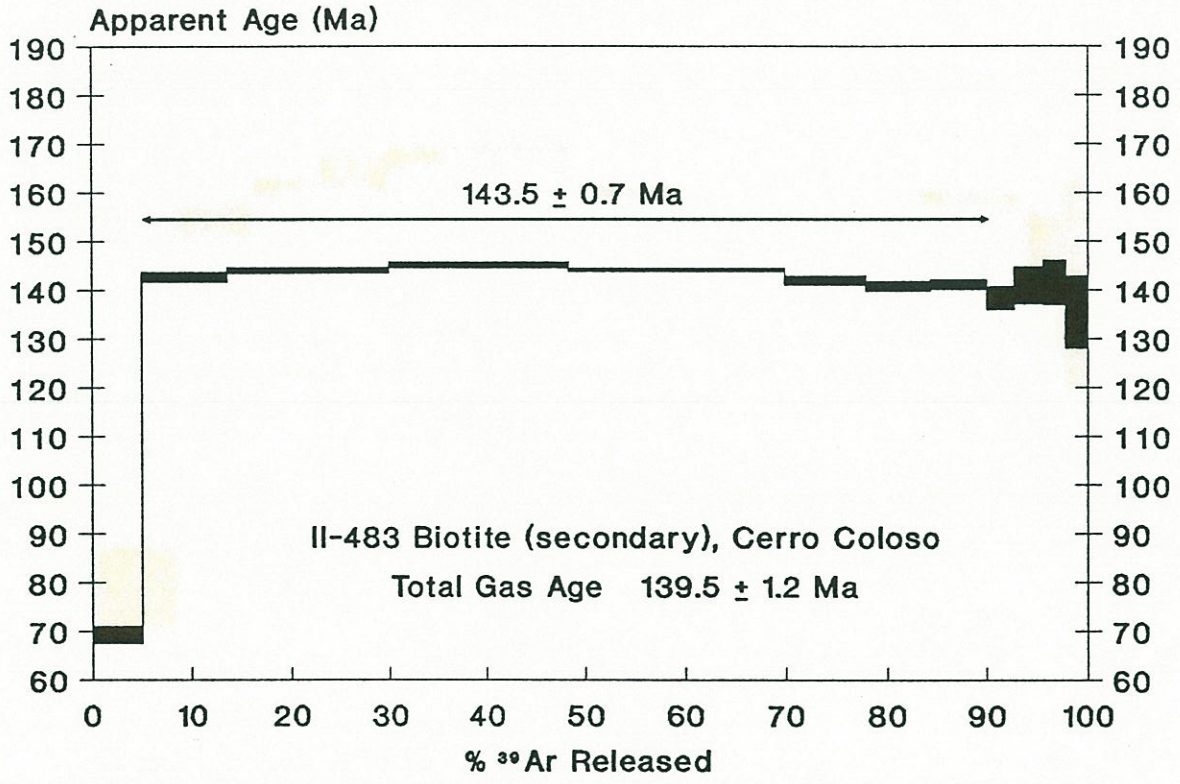


Figure A1.25. $^{40}Ar$-$^{39}Ar$ incremental-release age spectrum of secondary (recrystallized) biotite from a foliated gabbro of Cerro Coloso. Analytical uncertainties (±2σ) are represented by width of bars.

% C.I.I. = Interfering Isotopes Correction

J values were determined from six samples of the MMhb-1 hornblende standard (Alexander and others, 1978) included in each irradiated can. The potassium total decay constant and isotope abundances used for age calculations are those suggested by the IUGS Subcommission on Geochronology (Steiger and Jäger, 1977).

# APPENDIX 2. COMPILATION OF RADIOMETRIC AGES OF THE ANTOFAGASTA REGION

## A2.1 TABLES OF COMPILED RADIOMETRIC AGES

Table A2.1 Precambrian (?) - Lower Paleozoic Metamorphic Rocks

| Sample Identif. | Lat. S Long.W | Method & Material | Age (Ma) ± error | Lithology & Observations | Ref. |
|---|---|---|---|---|---|
| 84-22-1 | 22°40'(?)<br>68°58'(?)<br>Estimated | U-Pb Zir | 777 + 36 - 35<br>276 + 5 - 6 | Gneiss | (11) |
| | 23°14'50"<br>70°34'05"<br>Approx. | Sm-Nd Wr | 521 ± 55 | Amphibolite | (11) |
| 9545A-G-H | 21°35'20"<br>69°01'30" | Rb-Sr Wr | 485 ± 12 | Schist<br>Errorchron, MSWD 62.9 | (40) |
| S545 D | 21°35'20"<br>69°01'30" | K-Ar Mus | 422 ± 6 | Schist | (40) |
| S545 E | 21°35'20"<br>69°01'30" | K-Ar Mus | 418 ± 8 | Schist | (40) |
| S540 | 21°51'00"<br>69°07'00" | K-Ar Mus | 372 ± 3 | --------- | (40) |
| ANT-5A | 22°39'12"<br>68°59'13" | K-Ar Bt | 312 ± 15 | Amphibolite | (20) |
| ANT-9-10 | 22°39'17"<br>68°58'24"<br>Average | Rb-Sr Wr | 309 ± 11 | Schists & gneisses<br>Errorchron, MSWD 4.6<br>IR 0.7069 ± 0.0001 | (20) |
| MT-112b | 22°38'50"<br>68°58'36" | K-Ar Hb | 297 ± 13 | Schist | (20) |
| S5434 | ------- | K-Ar Bt | 293 ± 4 | ------- | (40) |
| Q-5 | 21°03'40"<br>68°52'20" | K-Ar Bt | 292 ± 17<br>297 ± 17 | Schist<br>Recalculated | (23)<br>(42) |
| ANT-6A | 22°39'20"<br>68°59'01" | K-Ar Mus | 283 ± 19 | Gneiss | (20) |
| ANT-7B | 22°39'45"<br>68°58'45" | K-Ar Hb | 283 ± 8<br>269 ± 9 | Amphibolite | (20) |

| Sample Identif. | Lat. S Long.W | Method & Material | Age (Ma) ± error | Lithology & Observations | Ref. |
|---|---|---|---|---|---|
| ANT-6B | 22°39'20" 68°59'01" | K-Ar Hb | 282 ± 8 | Amphibolite | (20) |
| ANT-3 | 22°39'08" 68°59'15" | K-Ar Mus K-Ar Bt | 276 ± 11 242 ± 8 | Amphibolite | (20) |
| ANT-10C | 22°39'07" 68°58'18" | K-Ar Mus | 275 ± 11 | Schist | (20) |
| 81150-152 81011 | 22°38'51" 68°58'42" Average | Rb-Sr Wr | 251 ± 50 | Schists, amphibolites Errorchron, MSWD 1100 IR 0.707 ± 0.004 | (36) |
| ANT-9i | 22°39'26" 68°58'29" | K-Ar Bt | 239 ± 7 | Gneiss or schist | (20) |
| MD-7A | 23°07'10" 70°33'35" | K-Ar Wr | 177 ± 8 | Amphibolite | (15) |
| MD-16 | 23°06'50" 70°33'20" | K-Ar Wr | 172 ± 12 | Amphibolite | (15) |
| MO-29A | 23°15'20" 70°30'00" | K-Ar Amp | 167 ± 8 | Amphibolite | (15) |

Table A2.2 Paleozoic Migmatites

| Sample Identif. | Lat. S Long.W | Method & Material | Age (Ma) ± error | Lithology & Observations | Ref. |
|---|---|---|---|---|---|
| QCH-66 | 21°04'32" 68°53'38" | U-Pb Zir | 1260 ± 30 480 ± 5 | Migmatite | (11) |
| QCHO-68 | 21°03'30" 68°52'15" Approx. | U-Pb Zir | 1213 + 28 - 25 415 ± 36 | Gneiss | (11) |
| S10-12 | 21°04'40" 68°52'30" | Rb-Sr Wr | 511 ± 82 | Migmatite Errorchron, MSWD 85.6 IR 0.7199 ± 0.082 | (40) |
| S-10 | 21°04'40" 68°52'30" | K-Ar Hb K-Ar Bt | 452 ± 11 269 ± 7 | Migmatite | (40) |

Table A2.3 Cambrian-Ordovician volcanic rocks

| Sample Identif. | Lat. S Long.W | Method & Material | Age (Ma) ± error | Lithology & Observations | Ref. |
|---|---|---|---|---|---|
| | 23°50'(?) 68°22'(?) | Nd-Sm Wr | 448 ± 145 | Basalt Errorchron | (11) |

Table A2.4 Ordovician-Silurian plutons

| Sample Identif. | Lat. S Long.W | Method & Material | Age (Ma) ± error | Lithology & Observations | Ref. |
|---|---|---|---|---|---|
| MQ156E | 24°25'(?) 68°27'(?) Estimated | U-Pb Zir | 502 ± 7 | Granodiorite | (11) |
| 84-15-01 | 23°47'(?) 68°22'(?) Estimated | U-Pb Zir | 491 + 68 - 59 | Diorite | (11) |
| H-73 (14) | 24°13'15" 68°27'40" | Rb-Sr Wr | 468 ± 100<br>478 ± 44 | Granite; Errorchron<br>Recalculated, MSWD 2.6 IR 0.7045 | (18)<br>(28) |
| 84-16-1 | 23°57'(?) 68°25'(?) Estimated | U-Pb Zir | 463 ± 26 | Granodiorite | (11) |
| L58-L60 | 23°47'00" 68°16'30" Average | Rb-Sr Wr | 452 ± 4 | Granite MSWD 0.8 IR 0.7113 ± 0.0084 | (28) |
| 84-18-05 | 23°54'(?) 68°17'(?) | U-Pb Zir | 450 + 11 - 102 | Granite | (11) |
| SO-3004 | 23°50'(?) 68°24'12" | K-Ar Mus + Ort | 444 ± 10 | Pegmatitic, granite | (13) |
| L5-L13 | 23°52'20" 68°17'00" Average | Rb-Sr Wr | 441 ± 8 | Monzogranite MSWD 5.5 IR 0.7102 ± 0.004 | (28) |
| Q-170 | 21°05'50" 68°52'20" | K-Ar Mus | 431 ± 10<br>438 ± 10 | Granite<br>Recalculated | (23)<br>(42) |

| Sample Identif. | Lat. S Long.W | Method & Material | Age (Ma) ± error | Lithology & Observations | Ref. |
|---|---|---|---|---|---|
| L-26 | 23°55'40" 68°24'50" | K-Ar Hb K-Ar Bt | 429 ± 12 425 ± 10 | Granodiorite | (28) |

Table A2.5 Devonian - Lower Carboniferous sedimentary and metasedimentary rocks

| Sample Identif. | Lat. S Long.W | Method & Material | Age (Ma) ± error | Lithology & Observations | Ref. |
|---|---|---|---|---|---|
| HAB-125A | 24°46'15" 70°24'20" | K-Ar Mus | 146 ± 4 | Metasedimentary rock Age rejuvenated by pluton intrusion | (22) |
| MAB-404 | 24°05'50" 70°12'30" | K-Ar Bt | 143 ± 4 | Phyllite Age rejuvenated by pluton intrusion | (22) |
| MAB-401 | 24°02'25" 70°14'00" | K-Ar Mus | 135 ± 4 | Phyllite Age rejuvenated by pluton intrusion | (22) |

Table A2.6 Carboniferous-Middle Triassic volcanic and subvolcanic rocks

| Sample Identif. | Lat. S Long.W | Method & Material | Age (Ma) ± error | Lithology & Observations | Ref. |
|---|---|---|---|---|---|
| SO-477 | 24°27'12" 68°33'30" | K-Ar Bt | 290 ± 7 | Welded tuff | (14) |
| MO-934 -942 | 24°20'30" 68°58'45" Average | Rb-Sr Wr | 271 ± 17 | Rhyolite IR 0.7060 | (13) |
| TO-733 | 23°17'42" 67°58'30" | K-Ar Bt | 268 ± 6 | Welded tuff | (13) |
| 81041-045 80195 | 22°43'45" 69°03'14" Average | Rb-Sr Wr | 233 ± 36 | Rhyolite, cryst. tuff MSWD 170, IR 0.7073 ± 0.0014 | (36) |

| Sample Identif. | Lat. S Long.W | Method & Material | Age (Ma) ± error | Lithology & Observations | Ref. |
|---|---|---|---|---|---|
| MO-950 -953 | 24°09'10" 68°53'25" Average | Rb-Sr Wr | 227 ± 8 | Rhyolite MSWD 0.01, IR 0.7046 | (13) |
| Q-3 | 21°13'45" 68°46'40" | K-Ar Ort | 114 ± 3* 116 ± 3* | Rhyolite Recalculated | (23) (42) |

Table A2.7 Carboniferous-Middle Triassic intrusive rocks

| Sample Identif. | Lat. S Long.W | Method & Material | Age (Ma) ± error | Lithology & Observations | Ref. |
|---|---|---|---|---|---|
| LB-301b | 21°27'58" 69°56'50" | K-Ar Bt | 322 ± 5 | Granite | (41) |
| LB-543 | 21°18'14" 69°46'55" | K-Ar Bt | 320 ± 5 | Granite | (41) |
| CP-68A | 21°47'05" 69°39'10" | K-Ar Bt | 318 ± 6 | Granite | (25) |
| CM-224 | 21°21'30" 68°48'50" | K-Ar Bt | 318 ± 7 324 ± 7 | Granodiorite Chloritized biotite Recalculated | (23) |
| 84-19-01 | 23 40'(?) 68°23'(?) Estimated | U-Pb Zir | 312 ± 24 | Diorite | (11) |
| MC-572 | 22°37'10" 68°52'47" | K-Ar Bt | 305 ± 4 | Granite | (26) |
| D-2 | 21°51'30" 68°55'30" | K-Ar Bt | 305 ± 8 311 ± 8 | Granite Recalculated | (23) (42) |
| 84-22-12 | 22°37'(?) 68°55'(?) Estimated | U-Pb Zir | 298 ± 1.5 | Granite | (11) |
| SO-232 | 24°17'18" 68°53'42" | K-Ar Mus | 298 ± 7 | Copper vein La Casualidad mine Imilac district | (14) |

| Sample Identif. | Lat. S Long.W | Method & Material | Age (Ma) ± error | Lithology & Observations | Ref. |
|---|---|---|---|---|---|
| CM-350 | 21°33'20" 68°55'00" | K-Ar Bt | 297 ± 10<br>302 ± 10 | Granite<br>Recalculated | (23)<br>(42) |
| ANT-8 | 22°41'30" 68°59'30" | K-Ar Bt | 293 ± 11<br>267 ± 6 | Tonalita | (20) |
| 444A-C | 25°54'20" 70°37'30" | U-Pb Zir<br>Rb-Sr Wr + Plg + Apa | 293 ± 14<br>238 ± 12 | Granite<br>IR 0.7086 ± 00084 | (12)<br>(7) |
| MC-542 | 22°46'00" 68°43'42" | K-Ar Bt | 291 ± 4 | Granodiorite | (26) |
| 10X-S1 | 21°20'30" 68°45'50" | K-Ar Wr | 287 ± 7<br>292 ± 7 | Diorite<br>Recalculated | (23)<br>(42) |
| 327 A-D | 25°32'30" 70°33'30" | Rb-Sr Wr | 285 ± 17 | Sienogranite<br>IR 0.7054 ± 0.0004 | (12)<br>(7) |
| MO-982 -987 | 24°15'15" 68°30'44" Average | Rb-Sr Wr | 285 ± 4 | Granite<br>IR 0.70571 | (14)<br>(13) |
| SO-302 | 24°09'20" 68°47'33" | K-Ar Bt | 279 ± 7 | Quartz monzonite | (14) |
| CM-373 | 21°34'20" 68°46'40" | K-Ar Bt + Amp | 272 ± 2<br>277 ± 23 | Diorite<br>Chloritized minerals<br>Recalculated | (23)<br>(42) |
| CM-330 | 21°34'00" 68°59'30" | K-Ar Bt | 271 ± 8<br>276 ± 8 | Granodiorite<br>Chloritized biotite<br>Recalculated | (23)<br>(42) |
| MO-964 -992 | 24°09'50" 68°46'50" Average | Rb-Sr Wr | 271 ± 7 | Granite<br>MSWD 2.6, IR 0.7055 | (13) |
| Z-713 | 25°39' 70°38' | K-Ar Bt<br><br>Ar-Ar Bt | 267 ± 8<br>272 ± 8<br>259 ± 8 | Granodiorite<br>Recalculated<br>Gradient: 260-293 Ma | (47)<br>(42)<br>(44) |
| 81013-018 | 22°35'00" 68°55'29" | Rb-Sr Wr | 266 ± 42 | Granodiorite, granite<br>MSWD 6.9, | (36) |
| 81113-121 | 22°45'49" 68°55'41" | | | IR 0.7062 ± 0.0004<br>Coord. range of sampled area | |

| Sample Identif. | Lat. S Long.W | Method & Material | Age (Ma) ± error | Lithology & Observations | Ref. |
|---|---|---|---|---|---|
| 79CF12-14 | 26°22'48" 70°37'12" | Rb-Sr Wr | 262 ± 5 | Granite IR 0.70635 ± 0.00018 | (39) |
| CM-228 | 21°31'30" 68°45'30" | K-Ar Bt | 260 ± 4 | Granodiorite Chloritized biotite | (23) |
| | | | 265 ± 4 | Recalculated | (42) |
| Q-4 | 21°09'00" 68°47'30" | K-Ar Bt | 247 ± 18 | Granodiorite Chloritized biotite | (23) |
| | | | 252 ± 18 | Recalculated | (42) |
| MS-150C | 25°48'24" 70°41'36" | K-Ar Bt | 244 ± 4 | Monzogranite | (30) |
| TO-436 | 23°45'40" 68°46'05" | K-Ar Bt | 232 ± 3 | Granodiorite Chloritized biotite | (34) |
| D-3 | 21°51'40" 68°57'40" | K-Ar Bt | 232 ± 7 | Granite | (23) |
| | | | 236 ± 7 | Recalculated | (42) |
| CM-89 | 21°31'30" 68°47'10" | K-Ar Wr | 227 ± 8 | Rhyolitic porphyry Altered rock | (23) |
| | | | 232 ± 8 | Recalculated | (42) |
| SO-77 | 24°02'47" 68°49'51" | K-Ar Bt | 227 ± 6 | Granite | (14) |
| SO-85 | 24°00'30" 68°47'48" | K-Ar Bt | 227 ± 6 | Granite | (14) |
| AL-24 | 22°26'44" 68°14'40" | K-Ar Bt | 225 ± 7 | Dacitic porphyry | (26) |
| SO-78 | 24°01'00" 68°49'45" | K-Ar Amp | 225 ± 7 | Quartz monzodiorite | (14) |
| MO-995 -1010 | 23°54'30" 68°49'05" Average | Rb-Sr Wr | 223 ± 3 | Granite MSWD 2.8, IR 0.7049 ± 0.0001 | (13) |
| 593 A-E | 25°50'00" 70°41'20" | Rb-Sr Wr | 222 ± 3 | Monzogranite IR 0.7131 ± 0.0002 | (12) (7) |
| 511/639 A-E | 25°49'10" 70°38'10" | Rb-Sr Wr | 220 ± 13 | Sienogranite IR 0.7134 ± 0.0007 | (12) (7) |

| Sample Identif. | Lat. S Long.W | Method & Material | Age (Ma) ± error | Lithology & Observations | Ref. |
|---|---|---|---|---|---|
| MO-943 -961 | 24°07'33" 68°53'25" Average | Rb-Sr Wr | 217 ± 4 | Granodiorite IR 0.7048 ± 0.0001 | (13) |
| 117 | 22°03'30" 68°43'58" | K-Ar Bt | 216 ± 8* | Granodiorite Chloritized biotite | (45) |
| 247 | 22°08'30" 68°49'25" | K-Ar Bt? | 206 ± 7* | Granodiorite | (45) |
| AR-1 | 22°06'45" 68°45'50" | K-Ar Bt | 202 ± 8* | Granite | (45) |
| ---- | 22°17'00" 68°53'30" Approx. | K-Ar Bt | 122 ± 3.8* | Elena Granodiorite East of Chuquicamata mine | (2) |
| CM-334 | 21°38'00" 68°50'40" | K-Ar Ort | 109 ± 2* 111 ± 2* | Rhyolitic porphyry Recalculated | (23) (42) |
| 226-B | 22°03'40" 68°50'40" | K-Ar Bt? | 103 ± 4* | Granodiorite | (45) |
| 10X | 21°20'20" 68°46'00" | K-Ar Wr | 89.8 ± 2.3* 91.9 ± 2.3* | Rhyolitic porphyry Recalculated | (23) (42) |

Table A2.8 Jurassic volcanic rocks

| Sample Identif. | Lat. S Long.W | Method & Material | Age (Ma) ± error | Lithology & Observations | Ref. |
|---|---|---|---|---|---|
| 8077-8098 | 22°21'08" 70°15'15" Average | Rb-Sr Wr | 186.5 ± 13.6 | Basaltic andesites La Negra Fm., MSWD 4.2 IR 0.7032 ± 0.0002 | (36) |
| HAB-510 | 24°27'30" 70°33'20" | K-Ar Bt | 160 ± 4 | Andesite La Negra Fm. | (22) |
| Omega | 22°40'12" 70°09'50" | K-Ar Wr | 142 ± 7 | Altered andesite Susana mine, Michilla district | (5) |

Table A2.9 Jurassic intrusive rocks

| Sample Identif. | Lat. S Long.W | Method & Material | Age (Ma) ± error | Lithology & Observations | Ref. |
|---|---|---|---|---|---|
| 84-02-03 | 23°52'20" 70°19'00" Approx. | U-Pb Zir | 207 ± 39 | Granite | (11) (9) |
| MD44-50 | 23°25'12" 70°35'15" 23°24'10" 70°36'15" | Rb-Sr Wr | 200 ± 10 | Gabbro, pegmatite IR 0.7034 Coord. range of 7 samples Mejillones peninsula | (15) |
| MS-150A | 25°48'20" 70°41'40" | K-Ar Bt | 198 ± 4 | Monzogranite | (30) |
| MJ-100 | 23°25'(?) 70°35'(?) Estimated | U-Pb Zir | 196 ± 4 | Gabbro Mejillones peninsula | (11) |
| MO-925 | 24°04'55" 70°10'45" | K-Ar Bt | 192 ± 5 | Granodiorite | (22) |
| MJ-109 | 23°27'40" 70°34'40" Approx. | U-Pb Zir | 191 ± 6 | Gabbro Mejillones peninsula | (11) (9) |
| Z-716 | 25°54' 70°34' | K-Ar Bt<br>+ Clo<br>K-Ar Bt | 189 ± 8.8<br>193.1 ± 8.8<br>186 ± 6 | Diorite<br>Recalculated | (47)<br>(42)<br>(44) |
| 625A | 25°52' 70°41' | Rb-Sr Wr + Fel + Bt | 187 ± 6 | Granodiorite IR 0.7110 ± 0.0003 | (12) |
| | | Rb-Sr Wr + Fel | 182 ± 12.5 | | (7) |
| MB-10969 | 23°20'50" 70°06'20" | K-Ar Bt | 182 ± 3 | Granite | (10) |
| MAB-12A | 24°56'02" 70°26'02" | K-Ar Bt<br>K-Ar Amp | 181 ± 4<br>176 ± 6 | Granodiorite | (22) |
| TOC-4 | 22°13' 69°43' | K-Ar Bt | 178 ± 2 | Quartz monzodiorite | (8) |

| Sample Identif. | Lat. S Long.W | Method & Material | Age (Ma) ± error | Lithology & Observations | Ref. |
|---|---|---|---|---|---|
| 84-35-1 | 23 46'(?)<br>70°09'(?)<br>Estimated | U-Pb Zir | 174 ± 16 | Granite | (11) |
| MO-902-<br>MO-911 | 23°50'<br>70°14'<br>Approx. | Rb-Sr Rt | 170 ± 28 | Monzodiorite, tonalite<br>MSWD 0.0,<br>IR 0.07315 ± 0.0001 | (22) |
| MAB-376 | 24°10'00"<br>70°01'00" | K-Ar Bt | 168 ± 4 | Granodiorite | (22) |
| MAB-12 | 24°56'02"<br>70°26'02" | K-Ar Bt | 165 ± 5 | Granodiorite | (22) |
| FK-92R | 24°55'30"<br>70°24'00" | K-Ar Act | 164 ± 11 | Copper vein<br>Mantos mine<br>Montecristo district | (22) |
| MAB-601 | 24°31'00"<br>70°01'55" | K-Ar Bt | 162 ± 4 | Granodiorite | (22) |
| HAB-508-A | 24°29'40"<br>70°34'05" | K-Ar Bt | 160 ± 4 | Granodiorite | (22) |
| TA-153 | 25°01'35"<br>70°15'25" | K-Ar Bt<br>+ Clo | 159 ± 3 | Granodiorite | (30) |
| MAB-220 | 24°24'15"<br>70°03'00" | K-Ar Bt | 158 ± 4 | Quartz monzodiorite | (22) |
| 8054-0754 | 22°24'00"<br>70°13'55"<br>22°29'28"<br>70°15'12" | Rb-Sr Wr | 158 ± 6 | Diorite, granite, monzodiorite<br>MSWD 0.8, IR 0.7033 ± 0.0001<br>Coord. range of sampled area | (36) |
| HAB-507 | 24°24'20"<br>70°32'00" | K-Ar Bt | 157 ± 4 | Diorite | (22) |
| 81099-110 | 22°11'21"<br>69°45'52"<br>22°16'13"<br>69°47'10" | Rb-Sr Wr | 156 ± 32 | Tonalite, monzodiorite, granite<br>MSWD 22, IR 0.7041 ± 0.0005<br>Coord. range of sampled area | (36) |
| 81075-080<br>and<br>Toc1-Toc7 | 22°00'11"<br>70°05'24"<br>22°08'21"<br>70°11'09" | Rb-Sr Wr | 155 ± 13 | Monzonite, monzodiorite, granite<br>MSWD 9.5, IR 0.7039 ± 0.0002<br>Coord. range of sampled area | (36) |

| Sample Identif. | Lat. S Long.W | Method & Material | Age (Ma) ± error | Lithology & Observations | Ref. |
|---|---|---|---|---|---|
| HAB-586 | 24°49'00" 70°21'07" | K-Ar Bt | 155 ± 4 | Gabbro | (22) |
| HAB-518 | 24°41'26" 70°24'00" | K-Ar Bt | 155 ± 4 | Gabbro | (22) |
| Alfa | 22°40'12" 70°09'48" | K-Ar Wr | 154 ± 8 | Gabbroic dike Crosscuts ore body Susana mine, Michilla. | (5) |
| HAB-243 | 24°23'30" 70°32'20" | K-Ar Bt | 154 ± 4 | Granodiorite | (22) |
| CO-002 | 23°31'30" 70°33'10" Approx. | U-Pb Zir | 153 ± 2 | Pyroxenite | (11) (9) |
| 84-33-02 | 23°46'30" 70°15'25" Approx. | U-Pb Zir | 153 ± 6 | Diorite | (11) (9) |
| 84-26-01 | 23°55'55" 70°18'50" Approx. | U-Pb Zir | 152 ± 10 | Granodiorite | (11) (9) |
| HAB-613 | 24°47'20" 70°30'00" | K-Ar Bt | 151 ± 4 | Diorite | (22) |
| HAB-650 | 24°29'40" 70°34'05" | K-Ar Bt | 150 ± 4 | Granodiorite | (22) |
| HAB-464 | 24°17'50" 70°21'40" | K-Ar Bt | 149 ± 4 | Quartz monzodiorite | (22) |
| HAB-769 | 24°18'45" 70°22'10" | K-Ar Bt | 149 ± 4 | Quartz diorite | (22) |
| Ta-104A | 25°23'10" 70°19"25" | K-Ar Bt | 149 ± 3 | Monzogranite | (30) |
| Stock 1 | 22°40'12" 70°09'50" | K-Ar Wr | 149 ± 4 | Gabbroic stock Crosscuts ore body Susana mine, Michilla. | (5) |
| MB-10330 | 23°25'30" 70°02'45" | K-Ar Hb | 149 ± 13 | Andesitic dike Crosscuts ore body, Mantos Blancos mine | (10) |

| Sample Identif. | Lat. S Long.W | Method & Material | Age (Ma) ± error | Lithology & Observations | Ref. |
|---|---|---|---|---|---|
| HAB-10 | 24°44'05" 70°34'10" | K-Ar Bt K-Ar Amp | 148 ± 4 141 ± 5 | Gabbro | (22) |
| HAB-617 | 24°48'10" 70°29'25" | K-Ar Bt | 148 ± 4 | Quartz monzodiorite | (22) |
| MO-798- MO-800 | 24°46'05" 70°33'00" | Rb-Sr Rt | 148 ± 2 | Tonalite, granite MSWD 0.1, IR 0.07339 | (22) |
| UCC-62 | 24°02'15" 70°27'30" | K-Ar Amp | 148 ± 17 | Gabbro | (21) |
| MAB-430 | 24°11'05" 70°10'00" | K-Ar Bt | 147 ± 4 | Monzogranite | (22) |
| M1 | 23°26'30" 70°06'65" | K-Ar Bt | 147 ± 1 | Granodiorite Mantos Blancos district | (10) |
| MB-10747 | 23°27'10" 70°05'15" | K-Ar Bt | 147 ± 4 | Granodiorite Mantos Blancos district | (10) |
| MB-10725 | 23°24'10" 70°01'50" | K-Ar Hb | 147 ± 13 | Andesitic dike | (10) |
| MAB-333 | 24°07'00" 70°16'25" | K-Ar Bt | 146 ± 4 | Monzogranite | (22) |
| HAB-708 | 24°24'20" 70°22'35" | K-Ar Bt | 146 ± 3 | Tonalite | (22) |
| MO-918- MO-923 | 24°07'40" 70°22'45" | Rb-Sr Rt | 145 ± 10 | Tonalite, monzodiorite MSWD 0.0, IR 0.07326 | (22) |
| HAB-412 | 24°33'31" 70°24'50" | K-Ar Bt | 144 ± 5 | Gabbro | (22) |
| HAB-134 | 24°45'00" 70°24'25" | K-Ar Bt | 144 ± 4 | Quartz monzonite | (22) |
| HAB-505 | 24°40'48" 70°29'33" | K-Ar Bt | 144 ± 4 | Granodiorite | (22) |
| HAB-341-A | 24°00'40" 70°08'55" | K-Ar Bt | 144 ± 4 | Monzodiorite | (22) |

| Sample Identif. | Lat. S Long.W | Method & Material | Age (Ma) ± error | Lithology & Observations | Ref. |
|---|---|---|---|---|---|
| MAB-405 | 24°06'10" 70°14'00" | K-Ar Bt | 143 ± 4* | Quartz diorite | (22) |
| HAB-525 | 24°37'43" 70°27'17" | K-Ar Bt | 143 ± 3* | Granodiorite | (22) |
| HAB-11-A | 24°42'40" 70°28'45" | K-Ar Bt | 142 ± 3* | Monzodiorite | (22) |
| HAB-648A | 24°23'35" 70°26'50" | K-Ar Wr | 139 ± 5* | Mylonitic andesitic porphyry | (22) |
| MO-908 | 23°59'55" 70°13'05" | K-Ar Bt | 138 ± 3* | Quartz monzodiorite | (22) |
| MO-911 | 24°32'05" 70°14'30" | K-Ar Amp | 135 ± 13* | Diorite Age of secondary amphibole | (22) |
| Beta | 22°40'12" 70°09'48" | K-Ar Wr | 133 ± 7* | Gabbroic stock Crosscuts ore body Susana mine, Michilla. | (5) |
| MO-912 | 24°03'25" 70°28'05" | K-Ar Amp | 128 ± 9* | Gabbro | (22) |
| Rho | 22°26' 70°10' | K-Ar Wr | 124 ± 8* | Diorite | (5) |
| HAB-19A | 24°58'50" 70°24'00" | K-Ar Amp | 123 ± 7* | Gabbro | (22) |
| HAB-209-B | 24°30'40" 70°19'15" | K-Ar Amp | 115 ± 9* | Diorite Age of secondary amphibole | (22) |
| MD-58 | 23°27'55" 70°36'50" | K-Ar Plg K-Ar Amp | 116 ± 7* 108 ± 7* | Gabbro | (15) |

Table A2.10 Lower Cretaceous volcanic rocks

| Sample Identif. | Lat. S Long.W | Method & Material | Age (Ma) ± error | Lithology & Observations | Ref. |
|---|---|---|---|---|---|
| UP-6 | 25°36' 70°12' | K-Ar Wr K-Ar Bt | 115 ± 11 111 ± 3 | Andesite | (44) |

| Sample Identif. | Lat. S Long.W | Method & Material | Age (Ma) ± error | Lithology & Observations | Ref. |
|---|---|---|---|---|---|
| Z-3-75 | 25°54' 69°55' | K-Ar Wr | 106 ± 3 | Andesite | (44) |
| 81130-136 | 22°17'42" 69°04'02" 22°19'19" 69°06'29" | Rb-Sr Wr | 105 ± 19 | Basaltic andesites MSWD 9.7, IR 0.7043 ± 0.0003 Coord. range of sampled area | (36) |
| ET-144 | 22°09' 69°41' | K-Ar Wr | 78 ± 3* | Andesite | (8) |

Table A2.11 Lower Cretaceous intrusive rocks

| Sample Identif. | Lat. S Long.W | Method & Material | Age (Ma) ± error | Lithology & Observations | Ref. |
|---|---|---|---|---|---|
| HAB-707 | 24°40'50" 70°27'45" | K-Ar Bt | 144 ± 5 | Syenogranite | (22) |
| HAB-604 | 25°00'00" 70°14'30" | K-Ar Bt | 144 ± 6 | Monzodiorite | (22) |
| MAB-608 | 24°05'50" 70°12'20" | K-Ar Bt | 144 ± 4 | Granodiorite | (22) |
| HAB-702 | 24°26'40" 70°28'05" | K-Ar Amp | 143 ± 6 | Syenogranite | (22) |
| HAB-397 | 24°29'15" 70°27'50" | K-Ar Bt | 143 ± 4 | Monzogranite | (22) |
| MAB-606 | 23°59'10" 70°14'40" | K-Ar Bt | 143 ± 3 | Granodiorite | (22) |
| HAB-475 | 24°25'30" 70°24'00" | K-Ar Bt | 142 ± 4 | Granodiorite | (22) |
| ------- | 24°04'37" 70°23'40" | K-Ar Bt | 140 ± 4 | Tonalite | (21) |
| MAB-242 | 24°12'20" 70°12'00" | K-Ar Bt | 140 ± 3 | Monzogranite | (22) |

| Sample Identif. | Lat. S Long.W | Method & Material | Age (Ma) ± error | Lithology & Observations | Ref. |
|---|---|---|---|---|---|
| HAB-225A | 24°04'05" 70°13'05" | K-Ar Bt | 140 ± 3 | Foliated tonalite | (22) |
| HAB-798 | 24°22'50" 70°20'40" | K-Ar Bt | 140 ± 3 | Monzogranite | (22) |
| ------- | 24°04'37" 70°23'40" | K-Ar Bt | 140 ± 4 | Tonalite | (21) |
| MAB-322 | 24°01'05" 70°22'00" | K-Ar Bt | 140 ± 4 | Granodiorite | (22) |
| HAB-414 | 24°34'30" 70°23'05" | K-Ar Bt | 139 ± 5 | Syenogranite | (22) |
| HAB-736 | 24°37'05" 70°21'55" | K-Ar Amp | 138 ± 7 | Tonalite | (22) |
| HAB-1 | 24°11'15" 70°22'02" | K-Ar Bt | 138 ± 3 | Quartz monzodiorite | (22) |
| MAB-485A | 24°00'40" 70°19'15" | K-Ar Bt | 137 ± 3 | Granodiorite | (22) |
| 16-MK-11-R | 25°42'15" 70°16'51" | K-Ar Bt | 136 ± 4 | Granodiorite | (38) |
| MAB-271 | 24°35'50" 70°13'50" | K-Ar Bt | 135 ± 3 | Monzogranito | (22) |
| HAB-143 | 24°38'50" 70°17'20" | K-Ar Bt | 133 ± 3 | Diorite | (22) |
| EMY-21 | 21°55'30" 69°43'30" | K-Ar Wr | 132 ± 8 | Altered rock Puntillas Cu prospect | (29) |
| MO-782- MO-784 | 24°38'40" 70°19'30" | Rb-Sr Rt + Bt | 131 ± 1 | Granodiorite MSWD 0.3, IR 0.07338 | (22) |
| MO-794- MO-796 | 24°57'40" 70°28'40" | Rb-Sr Rt | 131 ± 6 | Rhyolitic porph. (dike) MSWD 0.0, IR 0.07900 | (22) |
| HAB-648-B | 24°23'15" 70°27'00" | K-Ar Bt | 131 ± 5 | Monzogranite | (22) |

| Sample Identif. | Lat. S Long.W | Method & Material | Age (Ma) ± error | Lithology & Observations | Ref. |
|---|---|---|---|---|---|
| HAB-689 | 24°23'43" 70°26'34" | K-Ar Bt | 131 ± 5 | Granite | (21) |
| MAB-9 | 24°56'05" 70°25'15" | K-Ar Amp | 131 ± 5 | Foliated tonalite | (22) |
| MAB-16 | 24°57'50" 70°25'20" | K-Ar Bt<br>K-Ar Bt | 129 ± 3<br>123 ± 4 | Foliated tonalite | (22) |
| MAB-177 | 24°33'05" 70°11'15" | K-Ar Bt | 128 ± 3 | Granodiorite | (22) |
| MAB-84 | 24°52'15" 70°22'50" | K-Ar Bt | 128 ± 3 | Monzogranite | (22) |
| HAB-481A | 24°40'55" 70°15'45" | K-Ar Bt | 128 ± 3 | Granodiorite | (22) |
| HAB-937 | 24°54'35" 70°12'00" | K-Ar Amp | 127 ± 12 | Diorite | (22) |
| MAB-590 | 24°23'30" 70°15'20" | K-Ar Rt | 127 ± 5 | Diorite (dike) | (22) |
| MI-140 | 23°26'30" 70°32'05" | K-Ar Bt | 126.2 ± 3.8 | Quartz diorite | (11) |
| MAB-545 | 24°56'10" 70°17'25" | K-Ar Rt | 124 ± 5 | Andesitic dike | (22) |
| U-174 | 25°55' 70°12' | Ar-Ar Bt<br>K-Ar Bt | 124 ± 4<br>120 ± 3 | Diorite | (44) |
| HAB-577-B | 24°58'25" 70°24'55" | K-Ar Rt | 123 ± 4 | Dacitic porphyry | (22) |
| HAB-11 | 24°42'40" 70°08'45" | K-Ar Bt | 122 ± 3 | Monzogranite | (22) |
| La Gringa | 21°55'20" 69°43'30' | K-Ar Wr | 118 ± 15 | Altered dacitic porphyry Puntillas prospect | (42) |
| UP-25 | 25°42' 70°11' | K-Ar Bt | 117 ± 3 | Monzodiorite | (44) |

| Sample Identif. | Lat. S Long.W | Method & Material | Age (Ma) ± error | Lithology & Observations | Ref. |
|---|---|---|---|---|---|
| HAB-791 | 24°21'30" 70°20'50" | K-Ar Bt | 117 ± 4 | Monzodiorite | (22) |
| Z-1-75 | 25°57' 69°58' | Ar-Ar Hb | 115 ± 2.8 | Porphyry | (44) |
| UP-4 | 25°26' 70°28' | K-Ar Bt | 112 ± 4 | Granodiorite | (44) |
| TA-8c | 25°29'10" 70°12'05" | K-Ar Bt | 111 ± 2 | Granodiorite | (30) |
| UP-2N | 25°39' 70°10' | K-Ar Bt | 111 ± 3 | Monzodiorite | (44) |
| MAB-808 | 24°19'35" 70°22'20" | K-Ar Plg | 110 ± 4 | Andesite (dike) | (22) |
| TA-260 | 25°18"35" 70°01'10" | K-Ar Bt | 109 ± 2 | Granodiorite | (30) |
| HAB-266 | 24°52'50" 70°03'00" | K-Ar Bt | 108 ± 4 | Diorite | (22) |
| MAB-369 | 24°04'50" 70°03'05" | K-Ar Bt | 107 ± 3 | Granodiorite | (22) |
| MAB-698 | 24°06'05" 69°57'55" | K-Ar Bt | 100 ± 3 | Granodiorite | (22) |
| MO-932 | 24°04'25" 69°58'35" | K-Ar Bt | 98 ± 3 | Monzodiorite | (22) |

Table A2.12 Upper Cretaceous-Eocene volcanic rocks

| Sample Identif. | Lat. S Long.W | Method & Material | Age (Ma) ± error | Lithology & Observations | Ref. |
|---|---|---|---|---|---|
| JN-73A | 25°22'00" 69°25'40" | K-Ar Bt | 72 ± 2 | Crystalline tuff | (30) |
| BAP-148 | 24°56'10" 69°32'50" | K-Ar Wr | 60.2 ± 2.2 | Andesite Cachinal de la Sierra | (31) |

| Sample Identif. | Lat. S Long.W | Method & Material | Age (Ma) ± error | Lithology & Observations | Ref. |
|---|---|---|---|---|---|
| JN-337D | 25°06'30" 69°55'25" | K-Ar Wr | 59 ± 3 | Vitreous welded tuff | (30) |
| AG-21 | 25°48°10" 69°48'30" | K-Ar Wr | 59 ± 5 | Andesite | (30) |
| JN-623 | 25°51'30" 69°31'30" | K-Ar Hb | 57 ± 3 | Dacite | (30) |
| AW-10 | 25°37'35" 69°42'55" | K-Ar Wr | 54 ± 2 | Andesite | (30) |
| CM-331 | 21°34'00" 68°55'30" | K-Ar Wr | 50.6 ± 1.3<br>51.8 ± 1.3 | Andesite<br>Recalculated | (23)<br>(42) |
| CM-36 | 21°42'10" 68°49'00" | K-Ar Wr | 42.8 ± 1.2<br>43.8 ± 1.2 | Andesite<br>Recalculated | (23)<br>(42) |
| D-1 | 21°50'00" 68°50'40" | K-Ar Wr | 42.2 ± 2.3<br>43.2 ± 2.3 | Andesite<br>Recalculated | (23)<br>(42) |
| To-364 | 23°02'45" 68°39'05" | K-Ar Bt | 41.0 ± 3.6 | Welded tuff | (34) |
| TO432 | 23°31'10" 68°39'05" | K-Ar Plg | 39.9 ± 3.0 | Tuff | (34) |
| ESAD-2 | 24°15'02" 69°04'57" | K-Ar Wr | 35.4 ± 1.8* | Altered andesite La Escondida porph. copper | (1) |
| CAKAR-13 | 24°16'17" 69°04'11" | K-Ar Bt | 33.2 ± 1.4* | Altered andesite La Escondida porph. copper | (1) |
| CAKAR-14 | 24°16'11" 69°04'11" | K-Ar Bt | 32.8 ± 1.3* | Altered andesite La Escondida porph. copper | (1) |

Table A2.13 Upper Cretaceous-Eocene intrusive rocks

| Sample Identif. | Lat. S Long.W | Method & Material | Age (Ma) ± error | Lithology & Observations | Ref. |
|---|---|---|---|---|---|
| 81088-099 | 22°10'08" 69°37'13" | Rb-Sr Wr | 79.2 ± 14.8 | Quartz monzodiorites MSWD 0.34 | (36) |
| Average | | | IR 0.70421 ± 0.00019 | | |

| Sample Identif. | Lat. S Long.W | Method & Material | Age (Ma) ± error | Lithology & Observations | Ref. |
|---|---|---|---|---|---|
| AW-17 | 25°36'25" 69°40'10" | K-Ar Wr | 78 ± 5 | Porphyry | (30) |
| JN-787 | 25°27'00" 69°49'35" | K-Ar Bt | 75 ± 2 | Rhyolitic porphyry | (30) |
| | 22°04'15" 68°47'10" | K-Ar Bt | 68 ± 2.5 | Diorite | (45) |
| HAB-285 | 24°56'30" 70°00'50" | K-Ar Bt | 66.6 ± 2.2 | Dioritic porphyry | (21) |
| MAF-306 | 23°05'05" 68°39'30" | K-Ar Bt | 66.4 ± 1.4 | Monzonite | (34) |
| AW-42 | 25°51'25" 69°34'40" | K-Ar Wr | 66 ± 5 | Andesite | (30) |
| 80166-190 | 21°48'23" 68°37'34" 21°52'10" 68°40'38" | Rb-Sr Wr | 66 ± 24 | Gabbro, diorite MSWD 1.9, IR 0.70385 Coord. of the sampled area | (36) |
| 22P-S2 | 21°26'30" 68°50'40" | K-Ar Wr | 65.8 ± 1.7<br>67.3 ± 1.7 | Granite<br>Recalculated | (23)<br>(42) |
| D-6 | 21°52'00" 68°40'10" | K-Ar Bt | 65.1 ± 1.8<br>66.6 ± 1.8 | Gabbro (Cerro Colorado)<br>Recalculated | (23)<br>(42) |
| MAF-325C | 23°05'30" 68°42'30" | K-Ar Bt | 64.6 ± 11 | Tonalite | (34) |
| HAB-279 | 24°54'30" 69°59'10" | K-Ar Bt | 63.2 ± 2.3 | Rhyolitic porphyry | (21) |
| | 22°18'30" 69°10'00" Approx. | K-Ar Hb | 62.3 ± 3.3 | Granite | (4) |
| A-38 | 21°54'30" 68°37'45" | K-Ar Bt | 62.2 ± 2.4<br>63.6 ± 2.4 | Gabbro (Cerro Colorado)<br>Recalculated | (6)<br>(42) |
| | 22°16' 69°05' | K-Ar Amp | 61.8 ± 3.4 | Monzonite | (4) |
| HAB-5A | 24°40'45" 69°44'30" | K-Ar Wr | 60.9 ± 4.4 | Rhyolitic porphyry | (21) |

| Sample Identif. | Lat. S Long.W | Method & Material | Age (Ma) ± error | Lithology & Observations | Ref. |
|---|---|---|---|---|---|
| BAP-74 district | 24°58'52" 69°32'30" | K-Ar Ser (hypogene) | 59.2 ± 1.4 | Silver vein Cachinal de la Sierra | (31) |
| H-405 | 21°00'10" 68°41'00" | K-Ar Wr | 59.4 ± 1.2<br>60.8 ± 1.2 | Granodiorite<br>Recalculated | (6)<br>(42) |
| BAP-1 | 24°55'36" 69°33'30" | K-Ar Wr | 59.2 ± 2 | Dacitic porphyry Cachinal de la Sierra district | (31) |
| BAP-11-T | 24°57'18" 69°33'48" | K-Ar Wr<br>K-Ar Plg | 57.5 ± 2.3<br>56.4 ± 11.8 | Dacitic porphyry Cachinal de la Sierra district | (31) |
| BAP-40 | 24°58'44" 69°33'04 | K-Ar Plg | 55.8 ± 3.5 | Diorite Cachinal de la Sierra district | (31) |
| D-4 | 21°48'00" 68°50'30" | K-Ar Bt | 49.1 ± 1.2<br>50.2 ± 1.2 | Diorite<br>Recalculated | (23)<br>(42) |
| Los Picos Diorite | 22°16'30" 69°00'15" | K-Ar Bt | 45.1 ± 1.8 | Diorite W of Chuquicamata mine | (4) |
| D-5 | 21°52'45" 68°46'40" | K-Ar Wr | 44.7 ± 2.5<br>45.7 ± 2.5 | Diorite<br>Recalculated | (23)<br>(42) |
| 108 | 22°50' 69°20' | K-Ar Bt + Hb | 43.9 ± 1.6<br>44.9 ± 1.6 | Granodiorite Sierra Gorda district<br>Recalculated | (32)<br>(42) |
| M171 | 25°06'39" 69°32'32" | K-Ar Alu | 43.8 ± 1.2 | Alunite vein El Guanaco Au district | (31) |
| QCH-75 | 21°04'26" 68°54'37" | U-Pb Zir | 43.7 ± 3.8 | Monzodiorite | (11) |

Table A2.14 Upper Eocene-Oligocene intrusive rocks

| Sample Identif. | Lat. S Long.W | Method & Material | Age (Ma) ± error | Lithology & Observations | Ref. |
|---|---|---|---|---|---|
| 80103-107 | 21°55'08" 68°48'12" 21°55'41" 68°50'41" | Rb-Sr Wr | 38.7 ± 2.2 | Southern Granodiorite El Abra MSWD 1.0, IR 0.70451 Coord. range of sampled area | (36) |
| CAKAR-10 | 24°15'27" 69°04'19" | K-Ar Alu (hypogene) | 38.3 ±1.5** | Alunite vein La Escondida porph. copper | (1) |
| Atahualpa Diorite | 22°10'00" 68°57'30" | K-Ar Bt | 38.1 ± 1.0<br>39.0 ± 1.0 | Diorite (Chuquicamata)<br>Recalculated | (3)<br>(42) |
| Fortuna Gd. | 22°15'30" 68°54'10" | K-Ar Bt | 38.0 ± 0.3<br>38.9 ± 0.3 | Granodiorite<br>Recalculated | (2)<br>(42) |
| JB-241 | 20°59'40" 68°47'50" | K-Ar Bt | 37.2 ± 1.4<br>38.1 ± 1.4 | Monzonite (Q. Blanca)<br>Recalculated | (46)<br>(42) |
| 106 | 22°18' 68°55' | K-Ar Bt | 36.9 ± 1.2<br>37.8 ± 1.2 | Fortuna granodiorite<br>Recalculated | (32)<br>(42) |
| JB-238 | 21°00'00" 68°49'00" | K-Ar Bt | 36.5 ± 1.4<br>37.4 ± 1.4 | Monzonite (Q. Blanca)<br>Recalculated | (46)<br>(42) |
| Fortuna Gd. | 22°17'20" 68°56'00" | K-Ar Bt | 36.2 ± 1.4 | Granodiorite Chuquicamata district | (2) |
| Pajonal Diorite | 21°54' 68°49' | K-Ar Bt | 35.9 ± 0.7<br>36.7 ± 0.7 | Diorite (El Abra)<br>Recalculated | (3)<br>(42) |
| CAKAR-18 | 24°15'32" 69°04'30" | K-Ar Alu (hypogene) | 35.7 ± 1.4 | Alunite vein La Escondida porph. copper | (1) |
| East Porphyry | 22°16'40" 68°53'30" | K-Ar Bt | 34.8 ± 1.9<br>35.6 ± 1.9 | Granodioritic porphyry<br>Recalculated Chuquicamata | (4)<br>(42) |
| Southern Gd. | 21°55'30" 68°49' Approx. | K-Ar Bt | 34.6 ± 0.8<br>35.4 ± 0.8 | Granodiorite<br>Recalculated El Abra | (4)<br>(42) |
| Southern Gd. | 21°55'10" 68°49'30" | K-Ar Bt | 34.5 ± 0.5<br>35.3 ± 0.5 | Granodiorite<br>Recalculated El Abra | (3)<br>(42) |

| Sample Identif. | Lat. S Long.W | Method & Material | Age (Ma) ± error | Lithology & Observations | Ref. |
|---|---|---|---|---|---|
| Diorite El Abra | 21°54'45" 68°49'45" | K-Ar Bt | 34.2 ± 0.6<br>35.0 ± 0.6 | Diorite<br>Recalculated El Abra | (4)<br>(42) |
| Dacitic Porphyry | 21°54'45" 68°49'45" | K-Ar Bt | 34.2 ± 0.7<br>35.0 ± 0.7 | Dacitic porphyry<br>Recalculated El Abra | (4)<br>(42) |
| Chuqui Porphyry | 22°16'40" 68°53'30" | Rb-Sr Wr | 34.2 ± 4.0 | Granodioritic porphyry IR 0.7045 ± 0.0007 | (48) |
| Banco Porphyry | 22°16'40" 68°53'30" | K-Ar Bt | 33.8 ± 1.3 | Granodioritic porphyry Chuquicamata | (2) |
| CAZ-321 | 24°16'55" 69°03'15" | K-Ar Ser | 33.7 ± 1.4 | Altered ignimbrite La Escondida | (1) |
| ESAD-1 | 24°15'00" 69°04'42" | K-Ar Bt | 33.7 ± 1.3 | Mineralized breccia La Escondida | (1) |
| East Porphyry | 22°16'40" 68°53'30" | K-Ar Bt | 33.6 ± 0.9<br>34.4 ± 0.9 | Granodioritic porphyry<br>Recalculated Chuquicamata | (3)<br>(42) |
| Dacitic Porphyry | 21°55' 68°51' | K-Ar Bt | 33.2 ± 1.0<br>34.0 ± 1.0 | Dacitic porphyry<br>Recalculated El Abra | (32)<br>(42) |
| West Porphyry | 22°16'40" 68°53'30" | K-Ar Bt | 31.8 ± 0.9<br>32.6 ± 0.9 | Granodioritic porphyry<br>Recalculated | (3)<br>(42) |
| 11S-B3 | 21°20'50" 68°49'40" | K-Ar Wr | 31.7 ± 2.2<br>32.4 ± 2.2 | Quartz diorite<br>Recalculated Quebrada Puno | (23) |
| CAZ-241 | 24°16'27" 69°03'26" | K-Ar Ser | 31.6 ± 1.6 | Altered rhyolitic porph. La Escondida | (1) |
| CAKAR-11 | 24°16'11" 69°03'51" | K-Ar Ser | 31.5 ± 1.4 | Altered dacitic dike La Escondida | (1) |
| Sericitic Alteration | 22°16'40" 68°53'30" | K-Ar Ser | 31.2 ± 1.3 | Quartz-sericite rock Chuquicamata | (2) |
| CAKAR-12 | 24°16'11" 69°03'55" | K-Ar Wr | 31.0 ± 1.4 | Altered dacitic dike La Escondida | (1) |

| Sample Identif. | Lat. S Long.W | Method & Material | Age (Ma) ± error | Lithology & Observations | Ref. |
|---|---|---|---|---|---|
| Altered porphyry | 22°16'40" 68°53'30" | K-Ar Ser | 30.3 ± 1.2<br>31.0 ± 1.2 | Altered porphyry<br>Recalculated | (3)<br>(42) |
| 107 | 22°16'40" 68°53'50" | K-Ar Ser | 29.8 ± 0.9<br>28.7 ± 0.9<br>30.5 ± 0.9<br>29.4 ± 0.9 | Granodioritic porphyry<br>Potassic alteration<br>Recalculated<br>Do (Chuquicamata) | (32)<br><br>(42) |
| Quartz-Sericite | 22°16'40" 68°53'30" | K-Ar Ser | 28.0 ± 1.1 | Granodioritic porphyry Chuquicamata | (2) |

Table A2.15 Pyroclastic intercalations within Oligocene-Early Miocene sedimentary rocks

| Sample Identif. | Lat. S Long.W | Method & Material | Age (Ma) ± error | Lithology & Observations | Ref. |
|---|---|---|---|---|---|
| CM-326 | 21°35'40" 68°53'50" | K-Ar Bt | 34.7 ± 0.8<br>35.5 ± 0.8 | Ignimbrite<br>Recalculated | (23)<br>(42) |
| | 22°54'30" 68°14'10" | K-Ar Bt | 28.0 ± 6.0<br>28.6 ± 6.0 | Tuff<br>Recalculated | (43)<br>(42) |
| MC-777 | 22°53'45" 68°13'05" | K-Ar Bt | 24.9 ± 1.0 | Tuff | (26) |
| AW-8 | 25°40'35" 69°33'35" | K-Ar Wr | 24 ± 2 | Ignimbrite | (30) |

Table A2.16 Supergene Minerals

| Sample Identif. | Lat. S Long.W | Method & Material | Age (Ma) ± error | Lithology & Observations | Ref. |
|---|---|---|---|---|---|
| CAKAR-19 | 24°16"13" 69°03'52" | K-Ar Alu (supergene) | 18.0 ± 0.7 | Alunite vein La Escondida | (1) |
| CAKAR-15 | 24°16"19" 69°03'55" | K-Ar Alu (supergene) | 17.7 ± 0.7 | Alunite vein La Escondida | (1) |

| Sample Identif. | Lat. S Long.W | Method & Material | Age (Ma) ± error | Lithology & Observations | Ref. |
|---|---|---|---|---|---|
| CAKAR-17 | 24°16'27" 69°03'40" | K-Ar Alu (supergene) | 16.4 ± 0.7 | Alunite vein La Escondida | (1) |
| CAKAR-16 | 24°16"05" 69°04'11" | K-Ar Alu (supergene) | 14.7 ± 0.6 | Alunite vein La Escondida | (1) |
| KA-4235 | 23°26'05" 70°03'10" | K-Ar Nat (supergene) | 14 ± 7 | Atacamite-alunite vein | (10) |

Table A2.17 Miocene-Holocene volcanic rocks

| Sample Identif. | Lat. S Long.W | Method & Material | Age (Ma) ± error | Lithology & Observations | Ref. |
|---|---|---|---|---|---|
| JN-540 | 25°20'35" 69°01'05" | K-Ar Bt | 18.2 ± 0.6 | Welded tuff | (30) |
| JN-565 | 25°22'50" 69°01'25" | K-Ar Plg | 18.2 ± 6.2 | Dacite | (30) |
| JN-541 | 25°21'05" 69°01'10" | K-Ar Plg | 17.8 ± 10.5 | Dacite | (30) |
| RG-109 | 22°43'30" 68°06'20" | K-Ar Bt | 17 ± 2 | Dacite | (33) |
| JN-567B | 25°28'30" 69°05'05" | K-Ar Wr | 16.5 ± 1.5 | Andesite | (30) |
| A-168-1 | 21°44'00" 68°31'30" | K-Ar Wr | 15.2 ± 0.8<br>15.5 ± 0.8 | Andesite<br>Recalculated | (6)<br>(42) |
| JN-831 | 25°24'05" 69°01'48" | K-Ar Wr | 13.7 ± 0.7 | Andesite | (30) |
| JN-204-H | 25°18'30" 69°14'50" | K-Ar Wr | 13.7 ± 2 | Vitreous tuff | (30) |
| A-29-2 | 21°29'00" 68°25'15" | K-Ar Plg<br>K-Ar Bt | 13.6 ± 1.8<br>12.2 ± 0.5<br>13.9 ± 1.8<br>12.5 ± 0.5 | Andesite<br><br>Recalculated | (6)<br><br>(42) |

| Sample Identif. | Lat. S Long.W | Method & Material | Age (Ma) ± error | Lithology & Observations | Ref. |
|---|---|---|---|---|---|
| PG-300 | 24°01'20" 67°20'55" | K-Ar Wr | 11.7 ± 0.7 | Andesite | (16) |
| A-6-2 | 21°56'30" 68°32'30" | K-Ar Hb | 11.0 ± 0.5 | Andesite | (6) |
| | | K-Ar Bt | 10.5 ± 0.4 | | |
| | | K-Ar Plg | 10.4 ± 0.6 | | |
| | | | 11.2 ± 0.5 | Recalculated | (42) |
| | | | 10.7 ± 0.4 | | |
| | | | 10.6 ± 0.6 | | |
| PG-294 | 23°58'30" 67°29'30" | K-Ar Wr | 10.7 ± 0.5 | Andesite | (16) |
| A-3-2 | 21°58'15" 68°28'45" | K-Ar Bt | 10.7 ± 0.5 | Andesite | (6) |
| | | | 10.9 ± 0.5 | Recalculated | (42) |
| A-97 | 21°59'15" 68°27'30" | K-Ar Bt | 10.6 ± 0.5 | Andesite | (6) |
| | | | 10.8 ± 0.5 | Recalculated | (42) |
| A-23 | 22°14'30" 68°26'05" | K-Ar Bt | 10.6 ± 0.7 | Ignimbrite | (6) |
| | | | 10.8 ± 0.7 | Recalculated | (42) |
| To-6 | 23°56'50" 67°31'50" | K-Ar Wr | 10.5 ± 0.9 | Andesite | (34) |
| To-340 | 23°48'00" 68°30'00" | K-Ar Bt | 10.2 ± 0.6 | Volcanic ash | (34) |
| GMC-27 | 23°30'00" 67°23'45" | K-Ar Plg | 10.2 ± 1.7 | Andesite | (16) |
| PG-267 | 22°58'30" 67°07'40" | K-Ar Bt | 10.1 ± 0.5 | Pumice | (16) |
| 868 | 22°43' 68°14' | K-Ar Bt | 10.0 ± 0.4 | Ignimbrite | (37) |
| | | | 10.2 ± 0.4 | Recalculated | (42) |
| A-4-1 | 21°58'00" 68°27'00" | K-Ar Bt | 10.0 ± 0.5 | Ignimbrite | (6) |
| | | | 10.2 ± 0.5 | Recalculated | (42) |
| A-66 | 21°06'45" 68°39'30" | K-Ar Bt | 9.4 ± 0.4 | Ignimbrite | (6) |
| | | | 9.6 ± 0.4 | Recalculated | (42) |
| A2-2 | 21°57'15" 68°31'30" | K-Ar Bt | 9.4 ± 0.7 | Ignimbrite | (6) |
| | | | 9.6 ± 0.7 | Recalculated | (42) |

| Sample Identif. | Lat. S Long.W | Method & Material | Age (Ma) ± error | Lithology & Observations | Ref. |
|---|---|---|---|---|---|
| T-1 | 22°19'50" 68°02'30" | K-Ar Bt | 9.3 ± 0.6 | Ignimbrite | (24) |
| PG-274 | 23°06'10" 67°20'30" | K-Ar Plg | 9.1 ± 4.3 | Andesite | (16) |
| A-129 | 21°02'00" 68°29'00" | K-Ar Bt | 9.0 ± 0.4<br>9.2 ± 0.4 | Andesite<br>Recalculated | (6)<br>(42) |
| MC-5 | 22°06'30" 68°20'55" | K-Ar Bt | 9.0 ± 0.7 | Ignimbrite | (26) |
| MC-774 | 22°23'20" 68°22'25" | K-Ar Bt | 9.0 ± 1.2 | Ignimbrite | (26) |
| A-6-6 | 21°56'30" 68°32'30" | K-Ar Bt | 8.9 ± 0.5<br>9.1 ± 0.5 | Ignimbrite<br>Recalculated | (6)<br>(42) |
| A-164-1 | 21°06'15" 68°22'15" | K-Ar Bt | 8.9 ± 0.8<br>9.1 ± 0.8 | Andesite<br>Recalculated | (6)<br>(42) |
| AJ-49 | 22°15'00" 68°23'35" | K-Ar Bt | 8.8 ± 0.4 | Ignimbrite | (26) |
| A-117 | 21°05'00" 68°22'30" | K-Ar Bt | 8.7 ± 0.4<br>8.9 ± 0.4 | Andesite<br>Recalculated | (6)<br>(42) |
| A-1 | 22°18'55" 68°38'50" | K-Ar Bt | 8.5 ± 0.5<br>8.7 ± 0.5 | Ignimbrite<br>Recalculated | (6)<br>(42) |
| A-40 | 21°45'00" 68°39'00" | K-Ar Bt | 8.5 ± 1.4<br>8.7 ± 1.4 | Ignimbrite<br>Recalculated | (6)<br>(42) |
| A-40-2 | 21°49'45" 68°36'45" | K-Ar Bt<br>K-AR Bt | 8.5 ± 1.4<br>8.2 ± 1.2<br>8.7 ± 1.4<br>8.4 ± 1.2 | Ignimbrite<br><br>Recalculated | (6)<br><br>(42) |
| A-41 | 21°46'45" 68°37'45" | K-Ar Bt | 8.4 ± 0.4<br>8.6 ± 0.4 | Ignimbrite<br>Recalculated | (6)<br>(42) |
| A-118 | 21°00'30" 68°30'30" | K-Ar Bt | 8.3 ± 0.4<br>8.5 ± 0.4 | Andesite<br>Recalculated | (6)<br>(42) |
| A-25 | 22°14'40" 68°26'00" | K-Ar Bt | 7.8 ± 0.3<br>7.9 ± 0.3 | Ignimbrite<br>Recalculated | (6)<br>(42) |

| Sample Identif. | Lat. S Long.W | Method & Material | Age (Ma) ± error | Lithology & Observations | Ref. |
|---|---|---|---|---|---|
| To-310 | 23°09'00" 67°34'15" | K-Ar Wr | 7.8 ± 0.6 | Andesite | (34) |
| PG-263 | 22°49'40" 67°17'00" | K-Ar Bt | 7.6 ± 0.3 | Welded tuff | (16) |
| A-164-2 | 21°06'15" 68°22'15" | K-Ar Bt | 7.5 ± 0.4<br>7.6 ± 0.4 | Ignimbrite<br>Recalculated | (6)<br>(42) |
| To-181-2 | 23°33'15" 67°30'00" | K-Ar Wr | 7.5 ± 0.6 | Andesite | (34) |
| CM-372 | 21°34"10" 68°47'00" | K-Ar Bt | 7.34 ± 0.37<br>7.52 ± 0.37 | Ignimbrite<br>Recalculated | (23)<br>(42) |
| RG-162 | 22°43'30" 68°06'15" | K-Ar Bt | 7.0 ± 1.0 | Ignimbrite | (33) |
| 867 | 22°46' 68°05' | K-Ar Bt | 6.89 ± 0.07<br>7.06 ± 0.07 | Ignimbrite<br>Recalculated | (37)<br>(42) |
| T-5 | 22°15'05" 68°10'30" | K-Ar Bt | 6.8 ± 0.3<br>6.9 ± 0.3 | Ignimbrite<br>Recalculated | (24)<br>(42) |
| A-8814 | 22°14'30" 68°07'30" | K-Ar Bt | 6.2 ± 0.3<br>6.3 ± 0.3 | Ignimbrite<br>Recalculated | (6)<br>(42) |
| To-301-B | 23°11'10" 67°35'00" | K-Ar Bt | 5.8 ± 0.1 | Welded tuff | (34) |
| A-30 | 21°25'15" 68°26'00" | K-Ar Wr | 5.8 ± 0.4<br>5.9 ± 0.4 | Andesite<br>Recalculated | (6)<br>(42) |
| A-51 | 21°05'15" 68°21'30" | K-Ar Bt | 5.7 ± 0.3<br>5.8 ± 0.3 | Ignimbrite<br>Recalculated | (6)<br>(42) |
| A-31 | 21°25'15" 68°24'15" | K-Ar Wr | 5.7 ± 0.4<br>5.8 ± 0.4 | Andesite<br>Recalculated | (6)<br>(42) |
| PG-322 | 23°21'55" 67°07'50" | K-Ar Bt | 5.7 ± 0.4 | Vitreous tuff | (16) |
| A-11 | 22°01'50" 68°36'50" | K-Ar Bt | 5.6 ± 0.4<br>5.7 ± 0.4 | Ignimbrite<br>Recalculated | (6)<br>(42) |
| A-48 | 21°08'30" 68°19'00" | K-Ar Bt | 5.4 ± 0.3<br>5.5 ± 0.3 | Ignimbrite<br>Recalculated | (6)<br>(42) |

| Sample Identif. | Lat. S Long.W | Method & Material | Age (Ma) ± error | Lithology & Observations | Ref. |
|---|---|---|---|---|---|
| PG-115 | 23°47'50" 67°15'00" | K-Ar Bt | 5.1 ± 0.4 | Welded tuff | (16) |
| PG-126 | 23°37'25" 67°11'45" | K-Ar Wr | 4.9 ± 0.4 | Andesite | (16) |
| PG-323 | 23°21'45" 67°07'50" | K-Ar Wr | 4.9 ± 0.7 | Pumice | (16) |
| GMC-26 | 21°29'35" 67°28'25" | K-Ar Bt | 4.8 ± 0.6 | Welded tuff | (16) |
| A-34-2 | 21°19'45" 68°15'00" | K-Ar Bt | 4.7 ± 0.3 | Rhyolite | (6) |
| PG-265 | 22°54'25" 67°28'05" | K-Ar Wr | 4.6 ± 1.2 | Dacite | (16) |
| SP-16 | 23°45'05" 67°51'10" | K-Ar Wr | 4.6 ± 2.3 | Andesite | (34) |
| AI-7 | 22°23'15" 68°14'05" | K-Ar Bt | 4.5 ± 0.2 | Ignimbrite | (26) |
| GMC-22 | 23°24"40" 67°27'40" | K-Ar Bt | 4.5 ± 0.4 | Welded tuff | (16) |
| G-302 | 23°55'50" 67°17"05" | K-Ar Wr | 4.5 ± 0.9 | Basalt | (16) |
| GMC-28 | 23°27'55" 67°24'00" | K-Ar Bt | 4.4 ± 0.3 | Rhyolite | (16) |
| PG-205 | 23°16'40" 67°20'25" | K-Ar Bt | 4.4 ± 0.7 | Rhyolite | (16) |
| PU-30 | 22°43'45" 69°00'00" | K-Ar Bt | 4.27 ± 0.07 | Ignimbrite | (26) |
| 869 | 22°43' 68°14' | K-Ar Bt | 4.24 ± 0.05<br>4.34 ± 0.05 | Ignimbrite<br>Recalculated | (37)<br>(42) |
| To-219 | 23°02'55" 67°30'10" | K-Ar Bt | 4.2 ± 0.2 | Welded tuff | (34) |
| GMC-5 | 22°53'05" 67°28'55" | K-Ar Bt | 4.1 ± 0.4 | Welded tuff | (16) |

| Sample Identif. | Lat. S Long.W | Method & Material | Age (Ma) ± error | Lithology & Observations | Ref. |
|---|---|---|---|---|---|
| PG-223 | 23°02'55" 67°22'05" | K-Ar Bt | 4.1 ± 0.2 | Welded tuff | (16) |
| To-301-D | 23°10'50" 67°35'10" | K-Ar Bt | 4.0 ± 0.2 | Welded tuff | (34) |
| M-88 | 22°57'55" 67°10'05" | K-Ar Bt | 4.0 ± 0.3 | Welded tuff | (16) |
| P-99 | 22°57'40" 67°18'00" | K-Ar Bt | 4.0 ± 0.3 | Welded tuff | (16) |
| PG-218 | 22°54'25" 67°21'45" | K-Ar Bt | 4.0 ± 0.3 | Vitreous tuff | (16) |
| PG-278 | 23°03'05" 67°27'05" | K-Ar Bt | 3.8 ± 0.3 | Pumice | (16) |
| PG-279 | 23°03'05" 67°27'05" | K-Ar Bt | 3.8 ± 0.5 | Tuff | (16) |
| PG-295 | 23°56'35" 67°22'45" | K-Ar Bt | 3.8 ± 1.2 | Pumice | (16) |
| To-52 | 23°56'45" 67°50'40" | K-Ar Wr | 3.7 ± 0.4 | Andesite | (34) |
| GU-43 | 22°54'30" 67°28'30" | K-Ar Bt | 3.6 ± 0.1 | Rhyolite | (26) |
| To-186 | 23°32'15" 67°36'45" | K-Ar Wr | 3.6 ± 0.4 | Andesite | (34) |
| A-33 | 21°25'00" 68°21'30" | K-Ar Wr | 3.6 ± 1.2<br>3.69 ± 1.20 | Andesite<br>Recalculated | (6)<br>(42) |
| PG-221 | 22°58'10" 67°18'45" | K-Ar Wr | 3.5 ± 0.7 | Andesite | (16) |
| A-69 | 21°16'45" 68°28'30" | K-Ar Wr | 3.3 ± 0.3<br>3.38 ± 0.30 | Andesite<br>Recalculated | (6)<br>(42) |
| A-128 | 21°06'15" 68°29'15" | K-Ar Bt | 3.2 ± 0.3<br>3.28 ± 0.30 | Andesite<br>Recalculated | (6)<br>(42) |
| To-101 | 23°56'30" 68°10'00" | K-Ar Bt | 3.2 ± 0.3 | Welded tuff | (34) |

| Sample Identif. | Lat. S Long.W | Method & Material | Age (Ma) ± error | Lithology & Observations | Ref. |
|---|---|---|---|---|---|
| To-150 | 23°45'45" 67°51'10" | K-Ar Bt | 3.1 ± 0.7 | Welded tuff | (34) |
| To-167 | 23°19'05" 67°40'00" | K-Ar Bt | 3.0 ± 0.2 | Dacite | (34) |
| GMC-1 | 23°12'55" 67°27'55" | K-Ar Bt | 2.7 ± 0.2 | Andesite | (16) |
| 443 | 21°28'00" 68°17'00" | K-Ar | 2.5 ± 0.1<br>2.56 ± 0.1 | Andesite<br>Recalculated | (35)<br>(42) |
| PG-286-1 | 23°55'50" 67°27'50" | K-Ar Bt | 2.5 ± 0.3 | Welded tuff | (16) |
| PG-260 | 23°40'25" 67°23'15" | K-Ar Bt | 2.4 ± 0.4 | Welded tuff | (16) |
| PG-313 | 23°48'45" 67°29'15" | K-Ar Wr | 2.0 ± 0.3 | Andesite | (16) |
| To-221 | 23°07'00" 68°00'00" | K-Ar Bt<br>K-Ar Bt | 1.7 ± 0.3<br>1.3 ± 0.3 | Pumice | (34) |
| 492 | 21°48'00" 68°15'00" | K-Ar | 1.5 ± 0.1<br>1.54 ± 0.10 | Dacite<br>Recalculated | (35)<br>(42) |
| So-1007 | 24°40'45" 68°34'45" | K-Ar Bt | 1.5 ± 0.4 | Dacite | (17) |
| A-8815 | 22°14'15" 68°08'30" | K-Ar Wr | 1.1 ± 0.1<br>1.13 ± 0.10 | Andesite<br>Recalculated | (6)<br>(42) |
| MC-776 | 22°56'00" 67°58'55" | K-Ar Bt | 1.0 ± 0.2 | Ignimbrite | (26) |
| 354 | 21°18'00" 68°13'00" | K-Ar | 0.8 ± 0.1<br>0.82 ± 0.10 | Andesite<br>Recalculated | (35)<br>(42) |
| LI-2b | 22°53'40" 67°46'20" | K-Ar Bt | 0.8 ± 0.3 | Ignimbrite | (26) |
| T-3 | 22°24'50" 68°03'00" | K-Ar Wr | 0.8 ± 0.1 | Dacite (dome) | (24) |

| Sample Identif. | Lat. S Long.W | Method & Material | Age (Ma) ± error | Lithology & Observations | Ref. |
|---|---|---|---|---|---|
| T-2 | 22°19'10" 68°00'30" | K-Ar Bt | <1 | Ignimbrite | (24) |
| To-503 | 23°56'30" 68°06'30" | K-Ar Wr | <1 | Basaltic andesite | (34) |
| To-443 | 23°57'55" 68°07'45" | K-Ar Wr | <1 | Andesite | (34) |
| T-4 | 22°27'00" 67°57'50" | K-Ar Bt | <1 | Rhyolite (dome) | (24) |
| MC-15 | 22°11'10" 68°11'05" | K-Ar Bt | <1 | Dacite | (26) |
| So-1001 | 24°42'00" 68°32'50" | K-Ar Wr | <1 | Dacite | (17) |

Table A2.18 Miocene-Pliocene subvolcanic intrusive rocks

| Sample Identif. | Lat. S Long.W | Method & Material | Age (Ma) ± error | Lithology & Observations | Ref. |
|---|---|---|---|---|---|
| MDR-161 | 22°58'00" 67°03'40" | K-Ar Bt | 12.8 ± 0.5 | Rhyolitic porphyry | (16) |
| GMC-15 | 23°25'00" 67°22'15" | K-Ar Wr | 10.9 ± 0.4 | Dacitic porphyry | (16) |
| Siglia 2 | 23°49'10" 67°17'50" | K-Ar Hb | 10.0 ± 0.9 | Monzonite | (16) |
| PU-34 | 22°37'30" 67°58'50" | K-Ar Bt | 8.8 ± 0.1 | Dacitic porphyry | (26) |
| GMC-12 | 23°21'55" 67°19'20" | K-Ar Plg | 8.0 ± 2.0 | Dacitic porphyry | (16) |
| 866 | 22°18'45" 68°01'00" | K-Ar Bt | 7.53 ± 0.05<br>7.72 ± 0.05 | Dacitic porphyry<br>Recalculated | (37)<br>(42) |
| To-79 | 23°19'00" 67°44'00" | K-Ar Bt | 5.2 ± 0.8 | Dacitic porphyry | (34) |

| Sample Identif. | Lat. S Long.W | Method & Material | Age (Ma) ± error | Lithology & Observations | Ref. |
|---|---|---|---|---|---|
| To-183 | 23°27'40" 67°28'30" | K-Ar Bt | 4.8 ± 0.2 | Dacitic porphyry | (16) |

Table A2.19 Volcanic ash intercalations within Miocene-Holocene mudflow, alluvial and colluvial deposits

| Sample Identif. | Lat. S Long.W | Method & Material | Age (Ma) ± error | Lithology & Observations | Ref. |
|---|---|---|---|---|---|
| HAB-775 | 24°26'20" 70°20'43" | K-Ar Bt | 19 ± 1.2 | Volcanic ash | (19) |
| CAKAR-20 | 24°15'05" 69°04'49" | K-Ar Bt | 8.7 ± 0.4 | Volcanic ash | (1) |
| | 22°19'30" 68°53'55" | K-Ar Bt | 8.4 ± 0.4<br>8.6 ± 0.4 | Volcanic ash<br>Recalculated<br>Southern mine Chuquicamata | (27)<br>(42) |
| CAKAR-5 | 24°12'19" 69°04'08" | K-Ar Bt | 6.5 ± 0.2 | Volcanic ash | (1) |
| MAB-663 | 24°30'00" 70°20'00" | K-Ar Bt | 5.5 ± 1.0 | Volcanic ash | (19) |
| CAKAR-2 | 24°15'22" 69°04'09" | K-Ar Bt | 4.2 ± 0.2 | Volcanic ash | (1) |
| SC-1 | 23°31'10" 70°15'00" | K-Ar Bt | 3.0 ± 0.2 | Volcanic ash | (49) |
| KA-454 | 23°27'20" 70°06'20" | K-Ar Bt | 2.97 ± 0.07 | Rhyolitic ash | (10) |
| KA-3991 | 23°27'20" 70°06'20" | K-Ar Bt | 2.87 ± 0.07 | Rhyolitic ash | (10) |

## A2.2 OBSERVATIONS AND ABBREVIATIONS USED:

| | |
|---|---|
| * | : Age too young according to field observations. |
| ** | : Age too old according to field observations. |
| IR | : $^{87}Sr/^{86}Sr$ initial ratio |
| MSWD | : Mean Standard Weighted Deviation |
| K-Ar | : Potassium-Argon Dating |
| Ar-Ar | : $^{40}Ar$-$^{39}Ar$ Dating |
| Rb-Sr | : Rb-Sr Dating |
| Recalculated | : Old ages recalculated using the decay constants suggested by the IUGS. (Steiger and Jäger, 1977). |

## A2.3 MINERAL ABBREVIATIONS USED

| | |
|---|---|
| Act | : Actinolite |
| Alu | : Alunite |
| Amp | : Amphibole |
| Apa | : Apatite |
| Bt | : Biotite |
| Clo | : Chlorite |
| Fel | : Feldspar |
| Hb | : Hornblende |
| Mus | : Muscovite |
| Ort | : Orthoclase |
| Plg | : Plagioclase |
| Wr | : Whole rock |
| Ser | : Sericite |
| Zir | : Zircon |

## A2.4 REFERENCES CODE

(1) Alpers and Brimhall, 1988
(2) Alvarez and others, 1980
(3) Ambrus, 1977
(4) Ambrus, 1979
(5) Astudillo, 1984
(6) Baker, 1977
(7) Berg and others, 1983
(8) Boric, 1981
(9) Buchelt and Zeil, 1986
(10) Chavez, 1985
(11) Damm and others, 1986
(12) Damm and Pichowiak, 1981
(13) Davidson written comm.
(14) Davidson and others, 1985
(15) Diaz and others, 1985
(16) Gardeweg and Ramirez, 1985
(17) Gardeweg and others, 1984
(18) Halpern, 1978
(19) Herve, 1987
(20) Herve and others, 1985
(21) Herve and others, in prep.
(22) Herve and Marinovic, 1989
(23) Huete and others, 1977
(24) Lahsen and Munizaga, 1979
(25) Maksaev and Marinovic, 1980
(26) Marinovic and Lahsen, 1984
(27) Mortimer and others, 1977
(28) Mpodozis and others, 1983
(29) Munizaga and others, 1985
(30) Naranjo and Puig, 1984
(31) Puig and others, 1988
(32) Quirt, 1972
(33) Ramirez, 1979
(34) Ramirez and Gardeweg, 1982
(35) Roobol and others, 1974
(36) Rogers, 1985
(37) Rutland and others, 1965
(38) SERNAGEOMIN-JICA-MMAJ, 1986
(39) Shibata et al., 1984
(40) Skarmeta, 1983
(41) Skarmeta and Marinovic, 1980
(42) This study; recalculated age
(43) Travisany, 1978
(44) Ulriksen, 1979
(45) Vega and Bordones, 1981
(46) Vergara and Thomas, 1984
(47) Zentilli, 1974
(48) Zentilli and others, 1988
(49) Naranjo, 1987

# APPENDIX 3. CHEMICAL ANALYSES

Table A3.1 Upper Cretaceous - Eocene volcanic rocks

| Sample | II-1 | II-2 | II-2 | II-12 | II-14 | II-14 | II-15 | II-16 |
|---|---|---|---|---|---|---|---|---|
| $SiO_2$ | 59.11 | 70.77 | 69.89 | 62.77 | 61.46 | 62.39 | 53.70 | 54.70 |
| $TiO_2$ | 0.80 | 0.13 | 0.15 | 0.52 | 0.88 | 0.89 | 1.06 | 0.80 |
| $Al_2O_3$ | 16.08 | 11.86 | 12.04 | 17.04 | 16.93 | 16.66 | 17.30 | 14.45 |
| $Fe_2O_3$ | 4.94 | 1.22 | 1.17 | 3.15 | 4.68 | 4.69 | 5.36 | 5.63 |
| FeO | 0.44 | 0.01 | 0.02 | 0.93 | 0.84 | 0.99 | 1.62 | 0.36 |
| MnO | 0.10 | 0.01 | 0.01 | 0.08 | 0.09 | 0.09 | 0.12 | 0.15 |
| MgO | 2.44 | 0.68 | 0.68 | 1.84 | 1.64 | 1.61 | 4.13 | 2.74 |
| CaO | 4.95 | 0.67 | 0.62 | 3.92 | 3.50 | 3.59 | 3.67 | 5.13 |
| $Na_2O$ | 4.07 | 2.57 | 2.55 | 4.25 | 5.16 | 4.91 | 3.86 | 4.77 |
| $K_2O$ | 3.96 | 5.98 | 5.78 | 2.02 | 2.77 | 2.57 | 3.54 | 2.78 |
| $P_2O_5$ | 0.29 | 0.04 | 0.01 | 0.14 | 0.22 | 0.11 | 0.22 | 0.19 |
| $H_2O+$ | 0.75 | 2.59 | 2.63 | 1.68 | 1.11 | 1.11 | 3.03 | 2.30 |
| $H_2O-$ | 1.11 | 3.18 | 2.51 | 0.91 | 0.48 | 0.45 | 1.80 | 1.87 |
| $CO_2$ | 0.66 | 0.07 | 0.15 | 0.44 | 0.09 | 0.08 | 0.70 | 0.92 |
| S | 0.06 | 0.05 | | 0.01 | 0.11 | | 0.04 | 1.14 |
| Total | 99.68 | 99.82 | 98.21 | 99.70 | 99.96 | 100.14 | 100.15 | 97.93 |
| V | 104 | 16 | | 89 | 95 | | 169 | 114 |
| Cr | 33 | 9 | | 14 | 7 | | 51 | 40 |
| Ni | 18 | 12 | | 8 | 21 | | 19 | 17 |
| Cu | 50 | 5 | | 52 | 19 | | 23 | 17 |
| Zn | 82 | 35 | | 69 | 77 | | 87 | 67 |
| Rb | 87 | 141 | | 46 | 70 | | 75 | 83 |
| Sr | 895 | 137 | | 705 | 500 | | 440 | 499 |
| Y | 22 | 11 | | 13 | 30 | | 25 | 24 |
| Zr | 273 | 81 | | 146 | 219 | | 174 | 153 |
| Nb | 14 | 11 | | 7 | 16 | | 13 | 12 |
| Th | 10 | 17 | | <1 | 3 | | 1 | 4 |
| Ba | 1108 | 346 | | 699 | 805 | | 679 | 520 |
| Pb | 14 | 17 | | <1 | 15 | | 6 | 9 |
| Ga | 24 | 18 | | 23 | 20 | | 27 | 18 |

| Sample | II-17 | II-18 | II-19 | II-20 | II-21 | II-22 | II-23 | II-24 |
|---|---|---|---|---|---|---|---|---|
| $SiO_2$ | 68.68 | 63.76 | 75.18 | 75.28 | 52.10 | 62.40 | 60.94 | 62.17 |
| $TiO_2$ | 0.23 | 0.73 | 0.13 | 0.18 | 0.83 | 0.52 | 0.52 | 0.48 |
| $Al_2O_3$ | 14.03 | 13.37 | 11.86 | 11.98 | 14.38 | 16.53 | 16.32 | 16.09 |
| $Fe_2O_3$ | 1.90 | 4.83 | 0.36 | 1.10 | 6.07 | 4.85 | 5.06 | 3.97 |
| FeO | 0.15 | 0.95 | 0.04 | 0.17 | 0.26 | 0.01 | 0.01 | 0.57 |
| MnO | 0.16 | 0.11 | 0.01 | 0.02 | 0.07 | 0.11 | 0.11 | 0.10 |
| MgO | 0.27 | 1.87 | 0.45 | 0.18 | 4.66 | 1.71 | 1.51 | 1.08 |
| CaO | 3.79 | 3.83 | 0.60 | 0.66 | 7.11 | 4.73 | 5.08 | 5.48 |
| $Na_2O$ | 4.45 | 3.40 | 1.62 | 2.35 | 2.48 | 4.37 | 4.57 | 3.96 |
| $K_2O$ | 3.22 | 2.29 | 6.21 | 6.62 | 3.37 | 2.49 | 2.29 | 2.51 |
| $P_2O_5$ | 0.11 | 0.16 | 0.03 | 0.05 | 0.26 | 0.17 | 0.18 | 0.17 |
| $H_2O+$ | 0.65 | 2.11 | 1.39 | 0.61 | 2.27 | 0.53 | 0.95 | 0.50 |
| $H_2O-$ | 0.38 | 1.13 | 1.75 | 0.47 | 1.55 | 0.86 | 1.12 | 0.83 |
| $CO_2$ | 1.60 | 1.53 | 0.12 | 0.09 | 4.25 | 0.12 | 0.09 | 0.14 |
| S | 0.09 | 0.09 | 0.07 | 0.06 | 0.02 | 0.08 | 0.22 | 0.40 |
| Total | 99.71 | 100.16 | 99.82 | 99.82 | 99.68 | 99.47 | 98.97 | 98.45 |
| V | 15 | 113 | 9 | 16 | 175 | 70 | 66 | 71 |
| Cr | 7 | 43 | 11 | 8 | 193 | 15 | 13 | 9 |
| Ni | 13 | 17 | 19 | 16 | 59 | 11 | 11 | 10 |
| Cu | 1 | 17 | <1 | 6 | 208 | 35 | 31 | 30 |
| Zn | 27 | 65 | 30 | 27 | 89 | 62 | 55 | 55 |
| Rb | 98 | 74 | 190 | 156 | 53 | 54 | 55 | 62 |
| Sr | 288 | 308 | 91 | 102 | 863 | 531 | 537 | 561 |
| Y | 25 | 22 | 20 | 22 | 20 | 18 | 18 | 19 |
| Zr | 198 | 146 | 107 | 108 | 194 | 172 | 164 | 169 |
| Nb | 12 | 10 | 18 | 16 | 9 | 10 | 10 | 12 |
| Th | 2 | 6 | 27 | 22 | 8 | <1 | <1 | <1 |
| Ba | 835 | 481 | 538 | 657 | 1380 | 720 | 670 | 832 |
| Pb | 8 | 16 | 25 | 21 | 22 | 4 | 7 | 7 |
| Ga | 18 | 17 | 14 | 15 | 23 | 23 | 22 | 22 |

| Sample | II-25 | II-26 | II-27 | II-27 | II-28 | II-29 | II-31 | II-33 |
|---|---|---|---|---|---|---|---|---|
| $SiO_2$ | 62.51 | 75.18 | 54.19 | 53.98 | 44.72 | 68.20 | 69.75 | 64.03 |
| $TiO_2$ | 0.42 | 0.13 | 1.10 | 1.08 | 1.15 | 0.20 | 0.15 | 0.57 |
| $Al_2O_3$ | 15.72 | 12.00 | 16.42 | 16.27 | 13.53 | 11.24 | 13.37 | 16.21 |
| $Fe_2O_3$ | 4.01 | 0.92 | 6.10 | 6.46 | 7.52 | 1.34 | 1.03 | 3.14 |
| FeO | 0.13 | 0.01 | 0.04 | 0.04 | 0.06 | 0.01 | 0.08 | 0.35 |
| MnO | 0.11 | 0.02 | 0.09 | 0.08 | 0.22 | 0.02 | 0.10 | 0.07 |
| MgO | 1.56 | 0.20 | 1.89 | 1.98 | 1.84 | 0.48 | 0.18 | 0.98 |
| CaO | 5.55 | 0.43 | 6.16 | 6.10 | 12.41 | 1.71 | 2.39 | 2.99 |
| $Na_2O$ | 4.06 | 3.55 | 3.75 | 3.64 | 3.19 | 1.36 | 4.10 | 3.95 |
| $K_2O$ | 2.28 | 4.78 | 3.21 | 2.83 | 4.86 | 9.15 | 4.00 | 5.00 |
| $P_2O_5$ | 0.14 | 0.03 | 0.24 | 0.14 | 0.26 | 0.05 | 0.07 | 0.17 |
| $H_2O+$ | 0.66 | 1.20 | 1.00 | 1.00 | 1.25 | 1.88 | 0.74 | 0.81 |
| $H_2O-$ | 0.41 | 1.16 | 1.43 | 1.17 | 0.96 | 0.74 | 1.61 | 0.86 |
| $CO_2$ | 0.07 | 0.19 | 4.09 | 3.71 | 7.54 | 0.07 | 0.14 | 0.17 |
| S | 0.67 | 0.03 | 0.02 | | 0.43 | 1.02 | 0.69 | 0.18 |
| Total | 98.30 | 99.82 | 99.73 | 98.48 | 99.94 | 97.47 | 98.40 | 99.48 |
| V | 51 | 7 | 148 | | 92 | 18 | 2 | 43 |
| Cr | 7 | 12 | 98 | | 118 | 9 | 7 | 5 |
| Ni | 13 | 23 | 37 | | 53 | 34 | 17 | 24 |
| Cu | 27 | <1 | 21 | | 34 | 11 | 1 | 18 |
| Zn | 60 | 27 | 76 | | 60 | 20 | 68 | 56 |
| Rb | 63 | 153 | 109 | | 179 | 330 | 121 | 152 |
| Sr | 511 | 73 | 489 | | 502 | 1 | 131 | 429 |
| Y | 17 | 22 | 23 | | 24 | 17 | 24 | 35 |
| Zr | 171 | 103 | 268 | | 163 | 135 | 137 | 308 |
| Nb | 12 | 18 | 15 | | 14 | 17 | 14 | 14 |
| Th | <1 | 21 | 12 | | 1 | 24 | 13 | 19 |
| Ba | 709 | 554 | 664 | | 999 | 718 | 817 | 873 |
| Pb | 4 | 18 | 16 | | 4 | 24 | 21 | 18 |
| Ga | 17 | 18 | 23 | | 15 | 15 | 18 | 22 |

| Sample | II-34 | II-35 | II-36 | II-37 | II-38 | II-39 | II-40 | II-41 |
|---|---|---|---|---|---|---|---|---|
| $SiO_2$ | 50.36 | 54.50 | 57.68 | 58.37 | 69.31 | 69.80 | 70.38 | 2.82 |
| $TiO_2$ | 1.02 | 1.07 | 0.53 | 0.60 | 0.35 | 0.35 | 0.20 | 0.72 |
| $Al_2O_3$ | 17.08 | 17.57 | 17.49 | 17.83 | 15.19 | 15.41 | 13.15 | 15.13 |
| $Fe_2O_3$ | 6.58 | 4.20 | 5.27 | 5.42 | 2.12 | 1.98 | 1.59 | 4.97 |
| FeO | 1.02 | 3.22 | 0.13 | 0.39 | 0.01 | 0.15 | 0.04 | 0.13 |
| MnO | 0.12 | 0.13 | 0.12 | 0.13 | 0.07 | 0.05 | 0.05 | 0.05 |
| MgO | 2.44 | 3.48 | 2.30 | 2.06 | 0.27 | 0.30 | 0.22 | 0.98 |
| CaO | 9.89 | 7.34 | 7.32 | 6.74 | 1.43 | 1.32 | 1.68 | 4.00 |
| $Na_2O$ | 3.36 | 3.75 | 3.98 | 3.96 | 4.58 | 4.50 | 1.83 | 3.57 |
| $K_2O$ | 2.07 | 2.05 | 1.51 | 1.67 | 4.95 | 4.90 | 5.18 | 3.46 |
| $P_2O_5$ | 0.30 | 0.24 | 0.19 | 0.20 | 0.07 | 0.05 | 0.06 | 0.24 |
| $H_2O+$ | 1.02 | 1.07 | 0.53 | 0.61 | 0.67 | 0.52 | 2.01 | 0.99 |
| $H_2O-$ | 1.27 | 0.54 | 0.87 | 0.79 | 0.51 | 0.47 | 0.99 | 1.36 |
| $CO_2$ | 0.08 | 0.10 | 0.07 | 0.58 | 0.11 | 0.20 | 0.27 | 0.89 |
| S | 1.23 | 0.35 | 0.91 | 0.25 | 0.12 | 0.06 | 0.60 | 0.15 |
| Total | 99.48 | 99.61 | 98.90 | 99.60 | 99.76 | 100.06 | 98.25 | 99.46 |
| V | 158 | 169 | 80 | 114 | 11 | 13 | 14 | 83 |
| Cr | 60 | 33 | 8 | 14 | 7 | 2 | 3 | 42 |
| Ni | 30 | 26 | 7 | 9 | 28 | 24 | 15 | 20 |
| Cu | 87 | 71 | 39 | 46 | <1 | 7 | 10 | 32 |
| Zn | 78 | 86 | 64 | 71 | 49 | 44 | 30 | 59 |
| Rb | 30 | 61 | 27 | 33 | 181 | 184 | 132 | 87 |
| Sr | 1038 | 595 | 819 | 620 | 202 | 247 | 359 | 586 |
| Y | 21 | 28 | 16 | 18 | 39 | 34 | 15 | 18 |
| Zr | 210 | 233 | 149 | 144 | 406 | 409 | 156 | 212 |
| Nb | 7 | 10 | 9 | 9 | 17 | 17 | 10 | 10 |
| Th | 1 | 5 | <1 | <1 | 33 | 30 | 12 | 9 |
| Ba | 885 | 661 | 582 | 586 | 989 | 1435 | 885 | 850 |
| Pb | 3 | 8 | 5 | 6 | 24 | 26 | 22 | 15 |
| Ga | 21 | 23 | 18 | 23 | 19 | 19 | 18 | 20 |

| Sample | II-65 | II-65 | II-66 | II-66 | II-67 | II-68 | II-69 | II-69 |
|---|---|---|---|---|---|---|---|---|
| $SiO_2$ | 68.66 | 67.87 | 72.17 | 71.49 | 56.86 | 62.32 | 76.96 | 77.47 |
| $TiO_2$ | 0.28 | 0.32 | 0.13 | 0.15 | 0.58 | 0.52 | 0.08 | 0.08 |
| $Al_2O_3$ | 15.11 | 15.07 | 11.54 | 11.35 | 15.23 | 16.04 | 11.43 | 11.09 |
| $Fe_2O_3$ | 2.36 | 3.06 | 0.97 | 0.79 | 4.13 | 3.47 | 0.59 | 0.19 |
| FeO | 0.44 | 0.16 | 0.01 | 0.12 | 0.01 | 0.17 | 0.04 | 0.38 |
| MnO | 0.04 | 0.04 | 0.04 | 0.04 | 0.11 | 0.11 | 0.04 | 0.04 |
| MgO | 0.80 | 0.81 | 0.51 | 0.51 | 1.82 | 1.13 | 0.17 | 0.16 |
| CaO | 0.46 | 0.49 | 2.57 | 2.64 | 3.15 | 3.72 | 0.98 | 0.92 |
| $Na_2O$ | 1.83 | 1.88 | 2.87 | 2.86 | 1.60 | 3.41 | 4.12 | 4.04 |
| $K_2O$ | 6.25 | 6.02 | 4.72 | 4.33 | 5.75 | 4.19 | 3.12 | 2.81 |
| $P_2O_5$ | 0.12 | 0.05 | 0.04 | 0.01 | 0.17 | 0.16 | 0.06 | 0.02 |
| $H_2O+$ | 1.96 | 2.09 | 0.81 | 0.67 | 4.42 | 1.46 | 0.65 | 0.61 |
| $H_2O-$ | 1.42 | 1.21 | 0.99 | 0.97 | 5.38 | 2.05 | 0.45 | 0.50 |
| $CO_2$ | 0.07 | 0.07 | <0.01 | 0.00 | 0.60 | 0.83 | <0.01 | 0.16 |
| S | 0.02 | | 0.82 | | 0.09 | 0.01 | 0.23 | |
| Total | 100.02 | 99.14 | 98.19 | 95.93 | 99.89 | 99.59 | 99.92 | 98.47 |
| V | 24 | | 13 | | 54 | 51 | 6 | |
| Cr | 5 | | 6 | | 12 | 12 | 6 | |
| Ni | 27 | | 15 | | 17 | 16 | 11 | |
| Cu | 4 | | 6 | | 21 | 16 | 0 | |
| Zn | 63 | | 22 | | 59 | 63 | 18 | |
| Rb | 252 | | 154 | | 147 | 111 | 86 | |
| Sr | 153 | | 289 | | 514 | 440 | 91 | |
| Y | 22 | | 19 | | 24 | 23 | 17 | |
| Zr | 200 | | 114 | | 312 | 324 | 71 | |
| Nb | 16 | | 14 | | 15 | 17 | 11 | |
| Th | 18 | | 34 | | 7 | 16 | 12 | |
| Ba | 778 | | 610 | | 1495 | 1246 | 630 | |
| Pb | 26 | | 28 | | 36 | 21 | 19 | |
| Ga | 19 | | 16 | | 17 | 19 | 16 | |

| Sample | II-70 | II-71 | II-74 | II-75 | II-76 | II-77 | II-77 | II-78 |
|---|---|---|---|---|---|---|---|---|
| $SiO_2$ | 58.11 | 76.67 | 65.43 | 64.78 | 52.22 | 63.50 | 64.15 | 59.16 |
| $TiO_2$ | 0.88 | 0.08 | 0.63 | 0.67 | 1.07 | 0.62 | 0.67 | 0.92 |
| $Al_2O_3$ | 16.38 | 11.37 | 14.92 | 15.66 | 17.08 | 14.96 | 14.59 | 15.28 |
| $Fe_2O_3$ | 5.69 | 1.25 | 3.49 | 3.67 | 7.39 | 3.59 | 3.84 | 6.83 |
| FeO | 0.30 | 0.17 | 0.22 | 0.21 | 0.17 | 0.35 | 0.44 | 0.08 |
| MnO | 0.08 | 0.04 | 0.07 | 0.08 | 0.14 | 0.07 | 0.07 | 0.13 |
| MgO | 2.52 | 0.27 | 0.86 | 1.23 | 1.31 | 2.34 | 2.48 | 2.84 |
| CaO | 5.05 | 0.50 | 3.15 | 3.12 | 8.76 | 2.83 | 2.89 | 4.77 |
| $Na_2O$ | 3.15 | 3.18 | 3.86 | 4.03 | 3.45 | 2.84 | 2.82 | 3.25 |
| $K_2O$ | 3.12 | 4.48 | 4.12 | 4.01 | 2.25 | 4.31 | 3.93 | 2.63 |
| $P_2O_5$ | 0.20 | 0.04 | 0.18 | 0.18 | 0.26 | 0.15 | 0.08 | 0.20 |
| $H_2O+$ | 1.79 | 0.83 | 1.09 | 0.89 | 0.97 | 1.92 | 1.80 | 1.69 |
| $H_2O-$ | 2.02 | 0.36 | 1.11 | 0.95 | 1.40 | 1.63 | 1.36 | 0.97 |
| $CO_2$ | 0.55 | 0.26 | 0.07 | 0.01 | 3.14 | 0.42 | 0.49 | 0.66 |
| S | 0.01 | 0.06 | 0.21 | 0.17 | <0.01 | 0.04 | | 0.05 |
| Total | 99.85 | 99.56 | 99.41 | 99.66 | 99.61 | 99.57 | 99.61 | 99.45 |
| V | 148 | 6 | 61 | 67 | 203 | 88 | | 104 |
| Cr | 37 | 7 | 1 | 7 | 33 | 16 | | 48 |
| Ni | 16 | 33 | 21 | 21 | 24 | 24 | | 26 |
| Cu | 29 | 0 | 16 | 15 | 30 | 29 | | 33 |
| Zn | 79 | 56 | 60 | 58 | 74 | 64 | | 78 |
| Rb | 63 | 157 | 150 | 153 | 49 | 147 | | 74 |
| Sr | 772 | 174 | 293 | 352 | 567 | 295 | | 478 |
| Y | 18 | 49 | 31 | 29 | 23 | 24 | | 21 |
| Zr | 205 | 184 | 279 | 280 | 191 | 254 | | 166 |
| Nb | 11 | 20 | 17 | 16 | 12 | 12 | | 11 |
| Th | <1 | 23 | 16 | 19 | <1 | 17 | | <1 |
| Ba | 906 | 245 | 807 | 764 | 795 | 732 | | 665 |
| Pb | 10 | 25 | 23 | 17 | <1 | 25 | | 4 |
| Ga | 21 | 15 | 19 | 19 | 24 | 22 | | 18 |

| Sample | II-79 | II-80 | II-81 | II-82 | II-83 | II-84 | II-85 | II-90 |
|---|---|---|---|---|---|---|---|---|
| $SiO_2$ | 55.99 | 70.43 | 61.13 | 61.60 | 62.60 | 76.59 | 77.05 | 73.54 |
| $TiO_2$ | 1.02 | 0.22 | 0.93 | 0.88 | 0.90 | 0.10 | 0.08 | 0.12 |
| $Al_2O_3$ | 16.60 | 11.18 | 16.17 | 16.09 | 16.13 | 11.69 | 11.66 | 12.75 |
| $Fe_2O_3$ | 4.10 | 0.83 | 5.06 | 4.54 | 4.31 | 1.12 | 0.73 | 0.90 |
| FeO | 2.72 | 0.30 | 0.66 | 0.08 | 0.26 | 0.13 | 0.30 | 0.01 |
| MnO | 0.14 | 0.04 | 0.11 | 0.09 | 0.09 | 0.02 | 0.08 | 0.04 |
| MgO | 3.12 | 0.38 | 2.14 | 1.08 | 1.53 | 0.15 | 0.36 | 0.25 |
| CaO | 5.53 | 2.97 | 3.76 | 2.57 | 3.37 | 0.45 | 0.20 | 1.32 |
| $Na_2O$ | 2.76 | 2.79 | 4.31 | 3.26 | 4.54 | 2.31 | 1.87 | 2.93 |
| $K_2O$ | 2.76 | 4.57 | 3.12 | 5.02 | 3.39 | 5.81 | 5.75 | 5.46 |
| $P_2O_5$ | 0.20 | 0.06 | 0.18 | 0.25 | 0.26 | 0.04 | 0.03 | 0.05 |
| $H_2O+$ | 2.81 | 0.91 | 1.18 | 1.81 | 0.95 | 0.77 | 1.03 | 0.89 |
| $H_2O-$ | 1.33 | 1.77 | 0.97 | 2.07 | 0.74 | 0.40 | 0.52 | 1.06 |
| $CO_2$ | 0.54 | 0.12 | 0.05 | 0.31 | 0.56 | 0.10 | 0.15 | 0.21 |
| S | 0.01 | 0.99 | 0.03 | 0.04 | 0.03 | 0.05 | 0.03 | 0.01 |
| Total | 99.63 | 97.56 | 99.80 | 99.69 | 99.66 | 99.73 | 99.84 | 99.53 |
| V | 191 | 32 | 115 | 47 | 74 | 34 | 6 | 3 |
| Cr | 21 | 1 | 12 | 2 | 4 | 11 | 6 | 6 |
| Ni | 25 | 19 | 17 | 21 | 15 | 29 | 25 | 24 |
| Cu | 42 | 6 | 16 | 7 | 16 | 0 | 48 | 0 |
| Zn | 54 | 35 | 71 | 67 | 81 | 33 | 95 | 25 |
| Rb | 97 | 165 | 94 | 139 | 96 | 239 | 234 | 214 |
| Sr | 487 | 228 | 369 | 350 | 403 | 98 | 111 | 94 |
| Y | 26 | 24 | 29 | 30 | 29 | 22 | 20 | 21 |
| Zr | 193 | 197 | 267 | 293 | 295 | 89 | 74 | 108 |
| Nb | 9 | 14 | 15 | 16 | 17 | 10 | 11 | 16 |
| Th | 6 | 9 | 4 | 3 | 7 | 12 | 12 | 28 |
| Ba | 714 | 699 | 774 | 1215 | 951 | 686 | 1541 | 677 |
| Pb | 13 | 13 | 12 | 12 | 15 | 17 | 17 | 25 |
| Ga | 18 | 14 | 24 | 23 | 24 | 16 | 15 | 19 |

| SAMPLE | CAB-79 | CAB-69 | CAB-72 | CAB-83 | CAB-82 | CAB-81 |
|---|---|---|---|---|---|---|
| SiO2 | 60.13 | 61.59 | 61.61 | 63.50 | 63.51 | 64.08 |
| TiO2 | 1.17 | 0.83 | 1.00 | 0.67 | 0.62 | 0.63 |
| Al2O3 | 15.91 | 16.43 | 16.77 | 16.59 | 16.57 | 15.17 |
| Fe2O3 | 3.41 | 4.80 | 5.29 | 4.97 | 4.35 | 4.19 |
| FeO | 2.86 | 0.47 | 0.32 | 0.20 | 0.21 | 0.06 |
| MnO | 0.14 | 0.13 | 0.12 | 0.10 | 0.09 | 0.08 |
| MgO | 3.00 | 2.14 | 1.79 | 1.56 | 1.49 | 1.54 |
| CaO | 5.58 | 3.53 | 3.97 | 3.67 | 3.89 | 4.20 |
| Na2O | 4.30 | 4.15 | 4.64 | 4.06 | 4.21 | 3.49 |
| K2O | 2.01 | 3.59 | 3.00 | 3.19 | 3.29 | 3.87 |
| P2O5 | 0.32 | 0.25 | 0.31 | 0.25 | 0.20 | 0.15 |
| H2O+ | 1.48 | 1.36 | 0.98 | 1.30 | 1.16 | 1.36 |
| $CO_2$ | 0.05 | 0.36 | 0.12 | 0.31 | 0.26 | 1.22 |
| S | 0.01 | 0.01 | 0.01 | 0.01 | 0.03 | 0.05 |
| Total | 100.37 | 99.64 | 99.93 | 100.38 | 99.88 | 100.09 |
| La | 39.27 | 37.67 | 34.09 | 26.84 | 24.39 | 22.75 |
| Ce | 81.44 | 79.06 | 81.49 | 58.58 | 51.57 | 51.22 |
| Nd | 32.68 | 27.58 | 35.23 | 23.07 | 19.89 | 0.00 |
| Sm | 7.13 | 6.49 | 7.19 | 5.13 | 4.50 | 4.05 |
| Eu | 1.49 | 1.43 | 1.82 | 1.14 | 0.97 | 0.92 |
| Tb | 0.92 | 0.87 | 0.97 | 0.57 | 0.54 | 0.43 |
| Yb | 2.90 | 2.81 | 3.17 | 2.37 | 2.27 | 1.56 |
| Lu | 0.40 | 0.40 | 0.43 | 0.34 | 0.35 | 0.28 |
| Rb | 249 | 127 | 106 | 123 | 121 | 150 |
| Sr | 590 | 410 | 380 | 410 | 380 | 300 |
| Ba | 773.76 | 935.37 | 902.24 | 746.92 | 680.65 | 643.71 |
| Cs | 83.29 | 7.47 | 6.42 | 5.29 | 7.80 | 15.69 |
| U | 3.31 | 3.05 | 2.60 | 3.69 | 4.34 | 5.00 |
| Th | 13.72 | 11.63 | 10.53 | 12.12 | 13.16 | 21.61 |
| Hf | 5.91 | 6.54 | 6.45 | 4.68 | 4.08 | 3.31 |
| Sc | 17.51 | 14.39 | 14.33 | 8.63 | 9.27 | 10.90 |
| Ta | 1.22 | 1.28 | 1.10 | 0.80 | 0.80 | 0.90 |
| Cr | 64.46 | 19.03 | 5.23 | 3.79 | 4.28 | 31.12 |
| Ni | 29.09 | 10.94 | 7.14 | 5.27 | 3.38 | 12.35 |
| Co | 36.98 | 82.92 | 22.45 | 46.17 | 51.25 | 18.47 |

| SAMPLE | CAB-80 | CAB-77 | CAB-68 | CAB-85 | CAB-74 | CAB-73 | CAB-75 |
|---|---|---|---|---|---|---|---|
| SiO2 | 67.64 | 72.01 | 72.75 | 74.02 | 74.86 | 80.71 | 81.91 |
| TiO2 | 0.45 | 0.20 | 0.13 | 0.18 | 0.17 | 0.12 | 0.12 |
| Al2O3 | 14.87 | 12.43 | 12.98 | 12.98 | 13.05 | 9.65 | 8.82 |
| Fe2O3 | 1.76 | 1.27 | 0.99 | 1.06 | 1.03 | 0.72 | 0.72 |
| FeO | 0.64 | 0.01 | 0.01 | 0.05 | 0.01 | 0.01 | 0.01 |
| MnO | 0.08 | 0.04 | 0.05 | 0.04 | 0.04 | 0.03 | 0.04 |
| MgO | 0.71 | 0.07 | 0.13 | 0.13 | 0.12 | 0.18 | 0.12 |
| CaO | 2.55 | 2.62 | 2.10 | 1.13 | 1.34 | 0.94 | 1.08 |
| Na2O | 4.54 | 2.87 | 3.84 | 2.40 | 3.71 | 2.62 | 2.10 |
| K2O | 2.82 | 5.84 | 5.45 | 7.05 | 5.05 | 4.10 | 3.86 |
| P2O5 | 0.12 | 0.06 | 0.04 | 0.02 | 0.04 | 0.03 | 0.03 |
| H2O+ | 3.70 | 0.06 | 0.66 | 0.54 | 0.50 | 0.76 | 0.92 |
| $CO_2$ | 0.12 | 0.47 | 1.04 | 0.01 | 0.01 | 0.14 | 0.12 |
| S | 0.01 | 0.75 | 0.28 | 0.43 | 0.29 | 0.15 | 0.23 |
| Total | 100.01 | 99.24 | 100.45 | 100.04 | 100.22 | 100.16 | 100.08 |
| La | 37.46 | 31.53 | 35.73 | 34.13 | 34.79 | 24.78 | 23.5 |
| Ce | 75.76 | 61.48 | 71.62 | 74.13 | 72.74 | 47.46 | 51.19 |
| Nd | 21.79 | 0.00 | 17.13 | 16.09 | 20.38 | 13.60 | 13.66 |
| Sm | 4.96 | 3.76 | 4.15 | 4.09 | 4.00 | 2.90 | 2.76 |
| Eu | 0.99 | 0.63 | 0.62 | 0.78 | 0.65 | 0.40 | 0.46 |
| Tb | 0.59 | 0.43 | 0.48 | 0.50 | 0.46 | 0.31 | 0.32 |
| Yb | 2.15 | 1.84 | 2.00 | 1.77 | 1.92 | 1.44 | 1.25 |
| Lu | 0.32 | 0.28 | 0.28 | 0.28 | 0.29 | 0.21 | 0.20 |
| Rb | 144 | 200 | 160 | 223 | 190 | 153 | 143 |
| Sr | 380 | 124 | 132 | 174 | 111 | 91 | 72 |
| Ba | 942.31 | 779.76 | 876.68 | 1061.34 | 809.70 | 600.25 | 549.93 |
| Cs | 128.60 | 10.01 | 2.86 | 5.13 | 3.58 | 5.46 | 4.47 |
| U | 3.92 | 4.68 | 5.18 | 4.3 | 3.79 | 4.39 | 3.33 |
| Th | 15.74 | 20.24 | 21.16 | 21.89 | 20.12 | 14.52 | 14.09 |
| Hf | 4.99 | 4.31 | 3.92 | 4.17 | 3.75 | 2.52 | 2.70 |
| Sc | 4.39 | 2.23 | 2.18 | 2.07 | 2.23 | 1.59 | 1.54 |
| Ta | 1.36 | 1.34 | 1.60 | 1.62 | 1.56 | 1.17 | 1.09 |
| Cr | 3.31 | 2.03 | 2.03 | 1.81 | 1.48 | 1.62 | 1.48 |
| Ni | 0.00 | 0.57 | 0.00 | 0.45 | 0.10 | 0.00 | 1.00 |
| Co | 19.77 | 29.70 | 52.40 | 6.71 | 19.90 | 20.30 | 33.60 |

Table A3.2 Upper Cretaceous - Eocene intrusive rocks

| Sample | II-584 | II-585 | II-586 | II-587 | II-591 | II-592 | II-597 | II-598 |
|---|---|---|---|---|---|---|---|---|
| $SiO_2$ | 64.5 | 62.61 | 64.63 | 61.55 | 63.25 | 63.37 | 50.35 | 62.97 |
| $TiO_2$ | 0.76 | 0.75 | 0.69 | 1.08 | 0.95 | 0.73 | 1.12 | 0.81 |
| $Al_2O_3$ | 15.52 | 15.93 | 15.8 | 15.02 | 15.4 | 15.72 | 18.71 | 15.86 |
| $Fe_2O_3$ | 1.86 | 2.48 | 1.98 | 1.66 | 2.79 | 2 | 5.35 | 1.75 |
| FeO | 3.15 | 2.59 | 3.05 | 4.43 | 3.01 | 3.18 | 4.02 | 4 |
| MnO | 0.08 | 0.12 | 0.08 | 0.1 | 0.09 | 0.08 | 0.21 | 0.13 |
| MgO | 2.39 | 2.61 | 2.15 | 2.33 | 2.18 | 2.2 | 4.2 | 2.65 |
| CaO | 3.99 | 3.74 | 3.96 | 4.29 | 3.96 | 4.14 | 9.66 | 4.71 |
| $Na_2O$ | 3.53 | 3.57 | 3.51 | 3.32 | 3 | 3.56 | 3.51 | 3.35 |
| $K_2O$ | 3.59 | 3.8 | 3.38 | 4.24 | 4.64 | 3.19 | 1.62 | 3 |
| $P_2O_5$ | 0.14 | 0.17 | 0.12 | 0.27 | 0.22 | 0.13 | 0.41 | 0.14 |
| $H_2O+$ | 0.61 | 0.81 | 0.95 | 0.75 | 0.84 | 0.77 | 0.87 | 0.86 |
| $H_2O-$ | 0.31 | 0.38 | 0.35 | 0.35 | 0.44 | 0.39 | 0.27 | 0.25 |
| $CO_2$ | 0.16 | 0.15 | 0.12 | 0.00 | 0.08 | 0.05 | 0.11 | 0.06 |
| S | 0.004 | 0.012 | 0.009 | 0.003 | 0.024 | 0.005 | 0.006 | 0.012 |
| Total | 100.59 | 99.72 | 100.78 | 99.39 | 100.87 | 99.52 | 100.43 | 100.55 |
| V | 113 | 116 | 101 | 123 | 109 | 109 | 311 | 126 |
| Cr | 30 | 39 | 12 | 20 | 17 | 11 | 2 | 17 |
| Ni | 24 | 18 | 25 | 39 | 33 | 22 | 7 | 21 |
| Cu | 9 | 21 | 45 | 93 | 67 | 22 | 28 | 29 |
| Zn | 61 | 75 | 63 | 63 | 65 | 62 | 94 | 111 |
| Rb | 162 | 136 | 193 | 263 | 292 | 176 | 37 | 141 |
| Sr | 264 | 397 | 273 | 202 | 212 | 263 | 928 | 253 |
| Y | 29 | 21 | 27 | 42 | 38 | 27 | 23 | 32 |
| Zr | 300 | 257 | 233 | 432 | 439 | 268 | 107 | 237 |
| Nb | 14 | 12 | 9 | 16 | 16 | 9 | 6 | 9 |
| Th | 22 | 32 | 27 | 33 | 46 | 26 | <1 | 18 |
| Ba | 546 | 688 | 597 | 748 | 648 | 573 | 550 | 517 |
| Pb | 13 | 19 | 16 | 18 | 21 | 12 | <1 | 24 |
| Ga | 19 | 18 | 21 | 16 | 10 | 19 | 23 | 18 |

| Sample | II-607 | II-608 | II-611 | HAB-5A | HAB-279 | HAB-285 | II-428 | II-430 |
|---|---|---|---|---|---|---|---|---|
| $SiO_2$ | 63.17 | 54.33 | 64.44 | 51.91 | 73.67 | 73.72 | 59.29 | 60.82 |
| $TiO_2$ | 0.72 | 1.29 | 0.69 | 0.2 | 0.2 | 0.18 | 0.73 | 0.65 |
| $Al_2O_3$ | 15.8 | 15.78 | 16.22 | 17.17 | 13.19 | 13.05 | 16.76 | 17.1 |
| $Fe_2O_3$ | 1.8 | 4.45 | 2.02 | 0.09 | 1.31 | 1.35 | 4.2 | 5.01 |
| FeO | 3.34 | 5.21 | 2.89 | 0.01 | 0.29 | 0.34 | 1.58 | 0.65 |
| MnO | 0.08 | 0.18 | 0.08 | 0.01 | 0.08 | 0.06 | 0.1 | 0.13 |
| MgO | 2.15 | 4.08 | 2.15 | 0.03 | 0.25 | 0.32 | 3.47 | 2.21 |
| CaO | 4.07 | 7.1 | 4.22 | 0.98 | 1.64 | 1.29 | 5.3 | 4.92 |
| $Na_2O$ | 3.63 | 3.07 | 3.6 | 0.98 | 3.87 | 3.71 | 3.56 | 3.37 |
| $K_2O$ | 3.25 | 1.85 | 3.2 | 3.18 | 3.88 | 3.76 | 1.99 | 2.45 |
| $P_2O_5$ | 0.13 | 0.36 | 0.12 | 0.16 | 0.04 | 0.04 | 0.2 | 0.15 |
| $H_2O+$ | 0.98 | 1 | 0.96 | 6.07 | 0.65 | 0.96 | 2.38 | 1.88 |
| $H_2O-$ | 0.11 | 0.2 | 0.18 | 0.69 | 0.45 | 0.68 | 0 | 0 |
| $CO_2$ | 0.05 | 0.14 | 0.07 | 0.07 | 0.13 | 0.13 | 0.22 | 0.48 |
| S | 0.008 | 0.000 | 0.003 | >5.03 | 0.17 | 0.01 | 0.01 | 0.01 |
| Total | 99.29 | 99.04 | 100.84 | 86.58 | 99.82 | 99.60 | 99.79 | 99.83 |
| V | 101 | 259 | 103 | 52 | 14 | 12 | 132 | 113 |
| Cr | 15 | 52 | 11 | 3 | 6 | 6 | 26 | 10 |
| Ni | 25 | 26 | 21 | <1 | 23 | 14 | 10 | 14 |
| Cu | 37 | 88 | 54 | 4 | <1 | <1 | 45 | 45 |
| Zn | 73 | 91 | 56 | 13 | 32 | 37 | 61 | 79 |
| Rb | 176 | 87 | 155 | 8 | 177 | 139 | 56 | 90 |
| Sr | 278 | 301 | 331 | 436 | 174 | 92 | 660 | 397 |
| Y | 29 | 41 | 22 | 5 | 29 | 23 | 17 | 19 |
| Zr | 267 | 236 | 208 | 119 | 128 | 127 | 131 | 141 |
| Nb | 10 | 12 | 9 | 9 | 12 | 12 | 8 | 8 |
| Th | 26 | 11 | 14 | 13 | 19 | 19 | 5 | 17 |
| Ba | 675 | 512 | 775 | 525 | 334 | 416 | 520 | 589 |
| Pb | 14 | 9 | 11 | 16 | 14 | 21 | 4 | 11 |
| Ga | 17 | 24 | 19 | 21 | 18 | 19 | 19 | 21 |

| Sample | II-11 | II-13 | II-86 | II-87 | II-209 | II-367 | II-391 | II-416 |
|---|---|---|---|---|---|---|---|---|
| $SiO_2$ | 59.22 | 58.57 | 49.98 | 58.43 | 58.66 | 66.32 | 64.52 | 58.24 |
| $TiO_2$ | 0.77 | 0.95 | 1.28 | 1.1 | 0.8 | 0.47 | 0.58 | 0.93 |
| $Al_2O_3$ | 17.55 | 16.55 | 18.44 | 16.62 | 17.02 | 15.24 | 15.77 | 16.49 |
| $Fe_2O_3$ | 3.9 | 3.97 | 4.77 | 3.94 | 3.17 | 2.54 | 2.86 | 3.04 |
| FeO | 1.83 | 1.64 | 4.65 | 3.22 | 2.71 | 1.31 | 1.4 | 2.98 |
| MnO | 0.09 | 0.12 | 0.17 | 0.17 | 0.1 | 0.09 | 0.12 | 0.1 |
| MgO | 3.12 | 1.67 | 4.53 | 3.1 | 3.28 | 2.17 | 2.09 | 3.27 |
| CaO | 5.34 | 5.53 | 8.21 | 5.78 | 6.11 | 2.35 | 3.79 | 5.26 |
| $Na_2O$ | 4.52 | 4.03 | 3.3 | 3.46 | 3.57 | 3.01 | 3.81 | 3.64 |
| $K_2O$ | 2.18 | 2.28 | 1.3 | 2.59 | 1.94 | 3.34 | 3.15 | 2.61 |
| $P_2O_5$ | 0.16 | 0.22 | 0.19 | 0.18 | 0.2 | 0.14 | 0.14 | 0.22 |
| $H_2O+$ | 1.48 | 1.5 | 2.56 | 1.3 | 1.76 | 2.22 | 1.18 | 2.04 |
| $CO_2$ | 0.17 | 2.47 | 0.32 | 0.09 | 0.13 | 0.16 | 0.37 | 1.10 |
| S | 0.02 | 0.02 | <0.01 | 0.01 | <0.01 | 0.25 | 0.06 | 0.04 |
| Total | 100.35 | 99.52 | 99.67 | 99.99 | 99.74 | 99.62 | 99.85 | 99.96 |
| V | 134 | 98 | 248 | 165 | 130 | 62 | 86 | 135 |
| Cr | 36 | 11 | 10 | 17 | 24 | 4 | 11 | 36 |
| Ni | 18 | 21 | 11 | 20 | 12 | 17 | 16 | 26 |
| Cu | 38 | 12 | 50 | 47 | 55 | 17 | 45 | 64 |
| Zn | 77 | 58 | 97 | 99 | 74 | 62 | 84 | 76 |
| Rb | 75 | 80 | 43 | 96 | 64 | 118 | 112 | 108 |
| Sr | 508 | 386 | 561 | 476 | 481 | 236 | 382 | 462 |
| Y | 20 | 29 | 23 | 32 | 20 | 20 | 20 | 25 |
| Zr | 168 | 205 | 123 | 247 | 159 | 185 | 176 | 248 |
| Nb | 8 | 15 | 7 | 12 | 9 | 11 | 8 | 12 |
| Th | 1 | 6 | <1 | 7 | 3 | 13 | 15 | 22 |
| Ba | 770 | 571 | 642 | 808 | 563 | 748 | 726 | 658 |
| Pb | 9 | 18 | 6 | 15 | 8 | 19 | 9 | 16 |
| Ga | 23 | 21 | 25 | 21 | 25 | 20 | 17 | 26 |

| Sample | II-431 | II-441 | II-444 | II-456 | II-456 |
|---|---|---|---|---|---|
| $SiO_2$ | 66.04 | 69.98 | 62.48 | 77.57 | 76.01 |
| $TiO_2$ | 0.72 | 0.42 | 0.68 | 0.18 | 0.10 |
| $Al_2O_3$ | 14.79 | 14.22 | 16.55 | 11.54 | 11.93 |
| $Fe_2O_3$ | 2.39 | 1.71 | 3.2 | 0.36 | 0.00 |
| FeO | 1.68 | 1.16 | 1.82 | 0.09 | 0.45 |
| MnO | 0.06 | 0.05 | 0.09 | 0.01 | 0.02 |
| MgO | 1.67 | 1.03 | 2.37 | 0.10 | 0.13 |
| CaO | 3.15 | 2.59 | 4.73 | 1.37 | 1.31 |
| $Na_2O$ | 3.46 | 3.18 | 3.69 | 3.44 | 3.28 |
| $K_2O$ | 4.15 | 4.36 | 2.88 | 3.83 | 4.04 |
| $P_2O_5$ | 0.14 | 0.09 | 0.17 | 0.05 | 0.02 |
| $H_2O+$ | 1.16 | 0.62 | 0.96 | 0.58 | 0.51 |
| $H_2O-$ | | | | | 0.38 |
| $CO_2$ | 0.11 | 0.27 | 0.16 | 0.73 | 0.54 |
| S | 0.11 | <0.01 | 0.02 | 0.15 | |
| Total | 99.63 | 99.68 | 99.80 | 100.00 | 98.72 |
| V | 90 | 52 | 100 | 12 | |
| Cr | 18 | 3 | 9 | 4 | |
| Ni | 36 | 29 | 20 | 14 | |
| Cu | 55 | 73 | 36 | <1 | |
| Zn | 64 | 53 | 54 | 14 | |
| Rb | 228 | 227 | 109 | 146 | |
| Sr | 343 | 228 | 423 | 167 | |
| Y | 32 | 28 | 21 | 17 | |
| Zr | 360 | 217 | 172 | 123 | |
| Nb | 14 | 11 | 10 | 21 | |
| Th | 37 | 52 | 7 | 34 | |
| Ba | 715 | 668 | 676 | 286 | |
| Pb | 19 | 29 | 4 | 15 | |
| Ga | 22 | 20 | 21 | 16 | |

Table A3.3 Upper Eocene - Lower Oligocene intrusive rocks

| Sample | FT-19 | FT-20 | FT-21 | FT-22 | FT-44 | FT-46 | FT-47 | FT-62 |
|---|---|---|---|---|---|---|---|---|
| $SiO_2$ | 71.71 | 70.81 | 72.13 | 69.47 | 69.06 | 67.35 | 67.52 | 60.54 |
| $TiO_2$ | 0.13 | 0.11 | 0.10 | 0.17 | 0.31 | 0.36 | 0.59 | 0.64 |
| $Al_2O_3$ | 15.47 | 15.90 | 15.70 | 16.06 | 16.01 | 17.21 | 14.18 | 17.00 |
| $Fe_2O_3$ | 0.00 | 0.00 | 0.00 | 1.74 | 1.38 | 1.47 | 2.90 | 2.72 |
| FeO | 1.30 | 0.49 | 0.59 | 0.86 | 1.00 | 1.26 | 1.63 | 2.56 |
| MnO | 0.26 | 0.01 | 0.01 | 0.02 | 0.02 | 0.03 | 0.03 | 0.10 |
| MgO | 0.40 | 0.64 | 0.27 | 0.67 | 1.00 | 1.15 | 1.93 | 2.74 |
| CaO | 0.53 | 0.00 | 0.21 | 0.15 | 1.98 | 1.14 | 0.94 | 4.89 |
| $Na_2O$ | 4.75 | 4.74 | 3.27 | 5.03 | 4.18 | 5.36 | 2.68 | 3.70 |
| $K_2O$ | 3.55 | 5.20 | 5.17 | 4.36 | 3.50 | 2.30 | 4.66 | 2.60 |
| $P_2O_5$ | 0.09 | 0.02 | 0.05 | 0.11 | 0.13 | 0.20 | 0.16 | 0.19 |
| $H_2O+$ | 0.60 | 0.72 | 0.77 | 0.87 | 0.78 | 1.00 | 1.35 | 0.91 |
| $H_2O-$ | 0.45 | 0.24 | 0.29 | 0.19 | 0.17 | 0.60 | 0.90 | 0.51 |
| $CO_2$ | 0.56 | 0.00 | 0.05 | 0.00 | 0.05 | 0.00 | 0.00 | 0.00 |
| S | 0.45 | 0.24 | 0.29 | 0.19 | 0.00 | 0.00 | 0.01 | 0.03 |
| Total | 100.01 | 99.07 | 99.25 | 99.77 | 99.57 | 99.43 | 99.48 | 99.13 |
| V | 27 | 34 | 22 | 34 | 58 | 69 | 152 | 131 |
| Cr | 4 | 3 | 4 | 7 | 4 | 8 | 16 | 16 |
| Ni | 7 | 12 | 10 | 9 | 12 | 4 | 14 | 17 |
| Cu | 2365 | 3285 | 1385 | 376 | 2218 | 1218 | 11716 | 52 |
| Zn | 704 | 81 | 246 | 315 | 62 | 64 | 97 | 88 |
| Rb | 83 | 139 | 77 | 97 | 114 | 53 | 101 | 104 |
| Sr | 433 | 264 | 634 | 302 | 538 | 623 | 283 | 487 |
| Y | 8 | 14 | 14 | 12 | 16 | 11 | 23 | 17 |
| Zr | 115 | 110 | 121 | 110 | 137 | 137 | 237 | 133 |
| Nb | 9 | 9 | 9 | 8 | 8 | 11 | 13 | 9 |
| Th | 1 | <1 | <1 | <1 | 11 | <1 | 28 | 5 |
| Ba | 504 | 604 | 894 | 806 | 1117 | 664 | 1143 | 627 |
| Pb | 7 | <1 | 2 | 5 | 11 | 12 | 7 | 12 |
| Ga | 28 | 26 | 24 | 26 | 26 | 25 | 25 | 28 |

| Sample | FT-66 | FT-67 | FT-23 | FT-24 | FT-45 | FT-48 |
|---|---|---|---|---|---|---|
| $SiO_2$ | 66.49 | 70.93 | 62.74 | 65.03 | 65.49 | 58.55 |
| $TiO_2$ | 0.40 | 0.28 | 0.64 | 0.52 | 0.63 | 0.76 |
| $Al_2O_3$ | 17.20 | 16.32 | 17.26 | 16.36 | 16.18 | 17.92 |
| $Fe_2O_3$ | 1.82 | 0.15 | 2.30 | 1.93 | 1.81 | 2.75 |
| FeO | 1.37 | 0.79 | 2.40 | 1.92 | 2.62 | 3.03 |
| MnO | 0.04 | 0.01 | 0.10 | 0.07 | 0.08 | 0.09 |
| MgO | 1.19 | 0.86 | 2.20 | 1.71 | 2.01 | 2.95 |
| CaO | 1.95 | 1.61 | 4.78 | 3.97 | 3.53 | 6.07 |
| $Na_2O$ | 4.29 | 4.77 | 4.18 | 4.07 | 3.79 | 4.05 |
| $K_2O$ | 2.26 | 1.52 | 2.63 | 3.31 | 3.49 | 2.19 |
| $P_2O_5$ | 0.22 | 0.05 | 0.21 | 0.18 | 0.19 | 0.28 |
| $H_2O+$ | 1.05 | 1.01 | 0.49 | 0.54 | 0.70 | 0.42 |
| $H_2O-$ | 1.15 | 0.49 | 0.19 | 0.13 | 0.35 | 0.26 |
| $CO_2$ | 0.17 | 0.08 | 0.00 | 0.00 | 0.04 | 0.00 |
| S | 0.02 | 0.07 | 0.01 | 0.01 | 0.05 | 0.00 |
| Total | 99.62 | 98.94 | 100.13 | 99.75 | 100.96 | 99.32 |
| V | 77 | 45 | 107 | 82 | 103 | 143 |
| Cr | 9 | 9 | 7 | 11 | 8 | 11 |
| Ni | 3 | 3 | 19 | 14 | 20 | 13 |
| Cu | 472 | 57 | 60 | 49 | 205 | 63 |
| Zn | 88 | 44 | 79 | 68 | 56 | 59 |
| Rb | 90 | 53 | 85 | 106 | 136 | 70 |
| Sr | 534 | 487 | 629 | 559 | 465 | 768 |
| Y | 11 | 12 | 19 | 17 | 22 | 17 |
| Zr | 132 | 127 | 154 | 162 | 208 | 147 |
| Nb | 8 | 10 | 10 | 10 | 11 | 10 |
| Th | <1 | <1 | <1 | 10 | 15 | <1 |
| Ba | 709 | 295 | 713 | 699 | 22 | 632 |
| Pb | 8 | <1 | <1 | 6 | <1 | <1 |
| Ga | 28 | 29 | 23 | 24 | 29 | 28 |

| SAMPLE | ZCH-1 | ZCH-2 | ZCH-4 | ZCH-9 | ZCH-10 | ES4785 | ES10178 | ES5262 |
|---|---|---|---|---|---|---|---|---|
| SiO2 | 72.64 | 71.78 | 65.9 | 74.72 | 68.59 | 68.91 | 64.46 | 70.90 |
| TiO2 | 0.15 | 0.16 | 0.17 | 0.17 | 0.21 | 0.38 | 0.45 | 0.36 |
| Al2O3 | 12.68 | 13.59 | 14.35 | 11.22 | 16.03 | 12.97 | 16.63 | 10.70 |
| Fe2O3 | 0.67 | 0.4 | 0.09 | 0 | 0 | 0 | 0.69 | 0.57 |
| FeO | 0.46 | 1.13 | 1.54 | 2.25 | 2 | 1.28 | 1.26 | 1.56 |
| MnO | 0.01 | 0.01 | 1.19 | 0.01 | 0.01 | 0.02 | 0.01 | 0.01 |
| MgO | 0.35 | 0.33 | 0.5 | 0.32 | 0.6 | 0.46 | 1.25 | 1.12 |
| CaO | 2.3 | 2.02 | 2.51 | 1.35 | 1.5 | 1.89 | 4.14 | 4.05 |
| Na2O | 0.01 | 0.04 | 0.13 | 0.05 | 0.12 | 0.33 | 4.82 | 2.97 |
| K2O | 3.9 | 4.11 | 7.79 | 3.54 | 5.84 | 6.57 | 2 | 2.43 |
| P2O5 | 0.06 | 0.05 | 0.09 | 0.04 | 0.03 | 0.15 | 0.16 | 0.12 |
| H2O+ | 1.16 | 1.35 | 1.13 | 0.93 | 1.49 | 1.68 | 0.54 | 0.41 |
| H2O- | 0.39 | 0.37 | 0.75 | 0.11 | 0.1 | 0.94 | 0.21 | 0.23 |
| S | 1.80 | 2.10 | 2.40 | 2.40 | 1.80 | 1.80 | | |
| Total | 94.88 | 95.51 | 97.17 | 94.83 | 96.55 | 96.11 | 96.79 | 95.70 |
| La | 19.6 | 10.9 | 23.1 | 9.02 | 11.8 | 46.9 | 17.9 | 13.9 |
| Ce | 36 | 23.1 | 40.9 | 19.6 | 26.1 | 84.1 | 40.4 | 32.4 |
| Nd | 10.9 | 10.4 | 12.2 | 7.6 | 10.3 | 29.6 | 18.3 | 15.1 |
| Sm | 1.63 | 1.63 | 1.9 | 1.47 | 1.72 | 4.47 | 3.47 | 2.99 |
| Eu | 0.42 | 0.4 | 0.47 | 0.34 | 0.43 | 1.17 | 1.17 | 0.85 |
| Tb | 0.22 | 0.23 | 0.25 | 0.18 | 0.21 | 0.39 | 0.49 | 0.34 |
| Yb | 0.57 | 0.56 | 0.71 | 0.48 | 0.56 | 0.56 | 0.66 | 0.68 |
| Lu | 0.09 | 0.09 | 0.11 | 0.08 | 0.09 | 0.08 | 0.1 | 0.11 |
| Rb | 88 | 92 | 193 | 71 | 125 | 27 | 42 | 42 |
| Sr | 644 | 537 | 366 | 209 | 224 | 63 | 709 | 435 |
| Th | 4.9 | 4.1 | 5.2 | 3.7 | 4.1 | 3.1 | 3.5 | 1.9 |
| Hf | 3.6 | 2.9 | 3.1 | 2.4 | 3.2 | 2.9 | 3.7 | 2.7 |
| Sc | 2 | 2.3 | 3 | 2 | 4.3 | 2.8 | 4 | 4 |
| Ta | 0.8 | 1 | 0 | 1 | 0.8 | 2.3 | 1.3 | 0.3 |
| Co | 15.3 | 23.2 | 23.6 | 30.7 | 17.2 | 79 | 36.7 | 4.9 |

Major elements determined by atomic absorption spectrophotometry at Chemical Laboratory of SERNAGEOMIN in Santiago, Chile. Duplicate analyses and samples in the range II-500 - II-600 by the same method at Chemical Laboratory of the Department of Geology, Dalhousie University.

Trace elements (V, Cr, Ni, Cu, Zn, Rb, Sr, Y, Zr, Nb, Th, Ba, Pb, Ga) determined by X-Ray fluorescence by Kevin Cameron at Saint Mary's University.

Rare Earth Elements determined by instrumental neutron activation analyses (INAA).

Analyses of samples 'CAB' provided by Dr. Constantino Mpodozis. Major elements of these samples analysed by absorption spectrophotometry at Chemical Laboratory of the SERNAGEOMIN, Chile. REEs analysed by neutron activation at Cornell University, Ithaca, New York. Analytical procedure as described in Kay and others (1987).

# APPENDIX 4. K-Ar ANALYTICAL DATA

TABLE A4.1 K-Ar ANALYTICAL DATA

| Sample Ident. | Lat. S Long. W | Dated Mater. | %K | $^{40}Ar^*$ nl/g | %Ar Atm. | AGE Ma ± error‡ |
|---|---|---|---|---|---|---|
| II-RB-74 | 22°09'54" 70°12'36" | Plg | 2.705 | 18.563 | 16 | 168 ± 5 |
| Iquiqueña | 22°01'00" 70°11'35" | Bt | 5.118 | 34.345 | 21 | 165 ± 3 |
| LG 2 | 21°55'18" 69°43'30" | Wr | 0.653 | 3.085 | 86 | 118 ± 15 |
| RB-1 | 22°23'30" 70°13'40" | A-T | 0.180 | 1.224 | 49 | 167 ± 7 |
| II-RB-43 | 24°41'06" 70°32'36" | Alt Plg | 0.476 | 2.218 | 46 | 116 ± 10 |
| II-RB-48 | 25°05'30" 70°29'06" | Plg | 3.183 | 17.145 | 15 | 133 ± 4 |
| II-RB-51 | 25°05'30" 70°29'06" | Wr | 1.606 | 8.354 | 22 | 129 ± 4 |
| II-RB-52 | 25°05'30" 70°29'06" | Plg | 2.309 | 12.947 | 19 | 139 ± 5 |
| II-RB-63 | 25°50'48" 70°36'00" | Wr | 0.767 | 5.255 | 56 | 168 ± 7 |
| II-RB-9 | 22°15'24" 69°04'42" | Wr | 6.744 | 13.326 | 38 | 50.1 ± 1.4 |
| II-RB-36 | 22°52'18" 69°21'12" | Bt | 6.131 | 15.436 | 27 | 64 ± 2 |

| Sample Ident. | Lat. S Long. W | Dated Mater. | %K | $^{40}Ar^{*}$ nl/g | %Ar Atm. | AGE Ma ± error* |
|---|---|---|---|---|---|---|
| II-RB-37 | 22°54'48" 69°22'12" | Bt | 4.844 | 12.077 | 36 | 63 ± 2 |
| II-RB-34 | 22°50'30" 69°20'36" | Plg | 4.529 | 10.765 | 77 | 60 ± 4 |
| II-RB-38 | 22°54'24" 68°22'12" | Wr | 3.357 | 7.940 | 34 | 59.8 ± 2.0 |
| II-RB-19 | 23°02'10" 68°59'18" | Wr | 2.371 | 7.117 | 70 | 76 ± 4 |
| II-RB-22 | 23°00'36" 69°01'54" | Wr | 3.485 | 7.530 | 45 | 54.7 ± 2.0 |
| II-RB-20 | 23°02'12" 68°58'18" | Chl Hbl | 0.502 | 0.816 | 77 | 41.3 ± 4.4 |
| II-RB-25 | 23°09'54" 69°09'42" | Ser Wr | 4.090 | 7.044 | 22 | 43.8 ± 1.5 |
| II-RB-26 | 23°09'54" 69°09'42" | Ser Wr | 3.468 | 6.040 | 26 | 44.3 ± 1.5 |
| II-RB 68 | 23°25'12" 69°33'42" | Bt | 5.087 | 12.178 | 33 | 61 ± 2 |
| II-RB-65 | 23°25'12" 69°33'36" | Chl Bt | 0.560 | 0.731 | 87 | 33.2 ± 7.3 |
| II-473 | 24°05'30" 69°20'28" | Wr | 1.702 | 2.820 | 35 | 42.1 ± 1.5 |
| II-147 | 24°01'20" 69°08'10" | Bt | 6.877 | 14.936 | 12 | 55.0 ± 1.4 |

| Sample Ident. | Lat. S<br>Long. W | Dated Mater. | %K | $^{40}Ar^*$ nl/g | %Ar Atm. | AGE Ma ± error‡ |
|---|---|---|---|---|---|---|
| II-39 | 23°33'30"<br>69°16'55" | Wr | 3.92 | 8.044 | 53 | 52 ± 2 |
| II-68 | 24°05'15"<br>69°23'05" | Bt | 6.71 | 15.567 | 18 | 59 ± 1 |
| FT-67 | 20°55'30"<br>68°53'24" | Bt | 6.393 | 9.395 | 74 | 37.4 ± 3.1 |
| FT-67 | 20°55'30"<br>68°53'24" | Bt | 3.866 | 5.190 | 52 | 34.2 ± 1.8 |
| FT-66 | 20°59'30"<br>68°48'06" | Bt | 7.229 | 9.855 | 23 | 37.7 ± 0.9 |
| FT-66 | 20°59'30"<br>68°48'06" | Wr | 1.817 | 2.562 | 26 | 35.9 ± 1.2 |
| FT-43 | 22°14'12"<br>68°55'30" | Bt | 6.960 | 10.796 | 27 | 39.5 ± 1.1 |
| FT-23 | 22°20'48"<br>68°58'54" | Bt | 7.126 | 10.931 | 48 | 39.0 ± 1.2 |

‡ Analytical error at 95% confidence level (± 2σ)

Abbreviations of dated materials:

| | | |
|---|---|---|
| A-T | : | Actinolite - Tremolite |
| Alt | : | Altered |
| Bt | : | Biotite |
| chl | : | Chloritized |
| Hbl | : | Hornblende |
| Plg | : | Plagioclase |
| Wr | : | Whole rock |
| ser | : | sericitized |

All K-Ar age determinations done by Carlos Perez de Arce (Laboratory Technician) at the geochronological laboratory of SERNAGEOMIN in Santiago, Chile.

Argon isotopes analyzed using an AEI MS-10S mass spectrometer, with automated digital data recording.

Potassium analyzed by a Perkin Elmer 4000 atomic absorption spectrophotometer operating in emission mode with lithium standard at the Chemical Analytic Laboratory of SERNAGEOMIN, Chile.

Decay constants used for age calculations are those recommended by the Geochronological Subcommission of the IUGS (Steiger and Jäger, 1977).

# APPENDIX 5. ANALYTICAL DATA OF FISSION TRACK AGES

TABLE A5.1 ANALYTICAL DATA OF APATITE FISSION TRACK AGES FROM UPPER PALEOZOIC GRANITOIDS OF THE DOMEYKO CORDILLERA

| Sample | No. cryst. | $N_s$ | $\rho_s$ ($x10^5 cm^{-2}$) | $N_i$ | $\rho_i$ ($x10^5 cm^{-2}$) | $N_d$ | $\rho_d$ ($x10^4 cm^{-2}$) | $\chi^2$ test | U ppm |
|---|---|---|---|---|---|---|---|---|---|
| FT-64 | 26 | 530 | 3.67 | 824 | 5.70 | 870 | 1.225 | P | 15 |
| FT-63 | 41 | 1159 | 4.43 | 1881 | 7.19 | 870 | 1.225 | P | 20 |
| FT-58 | 37 | 389 | 2.43 | 629 | 3.93 | 870 | 1.225 | P | 10 |
| RECOUNT | 27 | 140 | 1.33 | 239 | 2.27 | 870 | 1.225 | P | 6 |
| FT-56 | 31 | 714 | 4.35 | 1389 | 8.47 | 870 | 1.233 | P | 24 |
| RECOUNT | 31 | 662 | 5.14 | 1229 | 9.53 | 870 | 1.233 | P | 26 |
| FT-32 | 51 | 369 | 1.43 | 989 | 3.84 | 1225 | 1.940 | P | 7 |
| FT-34 | 51 | 258 | 0.806 | 457 | 1.43 | 870 | 1.226 | P | 4 |
| FT-30 | 41 | 516 | 2.87 | 906 | 5.04 | 870 | 1.220 | P | 15 |
| FT-37 | 34 | 256 | 1.68 | 459 | 3.01 | 870 | 1.240 | P | 8 |
| FT-38 | 45 | 151 | 0.614 | 270 | 1.10 | 870 | 1.235 | P | 3 |
| FT-39 | 51 | 351 | 1.25 | 628 | 2.23 | 870 | 1.235 | P | 6 |
| FT-35 | 57 | 159 | 0.515 | 284 | 0.92 | 870 | 1.240 | P | 3 |
| FT-40 | 51 | 660 | 2.14 | 1957 | 6.36 | 1200 | 1.990 | P | 11 |
| RECOUNT | 24 | 453 | 1.78 | 1355 | 5.34 | 1200 | 1.990 | P | 9 |
| FT-25 | 34 | 394 | 2.59 | 772 | 5.07 | 870 | 1.206 | P | 13 |

TABLE A5.2 ANALYTICAL DATA OF APATITE FISSION TRACK AGES FROM UPPER PALEOZOIC GRANITOIDS OF SALAR DE PEDERNALES AREA

| Sample | No. cryst. | $N_s$ | $\rho_s$ ($x10^5 cm^{-2}$) | $N_i$ | $\rho_i$ ($x10^5 cm^{-2}$) | $N_d$ | $\rho_d$ ($x10^4 cm^{-2}$) | $\chi^2$ test | U ppm |
|---|---|---|---|---|---|---|---|---|---|
| FT-07 | 39 | 181 | 0.961 | 421 | 2.24 | 1472 | 1.860 | P | 4 |
| FT-04 | 31 | 2086 | 17.2 | 3218 | 26.6 | 870 | 1.193 | P | 74 |
| FT-03 | 27 | 859 | 8.14 | 2170 | 20.6 | 1472 | 1.920 | P | 36 |

TABLE A5.3 ANALYTICAL DATA OF APATITE FISSION TRACK AGES FROM CERROS DE MONTECRISTO PLUTON

| Sample | No. cryst. | $N_s$ | $\rho_s$ ($x10^5 cm^{-2}$) | $N_i$ | $\rho_i$ ($x10^5 cm^{-2}$) | $N_d$ | $\rho_d$ ($x10^4 cm^{-2}$) | $\chi^2$ test | U ppm |
|---|---|---|---|---|---|---|---|---|---|
| FT-14 | 16 | 697 | 6.15 | 1267 | 11.2 | 1200 | 1.975 | P | 19 |
| RECOUNT | 24 | 745 | 7.95 | 1305 | 13.9 | 1200 | 1.975 | P | 23 |
| FT-13 | 22 | 1056 | 10.8 | 1997 | 20.4 | 1225 | 1.940 | P | 34 |
| FT-12 | 41 | 1344 | 7.17 | 2574 | 13.7 | 1225 | 1.940 | P | 23 |
| FT-11 | 51 | 1666 | 6.66 | 3607 | 14.4 | 1225 | 1.940 | F | 26 |
| FT-9 | 38 | 891 | 4.75 | 1784 | 9.51 | 1225 | 1.940 | P | 17 |
| FT-8 | 40 | 667 | 4.27 | 1570 | 10.0 | 1225 | 1.940 | P | 17 |
| RECOUNT | 21 | 649 | 4.26 | 1523 | 10.0 | 1225 | 1.940 | P | 17 |

TABLE A5.4 ANALYTICAL DATA OF APATITE FISSION TRACK AGES FROM THE FORTUNA GRANODIORITE

| Sample | No. cryst. | $N_s$ | $\rho_s$ ($x10^5 cm^{-2}$) | $N_i$ | $\rho_i$ ($x10^5 cm^{-2}$) | $N_d$ | $\rho_d$ ($x10^4 cm^{-2}$) | $\chi^2$ test | U ppm |
|---|---|---|---|---|---|---|---|---|---|
| FT-16 | 31 | 1200 | 9.91 | 3690 | 30.50 | 1200 | 1.985 | P | 51 |
| FT-43 | 25 | 786 | 5.16 | 2853 | 18.7 | 1225 | 1.900 | P | 33 |
| FT-41 | 21 | 328 | 2.40 | 1059 | 7.75 | 1225 | 1.930 | P | 13 |
| FT-17 | 28 | 910 | 8.32 | 3272 | 29.9 | 1225 | 1.940 | F | 51 |
| FT-15 | 21 | 547 | 3.29 | 1906 | 11.5 | 1225 | 1.940 | P | 23 |
| FT-24 | 31 | 527 | 4.35 | 1941 | 16.0 | 1225 | 1.940 | P | 28 |

TABLE A5.5 ANALYTICAL DATA OF APATITE FISSION TRACK AGES FROM CHUQUICAMATA AND EL ABRA

| Sample | No. cryst. | $N_s$ | $\rho_s$ ($x10^5 cm^{-2}$) | $N_i$ | $\rho_i$ ($x10^5 cm^{-2}$) | $N_d$ | $\rho_d$ ($x10^4 cm^{-2}$) | $\chi^2$ test | U ppm |
|---|---|---|---|---|---|---|---|---|---|
| FT-19 | 53 | 302 | 1.46 | 1130 | 5.46 | 1200 | 1.965 | P | 9 |
| FT-44 | 22 | 1145 | 13.3 | 3680 | 42.8 | 1200 | 1.985 | F | 72 |
| FT-45 | 31 | 1191 | 9.65 | 3998 | 32.4 | 1225 | 1.890 | F | 58 |
| FT-48 | 31 | 1386 | 9.59 | 4460 | 30.9 | 1200 | 2.000 | F | 50 |

TABLE A5.6 ANALYTICAL DATA OF APATITE FISSION TRACK AGES FROM THE INTERMEDIATE DEPRESSION

| Sample | No. cryst. | $N_s$ | $\rho_s$ ($\times 10^5 cm^{-2}$) | $N_i$ | $\rho_i$ ($\times 10^5 cm^{-2}$) | $N_d$ | $\rho_d$ ($\times 10^4 cm^{-2}$) | $\chi^2$ test | U ppm |
|---|---|---|---|---|---|---|---|---|---|
| II-592 | 31 | 647 | 5.34 | 1335 | 11.0 | 1472 | 1.915 | P | 19 |
| II-611 | 21 | 451 | 5.50 | 834 | 10.2 | 1225 | 1.835 | P | 18 |
| II-607 | 25 | 516 | 3.77 | 1083 | 7.92 | 1225 | 1.855 | P | 15 |
| II-598 | 37 | 1074 | 3.85 | 2338 | 8.38 | 1225 | 1.875 | P | 15 |
| II-597 | 25 | 4589 | 47.0 | 6702 | 68.6 | 1200 | 1.985 | P | 115 |

TABLE A5.7 ANALYTICAL DATA OF FISSION TRACK AGES OF THE COASTAL CORDILLERA

| Sample | No. cryst. | $N_s$ | $\rho_s$ ($\times 10^5 cm^{-2}$) | $N_i$ | $\rho_i$ ($\times 10^5 cm^{-2}$) | $N_d$ | $\rho_d$ ($\times 10^4 cm^{-2}$) | $\chi^2$ test | U ppm |
|---|---|---|---|---|---|---|---|---|---|
| II-565 | 31 | 538 | 4.44 | 556 | 4.59 | 1472 | 1.865 | P | 8 |
| II-547 | 22 | 528 | 6.14 | 576 | 6.70 | 1472 | 1.760 | P | 13 |
| II-571 | 41 | 1387 | 8.66 | 1225 | 7.65 | 1472 | 1.890 | P | 13 |
| II-527 | 23 | 807 | 8.61 | 847 | 9.03 | 1472 | 1.815 | P | 17 |
| II-528 | 31 | 1597 | 13.2 | 1989 | 16.4 | 1472 | 1.875 | P | 29 |
| II-558 | 31 | 1608 | 13.3 | 1663 | 13.7 | 1472 | 1.900 | F | 24 |
| II-483 | 21 | 2640 | 32.2 | 3837 | 46.8 | 1472 | 1.800 | P | 87 |
| II-536 | 28 | 1399 | 10.4 | 1472 | 1.830 | 1472 | 1.830 | P | 19 |

All apatite analyses by external detector method using 0.5 for the $4\pi/2\pi$ geometry correction factor. Apatite ages calculated using dosimeter glass SRM614 and $\zeta$-614 = 11,515.7. Fish Canyon apatite with an age of 27.8 ± 0.2 Ma (Hurford and Hammerschmidt, 1985) and Durango apatite standards with an age of 31.4 ± 0.5 Ma (Green, 1985) were used for system calibration.

**No. cryst.** is the number of apatite crystals where tracks were counted; $N_s$ and $N_i$ are the number of spontaneous and induced tracks counted respectively; $N_d$ is the number of induced tracks counted in each dosimeter glass detector. Track densities ($\rho$) are in tracks per $cm^{-2}$.

$\chi^2$ test for Poissonian distribution at 95% confidence level is indicated by pass (P) or fail (F). Individual counting sheets have been filed in the records of the fission track laboratory of Dalhousie University.

# APPENDIX 6. Sr and Nd ISOTOPIC DATA REPRESENTATION

The ϵ notation of DePaolo and Wasserburg (1967) has been utilized in figures 7.3 and 7.4 for representation of Nd and $r isotopic data at any time (τ) relative to a chondritic uniform reservoir (CHUR).

$$\epsilon^{i}_{Nd} = \left[ \frac{(^{143}Nd/^{144}Nd)_{Sample(\tau)}}{(^{143}Nd/^{144}Nd)_{CHUR(\tau)}} - 1 \right] x\ 10^{4}$$

Where:

$$(^{143}Nd/^{144}Nd)_{Sample(\tau)} = (^{143}Nd/^{144}Nd^{Sample}_{(0)}) - (^{147}Sm/^{144}Nd^{Sample}_{(0)})\ [\ e^{\lambda T} - 1\ ]$$

$$(^{143}Nd/^{144}Nd)_{CHUR(\tau)} = (^{143}Nd/^{144}Nd^{CHUR}_{(0)}) - (^{147}Sm/^{144}Nd^{CHUR}_{(0)})\ [\ e^{\lambda T} - 1\ ]$$

$$\lambda^{147}Sm = 6.54\ x\ 10^{-12} a^{-1}$$

$$(^{143}Nd/^{144}Nd)^{CHUR}_{(0)} = 0.51264$$

$$(^{147}Sm/^{144}Nd)^{CHUR}_{(0)} = 0.1967$$

$$\epsilon^{i}_{Sr} = \left[ \frac{(^{87}Sr/^{86}Sr)_{Sample(\tau)}}{(^{87}Sr/^{86}Sr)_{CHUR(\tau)}} - 1 \right] x\ 10^{4}$$

Where:

$$(^{87}Sr/^{86}Sr)_{Sample(\tau)} = (^{87}Sr/^{86}Sr^{Sample}_{(0)}) - (^{87}Rb/^{86}Sr^{Sample}_{(0)})\ [\ e^{\lambda T} - 1\ ]$$

$$\left(^{87}Sr/^{86}Sr\right)_{CHUR(T)} = \left(^{87}Sr/^{86}Sr^{CHUR}_{(0)}\right) - \left(^{87}Rb/^{86}Sr^{CHUR}_{(0)}\right) \left[ e^{\lambda T} - 1 \right]$$

$$\lambda^{87}Rb = 1.42 \times 10^{-11} a^{-1}$$

$$\left(^{87}Sr/^{86}Sr\right)^{CHUR}_{(0)} = 0.7047$$

$$\left(^{87}Rb/^{86}Sr\right)^{CHUR}_{(0)} = 0.0847$$

# VITA

| | |
|---|---|
| Name: | Victor Maksaev |
| Birthdata: | December 24, 1952: Santiago, Chile |
| Post-Secondary Education: | Ph.D. Geology, Sept. 1986 - August 1990<br>Dalhousie University, Halifax, Nova Scotia, Canada.<br><br>M.Sc. Geology, Sept. 1985 - Sept. 1986 (courses only: subsequent transfer to a Ph.D. programme)<br>Dalhousie University, Halifax, Nova Scotia, Canada.<br><br>B.Sc. Geology, March, 1970 - December, 1975.<br>Universidad de Chile, Santiago, Chile. |
| Awards: | Izaak Walton Killam Memorial Scholarship, 1986 - 1990 (declined the academic year 1988 - 1989).<br><br>Dalhousie Graduate Fellowship: 1985 - 1986. |
| Experience: | 1981 - now: Geologist, Servicio Nacional de Geología y Minería (SERNAGEOMIN), Chile.<br>(on leave during graduate studies at Dalhousie).<br><br>1975 - 1981: Geologist of the Economic Geology Department, Instituto de Investigaciones Geológicas, Chile.<br><br>1973 - 1975: Part-time, Instituto de Investigaciones Geológicas, Chile. |
| Specialty: | Andean metallogeny; Origin of hydrothermal mineral deposits of the active margin of South America in relation to igneous and tectonic processes. Chronology of mineralizing and hydrothermal phenomena. |

Publications: Huete, C., **Maksaev, V.**, Moscoso, R., Ulriksen, C. and Vergara, H., 1977. Antecedentes geocronológicos de rocas intrusivas y volcánicas en la Cordillera de Los Andes comprendida entre la Sierra de Moreno y el Río Loa y los 21° y 22° Lat. Sur, II Región de Chile. Revista Geológica de Chile Nº 4, pp. 35-41.

**Maksaev, V.**, 1978. Geología del cuadrángulo Chitigua y sector occidental del cuadrángulo Cerro Palpana, Región de Antofagasta. Carta Geológica de Chile Nº 31, Instituto de Investigaciones Geológicas, 53 p.

**Maksaev, V.**, 1979. Las fases tectónicas Incaica y Quechua en la Cordillera de Los Andes del Norte Grande de Chile. II Congreso Geológico Chileno, Actas, V. 1, pp. B-63-77.

Escobar, F. and others, 1980. Mapa Geológico de Chile, Escala 1:1000000. **Maksaev, V.** in charge of the compilation of the region between 30°30' y 34°00' Lat. S. Servicio Nacional de Geología y Minería, Chile.

**Maksaev, V.** and Marinovic, N., 1980. Geología de los cuadrángulos Cerro de la Mica, Quillagua, Cerro Posada y Oficina Prosperidad, Región de Antofagasta. Carta Geológica de Chile Nos. 45, 46, 47 y 48, Instituto de Investigaciones Geológicas, Chile, 63 p.

Arias, J., Ulriksen, C., and **Maksaev, V.**, 1982. Potencial de mineralización de molibdeno en Chile. III Congreso Geológico Chileno, Actas, V. 3, pp. F1-34.

**Maksaev, V.**, Mpodozis, C., Moscoso, R., and Nasi, C., 1984. Las unidades volcánicas y plutónicas del Cenozoico Superior en la Alta Cordillera del Norte Chico (29°-31°S): Geología, alteración hidrotermal y mineralización. Revista Geológica de Chile Nº 21, pp. 11-51.

**Maksaev, V.**, 1984. Mesozoico a Paleógeno de la Región de Antofagasta. Apuntes del Seminario de Actualización de la Geología de Chile, Servicio Nacional de Geología y Minería. Miscelanea Nº 4, pp. C1-20.

Kay, S., **Maksaev, V.**, Moscoso, R., and Nasi, C., 1985. Evolution of Mid-Late Tertiary igneous rocks in the main Chilean Cordillera (29°-32°S); correlations with changes in slab geometry. Proceedings of the Final Symposium of Project IGCP 120 "Magmatic Evolution of The Andes". Comunicaciones Nº 35, pp.37-40, Universidad de Chile.

Nasi, C., Mpodozis, C., Cornejo, P., Moscoso, R., and **Maksaev, V.**, 1985. El Batolito Elqui-Limarí (Paleozoico Superior-Triásico): Características petrográficas, geoquímicas y significado tectónico. Revista Geológica de Chile Nº 25-26, pp. 77-111.

Boric, R., Díaz, F. and **Maksaev, V.**, 1985. Magmatic events and related metallogenesis in the Antofagasta Region, Northern Chile. Proceedings of the Final Symposium of the Project IGCP 120 "Magmatic Evolution of The Andes", Comunicaciones Nº 35, Universidad de Chile, pp. 37-40.

Mpodozis, C., Nasi, C., Moscoso, R., Cornejo, P., **Maksaev**, V. and Parada, M.A., 1985. The Late Palaeozoic-Early Triassic magmatic belt of the Chilean Frontal Range (28°-31°S): Igneous "stratigraphy" and tectonic setting. Proceedings of the Final Symposium of the Project IGCP 120 "Magmatic Evolution of The Andes", Comunicaciones Nº 35, Univ. de Chile, pp. 161-165.

Kay, S., **Maksaev, V.**, Moscoso, R., Mpodozis, C. and Nasi, C., 1987. Probing the evolving Andean lithosphere: Mid-Late Tertiary Magmatism in Chile (29°-30°30'S) over the modern zone of subhorizontal subduction. Journal of Geophysical Research, Vol. 92, Nº B7, pp. 6173-6189, June, 1987.

Kay, S., **Maksaev, V.**, Moscoso, R., Mpodozis, C., Nasi, C. and Gordillo, C.E., 1988. Tertiary Andean magmatism in Chile and Argentina between 28° and 33° S: Correlation of magmatic chemistry with a changing Benioff zone. Journal of South American Earth Sciences, Vol. 1, pp. 21-38.

**Maksaev, V.**, Boric, R., Zentilli, M. and Reynolds, P.H., 1988. Metallogenic implications of K-Ar, $^{40}Ar$-$^{39}Ar$ and fission track dates of mineralized areas in the Andes of Northern Chile. (in Spanish, with abstract in English), V Congreso Geológico Chileno, Actas, Tomo I, pp. B65 - B86.

**Maksaev, V.**, Zentilli, M. and Reynolds, P.H., 1988. $^{40}Ar$-$^{39}Ar$ geochronology of porphyry copper deposits of northern Chilean Andes. (in Spanish, with abstract in English). V Congreso Geológico Chileno, Actas, Tomo I, pp. B109-B133.

**Maksaev, V.** and Zentilli, M., 1988. Metallogenic framework of the large porphyry copper deposits of the Andes of northern Chile. (in Spanish, with Abstract in english ). V Congreso Geológico Chileno, Actas, Tomo I, pp. B181-B212.

**Maksaev, V.**, Gardeweg, M., Ramirez, C. and Zentilli, M., 1988. Fission track dating of El Laco and Incahuasi magnetite bodies in the Highplateau of the Antofagasta Region. (in Spanish, with Abstract in English). V Congreso Geológico Chileno, Actas, Tomo I, pp. B1-B23.

Nasi, C., Moscoso, R. y **Maksaev, V.**, 1989. Geología de la Hoja Guanta, Región de Coquimbo. Carta Geológica de Chile Nº 67, Servicio Nacional de Geología y Minería.

Boric, R., Díaz, F. y **Maksaev, V.**, 1990. Geología y Yacimientos Metalíferos de la Región de Antofagasta, Norte de Chile. Boletín Nº 40, Servicio Nacional de Geología y Minería de Chile (in press).

Published Abstracts:

Kay, S., **Maksaev, V.** and Gordillo, C., 1985. Middle-Late Tertiary volcanism over a section of the modern shallowly-dipping Andean Benioff zone ($29^0$-$32^0$S). Abstract, Transactions, American Geophysical Union, Vol. 66, Nº 18, p. 422, April 30, 1985.

**Maksaev, V.**, 1986. Metallogenic evolution and migration of the magmatic front in the Chilean Andes between $21^0$ and $26^0$ South. Abstract of the Atlantic Geoscience Society Colloquium, Canada, p. 17.

Zentilli, M. and **Maksaev, V.**, 1987. Metallogenie des Andes entre $21^0$ et $28^0$ S: Donnes Isotopiques. Abstract, Séminaire Andes Centrales, Abstracts Volume, ORSTOM, Bondy, Paris, France, January 14-16, 1987.

**Maksaev, V.**, Gardeweg, M., Ramírez, C. and Zentilli, M., 1988. Aplicación del método trazas de fisión (fission-track) a la datación de cuerpos de magnetita de El Laco e Incahuasi en el Altiplano de la Región de antofagasta. Abstract, Comunicaciones Nº 39, Universidad de Chile, p. 65.

**Maksaev, V.** y Zentilli, M., 1988. Marco metalogénico regional de los megadepósitos de tipo pórfido cuprífero del Norte Grande de Chile. Abstract, Comunicaciones Nº 39, Universidad de Chile, p. 62.

**Maksaev, V.**, Boric, R., Zentilli, M. y Reynolds, P.H., 1988. Significado metalogénico de dataciones K-Ar, $^{40}Ar$-$^{39}Ar$ y trazas de fisión de zonas mineralizadas en el Norte Grande de Chile. Abstract, Comunicaciones Nº 39, Universidad de Chile, p. 63.

**Maksaev, V.**, Zentilli, M. y Reynolds, P.H., 1988. Geocronología $^{40}Ar$-$^{39}Ar$ de depósitos de tipo pórfido cuprífero del Norte Grande de Chile. Abstract, Comunicaciones Nº 39, Universidad de Chile, p. 64.

Zentilli, M., Mulja, T., Walker, J. y **Maksaev, V.**, 1988. Efectos de la alteración hidrotermal en el contenido de oro en rocas miocenas del Complejo Volcánico Copiapó, Chile: Análisis preliminar. Abstract, Comunicaciones, Universidad de Chile, p. 80.

Zentilli, M., Doe, B.R., Hedge, C.E. and **Maksaev, V.**, 1988. Lead and strontium isotopes, and REE in ores and rocks from Chuquicamata and other Andean porphyry copper deposits: relationships with magmatism and tectonic evolution. Abstract, Symposium: Andean Magmatism and its Tectonic Setting, Geological Society of America Centennial Celebration, Denver, Colorado, U.S.A., Abstracts with Programs, Volume 20, pp. A7-A8.

Zentilli, M. and **Maksaev, V.**, 1989. Genesis of porphyry copper deposits in the Andes of northern Chile in relation to Tertiary magmatism and tectonic uplift: Fission track evidence. Abstracts, 28th International Geological Congress, Washington D.C., USA, Vol. 3, pp. 3-429-3-430.

Zentilli, M.; **Maksaev, V.**; Dickin, A. and Doe, B.R., 1990. Homogeneous source of porphyry copper deposits in the Chilean Central Andes: Restrictions from Pb, Nd, Sr isotopes and REE. Abstract, Geological Association of Canada - Mineralogical Association of Canada, Annual Meeting Vancouver '90, Programs with Abstracts, V. 15, p. A 144.

**Maksaev, V.**; Zentilli, M. and Reynolds, P.H., 1990. Metallogenic evolution of major porphyry copper deposits in the Andes of Northern Chile (21°-26°S): Thermochronological constraints. Abstract, Geological Association of Canada - Mineralogical Association of Canada, Annual Meeting Vancouver '90, Programs with Abstracts, V. 15, p. A 82.

## REFERENCES


ABELE, G., 1988. Geomorphological west-east section through the north Chilean Andes near Antofagasta. *In*: Bahlburg, H., Breitkreuz, C. and Giese, P. (Editors), The Southern Central Andes, Lecture Notes in Earth Sciences, V. 17, Springer-Verlag, Berlin-Heidelberg, pp. 153-168.

ABELE, G., 1989. The interdependence of elevation, relief and climate on the western slope of the Central Andes. Zentralblatt für Geologie und Paläontologie, Teil I, H.5/6, pp. 1127-1139.

AGUE, J.J. and BRIMHALL, G.H., 1989. Geochemical modelling of steady state fluid flow and chemical reaction during supergene enrichment of porphyry copper deposits. Economic Geology, V. 84, pp. 506-528.

AGUIRRE, L., 1985. The Southern Andes. *In*: Nairn, A.E.M. and others (Editors), The ocean basins and margins. Volume 7A, The Pacific Ocean, Plenum Press, New York and London, pp. 265-376.

AGUIRRE, L., CHARRIER, R., DAVIDSON, J., MPODOZIS, C., RIVANO, S., THIELE, R., TIDY, E., VERGARA, M. and VICENTE, J.C., 1974. Andean magmatism: Its paleogeographic and structural setting in the central part (30°-35°S) of the Southern Andes. Pacific Geology, Tokai University Press, Tokyo Japan, V. 8, pp. 1-38.

AHLFELD, F., 1940. Informe geológico sobre el volcán Ollagüe y sus yacimientos de azufre. DEMIPE, 7 p., Santiago.

ALARCON, B. and VERGARA, M., 1964. Nuevos antecedentes sobre la geología de la quebrada El Way. Publicación N°24, Instituto de Geología, Univ. de Chile, Santiago.

ALEXANDER, E.C., Jr., MICHELSON, G.M. and LANPHERE, M.A., 1978. MMhb-1: A new $^{40}Ar/^{39}Ar$ dating standart. Short paper, 4th International Conference on Geochronology, Cosmochronology, Isotope Geology, U.S. Geological Survey Open-File Report 78-701, pp. 6-8.

ALFARO, G., 1973. Geología y prospección de yacimientos de cobre en la zona de Tocopilla, Provincia de Antofagasta. (Unpublished report), Instituto de Investigaciones Geológicas.

ALLEN, C.R., 1962. Circum-Pacific faulting in the Philippines-Taiwan region. Journal of Geophysical Research, V. 67, pp. 4795-4812.
ALLEN, C.R., 1965. Transcurrent faults in continental areas. *In* A symposium on continental drift. Royal Society of London, Phil. Trans. A, V. 258, pp. 82-89.

ALLMENDINGER, R.W., 1986. Tectonic development, southeastern border of the Puna Plateau, northwestern Argentine Andes. Geological Society of America Bulletin, V. 97, pp. 1070-1082.

ALLMENDINGER, R.W., RAMOS, V. A., JORDAN, T.E., PALMA, M and ISACKS, 1983. Paleogeography and Andean structural geometry, northwest Argentina, Tectonics, V. 2, pp. 1-16.

ALPERS, C.N., 1986. Geochemical and geomorphological dynamics of supergene copper sulphide ore formation and preservation at La Escondida, Antofagasta, Chile. Part I: Tertiary climatic desiccation and erosion rates in the Atacama desert, Northern Chile: Optimal conditions for supergene enrichment and preservation of ore deposits. Ph.D. Thesis, University of California, Berkeley, U.S.A., 184 p.

ALPERS, C.N. and BRIMHALL, G.H., 1988. Middle Miocene climatic change in the Atacama Desert, northern Chile: evidence from supergene mineralization at La Escondida. Geological Society of America Bulletin, V. 100, pp. 1640-1656.

ALPERS, C.N. and BRIMHALL, G.H., 1989. Paleohydrologic evolution and geochemical dynamics of cumulative supergene metal enrichment at La Escondida, Atacama Desert, Northern Chile. Economic Geology, V. 84, pp. 229-255.

ALVAREZ, O., MIRANDA, J. and GUZMAN, P., 1980. Geología del Complejo Chuquicamata. *In*: Minería de Cobres Porfíricos, V. 2, pp. 314-364, Instituto de Ingenieros de Minas de Chile, Santiago, Chile.

ALVAREZ, O., and ARACENA, I., 1982. El Abra; uno de los grandes yacimientos de cobre aún no explorados. Minerales, V. 37, N° 160, pp. 25-36.

ALVAREZ, O. and ARACENA, I., 1985. Algunas consideraciones de la petrología y alteración del complejo plutónico de Chuquicamata, Chile. Actas IV Congreso Geológico Chileno, Antofagasta, V. 4, pp. 1-30.

ALVAREZ, O. and FLORES, R., 1985. Alteración y mineralización hipógena en el yacimiento de Chuquicamata, Chile. Actas IV Congreso Geológico Chileno, V. 2, pp. 3-78 - 3-100. Antofagasta.

ALVAREZ, O. and GUZMAN, P., 1985. Estimación de recursos y reservas en el yacimiento Chuqui Norte, Chuquicamata, Chile. Actas IV Congreso Geológico Chileno, V. 2, pp. 3-101 - 3-120. Antofagasta.

ALVAREZ, O. and MIRANDA, G., 1985. Geología y Mineralización del distrito minero El Inca. Actas IV Congreso Geológico Chileno, V. 2, Antofagasta, pp. 121-137.

AMBRUS, J., 1977. Geology of the El Abra Porphyry Copper Deposit, Chile. Economic Geology, V. 72, pp. 1062-1085.

AMBRUS, J., 1979. Emplazamiento y mineralización de los pórfidos cupríferos de Chile. Ph.D. thesis, Depto. de Cristalografía y Mineralogía, Facultad de Ciencias, Univ. de Salamanca, Spain, 314 p.

AMSTUTZ, G.C., CISTERNAS, M.E., DIAZ, L.L., FONTBONTE, Ll., FRUTOS, J., MAYER, CH., SCHMIDT, S.Th. and WAUSSCHKUHN, A., 1985. Relaciones sobre algunos yacimientos de Ag, Zn, Fe y Ba y las secuencias marinas Trasarco del Jurásico y Cretácico Inferior en el Norte de Chile. Actas IV Congreso Geológico Chileno, V. 4, pp. 3-435 - 3-451, Antofagasta.

ANDERSON, PH., 1980. Regional time-space distribution of porphyry copper deposits - a decisive test for the origin of metals in magma-related ore deposits. Proceedings of the Fifth Quadrennial IAGOD Symposium, Stuttgart, pp. 35-48.

ANDERSON, R.N. and GREW, P.C., 1977. Stress corrosion theory of crack propagation with applications to geophysics. Reviews on Geophysics and Space Physics, V. 15, pp. 77-104.

ANONYMOUS, 1947. Informe preliminar mina Don Rigoberto, Níquel y Cobalto, propiedad del Sr. G. Flores. (Unpublished report), IFMCA, 4 p. Taltal.

ANONYMOUS, 1967. Informe N° 1 Cubicación Mina Bella Esperanza, (Unpublished report), ENAMI, 1 p. (Rol N° 22280).

ANONYMOUS, 1975. Solicitud de estudio geológico en la zona Nevados de Poquis. Cia. Mra. El Esfuerzo, (Unpublished report), SERNAGEOMIN Archive N° 2530.

ARABASZ, W.J., 1968. Geologic structure of the Taltal area, northern Chile, in relation to the earthquake of December 28, 1966. Seismologic Society of America Bulletin, V. 58, pp. 835 - 842.

ARABASZ, W., 1971. Geological and geophysical studies of the Atacama fault zone in northern Chile, Ph.D. Thesis, California Inst. Technol., 264 p. Pasadena, California, USA.

ARABASZ, W.J. and ALLEN, C.R., 1972. Tectonics of northern Chile as reflected by the Atacama fault system. (Abstract), *In*: Conference on solid earth problems, V. 2 (Buenos Aires : Upper Mantle Symposium, 1972), pp. 443-444.

ARCULUS, R.J. and POWELL, R.J., 1986. Source component mixing in the regions of arc magma generation. Journal of Geophysical Research, V. 91, pp. 5913-5926.

ARMIJO, R. and THIELE, R., 1990. Active faulting in northern Chile: ramp stacking and lateral decoupling along a subduction plate boundary? Earth and Planetary Science Letters, V. 98, pp. 40-61.

ASHLEY, R.P. and SILBERMAN, M.L., 1976. Direct dating of mineralization at Goldfield, Nevada, by potassium-argon and fission-track methods. Economic Geology, V. 71, pp. 904-924.

ASTUDILLO, O., 1984. Geología y Metalogénesis del distrito minero Carolina de Michilla, Antofagasta, II Región, Chile. B.Sc. thesis, Depto. de Geociencias, U. del Norte, 131 p., Antofagasta.

ATHERTON, M.P., PITCHER, W.S. AND WARDEN, V. , 1983. The Mesozoic marginal basin of central Peru, Nature, V. 305, pp. 303-306.

AUBOUIN, J. and BORRELLO, A.V., 1966. Chaines andines et chaines alpines; regard sur la géologie de la Cordillere des Andes au parallele de l'Argentine Moyenne. Bull. Soc. Geol. de France, 7° Ser., T VIII, N°7, pp. 1050-1070.

AUBOUIN, J., BORRELLO, A.V., CECCIONI, G., CHARRIER, R., CHOTIN, P., FRUTOS, J., THIELE, R. and VICENTE, J.C., 1973. Esquisse paléogéographique et structurale des Andes meridionales. Revue de Géographie Physique et de Geologie Dynamique, V. 15, pp. 11-72.

AUDEBAUD, E., CAPDEVILA, R., DALMAYRAC, B., DEBELMAS, J., LAUBACHER, G., LEFEVRE, C., MAROCCO, R., MARTINEZ, C., MATTAUER, M., MEGARD, F., PAREDES, J. and TOMASI, P., 1973. Les traits geologiques essentiels des Andes Centrales (Pérou-Bolivie). Revue de Géographie Physique et de Geologie Dynamique, V. 15, pp. 73-114.

AUMENTO, F., 1969. The mid-Atlantic ridge near 45° N. Fission track and manganese cronology. Canadian Journal of Earth Sciences, V. 6, pp. 1431-1440.

AYDIN, A. and NUR, A., 1982. Evolution of pull-apart basins and their scale independence. Tectonics, V. 1, No.1, pp. 91-105.

AYDIN, A. and NUR, A., 1985. The types and role of stepovers in strike-slip tectonics. *In*: Bidle, K.T. and Christie-Blick, N. (Editors), Strike-slip Deformation, Basin Formation, and Sedimentation. Special Publications Soc. econ. Paleont. Miner., 37, pp.35-44.

BAEZA, L., 1984. Petrography and tectonics of the plutonic and metamorphic complex of Limon Verde and Mejillones Peninsula, Northern Chile. Ph.D. Thesis, Tubingen University, West Germany, 205 p.

BAEZA, L. and VENEGAS, R., 1985. Caracterización petrográfica - estructural de las rocas de basamento de la parte norte de la Península de Mejillones, Chile. Actas del IV Congreso Geológico Chileno, V. 1, pp. 2-35 - 2-55, Antofagasta.

BAKER, M.C.W., 1977. Geochronology and volcanology of Upper Cenozoic volcanic in north Chile, and southwest Bolivia. Ph.D. Thesis, Open University, Milton Keynes, 248 p., London.

BAKER, M.C.W., 1981. The nature and distribution of Upper Cenozoic ignimbrite centres in the Central Andes. J. Volcanol. Geotherm. Res., V. 11, pp. 293-315.

BAKER, M.C.W. AND FRANCIS, P.W., 1978. Upper Cenozoic volcanism in the Central Andes ages and volumes. Earth Planetary Science Letters, V. 41, pp. 175-187.

BAKER, R.C. AND GUILBERT, J.M., 1987. Regional structural control of porphyry copper deposits in Northern Chile. (Abstract), Geological Society of America, Abstracts with programs, Phoenix, Arizona, p. 578.

BALDWIN, J.A. and PEARCE, J.A., 1982. Discrimination of productive and nonproductive porphyrytic intrusions in the Chilean Andes. Economic Geology, V. 77, pp. 664-674.

BALLI, A.W., 1981. Thoughts on the tectonics of folded belts. *In*: McClay, K.R. and Price, N.J. (Editors), Thrust and nappe tectonics. Geological Society of London, Special Publication No. 9, pp. 13-32.

BANDY, M.C., 1938. Mineralogy of three sulphate deposits of northern Chile. The American Mineralogist, V. 23, No. 11, pp. 669-760.

BANKS, N.G. and PAGE, N.J., 1980. Some observations that bear on the genesis of porphyry copper deposits. Proceedings of the Fifth Quadrennial IAGOD Symposium, Stuttgart, pp. 49-73.

BARANZAGI, M. and ISACKS, B.L., 1976. Spatial distribution of earthquakes and subduction of the Nazca plate beneath South America, Geology, V. 4, pp. 686-692.

BARANZAGI, M. and ISACKS, B.L., 1979. Subduction of the Nazca plate beneath Peru: evidence from spatial distribution of earthquakes. Geophysical Journal of the Royal Astronomical Society, V. 57, pp. 537-555.

BARREIRO, B.A., 1984. Lead isotopes and Andean magmagenesis. *In*: Harmon, R.S. and Barreiro, B.A. (Editors), Andean Magmatism, chemical and isotopic constraints. Shiva Publishing Limited, pp. 21-30.

BARREIRO, B.A. and STERN, C.R., 1982. Pb isotopic composition of recent calc-alkaline volcanic rocks from the southernmost Andes, (Abstract) Transactions American Geophysical Union, V. 63, p. 1148.

BARREIRO, B.A. and CLARK, A.H., 1984. Lead isotopic evidence for evolutionary changes in magma-crust interaction, Central Andes, southern Peru. Earth and Planetary Science Letters, V. 69, pp. 30-42.

BATES, R. and JACKSON, J., 1980. (Editors), Glossary of Geology. American Geological Institute. Falls Church, Virginia, 749 p. Second Edition.

BECK, M.E., 1983. On the mechanism of tectonic transport in zones of oblique subducction. Tectonophysics, V. 93, pp. 1-11.

BECK, M.E., 1986. Model for Late Mesozoic-Early Tertiary tectonics of coastal California and western Mexico and speculations on the origin of the San Andreas fault. Tectonics, V. 5, N°1, pp. 49-64.

BELL, C.M., 1982. The Lower Paleozoic Metasedimentary Basement of the Coastal Ranges of Chile between 25°30' and 27°00' S. Revista Geológica de Chile N°17, pp. 21-29, Santiago.

BELL, M., 1984. Deformation produced by the subduction of a Paleozoic turbidite sequence in northern Chile, Geol. Soc. Am., J., V. 141, Part 2, p. 339-347.

BELL, M., 1987. The origin of the upper Paleozoic Chañaral mélange of N Chile. Journal of the Geological Society, London, V. 144, pp.599-610

BENJAMIN, M.T., JOHNSON, N.M. and NAESER, C.W., 1987. Recent rapid uplift in the Bolivian Andes: Evidence from fission-track dating. Geology, V. 15, pp. 680-683.

BERG, K. and BREITKREUZ, C., 1983. Mesozoische plutone in der Northchilenischen Küstenkordillere: petrogenese, geochronologie, geochemie und geodynamik mantelbetonter magmatite. Geotektonische Forsch., V. 66, 107 p.

BERG, K., BREITKREUZ, CH., DAMM, K.W., PICHOWIAK, S. and ZEIL, W., 1983. The North-Chilean Coast Range, an example for the development of an active continental margin. Geol. Rundschau, V. 72, N°2, pp. 715-731.

BERGER, G., 1975. $^{40}Ar/^{39}Ar$ step heating of thermally overprinted biotites, hornblendes and potassium feldspars from Eldora, Colorado. Earth Planetary Science Letters, V. 26, pp. 387-408.

BIESE, W., 1961. El Jurásico de Cerritos Bayos. Publicación N°19, Instituto de Geología, Univ. de Chile, 61 p., Santiago.

BIGAZZI, G., 1981. The problem of the decay constant $\lambda_f$ of $^{238}U$. Nuclear Tracks, V. 5, pp. 35-44.

BIRD, M.I., CHIVAS, A.R. and McDOUGALL, I., 1990. An isotopic study of surficial alunite in Australia. 2. Potassium-argon geochronology. Chemical Geology (Isotope Geoscience Section), V. 80, pp. 133-145.

BLOT, C., 1972. Volcanisme et séismes du manteau supérieur dans l'Archipel des Nouvelles-Hebrides, Bulletin Volcanology, V. 36, pp. 441-461.

BLOT, C., 1976. Volcanisme et sismicite dans les arcs insulaires. Collect Geophys. no. 13, ORSTOM, Paris, 206 p.

BOBENRIETH, L., 1980. Geología de los cuadrángulos Cerro Desamparado y Cerro Soledad, Regiones de Tarapacá y Antofagasta. B.Sc. thesis, Depto. Geología, Univ. de Chile, 171 p., Santiago.

BORIC, R., 1981. Cuadrángulos Estación Colupito y Toco. Región de Antofagasta, Carta Geológica de Chile N°49-50, Instituto de Investigaciones Geológicas, 52 p., Santiago.

BORIC, R., DIAZ, F. and MAKSAEV, V., 1985. Magmatic events and related metallogenesis in the Antofagasta Region, Northern Chile. (Expanded abstract) Final Symposium of Project IGCP 120 "Magmatic Evolution of the Andes", Comunicaciones N°35, Depto. Geología y Geofísica, Univ. de Chile, pp. 37-40.

BOTT, M.H.P., WAGHORN, G.D. and WHITTAKER, A., 1989. Plate boundary forces at subduction zones and trench-arc compression. Tectonophysics, v.170, pp. 1-15.

BREITKREUZ, C., 1985. Plutonism in the Central Andes. Zbl. Geol. Palaont, Teil I, H.9/10, pp. 1283-1293, Stuttgart.

BREITKREUZ, C. and BAHLBURG, H., 1985. Paleozoic Flysch Series in the Coastal Cordillera of Northern Chile. Geologische Rundschau, V. 74, N°3, pp. 565-572. Stuttgart.

BREITKREUZ, C., BAHLBURG, H., DELAKOWITZ, and PICHOWIAK, S., 1989. Paleozoic events in the Central Andes. Journal of South American Earth Sciences, V. 2, No.2, pp. 171-189.

BRERETON, N.R., 1972. A reappraisal of the $^{40}Ar/^{39}Ar$ stepwise degassing technique. Geophysical Journal of the Royal Astronomical Society, V. 27, pp. 449-478.

BRIMHALL, G.H., AGEE, C. and STOFFREGEN, R., 1985. The hydrothermal conversion of hornblende to biotite. Canadian Mineralogist, V. 23, pp. 369-379.

BROWN, M., 1989. Tectonic controls on Paleozoic-Mesozoic magmatism, The Andes, N. Chile. (Abstract), Geological Association of Canada - Mineralogical Association of Canada Annual Meeting, Programs with abstracts, V. 14, pp. A12-A13.

BROWN, L., KLEIN, J., MIDDLETON.R., SACKS, I.S. and TERA, F., 1982. $^{10}Be$ in Island-Arc Volcanoes and Implications for Subduction, Nature, V. 229, pp. 718-720.

BRUGGEN, J., 1942. Geología de la Puna de San Pedro de Atacama y sus formaciones de areniscas y arcillas rojas. *In* Congreso Panamericano de Ingeniería de Minas y Geología. An., V. 2, pp. 342-367.

BRUGGEN, J., 1950. Fundamentos de la Geología de Chile. Instituto Geográfico Militar, 378 p., Santiago, Chile.

BUCHELT, M. and ZEIL, W., 1986. Petrographische und geochemische Untersuchungen an Jurassischen Vulkaniten der Porphyrit Formation in der Küstenkordillere Nord-Chiles, Berliner Geowissenschaftliche Abhandlungen, V. 66, pp. 191-204.

BUCHELT, M. and TELLEZ, C., 1988. The Jurassic La Negra Formation in the area of Antofagasta, Northern Chile (lithology, petrography, geochemistry). *In*: Bahlburg, and others (Editors), The Southern Central Andes, Contributions to structure and evolution of an active continental margin. Lecture Notes in Earth Sciences 17, Springer-Verlag, pp. 171-182.

BUCHFIELD, B.C., MOLNAR, P. and SUAREZ, G., 1981. Possible thin-skin tectonics in the Eastern Andes of Bolivia and Peru (Abstract), EOS Transactions AGU, V. 62, p. 1047.

BURG, J.P. and IGLESIAS-PONCE DE LEON, M., 1985. Pressure-solution structures in a granite. Journal of Structural Geology, V. 7, N°3/4, pp. 431-436.

BURNHAM, C.W., 1979. Hydrothermal fluids at the magmatic stage. *In*: Barnes, H.L. (Editor), Geochemistry of hydrothermal ore deposits, Holt, Rinehart and Winston Inc., pp. 34-76.

BURNHAM, C.W., 1981. Convergence and mineralization, Is there a relation?, Geological Society of America, Memoir 154, pp. 761-768.

BURNHAM, C.W., 1981a. Physicochemical constraints on porphyry copper mineralization. *In*: Dickinson, W.R. and Payne. W. (Editors), Relations of tectonics to ore deposits in the Southern Cordillera. Arizona Geological Society Digest, Tucson, Arizona, Vol.XIV, pp. 71-77.

BURNHAM, C.W., 1985. Energy release in subvolcanic enviroments: Implications for Breccia Formation. Economic Geology, V. 80, pp. 1515-1522.

BURNHAM, C.W. and OHMOTO, H., 1980. Late-stage processes of felsic magmatism. Mining Geology Special Issue, N°8, pp. 1-11.

BURNOL, L., 1966. Estudio de los yacimientos de cobre en el sector de Tres Puntas-San Juan-Cobija, en la Región de Tocopilla, Prov. de Antofagasta. (Unpublished report), ENAMI Rol. N° 2053, Antofagasta, SERNAGEOMIN, Archive, 36 p.

BUSBY-SPERA, C.J. and SALEEBY, J.B., 1990. Intra-arc strike-slip fault exposed at batholithic levels in the southern Sierra Nevada, California. Geology, V. 18, pp. 255-259.

CABELLO, J., 1978. Exploración geoquímica y magnetometría en el distrito argentífero de Caracoles. B.Sc. thesis, Depto. Geología, Univ. de Chile, Santiago, 117 p.

CABELLO, J., 1986. Precious metals and Cenozoic volcanism in the Chilean Andes. Journal of Geochemical Exploration, V. 25, pp. 1-19.

CAMINOS, R., 1979. Cordillera Frontal. *In*: Leanza, A.F. (Editor), Geología Regional Argentina, Academia Nacional de Ciencias, Córdoba, Argentina, pp. 397-454.

CAMPANO, P., 1978. Contribution à l'étude de la distribution des élements tracés dans les roches volcaniques du Nord Chile. Ph.D. Thesis, University of Paris, 182 p.

CAMUS, F., 1985. Los yacimientos estratoligados de Cu, Pb-Zn y Ag de Chile. *In*: Frutos, J., Oyarzun, R. and Pincheira, M. (Editors), Geología y Recursos Minerales de Chile. Editorial de la Universidad de Concepción, pp. 547-635.

CANDE, S., 1983. Nazca-South America Plate Interactions 80 m.y. B.P. to present. (Abstract), EOS, V. 64, N°45, p. 65.

CANDE, S.C., HERRON, E.M. and HALL, B.R., 1982. The early Cenozoic tectonic history of the southeast Pacific. Earth and Planetary Science Letters, V. 57, pp. 63-74.

CANDE, S.C. and LESLIE, R.B., 1986. Late Cenozoic tectonics of the southern Chile trench. Journal of Geophysical Research, V. 91, No. B1, pp. 471-496.

CANDELA, P.A. and HOLLAND, H.D., 1984. The partitioning of copper and molybdenum between silicate melts and aqueous fluids. Geochimica et Geochimica Acta, V. 48, pp. 373-380.

CANDELA, P.A., and HOLLAND, H.D., 1986. A mass transfer model for copper and molybdenum in magmatic hydrothermal systems: the origin of porphyry-type ore deposits. Economic Geology, V. 81, pp. 1-19.

CARLIER, G., GRANDIN, G., LAUBACHER, G., MAROCCO, R. and MEGARD, F., 1982. Present knowledge of the magmatic evolution of the Eastern Cordillera of Peru. Earth Science Reviews, V. 18, pp. 253-283.

CARMICHAEL, I.S.E., TURNER, F.J. and VERHOOGEN, J., 1974. Igneous Petrology. McGraw Hill Inc., 739 p.

CASAMIQUELA, R., 1980. Notas sobre restos de un reptil Aetosaurio (*Thecodontia aetosauria*) de Quimal, Cordillera de Domeyko, Antofagasta, prueba de la existencia de Neotriásico continental en Los Andes del Norte de Chile (Comunicación). Actas Congreso Geológico Argentino de Paleontología y Bioestratigrafía, V. 1, pp. 135-142, Buenos Aires, Argentina.

CASTRO, A., 1985. The Central Extremadura Batholith: Geotectonic implications (European Hercynian belt). Tectonophysics, V. 120, pp. 57-68.

CATHLES, L.M., 1977. An analysis of the cooling of intrusives by groundwater convection which includes boiling. Economic Geology, V. 72, pp. 804-826.

CATHLES, L.M., 1981. Fluid flow and genesis of hydrothermal ore deposits. Economic Geology 75th Anniversary Volume, pp. 424-457.

CATHLES, L.M., GLEEN, W.E. and LENZI, G., 1979. Fluid flow study in naturally fractured igneous rocks: a case history. (Abstract) AIME annual meeting, New Orleans, 1979, Program, p.68.

CAVIEDES, C., 1973. A climatic profile of the north Chilean desert at latitude 20° S. *In*: Amiran, D.H.K. and Wilson, A.W. (Editors), Coastal Deserts: Their natural and human environments, University of Arizona Press, Tucson, Arizona, pp. 115-121.

CECCIONI, A. and FRUTOS, J., 1975. Primera noticia sobre el hallazgo de Paleozoico inferior marino en la Sierra de Almeyda, norte de Chile. Actas Congreso Argentino de Paleontología y Bioestratigrafía, V. 1, pp. 191-207, Tucumán, Argentina.

CHAPPELL, B. and WHITE, A., 1974. Two contrasting granite types. Pacific Geology, V. 8, pp. 173-174.

CHARRIER, R., 1973. Interruptions of spreading and the compressive tectonic phases of the Meridional Andes. Earth and Planetary Science Letters, V. 20, pp. 242-249.

CHARRIER, R., 1979. El Triásico en Chile y regiones adyacentes de Argentina: una reconstrucción plaeogeográfica y paleoclimática. Comunicaciones N°26, Dept. Geología, Univ. Chile, pp. 1-37.

CHARRIER, R., 1981. Mesozoic and Cenozoic stratigraphy of the Central Argentinean-Chilean Andes (32°-35°S) and chronology of their tectonic evolution. Zentralbl. Geol. Paleontol., Teil I, V. 3/4, pp. 344-355.

CHARRIER, R., and VICENTE, J.C., 1970. Liminary and geosyncline Andes: Major orogenic phases and synchronical evolution of the central and austral sectors of the southern Andes. Symposium on the results of Upper Mantle Investigations with emphasis on Latin America, Buenos Aires, Argentina, pp. 451-470.

CHAVEZ, W., 1983. The Geologic Setting of Disseminated copper sulfide mineralization of the Mantos Blancos copper-silver district, Antofagasta Province, Chile. AIME, Pre-print Number 193; AIME Annual Meeting, Geology Section, Atlanta, Georgia.

CHAVEZ, W., 1984. Alteration mineralogy and chemistry of rhyolitic and andesitic volcanic rocks of the Mantos Blancos copper-silver district, Chile: Society of Mining Engineers of AIME Pre-print, N° 84-153, 5 p.

CHAVEZ, W., 1985. Geological setting and the nature and distribution of disseminated copper mineralization of the Mantos district, Antofagasta Province, Chile. Ph.D. Thesis, California Univ., Berkeley, 142 p.

CHINN, D.S. and ISACKS, B.L., 1983. Accurate source depths and focal mechanisms of shallow earthquakes in western South America and in the New Hebrides Island Arc. Tectonics, V. 2, pp. 529-563.

CHONG, G., 1973. Reconocimiento geológico del área Catalina, Sierra de Varas y estratigrafía del Jurásico del Profeta, Provincia de Antofagasta. B.Sc. thesis, Depto. de Geol., U. de Chile, 284 p.

CHONG., G., 1976. Las relaciones de los sistemas Jurásico y Cretácico en la zona preandina del norte de Chile. Actas I Congr. Geol. Chileno, V. 1, pp. A21-A42, Santiago, Chile.

CHONG, D.G., 1977. Contribution to the knowledge of the Domeyko Range of Northern Chile. Geologische Rundschau, V. 66, pp. 374-404.

CHONG, G. and VON HILLEBRANDT, A., 1985. El Triásico preandino de Chile entre los 23°30' y 26°00' de Lat.S. Actas IV Congreso Geológico Chileno, V. 1, pp. 1-162-1-210, Antofagasta.

CHRISTIE-BLICK, N. and BIDDLE, K.T., 1985. Deformation and basin formation along strike-slip faults. *In*: Biddle, K.T. and Christie-Blick, N. (Editors), Strike-slip deformation, basin formation, and sedimentation. Society Econ. Paleontologists Mineralogists, Special Publication 37, pp. 1-34.

CHURCH, S.E., 1973. Limits of sediment involvment in the genesis of orogenic volcanic rocks. Contributions to Mineralogy and Petrology, V. 39, pp. 17-32.

CHURCH, S.E., 1976. The Cascade Mountains revisited: a re-evaluation in light of the new isotope data. Earth and Planetary Science Letters, V. 29, pp. 175-188.

CLARK, A.H., 1970. An occurrence of the assemblage native sulphur-covellite, "$Cu_{5,5}xFexS_{6,5}x$", Aucanquilcha, Chile, American Mineralogist, V. 55, pp. 913-918.

CLARK, A.H., MAYER, A.B.S., MORTIMER, C., SILLITOE, R.H., COOKE, R.U. and SNELLING, N.J., 1967a. Implications of the isotopic ages of ignimbrite flows, southern Atacama Desert, Chile. Nature, V. 215, pp. 723-724.

CLARK, A.H., COOKE, R.U, MORTIMER, C. and SILLITOE, R.H., 1967b. Relationships between supergene mineral alteration and geomorphology, Southern Atacama Desert, Chile - an interim report. Trans. Instn. Min. Metall. B, V. 76, pp. B89-B96.

CLARK, A.H., FARRAR, E., HAYNES, S.J., QUIRT, S., CONN, H. and ZENTILLI, M., 1970. K-Ar chronology of granite emplacement ans associated mineralization, Copiapó mining district, Atacama, Chile. (Abstract), Economic Geology, V. 65, p. 736.

CLARK, A.H.. and ZENTILLI, M., 1972. The evolution of metallogenic province at a consuming plate margin: The Andes between latitudes 26° and 29° south (Abstract): Canadian Mining Metallurg. Bull., 65 (719), 37 (1972), p. 261.

CLARK, A.H., CAELLES, J.C., FARRAR, E., HAYNES, S.J., LORTIE, R.B., Mc.BRIDE, S.L., QUIRT, G.S., ROBERTSON, R.C.R. and ZENTILLI, M., 1976. Longitudinal variations in the metallogenic evolution of the Central Andes: a progress report. *In*: Strong, D.F. (Editor), Metallogeny and Plate Tectonics. Geol. Assoc. of Canada, Special Paper N°14, pp. 23-58.

CLINE, J.S. and BODNAR, R.J., 1989. Partitioning of Cu and Cl in magmatic/hydrothermal systems: Application to the Yerington, Nevada, porphyry deposit. (Abstract): Geological Society of America, Abstracts with programs, 1989 Annual Meeting, St. Louis Missoury, p. A150.

CLOOS, M. and SHREVE, R.L., 1988. Subduction-channel model of prism accretion, melange formation, sediment subduction, and subduction erosion at convergent plate margins: 1. Background and description. Pure and Applied Geophysics, V. 128, Nos. 3/4, pp. 455-500.

COBBING, E.J., 1985. The tectonic setting of the Peruvian Andes. *In* Pitcher, W.S. et al. (Editors), Magmatism at a plate edge, The Peruvian Andes. Blakie, Glasgow and Halsted Press, New York, pp. 3-12.

COIRA, B., DAVIDSON, J., MPODOZIS, C. and RAMOS, V. , 1982. Tectonic and magmatic evolution of the Andes of northern Argentina and Chile. Earth Science Reviews, V. 18, p. 303-332.

COIRA, B.L. and COUKHARSKY, M., 1976. Efusividad tradio-hercínica en el borde oriental de la Cordillera Frontal, Zona del Arroyo del Tigre, Provincia de Mendoza, Rep. Argentina., Actas I Congreso Geológico Chileno, Santiago, T.2, pp. F105-F124.

COLLEY, H., TREOLAR, P.J. and DIAZ, F., 1989. Gold-silver mineralization in the El Salvador region, northern Chile. *In*: Keays, R.R., Ramsay, R.H. and Groves, D.I. (Editors) The Geology of Gold Deposits: The perspective in 1988. Economic Geology Monograph 6, pp. 208-217.

CONEY, P.J., 1970. The geotectonic cycle and the new global tectonics. Geological Society of America Bull., V. 81, pp. 739-748.

CORVALAN, J., 1965. Gelogía. *In*: Geografía Económica de Chile, Corporación de Fomento de la Producción, Santiago de Chile, pp. 35-82.

CORVALAN, J., SALAS, R. and MONTECINOS, F., 1968. Upper Tertiary volcanic rocks of Chile and the uplift of the Andes (Abstract). *In*: Abstracts 23rd International Geological Congress, Prague, pp. 42-43.

COULBOURN, W.T., 1981. Tectonic of the Nazca plate and the continetal margin of western South America, 18° to 23° S. *In*: Kulm, L.V.D. and others (Editors), Nazca Plate: Crustal formation and Andean Convergence. Geological Society of America, Memoir 154, pp. 587-618.

COURTY, G., 1907. Explorations géologiques dans l'Amerique du sud. *In*: Mission scientifique de G. de Crequi-Montefort et Sénéchal de la Grange, París, France., V. 14, 208 p.

COWAN, G.A. and ADLER, H.H., 1976. The variability of the natural abundance of $^{235}U$. Geochimica et Cosmochimica Acta, V. 40, pp. 1487-1490.

CROUGH, S.T., 1983. Apatite fission-track dating of erosion in the eastern Andes, Bolivia. Earth and Planetary Science Letters, V. 64, pp. 396-397.

CUMMINGS, D. and SCHILLER, G.I., 1971. Isopach map of the Earth's crust. Earth Science Reviews, V. 7, pp. 97-125.

DALMAYRAC, B., LAUBACHER, G., MAROCCO, R., MARTINEZ, C. and TOMASI, P., 1980. La Chaine Hercynienne d'Amerique du Sud, structure et evolution d'un orogene intracratónique. Geol. Rundschau, V. 69, pp. 1-21.

DALMAYRAC, B., LAUBACHER, G. and MAROCCO, R., 1980b. Caractères généraux de l'évolution géologique des Andes Péruviennes, Géologie des Andes Péruviennes, Trav. Doc. ORSTOM, 122, Paris, 501 p.

DALMAYRAC, B. and MOLNAR, P., 1981. Parallel thrust and normal faulting in Peru and constraints on the state of stress. Earth and Planetary Science Letters, V. 55, pp. 473-481.

DALRYMPLE, G.B. and LANPHERE, M.A., 1969. Potassium-Argon Dating, W.H. Freeman & Co., San Francisco, 258 p.

DALRYMPLE, G.B. and LANPHERE, M.A., 1971. $^{40}Ar/^{39}Ar$ technique of K-Ar dating, a comparison with the conventional technique. Earth and Planetary Science Letters, V. 12, pp. 359-372.

DALZIEL, I.W.D., 1986. Collision and Cordilleran orogenesis: an Andean perspective. *In*: Coward, M.P. and Ries, A.C. (Editors), Collision Tectonics, Geological Society Special Publication No. 19, pp. 389-404.

DALZIEL, I.W.D. and FORSYTHE, R., 1985. Andean evolution and the terrane concept. *In*: Howel, D.G. (Editor), Tectonostratigraphic terranes of the Circum-Pacific Region, Circum-Pacific Council of Energy and Mineral Resources, Earth Science Series #1, pp. 565-581.

DAMM, K.-W. and PICHOWIAK, S., 1981. Geodynamik und Magmengenese in der Kustenkordillere Nordchileszwischen Taltal und Chañaral. Geotek. Forsch., 61, 166 p.

DAMM, K.-W., PICHOWIAK, S. and TODT, W., 1986. Geochemie, petrologie und geochronologie der plutonite und des metamorphen grundgebirges in Nordchile. Berliner geowiss. Abh., (A), V. 66, pp. 73-146, Berlín.

DAMON, P.E., 1986. Batholith-volcano coupling in the Metallogeny of porphyry copper deposits. *In*: Friedrich, G.H., and others (Editors), Geology and Metallogeny of Copper Deposits, Proceedings of the Copper Symposium 27th International Geological Congress, Moscow, 1984, Springer-Verlag, pp. 216-234.

DASCH, E.J., 1981. Lead isotopic composition of metalliferous sediments from the Nazca Plate. Geological Society of America, Memoir 154, pp. 199-209.

DAVIDSON, J., 1984. Introducción a la Geología de Chile. *In*: Seminario Actualización de la Geología de Chile, Apuntes, pp. B1-B24, SERNAGEOMIN, Santiago.

DAVIDSON, J., MPODOZIS, C. and RIVANO, S., 1981a. Paleozoico de Sierra de Almeida al oeste de Monturaqui, Alta Cordillera de Antofagasta, Chile. Revista Geológica de Chile N°12. pp. 2-23, Santiago.

DAVIDSON, J., MPODOZIS, C. and RIVANO, S., 1981b. Evidencias de tectogénesis del Devónico Superior Carbonífero Inferior al oeste de Augusta Victoria, Antofagasta, Chile. Revista Geológica de Chile N°12, p. 78-86, Santiago.

DAVIDSON, J., RAMIREZ, C., GARDEWEG, M., HERVE, M. and BROOK, M., 1985. Calderas del Paleozoico Superior-Triásico Inferior y mineralización asociada a la Cordillera de Domeyko, norte de Chile. (Abstract), Comunicaciones N°35, Depto. Geología y Geofísica, Univ. de Chile, pp. 53-57, Santiago.

DAVIDSON, J.P., DUNGAN, M.A., FERGUSON, K.M. and COLUCCI, M.T., 1987. Crust-magma interactions and the evolution of arc magmas: The San Pedro-Pellado volcanic complex, southern Chilean Andes. Geology, V. 15, pp. 443-446.

DAVIDSON, J.P., FERGUSON, K.M., COLUCCI, M.T. and DUNGAN, M.A., 1988. The origin and evolution of magmas from the San Pedro-Pellado volcanic complex, S. Chile: multicomponent sources and open system evolution. Contributions to Mineralogy and Petrology, V. 100, pp. 429-445.

DAVIES, F.B., 1982. Pan-African granite intrusion in response to tectonic volume changes in a ductile shear zone from northern Saudi Arabia. Journal of Geology, V. 90, pp. 467-483.

DAVIES, J.F., 1989. Some temporal-spatial aspects of North American porphyry deposits. Economic Geology, V. 84, pp. 2300-2306.

DEFINIS, A. 1985. Antecedentes geológicos del yacimiento de cobre Santo Domingo, Taltal y discusión acerca de su relación con un sistema de filones gabrodioríticos. Actas IV Congreso Geológico Chileno, V. 2, pp. 3-204 - 3-215, Antofagasta.

DePAOLO, D.J. and WASSERBURG, G.J. (1976). Nd isotopic variations and petrogenetic models. Geophysics Research Letters, V. 3, pp. 249-252.

DERUELLE, B., 1982. Petrology of the Plio-Quaternary volcanism of the South-Central and Meridional Andes. Journal of Volcanology and Geothermal Research, V. 14, pp. 77-124.

DEWEY J., 1980. Episodicity, sequence, and style at convergent plate boundaries. *In*: Strangway, D. (Editor), The Continental Crust and its Mineral Deposits, Geological Association of Canada, Special Paper N°20, pp. 553-577.

DEWEY, J.F. and BIRD, F.M., 1970. Mountain belts and the new global tectonic. Journal of Geophysical Research, V. 75, pp. 2625-2647.

DIAZ, F., in prep. Geological investigation of mineralization associated with the Atacama Fault Zone, Northern Chile. M. Phil Thesis, Oxford Polytechnic, United Kingdom.

DIAZ, F., BEMBOW, M.S., BRAVO, N., GUTIERREZ, A, MONTTI, S., SALINAS, M. and VOGEL, S., 1981. Mapa metalogénico pronóstico de la III Región. (Unpublished report), CORFO-IIG, 9 Vol.

DIAZ, M., CORDANI, U., KAWASHITA, K., BAEZA, L., VENEGAS, R., HERVE, F. and MUNIZAGA, F., 1985. Edades radiométricas preliminares de Península Mejillones, Norte de Chile. Comunicaciones N°35, Depto. Geología, Univ. de Chile, pp. 59-67, Santiago.

DINGMAN, R.J., 1963. Cuadrángulo Tulor. Carta Geológica de Chile, N°11, 35 p., Instituto de Investigaciones Geológicas, Santiago.

DINGMAN, R.J., 1965. Pliocene age of the ash-flow deposits of the San Pedro area, Chile. U.S. Geological Survey, Professional Paper No. 525-C, pp. 63-67.

DODSON, M.H., 1973. Closure temperature in cooling geochronological systems. Contributions to Mineralogy and Petrology, V. 40, pp. 259-274.

DODSON, M.H., 1975. Kinetic processes and thermal history of the rocks. Carnegie Institution Washington, Yearbook 74, pp. 210-217.

DODSON, M.H., 1976. Kinetics processes and thermal history of slowly-cooling solids. Nature, V. 259, pp. 551-553.

DODSON, M.H., 1979. Theory of cooling ages. *In*: Jager, E. and Hunzinker, J.C. (Editors); Lectures in Isotope Geology, Springer-Verlag, New York, pp. 194-202.

DOE, B.R. and DELEVAUX, M.H., 1980. Lead isotope investigations in the Minnesota River Valley - I. Late and post-tectonic granites. Geological Society of America, Special Paper 182, pp. 105-112.

DONELICK, R.A., 1988. Etchable fission track length reduction in apatite: experimental observations, theory and geological applications. Ph.D. thesis, Rensselaer Plytechnic Institute, Troy, New York, 413 p.

DOSTAL, J., ZENTILLI, M., CAELLES, J.C. and CLARK, A.H., 1977. Geochemistry and origin of volcanic rocks of the Andes (26°-28°S). Contributions to Mineralogy and Petrology, V. 63, pp. 113-128.

DREYER, H. and SOTO, H., 1985. Geología de Mina Susana, un yacimiento novedoso en Carolina de Michilla. Actas IV Congreso Geológico Chileno, V. 2, pp. 3-354 - 3-382. Antofagasta.

DUDDY, I.R., GREEN, P.F., and LASLETT, G.M., 1988. Thermal annealing of fission tracks in apatite. 3. variable temperature behaviour. Chemical Geology (Isotope Geoscience Section), V. 73, pp. 25-38.

EASTOE, C.J., 1982. Physics and chemistry of the hydrothermal system at the Panguna porphyry copper deposit, Bougainville, Papua New Guinea, Economic Geology, V. 77, pp. 127-153.

EATON, G.P., 1962. Crustal structure and volcanism in Hawaii. *In*: MacDonald G.A. and Kuno, H. (Editors), The crust of the Pacific Basin. Geophysical Monographs, American Geophysical Union, 6, pp. 13-29.

ELLISON, R.A., KLINCK, B.A. and HAWKINS, M.P., 1989. Deformation events in the Andean orogenic cycle in the Altiplano and Western Cordillera, southern Peru. Journal of South American Earth Sciences, V. 2, No. 3, pp. 263-276.

EMMONS, W.H., 1927. Relations of the disseminated copper ores in porphyry to igneous intrusives. AIME Transactions, 75, pp. 795-815.

ENGLAND, P.C. and RICHARDSON, S.W., 1977. The influence of erosion upon mineral facies of rocks from different metamorphic environments. Journal of the Gological Society London, V. 134, pp. 201-213.

ENGLAND, P.C. and RICHARDSON, S.W., 1980. Erosion and the age dependence of continental heat flow. Geophysical Journal of the Royal Astronomical Society, V. 62, pp. 421-437.

ENGLAND, P.C. and THOMPSON, A.B., 1984. Pressure-temperature-time paths of regional metamorphism I. Heat transfer during the evolution of regions of thickened continental crust. Journal of Petrology, V. 25, Part 4, pp. 894-928.

EREMCHUK, J.E., MON, R., SUAYTER, L.E. and ZOSSI, M.M., 1981. Sismicidad y tectónica en los Andes del norte argentino. Revista de la Asociación Geológica Argentina, V. 36, pp. 197-203.

ERICKSEN, G.E., 1975. Metallogenic provinces of the southeastern Pacific region. U.S. Geological Survey, Open file Report (IR)CP-1, 52 p.

ERICKSEN, G.E., 1976. Metallogenic provinces of Southern Pacific Region. Am. Assoc. of Petroleum Geologists Bull. Memoir 25, pp. 527-537.

ERICKSEN, G.E., 1981. Geology and origin of the Chilean nitrate deposits. U.S.G.S. Professional Paper 1188, 37 p.

ERICKSEN, G.E., 1983. The Chilean Nitrate Deposits. American Scientist, V. 71, pp. 366-374.

ESPINOZA, S., 1981. Esbozo metalogénico del distrito de Michilla, II Región, Chile. Actas 1° Coloquio sobre volcanismo y metalogénesis, Depto. Geociencias, Univ. del Norte, Antofagasta, Chile, pp. 71-81.

ESPINOZA, S., 1982. Definición del tipo diseminado infravolcánico de súlfuros de cobre. Actas III Congreso Geológico Chileno, V. 3, Concepción, pp. E201-E219.

ESPINOZA, S., 1983. Geología y génesis de la mineralización cuprífera del sector Caleta Coloso, al sur de Antofagasta. Revista Geológica de Chile, N°19-20, pp. 81-91, Santiago.

ETHERIDGE, M.A. and WILKIE, J.C., 1979. Grain size reducction, grain boundary sliding and the flow strength of mylonites. Tectonophysics, V. 58, pp. 159-178.

FARMER. G.L. and DePAOLO, D.J., 1987. Nd and Sr isotope study of hydrothermally altered granite at San Manuel, Arizona: Implications for element migration paths during the formation of porphyry copper ore deposits. Economic Geology, V. 82, pp. 1142-1151.

FARRAR, E., CLARK, A.H., HAYNES, S.J., QUIRT, G.S., CONN, H. and ZENTILLI, M., 1970. K-Ar evidence for the post-Paleozoic migration of granitic foci in the Andes of northern Chile. Earth and Planetary Science Letters, V. 10, pp. 60-66.

FARRAR, E. and NOBLE, D.C., 1976. Timing of late Tertiary deformation in the Andes of Peru. Geological Society of America Bulletin, V. 87, pp. 1247-1250.

FEDOTOV, S.A., 1976. Mechanism of magma ascent and deep feeding channels of island arc volcanoes. Bulletin Volcanology, V. 39, pp. 241-254.

FEISS, P.G., 1978. Magmatic sources of copper in porphyry copper deposits. Economic Geology, V. 73, pp. 397-404.

FELLENBERG, E., 1975. Geología del cuadrángulo Cerro Jaspeado. (Unpublished report), Depto. Geociencias, Univ. del Norte, 56 p., Antofagasta.

FERRARIS, F., 1978. Cordillera de la Costa entre 24° y 25° Latitud Sur, Escala 1:250.000, Región de Antofagasta. Carta Geológica de Chile N°26, Instituto de Investigaciones Geológicas, Santiago.

FERRARIS, F., ROJAS, N., ORTIZ, F., et al., 1973. Geología y yacimientos metalíferos de la región de la mina Julia, distrito minero de Paposo, Prov. de Antofagasta, (Unpublished report), Instituto de Investigaciones Geológicas, 106 p., SERNAGEOMIN AArchive, Santiago, Chile.

FERRARIS, F. and DI BIASE, F., 1978. Hoja Antofagasta, Región de Antofagasta, Carta Geológica de Chile, N°30, 48 p., Instituto de Investigaciones Geológicas, Santiago.

FIELD, C.W. and DASCH, E.J., 1981. Epilogue: Geostill reconsidered. Geological Society of America, Memoir 154, pp. 817-824.

FIELD, C.W. and GUSTAFSON, L.B., 1976. Sulfur isotopes in the porphyry copper deposit at El Salvador, Chile. Economic Geology, V. 71, pp. 1533-1548.

FITCH, T.J., 1972. Plate convergence, transcurrent faults, and internal deformation adjacent to southeast Asia and the Western Pacific. Journal of Geophysical Research, V. 77, pp. 4432-4460.

FITCH, J.G., MILLER, J.A. and MITCHELL, J.G., 1969. A new approach to radio-isotopic dating in orogenic belts. *In*: Kent, P.E., Satlherthwaite, G.E. and Spencer, A.M. (Editors), Time and Place in Orogeny, Geological Society of London, Special Publication N°3, pp. 157-195.

FLECK, R.D., SUTTER, J.F. and ELLIOT, E., 1977. Interpretation of discordant $^{40}Ar/^{39}Ar$ age spectra of Mesozoic tholeiites from Antarctica. Geochimica et Cosmochimica Acta, V. 41, pp. 15-32.

FLEISCHER, R.L. and HART, H.R., 1972. Fission track dating: techniques and problems. *In*: Bishop, W.W. and others (Editors), Calibration of Hominid Evolution, Scottish Academic Press, Edinburgh, pp. 135-170.

FLEISCHER, R.L. and PRICE, P.B., 1964. Decay constant for spontaneous fission of $^{238}U$. Physical Review, V. 133, pp. B63-B64.

FLEISCHER, R.L., PRICE, P.B. and WALKER, R.M., 1965. Effects of temperature, pressure, and ionization on the formation and stability of fission tracks in minerals and glasses. Journal of Geophysical Research, V. 70, pp. 1497-1502.

FLEISCHER, R.L., PRICE, P.B. and WALKER, R.M., 1965b. Tracks of charged particles in solids. Science, V. 149, Number 3682, pp. 383-393.

FLEISCHER, R.L., PRICE, P.B. and WALKER, R.M., 1965c. Ion explosion spike mechanism for formation of charged particle tracks in solids. Journal of Applied Physics, V. 36, pp. 3645-3652.

FLEISCHER, R.L., PRICE, P.B. and WALKER, R.M., 1975. Nuclear tracks in solids: Principles and Applications. University of California Press, Berkeley, California, 605 p.

FLINT, S., 1985. On the paragenetic position of Atacamite in low temperature red bed deposits of northern Chile. Zbl. Geol. Palaont., Teil I, H 9/10, pp. 1617-1627, Stuttgart.

FLINT, S., 1985b. Alluvial fan and playa sedimentation in an Andean closed basin: the Pacencia Group, Antofagasta Province, Chile. Journal of the Geological Society London, V. 142, pp. 533-546.

FLINT, S., 1986. Sedimentary and diagenetic controls on red-bed ore genesis: the middle Tertiary San Bartolo Copper Deposit, Antofagasta Province, Chile. Economic Geology, V. 81, N°4, pp. 761-778.

FLINT, S., 1987. Diagenesis of Tertiary playa sandstones of Northern Chile; implications for Andean uplift and metallogeny. Sedimentology 34, pp. 11-29.

FLINT, S., CLEMMEY, H. and TURNER, P., 1986. Conglomerate-hosted copper mineralization in Cretaceous Andean molasse: the Coloso Formation of northern Chile. Geological Magazine, V. 123, N°5, pp. 525-536.

FLORES, R., 1976. Control de la mineralización de plata en el distrito minero de Caracoles, II Región, Antofagasta, Chile. B.Sc. thesis, Depto. de Geociencias, Univ. del Norte, Antofagasta, 78 p.

FLORES, R., 1985. Control del enriquecimiento supérgeno en el yacimiento Chuquicamata, Chile. Actas IV Congreso Geológico Chileno, V. 2, pp. 3-228 - 3-249, Antofagasta.

FLORES, H. and HEVIA, J., 1952. Antecedentes geológicos sobre la mina Despreciada de la Cía. Minera de Tocopilla. Memoria de la 1° Convención Interamericana de recursos minerales, pp. 43-51, México.

FLOYD, P.A. and WINCHESTER, J.A., 1978. Identification and discrimination of altered and metamorphosed volcanic rocks using immobile elements. Chemical Geology, V. 21, pp. 291-306.

FORSYTHE, R., 1982. The Late Paleozoic to Early Mesozoic evolution of southern South America: A plate tectonic interpretation. Journal of the Geological Society, London, V. 139, pp. 671-682.

FORTT, M.A., 1981. Geología general de los cuadrángulos Cerro Quimal, Laguna Tebinquiche, Llano de la Paciencia y Salar de Atacama, II Región. (Unpublished report), Instituto de Investigaciones Geológicas, 48 p., Santiago.

FREY, F.A., GERLACH, D.C., HICKEY, R.L., LOPEZ-ESCOBAR, L. and MUNIZAGA, F., 1984. Petrogenesis of the Laguna del Maule volcanic complex, Chile (36°S), Contributions to Mineralogy and Petrology, V. 88, pp. 133-149.

FRUTOS, J., 1970. Ciclos tectónicos sucesivos y direcciones estructurales sobreimpuestas en Los Andes del Norte Grande de Chile. *In*: Symposium on the results of Upper Mantle Investigations with emphasis on Latin America, Buenos Aires, Aregentina, V. 2, pp. 451-470.

FRUTOS, J., 1973. Sobre el posible control tectónico de los yacimientos de cobre porfírico en la cuenca Andina Chilena. Revista Geológica de Chile, N°1, pp. 103-113.

FRUTOS, J., 1975. Porphyry copper-type mineralization and geosynclinal tectonic evolution in the Chilean Andes. Ann. Soc. Géol. Belgique, 98, fasc.1, pp. 5-15.

FRUTOS, J., 1979. La razón Cu/Mo en los depositos porfíricos en relación al grado de evolución tectónica de las cadenas orogénicas. Actas II Congreso Geológico Chileno, 2, pp. C69-C88.

FRUTOS, J., 1981. Andean tectonics as a consequence of seafloor spreading, Tectonophysics, V. 72, pp. T21-T32.

FRUTOS, J., 1982. Andean metallogeny related to the tectonic and petrologic evolution of the Cordillera. Some remarkable points. *In*: Amstutz, G.C., and others (Editors), Ore Genesis. The state of the art, Springer-Verlag, pp. 493-507.

FRUTOS, J., 1985. La cordillera de los Andes. Palabras de presentación. *In*: Frutos and others (Editors), Geología y Recursos Minerales de Chile. Editorial de la Univ. de Concepción, pp. 3-9.

FRUTOS, J. and TOBAR, A., 1975. Evolution of the Southwestern Continental Margin of South America. *In*: Campbell, K.S.W. (Editor), Gondwana Geology, Gondwana Basins and Continental Margins, Papers presented to the III International Gondwana Symposium, Australian National University Press, Canberra, pp. 565-578.

FRUTOS, J. and OYARZUN, J., 1975. Tectonic and geochemical evidence concerning the genesis of El Laco magnetite lava flow deposits, Chile. Economic Geology, V. 70, pp. 988-990.

FRUTOS, J. and PINCHEIRA, M., 1985. Metalogénesis y yacimientos metalíferos chilenos. *In*: Frutos, J., Oyarzun, R. and Pincheira, M. (Editors), Geología y Recursos Minerales de Chile. Editorial de la Univ. de Concepción, pp. 469-487.

FUENZALIDA, H., 1965. Orografía y Clima. *In*: Geografía Económica de Chile. CORFO (texto refundido). Editorial Universitaria, Santiago, pp. 7-34 and 99-152.

FUTA, K. and STERN, C.R., 1988. Sr and Nd isotopic and trace element composition of Quaternary volcanic centers of the Southern Andes. Earth and Planetary Science Letters, V. 88, pp. 253-262.

GALBRAITH, R.F., 1981. On statistical models for fission track counts. Mathematical Geology, V. 13, pp. 471-488.

GALLI, O.C., 1967. Pediplain in northern Chile and the Andean uplift. Science, V. 158, pp. 653-655.

GAPAIS D. AND BARBARIN, B., 1986. Quartz fabric transition in a cooling syntectonic granite (Hermitage Massif, France). Tectonophysics, V. 125, pp. 357-370.

GARCIA, F., 1967. Geología del Norte Grande de Chile. Simposium sobre el Geosinclinal Andino, (1962), Soc. Geol. Chile N°3, 138 p., Santiago.

GARCIA, F., PEREZ, E. and CEBALLOS, E., 1962. El Ordovícico de Aguada de la Perdiz, Puna de Atacama, Prov. de Antofagasta. Minerales, N°77, pp. 52-60, Santiago.

GARDEWEG, M., CORNEJO, P. and DAVIDSON, J., 1984. Geología del volcán Llullaillaco, Altiplano de Antofagasta, Chile (Andes Centrales). Revista Geológica de Chile N°23, Santiago, pp. 21-37.

GARDEWEG, M. and RAMIREZ, C., 1984. Volcanismo del Cenozoico Superior del Altiplano Chileno (18°-28° Lat.S). In Seminario Actualización de la Geología de Chile, Apuntes, pp. E1-E31, SERNAGEOMIN, Santiago.

GARDEWEG, M. and RAMIREZ, C., 1985. Hoja Río Zapaleri. Carta Geológica de Chile N°66, SERNAGEOMIN, Santiago, Chile, 89 p.

GARDEWEG M. and RAMIREZ, C., 1987. La Pacana caldera and the Atana ignimbrite. A major ash-flow and resurgent caldera complex in the Andes of Northern Chile. Bull. Volcanol., V. 49, pp. 547-566.

GARRET, R.G., 1972. Compositions of biotites from unaltered and altered monzonitic rocks in the Bingham mining district, Utah. Economic Geology, V. 68, pp. 269-280.

GARY, M., McAFEE, R. and WOLF, C.L., 1972. (Editors), Glossary of Geology, American Geological Institute, Washington, D.C., 805 p.

GERLACH, D.C., FREY, F.A., MORENO, H. and LOPEZ-ESCOBAR, L., 1988. Recent volcanism in the Puyehue-Cordon Caulle region, southern Andes Chile (40.5°S): Petrogenesis of evolved lavas. Journal of Petrology, V. 29, pp.333-382.

GILL, J., 1981. Orogenic Andesites and Plate Tectonics. Minerals and Rocks 16, Springer Verlag, 385 p.

GILMOUR, P., 1982. Grades and tonnages of porphyry copper deposits. *In*: Titley, S.R. (Editor), Advances in Geology of the Porphyry Copper Deposits, Southwestern North America. The University of Arizona Press, pp. 7-35.

GLEADOW, A.J.W., 1981. Fission track dating methods: what are the real alternatives?. Nuclear Tracks, V. 5, pp. 3-14.

GLEADOW, A.J.W. and DUDDY, I.R., 1981. A natural long-term annealing experiment for apatite. Nuclear Tracks, V. 5, pp. 169-174.

GLEADOW, A.J.W., DUDDY, I.R., GREEN, P.F., AND LOVERING, J.F., 1986. Confined fission track lengths in apatite: a diagnostic tool for thermal history analysis. Contributions to Mineralogy and Petrology, V. 94, pp. 405-415.

GLEADOW, A.J.W. and LOVERING, J.F., 1977. Geometry factor for external detectors in fission track dating. Nuclear Track Detection, V. 1, pp. 99-106.

GOETZE, H.-J., SCHMIDT, S. and STRUNK, S., 1988. Central Andean gravity field and its relation to crustal structures. *In*: Bahlburg, H., Breitkreuz, C. and Giese, P. (Editors), The Southern Central Andes, Lecture Notes in Earth Sciences, V. 17, Springer-Verlag, pp.199-208.

GOETZE, H.J., 1989. Crustal structures and behaviour of Central Andes between 21° and 25° S, from recent geophysical research. (Abstract), 28th International Congress, Washington, U.S.A., V. 1, pp. 1-560 - 1-561.

GOUGH, D.I., 1973. Dynamic uplift of Andean mountains and island arcs. Nature, V. 242, pp. 39-41.

GREEN, P.F., 1981. A new look to statistics in fission track dating. Nuclear Tracks, V. 5, pp. 77-86.

GREEN, P.F., 1988. The relationship between track shortening and fission track age reduction in apatite: Combined influences of inherent instability, annealing anisotropy, length bias and system calibration. Earth and Planetary Science Letters, V. 89, pp. 335-352.

GREEN, P.F., 1989. Thermal and tectonic history of the East Midlands shelf (onshore UK) and surrounding regions assessed by apatite fission track analysis. Journal of the Geological Society, London, V. 146, pp. 755-773.

GREEN, P.F. and HURFORD, A.J., 1984. Thermal neutron dosimetry for fission track dating. Nuclear Tracks, V. 9, Nos. 3/4, pp. 231-241.

GREEN, P.F., DUDDY, I.R., GLEADOW, A.J.W., and TINGATE, P.R., 1985. Fission track annealing in apatite: track length measurements and the form of the Arrhenius plot. Nuclear tracks, V. 10, pp. 323-328.

GREEN, P.F., DUDDY, I.R., GLEADOW, A.J.W., TINGATE, P.R. and LASLETT, G.M., 1986. Thermal annealing of fission tracks in apatite. 1. A qualitative description. Chemical Geology (Isotope Geoscience Section), V. 59, pp. 237-253.

GREEN, P.F., LASLETT, G.M., HEGGARTY, K.A., GLEADOW, A.J.W. and LOWERING, J.F., 1989. Thermal annealing of fission tracks in apatite. 4. Quantitative modelling techniques and extension to geological timescales. Chemical Geology (Isotope Geoscience Section), V. 79, pp. 155-182.

GRUNDER, A., 1987. Low $\delta^{18}O$ silicic volcanic rocks at Calabozos Caldera Complex, Southern Andes: Evidence for upper-crustal contamination. Contributions to Mineralogy and Petrology, V. 95, pp. 71-81.

GUILBERT, J.M. and PARK, C.F., 1986. The geology of ore deposits. Freeman and Co., New York, pp. 405-426.

GUILD P.W., 1972. Distribution of metallogenic provinces in relation to major earth features. *In*: Petrascheck, W.E. (Editor), Metallogenetic and Geochemical Provinces, Springer-Verlag.

GUINEBERTEAU, B., BOUCHEZ, J.-L. and VIGNERESSE, J.-L., 1987. The Mortagne granite pluton (France) emplaced by pull-apart along a shear zone: Structural and gravimetric arguments and regional implication. Geological Society of America Bulletin, V. 99, pp. 763-770.

GUSTAFSON, L.B., 1979. Porphyry copper deposits and calc-alkaline volcanism. *In*: Mc Elhini, M.W. (Editor), The earth its origin, structure and evolution. Acad. Press., London, pp. 427-468.

GUSTAFSON, L.B., and HUNT, J.P., 1975. The porphyry copper deposit at El Salvador, Chile. Economic Geology, V. 70, N°5, pp. 857-912.

HAGGERTY, S.E., 1970. El Laco magnetite lava flow, Chile. Carnegie Institution Washington, Yearbook 68, pp. 329-330.

HALPERN, M., 1978. Geological significance of Rb-Sr isotopic data of northern Chile, crystalline rocks of the Andean orogen between latitudes 23° and 27° south. Geol. Soc. Am. Bull., V. 89, pp. 522-532.

HALPERN, M., 1979. Strontium isotope composition of rocks from the Disputada copper mine, Chile. Economic Geology, V. 74, pp. 129-130.

HANMER, S.K., 1982. Microstructure and geochemistry of plagioclase and microcline in naturally deformed granite. Journal of Structural Geology, V. 4, N°1, pp.197-213.

HANNAH, G.C., WESCOTT, C.H., LEMMEL, H.D., LEONARD, B.R., STORY, J.S. and ATTREE, P.M., 1969. Revision of values for the 2200 m/s neutron constants for four fissile nuclides. General Electric Corporation: Atomic Energy Review, V. 7, pp. 3-92.

HARMON, R.S., BARREIRO, B.A., MOORBATH, S., HOEFS, J., FRANCIS, P.W., THORPE, R.S., DERUELLE, B., McHUGH, J. and VIGLINO, J.A., 1984. Regional O-, Sr-, and Pb-isotope relationships in late Cenozoic calc-alkaline lavas of the Andean Cordillera. Journal of the Geological Society London, V. 141, pp. 803-822.

HARRINGTON, H., 1961. Geology of parts of Antofagasta and Atacama provinces of Northern Chile. Am. Assoc. Pet. Geol. Bull., V. 45, N°2, pp. 169-197.

HARRISON, T.M., 1981. Diffusion of $^{40}Ar$ in hornblende. Contributions to mineralogy and petrology, V. 78, pp.324-331.

HARRISON, T.M. and McDOUGALL, I., 1980. Investigations of an Intrusive contact, Northern Nelson, New Zealand. Thermal and Isotopic Constraints. Geochimica et Cosmochimica Acta, V. 44, pp.1985-2003.

HARRISON, T.M. and McDOUGALL, I., 1981. Excess $^{40}Ar$ in metamorphic rocks from Broken Hill, New South Wales: Implications for $^{40}Ar/^{39}Ar$ age specttra and the thermal history of the region. Earth Planetary Science Letters, V. 55, pp. 123-149.

HARRISON, T.M., DUNCAN, I. and McDOUGALL, I., 1985. Diffusion of $^{40}Ar$ in biotite: temperature, pressure and compositional effects. Geochimica et Cosmochimica Acta, V. 49, pp.2461-2468.

HARTLEY, A.J., 1987. Mesozoic-Recent evolution of the Andean forearc, northern Chile (22°-24°S). Ph.D. Thesis, University of Aston, U.K., 330 p.

HARTLEY, A.J., FLINT, S. and TURNER, P., 1988. A proposed lithostratigraphy for the Cretaceous Purilactis Formation, Antofagasta Province, Northern Chile. Actas V Congreso Geológico Chileno, III, pp. H83-H99.

HAWKESWORTH, C.J., 1982. Isotope characteristics of magmas erupted along destructive plate margins. *In*: Thorpe, R.S. (Editor), Andesites, John Wiley & Sons, pp. 549-571.

HAWKESWORTH, C.J., NORRY, M.J., RODDICK, J.C., BAKER, P.E., FRANCIS, P.W. and THORPE, R.S., 1979. $^{143}Nd/^{144}Nd$, $^{87}Sr/^{86}Sr$, and incompatible element variations in calc-alkaline andesites and plateau lavas from South America. Earth and Planetary Science Letters, V. 42, pp. 45-57.

HAWKESWORTH, C.J., HAMMIL, M., GLEDHILL, A.R., VAN CALSTEREN, P. and ROGERS, G., 1982. Isotope and trace element evidence for late stage intra-crustal melting in the high Andes. Earth Planetary Science Letters, V. 58, pp. 240-254.

HAYBA, D.O., BETHKE, PM., HEALD, P., and FOLEY, N.K., 1986. Geologic, mineralogic and geochemical characteristics of volcanic-hosted epithermal precious-metal deposits. *In*: Berger, B.R. and Bethke, P.M. (Editors), Geology and Geochemistry of epithermal systems. Society of Economic Geologists, Reviews in Economic Geology, V. 2, pp. 129-167.

HEALD, P., FOLEY, N.K. and HAYBA, D.O., 1987. Comparative anatomy of volcanic-hosted epithermal deposits: Acid-sulfate and adularia-sericite types. Economic Geology, V. 82, pp. 1-26.

HEMLEY, J.J. and JONES, W.R., 1964. Chemical aspects of hydrothermal alteration with emphasis on hydrogen metasomatism. Economic Geology, V. 59, pp. 538-569.

HEMPTON, M.R. and NEHER, K., 1986. Experimental fracture, strain and subsidence patterns over en échelon strike-slip faults: implications for the structural evolution of pull-apart basins. Journal of Structural Geology, V. 8, pp. 597-605.

HENLEY, R.W. and McNABB, A., 1978. Magmatic vapor plumes and groundwater interaction in prophyry copper emplacement. Economic Geology, V. 73, pp. 1-20.

HENRIQUEZ, F., 1975. Antecedentes preliminares sobre los yacimientos volcánicos de fierro El Laco, Antofagasta, Chile. Resumenes, II Congreso Ibero-Americano de Geología Económica, Buenos Aires, Argentina.

HENRIQUEZ, F., 1981. El yacimiento El Laco (Abstract). Actas del Primer Coloquio sobre volcanismo y metalogénesis, pp. 92-94, Depto. Geociencias, Univ. del Norte, Antofagasta.

HENRIQUEZ, F. and MARTIN, R.F., 1978. Crystal-growth textures in magnetite flows and feeder dykes, El Laco, Chile. Canadian Mineralogist, V. 16, pp. 581-589.

HERRMANN, R. and ZEIL, W., 1989. Tectonics and volcanism in the north Chilean longitudinal valley (24°30'-25°15'S). Zentralblatt für Geologie und Paläontologie, Teil I, H.5/6, pp. 1065-1073.

HERVE, F., 1982. Condiciones de formación de complejos metamórficos chilenos a partir de la química de anfíbolas en metabasitas. Actas III Congreso Geológico Chileno, V. 2, pp. D93-D115, Concepción.

HERVE, F., 1988. Late Paleozoic subduction and accretion in southern Chile. Episodes, V. 11, N°3, pp. 183-188.

HERVE, F., DAVIDSON, J., GODOY, E., MPODOZIS, C. and COVACEVIC, V., 1981. The Late Paleozoic in Chile: Stratigraphy, structure and possible tectonic fromework. Anais Acad. Brasil. Cienc., V. 53, N°2, pp. 361-373, Rio de Janeiro.

HERVE, F., MUNIZAGA, F., MARINOVIC, N., HERVE, M., KAWASHITA, K., BROOK, M. and SNELLING, N., 1985. Geocronología Rb-Sr y K-Ar del basamento cristalino de Sierra Limón Verde, Antofagasta, Chile. Actas IV Congreso Geológico Chileno, V. 3, pp. 4-235 - 4-253, Antofagasta, Chile.

HERVE, M., 1987. Movimiento normal de la falla Paposo, Zona de Falla Atacama, en el Mioceno, Chile. Revista Geológica de Chile, N°31, pp. 31-36.

HERVE, M., 1987a. Movimiento sinistral en el Cretácico Inferior de la Zona de Falla Atacama al norte de Paposo (24°S), Chile. Revista Geológica de Chile, N°31, pp. 37-42.

HERVE, M. and MARINOVIC, N., 1988. El Batolito Vicuña Mackenna (Jurásico Inferior-Cretácico). Características petrográficas y geoquímicas. Actas V Congreso Geológico Chileno, Santiago, V. 3, pp. I297-I319.

HERVE, M. and MARINOVIC, N., 1989. Geocronología y evolución del Batolito Vicuña Mackenna, Cordillera de la Costa, sur de Antofagasta (24°-25° S). Revista Geológica de Chile, Santiago, V. 16, N°1, pp. 31-50.

HERVE, M., MAKSAEV, V., MARINOVIC, N., MPODOZIS, C. and others, in preparation. Hoja Aguas Blancas. Carta Geológica de Chile, SERNAGEOMIN.

HICKEY, R.L., GERLACH, D.C. and FREY, F.A., 1984. Geochemical variations in volcanic rocks from central-south Chile (33°-42°S): Implications for their petrogenesis, *In*: Harmon, R.S. and Barreiro, B.A. (Editors), Andean Magmatism, chemical and isotopic constraints, Shiva Publishing Limited, pp. 72-95.

HICKEY, R.L., FREY, F.A., GERLACH, D.C. and LOPEZ-ESCOBAR, L., 1986. Multiple sources for basaltic rocks from the southern volcanic zone of the Andes (34°-41°S): Trace element and isotopic evidence for contributions from subducted oceanic crust, mantle, and continental crust. Journal of Geophysical Research, V. 91, No. B6, pp. 5963-5983.

HILDE, T.W.C., 1983. Sediment subduction versus accretion around the Pacific. Tectonophysics, V. 99, pp. 381-397.

HILDRETH, W. and MOORBATH, S., 1988. Crustal contributions to arc magmatism in the Andes of Central Chile. Contributions to Mineralogy and Petrology, V. 98, pp. 455-489.

HOFFSTETTER, B., FUENZALIDA, H., CECCIONI, G., 1957. Chile. *In*: Lexique Stratigraphique International, Centre de Recherches Scientifiques, V. 5, Fasc.7, París.

HOFFMAN, N.R.A. and McKENZIE, D.P., 1985. The destruction of geochemical heterogeneities by differential fluid motions during mantle convection. Geophysical Journal of the Royal Astronomical Society, V. 82, pp. 163-206.

HOLE, M.D., SAUNDERS, A.D., MARRINER, G.F., and TARNEY, J., 1984. Subduction of pelagic sediments: Implications for the origin of Ce anomalous basalts from the Mariana Islands. Journal of the Geological Society, V. 141, pp. 453-472.

HOLLINGWORTH, S.E. and RUTLAND, R.W.R., 1968. Studies of Andean uplift; PArt I: Post-Cretaceous evolution of the San Bartolo area, north Chile. Geol. Journal, V. 6, pp. 46-62.

HOLLISTER, V.F., 1978. Porphyry copper deposits of the Andean orogen. *In*: Hollister, V.F. (1978), Geology of porphyry copper deposits of the western hemisphere. Society of Mining Engs. of AIME, New York, pp. 5-32.

HOLLISTER, V.F. and BERNSTEIN, M., 1975. Copaquire, Chile: Its Geologic Setting and Porphyry Copper Deposit. Society of Mining Engineers, AIME, Transactions, V. 258, pp. 137-142.

HOLLY, F.R. and SCHOLL, D.W., 1989. The evolution of forearc structures along an oblique convergent margin, Central Aleutian Arc. Tectonics, V. 8, No.3, pp. 497-516.

HUETE, C., MAKSAEV, V., MOSCOSO, R., ULRIKSEN, C. and VERGARA, H., 1977. Antecedentes geocronológicos de rocas intrusivas y volcánicas en la Cordillera de Los Andes comprendida entre la Sierra de Moreno y el Río Loa y los 21° y 22° Lat.Sur, II Región, Chile. Revista Geológica de Chile, N° 4, pp. 35-41.

HUNT, J.P., 1977. Porphyry copper deposits. (Abstract), *In*: Volcanic processes in ore genesis. Special Publication No.7 of the Geological Society of London, p. 98.

HUNT, J.P., BRATT, J.A., and MARQUARDT, L., J.C., 1983. Quebrada Blanca, Chile: An enriched porphyry copper deposit. Mining Engineering, V. 35, pp. 636-644.

HURFORD, A.J., 1986. Application of the fission track dating method to young sediments: Principles, methodology and examples. *In*: Hurford, A.J., Jäger, E. and Ten Cate J.A.P. (Editors), Dating Young Sediments, CCOP Technical Publication 16, Issued by Technical Secretariat, Bangkok, Thailand, pp. 199-233.

HURFORD, A.J., 1990. Standarization of fission track dating calibration: Recommendation by the Fission Track Working Group of the I.U.G.S. Subcommission on Geochronology. Chemical Geology (Isotope Geoscience Section), V. 80, pp. 171-178.

HURFORD, A.J. and GREEN, P.F., 1983. The zeta age calibration of fission track dating. Chemical Geology (Isotope Geoscience Section) V. 1, pp. 285-317.

HURFORD, A.J. AND HAMMERSCHMIDT, K., 1985. $^{40}Ar$-$^{39}Ar$ and K-Ar dating of the Bishop and Fish Canyon Tuffs: calibration ages for fission track dating standards. Chemical Geology (Isotope Geoscience Section) V. 58, pp. 23-32.

HUTTON, D.W.H., 1982. A tectonic model for the emplacement of the Main Donegal Granite, NW Ireland. Journal of the Geological Society, London, V. 139, pp. 615-631.

HUTTON, D.W.H., 1988. Igneous emplacement in a shear-zone termination: The biotite granite at Strontian, Scotland. Geological Society of America Bulletin, V. 100, pp. 1392-1399.

ISACKS, B.L., 1988. Uplift of the central Andean plateau and bending of the Bolivian orocline. Journal of Geophysical Research, V. 93, No. B4, pp. 3211-3231.

ISHIHARA, S., 1977. The Magnetite-Series and Ilmenite-Series granitic rocks. Mining Geology, V. 27, pp. 293-305.

ISHIHARA, S., 1980. Significance of the Magnetite-Series and Ilmenite-Series of granitoids in mineral exploration. Proceedings of the Fifth Quadrennial IAGOD Symposium, E. Schweitzerbart'sche Verlagsbuchhandlung (Nagele U. Obermiller), pp. 309-312, Stuttgart.

ISHIHARA, S., 1981. The granitoid series and mineralization. Economic Geology 75$^{th}$ Anniversary Volume, pp. 458-484.

ISHIHARA, S., 1985. Concentration of heavy metals during granitoid magmatic processes. *In*: Sasaki, A. et al., (Editors), Mineral resources and engineering geology. John Wiley & Sons, pp. 24-27.

ISHIHARA, S., ULRIKSEN, C., SATO, K., TERASHIMA, S., SATO, T. AND ENDO, Y., 1984. Plutonic rocks of north-central Chile. Bulletin of the Geological Survey of Japan, V. 35, N°11, pp. 503-536.

ISHIHARA, S. and SASAKI, A., 1989. Sulfur isotopic ratios of the magnetite-series and ilmenite-series granitoids of the Sierra Nevada batholith - A reconnaissance study. Geology, V. 17, pp. 788-791.

JACOBS, D.C. and PARRY, W.T., 1974. Geochemistry of biotite in the Santa Rita stock and its associated potassic and phyllic alteration zones, Central Mining District, Grant County, New Mexico. (Abstract) Geological Society of America, Abstracts with Programs, V. 6, p. 809.

JACOBS, D.C. and PARRY, W.T., 1979. Geochemistry of biotite in the Santa Rita porphyry copper deposit, New Mexico. Economic Geology, V. 74, pp. 860-887.

JAEGER, J.C., 1968. Cooling and Solidification of Igneous Rocks. *In*: Hess, H.H. and Poldervaart, A. (Editors), Basalts, The Poldervaart Treatise on Rocks of Basaltic Composition, V. 2, Interscience Publishers. pp. 503-535.

JAFFEY, A.H., FLYNN, K.F., GLENDENIN, L.E., BENTLEY, W.C. and ESSLING, A.M., 1971. Precision measurements of the half-lives and specific activities of $^{235}U$ and $^{238}U$. Physical Review, V. 4, pp. 1889-1906.

JAMES, D.E., 1971. Plate tectonic model for the evolution of the central Andes: Geological Society of America Bulletin, V. 82, pp. 3325-3346.

JAMES, D.E., 1971b. Andean crustal and upper mantle structure. Journal of Geophysical Research, V. 76, pp. 3246-3271.

JAMES, D.E., BROOKS, C. AND CUYUBAMBA, A., 1975. Early evolution of the central Andean volcanic arc. Carnegie Institution Washington Yearbook, 74, pp. 247-250.

JARRARD, R.D., 1986. Relationships among subduction parameters. Reviews of Geophysics, V. 24, pp. 217-284.

JARRELL, O.W., 1944. Oxidation at Chuquicamata, Chile. Economic Geology, V. 39, No. 4, pp. 251-286.

JESINKEY, C., FORSYTHE, R.D., MPODOZIS, C. and DAVIDSON, J., 1987. Concordant late Paleozoic paleomagnetization from the Atacama Desert: Implications for tectonic models of the Chilean Andes. Earth and Planetary Science Letters, V. 87, pp. 461-472.

JICA-MMAJ-SERNAGEOMIN, 1986. Informe de estudios básicos sobre la exploración de recursos minerales del área al sur de Antofagasta, de la República de Chile. Fase I, (Unpublished report), 157 p.

JONES, D.L., COX, A., CONEY, P.J. and BECK, M., 1982. The growth of western North America. Scientific American, V. 247, pp. 70-84.

JORDAN, T.E., ISACKS, B.L., ALLMENDINGER, R.W., BREWER, J.A., RAMOS, V.A. and ANDO, C.J., 1983. Andean tectonics related to geometry of subducted Nazca plate. Geological Society of America Bulletin, V. 94, pp. 341-361.

JORDAN, T.E. and ALONSO, R.N., 1987. Cenozoic stratigraphy and basin tectonics of the Andes mountains, 20°-28°S. The American Association of Petroleum Geologists Bulletin, V. 71, No. 1, pp. 49-64.

JORDAN, T.E. and GARDEWEG, M., 1989. Tectonic evolution of the Late Cenozoic Central Andes (20°-33°S). *In*: Ben-Avraham, Z. (Editor), The evolution of the Pacific Ocean Margins, Oxford Monographs on Geology and Geophysics No.8, pp. 193-205.

JURGAN, V.H., 1974. Die marine kolkfolge der unterkreide in der quebrada El Way-Antofagasta, Chile. Geol. Rundschau, V. 63, pp. 490-516.

KAY, R.W., 1980. Volcanic arc magmas: Implications of a melting-mixing model for element recycling in the crust-upper mantle system. The Journal of Geology, V. 88, pp. 497-521.

KAY, R.W., SUN, S.-S. and LEE-HU, C.N., 1978. Pb and Sr isotopes in volcanic rocks from the Aleutians Islands and Pribilof Islands, Alaska, Geochimica and Cosmochimica Acta, V. 42, pp. 263-273.

KAY, S.M., MAKSAEV, V., MOSCOSO, R., MPODOZIS, C. and NASI, C., 1987. Probing the evolving Andean lithosphere: Mid-Late Tertiary magmatism in Chile (29°-30°30') over the modern zone of subhorizontal subduction. Journal of Geophysical Research, V. 92, N°B7, pp.6173-6189.

KAY, S.M., MAKSAEV, V., MOSCOSO, R., MPODOZIS, C., NASI, C. and GORDILLO, C.E., 1988. Tertiary Andean magmatism in Chile and Argentina between 28° and 33° S: Correlation of magmatic chemistry with a changing Benioff zone, Journal of South American Earth Sciences, V. 1, No.1, pp. 21-38.

KAY, S.M., RAMOS, V. A., MPODOZIS, C. and SRUOGA, P., 1989. Late Paleozoic to Jurassic silicic magmatism at the Gondwana margin: Analogy to the Middle Proterozoic in North America?, Geology, V. 17, pp. 324-328.

KAY, S.M. and KAY, R.W., 1989. Aleutian magmatism in space and time, *In*: Plafker, G. and Jones, D.L. (Editors), Cordilleran Orogen, Alaska, Decade of North American Geology, Geological Society of America (in press).

KAY, S.M., MPODOZIS, C., RAMOS, V.A. and MUNIZAGA, F., 1990. Magma source variations for mid to late Tertiary volcanic rocks erupted over a shallowing crust in the main Andean Cordillera (28°-33°S.). *In*: Harmon, R.S. (Editor) Andean Magmatism, Special Publication Geological Society of America (in press).

KLINIC, I.A. and BURNHAM, C.W., 1972. Partitioning of chloride between a silicate melt and coexisting aqueous phase from 2 to 8 kilobars. Economic Geology, V. 67, pp. 231-235.

KLOHN, E., 1961. Yacimientos de cobre y uranio en el distrito minero de Tocopilla, B.Sc. thesis, Depto. Geol. U. de Chile, 149 p.

KLOHN, W., 1972. Hidrografía de las zonas desérticas de Chile. (Unpublished) Programa de las Naciones Unidas para el Desarrollo. Santiago, 188 p.

KRAUSKOPF, K.B., 1979. Source rocks for metal-bearing fluids. In. Barnes, H.L1., (Editor), Geochemistry of hydrothermal ore deposits. Holt, Rinehart and Winston, Inc., pp. 1-33.

KULM, L.D., SCHWELLER, W.J. and MASIAS, A., 1977. A preliminary analysis of the subduction processes along the Andean Continental Margin, 6° to 45° S. *In*: Talwani, M. and Pitman, W.W. (Editors), Problems in the evolution of island-arcs, deep sea trenches and back-arc basins. American Geophysical Union, Maurice Ewing Series.

KUNTZ, J., 1928. Monografía minera de la provincia de Antofagasta. SONAMI, Santiago, Chile, 77 p.

LAHARIE, R., 1976. Recherches géomorphologiques sur le néogene du sud Pérou. Bulletin Institut Français d'Etudes Andins, V. 5, pp. 1-2, 9-37.

LAHSEN, A., 1969. Geología del área comprendida entre el Tatio y los cerros de Aiquina. (Unpublished report), Comité Geotérmico, CORFO, 75 p.

LAHSEN, A. and MUNIZAGA, F., 1979. Nuevos antecedentes cronológicos del volcanismo Cenozoico Superior de los Andes del Norte de Chile, entre los 19°00' y los 22°30' Lat.S. Actas II Congreso Geológico Chileno, Arica, Chile, V. 1, pp. F61-F82.

LARSON, R.L., and PITMAN, W.C., 1972. World-wide correlation of Mesozoic magnetic anomalies and its implications. Geological Society of America Bulletiun, V. 83, pp. 3645-3662.

LASLETT, G.M., KENDALL, W.S., GLEADOW, A.J.W. AND DUDDY, I.R., 1982. Bias in measurement of fission-track length distributions. Nuclear Tracks, V. 6, No 2/3, pp. 79-85.

LASLETT, G.M., GLEADOW, A.J.W.and DUDDY, I.R., 1984. The relationships between track length and track density in apatite. Nuclear Tracks, V. 9, No 1, pp. 29-38.

LASLETT, G.M., GREEN, P.F., DUDDY, I.R., AND GLEADOW, A.J.W., 1987. Thermal annealing of fission tracks in apatite: 2. a quantitative analysis. Chemical Geology (Isotope Geoscience Section), V. 65, pp. 1-15.

LAUBACHER, G., BOUCOT, A.J. and GRAY, J., 1982. Additions to Silurian stratigraphy, lithofacies, biostratigraphy and paleontology of Bolivia and southern Peru. J. Paleont., V. 56, pp. 1158-1170.

LAUBACHER, G. and MEGARD, F., 1985. The Hercynian basement: a review. *In* Pitcher, W.S. (Editor), Magmatism at a plate edge. The Peruvian Andes, Blakie, Glasgow and Halsted Press, New York, pp. 29-35.

LAUGHLIN, A.W., DAMON, P.E. and WATSON, B.N., 1968. Potassium-Argon dates from Toquepala and Michiquillay, Peru. Economic Geology, V. 63, pp. 166-168.

LEVI, B., 1969. Burial metamorphism of a Cretaceous volcanic sequence west from Santiago, Chile. Contributions to Mineralogy and Petrology, V. 24, pp. 30-49.

LEVI, B., 1970. Burial metamorphic episodes in the Andean Geosyncline, Central Chile. Geologische Rundschau, V. 59, pp. 994-1013.

LEVI, B. and CORVALAN, J., 1964. Metamorfismo regional en las rocas volcánicas del geosinclinal andino. Revista Minerales, N°86, Santiago, Chile, pp. 6-15.

LEVI, B. and CORVALAN, J., 1968. Espesor y distribución de los depósitos del geosinclinal andino en Chile central. Revista Minerales, N°101, Santiago, Chile, pp. 13-15.

LEVI, B., AGUIRRE, L., NYSTROM, J.O., PADILLA, H. and VERGARA, M., 1989. Low-grade regional metamorphism in the Mesozoic-Cenozoic volcanic sequences of Central Andes. J. Metamorphic Geol., V. 7, pp. 487-495.

LINDGREN, W., 1922. A suggestion for the terminology of certain mineral deposits. Economic Geology, V. 17, pp. 202-294.

LINDGREN, W., 1933. Mineral Deposits, Mc Graw-Hill, New York.

LLAUMET, C., 1979. Evaluación geológica del distrito minero El Guanaco, II Región, Chile. (Unpublished report), ENAMI, 49 p. (Rol N° 2389).

LOPEZ, M.V., 1939. The primary mineralization at Chuquicamata, Chile, S.A., Economic Geology, V. 34, N°6, pp. 674-711.

LOPEZ, M.V., 1942. Chuquicamata, Chile. In: Newhouse, W.H. (Ed.), Ore deposits as related to structural features. Princeton University Press, N.J., pp. 126-128.

LOPEZ-ESCOBAR, L., FREY, F.A. and VERGARA, M., 1977. Andesites and high-alumina basalts from the Central-South Chile High Andes: Geochemical evidence bearing on their petrogenesis. Contributions to Mineralogy and Petrology, V. 63, pp. 199-228.

LOPEZ-ESCOBAR, L., VERGARA, M. and FREY, F.A., 1981. Petrology and geochemistry of lavas from Antuco Volcano, a basaltic volcano of the Southern Andes (37°25'S). Journal of Volcanology and Geothermal Research, V. 11, pp. 329-352.

LOPEZ-ESCOBAR, L., 1982. Caracteristicas geoquímicas de rocas ígneas asociadas con pórfidos cupríferos chilenos. Revista Geológica de Chile, No.17, pp. 3-19.

LOPEZ-ESCOBAR, L., 1984. Petrology and chemistry of volcanic rocks of the Southern Andes. *In*: Harmon, R.S. and Barreiro, B.A. (Editors), Andean Magmatism, Chemical and Isotopic Constraints, Shiva Publishing Limited, England, pp. 47-71.

LOSERT, J., 1973. Genesis of copper mineralization and associated alterations in the Jurassic volcanics rocks of Buena Esperanza mining area. Publicación N°40, Depto. de Geología, Univ. de Chile, 104 p. Santiago.

LOSERT, J., 1974. Alteration and associated copper mineralization in the Jurassic volcanic rocks of Buena Esperanza mining area (Antofagasta Province, Northern Chile). *In* Klohn E. (Editor), Coloquio sobre fenómenos de alteración y metamorfismo en rocas volcánicas e intrusivas, pp. 51-85.

LOWELL, J.D., 1987. Curso de exploración geológico minera, aspectos prácticos. (Unpublished), Depto. de Geología y Geofísica, Univ. de Chile.

LOWELL, J.D., and GUILBERT, J.M. 1970. Lateral and vertical alteration--mineralization zoning in porphyry ore deposits: Econ. Geol., V. 65, pp. 373-408.

LYON-CAEN, H., MOLNAR, P. and SUAREZ, G., 1985. Gravity anomalies and flexure of the Brazilian Shield beneath the Bolivian Andes. Earth Planettary Science Letters, V. 75, pp. 81-92.

MAALOE, S. and WILLIE, P.J., 1975. Water content of a granite magma deduced from the sequence of crystallization determined experimentally with water undersaturated conditions. Contributions to Mineralogy and Petrology, V. 52, pp. 175-191.

MACELLARI, C.E., 1988. Cretaceous paleogeography and depositional cycles of western South America. Journal of South American Earth Sciences, V. 1, pp. 373-418.

MAKSAEV, V., 1978. Cuadrángulo Chitigua y sector occidental del cuadrángulo Cerro Palpana. Región de Antofagasta. Carta Geológica de Chile N°31, Instituto de Investigaciones Geológicas. Santiago, 55 p.

MAKSAEV, V., 1979. Las Fases Tectónicas Incaica y Quechua en la Cordillera de los Andes del Norte Grande de Chile. Actas II Congreso Geológico Chileno, Arica, V. 1, pp. B63-B77.

MAKSAEV, V. and MARINOVIC, N., 1980. Cuadrángulos Cerro de la Mica, Quillagua, Cerro Posada y Oficina Prosperidad, Región de Antofagasta. Carta Geológica de Chile, N°45-48, Instituto de Investigaciones Geológicas, Santiago, 63 p.

MAMMERICKX, J., HERRON, E. AND DAMON, L., 1980. Evidence for two fossil spreading ridges in the southeast Pacific. Geological Society of America Bulletin, Part I, V. 91, pp. 263-271.

MANN, P., HEMPTON, M.R., BRADLEY, D.C. and BURKE, K., 1983. Development of pull-apart basins. Journal of Geology, V. 91, pp. 529-554.

MARCH, W., 1931. Report on El Inca silver-lead district. (Unpublished report), Chile Exploration Co., 12 p., SERNAGEOMIN Archive N° 3452.

MARCH, W.S., 1935. Ore deposits at Potrerillos, Chile. XVI International Geological Congress, Copper Resources of the World, Washington D.C., V. 2., pp. 485-500.

MARCH, W., and ZEIHEN, L., 1948. Report on Scouting examination of San Miguel copper prospect, near Calama, Prov. of Antofagasta, Chile. (Unpublished report), Chile Exploration Co., 15 p., SERNAGEOMIN Archive N° 3469.

MARIN, C., 1973. Petrografía, alteración y mineralización del yacimiento cuprífero Exótica, provincia de Antofagasta. B.Sc. thesis, Depto. de Geología, Univ. de Chile, 120 p., Santiago.

MARINOVIC, N., 1979. Geología de los cuadrángulos Zapaleri y Nevados de Poquis, II Región, Antofagasta. B.Sc. thesis, Depto. Geología, Univ. de Chile, 75 p., Santiago.

MARINOVIC, N. and LAHSEN, A., 1984. Hoja Calama, Región de Antofagasta, Carta Geológica de Chile, N°58, 139 p., SERNAGEOMIN, Santiago.

MARQUILLAS, R.A. and SALFITY, J.A., 1988. Tectonic framework and correlations of the Cretaceous-Eocene Salta Group; Argentina. *In*: Bahlburg, H., Breitkreuz, C. and Giese, P. (Editors), The Southern Central Andes, Lecture Notes in Earth Sciences, V. 17, Springer-Verlag Berlin-Heidelberg, pp. 119-136.

MARSH, B.D., 1976. Mechanism of Benioff zone magmatism. American Geophysical Union, Monograph 19, pp. 337-350.

MARSH, B.D., 1978. On the cooling of ascending andesitic magma. Philosophical Transactions, Royal Society of London, Ser. A, V. 288, pp. 611-625.

MARTINEZ, R., 1978. Hallazgo de Mioceno marino en la Península de Mejillones, Antofagasta, Chile. II Congreso Argentino de Paleontología y Bioestratigrafía-I Congreso Latinoamericano de Paleontología, 28 p., Buenos Aires.

McDOUGALL, J.D., 1976. Fission-track dating. Scientific American, V. 235, No 6, pp. 114-122.

McDOUGALL, I. and HARRISON, T.M., 1988. Geochronology and thermochronology by the $^{40}Ar/^{39}Ar$ method. Oxford Monographs on Geology and Geophysics, N°9, Oxford University Press, New York, Clareton Press, Oxford, 212 p.

McKEE, E.H. and NOBLE, D.C., 1982. Miocene volcanism and deformation in the western Cordillera and high plateaus of south-central Peru. Geological Society of America Bulletin, V. 93, pp. 657-662.

McMILLAN, N.J., HARMON, R.S., MOORBATH, S., LOPEZ-EZCOBAR, L. and STRONG, D.F., 1989. Crustal sources involved in continental arc magmatism: A case study of volcan Mocho-Choshuenco, southern Chile, Geology, V. 17, pp. 1152-1156.

McMILLAN, W.J. and PANTELEYEV, A., 1980. Ore Deposits Models- 1. Porphyry Copper Deposits. Geoscience Canada, V. 7, No.2, pp. 52-63.

MEGARD, F., 1984. The Andean orogenic period and its major structures in central and northern Peru. Journal of the Geological Society of London, V. 141, pp. 893-900.

MEGARD, F., 1987. Cordilleran Andes and Marginal Andes: a review of Andean geology north of the Arica elbow (18°S). *In*: Monger, J.W.H. and Francheteau, J. (Editors), Circum-Pacific orogenic belts and evolution of the Pacific Ocean basin. American Geophysical Union - Geological Society of America, Geodynamic Series, V. 18, pp. 71-95.

MEGARD, F., 1989. The evolution of the Pacific Ocean Margin in South America north of Arica Elbow (18°S). *In*: Ben-Avraham, Z. (Editor), The evolution of the Pacific Ocean Margins, Oxford Monographs on Geology and Geophysics, No.8, pp. 208-230.

MEGARD, F., NOBLE, D.C., McKEE, E.H. and BELLON, H., 1984. Multiple pulses of Neogene compressive deformation in the Ayacucho intermontane basin, Andes of central Peru. Geological Society of America Bulletin, V. 95, pp. 1108-1117.

MEIJER, A., 1976. Pb and Sr isotopic data bearing on the origin of volcanic rocks from the Mariana island arc system. Geological Society of America Bulletin, V. 87, pp. 1358-1369.

MERRIHUE, C., 1965. Trace element determination and potassium-argon dating by mass spectrometry of neutron irradiated samples. (Abstract) Transactions American Geophysical Union, V. 46, p. 125.

MERRIHUE, C. and TURNER, G., 1966. Potassium-Argon dating by activation with fast neutrons. Journal of Geophysical Research, V. 71, N$^0$ 11, pp. 2852-2857.

MILLER, J.F. and HARRIS, N.B.W., 1989. Evolution of continental crust in the Central Andes; constraints from Nd isotope systematics. Geology, V. 17, pp. 615-617.

MINGRAMM, A., RUSSO, A., POZZO, A. and CAZAU, L., 1979. Sierras Subandinas. *In*: Segundo Simposio de Geología Regional Argentina, Academia Nacional de Ciencias, Cordoba, Argentina, V. 1, pp. 95-138.

MIRANDA, J., 1982. Prospección geológica de yacimientos de tipo pórfido cuprífero en el área de Puno-Pinchal, Segunda Región, Antofagasta. B.Sc. Thesis, Depto. Geología, Univ. Chile.

MIRANDA, J., 1986. Prospección geológica de yacimientos de tipo pórfido cuprífero en el área de Puno-Pinchal, Segunda Región, Antofagasta. (Abstract) Comunicaciones N°36, Depto. Geología, Univ. de Chile, pp. 54-55.

MITCHELL, A.H.G., 1973. Metallogenic belts and angle of dip of Benioff Zones. Nature Phys. Sci., V. 245, pp. 49-52.

MITCHELL, A.H.G and GARSON, M.S., 1972. Relationship of porphyry copper and circum-Pacific tin deposits to palaeo-Benioff zones. Trans. Inst. Min. Metal., Section B, pp. B10-B25.

MOLNAR, P., 1986. The structure of mountain ranges. Scientific American, V. 255, No. 1, pp. 70-79.

MONTAÑO, J.M., 1976. Estudio geológico de la zona de Caracoles y áreas vecinas, con énfasis en el Sistema Jurásico, Provincia de Antofagasta, II Región, Chile. Ph.D. thesis, Depto. Geol., Univ. de Chile, 169 p., Santiago.

MOORE, J.C., BYRNE, T., PLUMLEY, P.W., REID, M., GIBBONS, H. and COE, R.S., 1983. Paleogene evolution of the Kodiak Islands, Alaska: consequences of ridge-trench interactions in a more southerly latitude. Tectonics, V. 2, N°3, pp. 265-293.

MORAGA, A., CHONG, G., FORTT, M.A. and HENRIQUEZ, H., 1974. Estudio geológico del Salar de Atacama, Provincia de Antofagasta. Boletín N°29, Instituto de Investigaciones Geológicas, 50 p. Santiago.

MORRIS, J.D. and HART, S.R., 1983. Isotopic and incompatible element constraints on genesis of island arc volcanics from Cold Bay and Amak Islands, Aleutians, and implications for mantle structure. Geochimica et Cosmochimica Acta, V. 47, pp. 2015-2030.

MORRIS, J. and TERA, F., 1989. $^{10}Be$ and $^{9}Be$ in mineral separates and whole rocks from volcanic arcs: Implications for sediment subduction. Geochimica et Cosmochimica Acta, V. 53, pp. 3197-3206.

MORRIS, J., HARMON, R.S., TERA, F., LOPEZ-ESCOBAR, L., KLEIN, J. and MIDDLETON, R., 1987. $^{10}Be$, Sr, O and Pb isotope evidence for sediment subduction in the Southern Andes. *In*: Munizaga, F. (Editor), Proceedings International Symposium Magmatic Evolution of the Andes.

MORTIMER, C., 1973. The Cenozoic history of the southern Atacama desert, Chile. Journal of the Geological Society, London, V. 129, pp. 505-526.

MORTIMER, C., 1980. Drainaje evolution of the Atacama desert of northernmost Chile. Revista Geológica de Chile, N°11, Santiago, pp. 3-28.

MORTIMER, C., FARRAR, E. and SARIC, N., 1974. K-Ar ages from Tertiary lavas of the northernmost Chilean Andes. Geologische Rundschau, V. 63, pp. 484-490.

MORTIMER, C. and SARIC, N., 1972. Landform evolution in the coastal region of Tarapacá Province, Chile. Révue de la Géomorphologie Dynamique, V,21, pp. 162-170.

MORTIMER, C. and SARIC, N., 1975. Cenozoic studies in northernmost Chile. Geol. Rundschau, B, V. 64, pp. 395-420.

MORTIMER, C., MUNCHMEYER, C. and URQUETA, I., 1977. Emplacement of the Exotica orebody, Chile. Trans. Inst. Mining and Metall., Sect. B., pp. B121-B127.

MORTIMER, C., MUNCHMAYER, C. AND URQUETA, I., 1978. Emplazamiento del yacimiento Exótica, Chile, Rev. Geol. Chile, N°6, p. 41-51, Santiago.

MOSCOSO, R. and MPODOZIS, C., 1988. Estilos estructurales en el Norte Chico de Chile (28-31°S), Regiones de Atacama y Coquimbo. Revista Geológica de Chile, V. 15, N°2, pp. 151-166.

MPODOZIS, C., 1984. Dinámica de los márgenes continentales activos. *In*: Seminario Actualización de la Geología de Chile, Apuntes, Miscelanea N°4, SERNAGEOMIN, Santiago, Chile, pp. A1-A22.

MPODOZIS, C., HERVE, F., DAVIDSON, J. and RIVANO, S., 1983. Los granitoides de Cerros de Lila, manifestaciones de un episodio intrusivo y termal del Paleozoico Inferior en los Andes del Norte de Chile. Revista Geológica de Chile N°18, pp. 3-14, Santiago.

MPODOZIS, C. and RAMOS, V., (in press). The Andes of Chile and Argentina. *In*: Symposium on the Geology of the Andes and its Relation to Hydrocarbon and Mineral Resources, Earth Sciences Series. Held in Santiago, Chile, 1985.

MUKASA, S.B., 1986. Common Pb isotopic compositions of the Lima, Arequipa and Toquepala segments in the Coastal batholith, Peru: Implications for magmagenesis. Geochimica et Cosmochemica Acta, V. 50, pp. 771-782.

MUNCHMEYER, C. and URQUETA, I., 1974. Geología del yacimiento Exótica. In Klohn, E. (Editor), Coloquio sobre fenómenos de alteración y metamorfismo en rocas volcánicas e intrusivas. Publ. N°41, Depto. Geol. U. de Chile, pp. 213-253, Santiago.

MUNIZAGA, F. and MARINOVIC, N., 1979. Evidencias preliminares de un volcanismo Cenozoico Superior shoshonítico en el área del volcán Zapaleri, II Región Chile. Actas II Congreso Geológico Chileno, V. 3, Arica, Chile, pp. E237-E255.

MUNIZAGA, F., HUETE, C. and HERVE, F., 1985. Geocronología K-Ar y razones iniciales $^{87}Sr/^{86}Sr$ de la "Franja Pacífica" de "Desarrollos Hidrotermales". Actas IV Congreso Geológico Chileno, V. 4, pp. 357-379.

MUÑOZ, J., 1942. El mineral de Gatico. (Unpublished report), ENAMI, 32 p. (Rol N° 2020), SERNAGEOMIN Archive, Santiago, Chile.

MUÑOZ, J. and STERN, C.R., 1988. The Quaternary volcanic belt of the southern continental margin of South America: transvers structural and petrochemical variations across the segment 38°S and 39°S. Journal of South American Earth Sciences, V. 1, pp. 147-162.

MUÑOZ-CRISTI, J., 1950. Geología de Chile. *In*: Geografía Económica de Chile, Corporación de Fomento de la Producción, Santiago Chile, 1950, V. 1, pp. 55-187.

MUÑOZ-CRISTI, J., 1956. Chile. *In*: Handbook of South American Geology, Geological Society of America, Memoir 65, pp. 187-214.

MYERS. J.S., 1976. Erosion surfaces and ignimbrite eruption, measures of Andean uplift in northern Peru. Geological Journal, V. 11, Pt.1, pp. 29-44.

NAESER, C.W., 1967. The use of apatite and sphene for fission track age determinations. Geological Society of America Bulletin, V. 78, pp. 1523-1526.

NAESER, C.W., 1976. Fission track dating; theory and laboratory procedures. U.S. Geological Survey, Open File Report, 76-190.

NAESER, C.W. and FAUL, H., 1969. Fission track annealing in apatite and sphene. Journal of Geophysical Research, V. 74, pp. 705-710.

NAESER, C.W. and FORBES, R.B., 1978. Variation of fission track ages with depth in two deep drill holes. (Abstract) EOS. Transactions American Geophysical Union, V. 57, p. 353.

NANEY, M.T., 1983. Phase equilibria of rock-forming ferromagnesian silicates in granitic systems. American Journal of Science, V. 283, pp. 993-1033.

NANEY, M.T. and SWANSON, S.E., (1980). The effect of Fe and Mg on crystalllization in granitic systems. American Mineralogist, V. 65, pp. 639-658.

NARANJO, J.A., 1978. Geología del cuadrángulo El Salado, Región de Atacama. B.Sc. thesis, Depto. de Geología, Univ. de Chile, 117 p.

NARANJO, J.A., 1987. Interpretación de la actividad cenozoica superior a lo largo de la Zona de Falla Atacama, norte de Chile. Revista Geológica de Chile, N°31, pp. 43-56.

NARANJO, J.A. and PASKOFF, R., 1981. Estratigrafía de los depósitos cenozoicos de la región de Chiu-Chiu Calama, Desierto de Atacama, Revista Geológica de Chile N°13-14, Santiago, pp. 78-85.

NARANJO, J.A. and PUIG, A., 1984. Hojas Taltal y Chañaral, Regiones de Antofagasta y Atacama. Carta Geológica de Chile, N°62-63, SERNAGEOMIN, 140 p., Santiago.

NARANJO, J.A., HERVE, F., PRIETO, X. and MUNIZAGA, F., 1984. Actividad cretácica de la falla de Atacama al este de Chañaral; milonitización y plutonismo. Comunicaciones, N°34, pp. 57-66, Depto. Geología, Univ. de Chile.

NEUMANN, H., 1973. Mineralizaciones tipo cobre porfidico en Chile. Revista Geológica de Chile, N°1, pp. 67-73.

NEWMAN, A.C.D., 1970. The synergetic effect of hydrogen ions on the cation exchange of potassium in micas. Caly Minerals, V. 8, pp. 361-373

NICHOLS, I.A. and HARRIS, K.L., 1980. Experimental rare earth element partition coefficients for garnet, clinopyroxene and amphibole coexisting with andesitic and basaltic liquids. Geochimica et Cosmochimica Acta, V. 44, pp. 287-308.

NIEMEYER, H., URZUA, F., ACEÑOLAZA, F. and GONZALEZ, C., 1985. Progresos recientes en el conocimiento del Paleozoico de la Región de Antofagasta. Actas IV Congreso Geológico Chileno, V. 1, pp. 1-410-1-438, Antofagasta.

NISTERENKO, G.V., LOSERT, J., CHAVEZ, L. and NAUMOV, V.B., 1973. Temperaturas y presiones de formación de algunos yacimientos cupríferos de Chile. Revista Geológica de Chile, N°1, pp. 74-84.

NOBLE, D.C., McKEE, E.H., FARRAR, E., and PETERSEN, U., 1974. Episodic Cenozoic volcanism and tectonism in the Andes of Peru. Earth and Planetary Science Letters, V. 21, pp. 213-220.

NOBLE, D.C., McKEE, E.H. and MEGARD, F., 1978. Eocene uplift and unroofing of the coastal batholith near Lima, Central Peru. Journal of Geology, V. 86, pp. 403-405.

NOBLE, D.C., FARRAR, E. and COBBING, E.J., 1979. The Nazca Group of south-central Peru: Age, source and regional volcanic and tectonic significance. Earth and Planetary Science Letters, V. 45, pp. 80-86.

NORTON, D., 1978. Source-lines, source-regions, and pathlines for fluids in hydrothermal systems related to cooling plutons. Economic Geology, V. 73, pp. 21-28.

NUR, A. and BEN-AVRAHAM, Z., 1977. Lost Pacifica continent. Nature, V. 270, pp. 41-43.

NUR, A. and BEN-AVRAHAM, Z., 1981. Volcanic gaps and the consumption of aseismic ridges in South America. Geological Society of America, Memoir 154, pp. 729-740.

NUR, A. and BEN-AVRAHAM, Z., 1982. Oceanic plateaus, the fragmentation of continents, and mountain building. Journal of Geo[hysical Research, V. 87, pp. 3644-3661.

NUR, A. and BEN-AVRAHAM, Z., 1983. Displaced terranes and mountain building. *In*: Hsu, K.J. (Editor), Mountain building processes, London Academic Press, pp. 73-84.

OFFICER, H.G., 1922. Sulphur resources of Chile. Engineering and Mining Journal Press, New York.

OHMOTO, H. and KERRICK, D.M., 1977. Devolatilization equilibria in graphitic systems. Am. Jour. Sci., V. 277, pp. 1013-1044.

OJEDA, J.M., 1986. Escondida porphyry copper deposits, II Region Chile; exploration drilling and current geological interpretation. *In*: Papers presented at the Mining Latin America/Mineria Latinoamericana conference. (Smale Adams, K.B., Chairperson). Inst. Min. and Metall, London, United Kingdom, Meeting: Nov. 17-19, 1986. Santiago, Chile, pp. 229-318.

OLSON, 1989. The stratigraphic and structural setting of the Potrerillos porphyry copper district, Northern Chile. Revista Geologica de Chile, V. 16, N°1, pp. 3-30.

ORQUERA, W., 1987. Geología y geoquímica de alteración en el "Area de Superficie" de la mina de cobre Buena Esperanza, Chile. B.Sc. thesis, Depto. Geociencias, Universidad del Norte, Antofagasta, 221p.

ORTIZ, F., 1969. Informe geológico de la mina copucha, distrito minero de Sierra Gorda, Prov. de Antofagasta, Chile. (Unpublished report), ENAMI, 10 p., (Rol N° 22314).

OSORIO, R. and RIVANO, S., 1985. Paparchitidae (Ostracoda) del Paleozoico Superior en la Formación Pular (Harrington, 1961), Quebrada Pajonales, vertiente occidental de la Sierra de Almeyda, Antofagasta. Actas IV Congreso Geológico Chileno, V. 1, Area 1, pp. 439-457.

OYARZUN, J., 1974. Metallogenesis and volcanism in Chile: A review. In: Gonzalez-Ferrán, O. (Editor). Proceedings of the Symposium on Andean and Anctartic Volcanology Problems. (September 1974). IAVCEI Special Series, Printed by S. Tipografico F. Giannini & Figli, Napoli, Italy (1976), pp. 659-669.

OYARZUN, J., 1985. La metallogenie andine: cadre geologique, petrologique et geochimique et essai d'interpretation. Doctoral Thesis, Universite de Paris-Sud, Centre D'Orsay, France, 864 p.

OYARZUN, J., 1985b. Magmatismo y metalogénesis andina en Chile. *In*: Frutos, J., Oyarzun, R. and Pincheira, M. (Editors), Geología y Recursos Minerales de Chile. Editorial de la Univ. de Concepción, pp. 441-468.

OYARZUN, J. and FRUTOS, J., 1974. Porphyry copper and tin-bearing porphyries a discusion of genetic models. Physics of the Earth and Planetary Interiors, V. 9, pp. 259-263.

OYARZUN, J. and FRUTOS, J. 1980. Metallogenesis and porphyry deposits of the Andes (Southeastern Pacific Region) Mémoire du BRGM N°106. Colloque C.1, Resources minerales, Bureau de Recherches Geologiques et Minieres, pp. 50-62.

PACCI, D., HERVE, F., MUNIZAGA, F., KAWASHITA, K. and CORDANI, V., 1980. Acerca de la edad Precámbrica de la Formación Esquistos de Belén, Depto. de Parinacota, Chile, Revista Geológica de Chile, N°11, pp. 43-50.

PALACIOS, C., 1973. La zona de contacto del intrusivo granítico de Tocopilla con la formación volcánica La Negra y su influencia en la mineralización. B.Sc. thesis, Depto. Geología, Univ. de Chile, Santiago.

PALACIOS, C., 1977. Metamorfismo regional en rocas volcánicas jurásicas en el norte de Chile. Estudios Geológicos, V. 33, pp. 11-16, Spain.

PALACIOS, C., 1978. The Jurassic Paleovolcanism in Northern Chile. Dissertation submitted to Eberhard-Karls-Universtat zu Tubingen, 99 p.

PALACIOS, C., 1982. Volcanismo Jurásico en el sector sur de los Andes Centrales (22°-26° S), Chile. Actas Quinto Congreso Latinoamericano de Geología, V. 2, p. 83-96, Argentina.

PALACIOS, C., 1986. Subvolcanic Cooper deposits in the Coastal Range of Northern Chile. Zentralblatt für Geologie und Paläontologie, Teil I, 1985, H.9/10, Stuttgart, Juni 1986, pp. 1605-1615.

PALACIOS, C. and DEFINIS, A., 1981. Petrología del yacimiento Buena Esperanza, II Región, Norte de Chile. Actas Primer Coloquio sobre volcanismo y metalogénesis, Depto. Geociencias, Univ. del Norte, Antofagasta, pp. 48-67.

PALACIOS, C. and DEFINIS A., 1981b. Geología del yacimiento estratiforme Susana, distrito Michilla, Antofagasta. Actas Primer Coloquio sobre volcanismo y metalogénesis, Depto. Geociencias, Univ. del Norte, Antofagasta, pp. 82-91.

PALACIOS, C. and ESPINOZA, S., 1982. Geología y Petrología del Complejo Plutónico de la Cordillera de la Costa entre Tocopilla y el río Loa, norte de Chile. Actas III Congreso Geológico Chileno, V. 2, pp. D154-D171.

PALMER, A.R., 1983. The Decade of North American Geology 1983 Geologic Time Scale. Geology, V. 11, pp. 503-504.

PARADA, M.A., ARACENA, I. and TANAKA, H., 1987. The petrology of the Chuquicamata Plutonic Complex, Chile. Journal of the Japanese Association of Mineralogists, Petrologists and Economic Geologists, V. 82, pp. 177-188.

PARDO-CASAS, F. AND MOLNAR, P., 1987. Relative motions of the Nazca (Farallon) and South American plates since Late Cretaceous time. Tectonics, V. 6, N°3, pp. 233-248.

PARK, C.F. Jr., 1961. A magnetite "flow" in Northern Chile. Economic Geology, V. 56, pp. 431-441.

PARRISH, R.R., 1983. Cenozoic thermal evolution and tectonics of the Coast Mountains of British Columbia. 1. Fission track dating, apparent uplift rates, and patterns of uplift. Tectonics, V. 2, No 6, pp. 601-631.

PARSONS, A.B., 1933. The porphyry coppers. Amer. Inst. Min. Metall. and Petroleum Engineers, Rocky Mountains Fund Ser., New York, 581 p.

PARSONS, A.B., 1957. The porphyry coppers in 1956. Amer. Inst. Min. Metall. and Petroleum Engineers, Rocky Mountains Fund Ser., New York, 270 p.

PEARCE, J.A., 1983. Role of the sub-continental lithosphere in magma genesis at active continental margins. *In*: Hawkesworth, C.J. and Norry, M.J., (Editors), Continental basalts and mantle xenoliths, Shiva Publishing Limited, England, pp. 230-249.

PEÑA Y LILLO, O., 1927. Breve reseña sobre la minería en Chile. Boletín de la Sociedad Nacional de Minería, Santiago, V. 39, pp. 702-722.

PERELLO L.J. and MULLER, M.G., 1984. El horst de Sierra Castillo en la Cordillera de Domeyko, al occidente del Salar de Pedernales: sus fallas límites Barracas y Sierra Castillo. Comunicaciones No. 34, Depto. de Geología, Univ. de Chile, Santiago, pp. 47-55.

PEREZ D'ANGELO, E., 1983. Estado actual del conocimiento del Cambro-Ordovícico de Latino America, Segunda reunión del Grupo Internacional, Cartagena de Indias, Colombia, International Geological Correlation Program (IGCP), pp. 88-97.

PERFIT, M.R. and KAY, R.W., 1986. Comment on "Isotopic and incompatible element constraints on the genesis of island arc volcanics from Cold Bay and Amak Islands, Aleutians, and implications for mantle structure" by J.D. Morris and S.R. Hart. Geochemica et Cosmochemica Acta, V. 50, pp. 477-481.

PERRY, V.D., 1952. Geology of the Chuquicamata orebody. Mining Engineering, V. 4, N°12, pp. 116-1168.

PERRY, V.D., 1960. History of El Salvador development. Mining Engineering, V. 12, N°4, pp. 341-343.

PETERSEN, U., 1970. Metallogenic provinces in South America. Geologische Rundschau, V. 59, pp. 834-897.

PETERSEN, U., 1977. Introduction to the issue devoted to mineral deposits in the South American Cordillera. Economic Geology, V. 72, pp. 887-892.

PHILLIPS, W.J., 1973. Mechanical effects of retrograde boiling and its probable importance in the formation of some porphyry ore deposits. Institution of Mining and Metallurgy Transactions, V. 81, Sec. B, pp. 90-98.

PICHOWIAK, S. and BREITKREUZ, C., 1984. Volcanic dykes in the north Chilean Coast Range. Geologische Runschau, V. 73, pp. 853-868.

PILGER, R.H., 1983. Kinematics of the South American subduction zone from global plate reconstructions. *In*: Cabré, R. (Editor) Geodynamics of the eastern Pacific region, Caribbean and Scotia arcs, Geodynamics Series, V. 9, American Geophys. Union-Geol. Soc. of America, pp. 113-125.

PILGER, R.H., 1984. Cenozoic plate kinematics, subduction and magmatism: South American Andes. J. Geol. Soc. London, V. 141, pp. 793-802.

PITMAN, W.C.,III and ANDREWS, J.A., 1985. Subsidence and thermal history of pull-apart basins. *In*: Biddle, K.T. and Christie-Blick, N. (Editors), Strike-slip deformation, basin formation, and sedimentation. Society Econ. Paleontologists Mineralogists, Special Publication 37, pp. 45-49.

PRICE, P.B. and WALKER, R.M., 1962. Chemical etching of charged-particle tracks in solids. Journal of Applied Physics, V. 33, pp. 3407-3412.

PRICE, P.B. and WALKER, R.M., 1963. Fossil tracks of charged-particles in mica and the age of minerals. Journal of Geophysical Research, V. 68, pp. 4847-4862.

POHL, D.C., 1985. Supergene gold migration and enrichment, Sierra Gorda, Chile. (Abstract), EOS, V. 66, No. 46, pp. 1143.

POHL, D.C., 1986. Supergene gold transport in bromide groundwater. (Abstract), Geological Society of America, Abstracts with Programs 1986, p. 720.

PUIG, A., 1988. Geologic and metallogenic significance of the isotopic composition of lead in galenas of the Chilean Andes. Economic Geology, V. 83, pp. 843-858.

PUIG, A., DIAZ, S. and CUITIÑO, L., 1987. Hydrothermal systems related with a Paleocene cauldron complex in the Central Andes, Chile: El Guanaco, Cachinal de la Sierra and El Soldado mining districts, Antofagasta Region. (Abstract) IUGS/UNESCO Deposit Modelling Program Workshop, "Hydrothermal Systems in Volcanic Centers", pp. 27-28. Workshop held on November 9-18, 1987, Santiago, Chile.

PUIG, A., DIAZ, S. and CUITIÑO, L., 1988. Sistemas hidrotermales asociados a calderas en el arco volcánico paleógeno de la Región de Antofagasta, Chile: Distritos El Guanaco, Cachinal de la Sierra y el Soldado, Revista Geológica de Chile, V. 15, N°1, pp. 91-106.

QUEZADA, R., 1967. Informe geológico Centinela, Sierra Gorda, Provincia de Antofagasta. (Unpublished report), Instituto de Investigaciones Geológicas, 16 p. Santiago.

QUIRT, G.S., 1972. A potassium-argon geochronological investigation of the Andean mobile belt of north-central Chile. Ph.D. Thesis, Queen's University, Kingston, Canada, 240 p.

QUIRT, G.S., STEWARD, J., CLARK, A.H. and FARRAR, E., 1971. Potassium argon ages of porphyry cooper deposits in northern and central Chile. Geol. Soc. Am. Abstracts with Programs, V. 3, N°7, pp. 676-677.

RACZYNSKI, A. 1963. Geología del distrito minero de Tuina. B.Sc. thesis, Depto. Geología, Univ. de Chile, 117 p. Santiago.

RACZYNSKI, A., 1966. Informe geológico minas El Tesoro (minas Marieta y Leonor) Provincia de Antofagasta, Distrito de Sierra Gorda de Orenco Minas Ltda., Antofagasta, (Unpublished report), IIG-ENAMI, 20 p.

RAMIREZ, C., 1979. Edades potasio-argón de rocas volcánicas cenozoicas en la zona de San Pedro de Atacama-El Tatio, Región de Antofagasta. Actas II Congreso Geológico Chileno, Arica, V. 1, pp. F-31 - F-41.

RAMIREZ, C., and HUETE, C., 1981. Hoja Ollagüe, Escala 1:250.000, Región de Antofagasta. Carta Geológica de Chile N°40, Instituto de Investigaciones Geológicas, Santiago, Chile, 47 p.

RAMIREZ, C., and GARDEWEG, M., 1982. Hoja Toconao, Región de Antofagasta. Carta Geológica de Chile, SERNAGEOMIN, Santiago, N°54, 121 p.

RAMOS, V., 1988. Late Proterozoic-Early Paleozoic of South America - a collisional history. Episodes, V. 11, N°.3, pp. 168-174.

RAMOS, V., JORDAN, T.E., ALLMENDINGER, R.W., MPODOZIS, C., KAY, S.M., CORTES, J.M. and PALMA, M.A., 1986. Paleozoic terranes of the Central Argentine-Chilean Andes. Tectonics, V. 5, N°6, pp. 855-880.

READING, H.G., 1980. Characteristics and recognition of strike-slip systems. *In*: Ballance, F. and Reading, H.G. (Editors), Sedimentation in oblique-slip mobile zones. International Association of Sedimentologists, Special Publication No.4, Blackwell, England, pp. 7-26.

REUTTER, K.-J., GIESE, P., GOETZE, H.-J., SCHEUBER, E., SCHWAB, K., SCHWARTZ, G. and WIGGER, P., 1988. Structures and crustal development of the Central Andes between 21° and 25° S. *In*: Bahlburg, Ch., Breitkreuz, C. and Giese, P. (Editors), The Southern Central Andes, Lecture Notes in Earth Sciences, V. 17, pp. 231-261.

REYMER, A. and SHUBERT, G., 1984. Phanerozoic addition rates to the continental crust and crustal growth. Tectonics, V. 3, pp. 63-78.

REYNOLDS, P.H. and DASCH, E.J., 1971. Lead isotopes in marine manganese nodules and the ore growth curve. Journal of Geophysical Research, V. 76, No.21, pp. 5124-5129.

RICHARDS, J.P. and McDOUGALL, I., 1990. Geochronology of the Porgera gold deposit, Papua New Guinea: Resolving the effects of excess argon on K-Ar and $^{40}Ar$-$^{39}Ar$ age estimates for magmatism and mineralization. Geochimica et Cosmochimica Acta, V. 54, pp. 1397-1415.

RIVANO, S., SEPULVEDA, P., HERVE, M. and PUIG, A., 1985. Geocronología K-Ar de rocas intrusivas entre los 31°-32° latitud Sur, Chile. Revista Geológica de Chile, N°24, Santiago, Chile, pp. 63-74.

RIVERA, S., 1980. Geología del distrito aurífero San Cristobal, II Región Antofagasta. B.Sc. thesis, Depto de Geociencias, Univ. del Norte, Antofagasta. 202 p.

RIVERA, S. and STEPHENS, A.J., 1988. Campos geotermales fósiles de edad Terciario Inferior y mineralización asociada en la Región de Antofagasta. V Congreso Geológico Chileno, Actas, V. 1, pp. B39-B64.

RODGERS, D.A., 1980. Analysis of pull-apart basin development produced by *en echelon* strike-slip faults. *In*: Ballance, F. and Reading, H.G. (Editors), Sedimentation in oblique-slip mobile zones. International Association of Sedimentologists, Special Publication No.4, Blackwell, England, pp. 27-41.

ROEDER, D., 1988. Andean-age structure of Eastern Cordillera (Province of La Paz, Bolivia). Tectonics, V. 7, N°1, pp. 23-29.

ROGERS, D.P., 1968. The extrusive iron oxide deposits, "El Laco", Chile. (Abstract), Geol. Soc. Am. Abstracts with Programs, 1968, pp. 252-253.

ROGERS, G., 1985. A geochemical traverse across the North Chilean Andes. Ph.D. Thesis, Dept. of Earth Sciences, The Open University, Milton Keynes, U.K., 333 p.

ROGERS, G. and HAWKESWORTH, C.J., 1989. A geochemical traverse across the North Chilean Andes: evidence for crust generation from the mantle wedge. Earth and Planetary Science Letters, V. 91, pp. 271-285.

RONA, P.A. AND RICHARDSON E.S., 1978. Early Cenozoic global plate reorganization. Earth Planetary Science Letters, V. 40, pp. 1-11.

ROOBOL, M., FRANCIS, P.W., RIDLEY, W.I., RHODES, M. and WALKER, G.P.L., 1974. Physico-chemical characters of the Andean volcanic chain, between latitudes 21° and 22° South. *In*: Gonzales-Ferran, O. (Editor), Andean and Antarctic Volcanology Problems, Proceedings IAVCEI International Symposium on volcanology. Printed in 1976. pp. 450-464.

ROSE, A.W., 1970. Zonal relations of wallrock alteration and sulfide distribution at porphyry copper deposits. Economic Geology, V. 65, pp. 920-936.

ROSE, A.W. and BURT, D.M., 1979. Hydrothermal alteration. *In*: Barnes, H.L. (Editor) Geochemistry of hydrothermal ore deposits. Second Edition, Wiley-Interscience, pp. 173-235.

ROUTHIER, P., 1980. Ou sont les métaux pour l'avenir?. Les provinces metalliques. Essai de métallogénie globale. Memoire du BRGM, n°105, 410 p.

RUIZ, C. and ERIKSEN, G.E., 1962. Metallogenetic provinces of Chile, S.A. Economic Geology, V. 57, N°1, pp. 91-106.

RUIZ, C., AGUIRRE, L., CORVALAN, J., KLOHN, C., KLOHN, E., and LEVI, B., 1965. Geología y yacimientos metalíferos de Chile. Instituto de Investigaciones Geológicas, Santiago. 302 p.

RUIZ, C., AGUILAR, A., EGERT, E., ESPINOSA, W., PEEBLES, F., QUEZADA, R. and SERRANO, M., 1971. Strata-bound copper sulphide deposits of Chile. In Proceedings IMA-IAGOD, 7th General Meeting, Tokyo-Kyoto, Japan, 1970. Soc. Min. Geol. Japan, Special Issue 3, pp. 252-260.

RUIZ, C. and PEEBLES, F., 1988. Geología, distribución y génesis de los yacimientos metalíferos chilenos. Editorial Universitaria, 334 p.

RUTLAND, R.W.R., 1971. Andean orogeny and ocean floor spreading. Nature, V. 233, pp. 252-255.

RUTLAND, R., GUEST, J. and GRASTY, R., 1965. Isotope ages and Andean uplift. Nature, V. 208, No. 5011, pp. 677-678.

SALFITY, J.A., 1982. Evolución paleogeográfica del grupo Salta (Cretácico-Eogénico), Argentina. Actas Quinto Congreso Latinoamericano de Geología, V. 1, pp. 11-26. Buenos Aires.

SALFITY, J.A., MARQUILLAS, R.A., GARDEWEG, M., RAMIREZ, C. and DAVIDSON J., 1985. Correlaciones en el Cretácico superior del norte de Argentina y Chile. Actas, IV Congreso Geológico Chileno, Antofagasta, Chile, T.1, pp. 654-667.

SALES, R.W., 1954. Genetic relations between granites, porphyrites and associated copper deposits. Mining Engineering, 6, pp. 497-505.

SANCHEZ, J., 1968. Estudio geológico preliminar del distrito azufrero Aucanquilcha Polán, Provincia de Antofagasta. (Unpublished report), IIG-CORFO, 32 p.

SARIC, N., 1971. Evolución Cenozoica de la Cordillera de la Costa en la Provincia de Tarapacá. B.Sc. Thesis, Dept. Geología, Univ. de Chile, Santiago, 176 p.

SASAKI, A., ULRIKSEN, C., SATO, K. and ISHIHARA, S., 1984. Sulpur isotope reconnaissance of porphyry copper and manto-type deposits in Chile and the Philippines: Bulletin of the Geological Survey of Japan, V. 35, pp. 615-622.

SATO, T., 1984. Manto type copper deposits in Chile: a review. Bulletin of the Geological Survey of Japan. V. 35, p. 565-582.

SAWKINS, F.J., 1972. Sulfide ore deposits in relation to plate tectonics. Journal of Geology, V. 80, pp. 377-97.

SAWKINS, F.J., 1990. Metal deposits in relation to plate tectonics. Second Edition, Springer-Verlag, 461 p.

SAWYER, D.S, HSUI, A.T. and TOKSOZ, M.N., 1987. Extension, subsidence and thermal evolution of the Los Angeles Basin - a two dimensional model. Tectonophysiscs, V. 133, pp. 15-32.

SCHEUBER, E. and ANDRIESSEN, P.A.M., 1990. The kinematic and geodynamic significance of the Atacama fault zone, northern Chile. Journal of Structural Geology, V. 12, No 2, pp. 243-257.

SCHMITT, H., 1950. The origin of the "epithermal" mineral deposits. Economic Geology, V. 45, pp. 191-200.

SCHWAN, W., 1985. The worldwide active middle-late Eocene geodynamic episode with peaks at 45 and 37 m.y. B.P., and implications and problems of orogeny and sea-floor spreading. Tectonophysics, V. 115, pp. 197-234.

SCHWELLER, W.J., KULM, L.D. and PRINCE, R.A., 1981. Tectonics, structure and sedimentary framework of the Peru-Chile trench. *In*: Kulm, L.D. and others (Editors), Nazca Plate: Crustal Formation and Andean Convergence, Geological Society of America, Memoir 154, pp. 323-349.

SEGALL, P. and POLLARD, D.D., 1980. Mechanics of discontinuous faults, Journal of Geophysical Research, V. 85, No. B8, pp. 4337-4350.

SEPULVEDA, R., 1963. Estudio del yacimiento de cobre de Lomas Bayas en la provincia de Antofagasta. (Unpublished report), ENAMI, 29 p. (Rol N° 22250).

SERNAGEOMIN, 1989. Anuario de la minería de Chile. SERNAGEOMIN, Santiago Chile, 135 p.

SERRANO, M., 1960. Cooper-uranium deposits of Sierra Gorda mining district, Province of Antofagasta, Chile, (Unpublished report), Instituto de Investigaciones Geológicas, 73 p.

SHAW, H.R., 1980. The fracture mechanism of magma transport from the mantle to the surface. *In*: Hargraves, R.B. (Editor), Physics of magmatic processes, Princeton University Press, New Jersey, pp. 201-264.

SHEFFELS, B., BURCHFIELD, C. and MOLNAR, P., 1986. Deformational style and crustal shortening in the Bolivian Andes (Abstract), EOS Transactions AGU, V. 44, p. 1241.

SHEPPARD, S.M.F. and GUSTAFSON, L.B., 1976. Oxygen and hydrogen isotopes in the porphyry copper deposit at El Salvador, Chile. Economic Geology, V. 71, pp. 1549-1559.

SHEPPARD, S.M.F., NIELSEN, R.L. and TAYLOR, H.P. Jr., 1971. Oxygen and hydrogen isotope ratios in minerals from porphyry copper deposits: Economic Geology, V. 66, pp. 515-542.

SHIBATA, K., ISHIHARA, S. and ULRIKSEN, C., 1984. Rb-Sr ages and initial $^{87}Sr/^{86}Sr$ ratios of Late Paleozoic granitic rocks from northern Chile. Bulletin of the Geological Survey of Japan, V. 35, N°11, pp. 503-536.

SIBSON, R.H., MOORE, J.McM. and RANKIN, A.H., 1975. Seismic pumping - a hydrothermal fluid transport mechanism. Journal of the Geological Society London, V. 131, pp. 653-659.

SIBSON, R.H., 1985. Stopping of earthquake ruptures at dilational fault jogs. Nature, V. 316, pp. 248-251.

SIBSON, R.H., 1986. Brecciation processes in fault zones: inferences from earthquake rupturing. Pure and Applied Geophysics, V. 124, Nos. 1/2, pp. 159-175.

SIBSON, R.H., 1987. Earthquake rupturing as mineralizing agent in hydrothermal systems. Geology, V. 15, pp. 701-704.

SILLITOE, R.H., 1969. Studies of the controls and mineralogy of the supergene alteration of copper deposits, northern Chile. Ph.D. Thesis, University of London, 498 p.

SILLITOE, R.H., 1972. A plate tectonic model for the origin of porphyry copper deposits. Economic Geology, V. 67, pp. 184-197.

SILLITOE, R.H., 1972b. Relation of metal provinces in Western America to subduction of oceanic lithosphere. Geol. Soc. of America Bull., V. 83, pp. 813-818.

SILLITOE, R.H., 1973. The tops and bottoms of porphyry copper deposits. Economic Geology, V. 68, pp. 799-815.

SILLITOE, R., 1974. Tectonic segmentation of the Andes: Implications for magmatism and metallogeny: Nature, V. 250, pp. 542-545.

SILLITOE, R.H., 1976. Andean mineralization a model for the metallogeny of convergent plate margins. *In*: Strong, D.F. (Editor) Metallogeny and plate tectonics, Geol. Assoc. Canada, Special Paper, N°14, pp. 59-100.

SILLITOE, R.H., 1977. Permo-Carboniferous, Upper Cretaceous, and Miocene porphyry copper-type mineralization in the Argentinian Andes. Economic Geology, V. 72, pp. 99-109.

SILLITOE, R.H., 1980. Are porphyry copper deposits and Kuroko-type massive sulfide deposits incompatible?. Geology, V. 8, pp. 11-14.

SILLITOE, R.H., 1981. Regional aspects of the Andean porphyry copper belt in Chile and Argentina. Inst. Min. Metall. Transactions, Section B, V. 90, pp. 15-36.

SILLITOE, R.H., 1986. Space-time distribution, crustal setting and Cu/Mo ratios of Central Andean porphyry copper deposits: Metallogenic implications. *In*: Friedrich, G.H. and others (Editors), Geology and Metallogeny of copper deposits, Springer-Verlag, pp. 235-250.

SILLITOE, R.H., 1985. Epochs of intrusion-related copper mineralization in the Andes (Expanded abstract). Final Symposium of Project IGCP 120 "Magmatic Evolution of the Andes", Comunicaciones N° 35, Depto. Geología Univ. de Chile, pp. 225-226.

SILLITOE, R.H., 1988. Epochs of intrusion-related copper mineralization in the Andes. Journal of South American Earth Sciences, V. 1, N°1, pp. 89-108.

SILLITOE, R.H., MORTIMER, C. and CLARK, A.H., 1968. A chronology of landform evolution and supergene mineral alteration, southern Atacama Desert Chile: Trans. Inst. Mining. Metall., Section B, V. 77, pp. 166-169.

SILLITOE, R.H. and CLARK, A.H., 1969. Copper and copper sulfides as the initial products of supergene oxidation, Copiapó mining district, northern Chile. The American Mineralogist, V. 54, pp. 1684-1710.

SILLITOE, R. and NEUMANN, H., 1970. Centinela. (Unpublished report), Instituto de Investigaciones Geológicas, 4 p. Santiago.

SILLITOE, R.H. and SAWKINS, F.J., 1971. Geologic, mineralogic and fluid inclusion studies relating to the origin of copper bearing tourmaline breccia pipes, Chile. Economic Geology, V. 66, pp. 1028-1041.

SILLITOE, R.H., and GAPPE, I.M., (1984). Phillipine porphyry copper deposits: geologic setting and characteristics. CCOP Project Office, UNDP Technical Support for Regional Offshore Prospecting in East Asia (RAS/81/120), 89 p.

SILLITOE, R.H. and HART, S.R., 1984. Lead isotopic signatures of porphyry copper deposits in oceanic and continental settings, Colombian Andes. Geochimica et Cosmochimica Acta, V. 48, pp. 2135-2142.

SIMIC, D., 1971. Informe sobre la revisión de la documentación del distrito de cobre y molibdeno Sierra Gorda, Depto Antofagasta. Prov. Antofagasta. (Unpublished report), ENAMI, 52 p. Santiago (Rol N° 22312).

SIMPSON, C., 1985. Deformation of granitic rocks across the brittle-ductile transition. Journal of Structural Geology, V. 7, N°5, pp. 503-511.

SISSELMAN, R., 1978. Chile's Chuquicamata: looking to stay no. 1 in copper output. Engineering Mining Journal, V. 179, Aug. 1978, pp. 59-64.

SKARMETA, J., 1983. The structural geology of the Sierra de Moreno northern Chile. Ph.D. Thesis, Univ. of London, 309 p. London, U.K.

SKARMETA, J. and MARINOVIC, N., 1981. Hoja Quillagua, Región de Antofagasta. Carta Geológica de Chile, N°51, 63 p., SERNAGEOMIN, Santiago.

SKEWES, M.A., 1985. Biotitas en la zona de alteración potásica de cobre porfídico Los Pelambres. Actas, IV Congreso Geológico Chileno, Antofagasta, V. 2, pp. 341-353.

SPERA, F.J., 1980. Aspects of magma transport. *In*: Hargraves, R.B. (Editor), Physics of magmatic processes, Princeton University Press, New Jersey, pp. 265-323.

ST. AMAND, P. and ALLEN, C.R., 1960. Strike-slip faulting in northern Chile (Abstract), Geological Society of America Bulletin, V. 71, p. 1965.

STAUDER, W.M., 1973. Mechanism and spatial distribution of Chilean earthquakes with relation to subduction of the oceanic plate. Journal of Geophysical Research, V. 78, pp. 5033-5061.

STEIGER, R.H. and JAGER, E., 1977. Subcomission on Geochronology IUGS; convention on the use of decay constants in geo- and cosmochronology. Earth Planetary Science Letters, V. 36, N°3, pp. 359-367.

STEINMAN, G., 1929. Geologie von Peru. Carl Winters Univstatsbuchladlung, Heidelberg, 448 p.

STERN, C.R., 1988. Source region versus intra-crustal contamination in the petrogenesis of the Quaternary volcanic centers at the northern end (33-34°S) of the Southern Volcanic Zone of the Andes. Actas V Congreso Geológico Chileno, V. 3, pp. 129-143.

STERN, C.R., 1989. Pliocene to Present migration of the volcanic front, Andean Southern Volcanic Zone. Revista Geológica de Chile, V. 16, No. 2, pp. 145-162.

STERN, C.R., In Press. The role of tectonic erosion, sediment subduction, and source region contamination in magma genesis at the northern end (33-34°S) of the Southern Volcanic Zone of the Andes. Geological Society of America, Special Paper "Andean Magmatism and its tectonic setting", in press.

STOERTZ, G.E. and ERICKSEN, G.E., 1974. Geology of salars in northern Chile: U.S.G.S. Professional Paper 811, 65 p.

STOLL, W.C., 1964. Metallogenic belts, centers and epochs in Argentina and Chile. Economic Geology, V. 59, pp. 126-135.

STOLL, W.C., 1965. Metallogenic provinces of South America. Mining Magazine, V. 112, pp. 22-33, 90-99.

STORMER, J.C., Jr., 1975. A practical two-feldspar geothermometer. American Mineralogist, V. 60, pp. 667-674.

STRECKER, M.R., CERVENY, P., BLOOM. A.L. and MALIZIA, D., 1989. Late Cenozoic tectonism and landscape development in the foreland of the Andes: northern Sierras Pampeanas (26°-28°S), Argentina. Tectonics, V. 8, No. 3, pp. 517-534.

STRECKEISEN, A. and LE MAITRE, R.W., 1979. A chemical approximation to model QAPF classification of igneous rocks. Neues Jahrbuch Miner. Abh., V. 136, No. 2, pp. 169-206, Stuttgart, August, 1979.

SUAREZ, G., MOLNAR, P. and BURCHFIELD, B.C., 1983. Seismicity, fault plane solutions, depth of faulting, and active tectonics of the Andes of Peru, Ecuador and southern Colombia. Journal of Geophysical Research, V. 88, pp. 10403-10429.

SUAREZ, M., NARANJO, J.A. and PUIG., A., 1985. Estratigrafía de la Cordillera de la Costa, al sur de Taltal, Chile: etapas iniciales de la evolución andina. Revista Geológica de Chile, N°24, pp. 19-28.

SUN, S.,-S., 1980. Lead isotopic study of young volcanic rocks from mid-ocean ridges, ocean islands and island arcs. Philosophical Transactions Royal Society of London, Ser.A, V. 297, pp. 409-445.

SUTULOV, A., 1974. Copper porphyries. The University of Utah Printing Services, Salt Lake City, Utah, 200 p.

SWANSON, M.T., 1988. Pseudotachylite-bearing strike-slip duplex structures in the Fort Foster brittle zone, S. Maine. Journal of Structural Geology, V. 10, No.8, pp. 813-828.

SYLVESTER, A.G., 1988. Strike-slip faults. Geological Society of America Bulletin, V. 100, pp. 1666-1703.

TAYLOR, A.V., 1935. Ore deposits at Chuquicamata, Chile. XVI International Geological Congress, Washington, V. 2, pp. 473-484.

TAYLOR, H.P., 1974. The application of oxygen and hydrogen isotopic studies to problems of hydrothermal alteration and ore deposition. Economic Geology, V. 69, pp. 843-883.

TAYLOR, H.P., 1979. Oxygen and hydrogen isotope relationships in mineral deposits. *In*: Barnes, H.L. (Editor), Geochemistry of hydrothermal ore deposits, Second edition, John Wiley & Sons, pp. 236-277.

TAYLOR, 1984. Magmatic volatiles: isotopic variation of C, H and S. *In*: Valley, J.W. and others (Editors), Stable Isotopes in high temperature geological processes. Reviews in Mineralogy, Mineralogical Society of America, V. 16, pp. 185-225.

TAYLOR, R.P. and FRYER, B.J., 1982. Rare earth element geochemistry as an aid to interpreting hydrothermal ore deposits. *In*: Evans, A.M. (Editor) Metallization Associated with Acid Magmatism, John Wiley & Sons Ltd., pp. 357-365.

TERA, F., BROWN, L., MORRIS, J., SACKS, I.S., KLEIN, J. AND MIDDLETON, R., 1986. Sediment in island-arc magmas: inferences from $^{10}Be$. Geochimica et Cosmochimica Acta, V. 50, pp. 535-550.

THE GUINNESS BOOK OF RECORDS, 1990. McFarlan, D. (Editor), Guinness Publishing Ltd., 320 p.

THIEL, K. and HERR, W., 1976. The $^{238}U$ spontaneous fission decay constant redetermined by fission tracks. Earth and Planetary Science Letters, V. 30, pp. 50-56.

THOMAS, A., 1970. Beitrag zur tektonik Nordchiles. Geologische Rundschau, V. 59, pp. 1013-1027.

THOMPSON, J.D., 1978. Ocean deserts and ocean oases. Climatic change, V. 1, pp. 205-230.

THOMPSON, R.N., MORRISON, M.A., HENDRY, G.L. and PARRY, S.J., 1984. An assesment of the relative roles of crust and mantle in magma genesis: an elemental approach. Philosophical Transactions of the Royal Society London, Sec.A, V. 310, pp. 549-590.

THORPE, R.S., FRANCIS, P.W. and HARMON, R.S., 1981. Andean andesites and crustal growth. Philosophical Transactions Royal Society of London, Series A, V. 301, pp. 305-320.

THORPE, R.S., FRANCIS, P.W., HAMMILL, M. and BAKER, M.C.W., 1982. The Andes, *In*: Thorpe, R.S. (Editor), Andesites, John Wiley & Sons, pp. 187-205.

THORPE, R.S., FRANCIS, P.W. and O'CALLAGHAN, L., 1984. Relative roles of source composition, fractional crystallization and crustal contamination in the petrogenesis of Andean volcanic rocks. Philosophical Transactions Royal Society of London, Ser.A, V. 310, pp. 675-692.

TILTON, G.R., 1979. Isotopic studies of Cenozoic Andean calc-alkaline rocks. Carnegie Institution Washington, Yearbook 78, pp. 298-304.

TILTON, G.R., 1983. Evolution of depleted mantle: The lead perspective. Geochimica et Cosmochimica Acta, V. 47, pp. 1191-1197.

TILTON, G.R. and BARREIRO, B.A., 1980. Origin of lead in Andean calc-alkaline lavas, Southern Peru. Science, V. 210, pp. 1245-1247.

TILTON, G.R., POLLAK, R.J., CLARK, A.H., and ROBERTSON, R.C.R., 1981. Isotopic composition of Pb in Central Andean ore deposits. Geological Society of America, Memoir 154, pp. 791-816.

TITLEY, S.R., 1981. Geologic and geotectonic setting of porphyry copper deposits in the Southern Cordillera. *In*: Dickinson, W.R. and Payne, W.D. (Editors). Relations of tectonics to ore deposits in the Southern Cordillera. Arizona Geological Society Digest, V. XIV, pp. 79-97.

TITLEY, S.R., 1982. (Editor), Advances in Geology of the Porphyry Copper Deposits, Southwestern North America. The University of Arizona Press, Tucson, Arizona, 560 p.

TITLEY, S.R. and BEANE, R.E., 1981. Porphryry copper deposits, Part 1: geologic settings, petrology, and tectogenesis. Economic Geology 75th Anniversary Volume, pp. 214-234.

TOBAR, A., 1966. Estratigrafía del área Baquedano-Rencoret, Provincia de Antofagasta. B.Sc. thesis, Depto. de Geología, Univ. de Chile, 80 p., Santiago.

TOBAR A., 1977. Stratigraphy and structure of the El Salvador-Potrerillos region, Atacama, Chile. Ph.D. Thesis, University of California, 117 p.

TOBAR, A., 1981. Geología de Mantos Blancos (Abstract). Actas Primer Coloquio sobre volcanismo y metalogénesis. Depto. Geociencias, Univ. del Norte, pp. 68-69, Antofagasta.

TOSDAL, R.M., CLARK, A.H. and FARRAR, E., 1984. Cenozoic polyphase landscape and tectonic evolution of the Cordillera Occidental, southernmost Peru. Geological Society of America Bulletin, V. 95, pp. 1318-1332.

TRASK, F., 1968. Exótica ore reserves. (Unpublished report), Anaconda Co., 2 p.

TRAVISANY, V., 1976. Evaluación preliminar de los yacimientos de plata de la II Región (Antofagasta). (Unpublished report), Instituto de Investigaciones Geológicas, Santiago, 67 p.

TRAVISANY, V., 1978. Mineralización cuprífera en areniscas de la formación San Pedro en el distrito San Bartolo. B.Sc. thesis, Depto. Geología, Univ. de Chile, 71 p. Santiago.

TRAVISANY, V. and DIAZ, F., 1978. Estudio geológico y geoquímico del sector Nevados del Poquis, Etapa II, Proyecto Prospección y evaluación de elementos polimetálicos Alta Cordillera II Región. (Unpublished report), Instituto de Investigaciones Geológicas, V. 9, 38 p.

TREWARTHA, G.T., 1981. An introduction to climate (4th edition). New York, McGraw-Hill Book Co., 408 p.

TRIEP, E.G., and CARDINALI, C.B., 1984. Mecanismos de sismos en las Sierras Pampeanas occidentales. Actas IX Congreso Geológico Argentino, San Carlos de Barriloche, Argentina, pp. 61-80.

TUFIÑO, G., 1973. Antecedentes de geología del yacimiento Pampa Norte-Chuquicamata, B.Sc. thesis, Depto. Geología, Univ. de Chile, 85 p., Santiago.

TULLIS, J. and YUND, R.A., 1978. Experimental deformation of dry Westerly granite. Journal of Geophysical Research, V. 82, N°36, pp. 5705-5718.

TULLIS, J. and YUND, R.A., 1980. Hydrolytic weakening of experimentally deformed Westerly granite and Hale albite rock. Journal of Structural Geology, V. 2, N°4, pp. 439-451.

TURNER, G., 1968. The distribution of potassium and argon in chondrites. *In*: Ahrens, L.H. (Editor), The distribution of the elements, Pergamon Press, pp. 387-398.

TURNER, G., 1969. Thermal histories of meteorites by the $^{39}Ar$-$^{40}Ar$ method. *In*: Millman, P.M. (Editor), Meteorite Research, Riedel, pp. 407-417.

TURNER, G., 1970a. Argon-40/argon-39 dating of lunar rock samples. Proc. Apollo 11 Lunar Sci. Conf., Geochimica et Cosmochimica Acta, Suppl.1, V. 2, pp.1665-1684.

TURNER, G., 1970b. Thermal histories of meteorites. *In*: Runcorn, S.K. (Editor), Paleogeophysics, Academic Press, pp. 491-502.

TURNER, J. and MENDEZ, V., 1975. Geología del sector oriental de los departamentos de Santa Victoria e Iruya, Prov. de Salta. Bol. Acad. Nac. Cienc. LI (1-2): 11-24. Argentina.

TURNER, J. and MENDEZ, V., 1979. Puna. *In* Geología Regional Argentina, N°2, Academia Nacional de Ciencias, V. 1, pp. 13-56, Córdoba, Argentina.

ULRIKSEN, C., 1979. Regional geology, geochronology and metallogeny of the Coastal Cordillera of Chile between 25°30' and 26° south. M.Sc. Thesis Dalhousie University, Canada, 221 p.

UNESCO, 1980. Desertification in the region of Coquimbo, Chile. *In* Mabbutt, J.A. and FLORET, C. (Eds.), Case studies on desertification, London, England, UNESCO Natural Resources Series, N°18, pp. 52-14.

UNRUH, D.M. and TATSUMOTO, M., 1976. Lead isotopic composition and uranium, thorium, and lead concentrations in sediments and basalts from the Nazca plate. Initial Reports of the Deep Sea Drilling Project, U.S. Government Printing Office, Washington D.C., V. 34, pp. 341-347.

URIBE, F. and NIEMEYER, H., 1984. Franjas miloníticas en la Cordillera de la Costa de Antofagasta (Cuadrángulos Cerro Cristales, 24°00'-24°15' S) y la distribución del Basamento precámbrico. Revista Geológica de Chile N°23, Santiago, pp. 87-91.

UYEDA, S., 1987. Chilean vs Mariana type subduction zones with remarks on arc-volcanism and collision tectonics. In. Monger, J.W.H. and Francheteau, J., (Editors), Amer. Geophys. Union - Geol. Soc. of America, Geodynamic Series, V. 18, pp. 1-7.

UYEDA, S. and NISHWAKI, C., 1980. Stress field, metallogenesis and mode of subduction. *In*: Strangway, D., (Editor), The continental Crust and Its Mineral Resources, Geological Association of Canada, Special Paper 20, pp. 323-339.

VALDEBENITO, E., 1979. Geología de las fosforitas, Mejillones. B.Sc. thesis, Depto. Geología, Univ. de Chile, 152 p., Santiago.

VEGA, J. and BORDONES, L., 1981. Geología del cuadrángulo Cerros de Paqui y parte oeste del cuadrángulo Conchi, Prov. El Loa, II Región, Antofagasta, Chile. B.Sc. thesis, Depto. de Geociencias, Univ. del Norte, Antofagasta, 136 p.

VERGARA, H., 1978. Cuadrángulo Quehuita y sector occidental del cuadrángulo Volcán Miño, Región de Tarapacá. Carta Geológica de Chile, N°32, 44 p., Instituto de Investigaciones Geológicas, Santiago.

VERGARA, M., 1985. Geología de los distritos cupríferos Naguayán, Desesperado y El Morado, Segunda Región de Antofagasta, Chile. B.Sc. thesis, Depto. de Geociencias, Univ. del Norte, 80 p., Antofagasta.

VERGARA, H. and THOMAS, A., 1984. Hoja Collacagua, Región de Tarapacá. Carta Geológica de Chile N°59, SERNAGEOMIN, 79 p., Santiago.

VERNON, R.H., 1974. Controls of mylonitic compositional layering during non-cataclastic ductile deformation. Geological Magazine 111 (2), pp. 121-123.

VICENTE, J.C., 1970. Reflexiones sobre la porción meridional del sistema peripacífico oriental. *In*: Conference on Solid Earth Problems, Buenos Aires, Argentina, V. 1, pp. 158-184.

VICENTE, J.C., 1972. Aperçu sur l'organisation et l'evolution des Andes argentino-chiliennes centrales au parallèle de l'Aconcagua. *In*: 24th International Geological Congress, Montreal, Canada, Section 3, pp. 423-436.

VICENTE, J.C., CHARRIER, R., DAVIDSON, J., MPODOZIS, C. and RIVANO, S., 1973. La orogénesis Subhercínica: fase mayor de la evolución paleogeográfica y estructural de Los Andes Argentino-Chilenos Centrales. Actas V Congreso Geológico Argentino, V, Buenos Aires, Argentina, pp. 81-98.

VIDAL, C.E., 1985. Metallogenesis associated with the Coastal Batholith of Peru: a review. *In*: Pitcher, W.S. and others (Eds.). Magmatism at a plate edge. The Peruvian Andes, pp. 243-249.

VIDAL, PH. and CLAUER, N., 1981. Pb and Sr isotopic systematics of some basalts and sulfides from the East Pacific Rise at 21°N (project RITA). Earth and Planetary Science Letters, V. 55, pp. 237-246.

VILA, T., 1974. Geología y Geoquímica de los depósitos salinos, Provincia de Antofagasta. B.Sc. thesis, Depto. de Geología, Univ. de Chile.

WAGNER, G.A., 1968. Fission track dating of apatites. Earth and Planetary Science Letters, V. 4, pp. 411-415.

WAGNER, G.A. and REIMER, G.M., 1972. Fission track tectonics: the tectonic interpretation of fission track apatite ages. Earth and Planetary Science Letters, V. 14, pp. 263-268.

WAGNER, G.A., REIMER, G.M. and JAEGER, E., 1977. Cooling ages derived by apatite fission-track, mica Rb-Sr and K-Ar dating: The uplift and cooling history of the Central Alps. Memorie degli Instituti di Geologia e Mineralogia dell'Universita di Padova, V. 30.

WALCOTT, R.I., 1978. Geodetic strains and large earthquakes in the axial tectonic belt of north island, New Zealand. Journal of Geophysical Research, V. 83, pp. 4419-4429.

WEAVER, C.S., GRANT, W.C. and SHEMETA, J.E., 1987. Local crustal extension at Mount St. Helens. Washington. Journal of Geophysical Research, V. 92, B10, pp. 10,170-10,178.

WEERTMAN, J., 1971. Theory of water-filled crevices in glaciers applied to vertical magma transport beneath oceanic ridges. Journal of Geophysical Research, V. 76, pp. 1171-1183.

WEGNER, R., 1979. Die magnetit lavastrome von El Laco un Chile, und ihiere begleitenden gesteine. B.Sc. thesis, Albert-Ludwing University, 89 p., Freiburg Bremen, Germany.

WENDEL, C., 1941. Report on the Los Amigos mines of the Caracoles silver district. (Unpublished report), Chile Exploration Co., 7 p., SERNAGEOMIN Archive N°4411.

WENDEL, C., 1947. Report of reconnaissance examination of the Sierra Valenzuela copper district near Baquedano, Chile. (Unpublished report), Chile Exploration Co., Potrerillos, SERNAGEOMIN Archive N°4397, 17 p.

WENDEL, C. and WEISSENBORN, A. 1940. Report on the reconanaissance examination of the region in the vecinity of the Nevados de Poquis, Chile. (Unpublished report), Chile Exploration Co., 12 p., SERNAGEOMIN Archive N°4412.

WETZEL, W., 1927. Beitrage zur Erdgeschichte der mittleren Atacama. Neues Jahrb., Mineralogie, geologie und palaontologie, Ser. B, N°58, pp. 505-578.

WHITE, A.J.R. and CHAPPEL, B.W., 1977. Ultrametamorphism and granitoid genesis. Tectonophysics, V. 43, pp. 7-22.

WHITMAN, J.M., HARRISON, C.G.A. and BRASS, G.W., 1983. Tectonic evolution of the Pacific Ocean since 74 Ma. Tectonophysics, V. 99, pp. 241-249.

WHITNEY, J.A., 1988. The origin of granite: The role and source of water in the evolution of granitic magmas. Geological Society of America Bulletin, V.100, pp. 1886-1897.

WIGGER, P.J., 1988. Seismicity and crustal structure of the Central Andes, *In*: Bahlburg, H., Breitkreuz, C. and Giese, P. (Editors), The Southern Central Andes, Lecture Notes in Earth Sciences, V. 17, Springer-Verlag, pp.

WINCHESTER, J.A. and FLOYD, P.A., 1977. Geochemical discrimination of different magma series and their differentiation products using immobile elements. Chemical Geology, V. 20, pp. 325-343.

WOODCOCK, N.H., 1986. The role of strike-slip fault systems at plate boundaries. Royal Society of London Philosophical Transactions, Ser. A, V. 317, pp.13-29.

WOODCOCK, N.H. and FISHER, M., 1986. Strike-slip duplexes. Journal of Structural Geology, V. 8, No.7, pp. 725-735.

WORTEL, M.J.R. and CLOETINGH, S.A.P.L., 1985. Accretion and lateral variations in tectonic structure along the Peru-Chile Trench. Tectonophysics, V. 112, pp. 443-462.

YODER, H.S. Jr., 1976. Generation of basaltic magma. U.S. National Academy of Science, Washington, 265 p.

ZARTMAN, R.E., 1984. Lead, strontium, and neodymium isotopic characterization of mineral deposits relative to their geologic environments. Proceedings of the 27th International Geological Congress, V. 12, pp. 83-106.

ZARTMAN, R.E. and DOE, B.R., 1981. Plumbotectonics - The model. Tectonophysics, V. 75, pp. 135-162.

ZEIL, W., 1979. The Andes, A geological Review, Gebrüder Borntraeger, Berlin, Stuttgart.

ZEITLER, P.K., 1983. Uplift and cooling history of the N.W. Himalaya, northern Pakistan; evidence from fission-track and $^{40}Ar$-$^{39}Ar$ cooling ages. Unpublished Ph.D. thesis, Dartmouth College, 297 p.

ZEITLER, P.K., TAHIRKHELI, R.A.K., NAESER, C.W. and JOHNSON, N.M., 1982. Unroofing history of a suture zone in the Himalaya of Pakistan by means of fission-track annealing ages. Earth and Planetary Science Letters, V. 57, pp. 227-240.

ZENTILLI, M., 1974. Geological Evolution and metallogenic relationships in the Andes of northern Chile, between 26° and 29° South. Ph.D. Thesis, Queen's University, Kingston, Canada, 446 p.

ZENTILLI, M., 1975. Zonación regional y evolución metalogénica de los Andes entre las latitudes 26° y 29° Sur. Actas II Congreso Iberoamericano de Geología Económica. Tomo V, Buenos Aires, Argentina, pp 531-544.

ZENTILLI, M., DOE, B.R., HEDGE, C.E., ALVAREZ, O., TIDY, E. and DAROCA, J.A., 1988. Isótopos de plomo en yacimientos de tipo pórfido cuprífero, comparados con otros depósitos metalíferos en los Andes del norte de Chile y Argentina. Actas V Congreso Geológico Chileno, Tomo I, pp. B331-B369.

ZIMMERMANN, R.A., REIMER, G.M., FOLAND, K.A. and FAUL, H., 1975. Cretaceous fission track dates of apatites from northern New England. Earth and Planetary Science Letters, V. 28, pp. 181-188.

ZIMMERMANN, R.A. and GAINES, A.M., 1978. A new approach to the study of fission-track fading. *In*: Zartman, R.E. (Editor) Short papers of the fouth International Conference on Geocronology, Cosmochronology, Isotope Geology. USGS Open-file Report 78-701.

ZONESHAYN, L.P., SAVOSTIN, L.A. and SEDOV, A.P., 1984. Global Paleogeodynamic reconstructions for the last 160 million years. Geotectonics, V. 18, N°3, pp. 181-195.

ZONENSHAYN, L.P., SAVOSTIN, L.A., SEDOV, A.P. and VOLOKITINA, L.P., 1985. Paleogeodynamics world base maps and paleobathymetry for the last 70 Ma: an explanatory note. Tectonophysics, V. 116, pp. 189-207.